

**CLINCH RIVER
BREEDER REACTOR PROJECT**

**PRELIMINARY
SAFETY ANALYSIS
REPORT**

VOLUME 18

PROJECT MANAGEMENT CORPORATION

TABLE OF CONTENTS

<u>Section</u>		<u>Page</u>
1.0	<u>INTRODUCTION AND GENERAL DESCRIPTION OF THE PLANT</u>	1.1-1
1.1	<u>INTRODUCTION</u>	1.1-1
1.1.1	General Information	1.1-2
1.1.2	Overview of Safety Design Approach	1.1-3
1.1.3	Applicability of Regulatory Guides	1.1-5
1.2	<u>GENERAL PLANT DESCRIPTION</u>	1.2-1
1.2.1	Site	1.2-1
1.2.2	Engineered Safety Features	1.2-2
1.2.3	Reactor, Heat Transport and Related Systems	1.2-2
1.2.4	Steam Generator - Turbine and Related Systems	1.2-3
1.2.5	Offsite and Onsite Power	1.2-5
1.2.6	Instrumentation, Control and Protection	1.2-6
1.2.7	Auxiliary Systems	1.2-7
1.2.8	Refueling System	1.2-8
1.2.9	Radwaste Disposal System	1.2-9
1.2.10	Reactor Confinement/Containment System	1.2-9
1.2.11	Major Structures	1.2-10
1.3	<u>COMPARISON TABLES</u>	1.3-1
1.3.1	Comparisons with Similar Designs	1.3-1
1.3.2	Detailed Comparison with Fast Flux Test Facility	1.3-2
1.4	<u>IDENTIFICATION OF PROJECT PARTICIPANTS</u>	1.4-1
1.4.1	Functions, Responsibilities and Authorities of Project Participants	1.4-2
1.4.2	Description of Organizations	1.4-3
1.4.3	Interrelationships with Contractors and Suppliers	1.4-21a
1.4.4	General Qualification Requirement of CRBRP Project Participants	1.4-22
1.5	<u>REQUIREMENTS FOR FURTHER TECHNICAL INFORMATION</u>	1.5-1
1.5.1	Information Concerning the Adequacy of a New Design	1.5-2
1.5.2	Information Concerning Margin of Conservatism of Proven Design	1.5-28
1.5.3	References	1.5-47

TABLE OF CONTENTS (Cont'd.)

<u>Section</u>		<u>Page</u>
1.6	<u>MATERIAL INCORPORATED BY REFERENCE</u>	1.6-1
1.6.1	Introduction	1.6-1
1.6.2	References	1.6-1
	Appendix 1-A Flow Diagram Symbols	1.A-1
2.0	<u>SITE CHARACTERISTICS</u>	2.1-1
2.1	<u>GEOGRAPHY AND DEMOGRAPHY</u>	2.1-1
2.1.1	Site Location and Layout	2.1-1
2.1.2	Site Description	2.1-2
2.1.3	Population and Population Distribution	2.1-4
2.1.4	Uses of Adjacent Lands and Waters	2.1-8
2.2	<u>NEARBY INDUSTRIAL, TRANSPORTATION AND MILITARY FACILITIES</u>	2.2-1
2.2.1	Locations, Routes, and Descriptions	2.2-1
2.2.2	Evaluations	2.2-3
2.2.3	New Facility/Land Use Requirements	2.2-4c
2.3	<u>METEOROLOGY</u>	2.3-1
2.3.1	Regional Climatology	2.3-1
2.3.2	Local Meteorology	2.3-4
2.3.3	On-site Meteorological Monitoring Program	2.3-9
2.3.4	Short-Term (Accident) Diffusion Estimates	2.3-9
2.3.5	Long-Term (Average) Diffusion Estimates	2.3-13
2.4	<u>HYDROLOGIC ENGINEERING</u>	2.4-1
2.4.1	Hydrologic Description	2.4-1
2.4.2	Floods	2.4-6
2.4.3	Probable Maximum Flood (PMF) on Streams and Rivers	2.4-10
2.4.4	Potential Dam Failures (Seismically and Otherwise Induced)	2.4-21
2.4.7	Ice Flooding	2.4-31
2.4.8	Cooling Water Canals and Reservoirs	2.4-31a
2.4.9	Channel Diversions	2.4-32
2.4.10	Flooding Protection Requirements	2.4-32
2.4.11	Low Water Considerations	2.4-33
2.4.12	Environmental Acceptance of Effluents	2.4-42
2.4.13	Groundwater	2.4-44
2.4.14	Technical Specification and Emergency Operation Requirement	2.4-55

TABLE OF CONTENTS (Cont'd.)

<u>Section</u>		<u>Page</u>
2.5	<u>GEOLOGY AND SEISMOLOGY</u>	2.5-1
2.5.1	Basic Geologic and Seismic Information	2.5-1
2.5.2	Vibratory Ground Motion	2.5-20
2.5.3	Surface Faulting	2.5-27
2.5.4	Stability of Subsurface Materials	2.5-32
2.5.5	Slope Stability	2.5-48a
	Appendix 2-A Field Investigative Procedures	2A-1
	Appendix 2-B Laboratory Test Procedures	2B-1
	Appendix 2-C Report of Test Grouting Program	2C-1
	Appendix 2-D Report of Engineering Properties for Crushed Stone Materials from Commercial Suppliers	2D-1
	Appendix 2-E Extracts from U.S. Atomic Energy Commission AEC Manual	2E-1
	Supplement 1 to Chapter 2 Deleted	
	Supplement 2 to Chapter 2 Question and Responses Related to Chapter Two Information and Critical For NRC Docketing of CRBRP Environmental Report	1
3.0	<u>DESIGN CRITERIA - STRUCTURES, COMPONENTS EQUIPMENT AND SYSTEMS</u>	3.1-1
3.1	<u>CONFORMANCE WITH GENERAL DESIGN CRITERIA</u>	3.1-1
3.1.1	Introduction and Scope	3.1-1
3.1.2	Definitions and Explanations	3.1-2
3.1.3	Conformance with CRBRP General Design Criteria	3.1-8
3.2	<u>CLASSIFICATIONS OF STRUCTURES, SYSTEMS, AND COMPONENTS</u>	3.2-1
3.2.1	Seismic Classifications	3.2-1
3.2.2	Safety Classifications	3.2-2
3.3	<u>WIND AND TORNADO LOADINGS</u>	3.3-1
3.3.1	Wind Loadings	3.3-1
3.3.2	Tornado Loadings	3.3-2
3.4	<u>WATER LEVEL (FLOOD) DESIGN</u>	3.4-1
3.4.1	Flood Protection	3.4-1
3.4.2	Analysis Procedures	3.4-1a

TABLE OF CONTENTS (Cont'd.)

<u>Section</u>		<u>Page</u>
3.5	<u>MISSILE PROTECTION</u>	3.5-1
3.5.1	Missile Barrier and Loadings	3.5-4
3.5.2	Missile Selection	3.5-4a
3.5.3	Selected Missiles	3.5-7
3.5.4	Barrier Design Procedures	3.5-10
3.5.5	Missile Barrier Features	3.5-13c
3.6	<u>PROTECTION AGAINST DYNAMIC EFFECTS ASSOCIATED WITH THE POSTULATED RUPTURE OF PIPING</u>	3.6-1
3.6.1	Systems in Which Pipe Breaks are Postulated	3.6-1
3.6.2	Pipe Break Criteria	3.6-2
3.6.3	Design Loading Combinations	3.6-2
3.6.4	Dynamic Analysis	3.6-3
3.6.5	Protective Measures	3.6-8
3.7	<u>SEISMIC DESIGN</u>	3.7-1
3.7.1	Seismic Input	3.7-1
3.7.2	Seismic System Analysis	3.7-4a
3.7.3	Seismic Subsystem Analysis	3.7-11
3.7.4	Seismic Instrumentation Program	3.7-16
3.7.5	Seismic Design Control	3.7-20
	Appendix to Section 3.7 Seismic Design Criteria	3.7-A.1
3.8	<u>DESIGN OF CATEGORY I STRUCTURES</u>	3.8-1
3.8.1	Concrete Containment (Not Applicable)	3.8-1
3.8.2	Steel Containment System	3.8-1
3.8.3	Concrete and Structural Steel Internal Structures of Steel Containment	3.8-8
3.8.4	Other Seismic Category I Structures	3.8-22a
3.8.5	Foundation and Concrete Supports	3.8-35
	Appendix 3.8A Buckling Stress Criteria	3.8A-1
	Appendix 3.8-B Cell Liner Design Criteria	3.8-B.1
	Appendix 3.8-C Catch Pan and Fire Suppression Deck Design Criteria	3.8-C.1
3.9	<u>MECHANICAL SYSTEMS AND COMPONENTS</u>	3.9-1
3.9.1	Dynamic System Analysis and Testing	3.9-1
3.9.2	ASME Code Class 2 and 3 Components	3.9-3a
3.9.3	Components Not Covered by ASME Code	3.9-5
3.10	<u>SEISMIC DESIGN OF CATEGORY I INSTRUMENTATION AND ELECTRICAL EQUIPMENT</u>	3.10-1
3.10.1	Seismic Design Criteria	3.10-1

TABLE OF CONTENTS (Cont'd.)

<u>Section</u>		<u>Page</u>
3.10.2	Analysis, Testing Procedures and Restraint Measures	3.10-3
3.11	<u>ENVIRONMENTAL DESIGN OF MECHANICAL AND ELECTRICAL EQUIPMENT</u>	3.11-1
3.11.1	Equipment Identification	3.11-1
3.11.2	Qualification Test and Analysis	3.11-1
3.11.3	Qualification Test Results	3.11-1
3.11.4	Loss of Ventilation	3.11-2
3.11.5	Special Considerations	3.11-2
3A.0	<u>SUPPLEMENTARY INFORMATION ON SEISMIC CATEGORY I STRUCTURES</u>	3A.1-1
3A.1	Inner Cell System	3A.1-1
3A.2	Head Access Area	3A.2-1
3A.3	Control Building	3A.3-1
3A.4	Reactor Service Building (RSB)	3A.4-1
3A.5	Steam Generator Building	3A.5-1
3A.6	Diesel Generator Building	3A.6-1
3A.7	Deleted	
3A.8	Cell Liner Systems	3A.8-1
4.0	<u>REACTOR</u>	4.1-1
4.1	<u>SUMMARY DESCRIPTION</u>	4.1-1
4.1.1	Lower Internals	4.1-1
4.1.2	Upper Internals	4.1-3
4.1.3	Core Restraint	4.1-4
4.1.4	Fuel Blanket and Removable Radial Shield Regions	4.1-4
4.1.5	Design and Performance Characteristics	4.1-9
4.1.6	Loading Conditions and Analysis Techniques	4.1-9
4.1.7	Computer Codes	4.1-10
4.2	<u>MECHANICAL DESIGN</u>	4.2-1
4.2.1	Fuel and Blanket Design	4.2-1
4.2.2	Reactor Vessels Internals	4.2-118
4.2.3	Reactivity Control Systems	4.2-228
4.3	<u>NUCLEAR DESIGN</u>	4.3-1
4.3.1	Design Bases	4.3-1
4.3.2	Description	4.3-3
4.3.3	Analytical Methods	4.3-69
4.3.4	Changes	

TABLE OF CONTENTS (Cont'd.)

<u>Section</u>		<u>Page</u>
4.4	<u>THERMAL AND HYDRAULIC DESIGN</u>	4.4-1
4.4.1	Design Bases	4.4-1
4.4.2	Description	4.4-4
4.4.3	Evaluation	4.4-45
4.4.4	Testing and Verification	4.4-75
4.4.5	Core Instrumentation	4.4-80
5.0	<u>HEAT TRANSPORT AND CONNECTED SYSTEMS</u>	5.1-1
5.1	<u>SUMMARY DESCRIPTION</u>	5.1-1a
5.1.1	Reactor Vessel, Closure Head, and Guard Vessel	5.1-1a
5.1.2	Primary Heat Transport System	5.1-2
5.1.3	Intermediate Heat Transport System	5.1-5
5.1.4	Steam Generator System	5.1-7
5.1.5	Residual Heat Removal System	5.1-8
5.1.6	Auxiliary Liquid Metal System	5.1-9
5.1.7	Features for Heat Transport System Safety	5.1-10
5.1.8	Physical Arrangement	5.1-11
5.2	<u>REACTOR VESSEL, CLOSURE HEAD, AND GUARD VESSEL</u>	5.2-1
5.2.1	Design Basis	5.2-1
5.2.2	Design Parameters	5.2-4b
5.2.3	Special Processes for Fabrication and Inspection	5.2-7
5.2.4	Features for Improved Reliability	5.2-8
5.2.5	Quality Assurance Surveillance	5.2-10d
5.2.6	Materials and Inspections	5.2-11
5.2.7	Packing, Packaging, and Storage	5.2-11a
	Appendix 5.2.A Modifications to the High Temperature Design Rules for Austenitic Stainless Steel	5.2A-1
5.3	<u>PRIMARY HEAT TRANSPORT SYSTEM (PHTS)</u>	5.3-1
5.3.1	Design Bases	5.3-1
5.3.2	Design Description	5.3-9
5.3.3	Design Evaluation	5.3-33
5.3.4	Tests and Inspections	5.3-72
5.4	<u>INTERMEDIATE HEAT TRANSPORT SYSTEM (IHTS)</u>	5.4-1
5.4.1	Design Basis	5.4-1
5.4.2	Design Description	5.4-6
5.4.3	Design Evaluation	5.4-12

TABLE OF CONTENTS (Cont'd.)

<u>Section</u>		<u>Page</u>
5.5	<u>STEAM GENERATOR SYSTEM (SGS)</u>	5.5-1
5.5.1	Design Bases	5.5-1
5.5.2	Design Description	5.5-5
5.5.3	Design Evaluation	5.5-17
5.6	<u>RESIDUAL HEAT REMOVAL SYSTEMS</u>	5.6-1
5.6.1	Steam Generator Auxiliary Heat Removal System (SGAHRs)	5.6-1b
5.6.2	Direct Heat Removal Service (DHRS)	5.6-20
5.7	<u>OVERALL HEAT TRANSPORT SYSTEM EVALUATION</u>	5.7-1
5.7.1	Startup and Shutdown	5.7-1
5.7.2	Load Following Characteristics	5.7-2
5.7.3	Transient Effects	5.7-2a
5.7.4	Evaluation of Thermal Hydraulic Characteristics and Plant Design Heat Transport System Design Transient Summary	5.7-6
6.0	<u>ENGINEERED SAFETY FEATURES</u>	6.1-1
6.1	<u>GENERAL</u>	6.1-1
6.2	<u>CONTAINMENT SYSTEMS</u>	6.2-1
6.2.1	Confinement/Containment Functional Design	6.2-1
6.2.2	Containment Heat Removal	6.2-9
6.2.3	Containment Air Purification and Cleanup System	6.2-9
6.2.4	Containment Isolation Systems	6.2-10
6.2.5	Annulus Filtration System	6.2-14
6.2.6	Reactor Service Building (RSB) Filtration System	6.2-16
6.2.7	Steam Generator Building Aerosol Release Mitigation System Functional Design	6.2-17
6.3	<u>HABITABILITY SYSTEMS</u>	6.3-1
6.3.1	Habitability System Functional Design	6.3-1
6.4	<u>CELL LINER SYSTEM</u>	6.4-1
6.4.1	Design Base	6.4-1
6.4.2	System Design	6.4-1
6.4.3	Design Evaluation	6.4-1
6.4.4	Tests and Inspections	6.4-1
6.4.5	Instrumentation Requirements	6.4-1

TABLE OF CONTENTS (Cont'd.)

<u>Section</u>		<u>Page</u>
6.5	<u>CATCH PAN</u>	6.5-1
6.5.1	Design Base	6.5-1
6.5.2	System Design Description and Evaluation	6.5-1
6.5.3	Tests and Inspections	6.5-1
6.5.4	Instrumentation Requirements	6.5-1
7.0	<u>INSTRUMENTATION AND CONTROLS</u>	7.1-1
7.1	<u>INTRODUCTION</u>	7.1-1
7.1.1	Identification of Safety Related Instrumentation and Control Systems	7.1-1
7.1.2	Identification of Safety Criteria	7.1-1
7.2	<u>REACTOR SHUTDOWN SYSTEM</u>	7.2-1
7.2.1	Description	7.2-1
7.2.2	Analysis	7.2-13
7.3	<u>ENGINEERED SAFETY FEATURE INSTRUMENTATION AND CONTROL</u>	7.3-1
7.3.1	Containment Isolation System	7.3-1
7.3.2	Analysis	7.3-3
7.4	<u>INSTRUMENTATION AND CONTROL SYSTEMS REQUIRED FOR SAFE SHUTDOWN</u>	7.4-1
7.4.1	Steam Generator Auxiliary Heat Removal Instrumentation and Control Systems	7.4-1
7.4.2	Outlet Steam Isolation Instrumentation and Control System	7.4-6
7.4.3	Remote Shutdown System	7.4-8a
7.5	<u>INSTRUMENTATION AND MONITORING SYSTEM</u>	7.5-1
7.5.1	Flux Monitoring System	7.5-1
7.5.2	Heat Transport Instrumentation System	7.5-5
7.5.3	Reactor and Vessel Instrumentation	7.5-13
7.5.4	Fuel Failure Monitoring System	7.5-14
7.5.5	Leak Detection Systems	7.5-18
7.5.6	Sodium-Water Reaction Pressure Relief System (SWRPRS) Instrumentation and Controls	7.5-30
7.5.7	Containment Hydrogen Monitoring	7.5-33b
7.5.8	Containment Vessel Temperature Monitoring	7.5-33b
7.5.9	Containment Pressure Monitoring	7.5-33b
7.5.10	Containment Atmosphere Temperature	7.5-33c
7.5.11	Post Accident Monitoring	7.5-33c

TABLE OF CONTENTS (Cont'd.)

<u>Section</u>		<u>Page</u>
7.6	<u>OTHER INSTRUMENTATION AND CONTROL SYSTEMS REQUIRED FOR SAFETY</u>	7.6-1
7.6.1	Plant Service Water and Chilled Water Instrumentation and Control Systems	7.6-1
7.6.2	Deleted	
7.6.3	Direct Heat Removal Service (DHRS) Instrumentation and Control System	7.6-3
7.6.4	Heating, Ventilating, and Air Conditioning Instrumentation and Control System	7.6-3e
7.6.5	SGB Flooding Protection Subsystem	7.6-3f
7.7	<u>INSTRUMENTATION AND CONTROL SYSTEMS NOT REQUIRED FOR SAFETY</u>	7.7-1
7.7.1	Plant Control System Description	7.7-1
7.7.2	Design Analysis	7.7-16
7.8	<u>PLANT DATA HANDLING AND DISPLAY SYSTEM</u>	7.8-1
7.8.1	Design Description	7.8-1
7.8.2	Design Analysis	7.8-2
7.9	<u>OPERATING CONTROL STATIONS</u>	7.9-1
7.9.1	Design Basis	7.9-1
7.9.2	Control Room	7.9-1
7.9.3	Local Control Stations	7.9-6
7.9.4	Communications	7.9-6
7.9.5	Design Evaluation	7.9-6
8.0	<u>ELECTRIC POWER</u>	8.1-1
8.1	<u>INTRODUCTION</u>	8.1-1
8.1.1	Utility Grid and Interconnections	8.1-1
8.1.2	Plant Electrical Power System	8.1-1
8.1.3	Criteria and Standards	8.1-3
8.2	<u>OFFSITE POWER SYSTEM</u>	8.2-1
8.2.1	Description	8.2-1
8.2.2	Analysis	8.2-4
8.3	<u>ON-SITE POWER SYSTEMS</u>	8.3-1
8.3.1	AC Power Systems	8.3-1
8.3.2	DC Power System	8.3-44

TABLE OF CONTENTS (Cont'd.)

<u>Section</u>		<u>Page</u>
9.0	<u>AUXILIARY SYSTEMS</u>	9.1-1
9.1	<u>FUEL STORAGE AND HANDLING</u>	9.1-1
9.1.1	New Fuel Storage	9.1-3
9.1.2	Spent Fuel Storage	9.1-5
9.1.3	Spent Fuel Cooling and Cleanup System	9.1-20
9.1.4	Fuel Handling System	9.1-33
9.2	<u>NUCLEAR ISLAND GENERAL PURPOSE MAINTENANCE SYSTEM</u>	9.2-1
9.2.1	Design Basis	9.2-1
9.2.2	System Description	9.2-1
9.2.3	Safety Evaluation	9.2-3
9.2-4	Tests and Inspections	9.2-3
9.2-5	Instrumentation Applications	9.2-4
9.3	<u>AUXILIARY LIQUID METAL SYSTEM</u>	9.3-1
9.3.1	Sodium and NaK Receiving System	9.3-1a
9.3.2	Primary Na Storage and Processing	9.3-2
9.3.3	EVS Sodium Processing	9.3-9a
9.3.4	Primary Cold Trap NaK Cooling System	9.3-10
9.3.5	Intermediate Na Processing System	9.3-12
9.4	<u>PIPING AND EQUIPMENT ELECTRICAL HEATING</u>	9.4-1
9.4.1	Design Bases	9.4-1
9.4.2	Systems Description	9.4-2
9.4.3	Safety Evaluation	9.4-3
9.4.4	Tests and Inspections	9.4-3b
9.4.5	Instrumentation Application	9.4-3b
9.5	<u>INERT GAS RECEIVING AND PROCESSING SYSTEM</u>	9.5-1
9.5.1	Argon Distribution Subsystem	9.5-2
9.5.2	Nitrogen Distribution System	9.5-6
9.5.3	Safety Evaluation	9.5-10
9.5.4	Tests and Inspections	9.5-12
9.5.5	Instrumentation Requirements	9.5-12
9.6	<u>HEATING, VENTILATING AND AIR CONDITIONING SYSTEM</u>	9.6-1
9.6.1	Control Building HVAC System	9.6-1
9.6.2	Reactor Containment Building	9.6-12
9.6.3	Reactor Service Building HVAC System	9.6-25
9.6.4	Turbine Generator Building HVAC System	9.6-37
9.6.5	Diesel Generator Building HVAC System	9.6-40
9.6.6	Steam Generator Building HVAC System	9.6-45

TABLE OF CONTENTS (Cont'd.)

<u>Section</u>		<u>Page</u>
9.7	<u>CHILLED WATER SYSTEMS</u>	9.7-1
9.7.1	Normal Chilled Water System	9.7-1
9.7.2	Emergency Chilled Water System	9.7-4
9.7.3	Prevention of Sodium or NaK/Water Interactions	9.7-9
9.7.4	Secondary Coolant Loops (SCL)	9.7-12
9.8	<u>IMPURITY MONITORING AND ANALYSIS SYSTEM</u>	9.8-1
9.8.1	Design Basis	9.8-1
9.8.2	Design Description	9.8-2
9.8.3	Design Evaluation	9.8-5
9.8.4	Tests and Inspection	9.8-7
9.8.5	Instrumentation Requirements	9.8-8
9.9	<u>SERVICE WATER SYSTEMS</u>	9.9-1
9.9.1	Normal Plant Service Water System	9.9-1
9.9.2	Emergency Plant Service Water System	9.9-2
9.9.3	Secondary Service Closed Cooling Water System	9.9-4
9.9.5	River Water Service	9.9-11
9.10	<u>COMPRESSED GAS SYSTEM</u>	9.10-1
9.10.1	Service Air and Instrument Air Systems	9.10-1
9.10.2	Hydrogen System	9.10-3a
9.10.3	Carbon Dioxide System	9.10-4
9.11	<u>COMMUNICATIONS SYSTEM</u>	9.11-1
9.11.1	Design Bases	9.11-1
9.11.2	Description	9.11-3
9.12	<u>LIGHTING SYSTEMS</u>	9.12-1
9.12.1	Normal Lighting System	9.12-1
9.12.2	Standby Lighting Systems	9.12-2
9.12.3	Emergency Lighting System	9.12-3
9.12.4	Design Evaluation	9.12-4
9.13	<u>PLANT FIRE PROTECTION SYSTEM</u>	9.13-1
9.13.1	Non-Sodium Fire Protection System	9.13-1
9.13.2	Sodium Fire Protection System (SFPS)	9.13-13
9.13A	Overall Fire Protection Requirements -- CRBRP Design Compared with APCSB 9.5-1 & ASB 9.5-1	9.13A-1
9.14	<u>DIESEL GENERATOR AUXILIARY SYSTEM</u>	9.14-1
9.14.1	Fuel Oil Storage and Transfer System	9.14-1

TABLE OF CONTENTS (Cont'd.)

<u>Section</u>		<u>Page</u>
9.14.2	Cooling Water System	9.14-2
9.14.3	Starting Air Systems	9.14-4
9.14.4	Lubrication System	9.14-5
9.15	<u>EQUIPMENT AND FLOOR DRAINAGE SYSTEM</u>	9.15-1
9.15.1	Design Bases	9.15-1
9.15.2	System Description	9.15-1
9.15.3	Safety Evaluation	9.15-2
9.15.4	Tests and Inspections	9.15-2
9.15.5	Instrumentation Application	9.15-2
9.16	<u>RECIRCULATION GAS COOLING SYSTEM</u>	9.16-1
9.16.1	Design Basis	9.16-1
9.16.2	System Description	9.16-1
9.16.3	Safety Evaluation	9.16-6
9.16.4	Tests and Inspection	9.16-7
9.16.5	Instrumentation and Control	9.16-7
10.0	<u>STEAM AND POWER CONVERSION SYSTEM</u>	10.1-1
10.1	<u>SUMMARY DESCRIPTION</u>	10.1-1
10.2	<u>TURBINE GENERATOR</u>	10.2-1
10.2.1	Design Bases	10.2-1
10.2.2	Description	10.2-1a
10.2.3	Turbine Missiles	10.2-5
10.2.4	Evaluation	10.2-9
10.3	<u>MAIN STEAM SUPPLY SYSTEM</u>	10.3-1
10.3.1	Design Bases	10.3-1
10.3.2	Description	10.3-1
10.3.3	Evaluation	10.3-2
10.3.4	Inspection and Testing Requirements	10.3-2
10.3.5	Water Chemistry	10.3-3
10.4	<u>OTHER FEATURES OF STEAM AND POWER CONVERSION SYSTEM</u>	10.4-1
10.4.1	Condenser	10.4-1
10.4.2	Condenser Air Removal System	10.4-2
10.4.3	Turbine Gland Sealing System	10.4.3
10.4.4	Turbine Bypass System	10.4-4
10.4.5	Circulating Water System	10.4-5
10.4.6	Condensate Cleanup System	10.4-7

TABLE OF CONTENTS (Cont'd.)

<u>Section</u>		<u>Page</u>
10.4.7	Condensate and Feedwater Systems	10.4-9
10.4.8	Steam Generator Blowdown System	10.4-14
11.0	<u>RADIOACTIVE WASTE MANAGEMENT</u>	11.1-1
11.1	<u>SOURCE TERMS</u>	11.1-1
11.1.1	Modes of Radioactive Waste Production	11.1-1
11.1.2	Activation Product Source Strength Models	11.1-2
11.1.3	Fission Product and Plutonium Release Models	11.1-5
11.1.4	Tritium Production Sources	11.1-7
11.1.5	Summary of Design Bases for Deposition of Radioactivity in Primary Sodium on Reactor and Primary Heat Transfer Surfaces and Within Reactor Auxiliary Systems	11.1-7
11.1.6	Leakage Rates	11.1-10
11.2	<u>LIQUID WASTE SYSTEM</u>	11.2-1
11.2.1	Design Objectives	11.2-1
11.2.2	System Description	11.2-2
11.2.3	System Design	11.2-4
11.2.4	Operating Procedures and Performance Tests	11.2-5
11.2.5	Estimated Releases	11.2-6
11.2.6	Release Points	11.2-6
11.2.7	Dilution Factors	11.2-7
11.2.8	Estimated Doses	11.2-8
	Appendix 11.2A Dose Models: Liquid Effluents	11.2A-1
11.3	<u>GASEOUS WASTE SYSTEM</u>	11.3-1
11.3.1	Design Base	11.3-1
11.3.2	System Description	11.3-1
11.3.3	System Design	11.3-10
11.3.4	Operating Procedures and Performance Tests	11.3-11a
11.3.5	Estimated Releases	11.3-14
11.3.6	Release Points	11.3-15
11.3.7	Dilution Factors	11.3-17
11.3.8	Dose Estimates	11.3-17
	Appendix 11.3A Dose Models: Gaseous Effluents	11.3A-1
11.4	<u>PROCESS AND EFFLUENT RADIOLOGICAL MONITORING SYSTEM</u>	11.4-1
11.4.1	Design Objectives	11.4-1
11.4.2	Continuous Monitoring/Sampling	11.4-2
11.4.3	Sampling	11.4-3

TABLE OF CONTENTS (Cont'd.)

<u>Section</u>		<u>Page</u>
11.5	<u>SOLID WASTE SYSTEM</u>	11.5-1
11.5.1	Design Objectives	11.5-1
11.5.2	System Inputs	11.5-1
11.5.3	Equipment Description	11.5-1
11.5.4	Expected Volumes	11.5-3
11.5.5	Packaging	11.5-4
11.5.6	Storage Facilities	11.5-4
11.5.7	Shipment	11.5-4
11.6	<u>OFFSITE RADIOLOGICAL MONITORING PROGRAM</u>	11.6-1
11.6.1	Expected Background	11.6-1
11.6.2	Critical Pathways to Man	11.6-2
11.6.3	Sampling Media, Locations and Frequencies	11.6-4
11.6.4	Analytical Sensitivity	11.6-4
11.6.5	Data Analysis and Presentation	11.6-4
11.6.6	Program Statistical Sensitivity	11.6-5
12.0	<u>RADIATION PROTECTION</u>	12.1-1
12.1	<u>SHIELDING</u>	12.1-1
12.1.1	Design Objectives	12.1-1
12.1.2	Design Description	12.1-3
12.1.3	Source Terms	12.1-13
12.1.4	Area Radiation Monitoring	12.1-23
12.1.5	Estimates of Exposure	12.1-24
	Appendix to Section 12.1	12.1A-1
12.2	<u>VENTILATION</u>	12.2-1
12.2.1	Design Objectives	12.2-1
12.2.2	Design Description	12.2-1
12.2.3	Source Terms	12.2-3
12.2.4	Airborne Radioactivity Monitoring	12.2-3
12.2.5	Inhalation Doses	12.2-5
12.3	<u>HEALTH PHYSICS PROGRAM</u>	12.3-1
12.3.1	Program Objectives	12.3-1
12.3.2	Facilities and Equipment	12.3-3
12.3.3	Personnel Dosimetry	12.3-6
12.3.4	Estimated Occupancy Times	12.3-7
	Appendix 12A - Information Related to ALARA for Occupational Radiation Exposures	12A-1

TABLE OF CONTENTS (Cont'd.)

<u>Section</u>		<u>Page</u>
13.0	<u>CONDUCT OF OPERATIONS</u>	13.1-1
13.1	<u>ORGANIZATIONAL STRUCTURE OF THE APPLICANT</u>	13.1-1
13.1.1	Project Organization	13.1-1
13.1.2	Operating Organization	13.1-5
13.1.3	Qualification Requirements for Nuclear Plant Personnel	13.1-12
13.2	<u>TRAINING PROGRAM</u>	13.2-1
13.2.1	Program Description	13.2-1
13.2.2	Retraining Program	13.2-6
13.2.3	Replacement Training	13.2-6
13.2.4	Records	13.2-6
13.3	<u>EMERGENCY PLANNING</u>	13.3-1
13.3.1	General	13.3-1
13.3.2	Emergency Organization	13.3-2
13.3.3	Coordination with Offsite Groups	13.3-5
13.3.4	Emergency Action Levels	13.3-6
13.3.5	Protective Measures	13.3-7
13.3.6	Review and Updating	13.3-7
13.3.7	Medical Support	13.3-7
13.3.8	Exercises and Drills	13.3-8
13.3.9	Training	13.3-8
13.3.10	Recovery and Reentry	13.3-9
13.3.11	Implementation	13.3-9
	Appendix 13.3A	13.3A-1
13.4	<u>REVIEW AND AUDIT</u>	13.4-1
13.4.1	Review and Audit - Construction	13.4-1
13.4.2	Review and Audit - Test and Operation	13.4-1
13.5	<u>PLANT PROCEDURES</u>	13.5-1
13.5.1	General	13.5-1
13.5.2	Normal Operating Instructions	13.5-1
13.5.3	Abnormal Operating Instructions	13.5-2
13.5.4	Emergency Operating Instructions	13.5-2
13.5.5	Maintenance Instructions	13.5-3

Amend. 68
May 1982

TABLE OF CONTENTS (Cont'd.)

<u>Section</u>		<u>Page</u>
13.5.6	Surveillance Instructions	13.5-4
13.5.7	Technical Instructions	13.5-4
13.5.8	Sections Instruction Letters	13.5-4
13.5.9	Site Emergency Plans	13.5-4
13.5.10	Radiation Control Instructions	13.5-4
13.6	<u>PLANT RECORDS</u>	13.6-1
13.6.1	Plant History	13.6-1
13.6.2	Operating Records	13.6-1
13.6.3	Event Records	13.6-1
13.7	<u>RADIOLOGICAL SECURITY</u>	13.7-1
13.7.1	Organization and Personnel	13.7-1
13.7.2	Plant Design	13.7-3
13.7.3	Security Plan	13.7-6
14.0	<u>INITIAL TESTS AND OPERATION</u>	14.1-1
14.1	<u>DESCRIPTION OF TEST PROGRAMS</u>	14.1-1
14.1.1	Preoperational Test Programs	14.1-2
14.1.2	Startup Test Program	14.1-2
14.1.3	Administration of Test Program	14.1-3
14.1.4	Test Objectives of First-of-a-Kind Principal Design Features	14.1-6
14.2	<u>AUGMENTATION OF OPERATOR'S STAFF FOR INITIAL TESTS AND OPERATION</u>	14.2-1
15.0	<u>ACCIDENT ANALYSES</u>	15.1-1
15.1	<u>INTRODUCTION</u>	15.1-1
15.1.1	Design Approach to Safety	15.1-1
15.1.2	Requirements and Criteria for Assessment of Fuel and Blanket Rod Transient Performance	15.1-50
15.1.3	Control Rod Shutdown Rate and Plant Protection System Trip Settings	15.1-93
15.1.4	Effect of Design Changes on Analyses of Accident Events	15.1-105
15.2	<u>REACTIVITY INSERTION DESIGN EVENTS - INTRODUCTION</u>	15.2-1
15.2.1	Anticipated Events	15.2-5
15.2.2	Unlikely Events	15.2-34
15.2.3	Extremely Unlikely Events	15.2-51

TABLE OF CONTENTS (Cont'd.)

<u>Section</u>		<u>Page</u>
15.3	<u>UNDERCOOLING DESIGN EVENTS - INTRODUCTION</u>	15.3-1
15.3.1	Anticipated Events	15.3-6
15.3.2	Unlikely Events	15.3-29
15.3.3	Extremely Unlikely Events	15.3-38
15.4	<u>LOCAL FAILURE EVENTS - INTRODUCTION</u>	15.4-1
15.4.1	Fuel Assembly	15.4-2
15.4.2	Control Assemblies	15.4-42
15.4.3	Radial Blanket Assembly	15.4-51
15.5	<u>FUEL HANDLING AND STORAGE EVENTS - INTRODUCTION</u>	15.5-1
15.5.1	Anticipated Events (None)	15.5-4
15.5.2	Unlikely Events	15.5-4
15.5.3	Extremely Unlikely Events	15.5-23
15.6	<u>SODIUM SPILLS - INTRODUCTION</u>	15.6-1
15.6.1	Extremely Unlikely Events	15.6-4
15.7	<u>OTHER EVENTS - INTRODUCTION</u>	15.7-1
15.7.1	Anticipated Events	15.7-3
15.7.2	Unlikely Events	15.7-9
15.7.3	Extremely Unlikely Events	15.7-18
15.A	Appendix 15.A - Radiological Source Term for Assessment of Site Suitability	15.A-1
16.0	<u>TECHNICAL SPECIFICATIONS</u>	16.1-1
16.1	<u>DEFINITIONS</u>	16.1-1
16.1.1	Reactor Operating Condition	16.1-1
16.1.2	Reactor Core	16.1-2
16.1.3	Plant Protection System Instrumentation	16.1-3
16.1.4	Safety Limit	16.1-5
16.1.5	Limiting Safety System Setting (LSSS)	16.1-5
16.1.6	Limiting Conditions for Operation (LCO)	16.1-6
16.1.7	Surveillance Requirements	16.1-6
16.1.8	Containment Integrity	16.1-6
16.1.9	Abnormal Occurrence	16.1-6

TABLE OF CONTENTS (Cont'd.)

<u>Section</u>		<u>Page</u>
16.2	<u>SAFETY LIMITS AND LIMITING SAFETY SYSTEM SETTINGS</u>	16.2-1
16.2.1	Safety Limit, Reactor Core	16.2-1
16.2.2	Limiting Safety System Settings	16.2-1
16.3	<u>LIMITING CONDITIONS FOR OPERATION</u>	16.3-1
16.3.1	Reactor Operating Conditions	16.3-1
16.3.2	Primary Heat Transport System (PHTS)	16.3-2
16.3.3	Intermediate Heat Transport Coolant System	16.3-6
16.3.4	Steam Generation System (SGS)	16.3-7
16.3.5	Auxiliary Liquid Metal System	16.3-12
16.3.6	Inert Gas System Cover Gas Purification System	16.3-13
16.3.7	Auxiliary Cooling System	16.3-14
16.3.8	Containment Integrity	16.3-21
16.3.9	Auxiliary Electrical System	16.3-21
16.3.10	Refueling	16.3-24
16.3.11	Effluent Release	16.3-27
16.3.12	Reactivity and Control Rod Limits	16.3-31
16.3.13	Plant Protection System	16.3-34
16.4	<u>SURVEILLANCE REQUIREMENTS</u>	16.4-1
16.4.1	Operational Safety Review	16.4-1
16.4.2	Reactor Coolant System Surveillance	16.4-1
16.4.3	Containment Tests	16.4-3
16.4.4	HVAC and Radioactive Effluents	16.4-6
16.4.5	Emergency Power System Periodic Tests	16.4-10
16.4.6	Inert Gas System	16.4-13
16.4.7	Reactivity Anomalies	16.4-13
16.4.8	Pressure and Leakage Rate Test of RAPS Cold Box Cell	16.4-15
16.4.9	Pressure and Leakage Rate Test of RAPS Noble Gas Storage Vessel Cell	16.4-15a
16.5	<u>DESIGN FEATURES</u>	16.5-1
16.5.1	Site	16.5-1
16.5.2	Confinement/Containment	16.5-1
16.5.3	Reactor	16.5-2
16.5.4	Heat Transport System	16.5-5
16.5.5	Fuel Storage	16.5-7
16.6	<u>ADMINISTRATIVE CONTROLS</u>	16.6-1
16.6.1	Organization	16.6-1
16.6.2	Review and Audit	16.6-1
16.6.3	Instructions	16.6-4
16.6.4	Actions to be Taken in the Event of Reportable Occurrence in Plant Operation	16.6-6

TABLE OF CONTENTS (Cont'd.)

<u>Section</u>		<u>Page</u>
16.6.5	Action to be Taken in the Event a Safety Limit Is Exceeded	16.6-6
16.6.6	Station Operating Records	16.6-6
16.6.7	Reporting Requirements	16.6-7
16.6.8	Minimum Staffing	16.6-8
17.0	<u>QUALITY ASSURANCE - INTRODUCTION</u>	17.0-1
17.0.1	Scope	17.0-1
17.0.2	Quality Philosophy	17.0-1
17.0.3	Participants	17.0-2
17.0.4	Project Phase Approach	17.0-3
17.0.5	Applicability	17.0-3
17.1	<u>QUALITY ASSURANCE DURING DESIGN AND CONSTRUCTION</u>	17.1-1
17.1.1	Organization	17.1-1
17.1.2	Quality Assurance Program	17.1-2
17.1.3	References Referred to in the Text	17.1-6
17.1.4	Acronyms Used In Chapter 17 Text and Appendices	17.1-6a

TABLE OF CONTENTS (Cont'd.)

<u>Section</u>		<u>Page</u>
Appendix 17A	A Description of the Owner Quality Assurance Program	17A-1
Appendix 17B	A Description of the Fuel Supplier Quality Assurance Program	17B-1
Appendix 17C	A Description of the Balance of Plant Supply Quality Assurance Program	17C-1
Appendix 17D	A Description of the ARD Lead Reactor Manufacturer Quality Assurance Program	17D-1
Appendix 17E	A Description of the Architect-Engineer Quality Assurance Program	17E-1
Appendix 17F	A Description of the Constructor Quality Assurance Program	17F-1
Appendix 17G	RDT Standard F2-2, 1973, Quality Assurance Program Requirements	17G-1
Appendix 17H	A Description of the ARD Reactor Manufacturer Quality Assurance Program	17H-1
Appendix 17I	A Description of the GE-ARSD-RM Quality Assurance Program	17I-1
Appendix 17J	A Description of the ESG-RM Quality Assurance Program	17J-1
Appendix A	Computer Codes	A-1
Appendix B	General Plant Transient Data	B-1
Appendix C	Safety Related Reliability Program	C.1-1
Appendix D	Deleted	
Appendix E	Deleted	
Appendix F	Deleted	
Appendix G	Plan for Inservice and Preservice Inspections	G-1
Appendix H	Post TMI Requirements	H-1

Question 001.447 (F6.2.4.3)

In reference to Table F6.2-17, provide the time "prior to failure" for the midplane values given and for the "Damage Severity". Define "Primary Loading" and "Failure Loading".

Response:

The CRBRP Project has consolidated all considerations given Hypothetical Core Disruptive Accidents into report CRBRP-3 (References 10a and 10b, PSAR Section 1.6) and its associated references; consequently, PSAR Appendices D and F have been withdrawn in Amendments 24 and 60 respectively. The response to this question is now found in Sections 3.2.3 and 6.2.1 of Reference 15, PSAR Section 1.6.

60

Question 001.448 (F6.2.4.3.1)

Paragraph 5 on Page F6.2-64 is unclear due to a typographical error. Make the necessary correction.

Response:

This question requests clarification of information which is no longer a part of the current documentation. The Project has since consolidated all considerations given Hypothetical Core Disruptive Accidents into report CRBRP-3 (References 10a and 10b, PSAR Section 1.6) and its associated references; consequently, PSAR Appendices D and F have been withdrawn in Amendments 24 and 60 respectively.

60

Question 001.449 (F6.2.3.2.2)

As presently modeled in SAS, what is the partitioning of the fission gas released from the unrestructured fuel prior to melting (Gruber model) between the pin cavity, the plenum and the unrestructured fuel itself? Discuss what happens to the fission gas released from the unrestructured fuel at axial nodes that have no cavity.

Response:

The CRBRP Project has consolidated all considerations given Hypothetical Core Disruptive Accidents into report CRBRP-3 (References 10a and 10b, PSAR Section 1.6) and its associated references; consequently, PSAR Appendices D and F have been withdrawn in Amendments 24 and 60 respectively. The response to this question is now found in Sections 4.3 and 4.4 of Reference 10a, PSAR Section 1.6.

60

Question 001.450 (F6.2.3.4.3)

Explain why the gap ΔT in Figure 6.2-23 (400°C) is greater than the gap ΔT in Figure 6.2-33 (375°C), when the respective gaps are approximately 0.001 cm and 0.005 cm respectively.

Response:

The CRBRP Project has consolidated all considerations given Hypothetical Core Disruptive Accidents into report CRBRP-3 (References 10a and 10b, PSAR Section 1.6) and its associated references; consequently, PSAR Appendices D and F have been withdrawn in Amendments 24 and 60 respectively. The response to this question is now found in Sections 5.2 and 5.3 of Reference 15, PSAR Section 1.6.

60

Question 001.451 (F6.2.3.4.3)

Based on the statements that calculated fuel temperatures are unrealistically high and that "This condition would be conservative...", justify this conclusion considering the following:

- a) Early failures might be beneficial to the outcome of the accident;
- b) Assuming use of the burst failure criterion, the more restructuring, the higher the pin is likely to fail;
- c) The more restructuring, the less transient fission gas is available for pressurization;
- d) The unrealistic stimulation of early failures may introduce incoherence which would make the outcome non-conservative;
- e) Fuel-pellet clad contact (i.e., zero gap) may enhance local boiling and/or local secondary loading failures.

Response:*

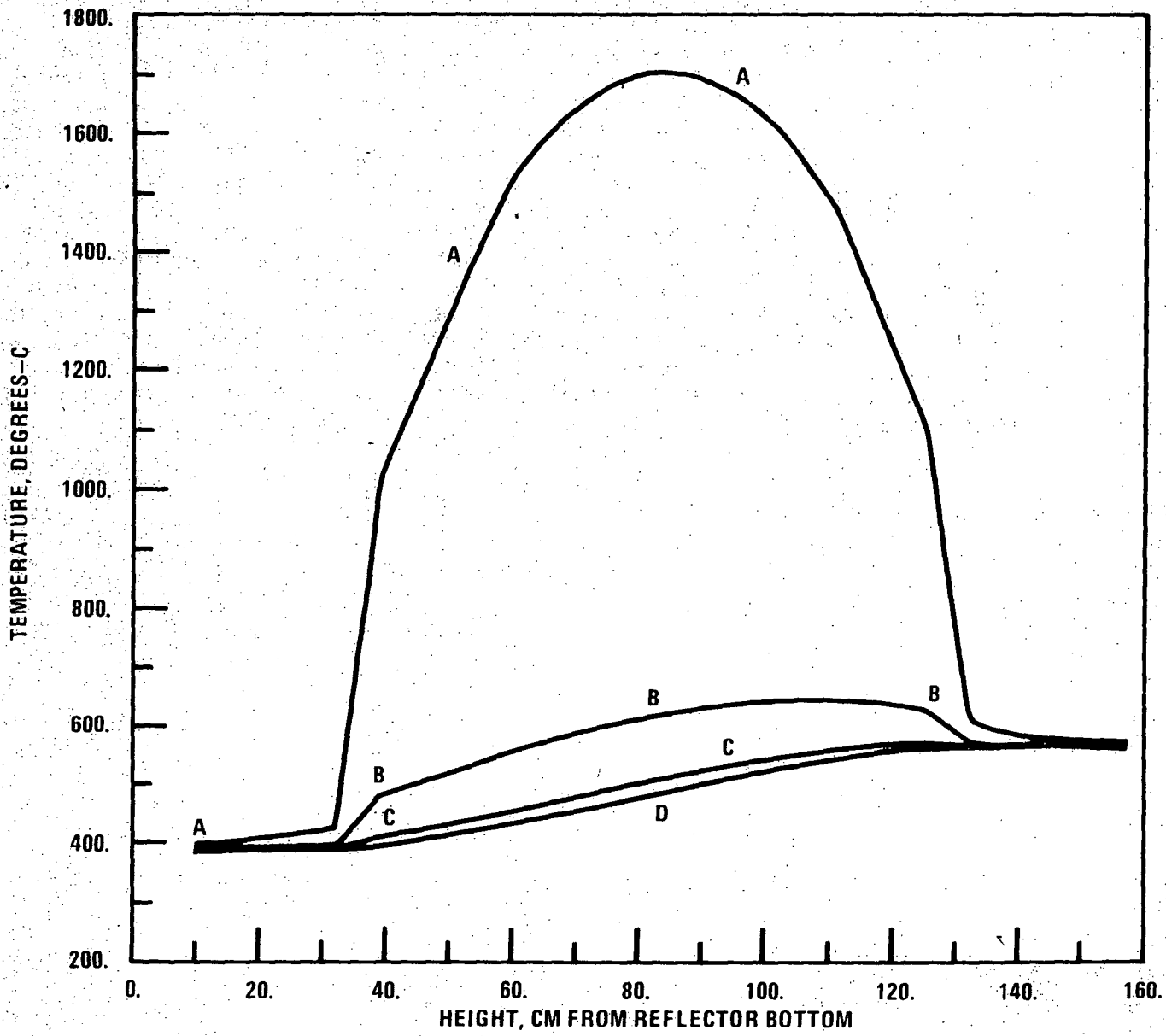
In order to clarify the statement that for the CRBR EOEC core representation in SAS3A, the calculated steady-state fuel temperatures are high and this would yield conservative predictions concerning transient behavior an EOEC TOP case was run where the minimum and maximum no-pressure conduction contribution to the gap conductance was set at 2 watts $\text{cm}^{-2} \text{sec}^{-1} \text{ } ^\circ\text{C}^{-1}$ ($3522 \text{ Btu ft}^{-2} \text{ hr}^{-1} \text{ } ^\circ\text{F}^{-1}$). The radiation and contact gap conductance contributions employed the same algorithm as the EOEC TOP base case. Figure Q001.451-1 shows the highest-power channel steady-state axial temperature profiles. As can be seen from comparison with Fig. 5-18. of Ref. 15, PSAR Section 1.6, the temperature drop across the fuel-cladding gap has been reduced by more than a factor of four.

The transient for this parametric was similar to the base case, i.e., fuel pin failure resulted in hydraulic sweepout of fuel and a benign accident termination. Figure Q001.451-2 gives the overall power and reactivity traces. These may be compared to Fig. 6-1 of Ref. 15, PSAR Section 1.6 for the base case. The high gap conductance case was more incoherent than the base case and the final net reactivity was not as low since fewer pins failed and less cavity fuel was available for sweepout following each pin failure. In general, these results do strongly suggest that it is indeed conservative to use a low steady-state gap conductance which increases as a TOP accident progresses (particularly, when in the SAS model transient fuel cracking is modeled as resulting in fuel-cladding contact). The specific points raised in the question can be addressed as follows:

*Note that Appendix F has been withdrawn. The text, upon which the question was based, can now be found in Section 5 of Reference 15, PSAR Section 1.6.

- (a) It is true that (1) early pin failures would be beneficial to the accident outcome, and (2) the first pin failure is at 12.65 sec in the high gap conductance case versus 12.00 sec in the base case. However, these observations miss the important point regarding the molten fuel present at pin failure. Figure Q001.451-3 and Figure 6-5 of Reference 15, PSAR Section 1.6, compare the fuel conditions versus time for the two cases. The base case has a centerline molten fuel fraction of over 40% at failure. The high gap conductance has a centerline molten fuel fraction of less than 30%. These pins fail with less molten fuel because of the greater transient fission gas availability due to the colder steady-state temperatures. In a slow transient, a reduction in the amount of molten fuel that is available for rapid mixing with sodium will reduce the extent of any fuel-coolant heat transfer. The fuel-coolant interaction pressures are thus lower in the high gap conductance case. In short, the absolute time into the transient is not relevant if the steady-state conditions are different. | 61
- (b) Figure Q001.451-4 and Figure 5-21 of Ref. 15, PSAR Section 1.6, compare the restructuring boundaries for the two cases. The differences are appreciable, but the high gap conductance case still has a central void extending over 55 cm., and pin failure is predicted to be only one SAS node lower, ~7 cm. This is not significant due to the reduced FCI. Figure Q001.451-5, and Q001.451-6, and Fig. 6-2 of Ref. 15, PSAR Section 1.6, compare the voiding reactivity. The high gap conductance parametric reduces the peak voiding reactivity in Channel 8 from ~9 cents to ~6.5 cents. (Channel 5 no longer even fails due to the increased incoherence). Figure Q001.451-7, and Figure 6-4 of Ref. 15, PSAR Section 1.6, compare the voiding profiles in Channel 8. The lower FCI zone interface was pushed downward almost 10 cm more in the base case. In the context of the burst failure criterion, there is not a strong sensitivity of the pin failure location to the degree of restructuring. | 60 | 31
- (c) Figure Q001.451-8 and Figure 5-22 of Ref. 15, PSAR Section 1.6, compare the steady-state fission gas retention. There is obviously more fission gas available with the lower steady-state fuel temperatures. As pointed out above, this results in pin failure with a smaller amount of molten fuel. With more restructuring, more fuel must melt to get sufficient pressurization for pin failure. The base case had 45.4 gm of molten fuel in the pin cavity at failure; the high gap conductance parametric had 23.6 gm. In a slow TOP accident, less transient fission gas availability is a conservative assumption. | 60 | 31
- (d) As discussed in point (a), it is the time from which fuel first starts to melt that is important. In the base case, initial fuel melting produced little pressurization in the peak pins; the lower power pins were allowed to get closer to their failure thresholds. In the high gap conductance case, initial fuel melting failed the peak pins terminating the transient. There will be more incoherence if the gap conductance is increased.

- (e) The peak coolant temperature was reduced from 869°C in the base case to 809°C in the high gap conductance case at pin failure. These temperatures are both significantly below the local sodium saturation temperature of 1049°C corresponding to a pressure of 3.8 atm. The reduced Doppler feedback is responsible for higher powers and hence the higher temperatures in the base case. The Doppler feedback is reduced since the steady-state temperatures are higher and since, at a given power, the transient fuel temperatures do not rise quite as rapidly due to the increasing gap conductance as a function of time and due to a higher energy input into fuel phase translations (melting) versus a continuing increase in solid fuel temperatures. Local boiling is more likely to be enhanced by fuel-pellet clad contact when such contact does not exist at steady-state but occurs purely in the transient behavior mode. This is the situation treated in the base case. Finally, local secondary loading failures are not treated in the current model, and are hence irrelevant to the present discussion, although it may be suggested that due to the hotter cladding resulting from higher power and temperatures, such failures may be more likely in the base case.



CHANNEL A B C D E
 8 FUEL-1 FUEL-0 CLAD-MID COOLANT STRUCT.

Figure Q001.451-1 Steady-state Axial Temperature Profiles for the Q001.451 Parametric.

11-76-P0802-7

Q001.451-4

Amend. 30
 Nov. 1976

Q001.451-5

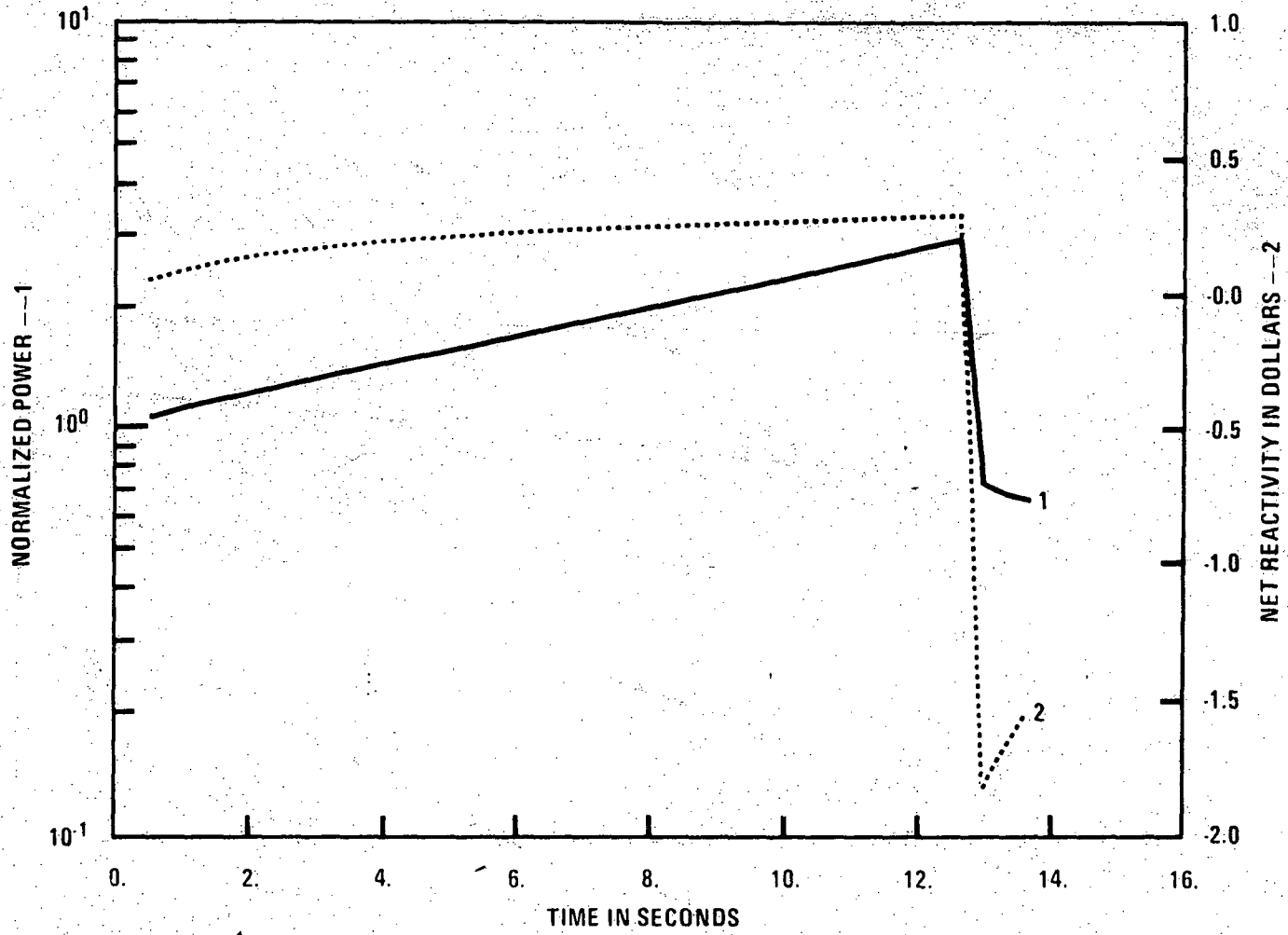


Figure Q001.451-2 Power and reactivity profiles for the Q001.451 Parametric.

Amend. 30
Nov. 1976

11-76-P0802-2

Q001.451-6

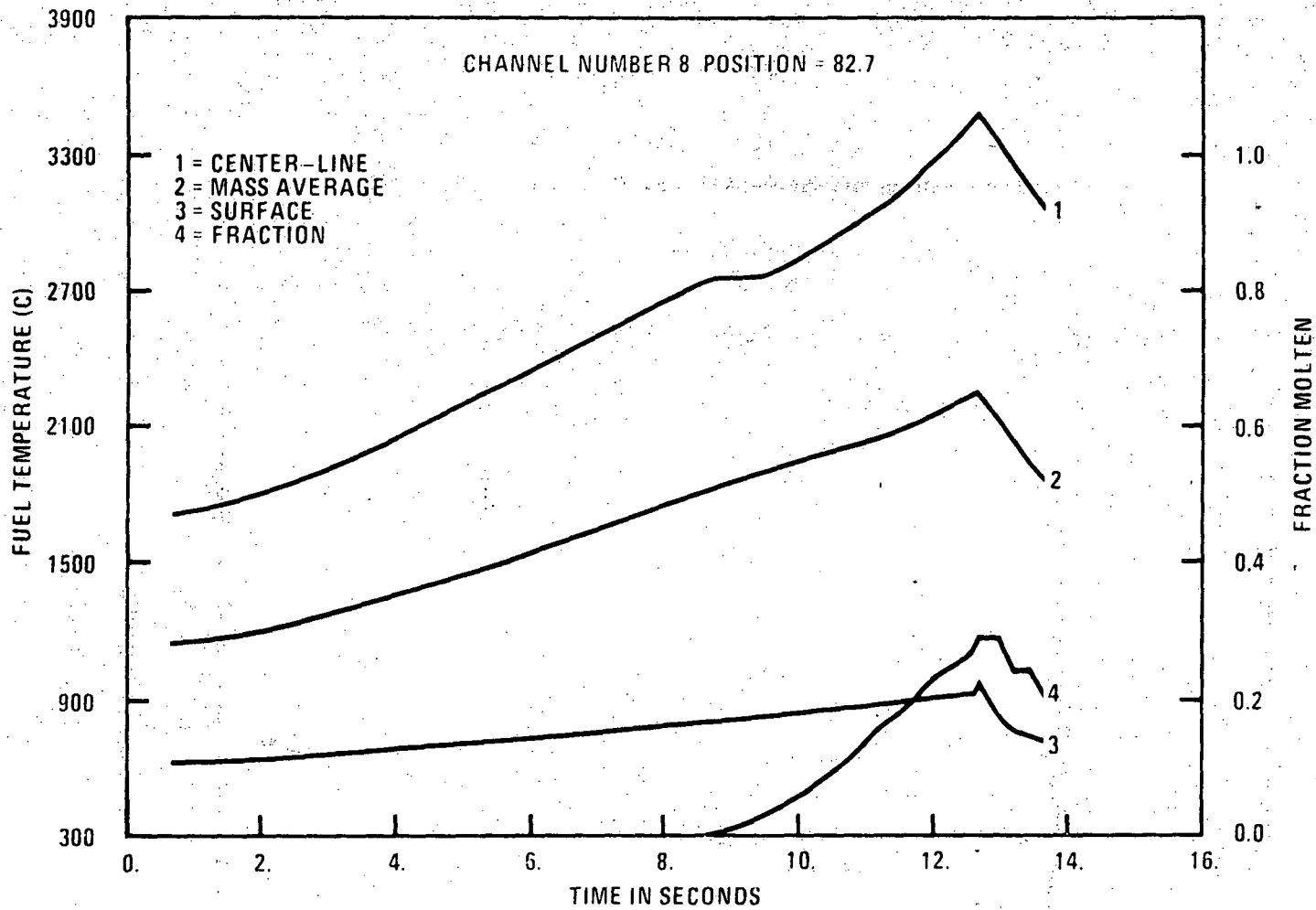


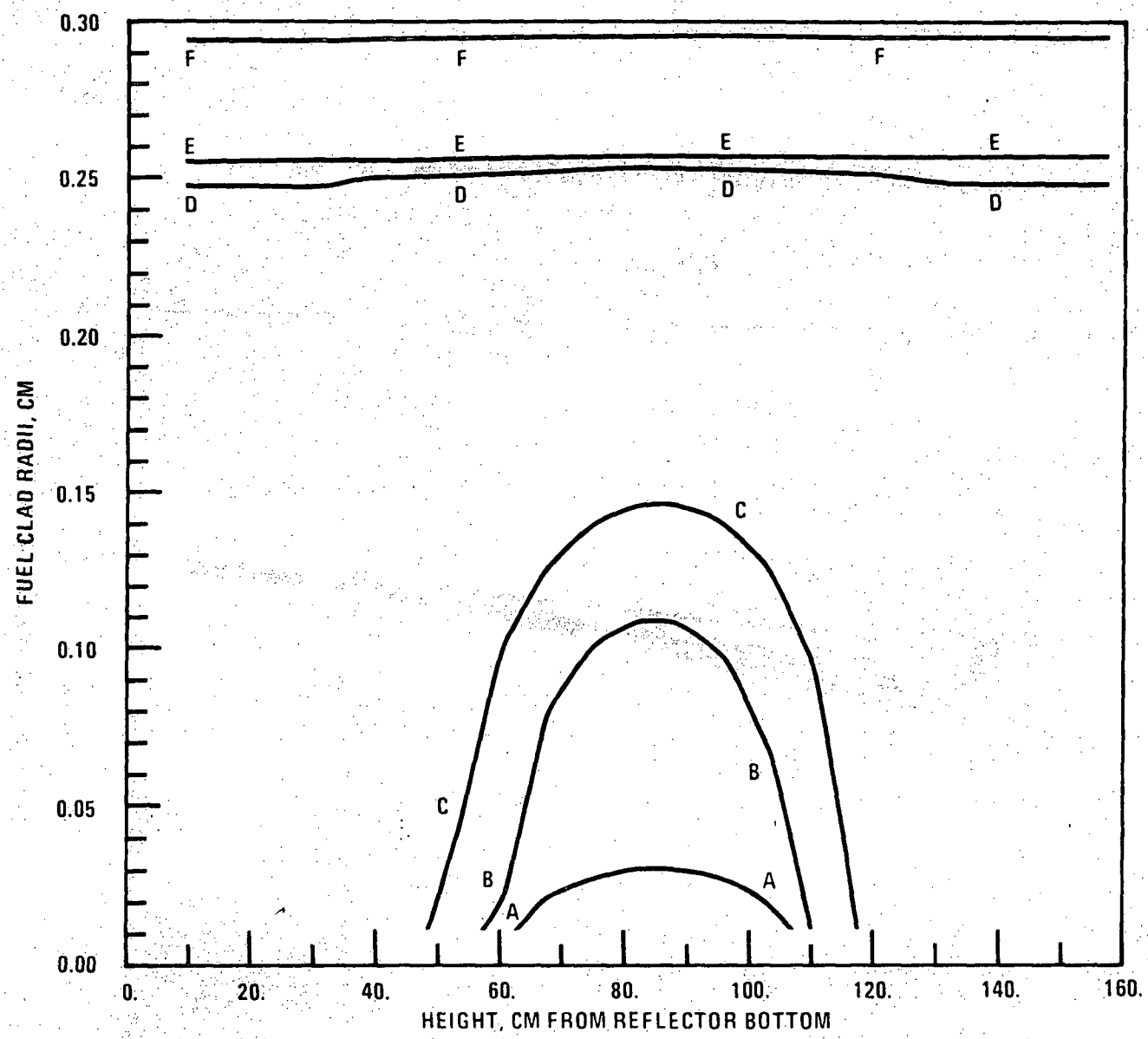
Figure Q001.451-3 Transient Fuel Temperatures for the Q001.451 Parametric.

Amend. 30
NOV. 1976

11-76-P0802-3

Q001.451-7

Amend. 30
Nov. 1976



CHANNEL A B C D E F
8 FUEL-I COL/EQA EQA/UNR FUEL-O CLAD-I CLAD-O

Figure Q001.451-4 Restructuring Boundaries for the Q001.451 Parametric

Q001.451-8

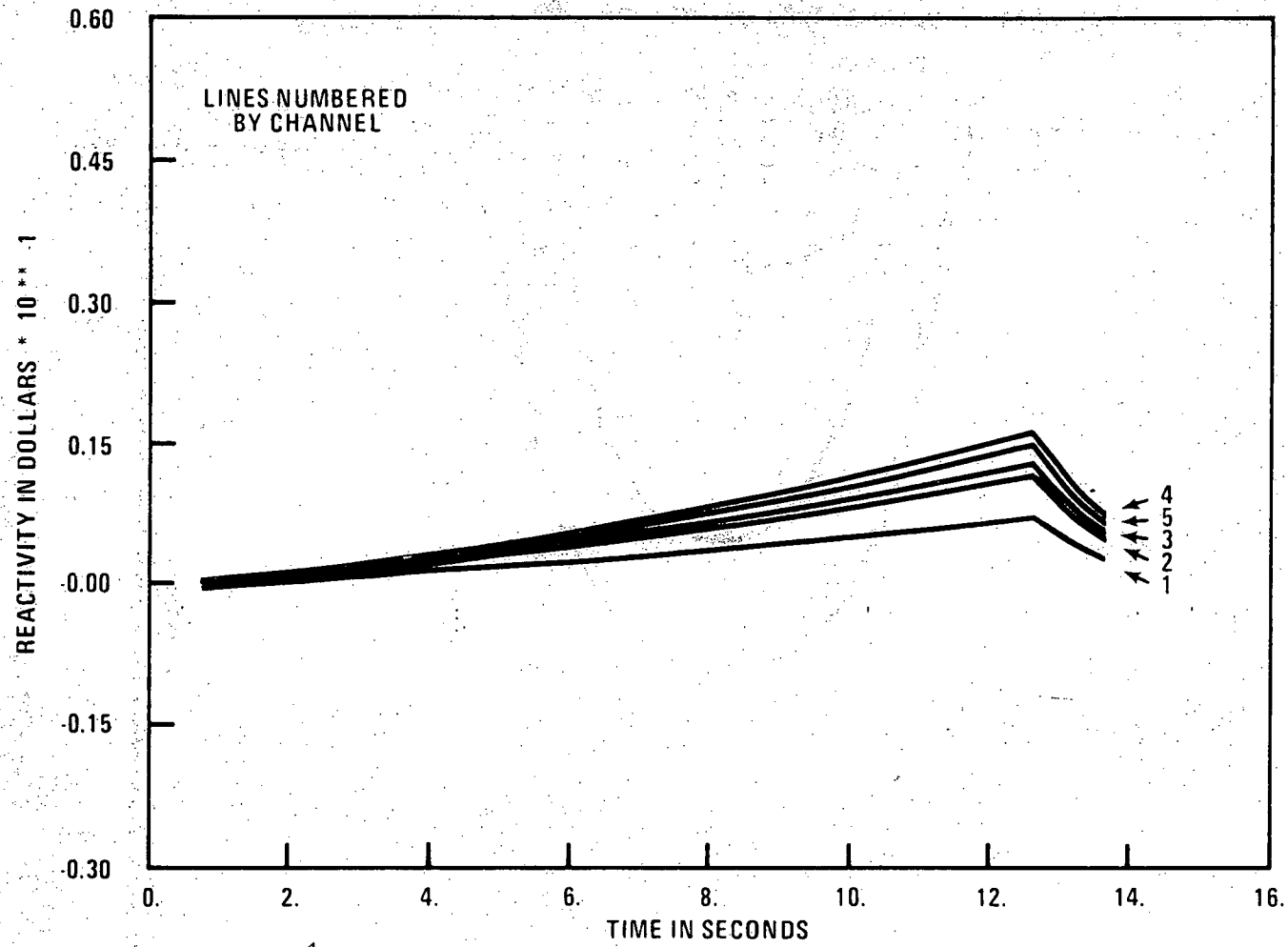


Figure Q001.451-5 Sodium Voiding Reactivity for the Q001.451 Parametric for Channels 1-5.

11-76-P0802-4

Amend. 30
Nov. 1976

Q001.451-9

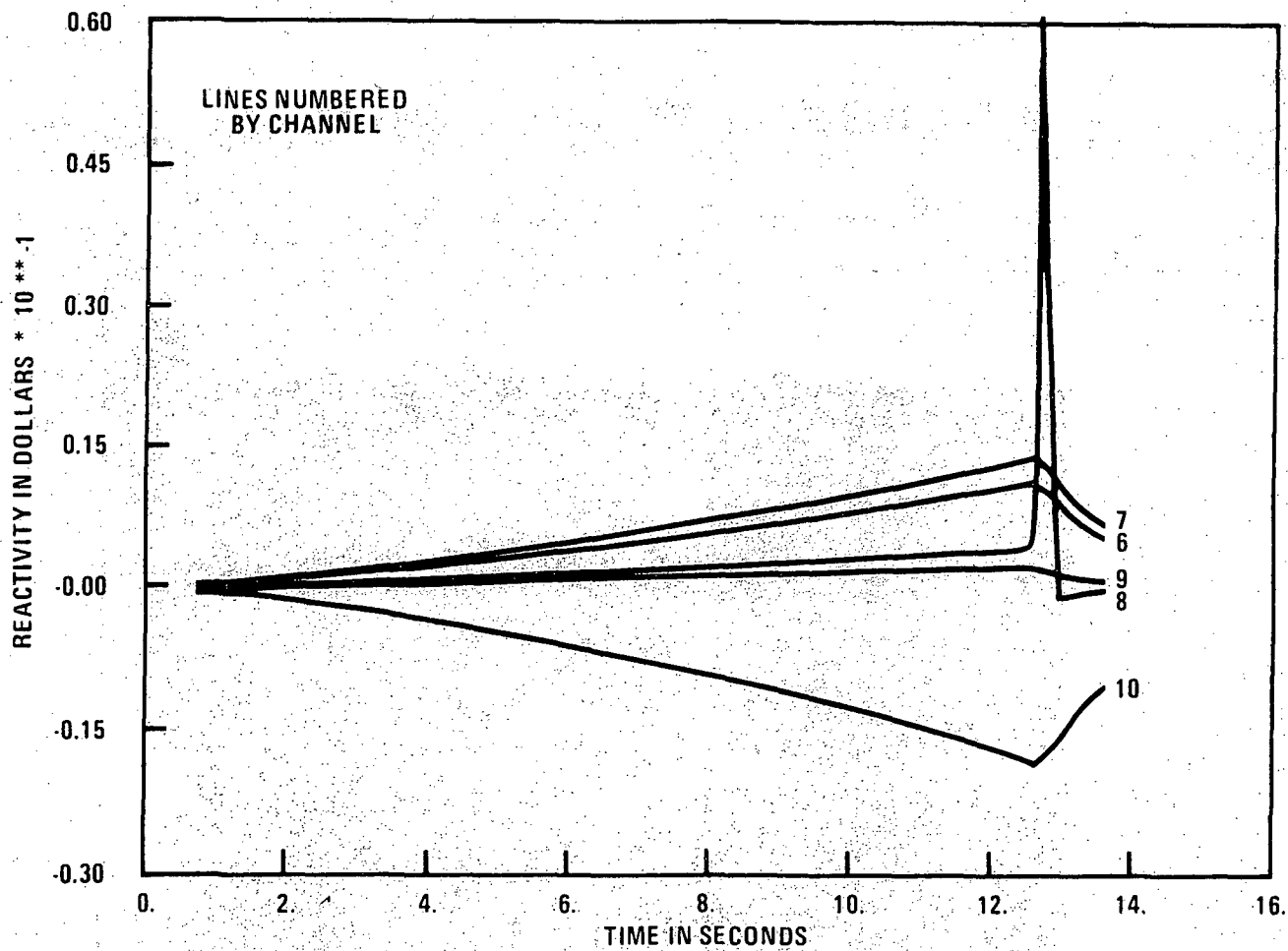


Figure Q001.451-6 Sodium Voiding Reactivity for the Q001.451 Parametric for Channels 6-10.

Amend. 30
Nov. 1976

11-76-P0802-5

Q001.451-10

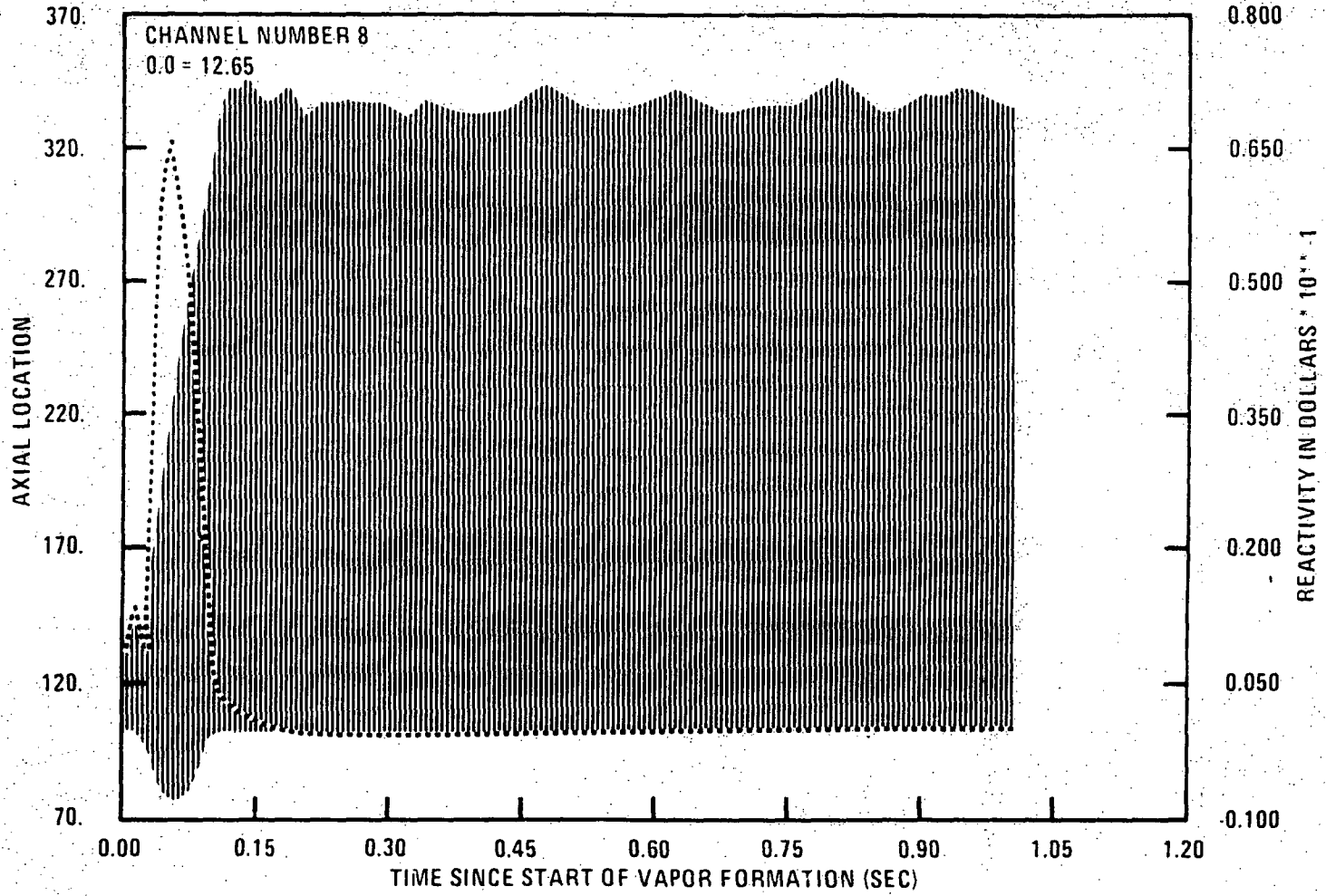


Figure Q001.451-7 FCI Zone Interfaces for the Q001.451 Parametric.

Amend. 30
Nov. 1976

11-76-P0802-1

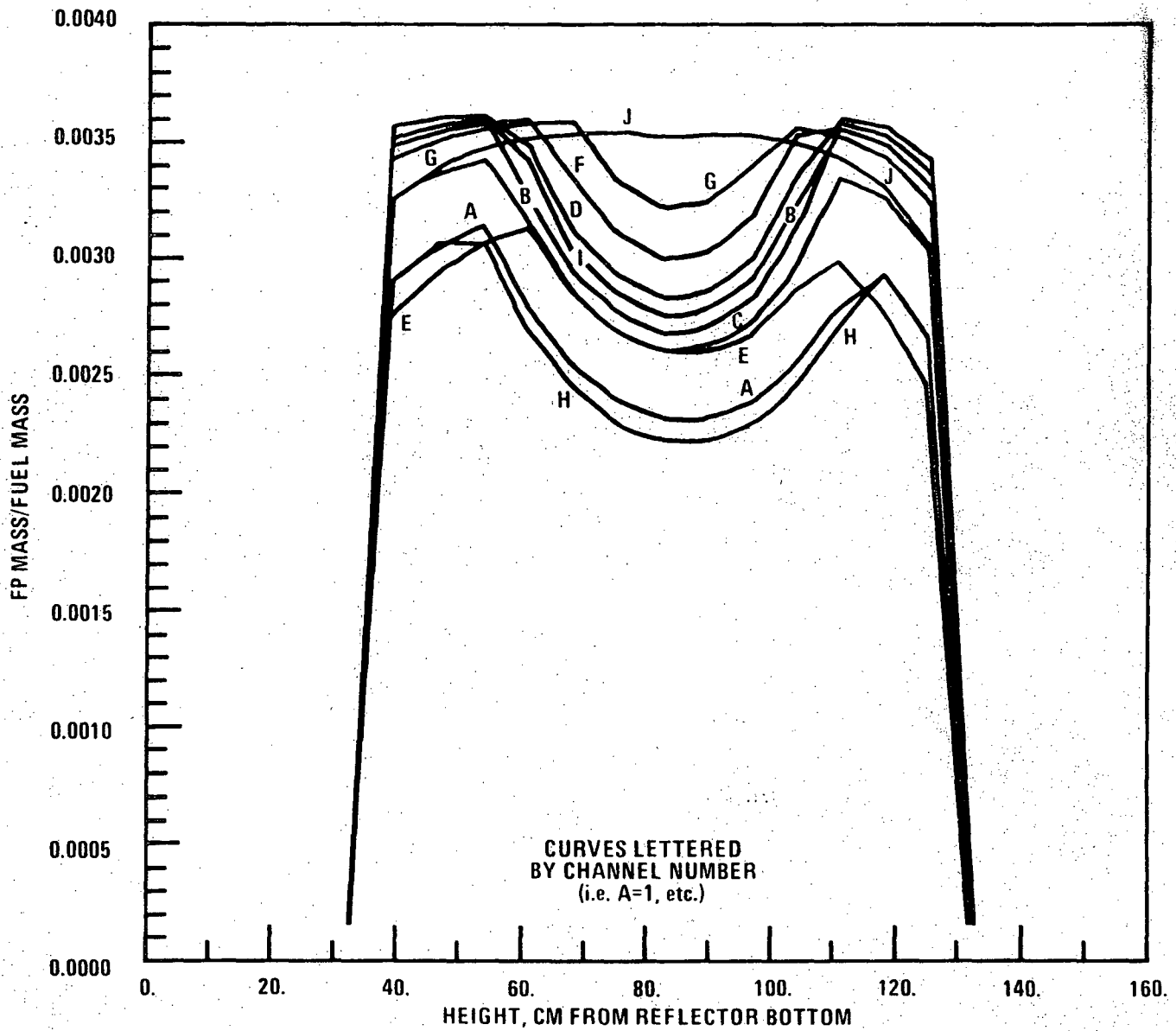


Figure Q001.451-8 Steady-State Fission Gas Retention for the Q001.451

11-76-P0802-8

Q001.451-11

Amend. 30
Nov. 1976

Question 001.452 (Section F6.2.4)

On page F6.2-42 it is stated that failures are predicted at the core mid-plane. Identify the failure criterion used in this prediction.

Response:

The CRBRP Project has consolidated all considerations given Hypothetical Core Disruptive Accidents into report CRBRP-3 (References 10a and 10b, PSAR Section 1.6) and its associated references; consequently, PSAR Appendices D and F have been withdrawn in Amendments 24 and 60 respectively. The response to this question is now found in Section 4.3.2.2 of Reference 10a, PSAR Section 1.6.

60

Question 001.453 (F6.2.4.3.1)

Reference is made to Figure F6.2-99. Describe the "BOEC SASBLOK comparison W/ANL Base Case" noted on the figure.

Response:

This question requests clarification of information which is no longer a part of the current documentation. The Project has since consolidated all considerations given Hypothetical Core Disruptive Accidents into report CRBRP-3 (References 10a and 10b, PSAR Section 1.6) and its associated references; consequently, PSAR Appendices D and F have been withdrawn in Amendments 24 and 60 respectively.

60

Question 001.454 (F6.2.4.3.1)

It is not clear why a SASBLOK analysis was performed on the initial failure (Channel 10) but not the subsequent failure in Channel 2. Explain this course in the analyses.

Response:*

60

A SASBLOK analysis was not performed for the failure in Channel 2 since the total reactivity of \$3.20 had been inserted and the negative fuel motion reactivity from Channel 2 was sufficient to neutronically terminate the accident. The primary purpose of the SASBLOK procedure is to allow the SAS calculation of the transient to continue, beyond the termination of the SAS/FCI calculations in the failed channels, until neutronic shutdown can be shown to occur. When the failure of Channel 2 occurs at 32.98 seconds the total reactivity of \$3.20 has already been inserted. The failure of Channel 2 renders the reactor \$-4.35 subcritical, which neutronically terminates the transient. A SASBLOK analysis of the failure in Channel 2 would not provide any additional information about the course of the transient since the total reactivity has been inserted and the negative fuel motion reactivity from Channel 2 results in a final subcritical state.

60

*Note that Appendix F has been withdrawn. The text, upon which the question was based, can now be found in Section 6 of Reference 15, PSAR Section 1.6.

60

Q001.454-1

Amend. 60
Feb. 1981

Question 001.455 (F6.2.4.3.2.1)

Considering differences in the low ramp rate accident relative to 10¢/sec base case, there is no mention of clad failure in the plenum region prior to pin failure in the core region. Because of the relatively high plenum region clad temperatures for low ramp rates, the possibility of failure in this region above the core is increased. Discuss the possibility of such failure and the sequence of events following such failures. Include in your considerations the degraded condition of the cladding (due to, for example, cesium attack), the core voiding progression, the driving forces for fuel motion once core area failures have occurred. Comment on the applicability (or lack of applicability) of the TREAT E7 test in which fission gas is thought to have been released prior to fuel motion.

Response: *

The SAS3A code calculates the cladding strength at the axial nodes in the upper blanket and in the plenum region based on the clad loading and temperature. The calculated cladding strength is compared with the clad failure strength data to determine if cladding failure will occur. Cladding failure in the plenum region was not predicted to occur in the BOEC and EOEC 2.4 and 10¢/sec. best-estimate TOP analyses. The possibility of cladding failure in the plenum region is much lower than in the active core region even though the cladding temperatures are somewhat higher above the core, because the clad loading due to circumferential stresses in the plenum is much less than in the active core region as discussed below.

In order for cladding failure to occur in the plenum region before it occurs in the core region, the effect of higher cladding temperature in the plenum region must be greater than the effects of higher clad loading and greater cladding ductility degradation due to fluence effects in the core region. Table Q001.455-1 lists the factors that must be considered in comparing the effects of clad loading relative to its strength in the plenum and core regions for the first channel to fail in the BOEC 2.4 ¢/sec. TOP transient. As shown in the Table, the circumferential stress in the cladding is almost an order of magnitude larger in the core region of Channel 2 than in the plenum region at the time of the predicted failure. The Channel 2 plenum region is the most likely to experience failure of any of the plenum regions in the ten SAS3A channels because maximum plenum pressure is calculated to occur in Channel 2.

The strength of cladding in the plenum region can be estimated directly from Fuel Cladding Transient Test (FCTT) data (Reference Q001.455-1) since the fluence in the plenum region of CRBRP is low. FCTT specimen PNL 10-63-Q closely approximates CRBR plenum - region cladding. This specimen failed at 43.2 Ksi (3.0×10^9 dynes/cm²) under a 10⁰F/sec. thermal ramp. This value of strength is slightly too high because the specimen failure temperature was 1483⁰F (806⁰C). A lower limit of 28.8 Ksi (2.0×10^9 dyne/cm²) is provided by specimen N-035-I, which failed at 1630⁰F (887⁰C).

*Note that Appendix F has been withdrawn. The text upon which the question was based, can now be found in Reference Q001.455-1 and Q001.455-2.

Interpolating with respect to failure temperature, a best estimate for plenum region cladding strength at 837°C is 37.7 Ksi (2.6×10^9 dynes/cm²) at the time Channel 2 failed in the core region. The Channel 2 plenum region is not likely to fail with a calculated circumferential stress of 2.9 Ksi (2.0×10^8 dyne/cm²) at any time before the time of failure in the core region, despite its high temperature.

Table Q001.455-1 lists the factors that cause low strength in the core-region cladding. The primary effects are fluence and the fuel adjacency effect. This latter effect is believed to promote intergranular failure by injecting helium into the cladding. In cladding with pretransient temperature above 950-1000°F (510-538°C), this helium weakens the grain boundaries and promotes failure at low stresses and low uniform elongation. Increasing fluence probably adds to this effect. Other effects, such as cladding wastage, are believed to be of secondary importance. The strain rate is not expected to significantly influence strength as long as the pretransient cladding temperature is above 950-1000°F and failure is intergranular.

Cesium effects are expected to increase the likelihood of cladding failure in the core region or near the ends of the fuel column. Failure in the plenum region due to cesium effects is not likely because cesium appears to be immobilized near the fuel-blanket interface by the low fuel-cladding gap temperature in this region or by oxygen in the blanket pellets.

The possibility of cladding failure in the plenum prior to cladding failure in the core is therefore expected to be very low, as shown by the SAS3A transient cladding strength and temperature calculations in the plenum as well as the active core region, and as indicated by the discussion of the factors affecting cladding strength in Table Q001.455-1.

Effects of Plenum Region Failure

If it is postulated that fission gas will be released from the plenum region before cladding failure occurs in the core region, then the following sequence of events may occur.

The release of fission gas from the plenum region may produce a fission gas bubble or void in the coolant channel. Should the lower interface of the bubble move down into the core region, pin failures may occur due to the resultant cladding temperature increase. The driving force for fuel motion, once clad failure has occurred in the core region, is the fission gas pressure inside the fuel central cavity which does not communicate with the fission gas plenum. The molten fuel and fission gas mixture inside the pin would be ejected into the voided region of the channel and freeze on cladding in the areas adjacent to the failure location. When the sodium re-enters this section of the channel, a mild fuel-coolant interaction may occur. Sodium flow will eventually be re-established in the entire channel.

If the cladding fails in the upper one-third of the core as predicted by current models, a negative reactivity component, due to fuel motion inside the pins, would tend to decrease the reactor power. However, positive

reactivity would be added due to the voiding in the channel. The overall effect may be to slow the reactor power increase slightly, but as the reactivity continues to increase due to the continued control rod withdrawal, other channels will eventually fail in the active core region, resulting in a fuel-coolant interaction fuel sweepout and neutronic shutdown.

If the cladding fails near the core axial midplane, the positive reactivity addition due to fuel motion may increase the reactor power, resulting in earlier failure of other channels in the core. However, the additional failures are expected to be at axial locations above the midplane, resulting in fuel sweepout and neutronic shutdown. If the additional failures occur at the core midplane, the energetics should be of the same order of magnitude as calculated for the forced midplane failure case.

The scenario described above assumes that the plenum failure occurs at a certain time during the transient, and that the void enters the core region and remains in the core region long enough to cause an increase in the core cladding temperature, causing the cladding to fail. The possibility that the plenum failure will cause a failure in the core region thus depends on: 1) the time during the transient at which the plenum fails, 2) the extent of voiding in the channel, 3) the core cladding temperatures, and 4) the length of time that the void remains in the core region. Therefore, even if fission gas release due to plenum failure does occur, it would not necessarily promote failures in the core region or result in energetics greater than the energetics which result from the accident scenarios in the best estimate cases.

Applicability of TREAT E-7 Test to CRBRP

The results of the TREAT E-7 test are unlike those of any other TREAT TOP test. The discussion of the TREAT E-7 test in Reference Q001.455-2 (pp. III-62 to III-70) indicated that the initial failure of the hottest edge pin in the irradiated pin test section resulted in gas release through a pin hole crack in the cladding near the upper end of the fuel column boundary possibly along a grain in the cladding.

The mechanism and axial location of failure of the other rods in the test section has not been determined. Although the initial pin failure resulted in fission gas release, it cannot be determined to what extent the failure of the other pins may have been caused by the fission gas induced sodium voiding. Therefore, the TREAT E-7 test provides no clear information regarding the effect of fission gas release on pin failure propagation relative to the CRBRP.

References:

- Q001.455-1: T. C. Chawla, et al., "The Recovery of Coolant Flow Following Rapid Release of Fission Gas from a Postulated Multiple Pin Failure", ANL/RAS 75-3, February 1975
- Q001.455-2: L. W. Dietrich, et al., "Final Summary Report on Fuel Dynamics Tests H2 and H4", ANL/RAS 74-8, 1974

TABLE Q001.455-1

COMPARISON OF FACTORS AFFECTING CLADDING STRENGTH IN CRBR
BOEC CHANNEL 2 CORE AND PLENUM REGIONS DURING A 2.4 ϕ /SEC TOP EVENT

<u>Factor</u>	<u>Relative Value at Predicted Core Failure Location in Channel 2</u>	<u>Relative Value in Plenum Region in Channel 2</u>
Cladding Circumferential Stress ⁽¹⁾	27.4 Ksi (1.9×10^9 dynes/cm ²)	2.9 Ksi (2.0×10^8 dynes/cm ²)
Cladding Temperature ⁽¹⁾	712°C (1313°F)	837°C (1538°F)
Pretransient Fluence (E>0.1 Mev)	$> 1 \times 10^{23}$ n/cm ²	$\sim 1.5 \times 10^{22}$ n/cm ²
Fuel Adjacency Effects on Cladding Properties	Yes	No
Pretransient Cladding Temperature	$> 538^\circ\text{C}$ ($>1000^\circ\text{F}$)	$>538^\circ\text{C}$ ($>1000^\circ\text{F}$)
Cladding Wastage	Greater	Less

Note:

(1) At time of predicted failure in the core region in Channel 2.

Question 001.456 (F6.2.4.3)

In Section F6.2.4.3.2.1.2 (page F6.2-66) explain the statement "as the ramp rate is increased . . . thr probability of sodium boiling in the fresh pin Channel 9 increases.

Response:

This question requests clarification of information which is no longer a part of the current documentation. The Project has since consolidated all considerations given Hypothetical Core Disruptive Accidents into report CRBRP-3 (References 10a and 10b, PSAR Section 1.6) and its associated references; consequently, PSAR Appendices D and F have been withdrawn in Amendments 24 and 60 respectively.

60

Question 001.457 (F6.2.4.3.2.1.2)

Correct typographical errors in Figure F6.2-99F.

Response

This question requests clarification of information which is no longer a part of the current documentation. The Project has since consolidated all considerations given Hypothetical Core Disruptive Accidents into report CRBRP-3 (References 10a and 10b, PSAR Section 1.6) and its associated references; consequently, PSAR Appendices D and F have been withdrawn in Amendments 24 and 60 respectively.

60

Question 001.458 (F6.2.4.3.2.2)

Assume that the "Smith correlation" is valid and that the power in Channel 9 is correct (i.e., not too high), is fresh fuel failure still expected prior to irradiated fuel failure? In your discussion consider the capability of the fresh ductile cladding to accommodate primary and secondary loading.

Response: *

| 60

The Smith correlation for fission gas release in irradiated fuel was not used in the best estimate BOEC TOP analyses since the experimental fission gas release data in Ref. Q001.458-1 indicates that fission gas release from unrestructured fuel begins before the solidus temperature of 2767°C is reached, whereas the Smith model assumes no fission gas release until the solidus temperature is reached. The Smith correlation was used primarily to determine if a significantly different accident scenario would result using this correlation as opposed to the best estimate modified Gruber correlation for irradiated fuel. The results of these analyses, presented in Section 6.2.3.1 of Ref. 15, PSAR Section 1.6, indicated that a significantly different accident scenario would not result, and that the energetics were expected to be on the same order of magnitude using either model.

| 60

However, if the Smith correlation is assumed to be valid and the power in Channel 9 is correct, the failure of fresh fuel is expected to occur prior to irradiated fuel failure. This is true because fresh fuel would fail due to coolant voiding and local overheating before high plastic strains occurred in the cladding and because irradiated cladding would experience no plastic straining until after coolant voiding occurred in Channel 9. The technical basis for these statements are as follows.

A review of the SAS analysis shows that, using the Burst Pressure criterion, the ratio of calculated stress to burst stress is only 0.39 in the worst irradiated channel (Channel 2) when failure occurs in Channel 9 (where the ratio is ~1.0 at failure). This is true even though Channel 2 cladding strength is reduced in the SAS model to account for irradiation effects and wastage. As shown in Table 4-1 of Ref. 15, PSAR Section 1.6 (Pointer 53), the burst strength of Channel 2 is decreased 16% to account for cladding wastage. Furthermore, as shown in Figure 3-3 of Ref. 15, PSAR Section 1.6, the burst strength of irradiated cladding at 854°C is reduced by an additional 36% to account for irradiation effects. As a result of these adjustments, the burst strength of irradiated Channel 2 is slightly lower than the strength of Channel 9, even though Channel 2 is colder by 137°C (246°F). Channel 2 does not fail because the pressure in the central fuel cavity is only half that of Channel 9.

| 60

For failure to occur first in irradiated fuel, an additional factor of 2.0 decrease in strength would have to be postulated; this would not be consistent with data currently available.

*Note that Appendix F has been withdrawn. The text, upon which the question was based, can now be found in Section 6 of Reference 15, PSAR Section 1.6.

| 60

If a failure criterion based on stress is assumed not to be applicable, and the present analysis is assumed to predict failure too early for fresh cladding, the course of the accident described in Section 6.2.3.1 of Ref. 15, PSAR Section 1.6, would change very little. The reason for this is that incipient coolant boiling occurred 0.180 seconds before the predicted time of failure in Channel 9. As shown in Figure 6-68 of Reference 15, PSAR Section 1.6, gross void formation in Channel 9 is imminent at 12.25 seconds, so failure of Channel 9 by localized overheating would be expected within a short time. |60

Since the fresh cladding in Channel 9 is expected to fail very near 12.25 seconds whether or not one accepts stress as a failure criterion, the only possibility for irradiated fuel to fail first is for irradiated cladding to obey a strain-based failure law and for the plastic strain in Channel 2 to be close to the failure value at 12.25 seconds or earlier. In fact, the analysis shows that Channel 2 is below the yield point at 12.25 seconds; the stress is 0.61×10^9 dyne/cm² (8845 psi) while the yield point is 1.35×10^9 dyne/cm² (19575 psi) at the "worst" axial section of Channel 2. Clearly, plastic strain in Channel 2 would not begin until well after failure in Channel 9.

In conclusion, the probability that fresh cladding will have such high ductility that irradiated fuel will fail first in the analysis of Section 6.2.3.1 of Ref. 15, PSAR Section 1.6, is negligible. This is true because 1) fresh cladding will fail by coolant voiding and local overheating before it accumulates high plastic strains, and 2) irradiated cladding will experience no plastic strain until after Channel 9 voids. |60

Reference:

Q001.458-1: A. D. Slagle, C. A. Hinman and E. T. Weber, "Experiments on Melting and Gas Release Behavior of Immediate Fuel", Hanford Engineering Development Laboratory, 1974. (HEDL-TME 74-17). |60

Question 001.459 (F6.2.4.3.2.2)

There appears to be inconsistencies in the text (page F6.2-68, 2nd paragraph) and in Figures F6.2-102 and 103 when referring to channel numbers. Make the necessary corrections.

Response:

This question requests clarification of information which is no longer a part of the current documentation. The Project has since consolidated all considerations given Hypothetical Core Disruptive Accidents into report CRBRP-3 (References 10a and 10b, PSAR Section 1.6) and its associated references; consequently, PSAR Appendices D and F have been withdrawn in Amendments 24 and 60 respectively.

60

Question 001.460 (F6.2.4.3.2.3)

Within the limitations of the DEFORM model you develop a mechanistic strain failure model for TOP accident analysis. It is stated that, based on these failure models, pins will fail by the burst pressure criterion before the strain failure criterion is satisfied. In order to demonstrate a strain-failure accident progression, strain failure is forced by reducing the failure strain in fresh pins from 1% to 0.2%. A fresh pin failure strain of 0.2% is, as stated in the PSAR, unrealistically low. However, an irradiated pin failure strain of 0.05% is not. Failure strains as low as 0.04% have been measured as part of the FCTT experiments. Perform an analysis where the irradiated channel failure strains are 0.05%, similar to that described at the top of page F6.2-71. Furthermore, discuss the possibility that the strain failure criterion will be satisfied before the burst pressure criterion in light of the following:

- a) An irradiated failure strain of 0.05% to 0.10% is more realistic than the 0.5% used;
- b) At any given time during the transient, DEFORM under predicts total strain because fuel swelling and fission gas loading are not taken into account;
- c) The increased gas volume attributed to cladding strain is not accounted for in the burst model, thus giving the burst model unrealistically high bottle pressure.

Response: *

160

Analysis of the BOEC 10¢/sec TOP accident scenario using an irradiated pin plastic failure strain of 0.05% indicates that Channel 2, which had the smallest pre-transient gap width, would reach 0.05% permanent strain at the axial mid-plane at approximately 10.84 sec into the transient. The failure was forced to occur at this time. The positive fuel motion reactivity effect resulted in a power increase from approximately 3.5 times steady-state power at the time of Channel 2 failure to approximately 16 times nominal at 10.89 sec. At this time the clad plastic strain in the irradiated Channels 4 and 8 had increased to 0.03% and 0.04%, respectively. Although the reactor power then began to slowly decrease due to the negative reactivity effect of fuel motion in the expanding Channel 2 fuel-coolant interaction zone, Channels 4 and 8 reached the strain failure value of 0.05% near the axial midplane at approximately 10.9 seconds. The predicted failure scenario using a constant plastic strain failure value of 0.05% are not thought to be realistic for the reasons explained in part a) below.

- a) The use of a constant failure strain value is an oversimplification of a complex phenomenon. The failure strain is dependent on the steady state cladding irradiation temperature, the transient cladding temperature, the transient strain rate and the neutron fluence.

*Note that Appendix F has been withdrawn. The text, upon which the question was based, can now be found in Section 6 of Reference 15, PSAR Section 1.6.

160

Amend. 60
Feb. 1981

Irradiated failure strains on the order of 0.05% measured in the FCTT tests occurred in cladding which was irradiated at steady state cladding temperatures in the range of 700 to 885°F, which corresponds to CRBR temperatures below the core midplane at CRBR fluences. An irradiated failure strain value on the order of 0.2% or greater is thought to be realistic in the region above the core midplane where the pin is expected to fail. (See Reference Q001.460-1). Specifying a failure strain value of 0.05% in effect forces the pins to fail near the core midplane since the permanent deformation (which first occurs near the midplane) is sufficient to produce this low value of strain before permanent deformation begins in the region above the core midplane.

Although an irradiated strain failure correlation (as opposed to a constant value) was not available for use in the CRBRP analyses, a strain failure criterion may result in a different pin failure sequence and lower axial failure locations than were predicted with the burst pressure criterion. 160

The accident energetics are expected to be of the same order of magnitude as the energetics resulting from the burst pressure criterion predictions of pin failure. Should this not be the case, the energetics that would result would be bounded by the energetics resulting from the forced midplane failure case presented in Section 6.2.3.4 of Reference 15, PSAR Section 1.6. 160

- b) The cavity pressure at the time that the DEFORM predictions resulted in a failure strain of 0.05% was not significantly greater than the steady state cavity pressure. The effects of neglecting fission gas loading become important when the cavity pressure begins to rapidly increase to hundreds of atmospheres, as exemplified in Figure 6-69 of Ref. 15, PSAR Section 1.6. Similarly, fuel swelling effects would not become important until the rate of fission gas release becomes large. As the transient progresses the effect of not taking fuel swelling and fission gas loading into account in DEFORM will tend to underpredict the total strain. However, since DEFORM does not allow molten fuel to relocate axially in the cavity, the pressure loading caused by expanding molten fuel constrained to remain at a fixed axial location will produce a loading component which results in strain overprediction. The above limitations in DEFORM do not allow a general conclusion to be made as to whether a strain failure criterion will be satisfied before the burst pressure criterion. 160
- c) Although the increased gas volume attributed to cladding strain is not accounted for in the burst model, the burst model is not thought to give unrealistically high cavity pressure. The cavity volume may be increased by clad straining but may be decreased by fuel swelling due to fission gas bubble growth and expansion at the grain boundaries in irradiated fuel. The overall effect of these two competing phenomena on the cavity volume is not accounted for in current models. However, if it was assumed that the burst model cavity pressure is too high due to not accounting for the increased volume attributed to cladding strain, the cavity pressure would be lower and the pin would tend to fail later. This delay in burst model predicted failure time would add to the time difference which already exists between the early failure time predicted with a constant strain failure criterion of 0.05% and the later failure time predicted with the burst pressure failure model.

Reference

- Q001.460-1 Sodium Cooled Reactor Core Emergency Program, Forty-fourth Quarterly Report, Aug.-Oct. 1972 GEAP-10028-44; pp 2-22 to 2-30.

Question 001.461 (F6.2.4.3.2.3.2)

In regard to the HEDL Empirical Failure Correlation, update the Damage Parameter correlation to include those TREAT tests not summarized in References 7 and 11. In particular, include the low-power HUT tests. Describe the results of those low-power tests impact on pin failure times and locations. Provide information, if known, on the failure location and mode, and the diagnostics for determining the location and mode for each of the transient tested pins used to derive and evaluate the Damage Parameter correlation.

Response:*

160

The HEDL Empirical Failure Correlation (the Damage Parameter correlation) has been recently extended and modified to include data from TREAT tests not formerly included; in particular, the low-power HUT tests. This new correlation, described in the attached Appendix A, has been named the Failure Potential correlation.

The following comparison of FFTF core analysis shows the effects of this new correlation upon fuel pin cladding failure times and location. In this study, the Failure Potential correlation results (including the low-power HUT tests) are compared with the Damage Parameter correlation (which did not contain the HUT data).

A twenty-channel model of the FFTF Beginning of Cycle 4 (BOC-4) core was constructed for the MELT-III (Reference Q001.461-1) code. An analysis was made using MELT-III, containing the SIEX code (Reference Q001.461-2) as a subroutine, and assuming a 50¢/sec reactivity insertion. The results obtained from both cases are given in Table Q001.461-1 for the first three failing channels. The failure node changes at most by one (both up and down) and the failure time is about 0.5 sec later using the Failure Potential correlation.

To investigate the sensitivity of the predicted failure node to wide variations in the correlations parameters of the Failure Potential, a 2-channel model was constructed and run using MELT-III with a 50¢/sec reactivity insertion. Two of the parameters (a and c) were varied over a 2σ range. The parameter d was not varied since the experimental pins were all of nominal FFTF smear density. The parameter b was not varied since the level of significance, from the T test, was found to be small. A detailed statistical analysis of the Failure Potential correlation is given in Reference Q001.461-3. The results are presented in Table Q001.461-2. The failure node is noted to change a maximum of only one axial level from the value obtained when using the "best" values for the parameters.

As shown in Table Q001.461-1 the Failure Potential correlation predicts a somewhat later failure time than the Damage Parameter correlation but the same relative pin failure sequence and axial failure location is predicted by both correlations. The later failure time predicted by the Failure Potential Criterion is in qualitative agreement with the later failure time predicted in the SAS3A comparisons with the Damage Parameter correlation, as shown in Tables 6-2 and 6-6 of Ref. 15, PSAR Section 1.6. The axial failure locations predicted by SAS3A, the Damage Parameter correlation and the Failure Potential correlation are in very good agreement.

*Note that Appendix F has been withdrawn. The text, upon which the question was based, can now be found in Section 6 of Reference 15, PSAR Section 1.6.

60

Amend. 60
Feb. 1981

References

- Q001.461-1 A. E. Walter, et al., "MELT-III, A Neutronics, Thermal-Hydraulics Computer Program for Fast Reactor Safety Analysis," Hanford Engineering Development Laboratory, December 1974, (HEDL-TME 74-47).
- Q001.461-2 D. S. Dutt, et al., "SIEX-A Correlated Code for the Prediction of Liquid Metal Fast Breeder Reactor Fuel Thermal Performance," Hanford Engineering Development Laboratory, December 1974, (HEDL-TME 74-55).
- Q001.461-3 P. Wilburn, et. al., "Sensitivity of LMFBR Hypothetical Accident Analysis to Variations in an Emperical Fuel Pin Failure Criterion," to be presented at International Meeting on Fast Reactor Safety in Chicago, October 6-8, 1976.

Table Q001.461-1.

FUEL PIN CLADDING FAILURE TIME AND NODE FOR 20-CHANNEL BOC-4 FFTF CORE

<u>CHANNEL</u>	<u>DAMAGE PARAMETER</u>		<u>FAILURE POTENTIAL</u>	
	<u>FAILURE TIME</u>	<u>FAILURE* NODE</u>	<u>FAILURE TIME</u>	<u>FAILURE* TIME</u>
1	2,6380	17	3,1240	16
3	2,7000	16	3,1485	17
4	2,7075	16	3,2225	16

* NOTE: 18 axial nodes in core (2" each) numbered 1 to 18 from bottom to top.

Table Q001.461-2

EFFECT OF PARAMETRIC VARIATION ON LOCATION OF FUEL PIN CLADDING FAILURE
 (FOR FAILURE POTENTIAL PARAMETERS a AND c **)

	a = 288	a = 440	a = 671
c = 1.58	NODE = 16*	NODE = 16	NODE = 16
c = 0.65	NODE = 16	NODE = 16	NODE = 16
c = 0.	NODE = 16	NODE = 16	NODE = 15

* NOTE: 18 axial nodes in core (2" each)
 numbered 1 to 18 from bottom to top.

** NOTE: See Appendix A

APPENDIX A to Q001.461

EMPIRICAL CORRELATION OF TOP FUEL PIN FAILURE THRESHOLDS

I.0 INTRODUCTION

The transient overpower (TOP) experimental program for irradiated fuel pins has conducted tests of EBR-II irradiated fuel pins in the TREAT facility.⁽¹⁾ These pins consist of 13.5 inch long fuel columns, and possess fuel microstructures with relatively little axial variation. The TREAT tests have been viewed as tests of differing portions of an FTR pin. Pending development of a mechanistic fuel pin transient code qualified against the TREAT tests, and use thereof to define fuel pin cladding failure thresholds for an FTR fuel pin, attempts have been made to develop empirical correlations of the fuel pin cladding failure thresholds as revealed in the TREAT tests. The Damage Parameter (DP) correlation,⁽²⁾ currently programmed into the MELT-III code,⁽³⁾ was such an empirical correlation. The DP correlation, however, was found to not satisfactorily correlate failure thresholds of low power microstructure fuel pins.

2.0 REVISED CORRELATION

The correlation has been substantially revised and the revised version now satisfactorily correlates the original five data points plus an additional seven data points, including two low power microstructure tests. The revised correlation, hereafter called the "Failure Potential" (FP) correlation to distinguish it from the DP, is defined as follows:

$$FP = a \left(\frac{\Delta H}{Y} \right)_{\text{time avg}} t^b e^{cs} D^d$$

where:

FP = Failure Potential

ΔH = Enthalpy (energy content per unit mass) upset of fuel in the noncolumnar grain region over that at steady-state operation, J/g

γ = Cladding burst strength as defined by FCTT tests⁽⁴⁾ on unirradiated 20% CW 316SS heated at a rate of 200F°/sec, psi

t = Time into transient, seconds

s = Variable representing fuel structural features

$$= 0.9 nV_f - g$$

g = Fuel-cladding gap at steady state operation, mils

V_f = Volume fraction of noncolumnar grain region of fuel

D = Available void volume, expressed as fraction of volume inside cladding not occupied by 100% dense fuel, relative to that for a nominal FFTF fuel pin

$$= (1. - Pd)/0.15$$

Pd = Planar smear density = $Td (R_f/R_{ci})^2$

Td = Pellet density, fraction of theoretical

Rf = As-fabricated outer fuel pellet radius

Rci = As-fabricated inner cladding radius

a,b,c,d, = Adjustable parameters

$$= 440.0, 0.09, 0.65, - 1.27, \text{ respectively.}$$

The values of the adjustable parameters were determined using linear regression techniques. The defining equation was solved for the variable $(\frac{\Delta H}{V})$ time average which was then used as the dependent variable. The equation was linearized by taking the logarithm of both sides.

As with the DP, the value of the FP is calculated for several axial locations along the pin as the transient proceeds. Failure is presumed at the time and location of the first axial location to achieve an FP value of 1.0.

3.0 DISCUSSION OF CORRELATION

The form of the FP correlation is similar in some respects yet substantially different from the DP correlation. Philosophically, the FP correlation seems the most satisfying of the two because it is the simplest. The concepts of enthalpy thresholds and of enthalpy "decay" used in the DP correlation were eliminated in the FP correlation. The best (tightest fit) correlation was obtained with the 200F°/sec unirradiated cladding strength data. Data for strength as a function of fluence did not extend to a high enough fluence to avoid extrapolation.

The available void volume term was introduced as an aide to correlating test results. Some test pins differed significantly in this regard from nominal FFTF specifications. Inasmuch as the available void volume represents the ultimate capability of the fuel pin to accommodate fission gas pressure and fuel expansions of any sort without cladding deformation, it seems reasonable to include it as a variable in the correlation. This term operates only for fuel pins that deviate from nominal FFTF specifications.

The microstructural variable, s , was defined in the course of revising the correlation. Originally, the V_f and g variables were used as independent variables in the form:

$$V_f^{c_1} e^{-cg}$$

It was noted the values of c_1 and c bore substantially the same ratio to each other regardless of circumstances; that is, one appeared to be a fixed multiple of the other, implying the two variables were not independent. The two were collapsed into a single independent variable "s" as follows:

$$\ln(V_f^{c_1} e^{-cg}) = c_1 \ln V_f - cg \quad (1)$$

Noting that $c_1 = 0.9 c$ equation (1) becomes:

$$c_1 \ln V_f - cg = c (0.91 \ln V_f - g) \quad (2)$$

Defining "s" as being equal to the expression in the parenthesis in equation (2) the original expression becomes:

$$V_f^{c_1} e^{-cg} = e^{cs}$$

The data base for the FP correlation is identified in Table 1, which shows steady state characterization for the fuel pins tested in the data base. Test HUT 3-3A was included in the data base as it is regarded as an incipient failure even though no failure was actually observed in the test. The values of the FP calculations for the data base and for other selected tests are shown in Figure 1 as a function of steady-state power.

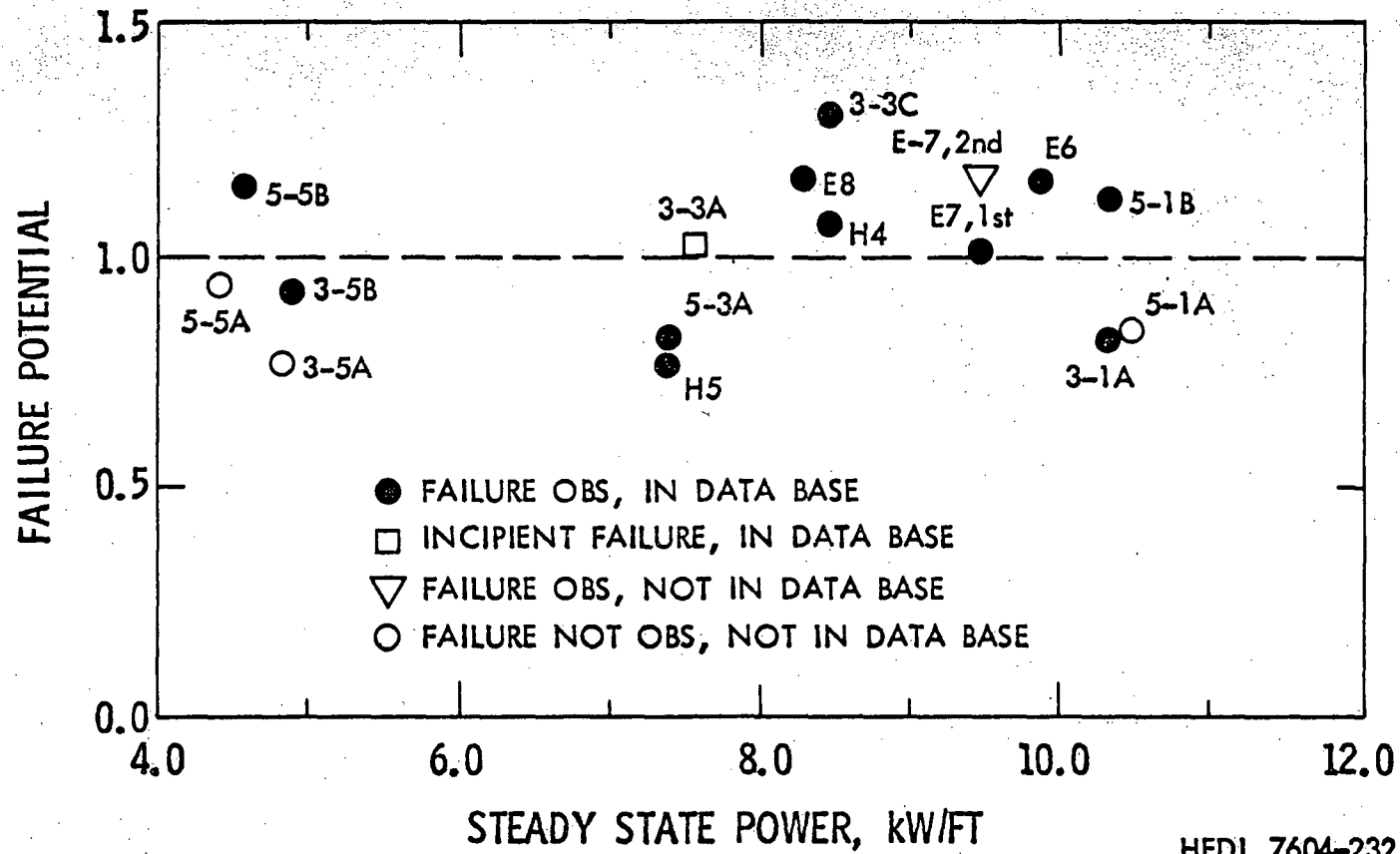
The value of FP is correlated to a standard deviation of $\pm 16\%$ for the twelve data points. As another expression of the precision of the correlation, the observed and predicted fuel pin failure times for the eleven data points, excluding HUT 3-3A, are tabulated in Table 2. As can be seen, the 3\$/sec ramp rate fuel pin failure times were predicted with average error of ~ 34 msec, and the 50¢/sec ramp rate test failure times were predicted with an average error of ~ 150 msec.

Additional development work on the correlation is planned to improve the statistical characteristics, and to improve the time weighting procedure for transient characterization.

4.0 APPLICATION TO TREAT TOP TESTS

The failure time for test HOP 3-3C was taken as 0.8 second into the transient as was used in the DP correlation development. Subsequently, the experimenters have concluded that failure occurred at 1.0 second into the transient. However, on careful examination of the test thermocouple traces, which are used to establish failure times, it is believed that there is basis, though not conclusive, for considering failure to have occurred at 0.8 second into the transient.

0001.461A-5



HEDL 7604-232

FIGURE 1. Failure Potential vs Local SS Pin Power

Amend. 25
Aug. 1976

TABLE I
DATA BASE STEADY STATE CHARACTERIZATION FOR FAILURE POTENTIAL CORRELATION

<u>Test</u>	<u>Midplane Power kW/ft</u>	<u>Exposure Mwd/MTM</u>	<u>Vol Frac⁽¹⁾ Non-Col gr</u>	<u>Steady-State⁽¹⁾ Fuel-Cladding Gap, mils</u>	<u>S</u>	<u>Available Void Volume</u>
HUT 5-5B	5.14	44800	1.0	0.74	-0.74	1.075
5-3A	8.38	49900	0.873	0.21	-0.332	0.998
5-1B	11.66	47000	0.580	0.0	-0.49	1.023
3-5B	5.51	48100	1.0	0.63	-0.63	1.081
HOP 3-3C	8.44	29800	0.942	0.35	-0.404	0.695
HUT 3-3A	8.56	51200	0.879	0.15	-0.266	0.991
3-1A	11.67	47000	0.576	0.0	-0.496	1.025
H4	10.11	40800	0.665	0.04	-0.407	1.029
H5	8.79	31100	0.903	0.45	-0.542	0.707
E6	10.94	44000	0.682	0.05	-0.394	1.011
E7	9.72	39500	0.682	0.02	-0.366	1.039
E8	8.50	50500	0.856	0.09	-0.250	0.469

1. As Calculated by the SIEX Code Using Time Averaged Irradiation History at Location of Failure.

0001.461A-6

Amend. 25
Aug. 1976

TABLE 2

COMPARISON OF OBSERVED AND PREDICTED FAILURE TIMES

Test	Ramp Rate	Failure Times ⁽¹⁾		Error (Obs-Pred) Seconds	% ⁽²⁾ Deviation
		Observed Seconds	Pred Seconds		
HUT 3-5B	3\$/sec	0.80	0.82	-0.020	-2.5
HOP 3-3C	3\$/sec	0.80	0.70	0.100	12.5
HUT 3-1A	3\$/sec	0.695	0.73	-0.035	-5.0
E6	3\$/sec	0.585	0.565	0.020	3.4
HUT 5-5B	50¢/sec	4.8	4.63	0.170	+4.0
HUT 5-3A	50¢/sec	3.20	3.40	-0.200	-6.2
HUT 5-1B	50¢/sec	3.68	3.56	0.120	+3.3
H5	50¢/sec	1.901	2.10	-0.200	-10.8
H4	50¢/sec	0.936	0.84	0.096	+10.3
E8	3\$/sec	0.5	0.47	0.03	6.0
E7 (1st)	3\$/sec	0.4	0.4	~0.0	0.0
(2nd)	3\$/sec	0.45	0.4	0.05	11.1

1. Time into spike transient
2. Relative to observed time of failure

The FP for the E7 and E8 tests was calculated for one of the hot peripheral pins in the seven pin bundle. These pins were subject to a marked asymmetric power distribution. The FP calculation was based on the rod average enthalpy, and on the hottest cladding section around the pin. Significant circumferential cladding temperature variations also existed for the central irradiated pins in tests H4, H5, and E6. The hottest cladding temperature was used in the FP calculation for those tests also.

Application of the correlation to the TREAT tests was complicated because of use of the time averaged value of the transient sensitive parameter. The steady-state enthalpy was frequently reached significantly earlier than the start of the spike transient, resulting in two fundamentally differing portions of the transient. The portion prior to start of the spike transient tended to "dilute" the spike portion of the transient and artificially depressed the FP. To avoid this problem, the correlation was applied separately to the two parts of the transient, values of the FP for the two parts being added to obtain the overall FP for the test.

FP values are shown in Figure 1 for several tests in which no failure occurred. The time average feature was felt to yield artificial results beyond achievement of the most severe conditions (maximum fuel enthalpy and cladding temperature) since the FP continues to increase almost indefinitely despite declining severity of conditions. Some increase in potential for failure may be reasonable after reaching peak conditions, since failure was attained in at least one test (HUT 3-5B) after that time. However, in the absence of any other rational criteria, the calculation is disregarded in nonfailure tests after peak conditions have been reached.

5.0 DETERMINATION OF EXPERIMENTAL FAILURE TIME AND LOCATION

Failure time is established in the ANL Mark II loop tests and the HEDL static capsule (TOP) tests with considerably more certainty than is the failure location. Failure time is established in the former tests

by pressure spikes, and in the absence thereof, by flowmeter deviation from the norm.⁽⁵⁾ These signals are normally not ambiguous. The failure time indications are felt to be accurate without corrections since both types of indications basically entail a pressure wave propagation, and should involve less than 1 msec delay. See Reference 1 or 5 for further details on establishment of ANL test failure times.

Time of deviation of thermocouple traces from the normal trend was the criteria for failure time in the HEDL static capsule tests. In most static capsule tests, the indication was an abrupt, almost infinite rate of temperature rise to failure of the thermocouple.⁽¹⁾ The earliest time of trend deviation was taken as the time of failure. Thermocouple time lag was not felt to be applicable since time lag is composed largely of heat transfer resistance and thermocouple heat capacity effects, and is useful primarily to establish temperature accuracy. The time lag should not affect the time of initial deviation; only time of material transport (i.e., travel time of molten fuel to the thermocouple) should be relevant. No attempt has been made to estimate the delay in failure time indication that would derive from such material transport; such delay is felt to be insignificant.

The location of failure has been clearly established from post-test examination for only three tests, HOP 3-3C (axial midplane), E6 (10 - 10.5 inches above the bottom of the fuel column), and H5 (~11 inches above the fuel column bottom). The experimenters have estimated a failure location in the top inch of one of the three highest powered peripheral pins in the E7 test. This estimate was based on the differences in failure time indications of the upper and lower flowmeters, and is regarded as tentative only.

Other than for test HOP 3-3C, the experimenters have concluded that in the HEDL static capsule tests, all test pins failed in the top half, based primarily on the time sequence of thermocouple failure.

For use in the FP correlation, the value of FP at the confirmed location of failure was used for tests HOP 3-3C, H5 and E6. For tests H4, E7, and E8, the highest value of FP anywhere along the pin was used. These occurred at 11.25, 8.1, and 8.1 inches above the bottom of the fuel column respectively.

The value of the FP computed at the highest point of the flat, high power zone in the central portion of the pin (~10 inches above the bottom of the fuel column) was used for all of the HUT tests. The value of the FP was also calculated at the axial midplane for these tests. The FP at axial midplane was found to be nearly the same for the HUT 3-5A, 5-5A, and 3-3A tests, and was significantly lower than the highest high power location for the balance of the tests. A more extensive investigation of FP variation with axial location is planned for the HEDL tests.

6.0 DETERMINATION OF FAILURE MODE

The failure mode has been identified for two of the fuel pins tested in the data base, ANL test H5 and HEDL test HOP 3-3C. The experimenters have concluded that the irradiated fuel pin tested in test H5 failed due to fuel-cladding mechanical interaction. The basis for this conclusion is documented in Reference 6.

The following summarizes the experimenter's conclusions as to mode of failure for the HOP 3-3C test, and the basis for the conclusions.

From examinations performed on the HOP 3-3C fuel pin sections and cladding failure area, it was concluded that the failure mechanisms and mode for this fuel pin were similar to fuel pin failures experienced in previous tests. The internal loading mechanism was believed to be differential thermal expansion combined with a threshold type loading caused by the action of fission gas both within the grains and in the grain boundaries. The latter is postulated to be the major contributor to the threshold type loading where the gas pressure in the grain boundaries exceeds the strength of the grain boundaries and a large increase in overall fuel volume occurs, thereby loading the cladding beyond its

strength capabilities.

Examination of the cladding failure area revealed that the probable mode of failure was intergranular. While the initial failure occurred near the fuel column axial midplane, identification of the original cladding breach was not possible because of extensive melting caused by the escape of molten fuel and NaK coolant voiding. Also, multiple cladding breaches in the same general failure location were possible because of the many intergranular fracture paths available and the loading character of fuel cladding mechanical interaction. Once the hot fission gas and molten fuel had been vented from the pin, it was possible for any subsequent fractures to remain cooled by the NaK. Two examples of this exist, one in the upper half of the pin which was partially destroyed by external contact of molten fuel, and the other which separated the pin into two. Both exhibited intergranular fracture characteristics.

The orientation of one of the unmelted fractures in PNL 17-34 demonstrates a strong axial stress from the fuel-cladding mechanical interaction at that location. Abundant cavitation and other microstructural features immediately beneath the fracture surface are consistent with a temperature of 1700 to 2000°F for this particular fracture. Post-transient calculations indicated that the cladding temperature did not exceed 1400°F. Apparently NaK voiding produced by the first cladding breach elevated the cladding temperature in this region prior to the fracture.

7.0 TOP TEST THERMAL TRANSIENT CALCULATION FOR FAILURE POTENTIAL CORRELATION

The test fuel pin thermal transient histories were calculated with particular effort to ensure consistency with the procedures used in the MELT-III code. Steady state characterizations were performed with the documented version of the SIEX code,⁽⁷⁾ also used in MELT-III. No attempts were made to force solutions to conform to sibling pin PIE results. The characterizations used as-fabricated parameters and time-averaged EBR-II irradiation histories supplied by the HIST code.

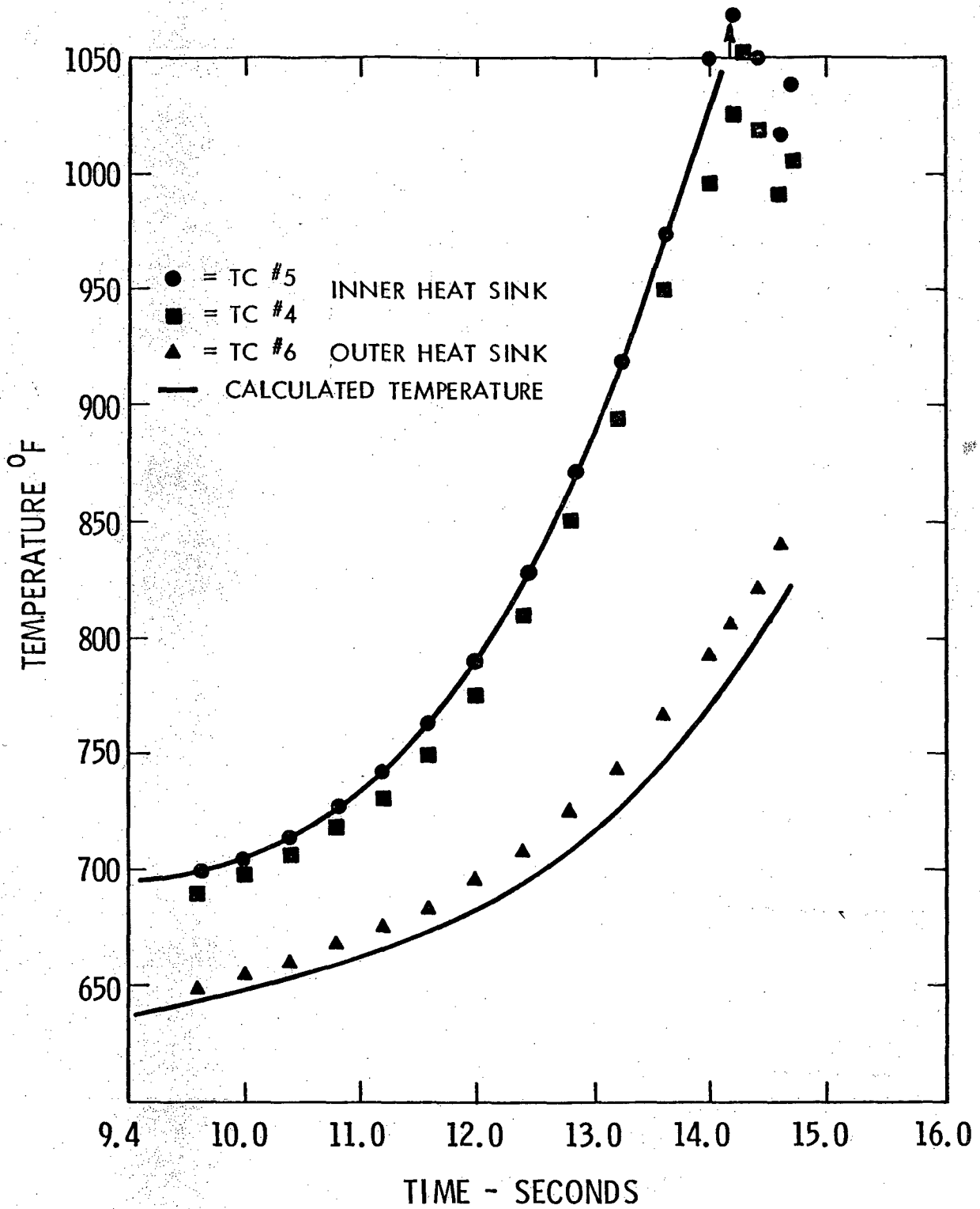
Thermal transients for the HEDL static capsule tests were calculated with the ARGUS⁽⁸⁾ subroutine used for heat transfer calculations in the PECT-2T code. A free standing version was used with the HEDL transient gap conduction model as applied in COBRA-3M and MELT-III. Gap closure was computed with volume-average-temperature-based differential thermal expansion applied to the cold gap as predicted by the SIEX correlated model.

The power coupling (relation between TREAT facility power and fuel pin power) was treated as an adjustable parameter. The power coupling was adjusted to obtain a good match to axial midplane inner heat sink thermocouple traces in the spike transient. Generally good, though not perfect, matches were obtained. Examples are shown in Figure 2 (HUT 5-5B) and Figure 3 (HUT 3-5B). The match for HUT 3-5B was the poorest obtained; the match for HUT 5-5B was typical. The axial melt fractions were then compared with the experimentally determined melt fractions where the latter were available. Excellent agreement was obtained in all cases, as is shown in Table 3 along with other results of the calculations.

Calculations were performed for the ANL tests with the HEDL version of the COBRA-3M code. Salient features of the code have been described in References 2 and 9. Two changes in procedure were made: from that described in Reference 2:

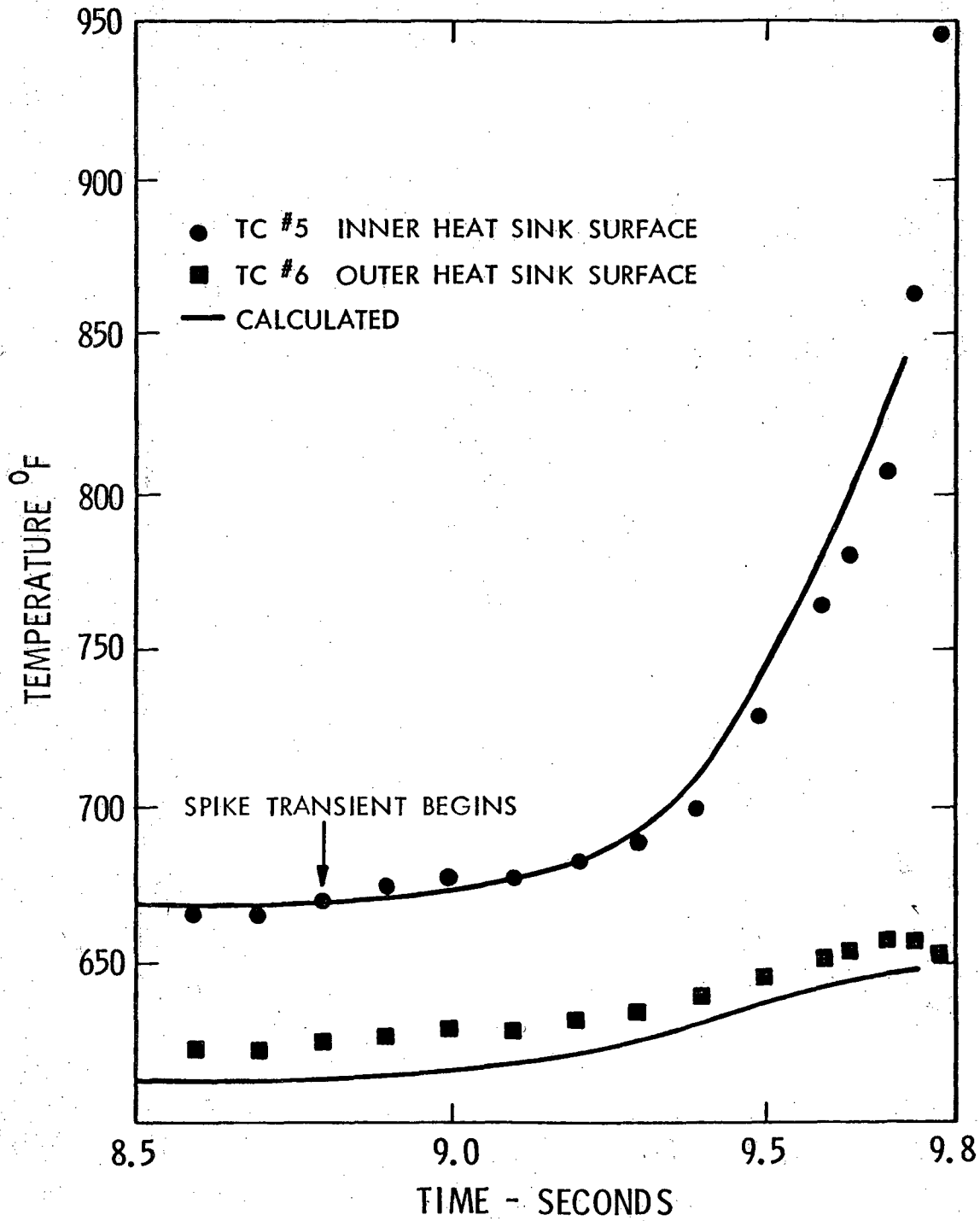
The code was altered to allow axial variations in fuel restructuring. The radial nodes were defined on an equal radial increment basis rather than on an equal areal increment basis.

The latter change was made upon indications that there were significant discrepancies between ARGUS and COBRA calculations (500-600F°) for 3\$/sec tests. The ARGUS calculations were assumed to be the most accurate as a finer radial node grid (20 vs 9) had been used than was possible in the COBRA calculations. Upon making the foregoing changes in COBRA radial node definition, agreement was again obtained (within 50 to 100 F°). Good agreement between the two codes was found without the above change for the 50¢/sec ANL tests.



HEDL 7605-76.1

FIGURE 2. Comparison of Calculated and Observed Heat Sink Temperature at Axial Midplane for Test HUT 5-5B.



HEDL 7605-73.2

FIGURE 3. Comparison of Calculated and Observed Heat Sink Temperatures at Axial Midplane for Test HUT 3-5B.

TABLE 3

TRANSIENT OVERPOWER TEST RESULTS

Test	Steady State Characterization			Transient Characterization			
	Midplane Power kW/ft	Exposure MWd/MTM	Ramp Rate	Pin Failed	Cladding Midwall ⁽¹⁾ Temp °F (Calculated)	Axial Melt Area % Calc	Midplane Fuel Fraction % Obs
HUT 5-5A	5.01	44000	50¢/sec	No	1477	30	36
5-5B ⁽³⁾	5.14	44800	50¢/sec	Yes	1714	49(2)	NA
5-3A ⁽³⁾	8.38	49900	50¢/sec	Yes	1514	47(2)	NA
5-1A	11.85	47700	50¢/sec	No	1548	57	55
5-1B ⁽³⁾	11.66	47000	50¢/sec	Yes	1682	65(2)	NA
3-5A	5.45	47600	3\$/sec	No	1573	0	0
3-5B ⁽³⁾	5.51	48100	3\$/sec	Yes	1634	61	65
HOP 3-3C ⁽³⁾	8.44	29800	3\$/sec	Yes	1393	34	40
HUT 3-3A ⁽³⁾	8.56	51200	3\$/sec	No	1498	53	50
3-1A ⁽³⁾	11.67	47000	3\$/sec	Yes	1525	73(2)	NA
H4 ⁽³⁾	10.11	40800	50¢/sec	Yes	1393	30(2)	NA
H5 ⁽³⁾	8.79	31100	50¢/sec	Yes	1378	25	25-30
E6 ⁽³⁾	10.94	44000	3\$/sec	Yes	1703	78(2)	NA

1. Quoted for failure location if known; otherwise, at 80% of fuel column height.

2. Quoted for observed time of pin failure.

3. Included in FP data base.

Q001.461A-15

Amend. 25
Aug. 1976

Results for the ANL tests have also been tabulated in Table 3. As can be seen, good agreement on areal melt fraction was obtained with experimental observations for the one ANL test (H5) for which a comparison was possible.

REFERENCES

1. R. E. Baars (compiler), Base Technology Support Document--Prefailure Transient Behavior and Failure Threshold Status Report: January, 1975 HEDL-TME 75-47, November, 1975.
2. J. H. Scott, et al, Microstructural Dependence of Failure Threshold in Mixed Oxide LMFBR Fuel Pins, HEDL-TME 75-9, October, 1975.
3. Alan Waltar, et al, MELT-III A Neutronics, Thermal-Hydraulics Computer Program for Fast Reactor Safety Analysis, HEDL-TME 74-47, December, 1974.
4. C. W. Hunter, et al, Mechanical Properties During Simulated Overpower Transients of Fast Reactor Cladding Irradiated from 700-1000°F, HEDL-TME 75-28, June, 1975.
5. L. W. Deitrich, et al, Summary and Evaluation--Fuel Dynamics Transient Overpower Experiments, ANL/RAS 74-8, June, 1974.
6. A. E. Wright, et al, Transient Overpower Test H5 on FFTF-Type "Intermediate Power" Fuel, ANL/RAS 75-27, June, 1975.
7. D. S. Dutt and R. B. Baker, SIEX A Correlated Code for the Prediction of Liquid Metal Fast Breeder Reactor (LMFBR) Fuel Thermal Performance, HEDL-TME 74-55, June, 1975.
8. D. F. Shoerberle, et al, A Method of Calculating Transient Temperatures in a Milliregion, Assymetric, Cylindrical, Configuration, the ARGUS Program, 1089/RE248, Written in FORTRAN-II, ANL-6654, November, 1963.
9. W. W. Marr, COBRA-3M: A Digital Computer Code for Analyzing Thermal-Hydraulic Behavior in Pin Bundles, ANL-8131, March, 1975.

Question 001.462 (F6.2.4)

In Sections F6.2.4.4.2.4 and F6.2.4.4.2.5 midplane failure and zero fuel axial expansion reactivity are considered as independent parametric variations on the EOE TOP base case. If failures occur at the midplane there is reason to believe that they will be caused by fuel pellet clad interaction as demonstrated when the strain failure criterion is used in Section F6.2.4.3.2.3. Thus midplane failure may be accompanied by zero axial expansion. Re-evaluate F6.2.4.4.2.4 based on this assumption.

Response:

The CRBRP Project has consolidated all considerations given Hypothetical Core Disruptive Accidents into report CRBRP-3 (References 10a and 10b, PSAR Section 1.6) and its associated references; consequently, PSAR Appendices D and F have been withdrawn in Amendments 24 and 60 respectively. The response to this question is now found in Sections 4.4.2.1, 4.4.2.2 and 4.3.2.2 of Reference 10a, PSAR Section 1.6.

24

60

Question 001.463 (F6.2.4)

Correct the several typographical errors in section F6.2.4.4.3.1.

Response

This question requests clarification of information which is no longer a part of the current documentation. The Project has since consolidated all considerations given Hypothetical Core Disruptive Accidents into report CRBRP-3 (References 10a and 10b, PSAR Section 1.6) and its associated references; consequently, PSAR Appendices D and F have been withdrawn in Amendments 24 and 60 respectively.

60

Question 001.464 (F6.2.5)

Justify leaving in the control assemblies with sodium in for the disrupted core calculation described in the last paragraph of section F6.2.5.2.4.

Response:*

60

Removing the control assemblies completely, i.e., filling the space with molten fuel would lead to very little difference in the computed critical height of the pool. To totally homogenize the core region with molten fuel, that is, to remove the sodium from the control assemblies and substitute fuel instead, (thus considering the effect of melting through the control sub-assembly walls) might lower the critical height slightly (probably 1-2 cm). However, the fraction of the total fuel inventory required to achieve criticality would change very little.

60

*Note that Appendix F has been withdrawn. The text, upon which the question was based, can now be found in Section 4 of Reference 10a, PSAR Section 1.6.

60

Question 001.465 (F6.2.3.2.1)

The best-estimate base case fuel-pin failure criterion is the Burst Pressure Criterion. It is assumed appropriate for predicting pin-failure threshold and location. Provide a justification for this model based on transient experiments. Include in the discussion the appropriateness of this criterion for fresh fuel. Summarize, for the transient tests, the failure location, if known, and the failure mode (primary vs. secondary loading).

Response:*

160

The failure of CRBRP fuel pins during overpower excursions is a complex interaction of several physical processes. For irradiated pins, the primary processes are considered to be:

- o differential thermal expansion of fuel-cladding
- o fuel volume increase at solid-liquid phase change
- o transient fission gas (FG) induced fuel swelling
- o entrapment of released FG by molten fuel extrusion into fuel cracks and fuel-clad gap.

The selection of the burst pressure criteria for the cladding reflects a judgement that the ultimate cladding loading is of the primary type. That is, small volume increases due to cladding strain will not significantly reduce the pressure loading produced by the heated, constrained gas bubbles. The failure criterion is based upon the mechanisms of differential thermal expansion and fuel volumetric phase change producing the internal pin conditions of gas entrapment and volume constraint leading to primary cladding loading.

The experimental justification for the burst pressure failure criteria of irradiated fuel lies in evidence supporting the individual physical processes, listed above, and engineering judgements on integral fuel failure tests in TREAT. The appropriate physical process and its experimental support are the following:

1. The transient release of FG during fuel thermal upset is supported by differential plenum gas content measurements following TREAT irradiations (Reference Q001.465-1), detailed pre-and-post transient fuel retained FG distributions (Reference Q001.465-2), and out-of-pile heating experiments which measure real time gas release (Reference Q001.465-3).
2. The ability of released FG to produce hydraulic forces in a molten fuel region was demonstrated by the extended motion of fuel materials and prediction of cladding strain using a FG pressure model (C3C) in the GE TREAT series III and V experiments (References Q001.465-4, 5).

*Note that Appendix F has been withdrawn. The text, upon which the question was based, can now be found in Section 6 of Reference 15, PSAR Section 1.6.

60

3. The capability of transient heated oxide fuel pins to entrap molten material and fission gas, if present, is supported by Argonne experiments which led to crucible (unclad fuel) and gas bottle (clad) formations (References Q001.465-6, 7).

The sum of the above information forms an experimental basis for the irradiated fuel pin failure model employed in Reference 15, PSAR Section 1.6.

In fresh fuel pins, the attainment of primary loadings by the above discussed mechanisms is less probable due to the much smaller gas content (FG and manufactured porosity). In the CRBRP, after each refueling, the fresh fuel pins will have a minimum burnup ~1-5 full power days prior to attainment of full power reactor operation. (Substantially longer for initial startup.) There is no a priori reason to not apply the model as long as the proper amount of gas content is represented. Indeed in the ANL experiments on zero burnup material (Reference Q001.465-7), the presence of some gas in fresh fuel, and the TREAT C4A and C4B behavior (Reference Q001.465-8) indicate that a primary failure loading is possible. Also, in fresh or zero burnup fuel pins, the burst pressure model will not result in substantial loading until local straining of the cladding is already in progress. Thus, for unterminated, reasonably rapid energy additions, a model of this type can predict the time of failure well (Reference Q001.465-9) and, with proper interpretation, be usefully employed.

The calculation in Reference 15, PSAR Section 1.6 did not concentrate on the failure criteria for fresh fuel since appropriate strain criteria (sodium boiling did not occur) would indicate an increase in the fuel pin capability to withstand melting and thus a later failure time. The application of a strain criterion would thus increase confidence in Reference 15, PSAR Section 1.6 best estimate conclusion that the prior failure of irradiated fuel and associated fuel motion phenomena would dominate the reactor response.

The LMFBR Base Program state-of-the-art in fuel pin integral response to overpower transients and fuel pin failure threshold was recently published by the HEDL staff (Reference Q001.465-10). Two of the HEDL conclusions with regard to failure mechanisms are noteworthy:

- o (p. 56) "It can be concluded that differential thermal expansion is potentially a contributor to any failure, but that in most cases it is not possible to clearly identify differential expansion as the principal failure mechanism."
- o (p. 92) "Tests H0P3-3C and H5 were conducted on sibling PNL 17 fuel pins with intermediate power-level fuel microstructure, but the transient rates were 3\$/sec and 50¢/sec, respectively. Although there was a large difference in transient rate, similarity in cladding temperatures at failure indicates that the loading must have been of the primary type."

Finally, the HEDL proposed empirical damage correlation incorporates the basis of a burst pressure criterion in that the fuel pin damage is directly proportional to the ratio of thermal upset in the gas bearing fuel region (related to thermal expansion and FG release) to clad mechanical strength.

The burst pressure failure criterion employed in Ref. 15, PSAR Section 1.6, is thus seen to have experimental justification in its elemental parts and integral support within the base technology assessment of fuel pin response to over-power transients. |60

Table Q001.465-1 provides a summary of available failure location and mode information abstracted from References Q001.465-4, 5, 8, 10, 11.

References:

- Q001.465-1 G.E. Culley, et al., "Response of an EBR-II Irradiated Mixed Oxide Fuel Pin to an Overpower Transient in TREAT," Proc. Fast Reactor Fuel Element Technology (New Orleans, La.) April 1971, pp. 657-678.
- Q001.465-2 D. Stahl and T. J. Patrician, "Fission-Gas Behavior During a Mild Overpower Transient," Argonne National Laboratory, February 1974, (ANL 8069).
- Q001.465-3 E.T. Weber, O.D. Slagle, C.A.Hinman, "Laboratory Studies on Melting and Gas Release Behavior of Irradiated Fuels," Proc. Fast Reactor Safety Meeting, April 1974, (CONF-740401) pp. 641-63.
- Q001.465-4 J.E. Hanson and J.H. Field, "Experimental Studies of Transient Effects in Fast Reactor Fuels, Series III, Pre-Irradiated Mixed Oxide (Pu_2-UO_2) Irradiated Final Report, Transient Irradiations," General Electric Co., July 1967, (GEAP-4469).
- Q001.465-5 T. Hikido and J.H. Field, "Molten Fuel Movement in Transient Overpower Tests of Irradiated Oxide Fuel," General Electric Co., September 1969, (GEAP-13543).
- Q001.465-6 "Reactor Development Physics Progress Report", Argonne National Laboratory, February, 1974 (ANL-ROP-2b), p. 5.4.
- Q001.465-7 B.J. Wrona, "Transient Response of Clad UO_2 ," Trans. Am., Nucl. Soc., 22, 420 (November, 1975).
- Q001.465-8 G.R. Thomas and J.H. Field, "Transient Overpower Irradiation of Axially Restrained, Zero Burnup Fast Reactor Fuel Specimens", General Electric Co., September 1969, (GEAP-13562).
- Q001.465-9 R.G. Stuart and G.R.Thomas, "Effects on Fission Gas on Transient Overpower Fuel Rod Failure," Trans. Am. Nucl. Soc. 13, 654. (1970).
- Q001.465-10 R.E. Baars, et al., "Base Technology FSAR Support Document - Prefailure Transient Behavior and Failure Threshold Status Report," Hanford Engineering Development Laboratory, January 1975, (HEDL-TRE 75-47), pp. 56 & 92.
- Q001.465-11 L.W. Dietrich, et al., "Summary and Evaluation - Fuel Dynamics Transient Overpower Experiments," Argonne National Laboratory, June 1974, (ANL/RAS 74-8).

Table Q001.465-1

FAILURE INFORMATION ON TREAT TRANSIENTS

<u>TREAT TESTS</u> <u>General Electric</u>	<u>No. of Pins</u>	<u>Fuel Burnup</u>	<u>Failure Location</u>	<u>Failure Mode</u>
C2C	1	Zero	Bottom	Cladding melt
C3C	1	65 GWD/T	Bottom end cap	Ejection through special needle assembly
C4A	1	Zero	Above midplane	Mechanical, believed secondary loading
C4B	1	Zero	Midplane downward for 5 in.	Mechanical, believed secondary loading
C5A	1	18 GWD/T	Upper section	Mechanical, believed primary loading
C5B	1	18 GWD/T	No clad failure	Ejection into upper annular blanket
<u>ANL</u>				
H2	1	Zero	Believed near top	Sodium boiling, probably clad melt
H4	7	1-4, 5 a/o 6-Zero	Central pin, Upper third of pin	Mechanical, possibly primary FG loading
H5	7	1-3.4 a/o 6-Zero	Central pin, Upper third of pin	Mechanical, possibly primary FG loading
E2	7	1-Zero 6-Hollow	Central, near top	Believed to be clad melting
F3	3	5.5 a/o	Unknown	Unknown, possible FG loading
E4	1	Zero	Near top	Unknown, believed clad melting
E6	7	1-4.5 a/o 6-Zero	Above midplane	Unknown, preboiling indicated, pin hole leak suspected
E7	7	4.5 a/o	Unknown, believed near top	Unknown, believed to be pin hole failure in edge pin

TREAT TESTS
ANL

No. of Ptns

Fuel Burnup

Failure Location

Failure Mode

E8

7

51 GWD/T

Near top

Believed primary loading

HEDL

HOP 3-3C

1

27 GWD/T

Near fuel mid-plane

Primary Loading

HUT 5-3A

1

45 GWD/T

Just below fuel midplane

Unknown

Question 001.466 (F3.2.1.2)

Provide a detailed description of the FØRE-II analysis of the initial phase of the continuous rod withdrawal accident.

Response:

The basic FØRE-II computer code structure is described in detail in Reference Q001.466-1. Modifications which have been incorporated in the ARD version of the code are discussed in the response to NRC Question 001.312.

Further definition of the initial reactor conditions, assumptions, conservatisms, and results for a Control Assembly Withdrawal at Power transient can be found in Chapter 15.0 (Sections 15.2 and 15.2.1.2). The difference in the analysis is the Ref. 15, PSAR Section 1.6 assumption that no shutdown system action is taken. Whereas, the curves shown by Figures 15.2.1.2-1 to -4, are "turned-around" after an appropriate control system delay, the reactor power and core temperatures would continue to monotonically increase for the HCDA initiation analysis. From the initial steady state operating condition at full power, a linear reactivity insertion of 2.4¢/sec. was input to the FØRE-II code, and the resultant temperatures calculated. Since reactor trip was precluded, the core flow and inlet temperature were maintained at their operating values. Boiling was conservatively assumed to occur when the hot channel maximum coolant temperature reached 1700°F. Since maximum temperatures occur at full flow, the actual saturation temperatures would be at least 100°F higher than this temperature. For fresh fuel pins with worst case temperatures as analyzed in Reference 15, PSAR Section 1.6, a solidus temperature of 5000°F was used for the incipience of melting (see Section 4.4.2.6.12). Typical results for the increase in maximum coolant and fuel temperatures for the hot rod in #6 fuel assembly are shown in Figure Q001.466-1.

|60

|60

|60

|60

Reference:

Q001.466-1: J. N. Fox, et al., "FØRE-II: A computational Program for the Analysis of Steady-State and Transient Reactor Performance", GEAP-5273, September 1966.

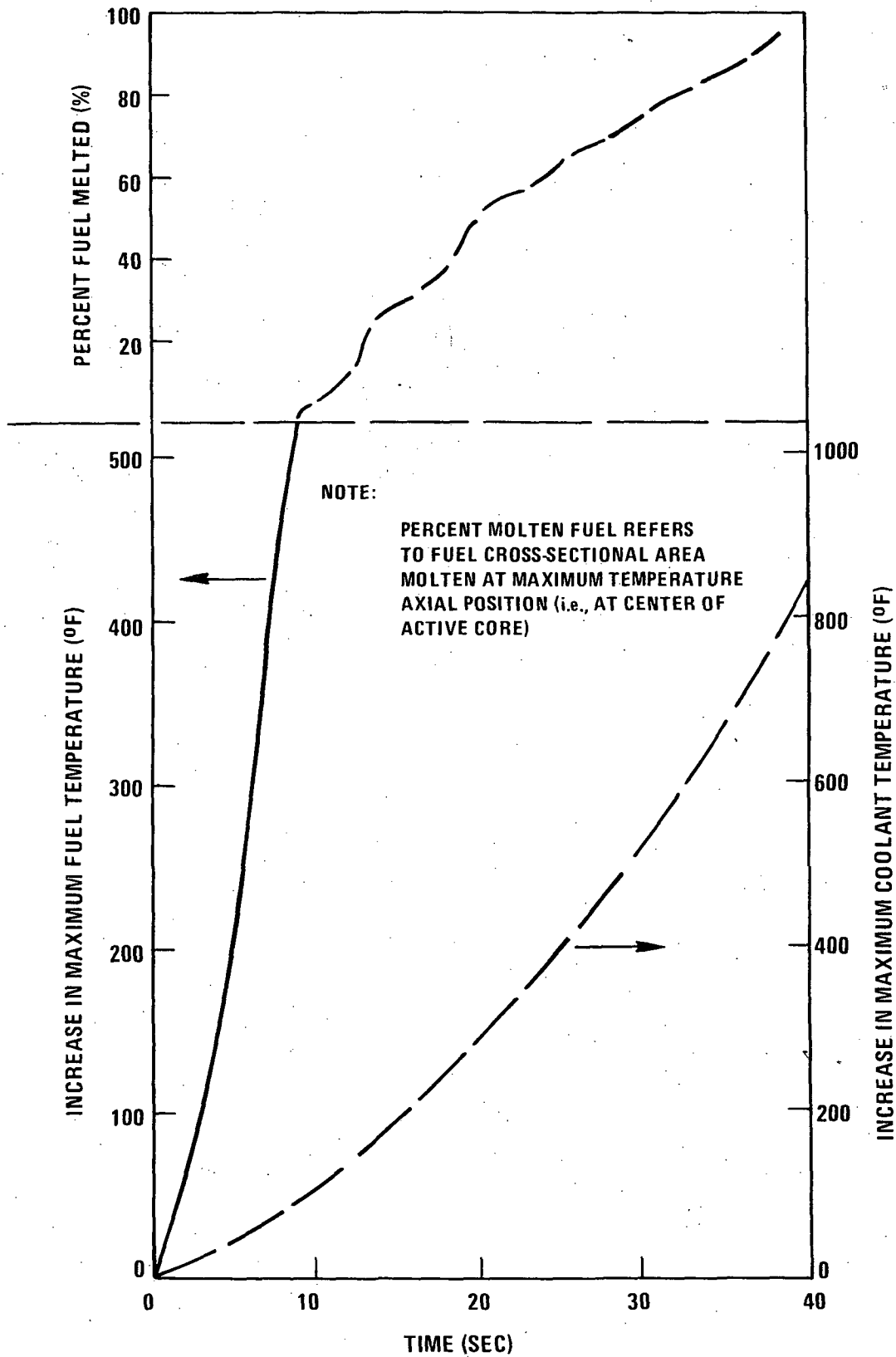


Figure Q001.466-1. Variation In F/A #6 Hot Channel Temperatures For Control Assembly Withdrawal At Power With Shutdown System Failure

7683-162

Amend. 60
 Feb. 1981

Q001.466-2

Question 001.467 (F3.2)

Identify the analysis on which Figure F3.2-3 is based.

Response:

This question requests clarification of information which is no longer a part of the current documentation. The Project has since consolidated all considerations given Hypothetical Core Disruptive Accidents into report CRBRP-3 (References 10a and 10b, PSAR Section 1.6) and its associated references; consequently, PSAR Appendices D and F have been withdrawn in Amendments 24 and 60 respectively.

Question 001.468 (F6.2.3.3)

Provide SAS-3A input decks for the four base cases (EOEC TOP & LOF, BOEC TOP & LOF).

Response:

The requested input decks have been supplied under separate cover.

Question 001.469 (F6.2.3.3)

There are uncertainties associated with the use of simplified models for steady-state fuel categorization such as SSFUEL in SAS3A which have an impact in the outcome of a TOP accident. Provide analysis and/or experimental evidence together with estimates of uncertainties by which basic fuels categorization such as those dealing with structuring isotherms, fission gas retention, gap closure, gap conductance, fuel and cladding swelling, and fuel cracking are judged.

Response:*

The uncertainties associated with the use of the simplified SSFUEL Model for steady state fuel categorization in the SAS Code analysis of TOP accidents have been estimated by comparison with fuel micro-structure calculations obtained with the experimentally correlated SIEX Code. In addition, comparisons of SAS3A results and results from SIEX, COBRA-3M and Damage Parameter analyses indicate the steady state uncertainties will not significantly affect the overall accident scenario or energetics.

Estimates of the uncertainties in the SAS3A steady state fuel categorization were obtained by comparing the steady state fuel and cladding temperatures, the fuel restructuring, the gap width, the gap conductance and the fission gas retention calculated by SAS3A using SSFUEL with corresponding values calculated by the experimentally correlated SIEX code. (Reference Q001.469-1). 160

The SIEX code has been specifically developed at the Hanford Engineering Development Laboratory (HEDL) to correlate existing data into a code which can be used to predict the fuel pin thermal performance in an LMFBR. Provided with the axial power profile, the burnup, the coolant flow rate per pin, and geometric data for an LMFBR pin, the SIEX code predicts the fuel restructuring, fuel temperatures, gap widths, gap conductances, generated fission gas, volume of fission gas released, and the plenum pressure.

To provide a basis for evaluation of the effects of the simplified models in SSFUEL on the outcome of a TOP accident, input data for the SIEX code was derived from the SAS3A code input deck listed in Table 4-1 of Ref.15, PSAR Section 1.6, for each of the 10 channels of the BOEC core and a SIEX prediction of the fuel pin characteristics was made for each channel. 60

A comparison of the SAS and SIEX calculated gap width, gap conductance, fuel pin temperatures and fuel microstructure for Channel 2 in the BOEC core are shown in Figures Q001.469-1 to Q001.469-4. Channel 2 represents 18 sub-assemblies of high power (8.6 KW/ft average) and high burnup (53,600 MWD/MT) irradiated pins. Channel 2 also has the smallest steady-state gap in the BOEC core, as shown in Figure 5-13 of Ref. 15, PSAR Section 1.6. 160

The primary reason for the differences between the SAS and SIEX calculated values of the parameters in Figure Q001.469-2 to 4 is the difference in gap conductance, shown in Figure Q001.469-1.

The gap conductance equation used in the SAS analysis of CRBR hypothetical transients is given in Pointer 31 in Section 4 of Ref. 15, PSAR Section 1.6. 160

*Note that Appendix F has been withdrawn. The text, upon which the question was based, can now be found in Sections 3, 4 and 5 of Reference 15, PSAR Section 1.6.

In the SIEX code, the gap conductance is computed by a rather complex relationship which has been documented in the description of this code. This correlation depends on the gap width, the jump distances and the thermal conductivity of the gaseous mixture in the gap, which in turn is dependent upon temperature as well as the composition of the mixture. The gap conductance in the SIEX code is completely determined from internal well-established correlations that have been built in. The correlations built into the SIEX code were determined from fuel melt and restructuring patterns obtained in a large number of experiments as is described in the SIEX document. In Figure Q001.469-1 the gap conductances in both cases include the radiation terms. The SAS profile shows the input "minimum" value at the ends of the pin.

Figure Q001.469-4 compares the SAS and SIEX predictions of gap width. As can be seen, SIEX predicts a smaller gap than SAS. The gap width is dependent on the expansion of the fuel and the expansion of the cladding due to temperature changes, and the swelling of the fuel and cladding due to burnup. SAS has a simple swelling correlation in which the percent swelling is a constant times the atomic percent burnup at the axial node for each type of fuel. SIEX also uses swelling in determination of the gap width, but it uses a built-in correlation.

A comparison of the SAS and SIEX code predictions for steady-state axial temperature profiles of the coolant, the inner surface of the cladding, the fuel outer surface, and the fuel inner radius in Channel 2, are given in Figure Q001.469-3 as a function of axial distance. The small difference noted in the coolant temperature profiles can be explained in the different method by which heat capacity is handled in the SAS and SIEX codes. SAS uses the heat capacity relationship directly as given in the tabular input. That is, in the iterative procedure for determination of the coolant temperature at any axial node, the temperature iterate is used as the value for entry to the heat capacity table to get the corresponding heat capacity for this node. SIEX, however uses effectively an integrated average heat capacity between the inlet and exit temperatures of the node. This more accurate representation is accomplished by integrating the heat capacity relationship to determine enthalpy as a function of temperature for the coolant and then using enthalpies in the energy equations instead of $C_p T$. The difference in the overall integral obtained across the core is zero because the overall coolant temperature change is determined solely by the amount of power input to the core of the reactor.

The small discrepancy noted in the predictions of inner cladding temperature can be explained by two effects. First, the differences in coolant temperatures are directly propagated to the cladding, and secondly, the SAS code envelops a constant value for the cladding thermal conductivity, whereas the SIEX utilizes a temperature dependence for this property.

When the fuel surface curves are examined, the difference in the gap width and conductances becomes apparent in the calculated temperature at the fuel surface, especially at the top and bottom of the core.

The inspection of the fuel inner radius temperatures shows that when the fuel surface temperatures are approximately in agreement, and since common values of thermal conductivity are used in the two codes, SIEX and SAS predict approximately the same centerline temperatures.

Figure Q001.469-4 compares the prediction of fuel microstructure for the two codes. SSFUEL in SAS predicts a greater amount of restructuring than SIEX. This is due to the algorithm employed in SSFUEL and the higher fuel temperatures predicted by SSFUEL as seen in Figure Q001.469-3.

The calculated fuel microstructure and the steady state fission gas release correlations result in SIEX and SAS fission gas retention values of 18.6% and 27.4%, respectively, in Channel 2. Although SIEX predicts more steady state fission gas release than SAS in Channel 2, the effect of fission gas loading on cladding failure during hypothetical transients depends on the transient fission gas release as well as the steady state (pre-transient) fuel microstructure.

The overall effect of the above differences in steady state fuel microstructure, gap width, gap conductance and fission gas retention is not expected to significantly effect the outcome of the TOP events analyzed. This statement is supported by the comparisons of failure predictions obtained using the SIEX, COBRA-3M and HEDL Empirical Failure Correlation (Damage Parameter) analyses with the SAS3A best estimate analyses of the 50 ϕ /sec. TOP transients in the BOEC and EOEC cores. These comparisons are presented in Sections 6.1.3.2 and 6.2.3.2 of Ref. 15, PSAR Section 1.6. The details of the pin failure sequence change somewhat due to the steady state fuel categorization differences noted above, but the overall course of the accident scenario and the magnitude of the accident energetics are not expected to differ significantly from the SAS3A TOP analyses presented in Ref. 15, PSAR Section 1.6.

References:

- Q001.496-1: D. S. Dutt, et al., "SIEX - A correlated Code for the Prediction of Liquid Metal Fast Breeder Reactor Fuel Thermal Performance", Hanford Engineering Development Laboratory, Richland, WA, June 1975 (HEDL-TME 74-55).

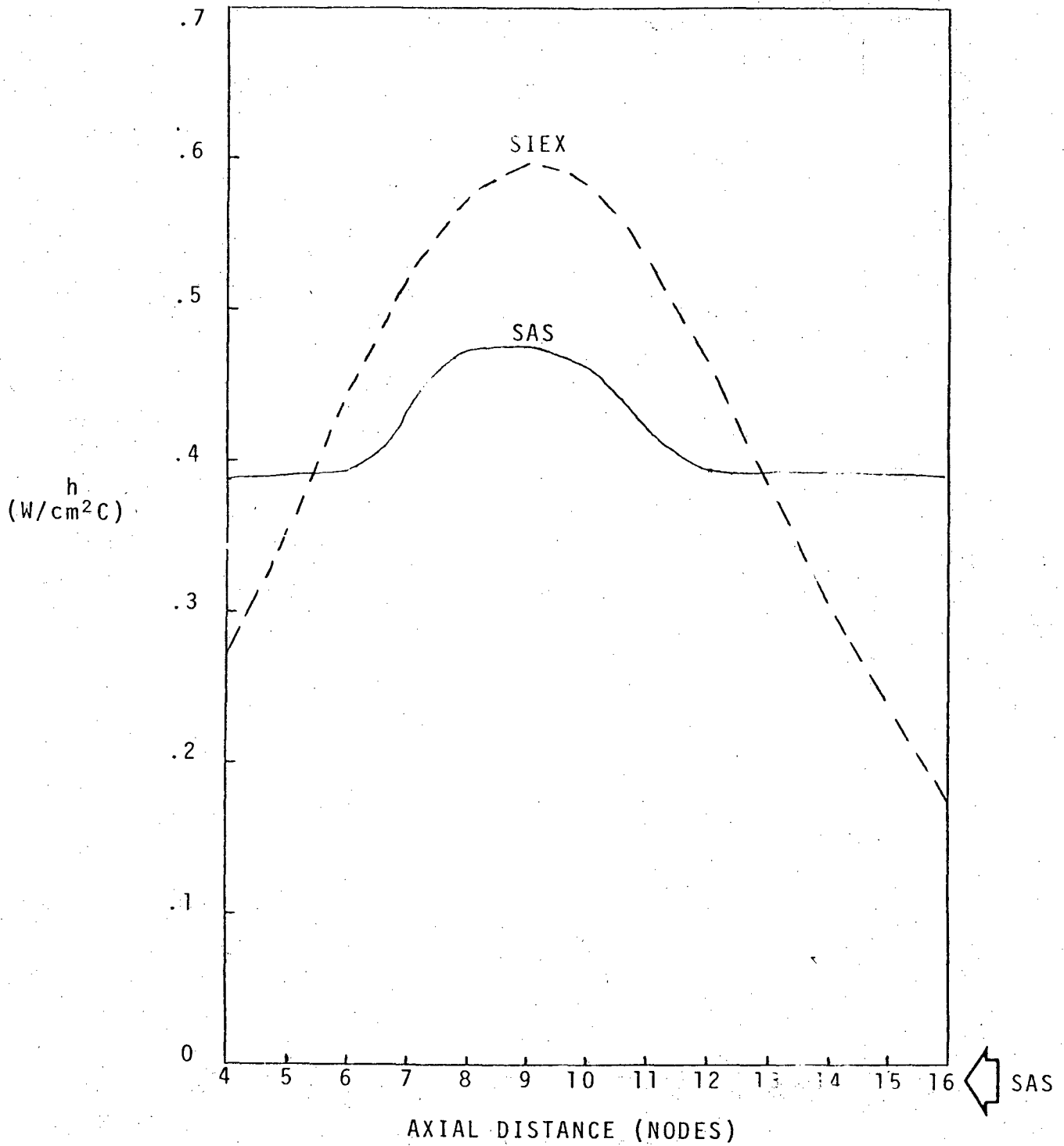


Figure Q001.469-1 GAP Conductance (Channel 2)

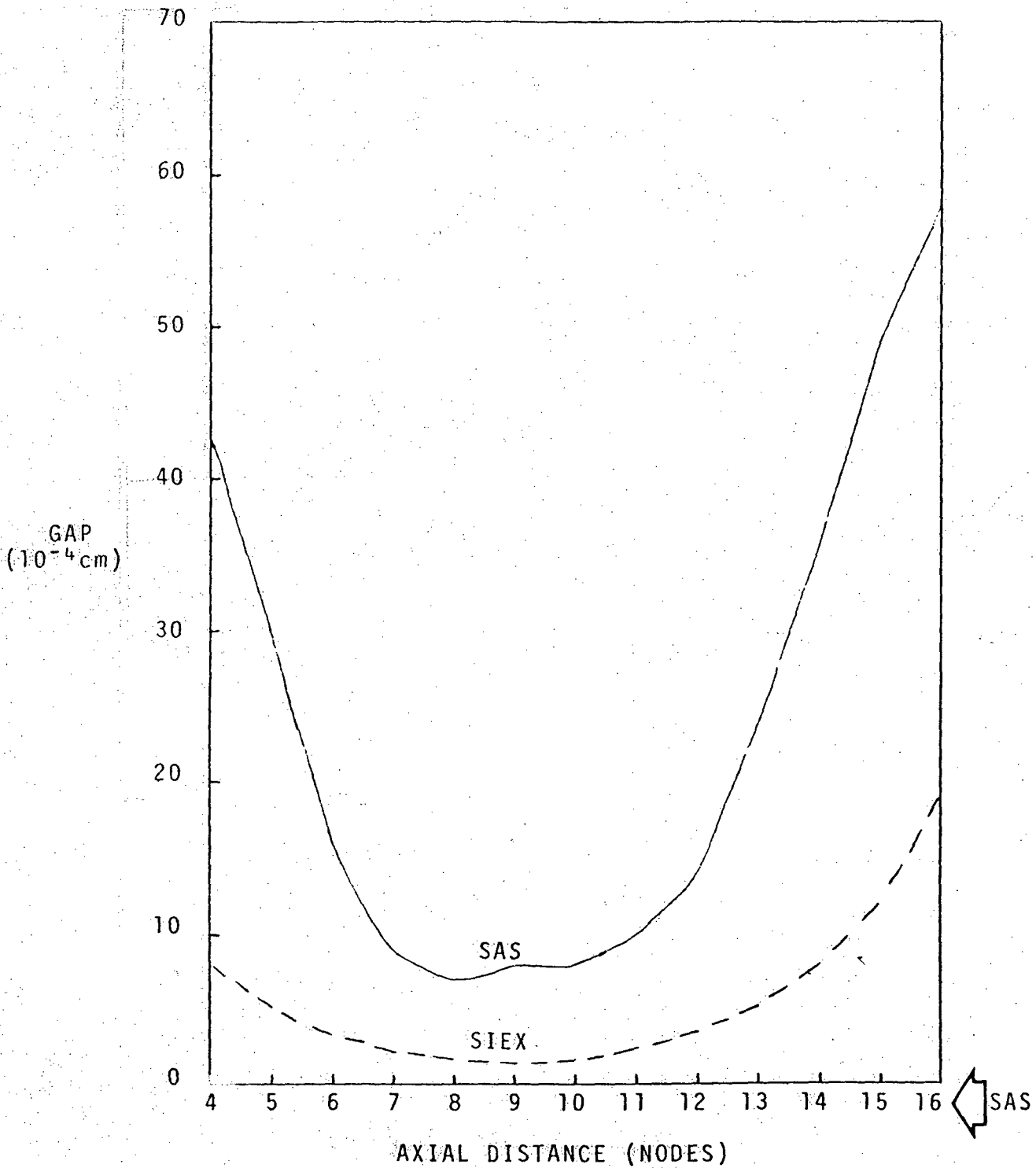


Figure Q001.469-2 Gap Width (Channel 2)

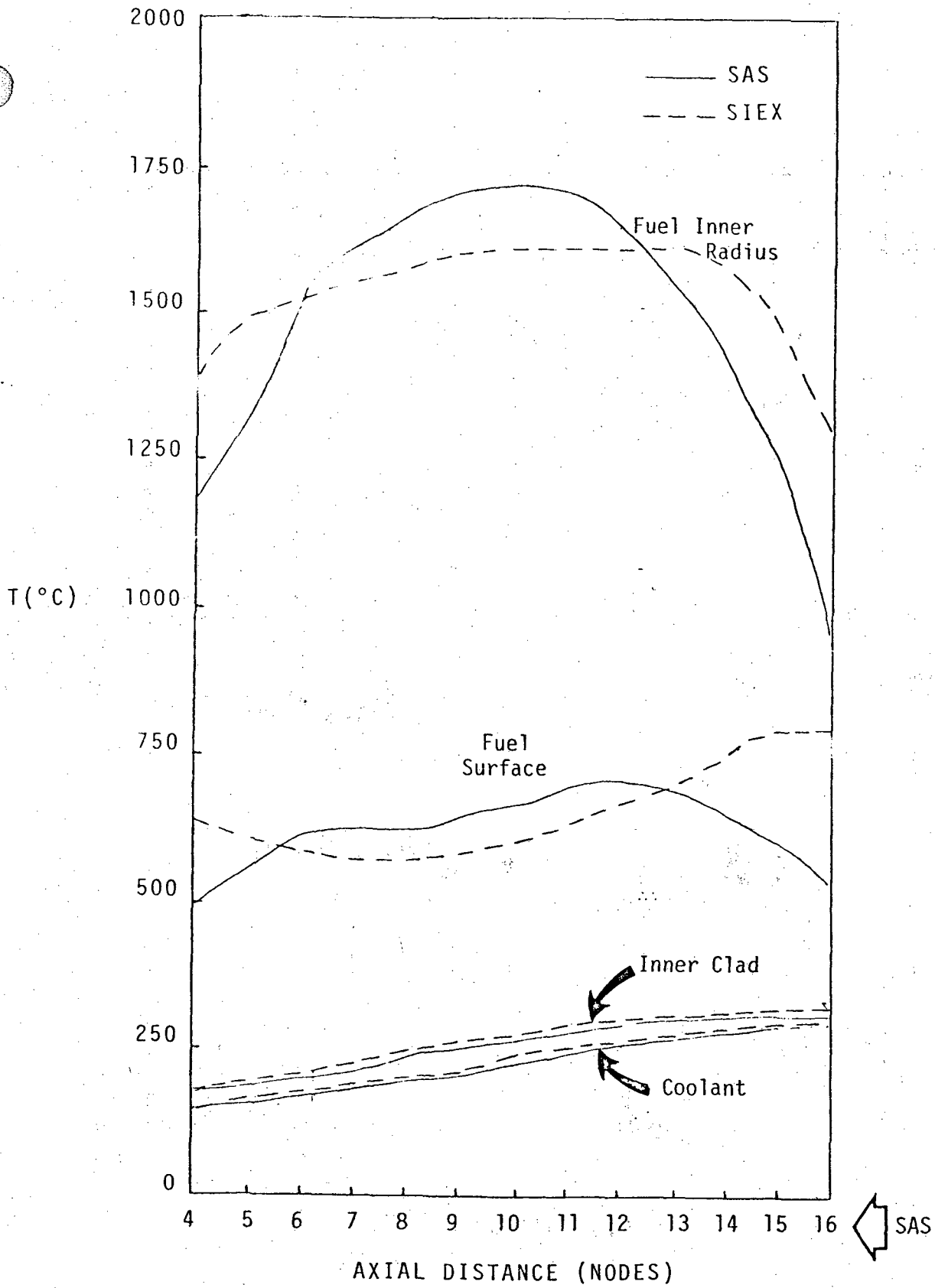


Figure Q001.469-3 Fuel Pin Temperatures (Channel 2)

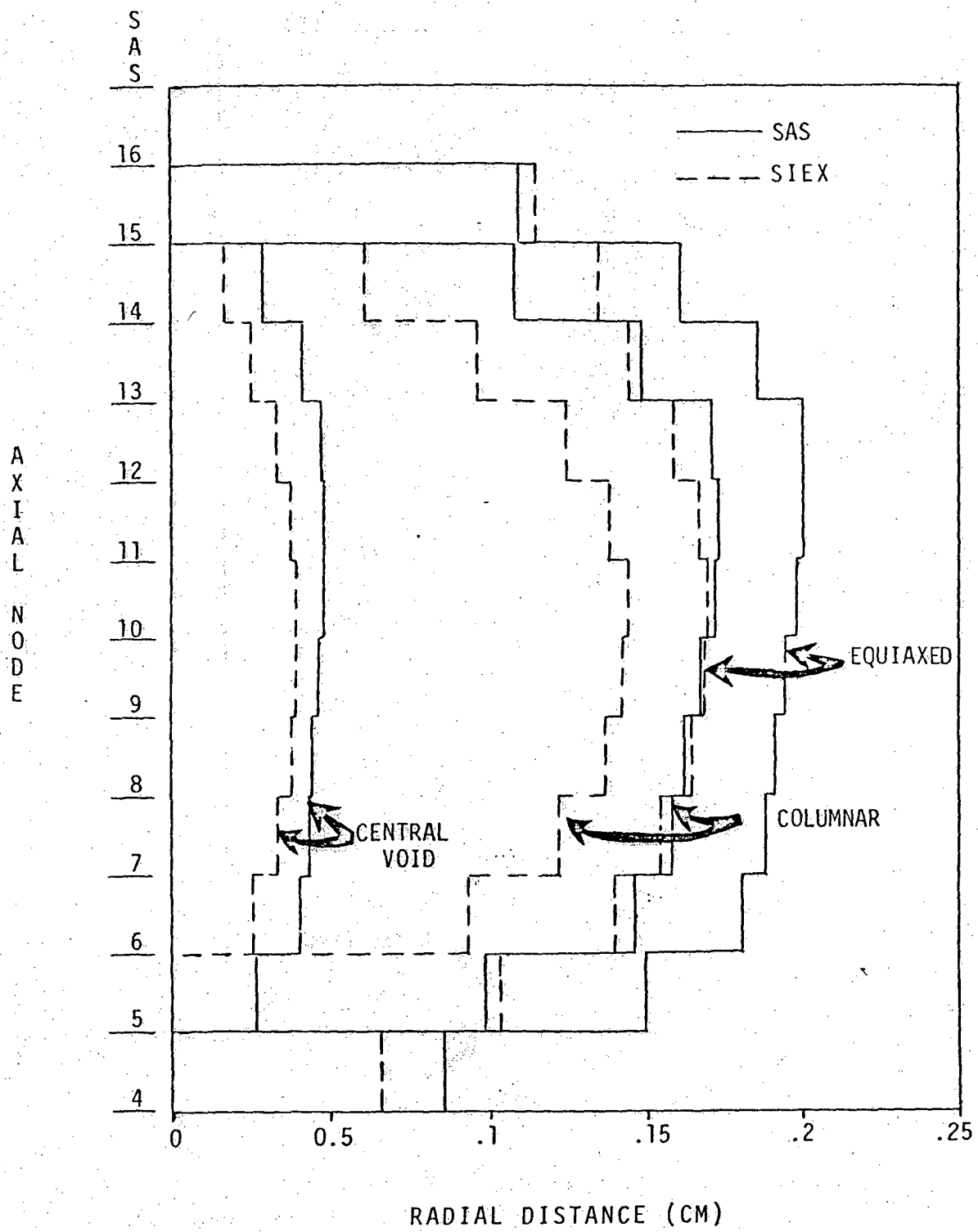


Figure Q001.469-4 Fuel Restructuring Patterns (Channel 2)

Question 001.470 (F6.2.3.2.2, F6.2.3.2.3)

Provide a summary of the experimental evidence and their applicability to CRBRP supporting SAS/FCI and PLUTO and include comparison of predicted vs. observed measurements indicative of the "violence" of the FCI, the extent and duration of sodium voiding, and the fuel motion in the channel.

Response:*

| 60

The experimental evidence supporting PLUTO and SAS/FCI is summarized below.

| 60

TREAT experiments have been used to model the fuel-coolant interaction phenomenon with SAS/FCI and PLUTO.

The experimental evidence directly supporting the PLUTO fuel-coolant interaction predictions includes the E4, N4, E7 and E8 TREAT tests. The PLUTO analysis of the E4 test indicated that the predicted upper and lower slug velocities and the fuel-coolant heat transfer calculation agreed reasonably well with the experimental results. The PLUTO analysis of the sodium reentry event in the H4 test indicated that the PLUTO compressible hydrodynamics calculations produced reasonably good agreement with the test results. The PLUTO analysis of the E7 test showed that the rapid sodium voiding was simulated with PLUTO. Finally, the PLUTO analysis of the E8 test, which modeled an overpower situation using irradiated fuel with a linear power density closely approximating the average linear power density in CRBRP, indicated that the phenomena which occurred during the first tens of milliseconds after pin failure are modelled reasonably well in PLUTO.

The good agreement between the PLUTO predictions of the E4, H4, E7 and E8 TREAT experiments with the actual results of these experiments directly supports the applicability of PLUTO for use in CRBR accident analyses studies. Since comparison calculations of PLUTO predictions with SAS/FCI predictions of coolant voiding and fuel motion have shown that the SAS/FCI predictions are conservative relative to PLUTO predictions (Reference Q001.470-1), the PLUTO analyses support the SAS/FCI calculations in the CRBR analysis of hypothetical transient overpower events.

| 60

Reference:

Q001.470-1: H. U. Wider, et al., "An Improved Analysis of Fuel Motion During an Overpower Excursion", Proc. Fast Reactor Safety Meeting (Beverly Hills, CA), April 1974 (Conf. -740401), pp 1541-1555.

| 60

*Note that Appendix F has been withdrawn. The text, upon which the question was based, can now be found in Section 3 of Reference 15, PSAR Section 1.6.

| 60

Question 001.471 (F6.2.4.3.1)

Describe how the recent low power HUT tests (5-5B, 3-5B, 5-5A, 3-5A) have helped to resolve some of the uncertainties described on page F6.2-63 in the transient behavior of low power pins. Discuss the implications these better understandings have on TOP analyses.

Response:

The CRBRP Project has consolidated all considerations given Hypothetical Core Disruptive Accidents into report CRBRP-3 (References 10a and 10b, PSAR Section 1.6) and its associated references; consequently, PSAR Appendices D and F have been withdrawn in Amendments 24 and 60 respectively. The response to this question is now found in Section 6.2.1 of Reference 15, PSAR Section 1.6.

| 37

| 60

Question 001.472 (F6.2-4.3, F6.2.4.4)

Since midplane failures for the base case result in hydrodynamic disassembly while base case failures higher in the core result in sweepout termination, there exists an axial location above which the accident results in hydraulic shutdown and below which the accident results in core disassembly. Specify that axial position for the BOEC & EOEK cases. Is this value symmetric, i.e., does it hold for failures below the midplane?

Response:

The CRBRP Project has consolidated all considerations given Hypothetical Core Disruptive Accidents into report CRBRP-3 (References 10a and 10b, PSAR Section 1.6) and its associated references; consequently, PSAR Appendices D and F have been withdrawn in Amendments 24 and 60 respectively. The response to this question is now found in Section 4.3.2.2 of Reference 10a, PSAR Section 1.6.

60

Question 001.473 (Figure 6.2-24 Yellow, Figure 6.2-34 Yellow)

Provide figures of radial gap profiles, using such steady codes as CYGRO or LIFE, and compare them with the results shown in Figures F6.2.24 and 34. Discuss the effects of fuel and clad swelling.

Response:*

60

The SAS3A radial gap profiles shown in Figs. 5-13 and 5-20 of Ref. 15, PSAR Sect. 1.6 present average gaps that are obtained by representing groups of subassemblies with similar neutronic, thermal and hydraulic characteristics by a single average fuel pin. The subassembly channel selections for the BOEC and EOEC cores are shown in Figs. 4-2 and 4-3 of Reference 15, PSAR Section 1.6, respectively. To compute similar radial gap profiles using CYGRO or LIFE, the same subassembly averaging process as in the SAS3A BOEC and EOEC models would be necessary. Such a calculation is not necessary for preliminary core design analysis and therefore has not been done.

60

However, as part of the Appendix F study of various phenomenological uncertainties, SIEX (Ref. Q001.473-1) models of the fuel pins represented by SAS BOEC core Channels 4 and 10, and EOEC core Channels 5 and 8 were developed by HEDL. Table Q001.473-1 presents a comparison of the SAS3A and SIEX calculated radial gap profiles for these channels. It is seen that the SIEX calculated gaps are smaller than the SAS3A calculated gaps.

The significance of using smaller steady state gaps in the SAS3A analysis is qualitatively discussed below; Although gaps smaller than those computed by the steady state fuels categorization routine in the SAS3A code are indicated by limited SIEX calculations, this cannot be generalized to all channels in the core.

The fuel pin steady state conditions (including radial gap size) are the initial conditions for transient fuel pin response calculations. The SIEX calculated steady state fuel pin conditions were used in the COBRA-3M analysis of the two BOEC and two EOEC Channels during a TOP 50 cents per second transient. The Damage Parameter (Ref. Q001.473-2) was used with the COBRA transient calculations to predict failure time and axial location in these four channels.

Table 6-6 in Reference 15, PSAR Section 1.6 presents a comparison of the SAS3A BOEC TOP channel failure sequence, using the burst pressure failure criteria, along with the Damage Parameter failure estimates in Channels 4 and 10. The correlated SIEX/COBRA-3M/Damage Parameter methodology predicts failure at a slightly earlier time in a different irradiated channel than does SAS3A. This difference is due to two factors. First the thermal response of the channels during the transient will differ due to the difference in initial fuel pin steady state conditions (including the radial gaps), and

60

*Note that Appendix F has been withdrawn. The text, upon which the question was based, can now be found in Section 5 of Reference 15, PSAR Section 1.6.

60

second, the mechanistic burst pressure failure model is a first principles attempt to predict failure, whereas the Damage Parameter failure criterion is an empirical correlation.

Since the axial failure locations were calculated by both failure models to be at similar elevations in the upper half of the core region, an autocatalytic event is not expected, and the failure energetics are expected to be of the same order as the failure energetics which resulted from the SAS3A analysis.

A similar conclusion was drawn for the EOE TOP 50 cents per second failure model comparison presented in Table 6-2, Ref. 15, PSAR Section 1.6.

160

In the LOF transient, the gap size will have little effect on the cladding temperatures prior to sodium voiding due to the high liquid sodium heat transfer coefficient. However, once voiding occurs, the smaller gap will result in lower fuel temperatures; fuel melting will occur later and the fuel slumping criterion will be satisfied slightly later. Therefore gap size may affect the timing but is not expected to significantly affect the sequence of events or the energetics in the LOF transient.

In conclusion, the fuel-clad steady state radial gaps in selected BOEC and EOE channels calculated using the SIEX steady state fuels categorization code were found to be smaller than the radial gaps calculated by the SAS3A code but the differences are not expected to result in significant difference in accident progression or energetics.

References:

- Q001.473-1. D. S. Dutt and R. B. Baker, SIEX--A Correlated Code for the Prediction of Liquid Metal Fast Breeder Reactor (LMFBR) Fuel Thermal Performance, HEDL-TME 74-55, June 1975.
- Q001.473-2. Scott, et al., "Microstructural Dependence of Failure Threshold in Mixed Oxide LMFBR Fuel Pins," HEDL-TME 75-9, October 1974 (See reference 7 of Section F6.2 of the PSAR).

TABLE Q001.473-1

FUEL-CLADDING RADIAL GAPS (CM)

SAS AXIAL NODE(1)	EOEC CHANNEL 5		EOEC CHANNEL 8		BOEC CHANNEL 4		BOEC CHANNEL 10	
	SIEX	SAS	SIEX	SAS	SIEX	SAS	SIEX	SAS
4	.0021	.0051	.0015	.0048	.0012	.0043	.0024	.0054
5	.0016	.0046	.0010	.0038	.0008	.0035	.0019	.0049
6	.0012	.0037	.0006	.0024	.0006	.0023	.0015	.0044
7	.0009	.0027	.0004	.0012	.0004	.0011	.0012	.0040
8	.0008	.0020	.0002	.0009	.0003	.0009	.0011	.0035
9	.0007	.0016	.0001	.0008	.0003	.0009	.0010	.0032
10	.0007	.0015	.0001	.0008	.0003	.0010	.0011	.0035
11	.0007	.0018	.0002	.0008	.0004	.0014	.0013	.0040
12	.0009	.0022	.0003	.0011	.0006	.0022	.0016	.0046
13	.0012	.0030	.0006	.0017	.0009	.0032	.0019	.0050
14	.0016	.0040	.0010	.0028	.0013	.0046	.0024	.0054
15	.0023	.0052	.0016	.0043	.0018	.0052	.0029	.0058
16	.0031	.0060	.0024	.0056	.0027	.0060	.0036	.0064

NOTE:

- (1) SAS AXIAL HEAT TRANSFER NODE. SEE FIG. 4-6 ON PAGE 4-36 OF REF. 15, PSAR SECTION 1.6 FOR NODAL SPACING IN THE CORE. NODE 10 IS AT THE CORE MIDPLANE.

60

Question 001.474 (F6.2.3.2.1)

For the "Burst Irradiated Clad" strength curve shown in Figure F6.2-14, provide the data points from reference 18 from which the curve was generated. (The strength values seem high in the range of temperatures from 500°C to 800°C based on the 10°F/sec values found in reference 18).

Response:

The CRBRP Project has consolidated all considerations given Hypothetical Core Disruptive Accidents into report CRBRP-3 (References 10a and 10b, PSAR Section 1.6) and its associated references; consequently, PSAR Appendices D and F have been withdrawn in Amendments 24 and 60 respectively. The response to this question is now found in Section 3.2.3 of Reference 15, PSAR Section 1.6.

60

Question 001.475 (F6.2.6.1)

For a meaningful disassembly calculation the initial core conditions must be defined and justified. For example, it is stated that the fuel should be assumed to behave as an inviscid fluid in the VENUS calculations, however, Table F6.2-21 to 24 show core (i.e., fuel) temperatures below melting. Provide a clarification of this discrepancy. In addition more information is needed to explain and support the criteria of the transition to VENUS. More specifically, describe how the VENUS rate ramp is formulated from the SAS3A output. A complete set of VENUS input parameters for the Appendix F VENUS runs should be provided.

Response:

The CRBRP Project has consolidated all considerations given Hypothetical Core Disruptive Accidents into report CRBRP-3 (References 10a and 10b, PSAR Section 1.6) and its associated references; consequently, PSAR Appendices D and F have been withdrawn in Amendments 24 and 60 respectively. The response to this question is now found in Section 11.1 of Reference 15, PSAR Section 1.6.

Question 001.476 (F6.2.6.1, F6.2.6.2.1)

Describe how it is decided whether a core is "full" or partially voided, and how the distribution of Na is determined for VENUS inputs. In connection with an energetic disassembly, discuss the reasons for not having considered the sodium entrainment during the ejection of the fuel in the sodium pool and the resulting increase of the work potential due to the resultant mixing.

Response:*

160

Examination of the SAS3A output at the point where initial conditions for VENUS-II are compiled determines the amount of sodium present. Some channels are totally voided, some are partially voided, and some are still filled with sodium. The sodium distribution for VENUS-II is determined by geometrically mapping the SAS3A channel conditions onto the VENUS R-Z grid. The actual sodium distributions are either smeared within a VENUS region or mapped pointwise. Calculations are provided in Section 11 of Reference 15, PSAR Section 1.6, using both techniques to account for the sodium effect on the disassembly.

With regard to the second part of the question, the existing experimental data supports a judgment that the entrainment of sodium into the expanding fuel bubble will result in a quenching of the fuel vapor without the generation of significant sodium vapor pressures. This subject is further discussed in Section 12 of Ref. 15, PSAR Section 1.6, and Section 4.5 of Ref. 10a, PSAR Section 1.6.

*Note that Appendix F has been withdrawn. The text, upon which the question was based, can now be found in Section 11 of Reference 15, PSAR Section 1.6.

60

Question 001.477 (F6.2.6.2, F6.2.6.2.1)

Following a non-energetic core meltdown, or even a very mild disassembly, there is a potential for molten fuel and steel to transfer their energy to liquid sodium (initially in the core or subsequently re-entering the core from the pool above), thus making the sodium vapor the working fluid. Consider both fuel and stainless steel as interacting with sodium and provide a quantitative assessment of the energetics following such potential interactions. Provide a justification of the most important parameters used in these assessments, especially their experimental base.

Response:

The CRBRP Project has consolidated all considerations given Hypothetical Core Disruptive Accidents into report CRBRP-3 (References 10a and 10b, PSAR Section 1.6) and its associated references; consequently, PSAR Appendices D and F have been withdrawn in Amendments 24 and 60 respectively. The response to this question is now found in Sections 4.5.1 and 4.5.2 of Reference 10a, PSAR Section 1.6.

Question 001.478 (F6.2.6.1)

Clarify the discrepancy of the initial conditions shown in the last column of Table F6.2.21 and the corresponding case 5* of Table 4.4-1 of ANL/RAS 75-29.

Response:

This question requests clarification of information which is no longer a part of the current documentation. The Project has since consolidated all considerations given Hypothetical Core Disruptive Accidents into report CRBRP-3 (References 10a and 10b, PSAR Section 1.6) and its associated references; consequently, PSAR Appendices D and F have been withdrawn in Amendments 24 and 60 respectively.

60

Question 001.479 (F6.2.6.1)

Discuss the potential for autocatalytic effects (from relative clad, fuel, and coolant motion) during the early phase of the energy production part of the hydrodynamic disassembly.

Response:

The CRBRP Project has consolidated all considerations given Hypothetical Core Disruptive Accidents into report CRBRP-3 (References 10a and 10b, PSAR Section 1.6) and its associated references; consequently, PSAR Appendices D and F have been withdrawn in Amendments 24 and 60 respectively. The response to this question is now found in Section 4.4.2.2 of Reference 10a, PSAR Section 1.6.

60

Question 001.480 (F6.2.6)

It has been shown by S. J. Board et. al., (Nature 254, 319-321, 1975) that mixed molten fuel and sodium could result into a vapor explosion, or detonation, if subjected to a strong shock wave or a pressure pulse. Examine if such conditions could potentially exist in the CRBRP.

Response:

The initial conditions assumed by S. J. Board, et. al., for a theoretical model for a vapor explosion (Reference Q001.480-1,2) can be summarized as follows when the theory is applied to a LMFBF core during a HCDA. A coarse mixture of molten fuel droplets in liquid sodium is subjected to a shock wave which strips the vapor blankets off the hot droplets, and fragments them. Heat is rapidly transferred to the sodium which then vaporizes and expands so rapidly that a strong self-sustaining detonation wave is generated even though there is not chemical reaction.

The potential for the occurrence of vapor explosions in LMFBF's has been studied for many years at ANL. The study has led to the conclusion that the potential is low because (Reference Q001.480-3) "initial conditions and alternate triggering events necessary to cause large-scale thermal "explosions" have not been identified in the LMFBF system." This conclusion is based on a large number of considerations and results (References Q001.480-3,4,5,6) which will be summarized here. For a loss-of-flow type of HCDA, calculations and tests have shown that the liquid sodium boils out of the core before the fuel penetrates through the cladding. Furthermore, the re-entry of liquid sodium into the core is retarded by evaporation of the sodium as it re-enters as well as plugging due to cladding and fuel relocation. The fuel in the core is probably in a "drop fluidized" state (Reference Q001.480-6), so that if any liquid sodium does re-enter the core it cannot contact a large volume of liquid fuel, and "experiments have shown that only non-energetic events occur when the hot material is predispersed or is in a state of flashing prior to being mixed with the working fluid" (Reference Q001.480-3).

For a transient overpower type of HCDA, calculations indicate that liquid fuel can penetrate through the cladding and cause a coarse mixture of molten fuel and liquid sodium to exist throughout a fraction of the core. However, even in this case an extensive vapor explosion is extremely unlikely. The cladding which initially separates the liquids (fuel and sodium) does not melt until after the sodium boils away from the cladding (Reference Q001.480-3) and even after the fuel penetrates through the cladding, most of the fuel and coolant continues to be separated by cladding. This is ignored by the theoretical model for a vapor explosion postulated in S. J. Board, et. al. Consideration of the pressure waves, surface instabilities, and cladding relocations which occur as the liquid fuel penetrates through the cladding (Reference Q001.480-3) indicates that the two liquids do not become finely mixed. Furthermore, the liquid fuel remaining within the cladding becomes dispersed in vapor so that it will not support a vapor explosion. Little or no increase in work potential over that for expanding fuel can be expected because of the small area of contact and low heat transfer rate between the fuel and sodium in the core (Reference Q001-480-3).

Potentially, the most quantitative and generally applicable criterion to demonstrate whether a large-scale thermal explosion can occur in the CRBRP is probably the spontaneous nucleation criterion (References Q001.480-3,4,5). This criterion indicates that for the specific liquids, UO_2 and Na, vapor explosions cannot occur (Reference Q001.480-7). Calculations indicate that the surface temperature when molten UO_2 contacts liquid Na is well below the "spontaneous nucleation temperature" and that this prevents explosive interaction. However, in its present state of development, the validity of the criterion is subject to some uncertainty (References Q001.480-8,9). Nevertheless, it appears that further development of the spontaneous nucleation criterion might conclusively demonstrate that a powerful vapor explosion due to fuel coolant interaction is not just extremely unlikely but is impossible in the CRBRP during a TOP type of HCDA.

References

- Q001.480-1 S. J. Board, et. al., "Detonation of Fuel Coolant Explosions", Nature V. 254, p. 319, March 27, 1975.
- Q001.480-2 S. J. Board and R. W. Hall, "Propagation of Thermal Explosions, Part 2, A Theoretical Model", RD/B/N-3249, Central Electricity Generating Board, Research Department, Berkeley Nuclear Laboratories, United Kingdom, December 1974.
- Q001.480-3 H. K. Fauske, "LMFBRs and Vapor Explosions, ANS Transactions, V. 22, p. 411, November 1975.
- Q001.480-4 R. E. Henry and H. K. Fauske, "Nucleation Characteristics in Physical Explosions", ANS Transactions, V. 22, p 412, November 1975.
- Q001.480-5 R. E. Henry, et. al., "Vapor Explosions with Subcooled Freon", ANS Transactions, V. 22, p. 413, November 1975.
- Q001.480-6 H. K. Fauske, "Boiling Flow Regime Maps on LMFBR HCDA Analysis," ANS Transactions, V. 22, p. 385, November 1975.
- Q001.480-7 H. K. Fauske, "Some Aspects of Liquid-Liquid Heat Transfer and Explosive Boiling", Proc. of the Fast Reactor Safety Meeting, Beverly Hills, Ca., April 1974.
- Q001.480-8 V. H. Arakeri, et. al., "Interaction of Molten Tin with Water: Effect of Temperature Stratification in the Coolant," ANS Transactions V. 22, p. 415, November 1975.
- Q001.480-9 D. R. ARMstrong, Laboratory Experiments on Mechanisms of Fragmentation and Pressure Generation, ANL-RDP-2, February 1972, p. 8.31.

Question 001.481 (F6.2.1)

It is stated in paragraph F6.2.1 that many of the energetic analyses reported therein were performed by Argonne National Laboratory and documented in ANL/RAS 75-29. In paragraph 4.4.2 of this report it is mentioned that prototypic in-reactor tests are in progress to verify the analysis. Provide a description including status and schedule of your R&D program for the verification of the analysis provided in the PSAR. Describe how the results of such a program will be utilized.

Response:

The CRBRP Project has consolidated all considerations given Hypothetical Core Disruptive Accidents into report CRBRP-3 (References 10a and 10b, PSAR Section 1.6) and its associated references; consequently, PSAR Appendices D and F have been withdrawn in Amendments 24 and 60 respectively. The response to this question is now found in Appendix A of Reference 10a, PSAR Section 1.6.

60

Question 001.482 (F6.2.6.3)

In the transition phase recriticality considerations of paragraph F6.2.6.3 it is assumed that plugs will form in the upper axial blanket. The corresponding paragraph of ANL/RAS 75-29, based on Reference 3.3, calculates that thick and complete blockages, which could limit the dispersion of the fuel, will not form. However, Reference 3.3 does not deal with the calculation of thick and complete blockages as claimed. Specify what is meant by complete blockages and what is their role in the evolution of the accident. Provide a more thorough analytical and experimental basis (than that provided in paragraph F6.2.6.3) for the formation of blockages. Provide a description, including that status and schedule of your R&D program to address this question. Provide an assessment of the situation when an upper blockage is formed and dispersing is provided through pressure relief downward.

Response:

The CRBRP Project has consolidated all considerations given Hypothetical Core Disruptive Accidents into report CRBRP-3 (References 10a and 10b, PSAR Section 1.6) and its associated references; consequently, PSAR Appendices D and F have been withdrawn in Amendments 24 and 60 respectively. The response to this question is now found in Section 4.2.3 of Reference 10a, PSAR Section 1.6.

Question 001.483 (F6.2.4)

Describe the physical aspects of lower plenum pressurization during voiding in LOF transients. Identify all aspects of the calculation that affect the magnitude of the pressurization and provide the sensitivity to, and justification for, the selection of the parameters. Provide and justify the core vapor flows and corresponding pressure drops as a function of time during the changing phase for a typical calculation.

Response:

The response to Question 001.265 describes the physical aspects of lower plenum pressurization during voiding in LOF transients. The response to Question 001.265 also discusses the parameters influencing the magnitude of the pressurization.

The experimental basis for the sodium voiding model used in the calculation of the core vapor flows and corresponding pressure drops is described in Reference Q001.483-1.

Following the initiation of voiding, pressure spikes could occur in the lower plenum. The effect of lower plenum pressure spikes on clad motion as predicted by SAS is discussed in Section 4.4 of Reference 10a, PSAR Section 1.6.

160

Reference:

Q001.483-1 Stevenson, M.G., et. al., "Report on the Analysis of the Initiating Phase of a Loss-of-Flow (Without Scram) Accident in the FTR", ANL/RAS 74-24, pp. 35-43, September 1974.

Question 001.484 (F6.2.4.1, F6.2.4.2, F6.3.4.2.4)

The interpretation of the phenomenology of the accident seems to have been connected with the two burst phenomenon. In view of the limitation of the channel selection which has been imposed (note restriction discussion on pages F6.2-39, 40) discuss the degree to which this scenario can be considered predictable under any reasonable channel configuration. Is it possible that a different scenario can evolve and that a basically different behavior could result from a different channel selection?

Response

The CRBRP Project has consolidated all considerations given Hypothetical Core Disruptive Accidents into report CRBRP-3 (References 10a and 10b, PSAR Section 1.6) and its associated references; consequently, PSAR Appendices D and F have been withdrawn in Amendments 24 and 60 respectively. The response to this question is now found in Section 4.4 and Ref. 4-2 of Reference 10a, PSAR Section 1.6.

Question 001.485 (F6.2.5.1.2.1)

For one of the cases discussed in this section, the peak fuel vapor pressure is given as 680 atm and the average temperature of the hot 28.5% of the fuel as 5730 K. The corresponding peak temperature will be in the area of the critical temperature of the fuel. Discuss the equation of state in the neighborhood of the critical point and the possible effects on the computed work during disassembly.

Response:

The numbers in the question are from a SAS3A run for a case in which disassembly would have occurred prior to reaching the stated temperature and pressure conditions. A VENUS calculation was performed to conclude this analysis. From this calculation, the peak fuel temperature was determined to be 5797°K. Other VENUS cases were also run and reported in Reference 10a, PSAR Section 1.6. In these calculations, the average temperature of the fuel core ranged between 4500-4600°K; the peak fuel temperatures were of the order of 5900-6400°K. In no case did the peak fuel temperature approach the critical temperature which is above 7000°K (see Table 5 of Reference Q001.485-1). A discussion of the equation of state near the critical point thus seems irrelevant, both for this case and others reported in Reference 10a, PSAR Section 1.6. What is relevant, though, is that those portions of the core that do achieve high fuel temperatures during hydrodynamic disassembly will contribute the dominant portion of the work.

Reference

Q001.485-1 E. A. Fischer, P. R. Kinsman, and R. w. Ohase, "Critical Assessment of Equation of State Data for UO₂", J. Nucl. Matls 59, 125-136 (1976).

Question 001.486 (F6.2.4.2.2.1)

Explain why in this case the clad solidus point is taken from the inner clad node next to the fuel.

Response:*

160

The reference to the clad solidus point being taken at the inner clad node is to emphasize that the clad solidus time in Table 7-1 of Ref. 15, PSAR Section 1.6, is not the time clad motion begins. In the SAS3A code, the clad solidus time is that time at which a node begins to melt (reaches clad solidus) while the clad does not begin to relocate until all but the outer node, 5% of the clad, has completely melted (reached clad liquidus). Since the inner clad node is hottest, that node usually reaches the solidus temperature first.

160

*Note that Appendix F has been withdrawn. The text, upon which the question was based, can now be found in Section 7 of Reference 15, PSAR Section 1.6.

160

Question 001.487 (F6.2.4.1.3)

A massive amount of fuel motion is calculated by SAS3A and it is known that perturbation theory over-predicts the negative reactivity effect. Provide an analysis in which fuel motion reactivity effects are not treated by perturbation theory. Relate your analysis to the fuel motion reactivity measurements which have recently been conducted on the ZPPR facility in Idaho.

Response:

In order to make a statement regarding what effect the reactivity treatment errors incurred by SAS3A may have on the course of the scenarios it predicts for CRBR, it is necessary to look more closely at the actual material relocations it predicts for such cases. In the case of the LOF scenario the first significant material motion which occurs in such scenarios is the voiding of the core and upper axial blanket of the high-power subassemblies. As pointed out in Reference Q001.487-1, first-order perturbation theory is generally adequate for predicting the voiding reactivity effect. As voiding progresses to the medium power subassemblies, a relatively small amount of cladding relocation upward from the upper core regions of the first subassemblies to void is predicted by SAS3A prior to fuel motion if the CLAZAS model is utilized. Because of the small amount of cladding involved, first order perturbation theory generally would provide adequate predictions of this reactivity effect prior to the start of fuel motion.

In considering the subsequent fuel motion reactivity errors which could result from the SAS3A first-order perturbation treatment in such scenarios, two important facts must be emphasized. The first is that, in comparison to the ZPPR Assembly 5 fuel relocation experiments, the amount and extent of fuel relocation predicted by SAS3A in a given local region is almost always less than the experiments are designed to model prior to the time that the reactor becomes several dollars subcritical. The second is that the reactivity worth used in SAS3A are based on a linearized treatment of the diffusion constant change in the leakage term. This consistently results in errors in the perturbation theory estimate of the leakage component of the reactivity which are opposite in sign to the error introduced by utilizing the initial state real and adjoint fluxes. To the extent that the two errors tend to cancel one another, first order perturbation theory with the linearized leakage treatment will account more accurately for initial fuel motion reactivity effects than will the corresponding non-linear leakage treatment.

In order to test the degree to which this error cancellation brings the first order treatment with linearized leakage closer to a true space-time reactivity treatment, the following comparison was carried out. An EOE LOF case was limited initial fuel motion and with the CLAZAS clad motion, was rerun in a mode where restart files were written sequentially every few SAS3A heat transfer time steps. The SAS3A material and temperature distributions were mapped onto the same two-dimensional cylindrical grid as was used for the steady-state neutronics calculations. A special version of the FX2 code (See Ref. Q001.487-2) was prepared which could accept these

60

material and temperature distribution snapshots and which, by linearly interpolating on a mesh-cell-by-mesh-cell basis between successive snapshots, could utilize them as continuous driving functions over the course of the transient. Using a 9 group cross section set generated in the same fashion as was the 27 group set, FX2 transient calculations were made to assess the reactivity trace generated by each of the three options implemented in FX2 - a quasistatic space-time reactivity model, a first-order perturbation model with nonlinear leakage, and a first order perturbation model with the linearized leakage treatment. The resulting reactivity histories are displayed on the accompanying Fig. Q001.487-1.

The solid line on Fig. Q001.487-1 is the reactivity trace generated by the space-time model with a fine shape function recalculation time mesh. The reactivity trace generated by the first order perturbation model using the nonlinear leakage treatment is shown as the dashed line on Fig. Q001.487-1. As can be seen, this model consistently underpredicts the reactivity compared to the space-time model because of its chronic overprediction of the negative leakage component. The reactivity predicted by the first order perturbation model with linearized leakage treatment is shown on Fig. Q001.487-1 by the small triangles.

The agreement seen here between the space-time model and the linearized first order perturbation model indicates that the use of a linearized first order perturbation theory reactivity model for the SAS3A analyses of LOF accidents in CRBR represents an adequate treatment.

Two points can be made in relating the ZPPR Assembly 5 fuel relocation experimental results to the SAS3A calculations for CRBR. The first is that it is not surprising that the true fuel worth distribution took on a double-humped axial shape, with central minimum at the core midplane, when such large dense regions of fuel were formed away from the core midplane in the slumped-out configuration (Ref. Q001.487-3). The second point is that the large coherent fuel relocations modeled in these experiments represent gross exaggerations of the degree and amount of fuel relocation generally predicted by SAS3A to have occurred in any local region by the time that the neutronics part of the LOF transient of concern has been effectively terminated.

References:

- Q001.487-1: H. Hummel and D. Okrent, Reactivity Coefficients in Large Fast Power Reactors, American Nuclear Society, 1970, pp. 106-112.
- Q001.487-2: D. R. Ferguson, T. A. Daly and E. L. Fuller, "Improvements of and Calculations with Two-Dimensional Space-Time Kinetics Code FX2", Proc. Conf. Mathematical Models and Computation Techniques for Analysis of Nuclear Systems CONF-730414, V.2, pp IX-59 (1973).
- Q001.487-3: ANL-ROP-42, pp. 6.8-6.11.

Q001.487-3

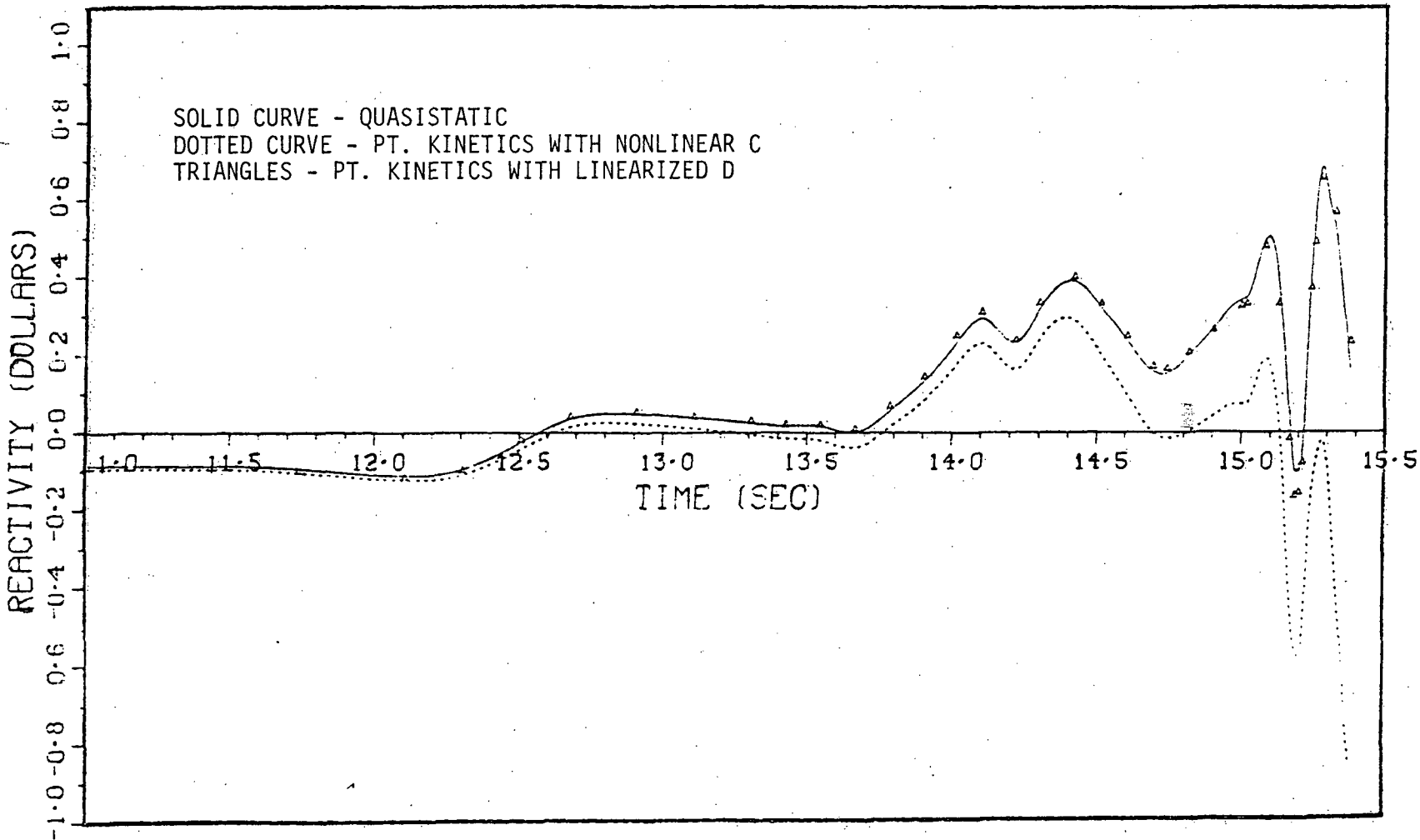


Figure Q001.487-1 ACCURACY OF POINT KINETICS REACTIVITY
IN A CRBR EEC LOF TRANSIENT

Amend. 60
Feb. 1981

Question 001.488 (F6.2.3.3)

Provide analysis in which worths and relative powers are computed from a HEX-Z representation of the core for both the BOEC and EOEC cases.

Response: *

Analysis has been performed using VENTURE (a 3-D diffusion theory code) (Reference Q001.488-1) for a one third reactor sector.

The results of the HEX-Z analysis for the beginning of equilibrium cycle (BOEC) and the end of equilibrium cycle (EOEC) are presented in Figures Q001.488-1 through Q001.488-86.

Figure Q001.488-1 provides both the assembly numbering scheme and the length of time that each assembly would have been in the core. Figures Q001.488-2 through 34 and Figures Q001.488-35 through 67 are the axial power density distribution for the 36 inch core height averaged over an assembly for BOEC and EOEC, respectively. The height above the bottom of the core corresponds to the distance above the core/lower axial blanket interface.

The material worths for the removal of sodium, stainless steel, and fuel were calculated using first order perturbation theory with three dimensional fluxes. The three material worths calculated are presented for each assembly in Figures Q001.488-69 through 77 for BOEC and 78 through 79 for EOEC.

Reference:

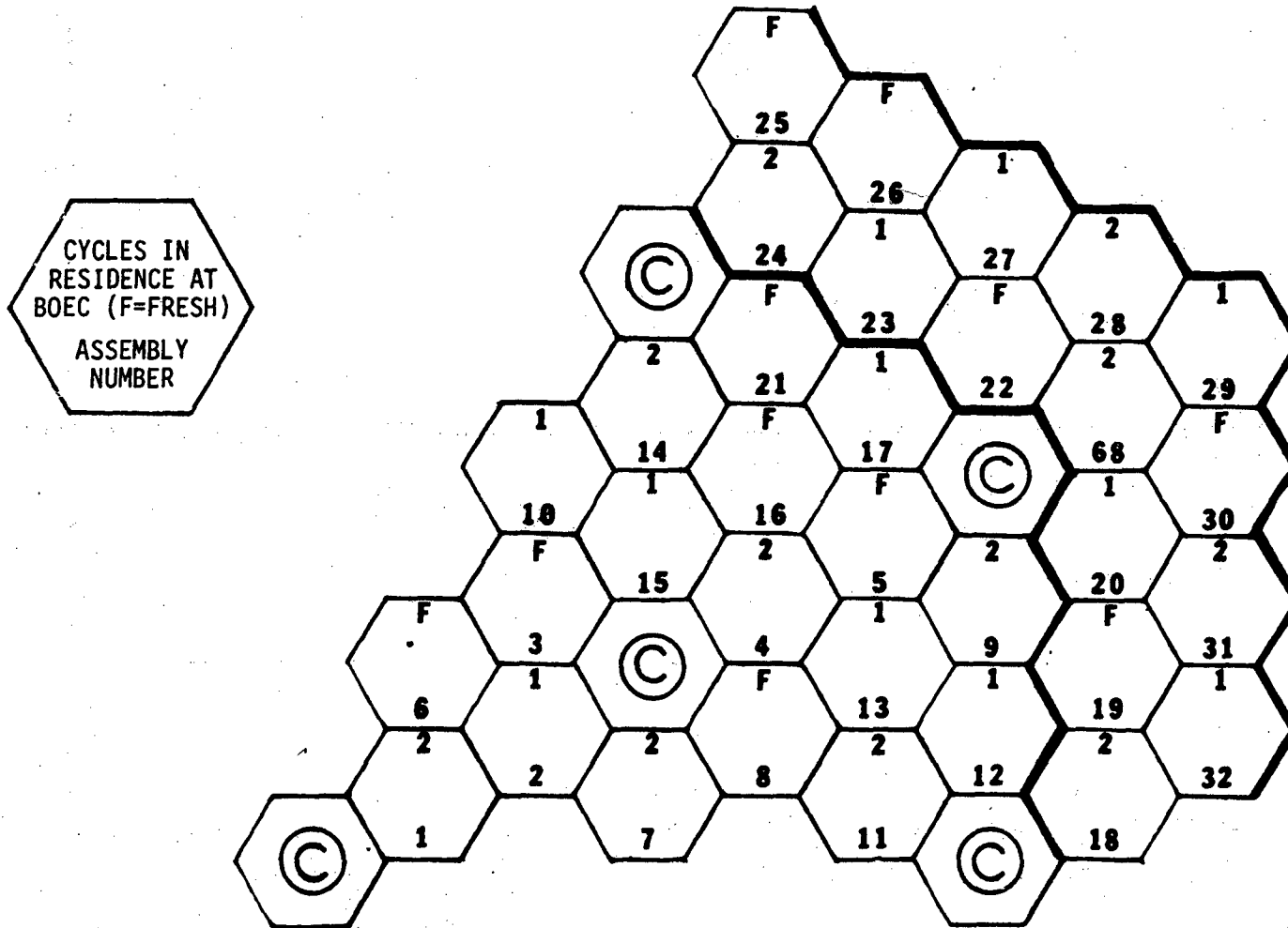
Q001.488-1: D. R. Vondy, T. B. Fowler, G. W. Cunningham, "VENTURE, A Code Block for Solving Multigroup Neutronics Problems Applying the Finite-Diffusion-Theory Approximation to Neutron Transport", ORNL-5062, October 1975.

*Note that Appendix F has been withdrawn. The text upon which the question was based, can now be found in Section 5 of Reference 15, PSAR Section 1.6.

60

FIGURE Q001.488-1

ASSEMBLY NUMBERING SCHEME AND FUEL BURNUP

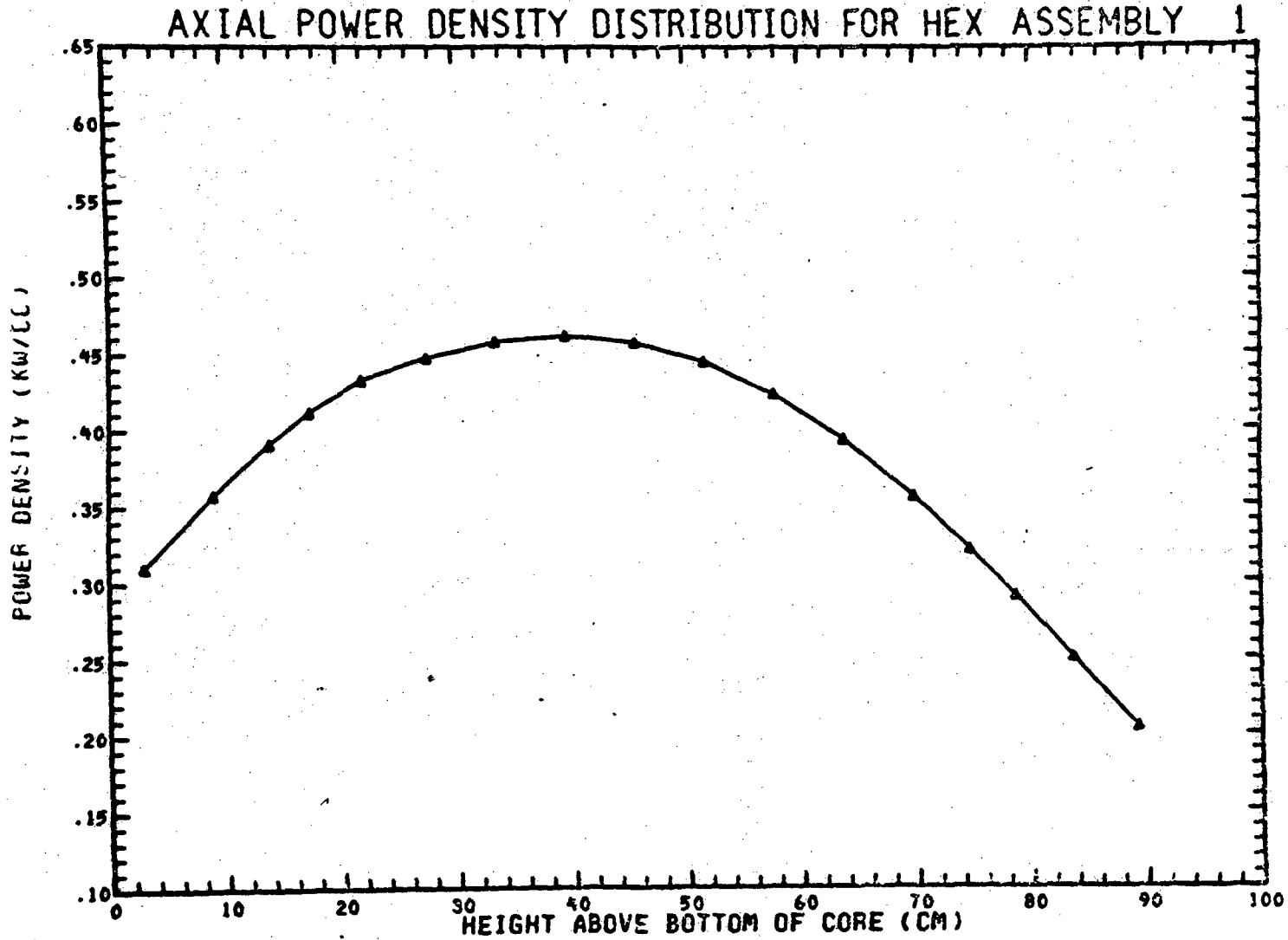


Q001.488-2

Amend. 60
Feb. 1981

FIGURE Q001.488-2

(BEGINNING OF EQUILIBRIUM CYCLE)



TOTAL POWER FOR THIS ASSEMBLY= .4486E+01 MEGAWATTS

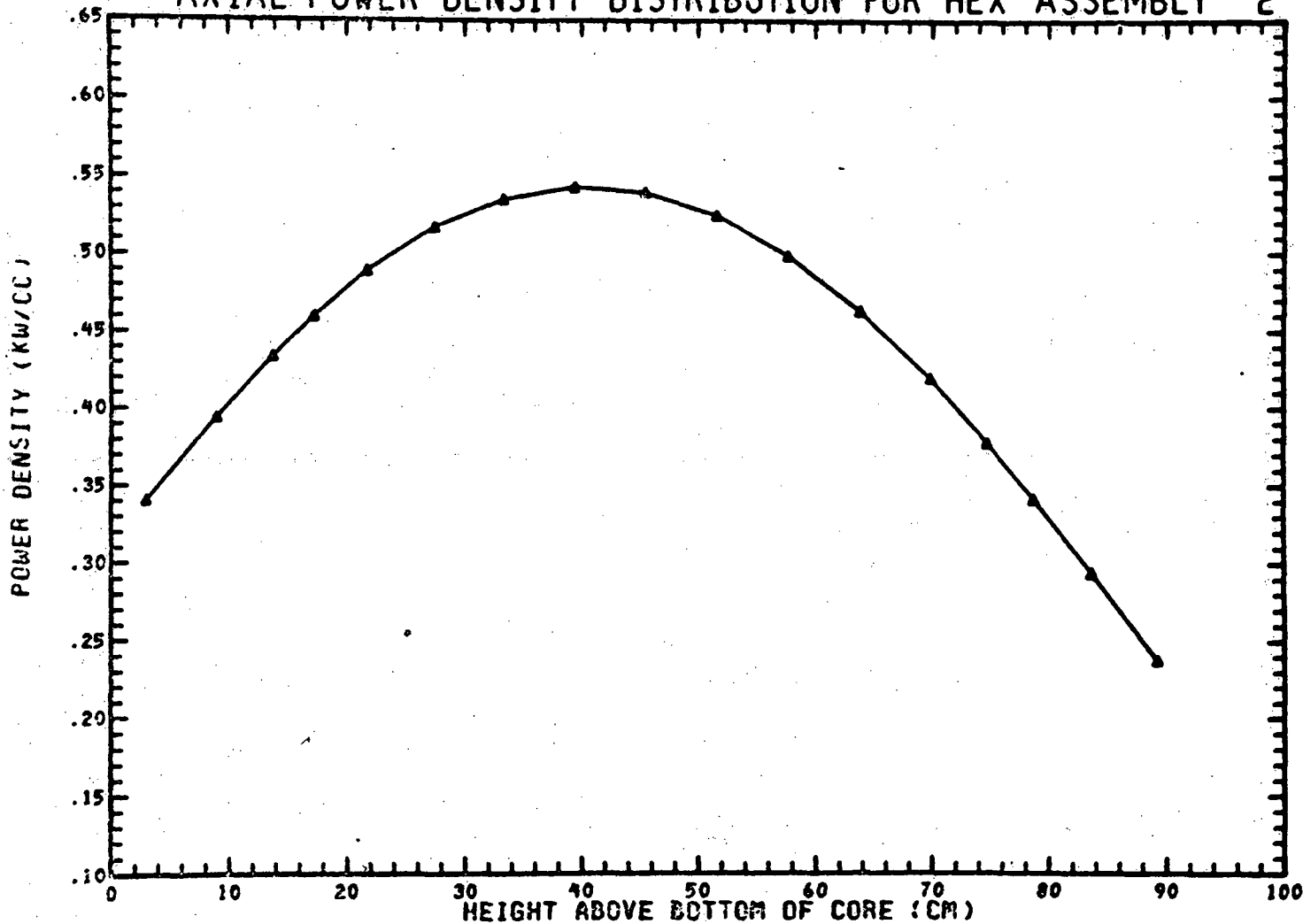
Q001.488-3

Amend. 60
Feb. 1981

FIGURE Q001.488-3

(BEGINNING OF EQUILIBRIUM CYCLE)

AXIAL POWER DENSITY DISTRIBUTION FOR HEX ASSEMBLY 2



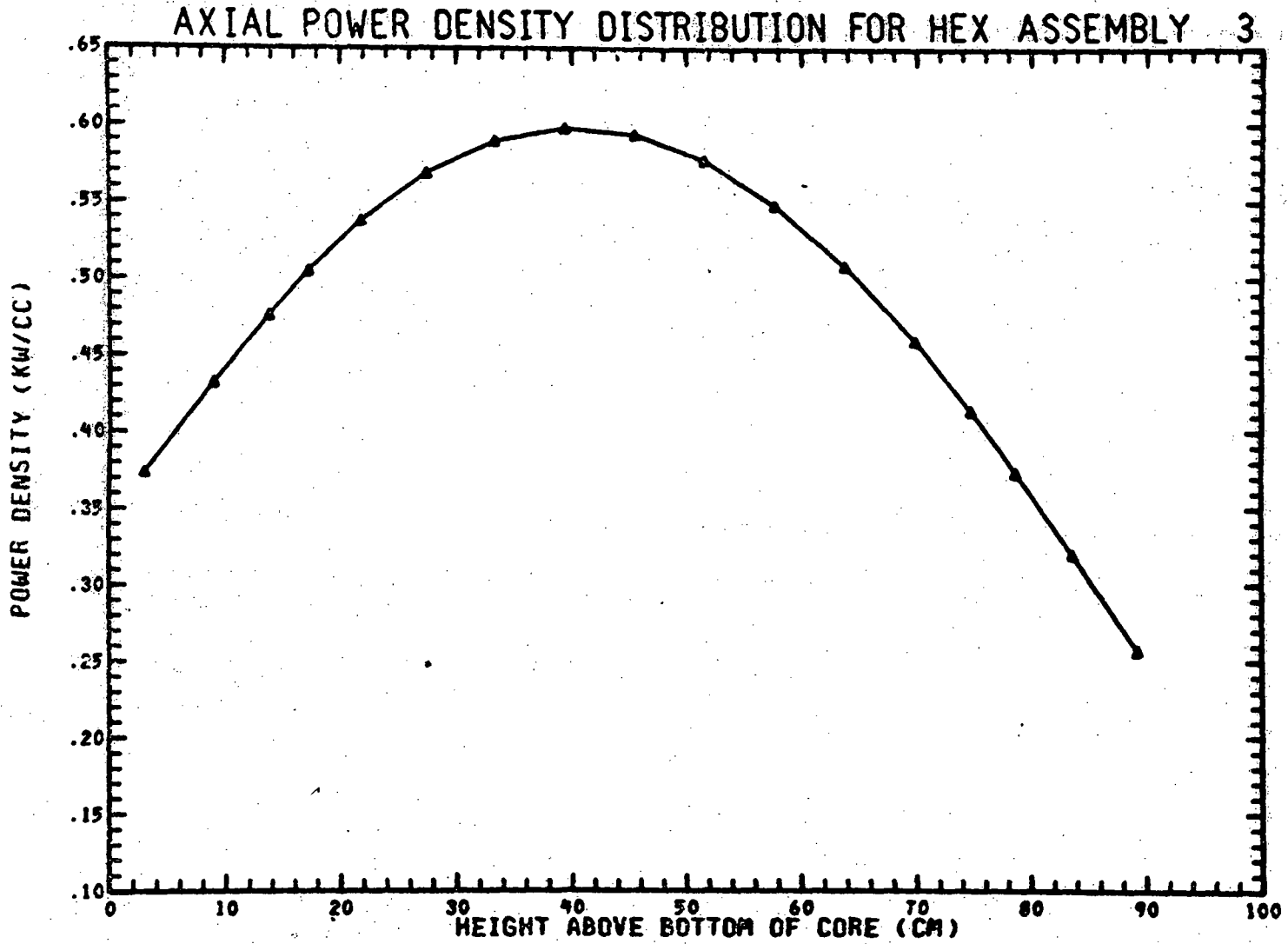
TOTAL POWER FOR THIS ASSEMBLY= .5192E+01 MEGAWATTS

Q001.488-4

Amend. 60
Feb. 1981

FIGURE Q001.488-4

(BEGINNING OF EQUILIBRIUM CYCLE)



Q001.488-5

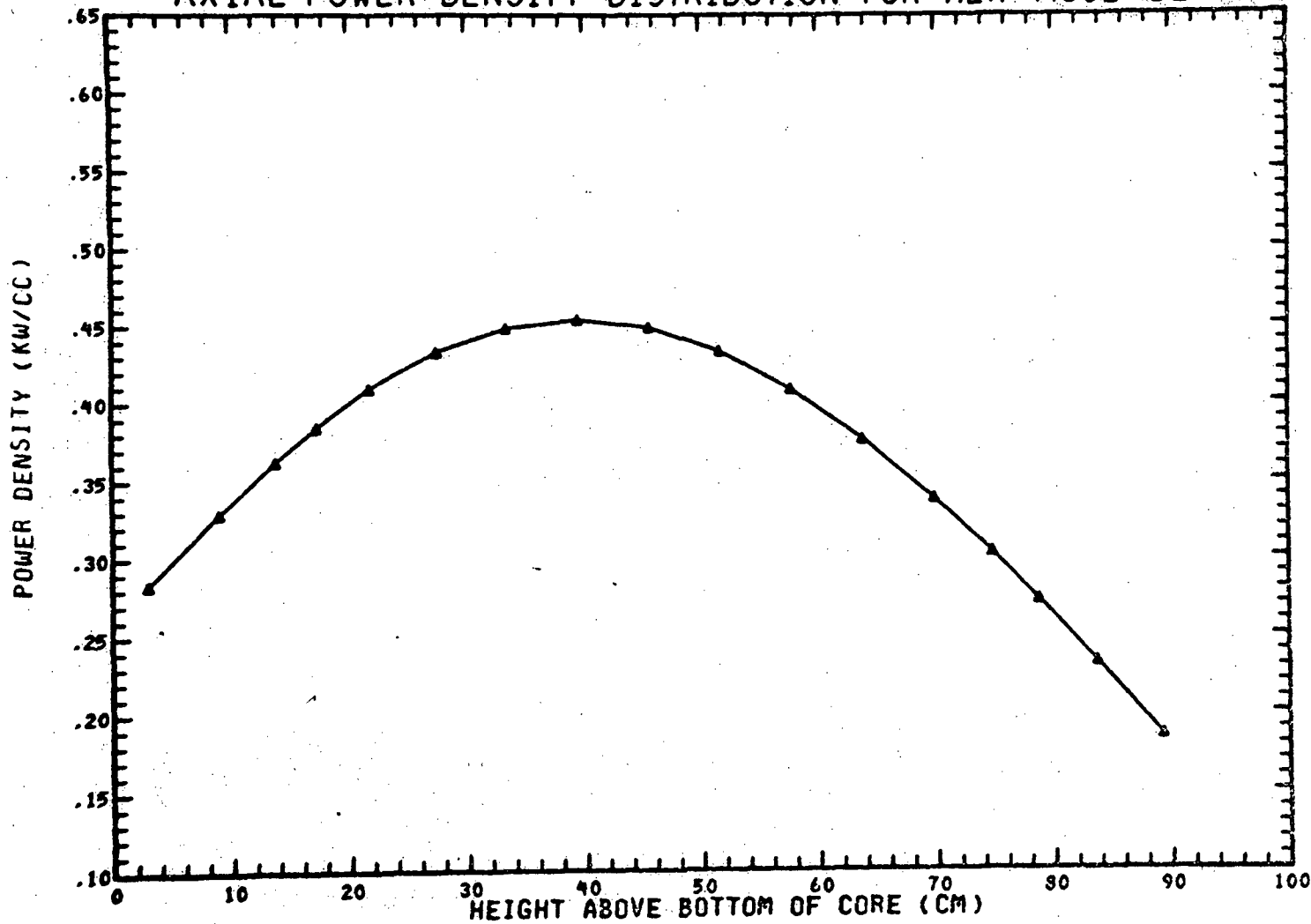
Amend. 60
Feb. 1981

TOTAL POWER FOR THIS ASSEMBLY= .5697E+01 MEGAWATTS

FIGURE Q001.488-5

(BEGINNING OF EQUILIBRIUM CYCLE)

AXIAL POWER DENSITY DISTRIBUTION FOR HEX ASSEMBLY 4



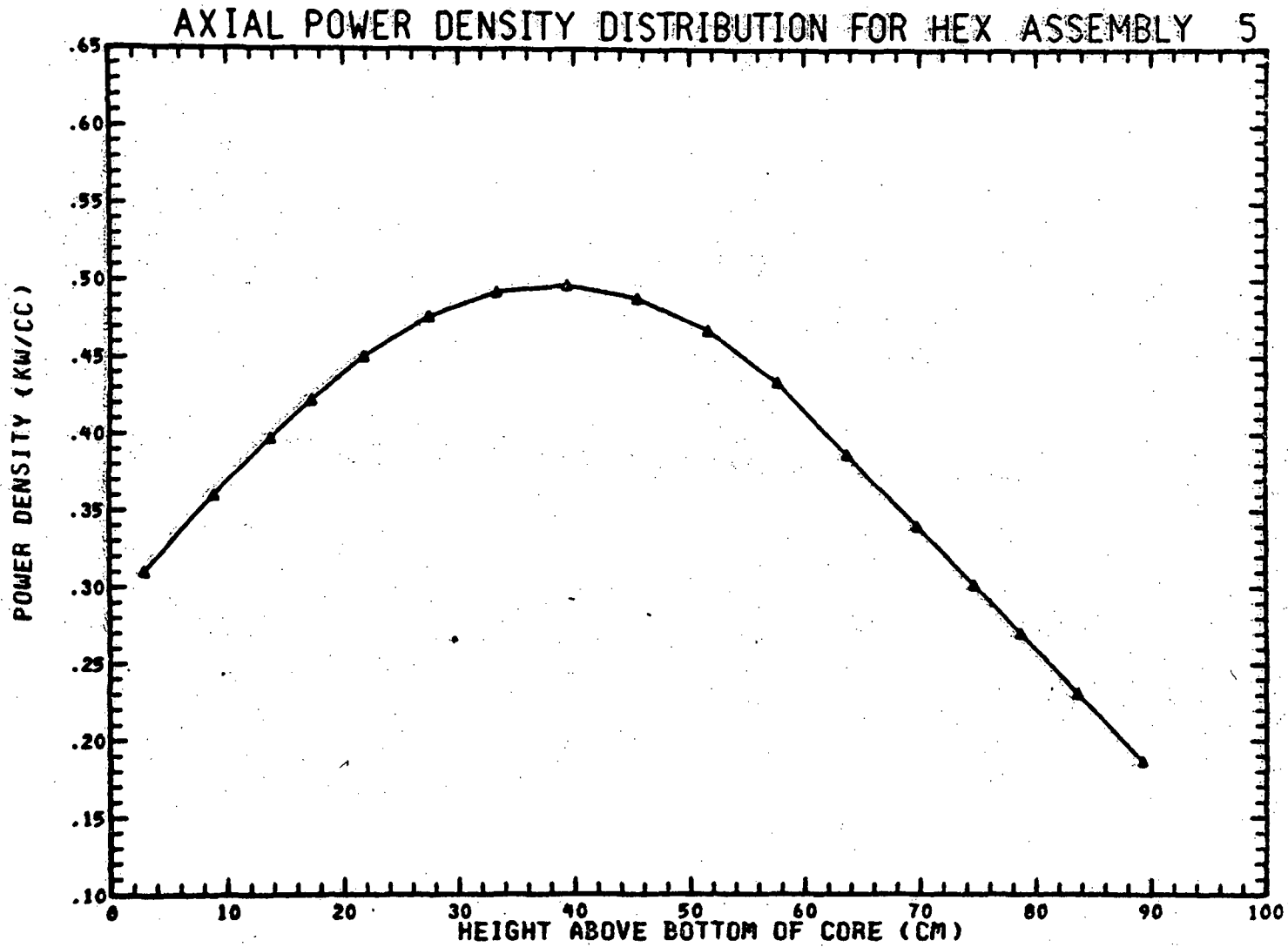
TOTAL POWER FOR THIS ASSEMBLY= .4275E+01 MEGAWATTS

Q001.488-6

Amend. 60
Feb. 1981

FIGURE Q001.488-6

(BEGINNING OF EQUILIBRIUM CYCLE)



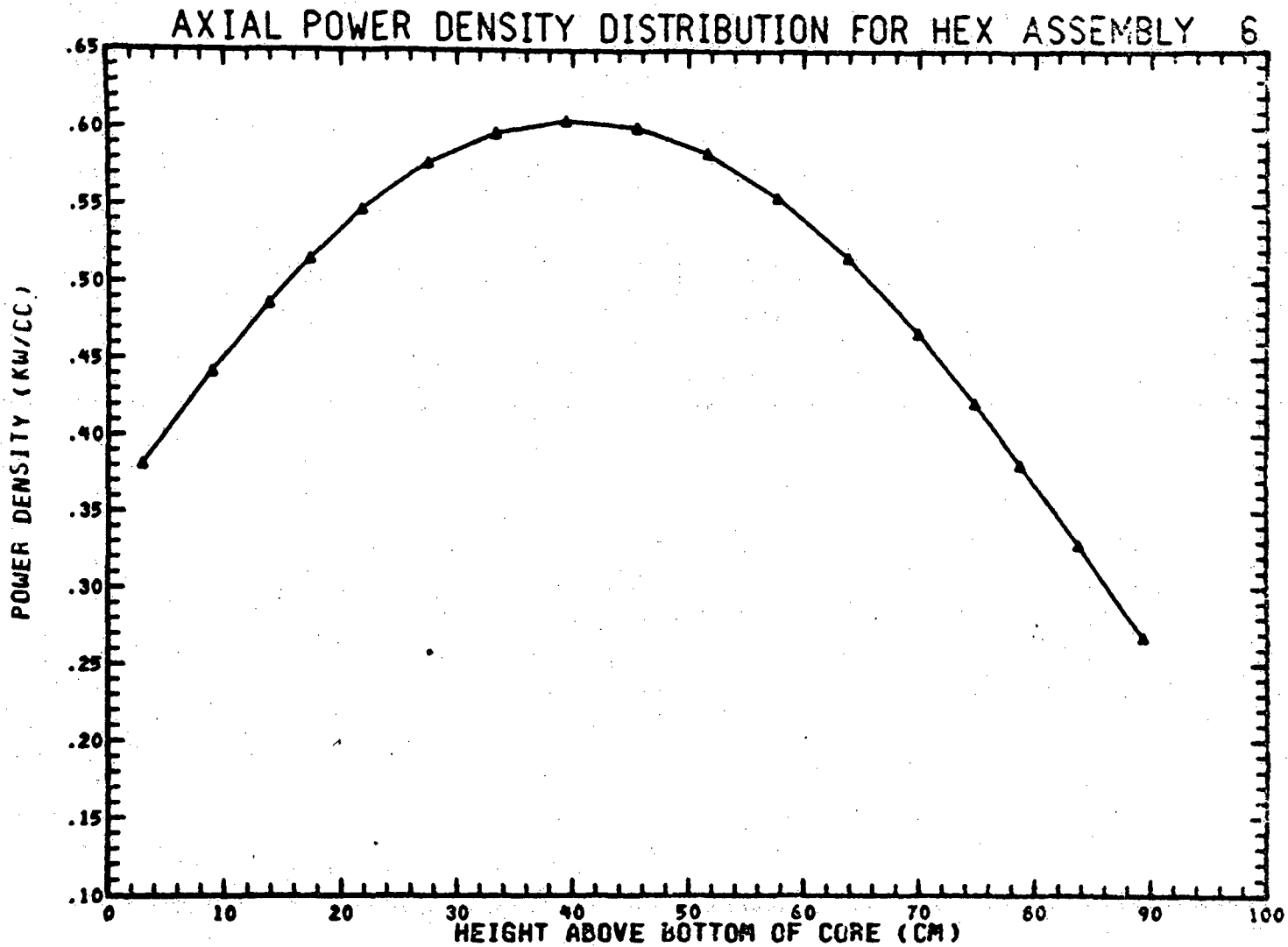
TOTAL POWER FOR THIS ASSEMBLY= .4570E+01 MEGAWATTS

Q001.488-7

Amend. 60
Feb. 1981

FIGURE Q001.488-7

(BEGINNING OF EQUILIBRIUM CYCLE)



TOTAL POWER FOR THIS ASSEMBLY= .5793E+01 MEGAWATTS

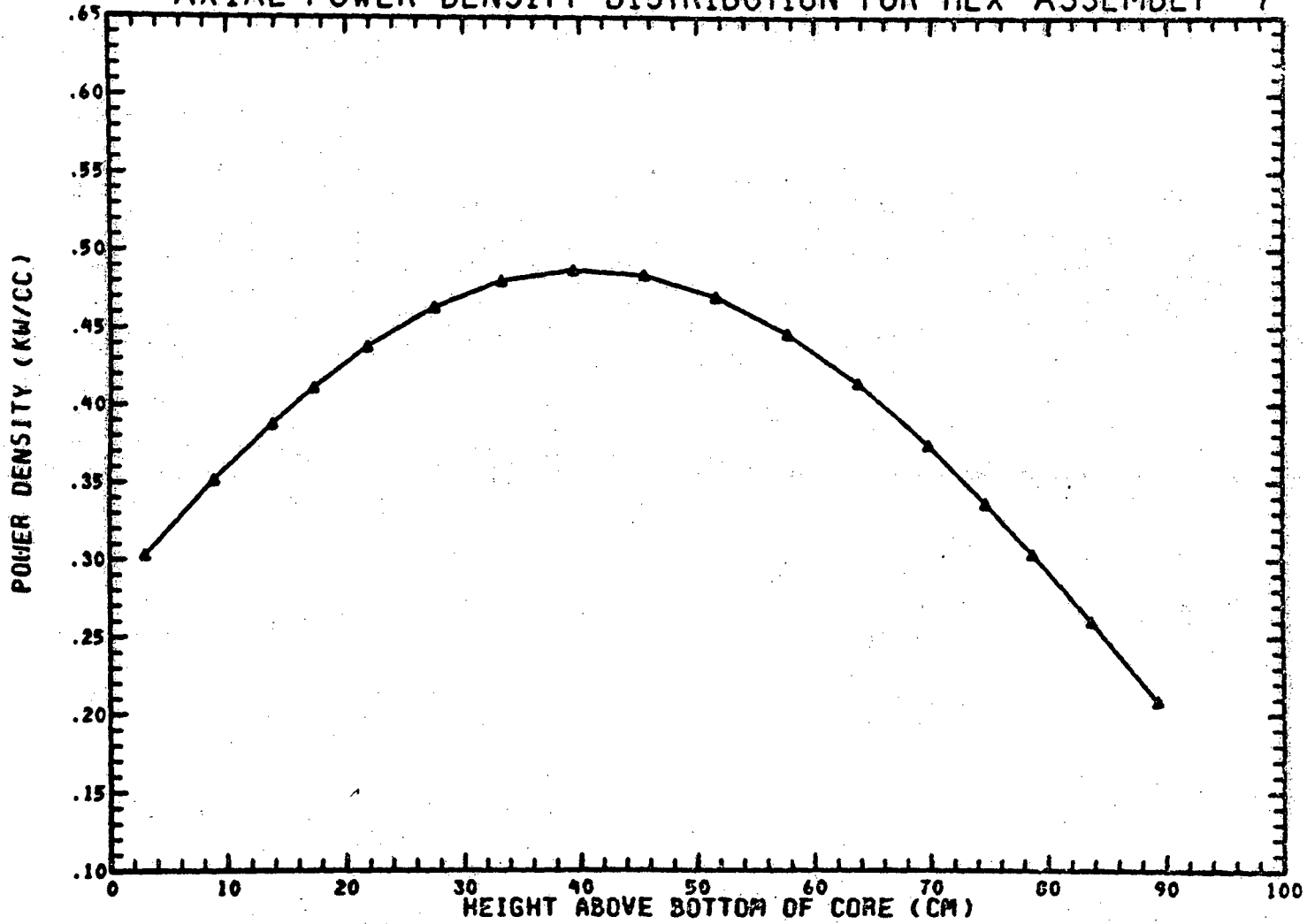
Q001.488-8

Amend. 60
Feb. 1981

FIGURE Q001.488-8

(BEGINNING OF EQUILIBRIUM CYCLE)

AXIAL POWER DENSITY DISTRIBUTION FOR HEX ASSEMBLY 7



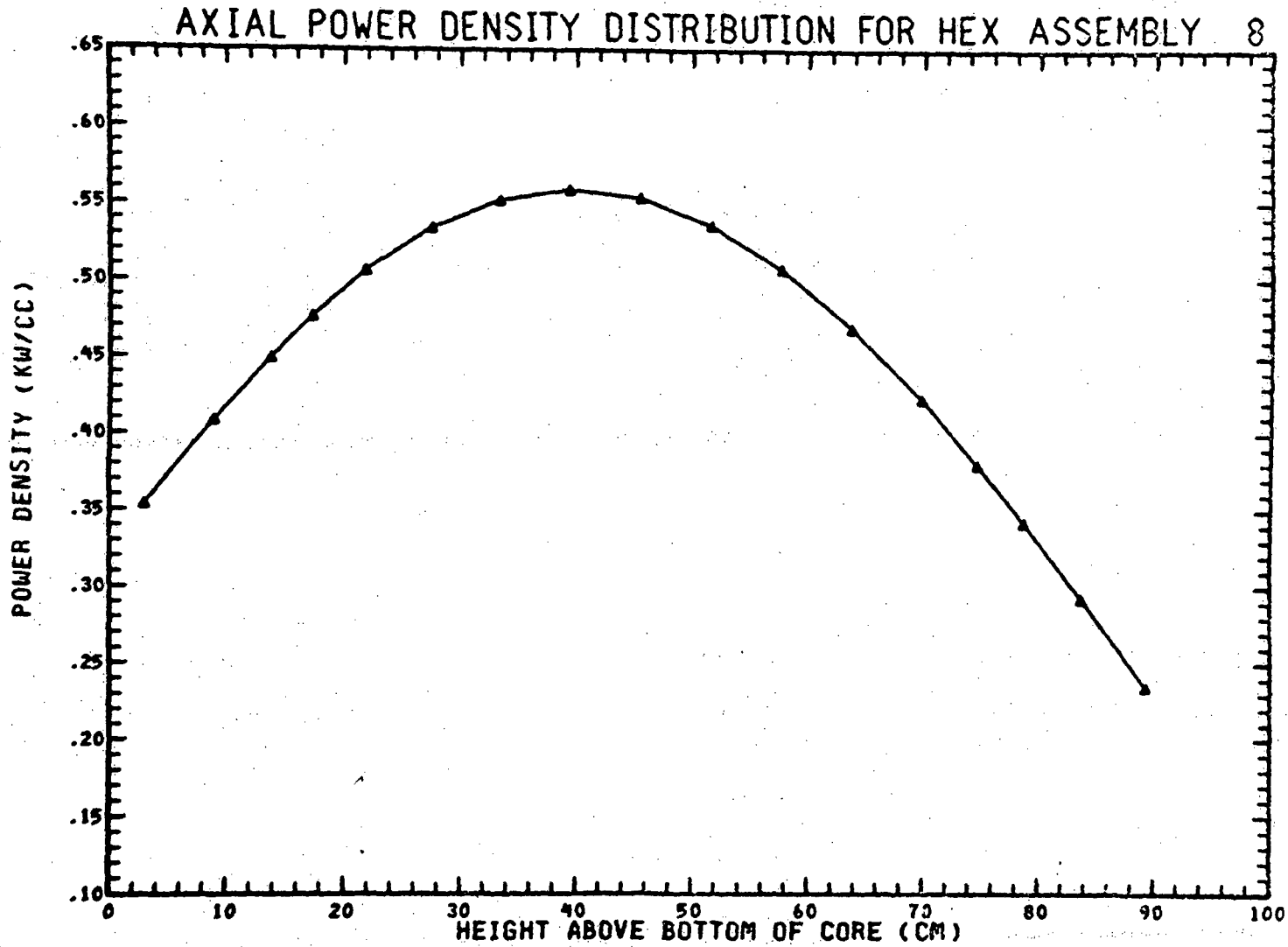
TOTAL POWER FOR THIS ASSEMBLY= .4639E+01 MEGAWATTS

Q001.488-9

Amend. 60
Feb. 1981

FIGURE Q001.488-9

(BEGINNING OF EQUILIBRIUM CYCLE)



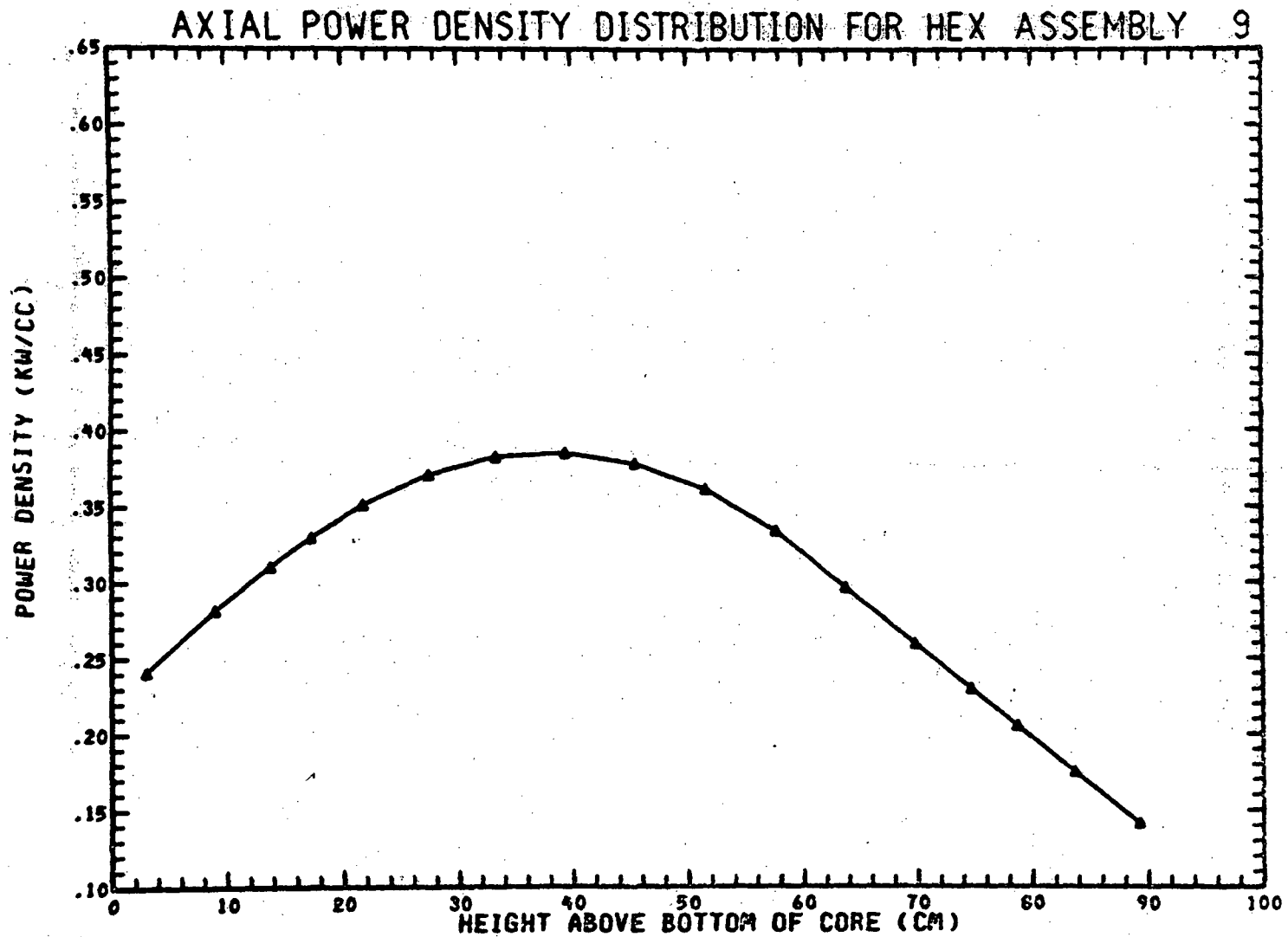
TOTAL POWER FOR THIS ASSEMBLY= .5309E+01 MEGAWATTS

Q001.488-10

Amend. 60
Feb. 1981

FIGURE Q001.488-10

(BEGINNING OF EQUILIBRIUM CYCLE)



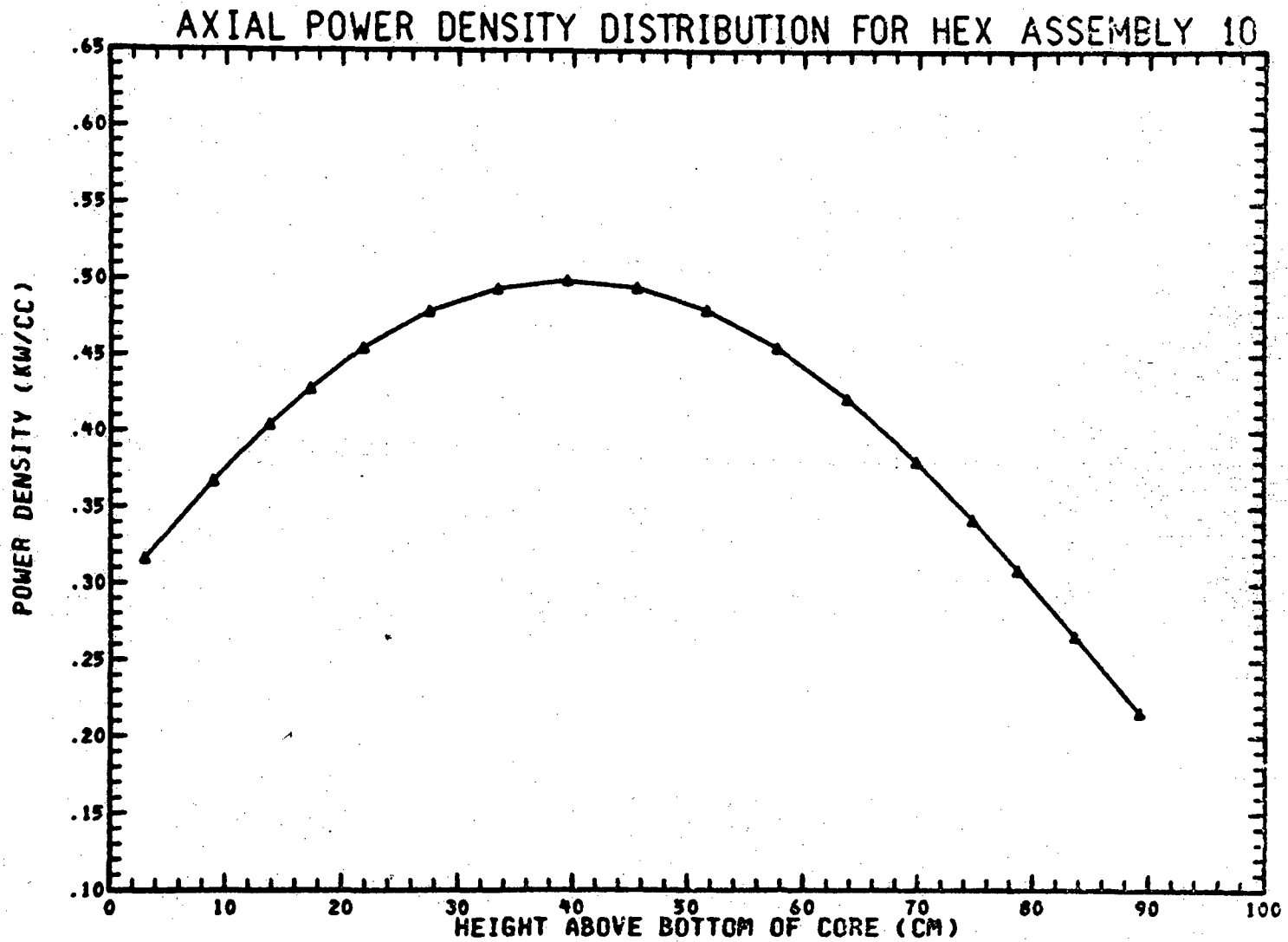
TOTAL POWER FOR THIS ASSEMBLY = .3533E+01 MEGAWATTS

Q001.488-11

Amend. 60
Feb. 1981

FIGURE Q001.488-11

(BEGINNING OF EQUILIBRIUM CYCLE)



Q001.488-12

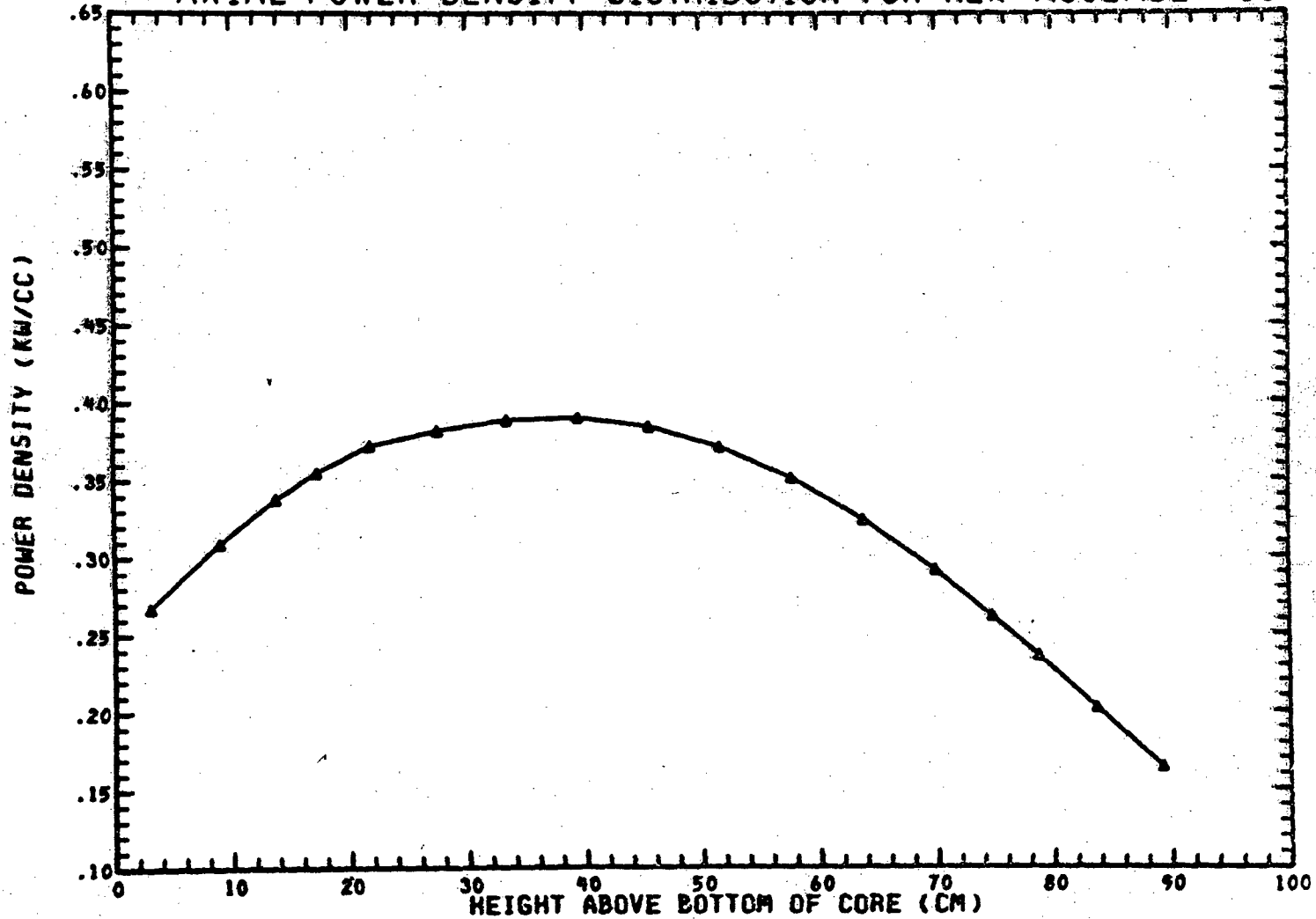
Amend. 60
Feb. 1981

TOTAL POWER FOR THIS ASSEMBLY= .4769E+01 MEGAWATTS

FIGURE Q001.488-12

(BEGINNING OF EQUILIBRIUM CYCLE)

AXIAL POWER DENSITY DISTRIBUTION FOR HEX ASSEMBLY 11



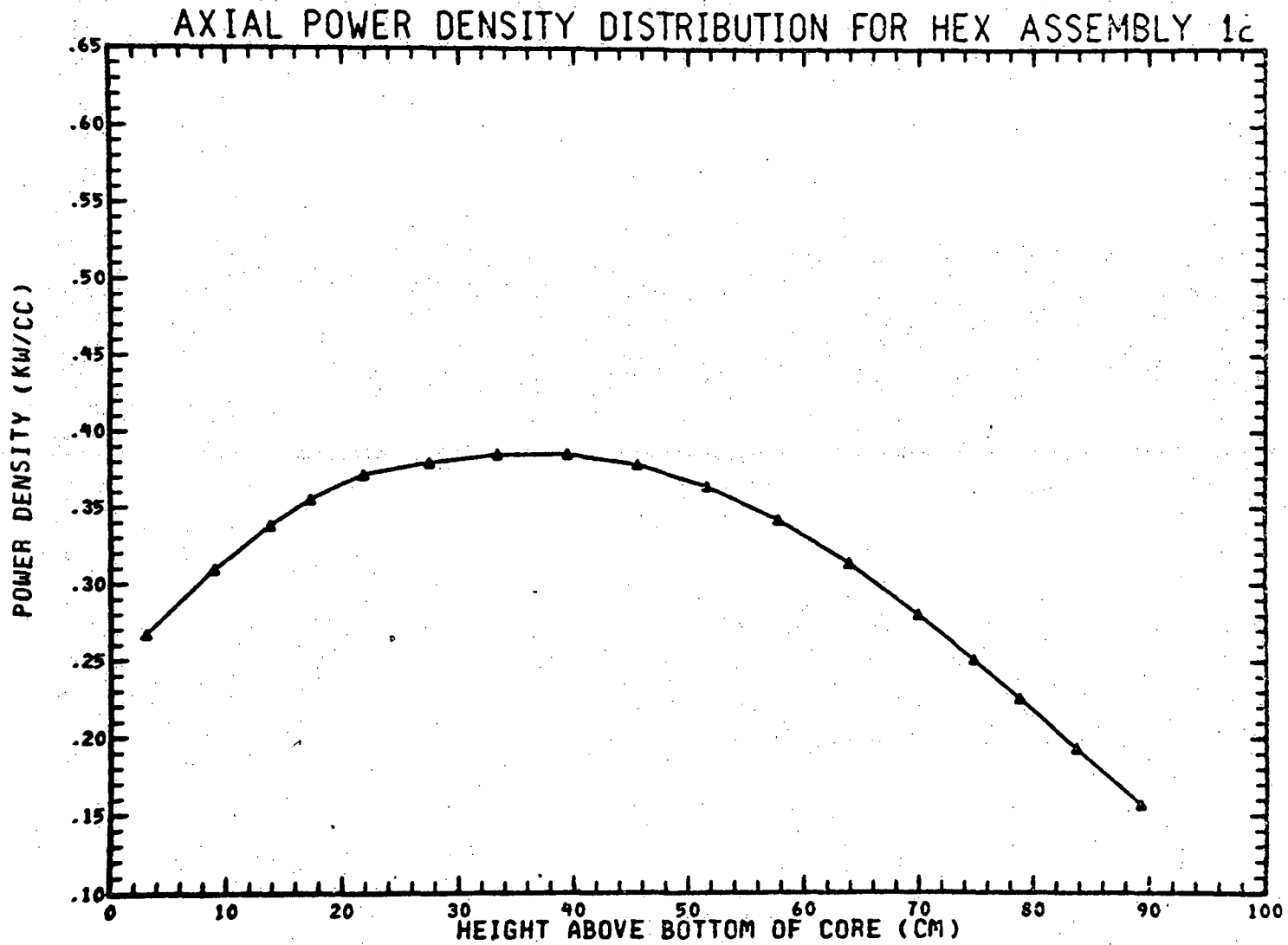
TOTAL POWER FOR THIS ASSEMBLY = .3768E+01 MEGAWATTS

Q001.488-13

Amend. 60
Feb. 1981

FIGURE Q001.488-13

(BEGINNING OF EQUILIBRIUM CYCLE)



TOTAL POWER FOR THIS ASSEMBLY= .3704E+01 MEGAWATTS

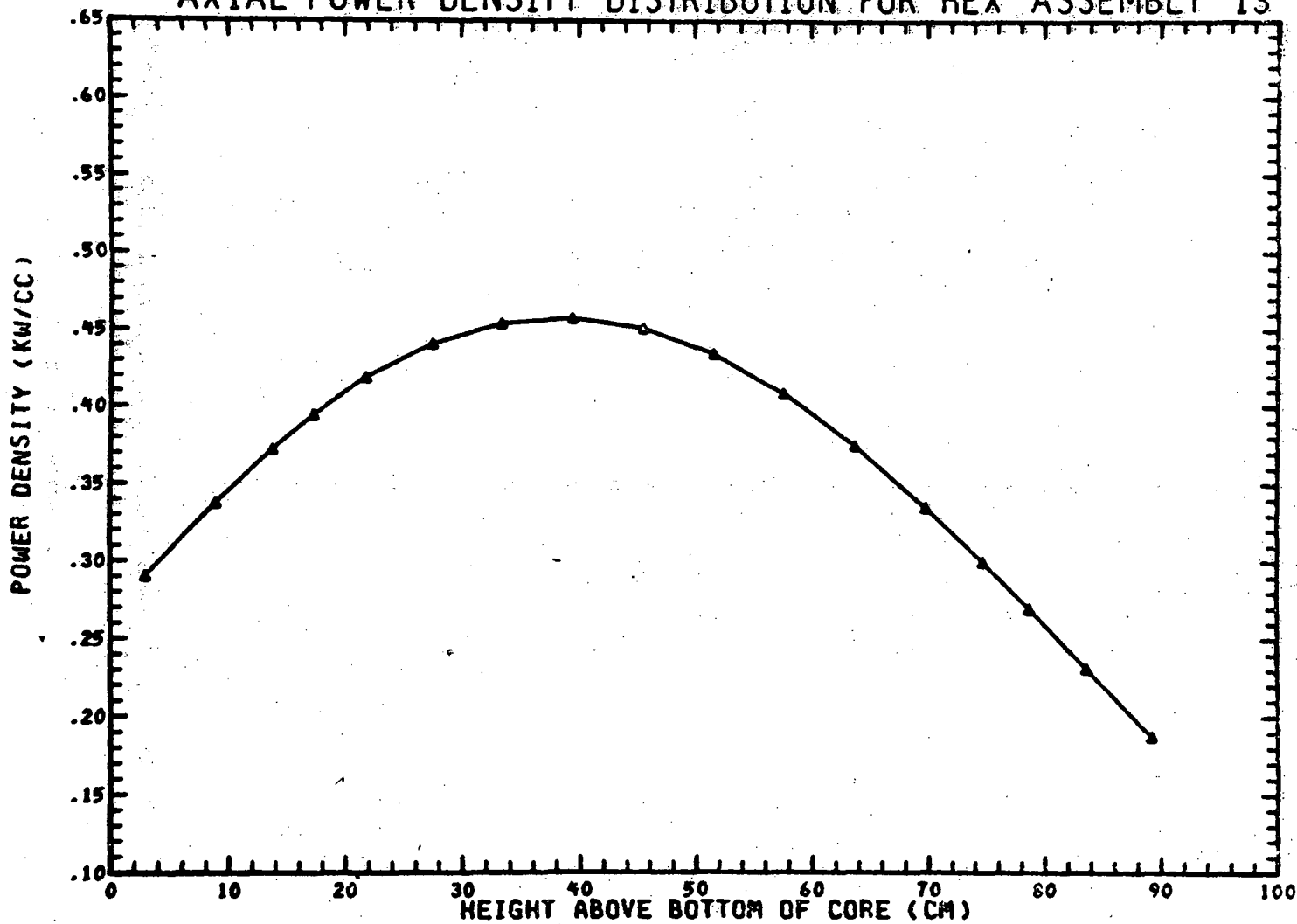
Q001.488-14

Amend. 60
Feb. 1981

FIGURE Q001.488-14

(BEGINNING OF EQUILIBRIUM CYCLE)

AXIAL POWER DENSITY DISTRIBUTION FOR HEX ASSEMBLY 13



TOTAL POWER FOR THIS ASSEMBLY= .4314E+01 MEGAWATTS

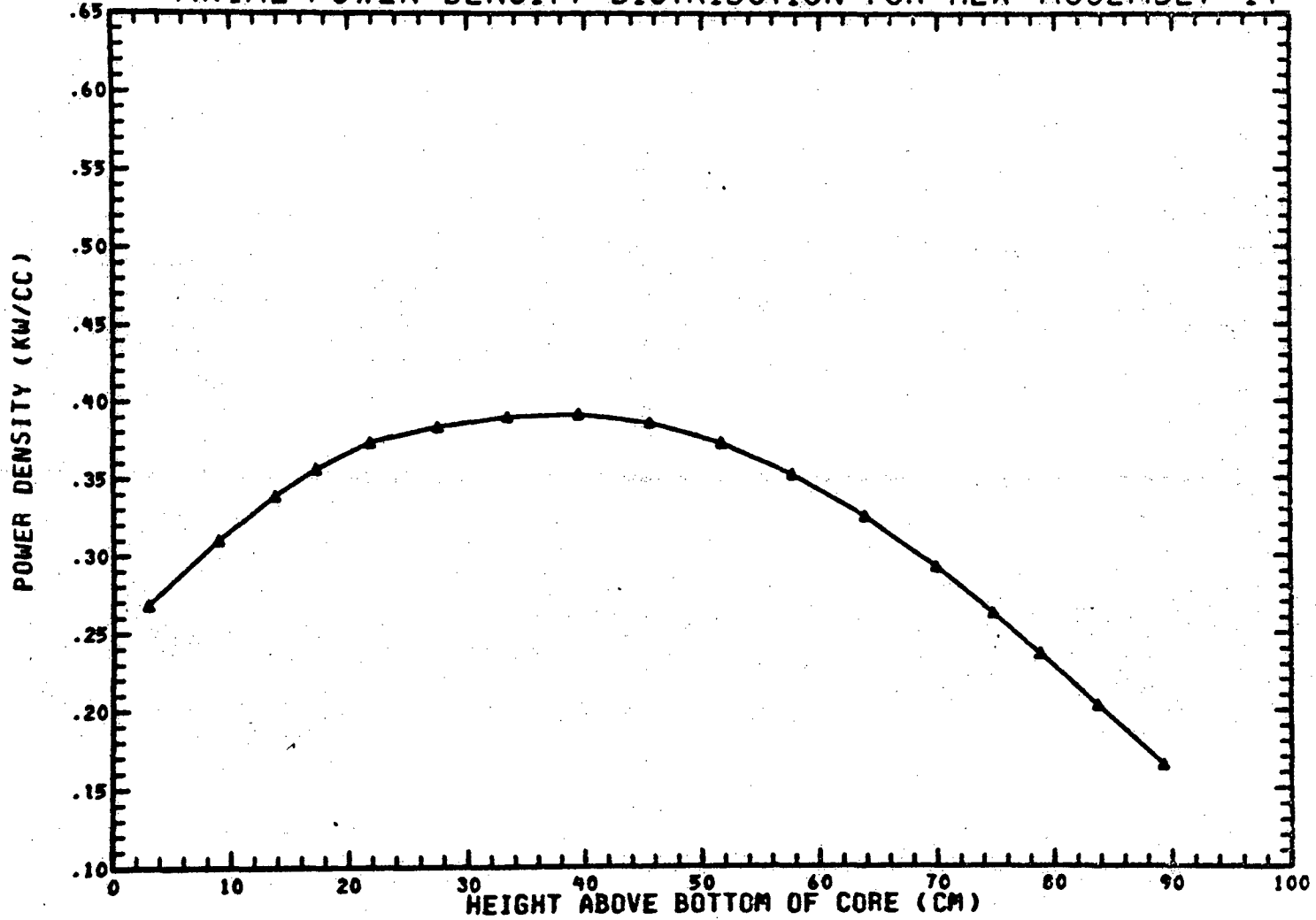
Q001.488-15

Amend. 60
Feb. 1981

FIGURE Q001.488-15

(BEGINNING OF EQUILIBRIUM CYCLE)

AXIAL POWER DENSITY DISTRIBUTION FOR HEX ASSEMBLY 14



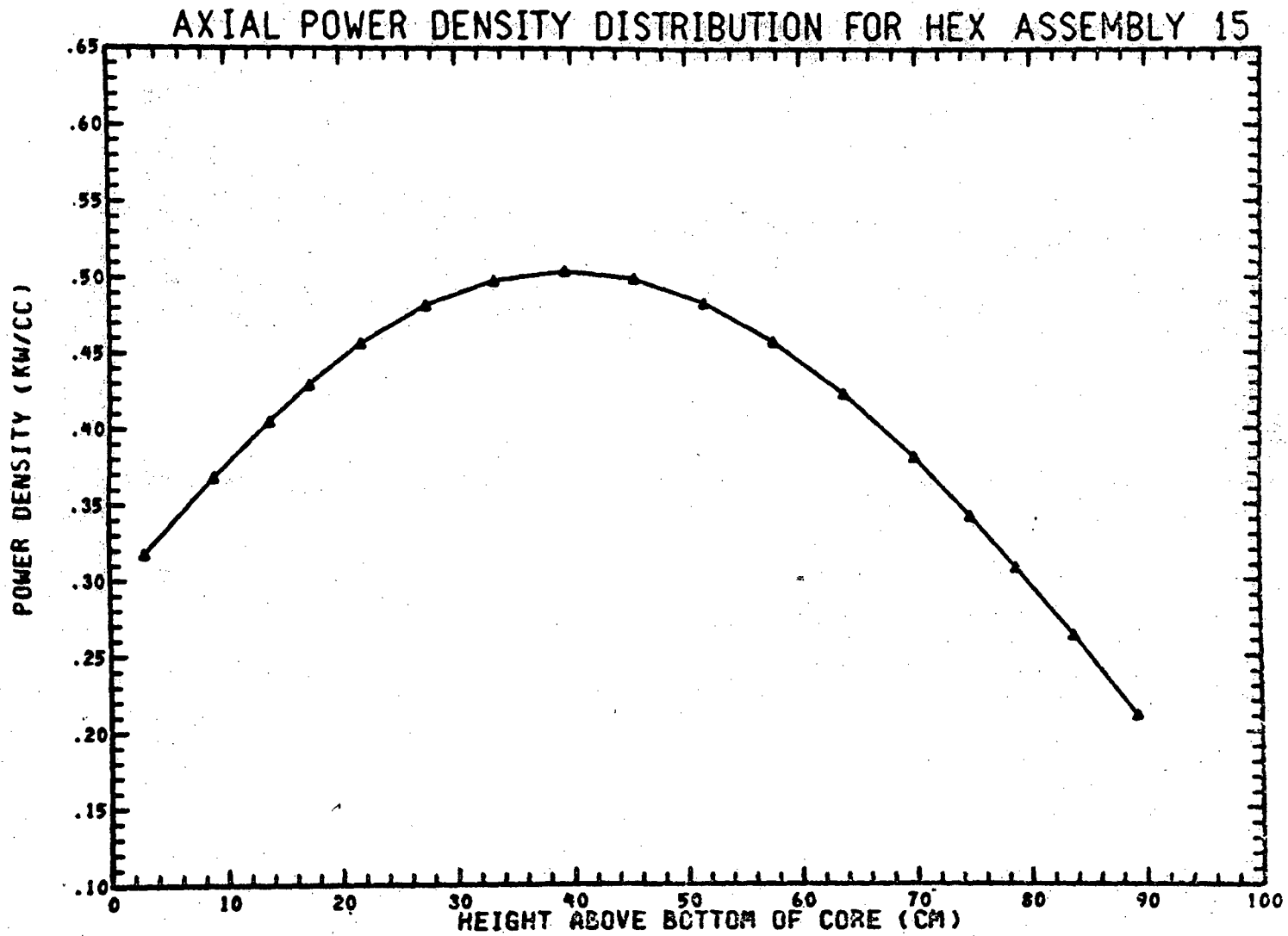
TOTAL POWER FOR THIS ASSEMBLY = .3783E+01 MEGAWATTS

Q001.488-16

Amend. 60
Feb. 1981

FIGURE Q001.488-16

(BEGINNING OF EQUILIBRIUM CYCLE)



TOTAL POWER FOR THIS ASSEMBLY= .4786E+01 MEGAWATTS

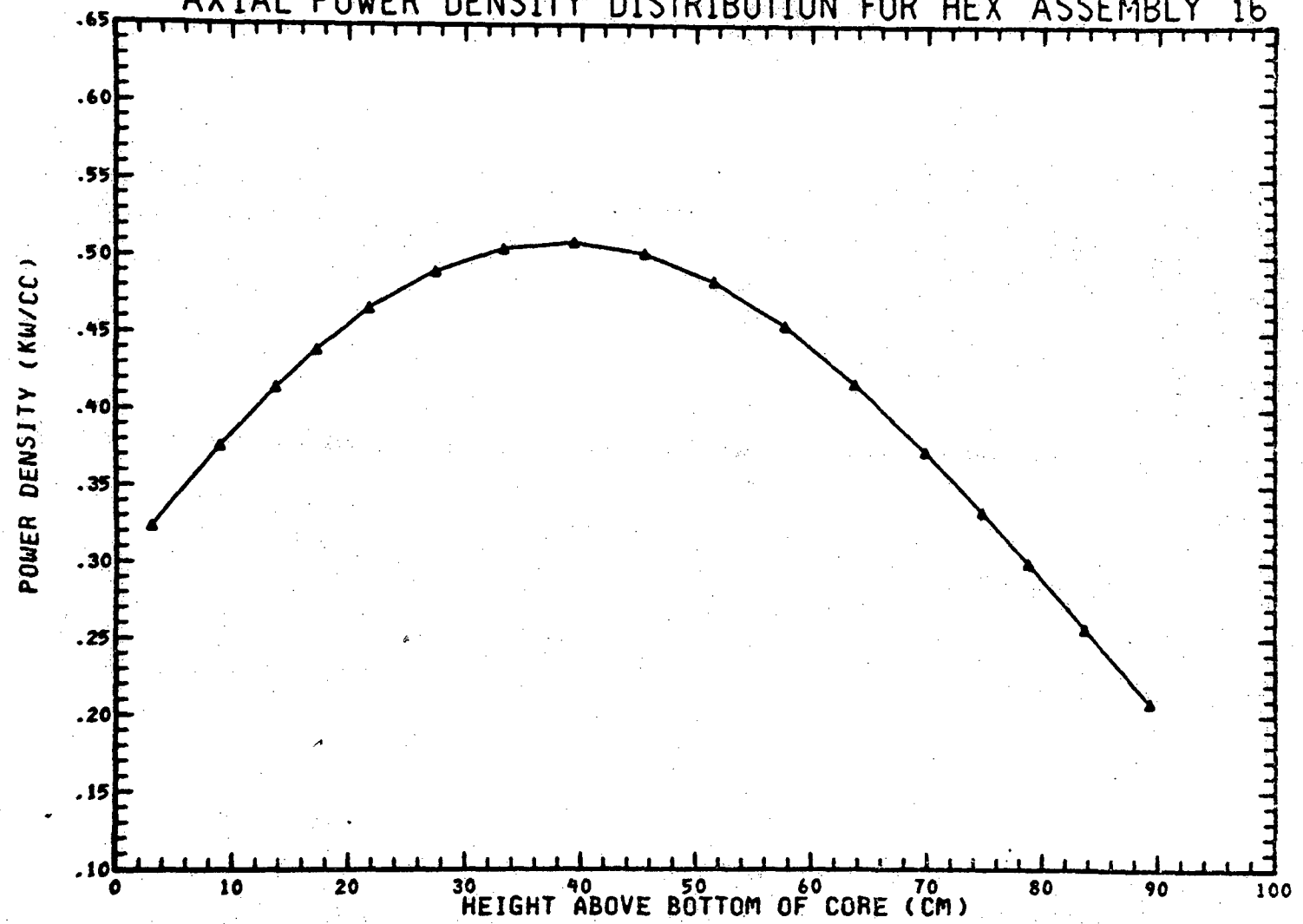
Q001.488-17

Amend. 60
Feb. 1981

FIGURE Q001.488-17

(BEGINNING OF EQUILIBRIUM CYCLE)

AXIAL POWER DENSITY DISTRIBUTION FOR HEX ASSEMBLY 16



TOTAL POWER FOR THIS ASSEMBLY= .4801E+01 MEGAWATTS

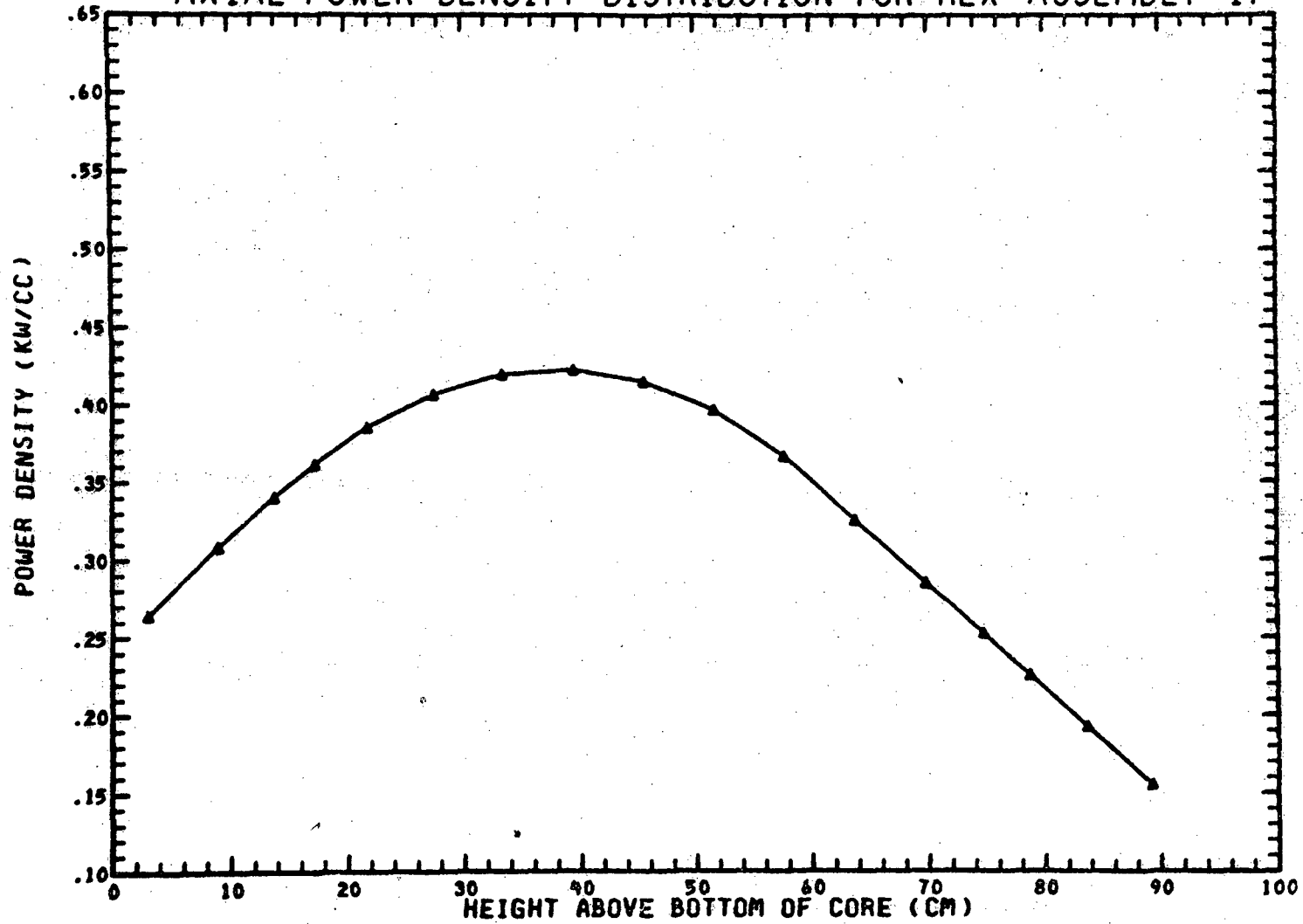
Q001.488-18

Amend. 60
Feb. 1981

FIGURE Q001.488-18

(BEGINNING OF EQUILIBRIUM CYCLE)

AXIAL POWER DENSITY DISTRIBUTION FOR HEX ASSEMBLY 17



TOTAL POWER FOR THIS ASSEMBLY= .3874E+01 MEGAWATTS

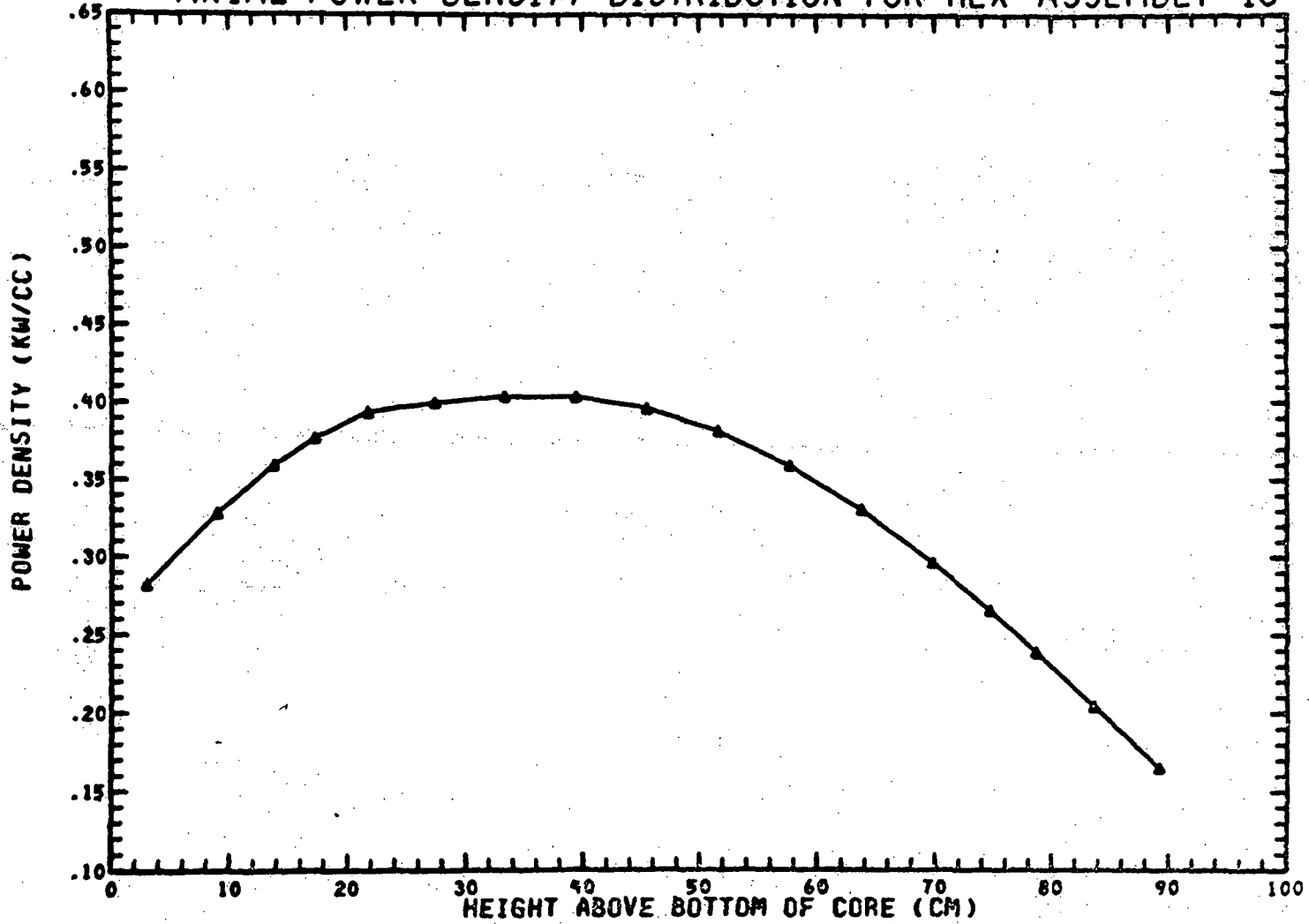
Q001.488-19

Amend. 60
Feb. 1981

FIGURE Q001.488-19

(BEGINNING OF EQUILIBRIUM CYCLE)

AXIAL POWER DENSITY DISTRIBUTION FOR HEX ASSEMBLY 18



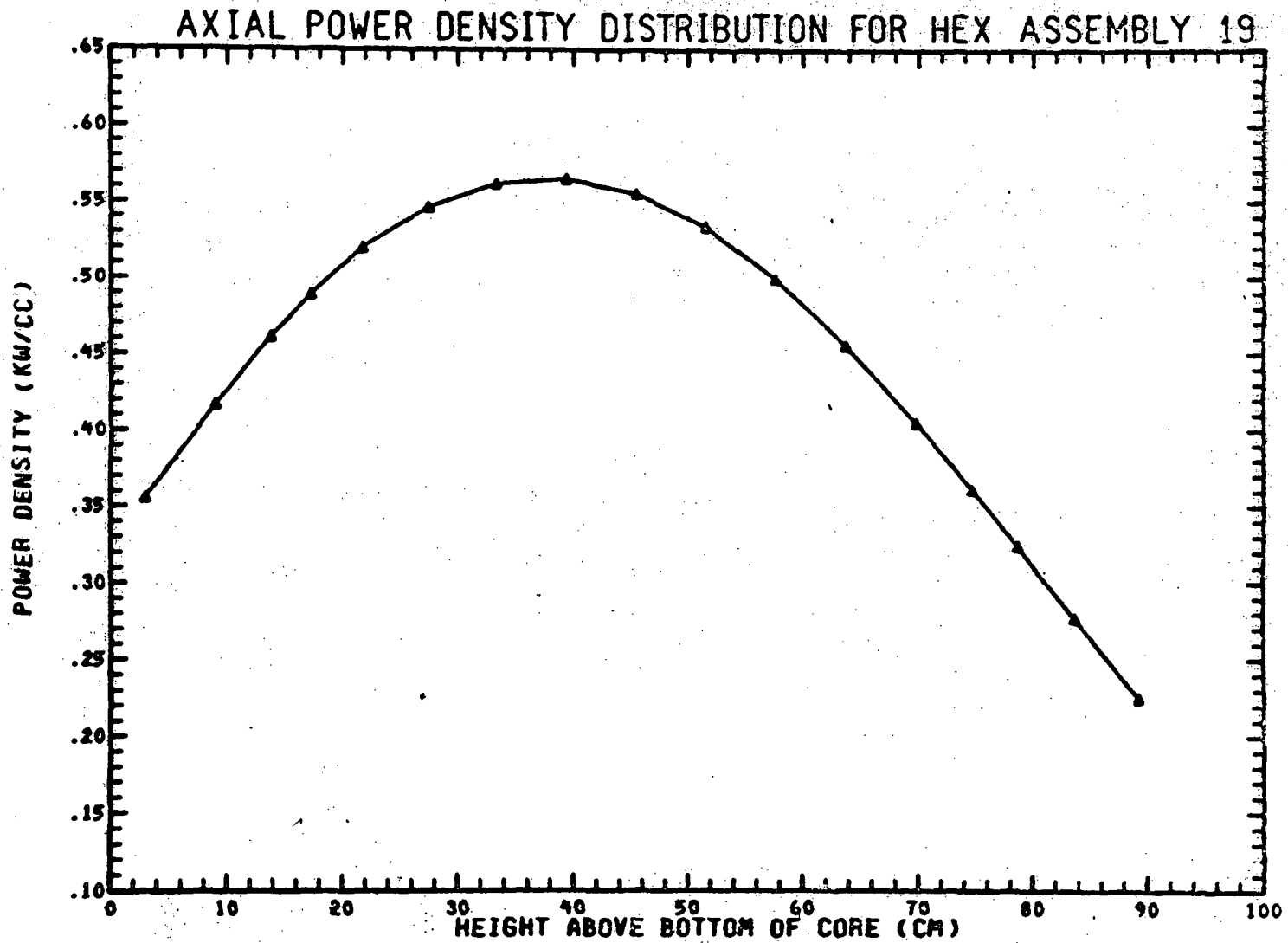
TOTAL POWER FOR THIS ASSEMBLY= .3900E+01 MEGAWATTS

Q001.488-20

Amend. 60
Feb. 1981

FIGURE Q001.488-20

(BEGINNING OF EQUILIBRIUM CYCLE)



Q001.488-21

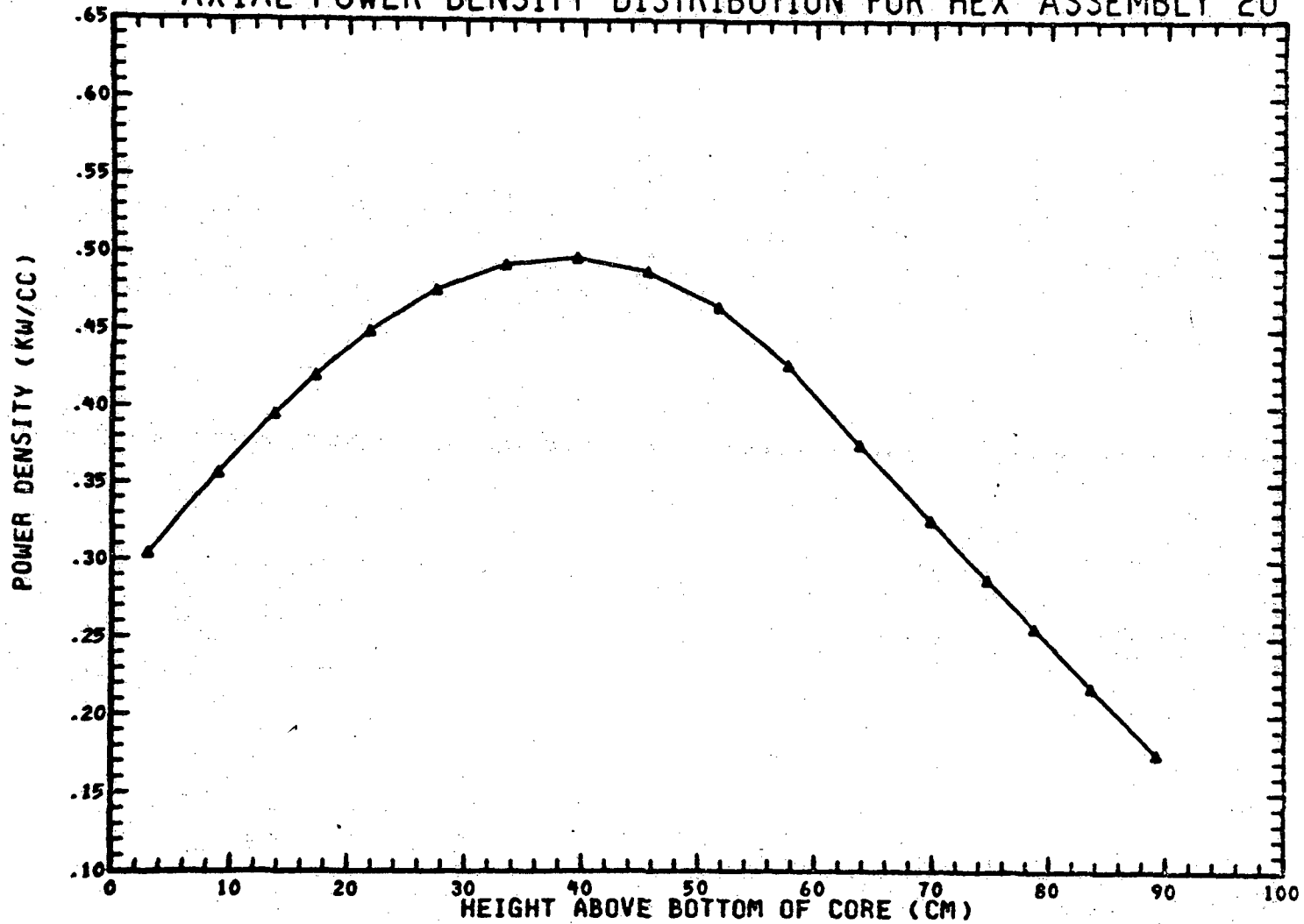
Amend. 60
Feb. 1981

TOTAL POWER FOR THIS ASSEMBLY = .5290E+01 MEGAWATTS

FIGURE Q001.488-21

(BEGINNING OF EQUILIBRIUM CYCLE)

AXIAL POWER DENSITY DISTRIBUTION FOR HEX ASSEMBLY 20



Q001.488-21

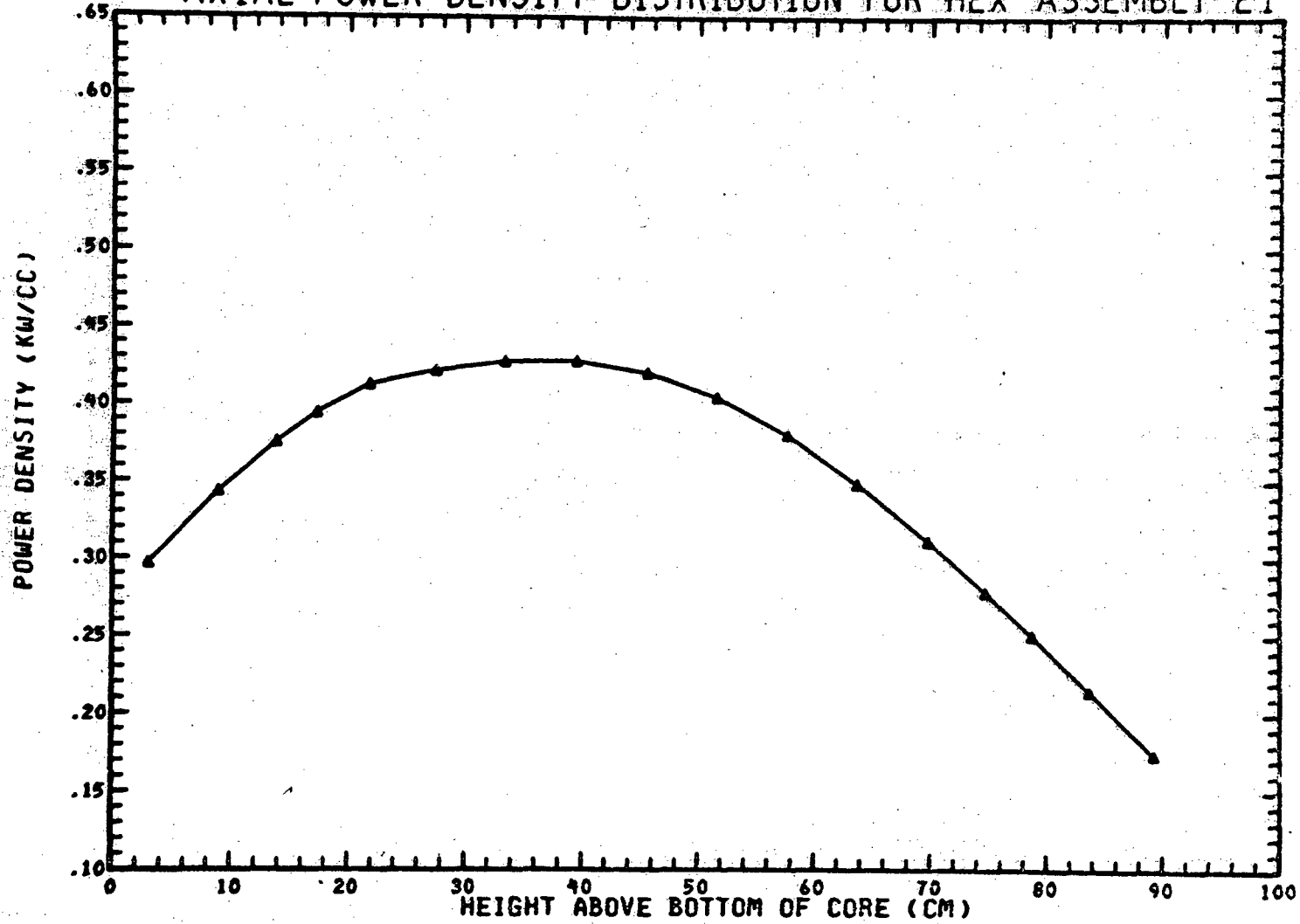
Amend. 60
Feb. 1981

TOTAL POWER FOR THIS ASSEMBLY= .4498E+01 MEGAWATTS

FIGURE Q001.488-22

(BEGINNING OF EQUILIBRIUM CYCLE)

AXIAL POWER DENSITY DISTRIBUTION FOR HEX ASSEMBLY 21



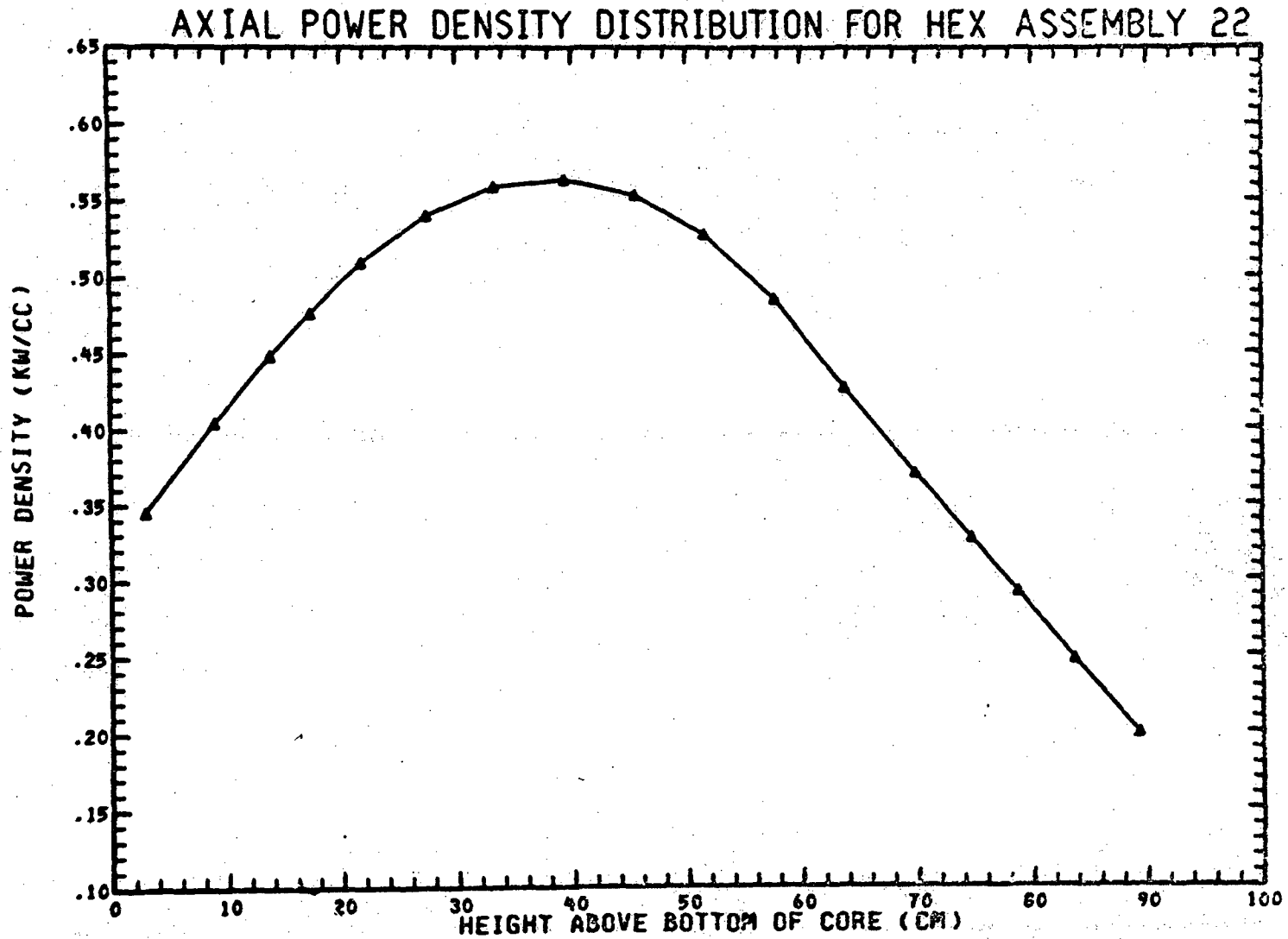
TOTAL POWER FOR THIS ASSEMBLY= .4111E+01 MEGAWATTS

Q001.488-23

Amend. 60
Feb. 1981

FIGURE Q001.488-23

(BEGINNING OF EQUILIBRIUM CYCLE)



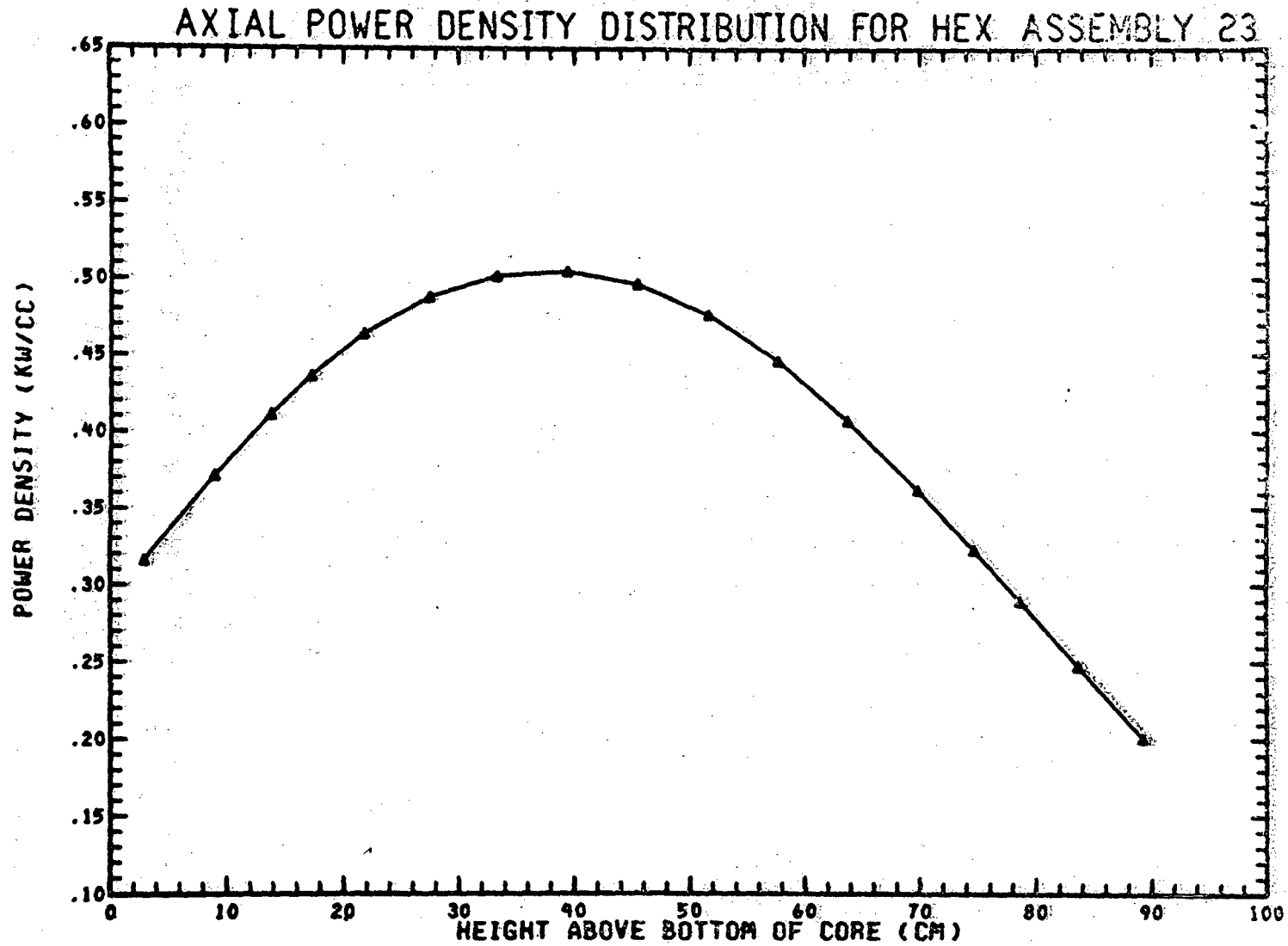
Q001.488-24

Amend. 60
Feb. 1981

TOTAL POWER FOR THIS ASSEMBLY= .5107E+01 MEGAWATTS

FIGURE Q001.488-24.

(BEGINNING OF EQUILIBRIUM CYCLE)



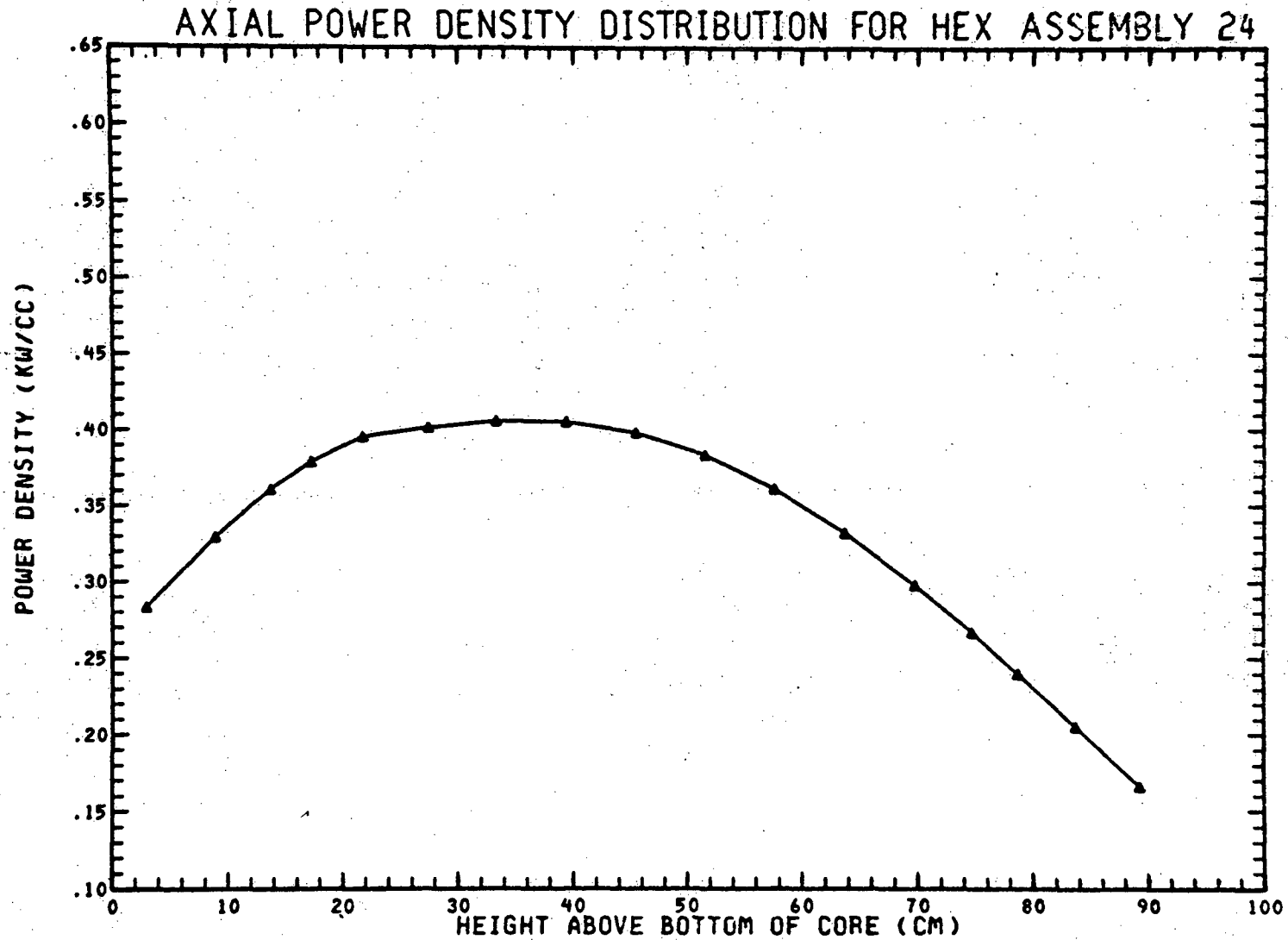
TOTAL POWER FOR THIS ASSEMBLY= .4724E+01 MEGAWATTS

Q001.488-25

Amend. 60
Feb. 1981

FIGURE Q001.488-25

(BEGINNING OF EQUILIBRIUM CYCLE)



TOTAL POWER FOR THIS ASSEMBLY= .3922E+01 MEGAWATTS

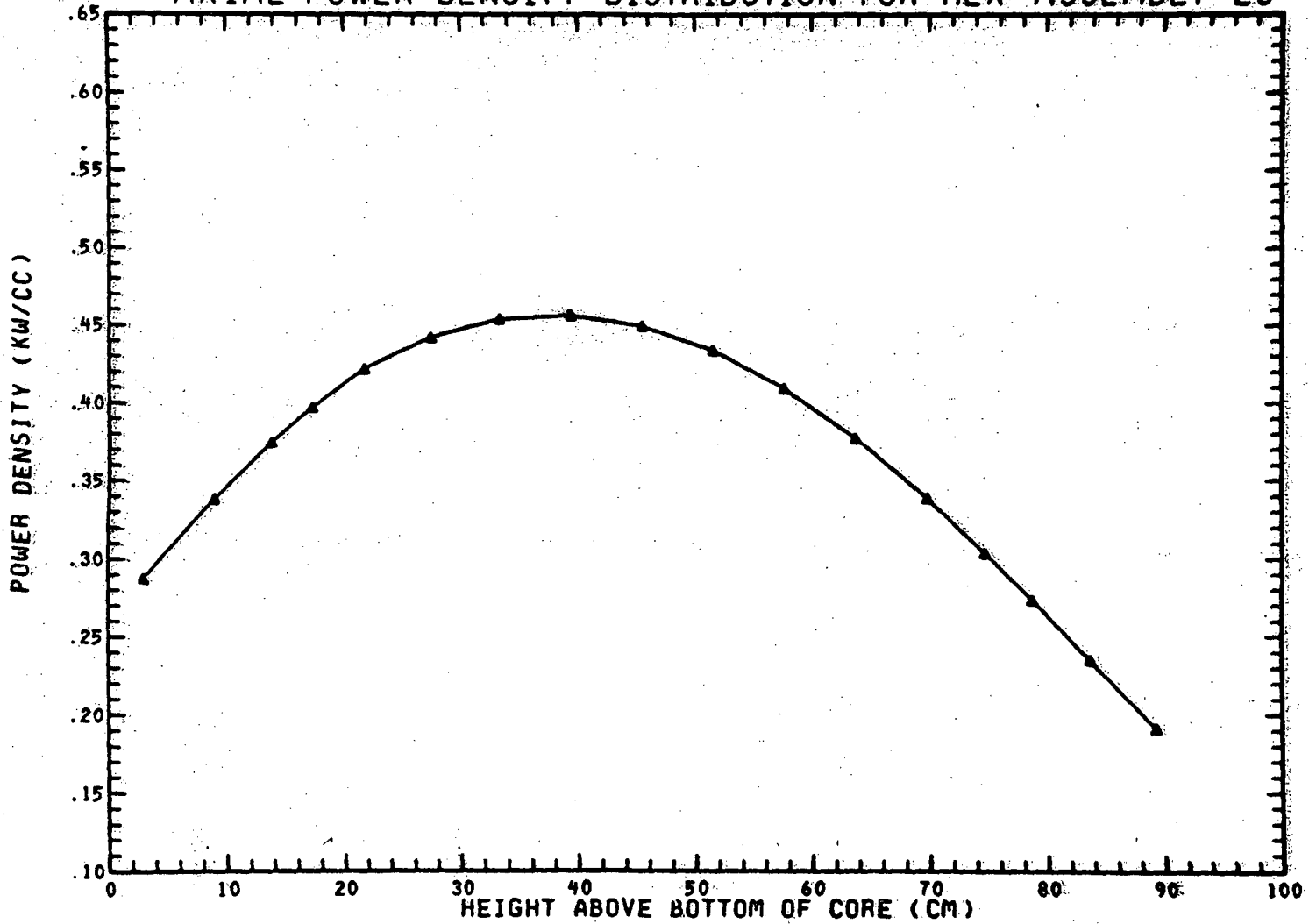
Q001.488-26

Amend. 60
Feb. 1981

FIGURE Q001.488-26

(BEGINNING OF EQUILIBRIUM CYCLE)

AXIAL POWER DENSITY DISTRIBUTION FOR HEX ASSEMBLY 25



TOTAL POWER FOR THIS ASSEMBLY= .4332E+01 MEGAWATTS

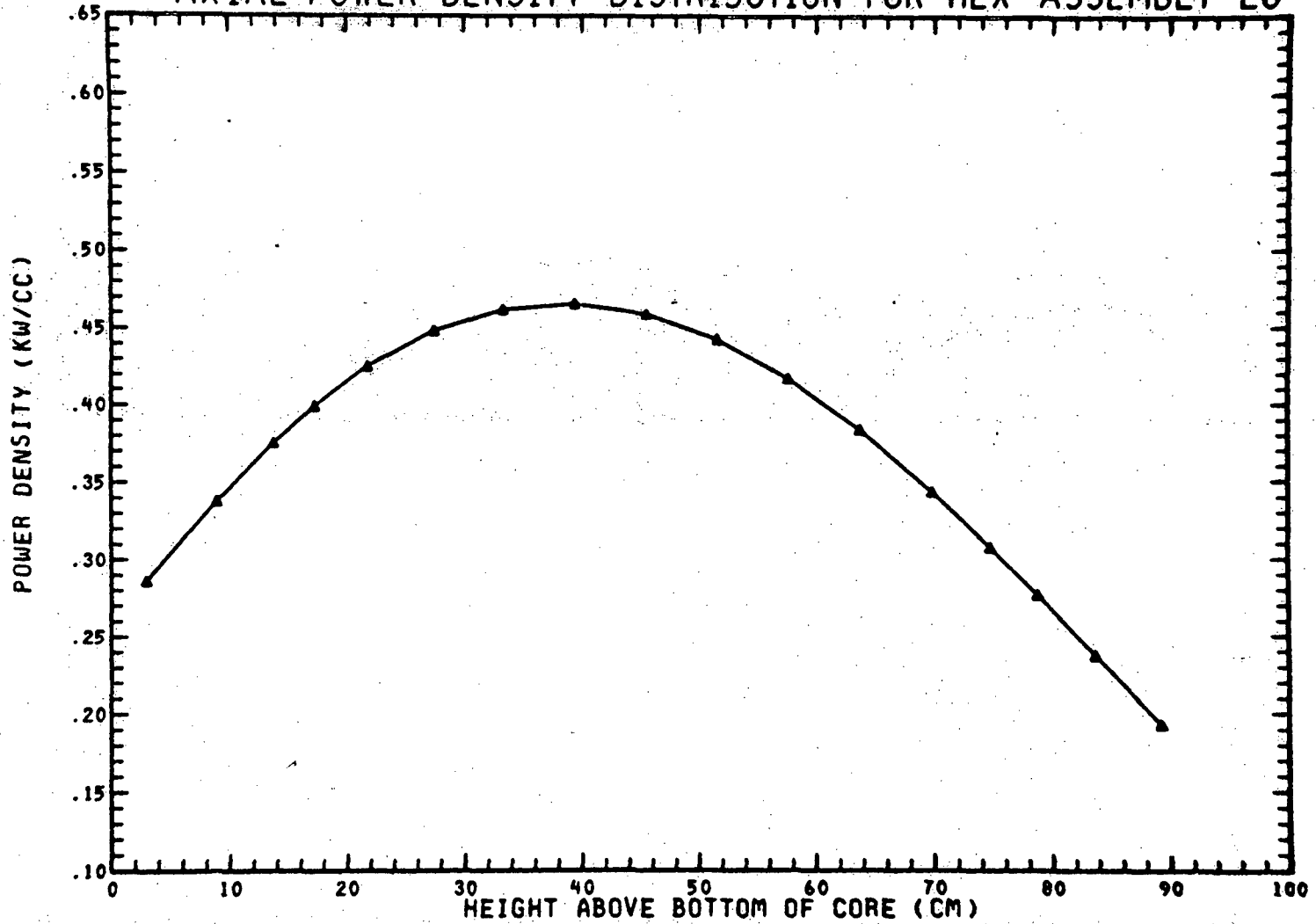
Q001.488-27

Amend. 60
Feb. 1981

FIGURE Q001.488-27

(BEGINNING OF EQUILIBRIUM CYCLE)

AXIAL POWER DENSITY DISTRIBUTION FOR HEX ASSEMBLY 26



Q001.488-28

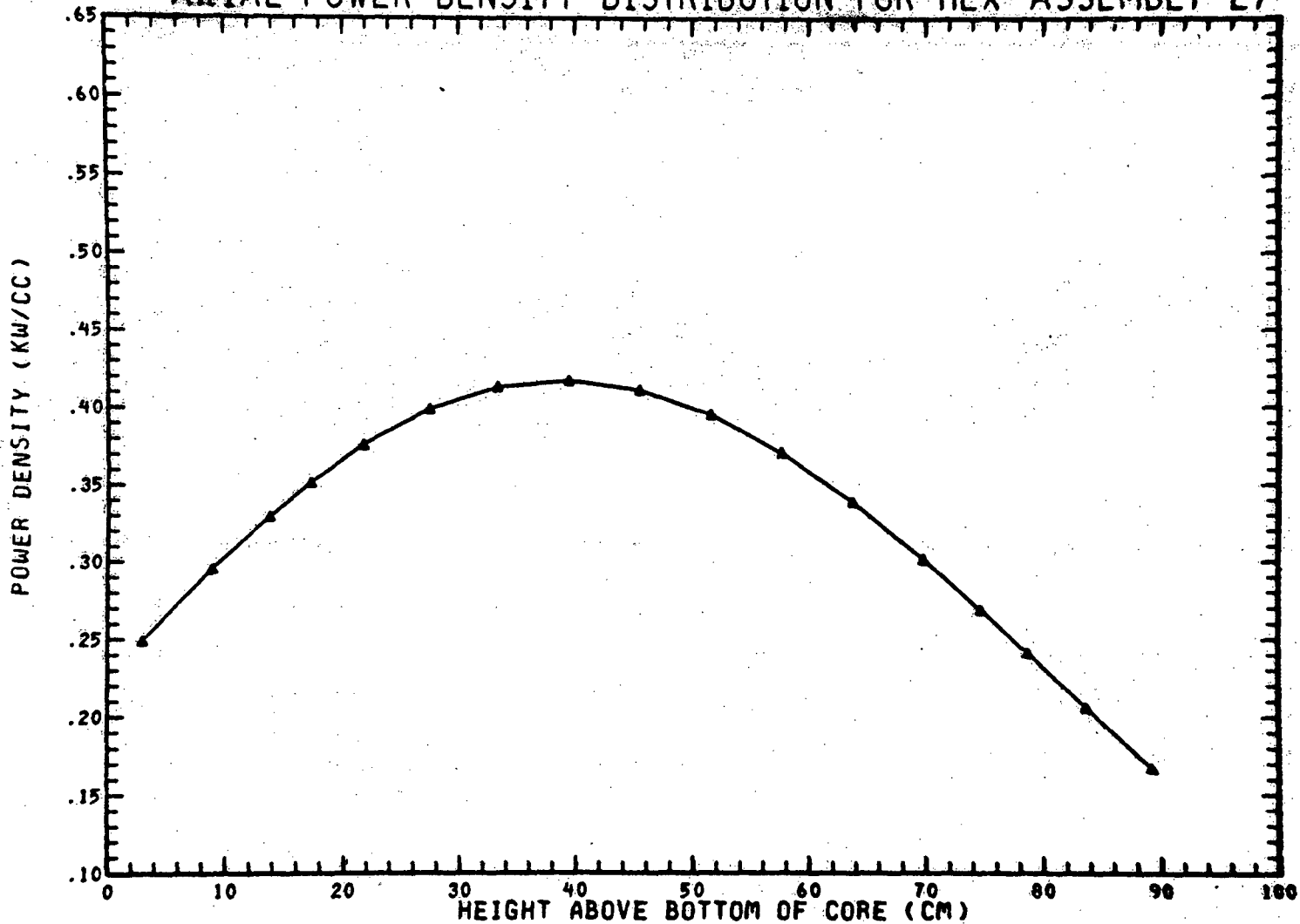
Amend. 60
Feb. 1981

TOTAL POWER FOR THIS ASSEMBLY= .4386E+01 MEGAWATTS

FIGURE Q001.488-28

(BEGINNING OF EQUILIBRIUM CYCLE)

AXIAL POWER DENSITY DISTRIBUTION FOR HEX ASSEMBLY 27



TOTAL POWER FOR THIS ASSEMBLY = .3881E+01 MEGAWATTS

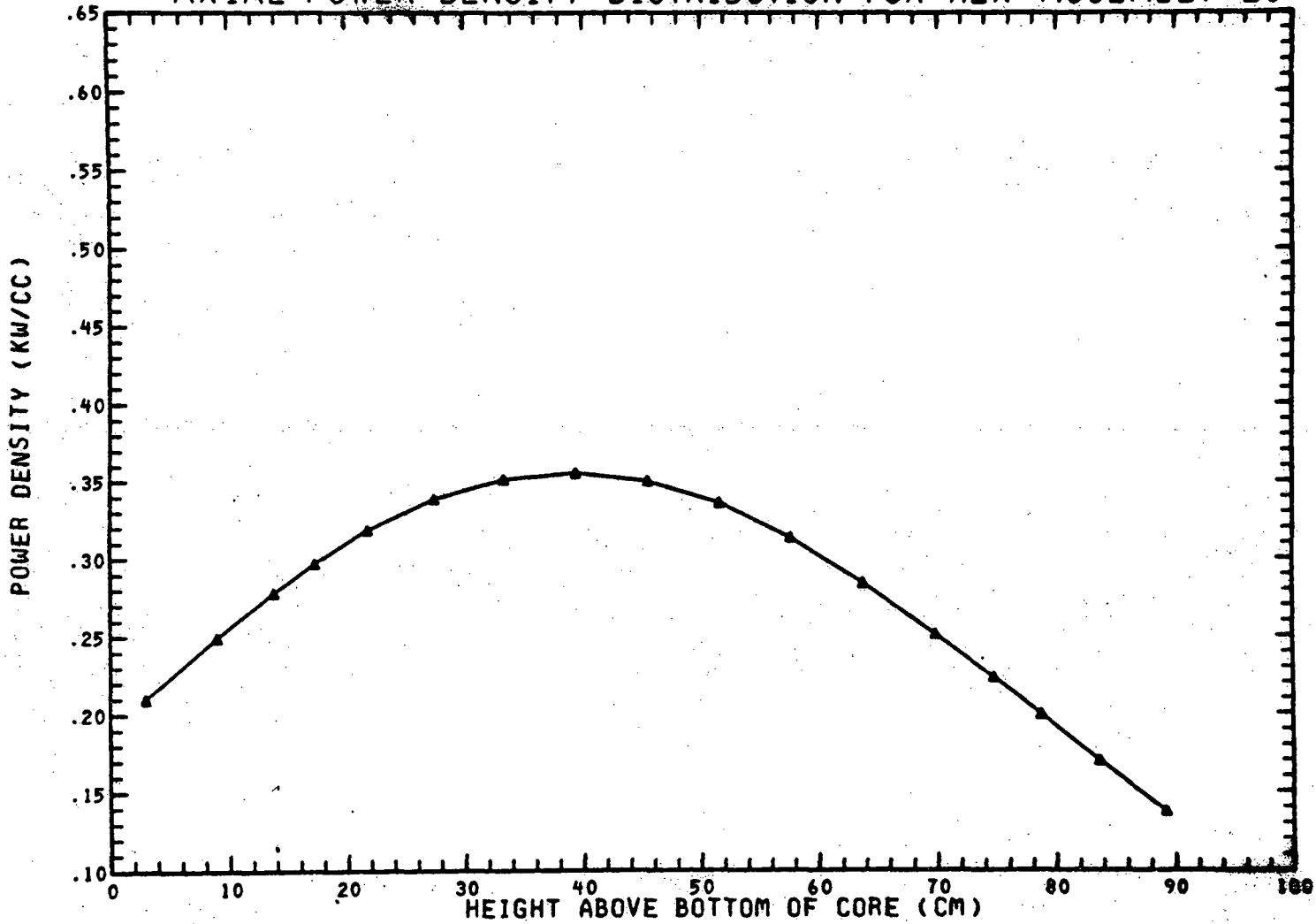
Q001.488-29

Amend. 60
Feb. 1981

FIGURE Q001.488-29

(BEGINNING OF EQUILIBRIUM CYCLE)

AXIAL POWER DENSITY DISTRIBUTION FOR HEX ASSEMBLY 28



TOTAL POWER FOR THIS ASSEMBLY= .3272E+01 MEGAWATTS

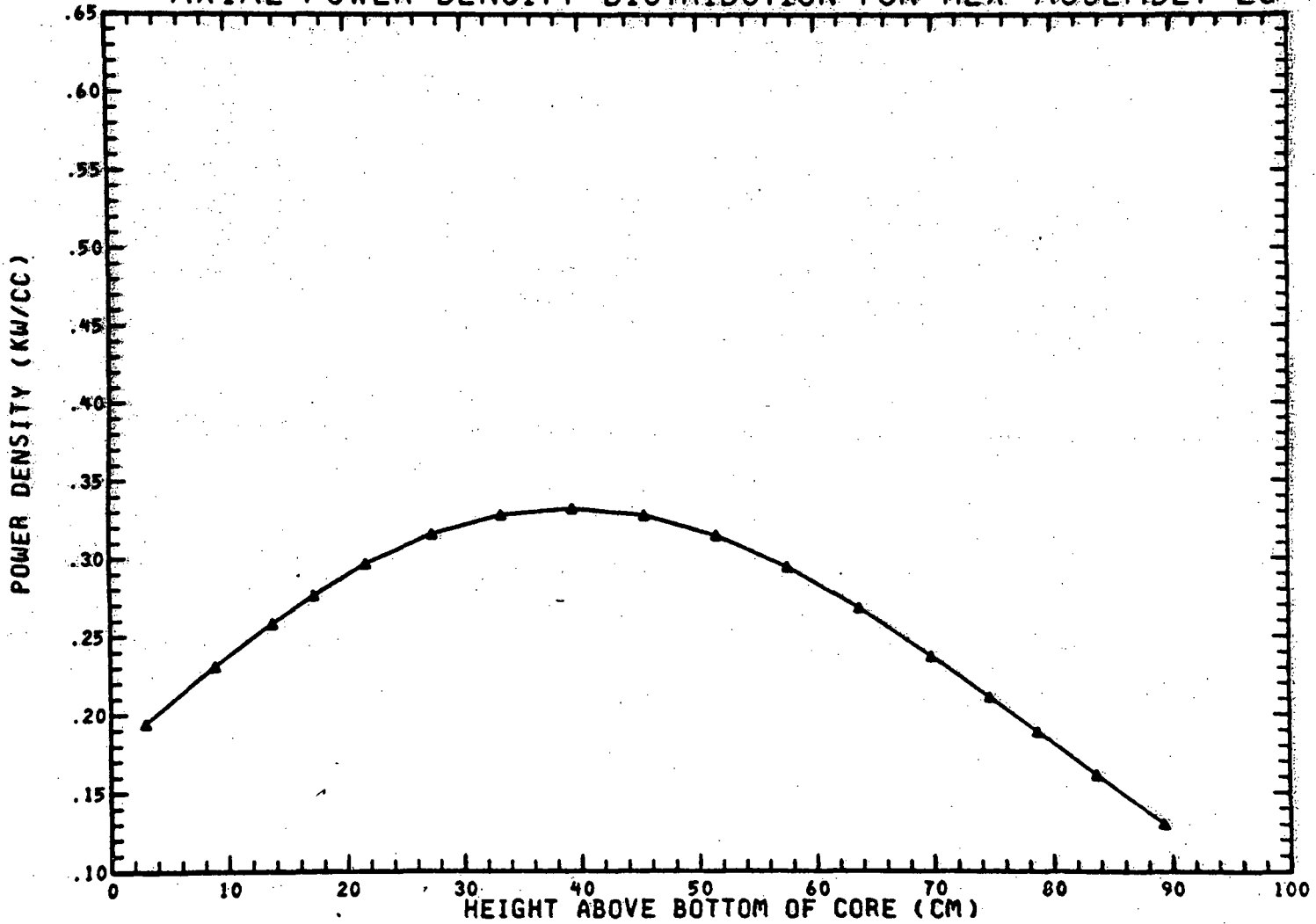
Q001.488-30

Amend. 60
Feb. 1981

FIGURE Q001.488-30

(BEGINNING OF EQUILIBRIUM CYCLE)

AXIAL POWER DENSITY DISTRIBUTION FOR HEX ASSEMBLY 29

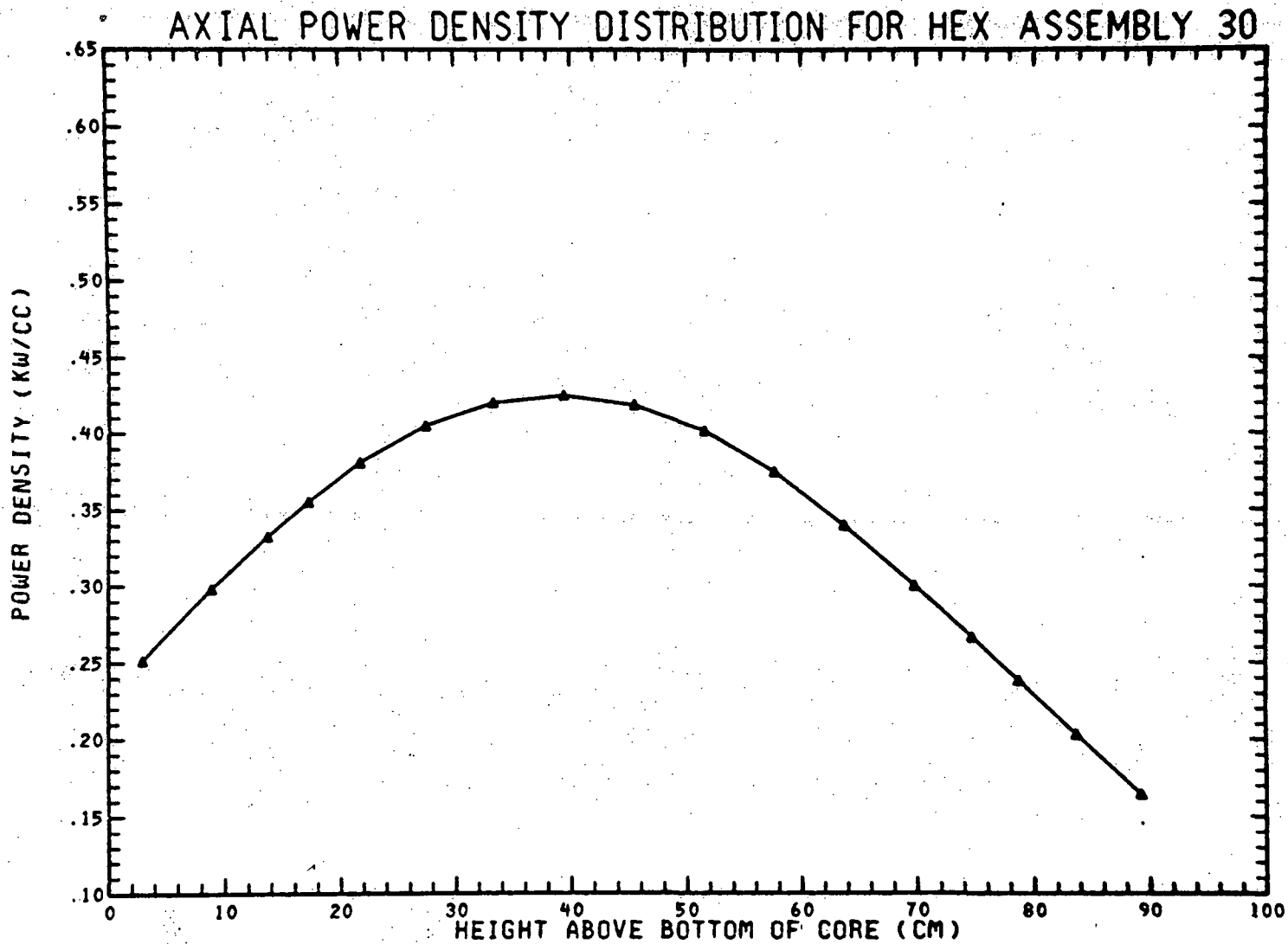


TOTAL POWER FOR THIS ASSEMBLY= .3064E+01 MEGAWATTS

Q001.488-3.1

Amend. 60
Feb. 1981

FIGURE Q001.488-31
(BEGINNING OF EQUILIBRIUM CYCLE)



TOTAL POWER FOR THIS ASSEMBLY= .3912E+01 MEGAWATTS

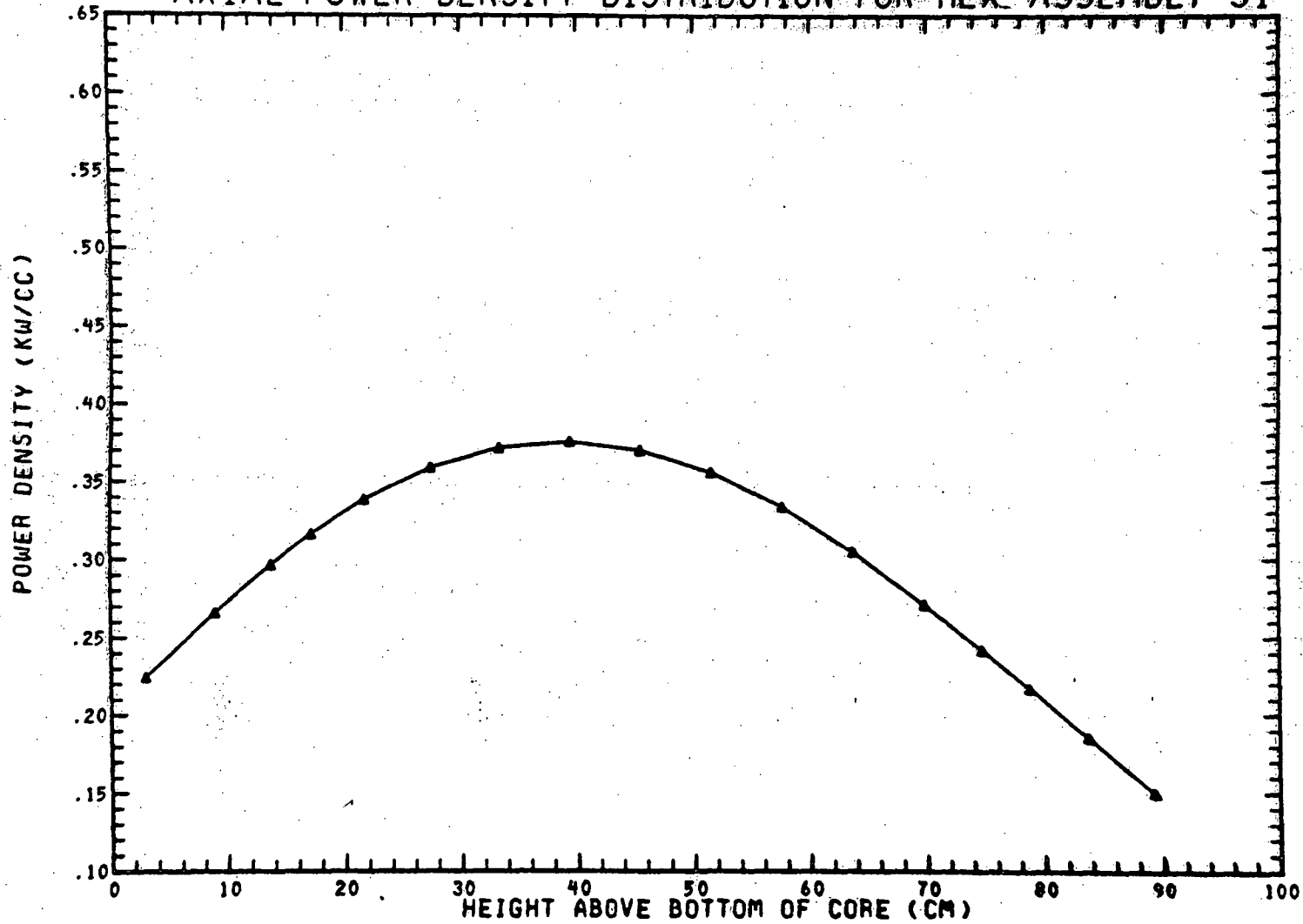
Q001.488-32

Amend. 60
Feb. 1981

FIGURE Q001.488-32

(BEGINNING OF EQUILIBRIUM CYCLE)

AXIAL POWER DENSITY DISTRIBUTION FOR HEX ASSEMBLY 31



TOTAL POWER FOR THIS ASSEMBLY= .3491E+01 MEGAWATTS

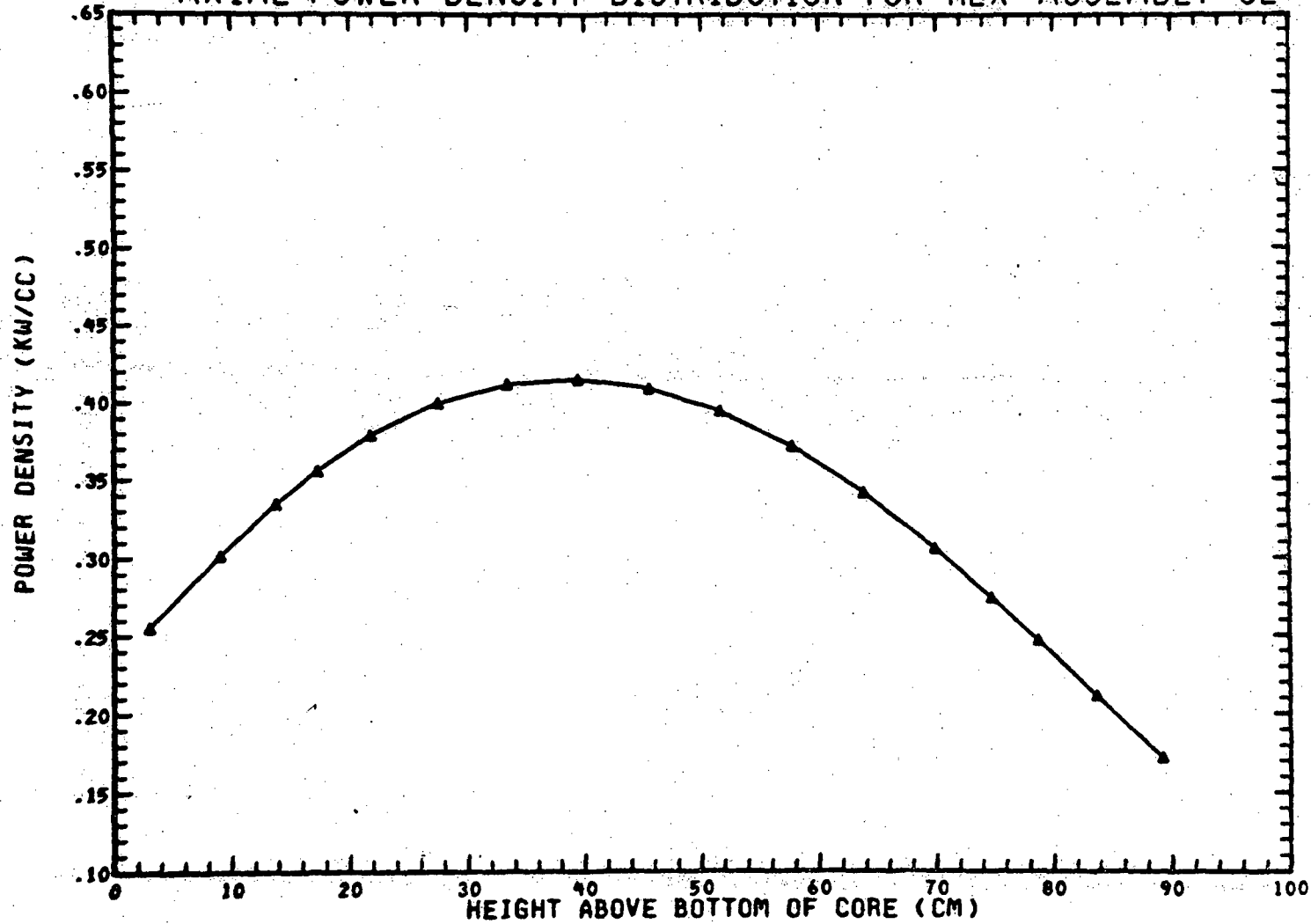
Q001.488-33

Amend. 60
Feb. 1981

FIGURE Q001.488-33

(BEGINNING OF EQUILIBRIUM CYCLE)

AXIAL POWER DENSITY DISTRIBUTION FOR HEX ASSEMBLY 32



TOTAL POWER FOR THIS ASSEMBLY = .3909E+01 MEGAWATTS

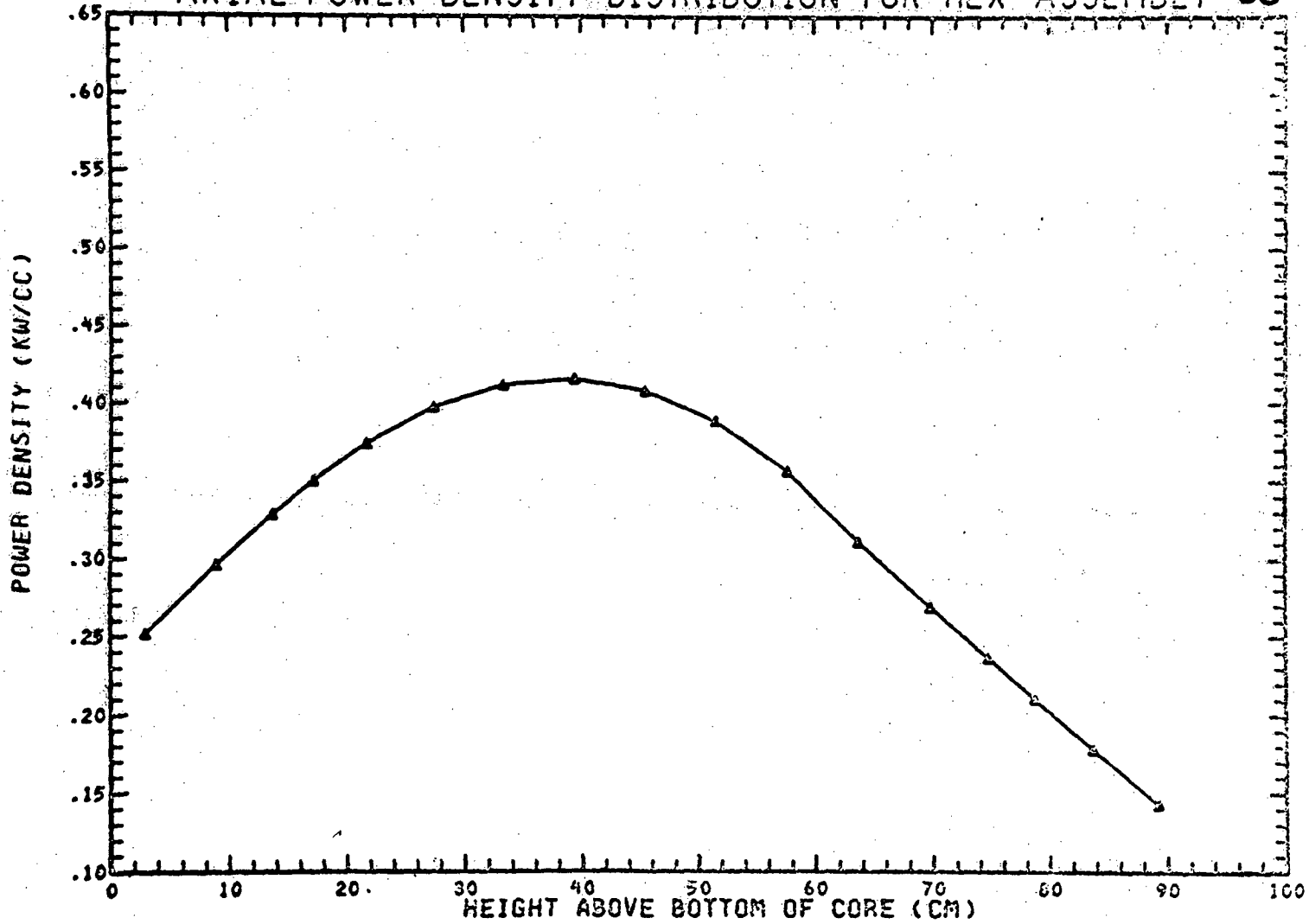
Q001.488-34

Amend. 60
Feb. 1981

FIGURE Q001.488-34

(BEGINNING OF EQUILIBRIUM CYCLE)

AXIAL POWER DENSITY DISTRIBUTION FOR HEX ASSEMBLY 68



TOTAL POWER FOR THIS ASSEMBLY= .3743E+01 MEGAWATTS

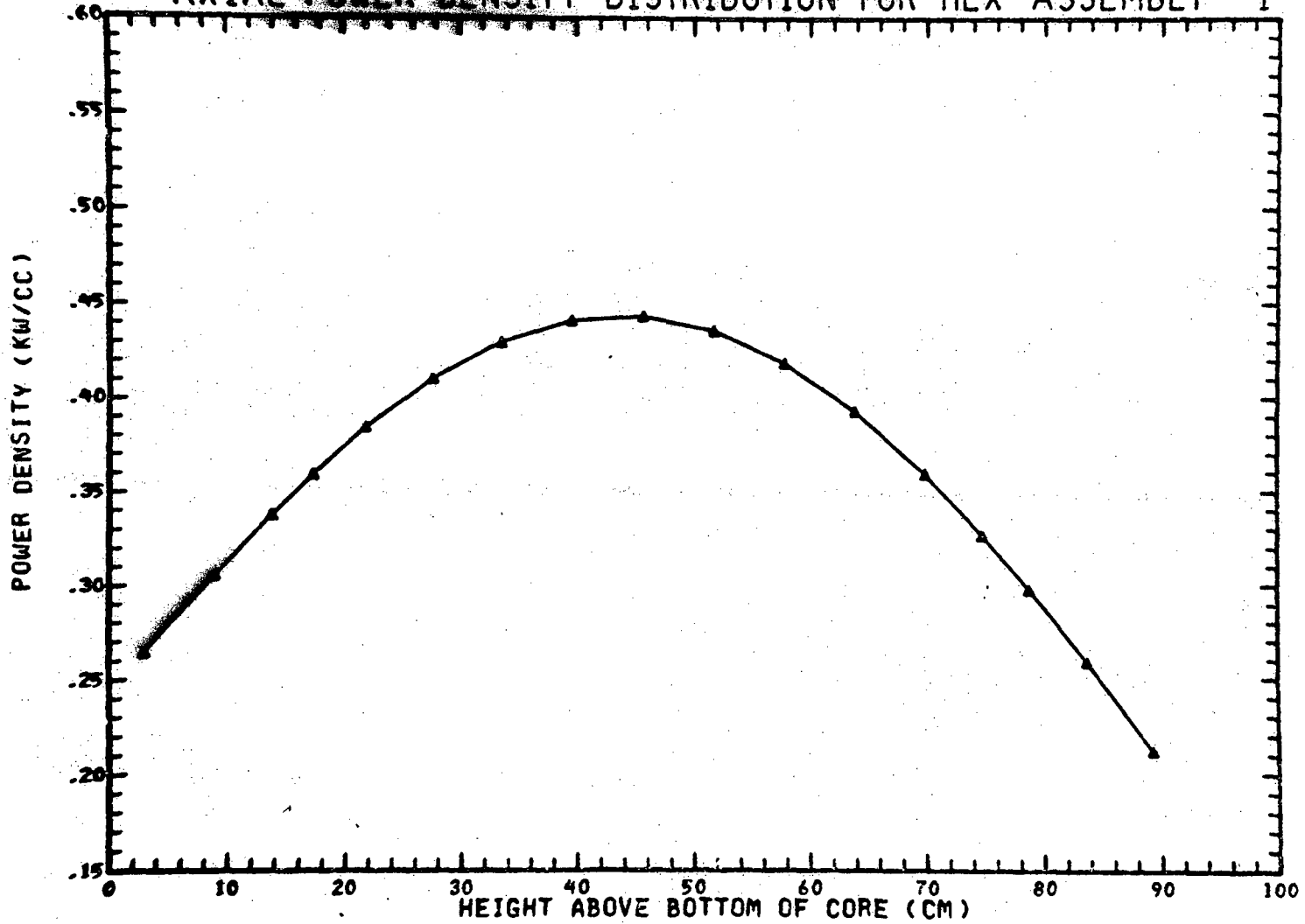
Q001.488-35

Amend. 60
Feb. 1981

FIGURE Q001.488-35

(END OF EQUILIBRIUM CYCLE)

AXIAL POWER DENSITY DISTRIBUTION FOR HEX ASSEMBLY 1



TOTAL POWER FOR THIS ASSEMBLY= .4264E+01 MEGAWATTS

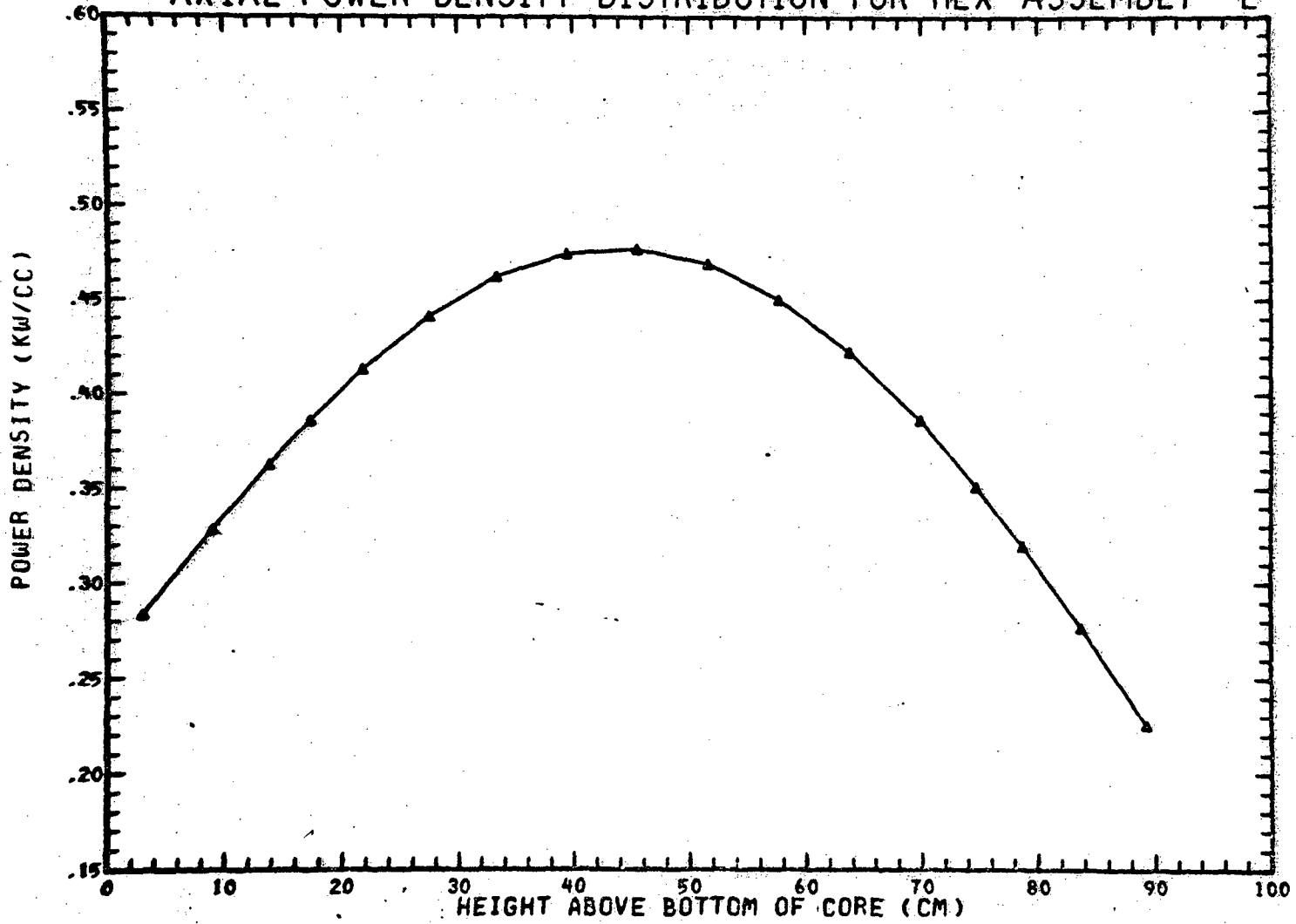
Q001.488-36

Amend. 60
Feb. 1981

FIGURE Q001.488-36

(END OF EQUILIBRIUM CYCLE)

AXIAL POWER DENSITY DISTRIBUTION FOR HEX ASSEMBLY 2



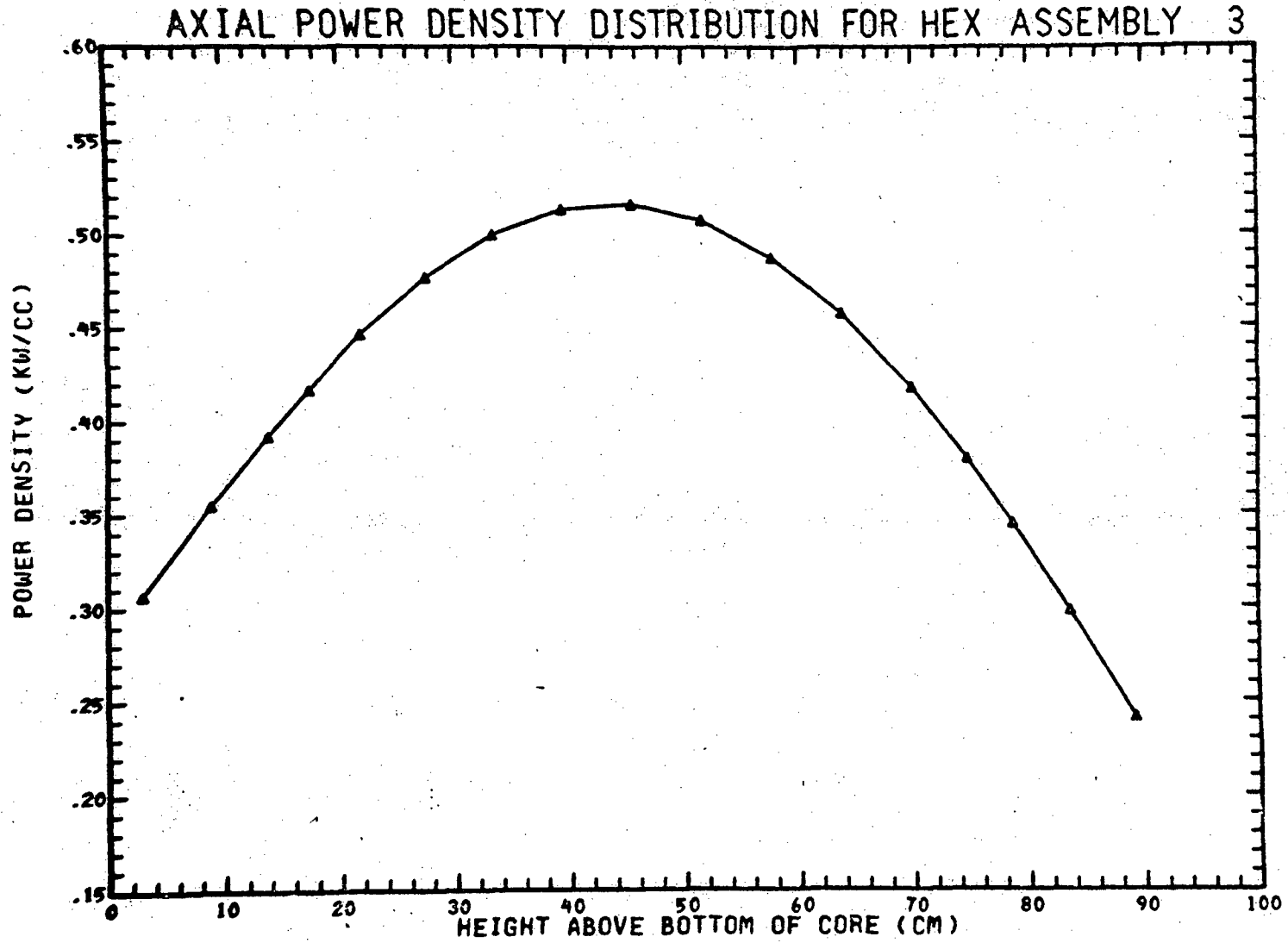
TOTAL POWER FOR THIS ASSEMBLY = .4579E+01 MEGAWATTS

Q001.488-37

Amend. 60
Feb. 1981

FIGURE 0001.488-37

(END OF EQUILIBRIUM CYCLE)



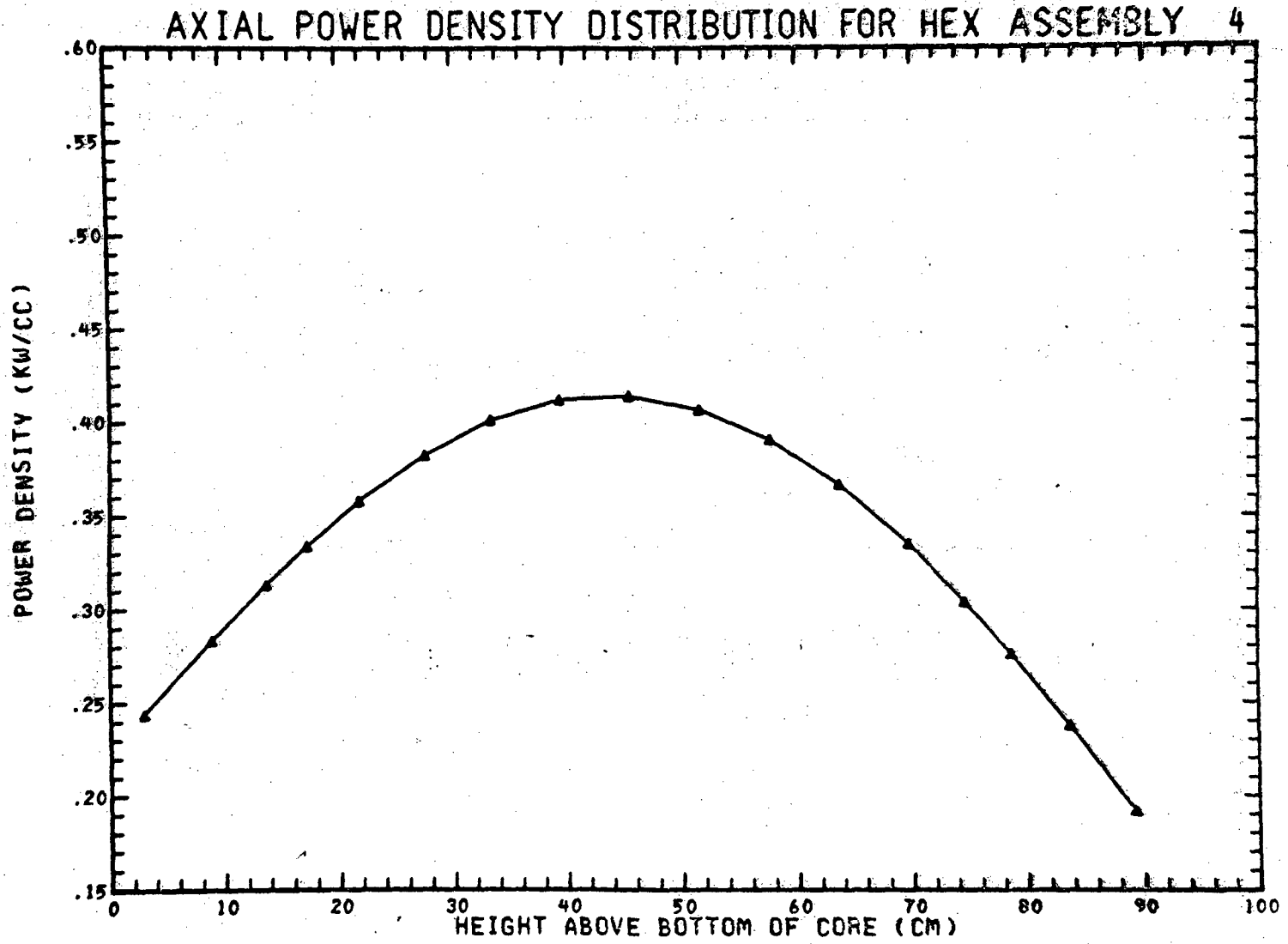
TOTAL POWER FOR THIS ASSEMBLY = .4947E+01 MEGAWATTS

0001.488-38

Amend. 60
Feb. 1981

FIGURE Q001.488-38

(END OF EQUILIBRIUM CYCLE)



TOTAL POWER FOR THIS ASSEMBLY= .3960E+01 MEGAWATTS

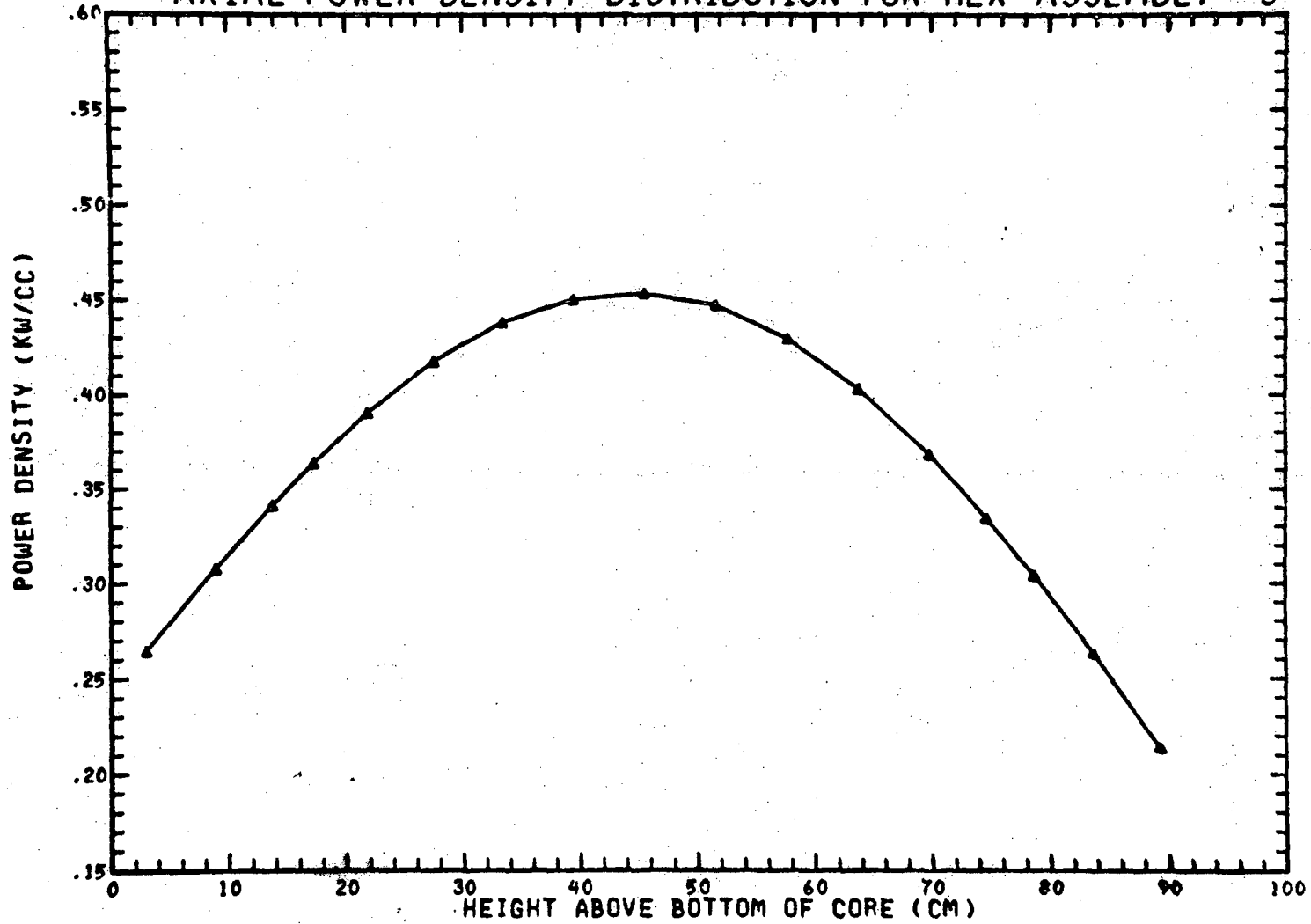
Q001.488-39

Amend. 60
Feb. 1981

FIGURE Q001.488-39

(END OF EQUILIBRIUM CYCLE)

AXIAL POWER DENSITY DISTRIBUTION FOR HEX ASSEMBLY 5



Q001.488-40

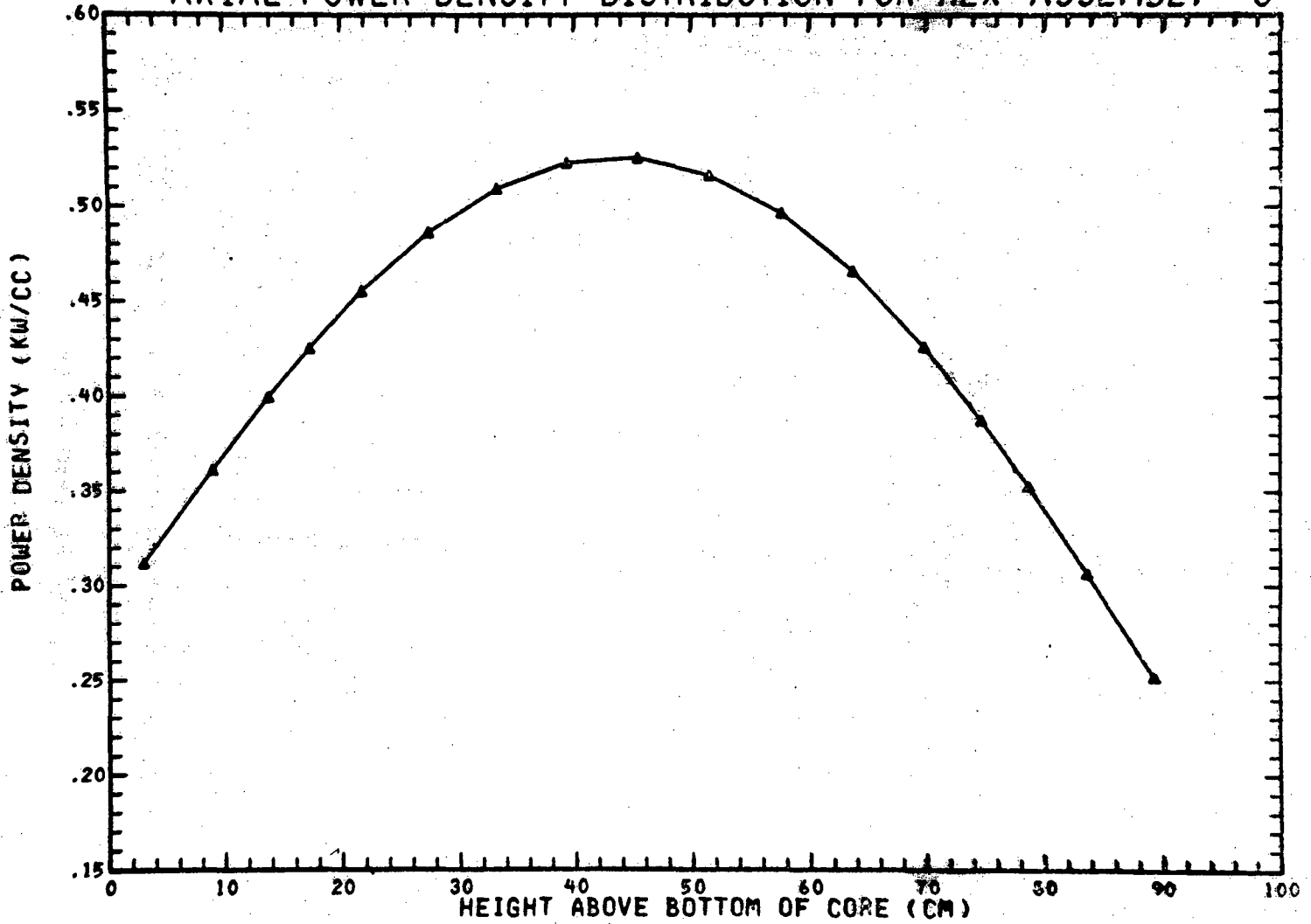
Amend. 60
Feb. 1981

TOTAL POWER FOR THIS ASSEMBLY = .4342E+01 MEGAWATTS

FIGURE Q001.488-40

(END OF EQUILIBRIUM CYCLE)

AXIAL POWER DENSITY DISTRIBUTION FOR HEX ASSEMBLY 6



TOTAL POWER FOR THIS ASSEMBLY = .5048E+01 MEGAWATTS

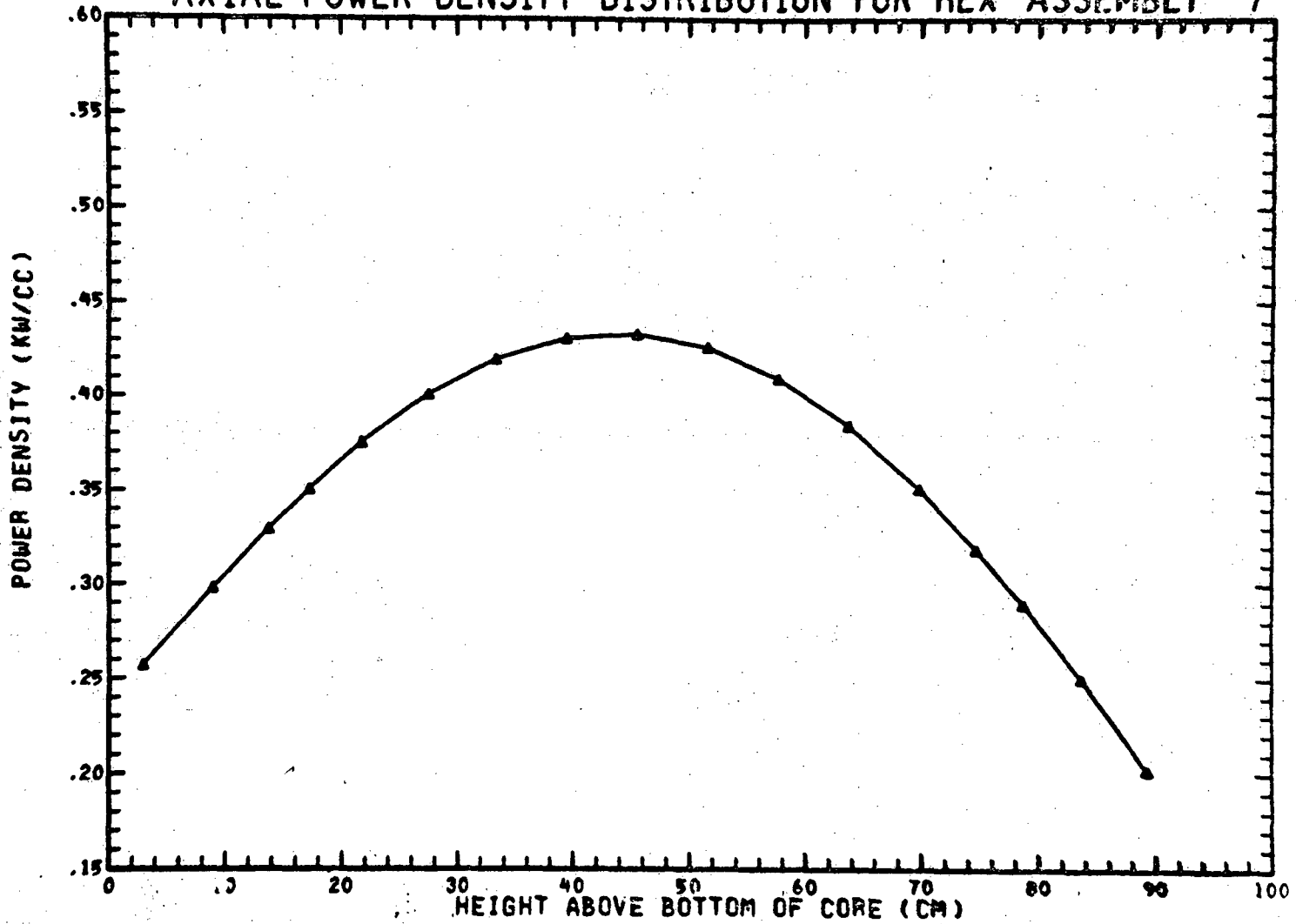
Q001.488-41

Amend. 60
Feb. 1981

FIGURE Q001.488-41

(END OF EQUILIBRIUM CYCLE)

AXIAL POWER DENSITY DISTRIBUTION FOR HEX ASSEMBLY 7



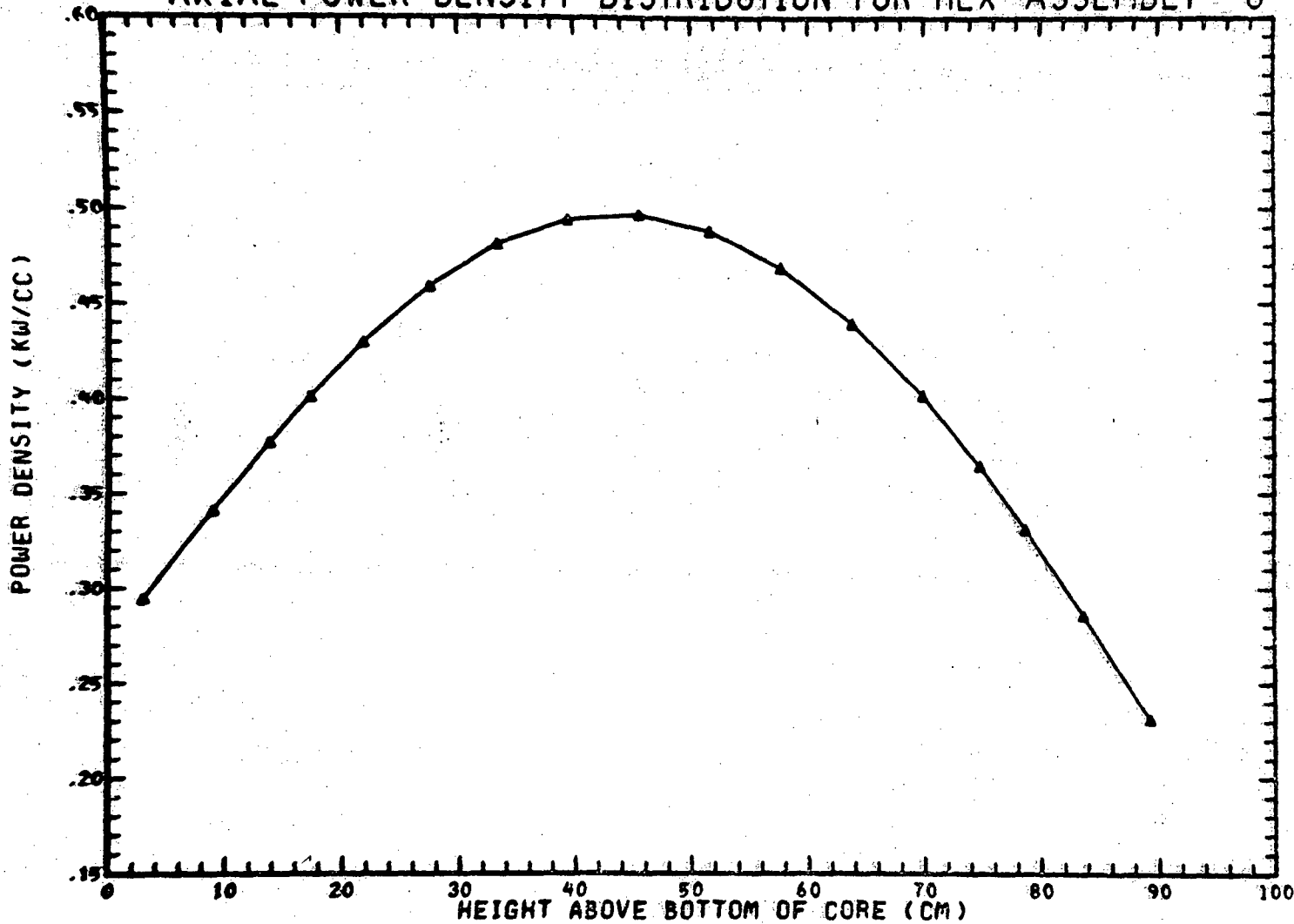
Q001.488-42

TOTAL POWER FOR THIS ASSEMBLY= .4155E+01 MEGAWATTS

Amend. 60
Feb. 1981

(END OF EQUILIBRIUM CYCLE)

AXIAL POWER DENSITY DISTRIBUTION FOR HEX ASSEMBLY 8



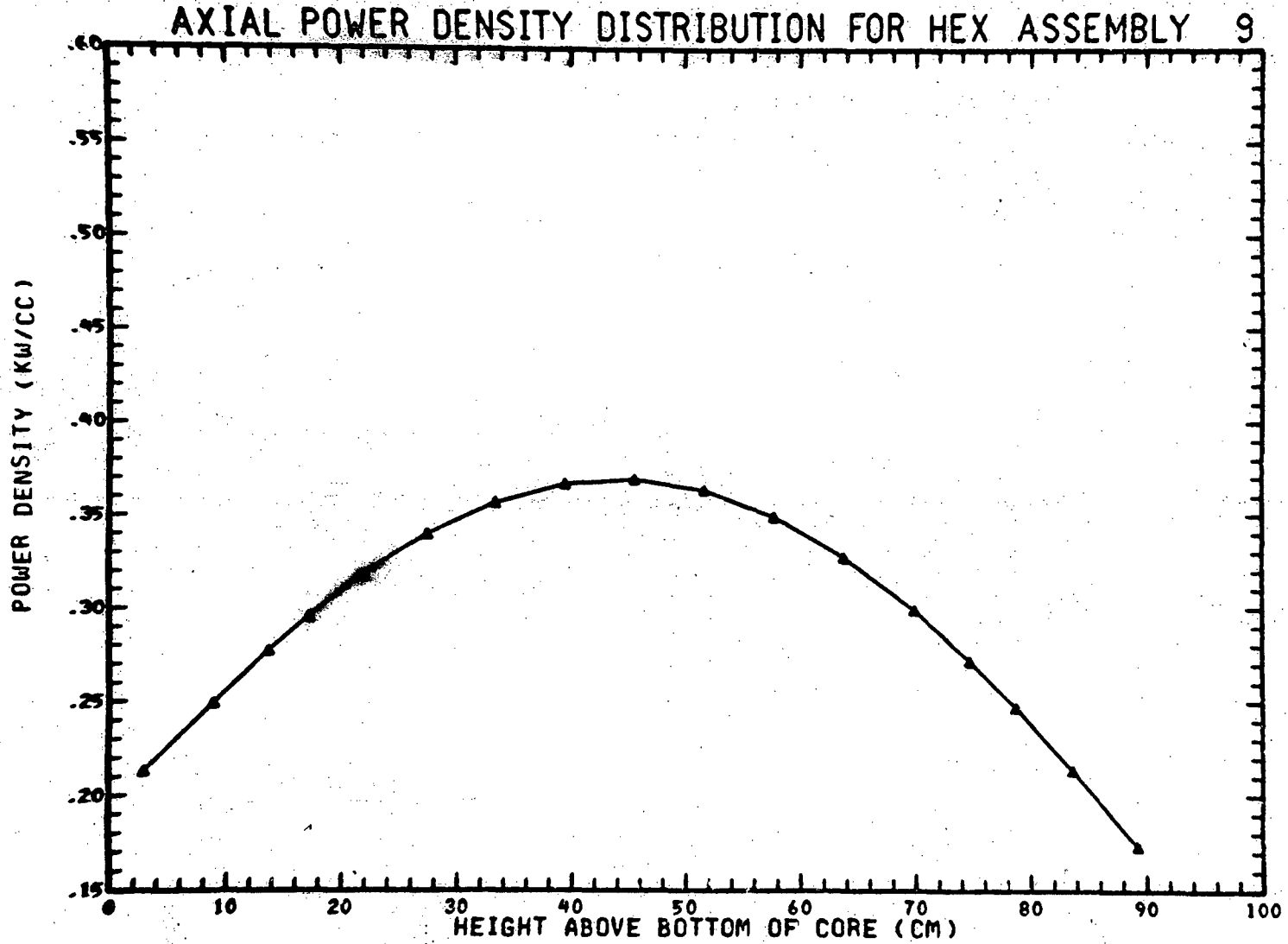
TOTAL POWER FOR THIS ASSEMBLY = .4760E+01 MEGAWATTS

Q001.488-43

Amend. 60
Feb. 1981

FIGURE Q001.488-43

(END OF EQUILIBRIUM CYCLE)



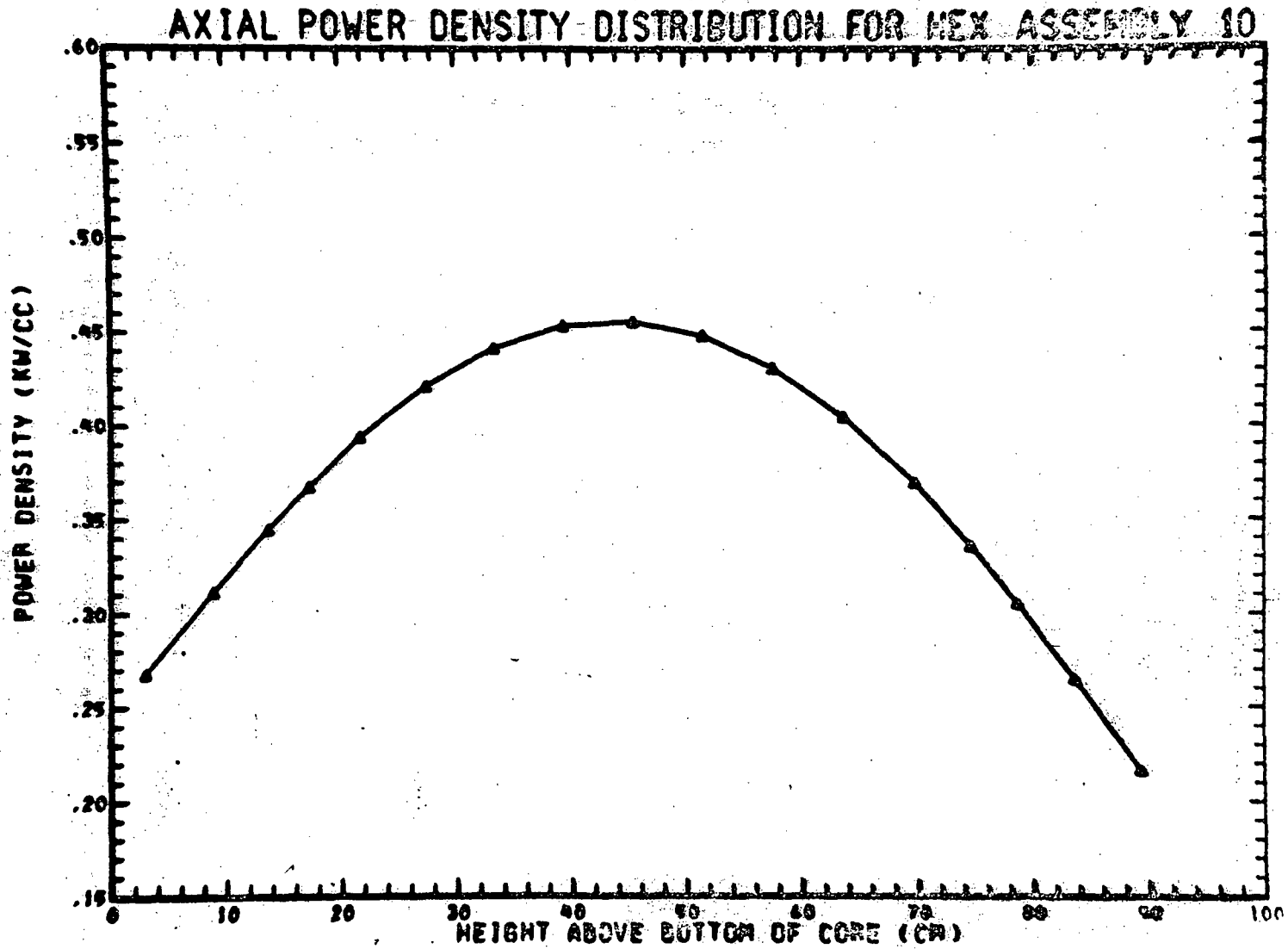
TOTAL POWER FOR THIS ASSEMBLY= .3530E+01 MEGAWATTS

Q001.488-44

Amend. 60
Feb. 1981

FIGURE Q001.488-44

(END OF EQUILIBRIUM CYCLE)



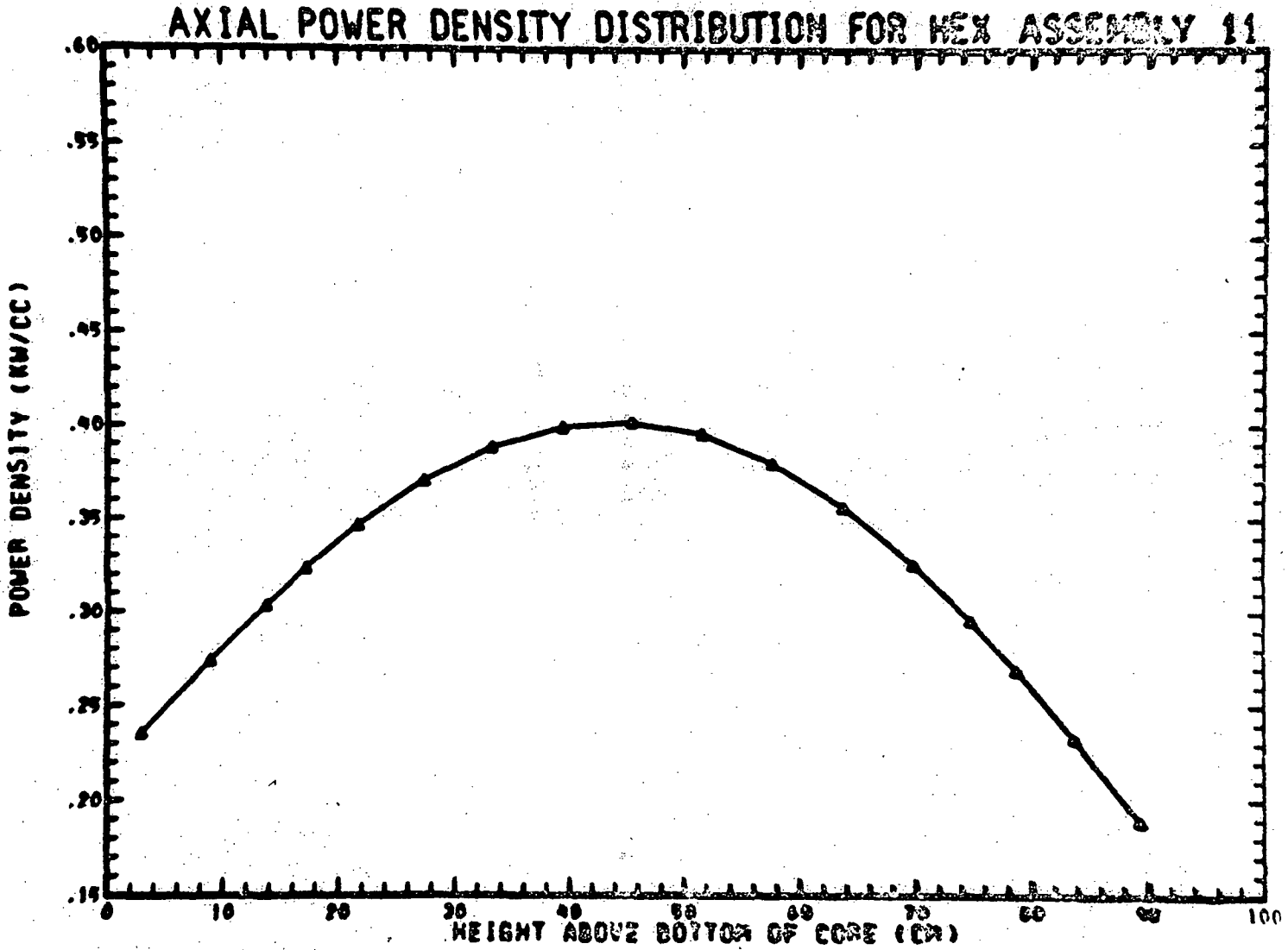
Q001.488-45

Amend. 60
Feb. 1981

TOTAL POWER FOR THIS ASSEMBLY = 0.9367 ± 0.01 MEGAWATTS

FIGURE Q001.488-45

(END OF EQUILIBRIUM CYCLE)



TOTAL POWER FOR THIS ASSEMBLY = $.3808E+01$ KW/CC

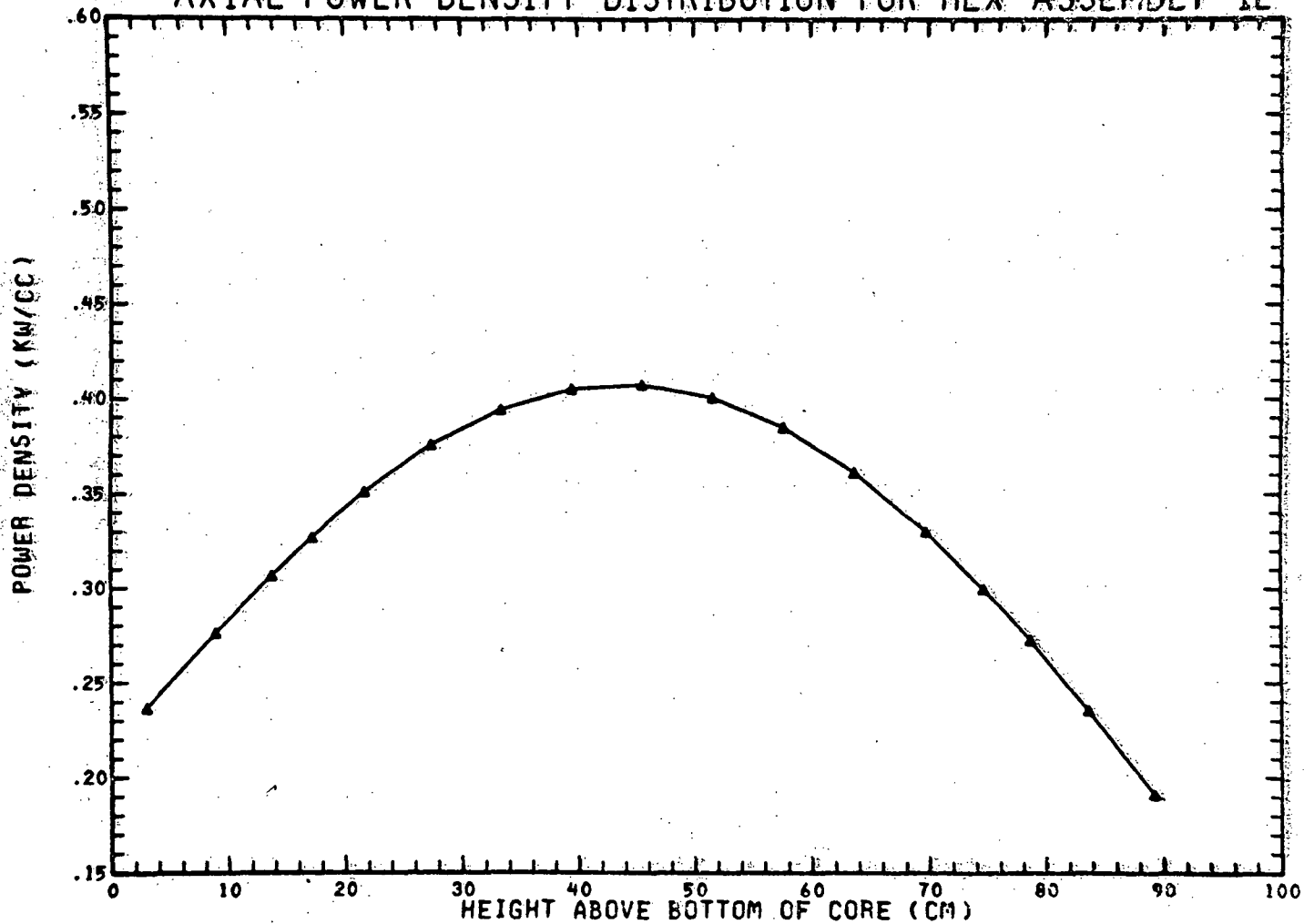
Q001.488-46

Amend. 60
Feb. 1981

FIGURE Q001.488-46

(END OF EQUILIBRIUM CYCLE)

AXIAL POWER DENSITY DISTRIBUTION FOR HEX ASSEMBLY 12



TOTAL POWER FOR THIS ASSEMBLY = .3896E+01 MEGAWATTS

Q001.488-47

Amend. 60
Feb. 1981

Question 001.488 (F6.2.3.3)

Provide analysis in which worths and relative powers are computed from a HEX-Z representation of the core for both the BOEC and EOEC cases.

Response: *

Analysis has been performed using VENTURE (a 3-D diffusion theory code) (Reference Q001.488-1) for a one third reactor sector.

The results of the HEX-Z analysis for the beginning of equilibrium cycle (BOEC) and the end of equilibrium cycle (EOEC) are presented in Figures Q001.488-1 through Q001.488-86.

Figure Q001.488-1 provides both the assembly numbering scheme and the length of time that each assembly would have been in the core. Figures Q001.488-2 through 34 and Figures Q001.488-35 through 67 are the axial power density distribution for the 36 inch core height averaged over an assembly for BOEC and EOEC, respectively. The height above the bottom of the core corresponds to the distance above the core/lower axial blanket interface.

The material worths for the removal of sodium, stainless steel, and fuel were calculated using first order perturbation theory with three dimensional fluxes. The three material worths calculated are presented for each assembly in Figures Q001.488-69 through 77 for BOEC and 78 through 79 for EOEC.

Reference:

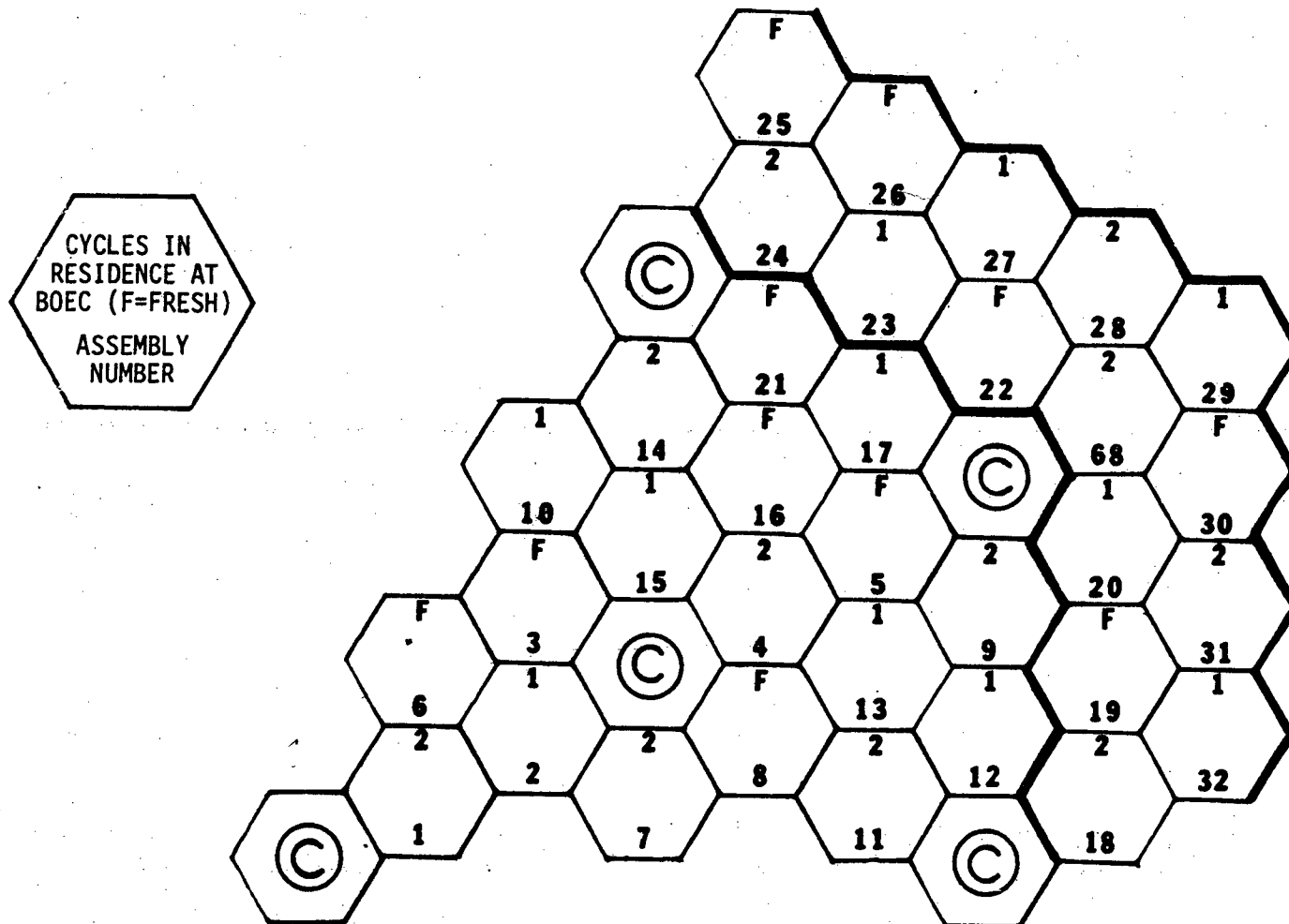
Q001.488-1: D. R. Vondy, T. B. Fowler, G. W. Cunningham, "VENTURE, A Code Block for Solving Multigroup Neutronics Problems Applying the Finite-Diffusion-Theory Approximation to Neutron Transport", ORNL-5062, October 1975.

*Note that Appendix F has been withdrawn. The text upon which the question was based, can now be found in Section 5 of Reference 15, PSAR Section 1.6.

60

FIGURE Q001.488-1

ASSEMBLY NUMBERING SCHEME AND FUEL BURNUP

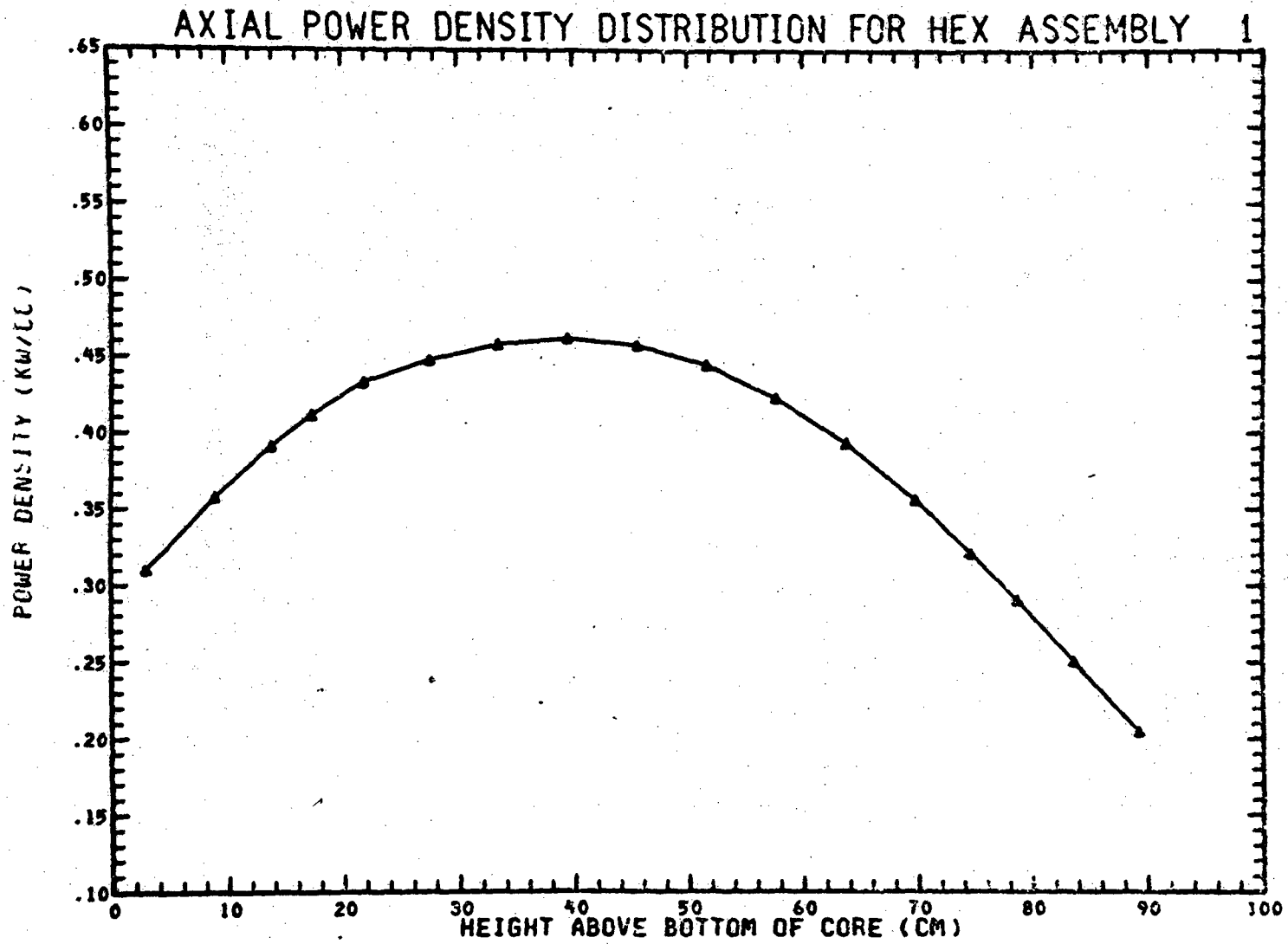


Q001.488-2

Amend. 60
Feb. 1981

FIGURE Q001.488-2

(BEGINNING OF EQUILIBRIUM CYCLE)



TOTAL POWER FOR THIS ASSEMBLY= .4486E+01 MEGAWATTS

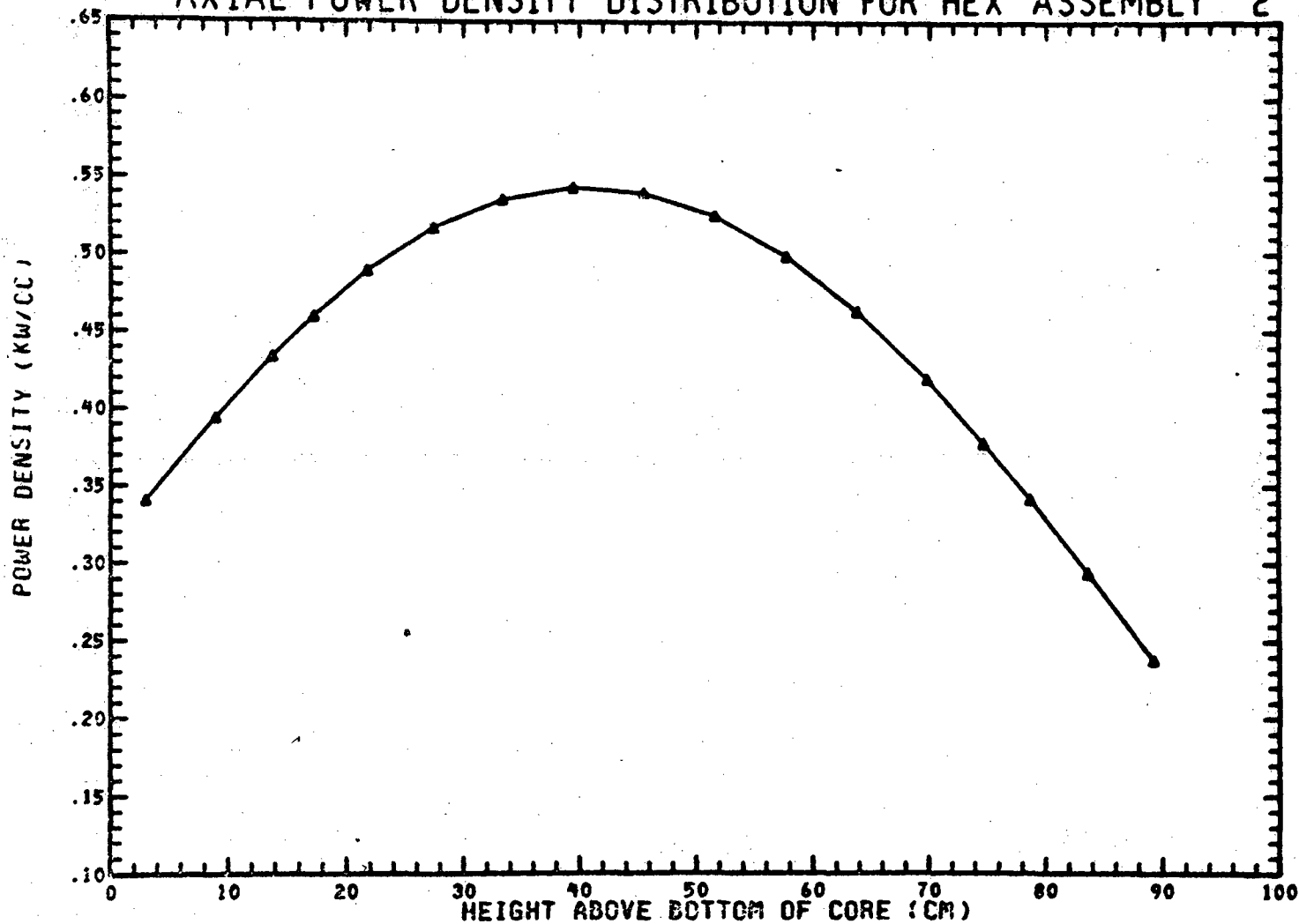
Q001.488-3

Amend. 60
Feb. 1981

FIGURE Q001.488-3

(BEGINNING OF EQUILIBRIUM CYCLE)

AXIAL POWER DENSITY DISTRIBUTION FOR HEX ASSEMBLY 2



TOTAL POWER FOR THIS ASSEMBLY= .5192E+01 MEGAWATTS

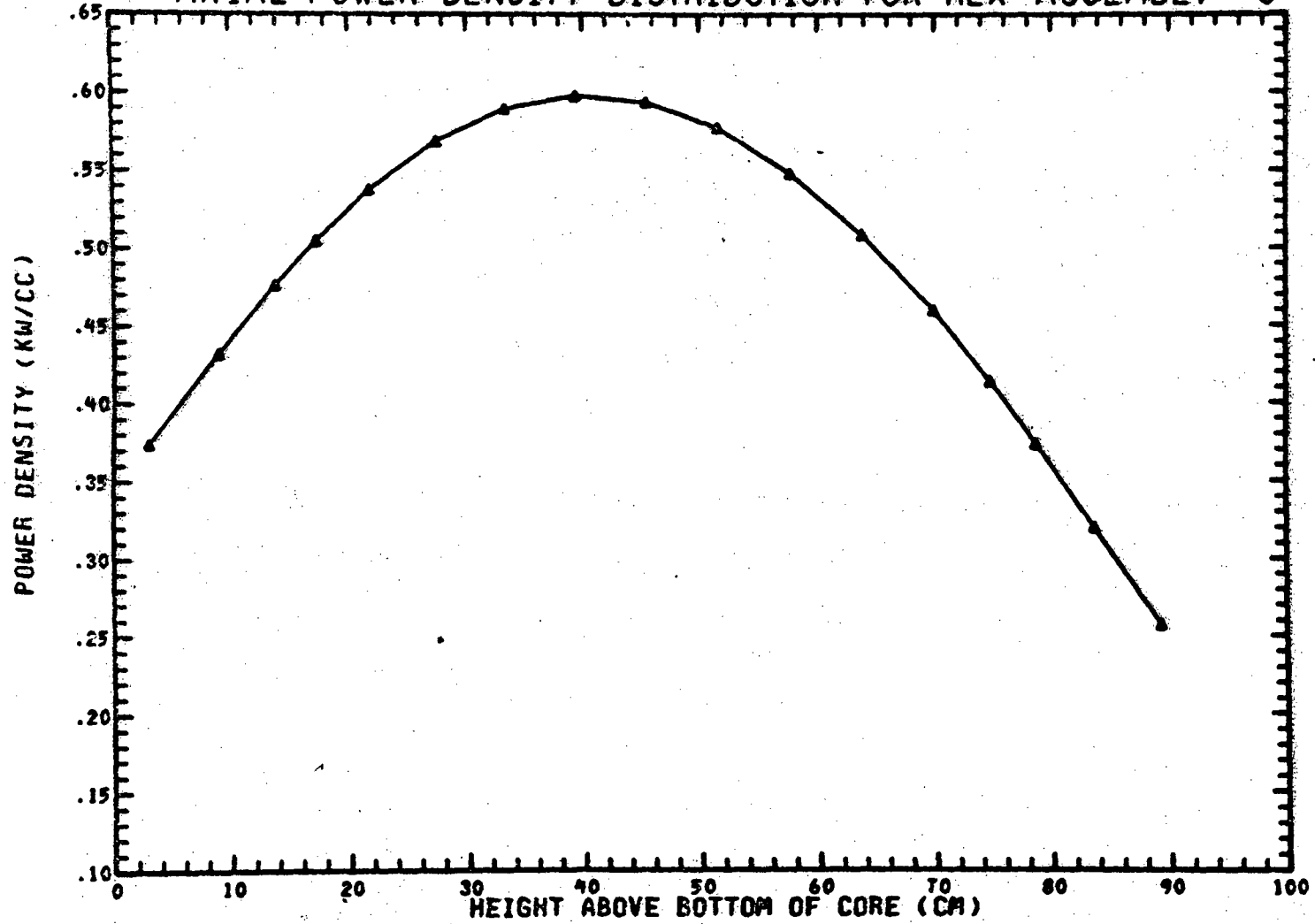
Q001.488-4

Amend. 60
Feb. 1981

FIGURE Q001.488-4

(BEGINNING OF EQUILIBRIUM CYCLE)

AXIAL POWER DENSITY DISTRIBUTION FOR HEX ASSEMBLY 3



TOTAL POWER FOR THIS ASSEMBLY= .5697E+01 MEGAWATTS

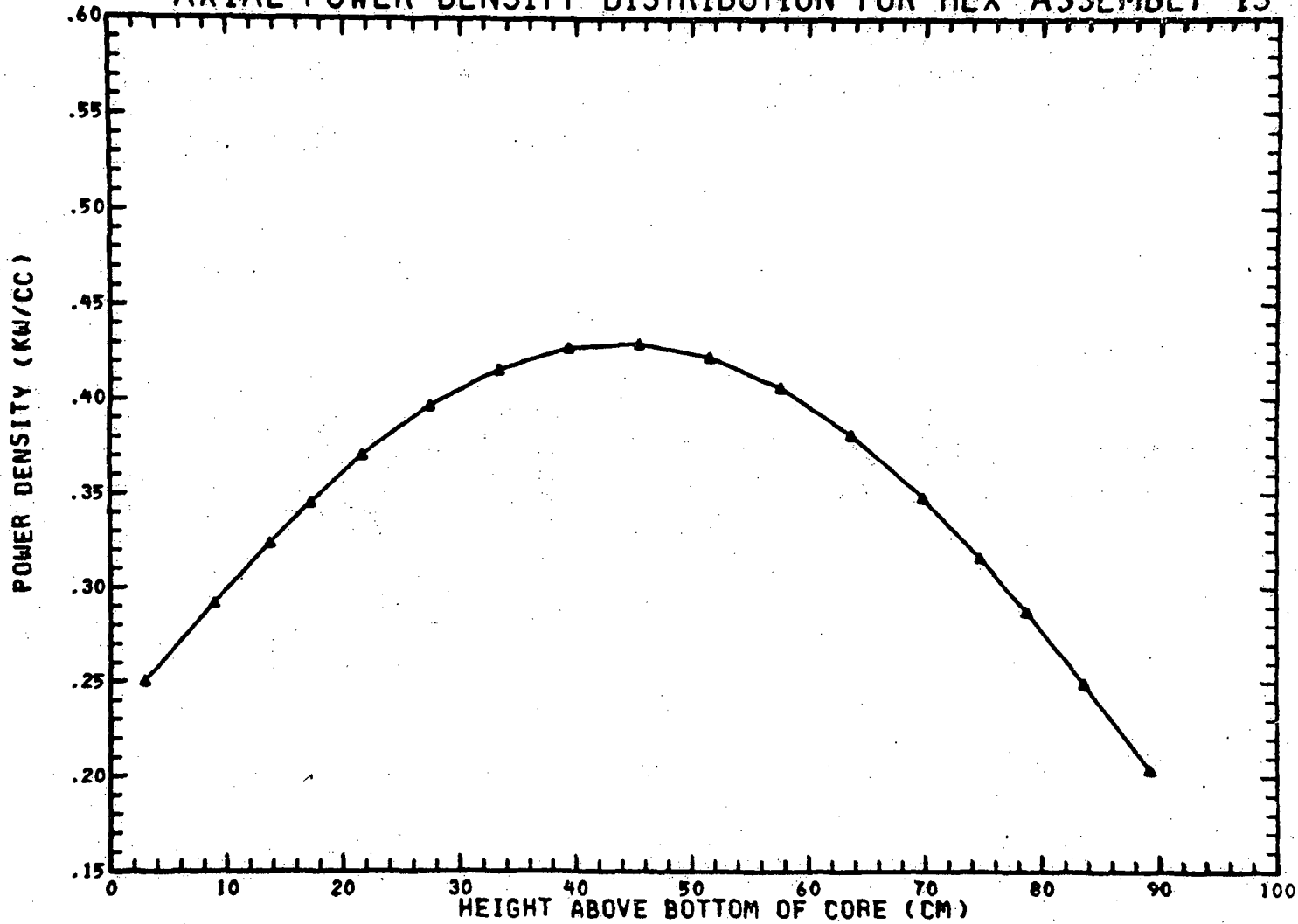
Q001.488-5

Amend. 60
Feb. 1981

FIGURE Q001.488-47

(END OF EQUILIBRIUM CYCLE)

AXIAL POWER DENSITY DISTRIBUTION FOR HEX ASSEMBLY 13



TOTAL POWER FOR THIS ASSEMBLY= .4112E+01 MEGAWATTS

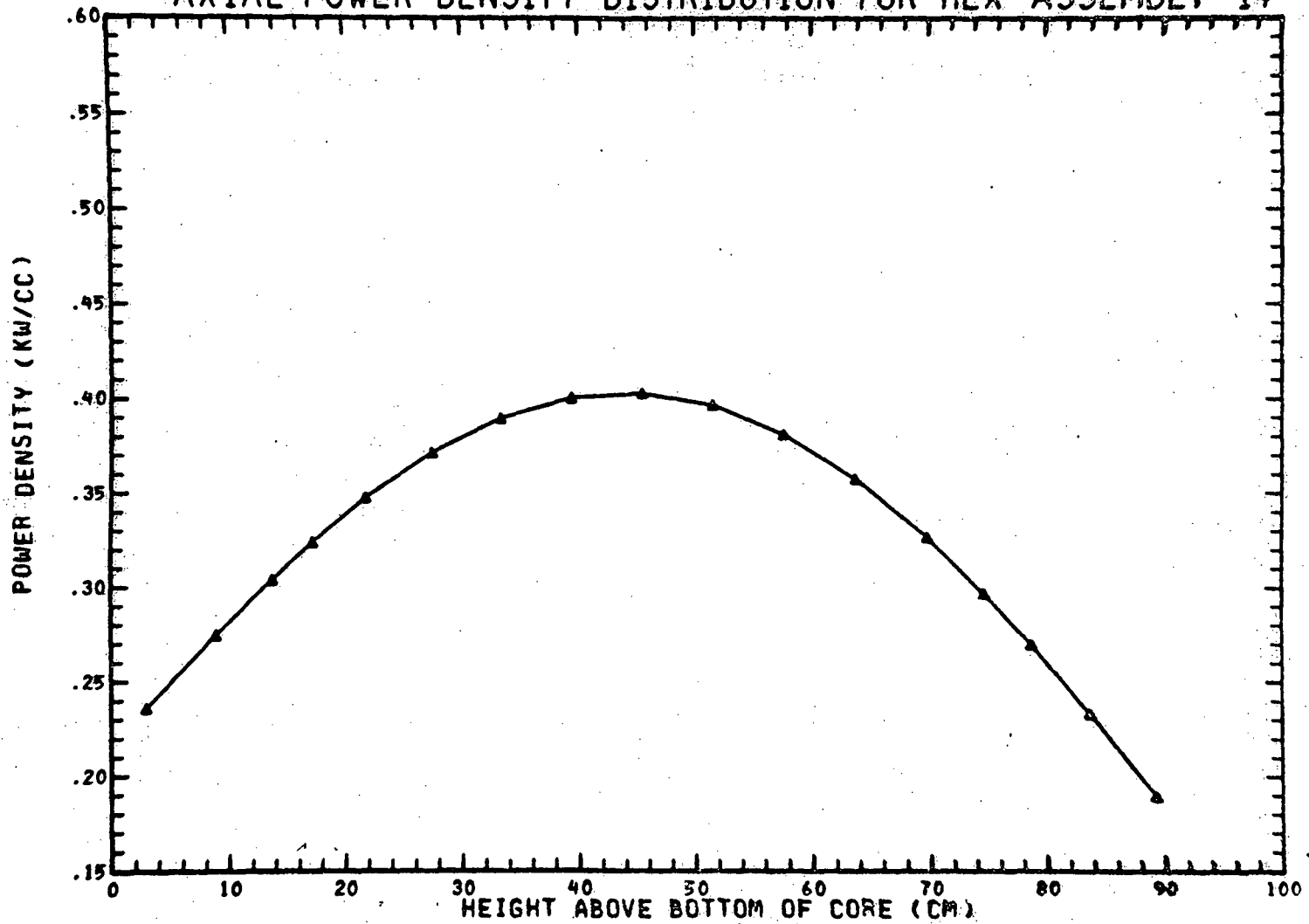
Q001.488-48

Amend. 60
Feb. 1981

FIGURE Q001.488-48

(END OF EQUILIBRIUM CYCLE)

AXIAL POWER DENSITY DISTRIBUTION FOR HEX ASSEMBLY 14



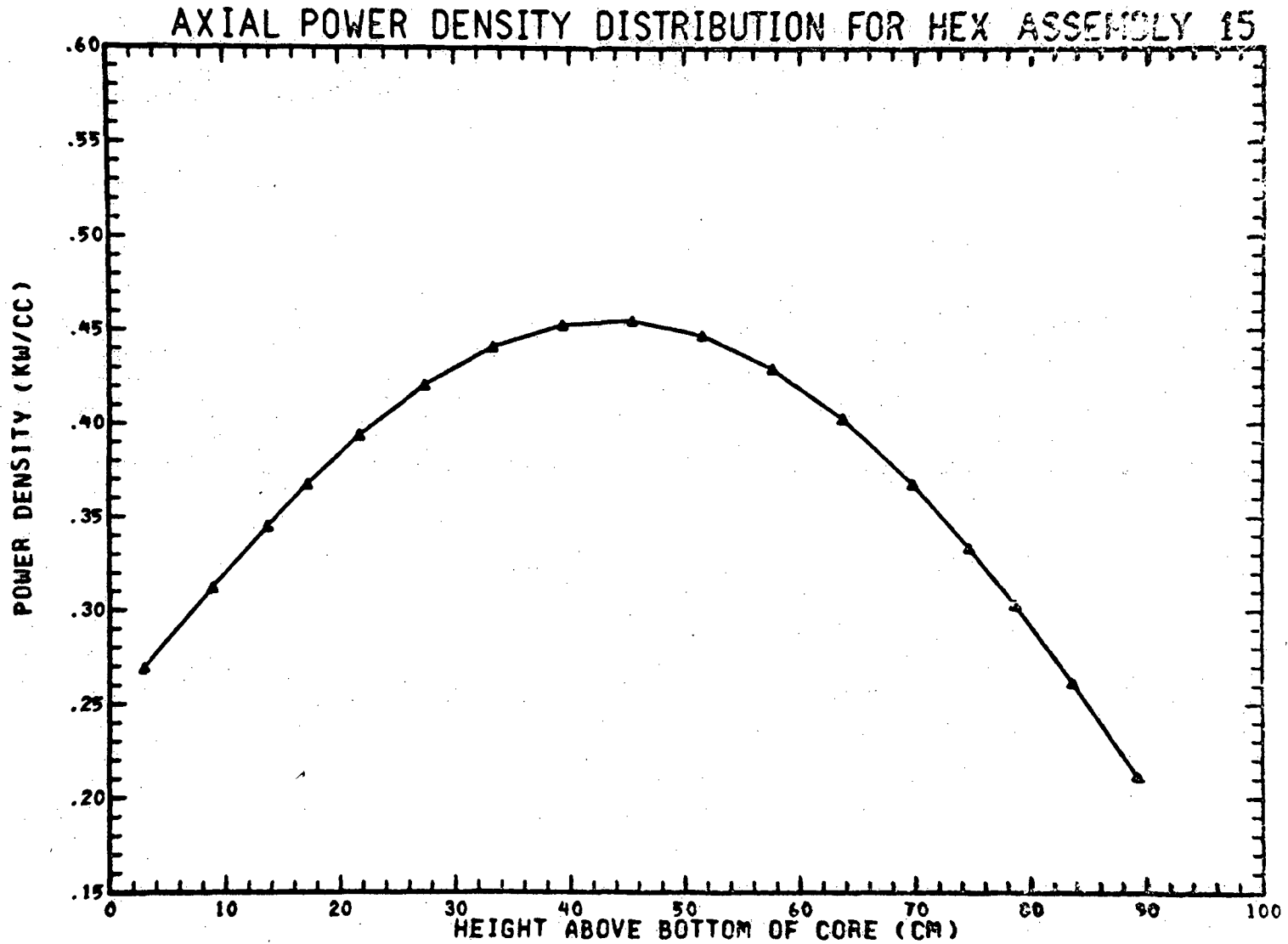
TOTAL POWER FOR THIS ASSEMBLY = .3858E+01 MEGAWATTS

Q001.488-49

Amend. 60
Feb. 1981

FIGURE Q001.488-49

(END OF EQUILIBRIUM CYCLE)



TOTAL POWER FOR THIS ASSEMBLY = .4357E+01 MEGAWATTS

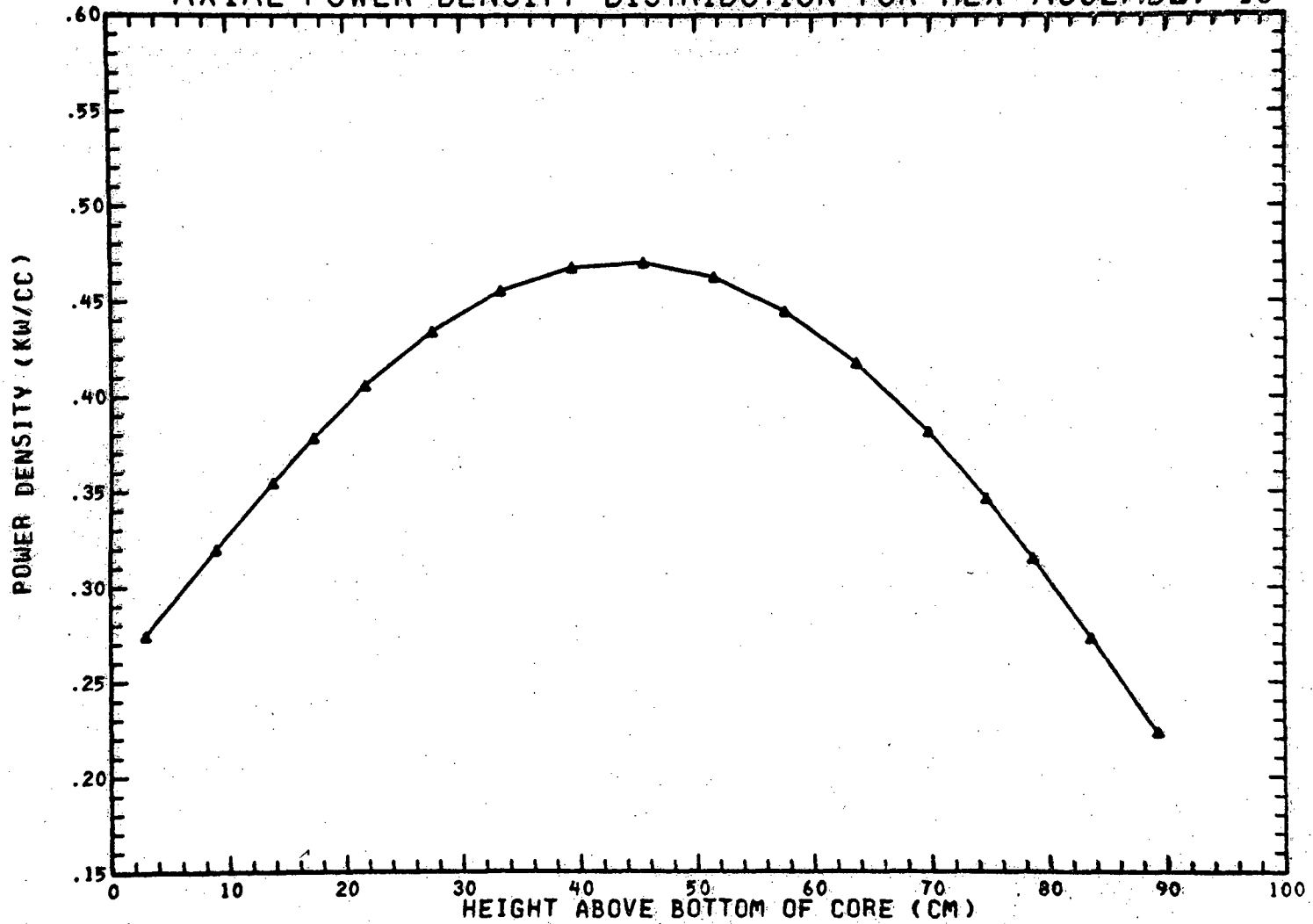
Q001.488-50

Amend. 60
Feb. 1981

FIGURE Q001.488-50

(END OF EQUILIBRIUM CYCLE)

AXIAL POWER DENSITY DISTRIBUTION FOR HEX ASSEMBLY 16



TOTAL POWER FOR THIS ASSEMBLY= .4506E+01 MEGAWATTS

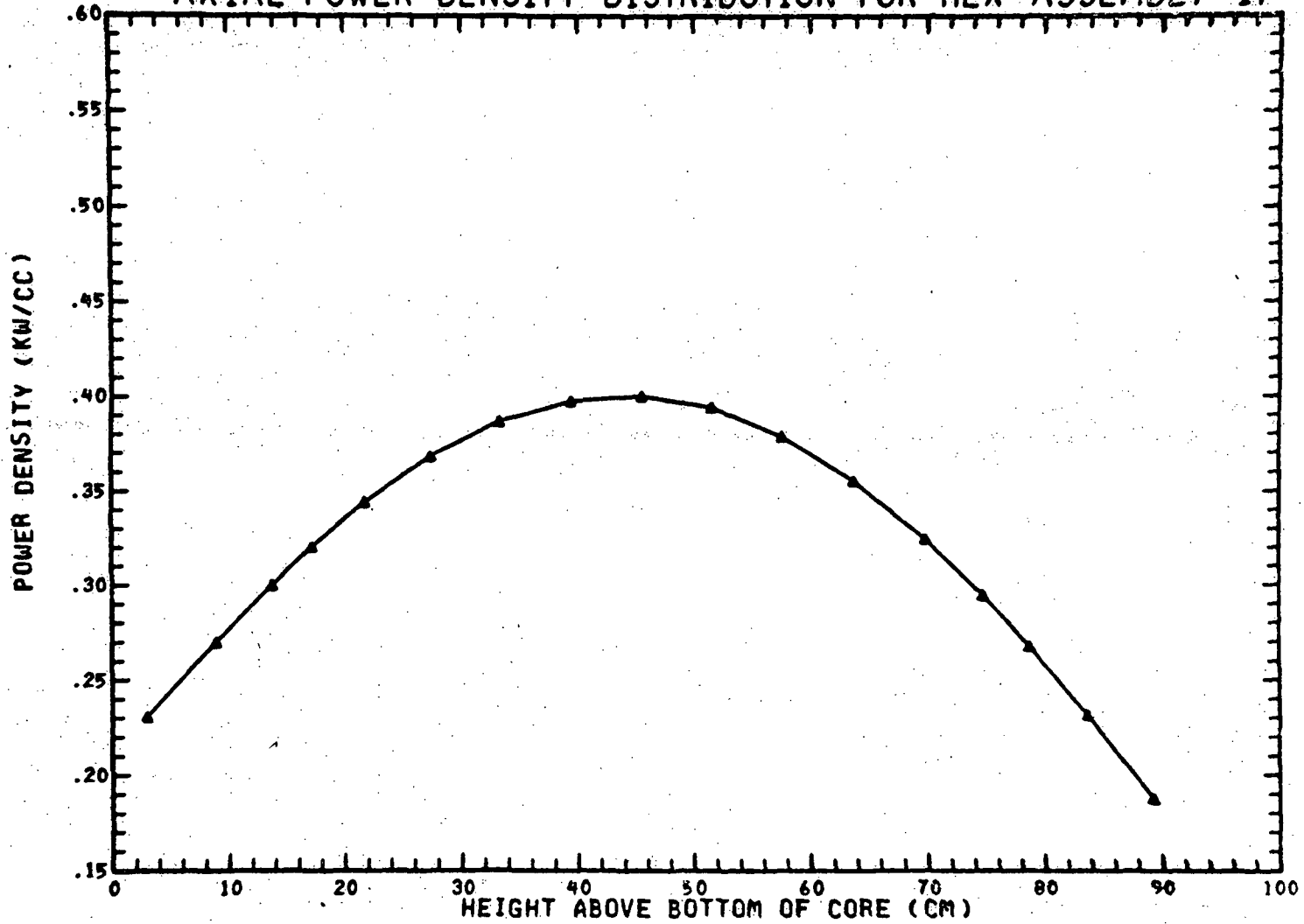
Q001.488-51

Amend. 60
Feb. 1981

FIGURE Q001.488-51

(END OF EQUILIBRIUM CYCLE)

AXIAL POWER DENSITY DISTRIBUTION FOR HEX ASSEMBLY 17



Q001.488-52

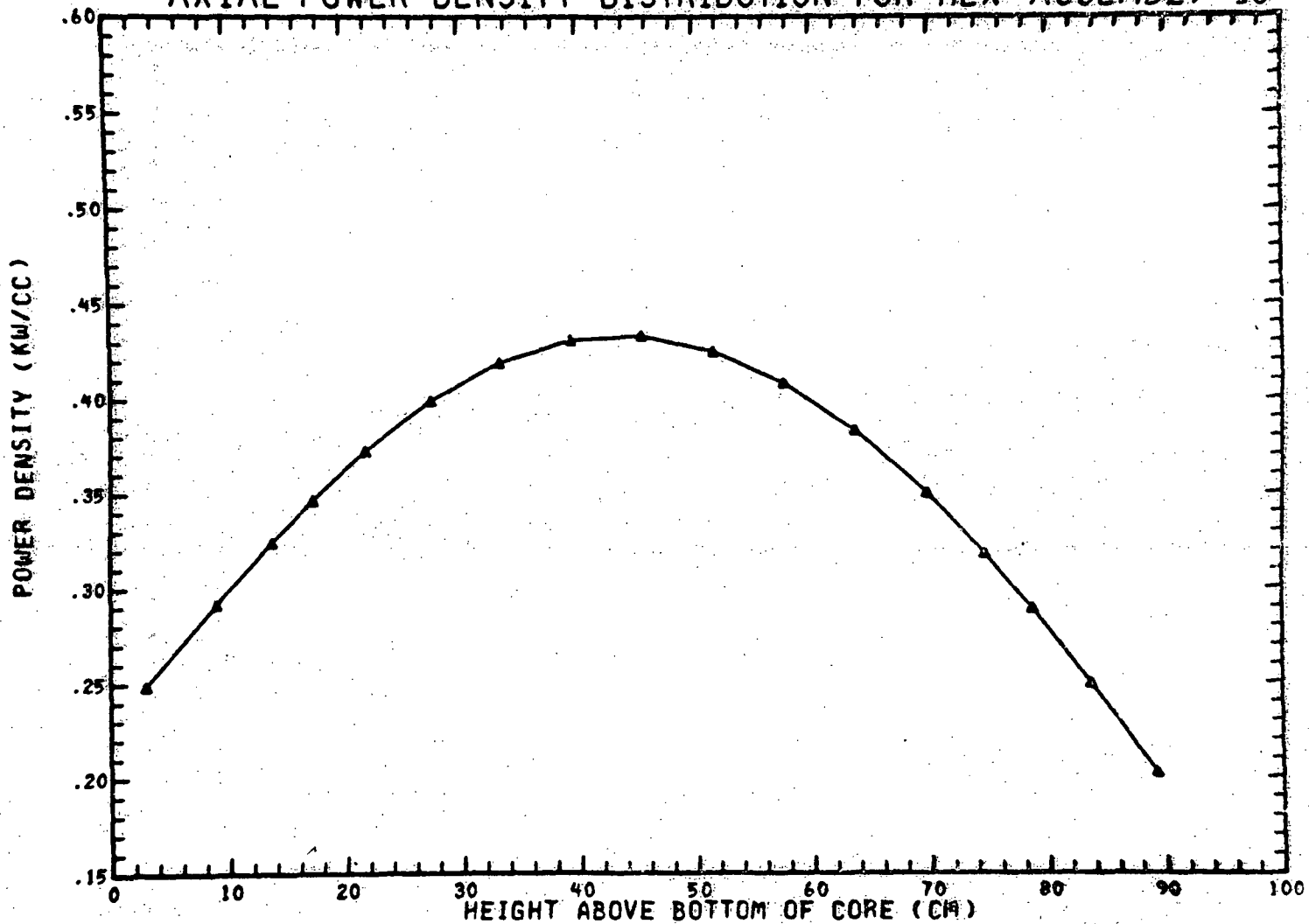
TOTAL POWER FOR THIS ASSEMBLY= .3820E+01 MEGAWATTS

Amend. 60
Feb. 1981

FIGURE Q001.488-52

(END OF EQUILIBRIUM CYCLE)

AXIAL POWER DENSITY DISTRIBUTION FOR HEX ASSEMBLY 18



TOTAL POWER FOR THIS ASSEMBLY = .4131E+01 MEGAWATTS

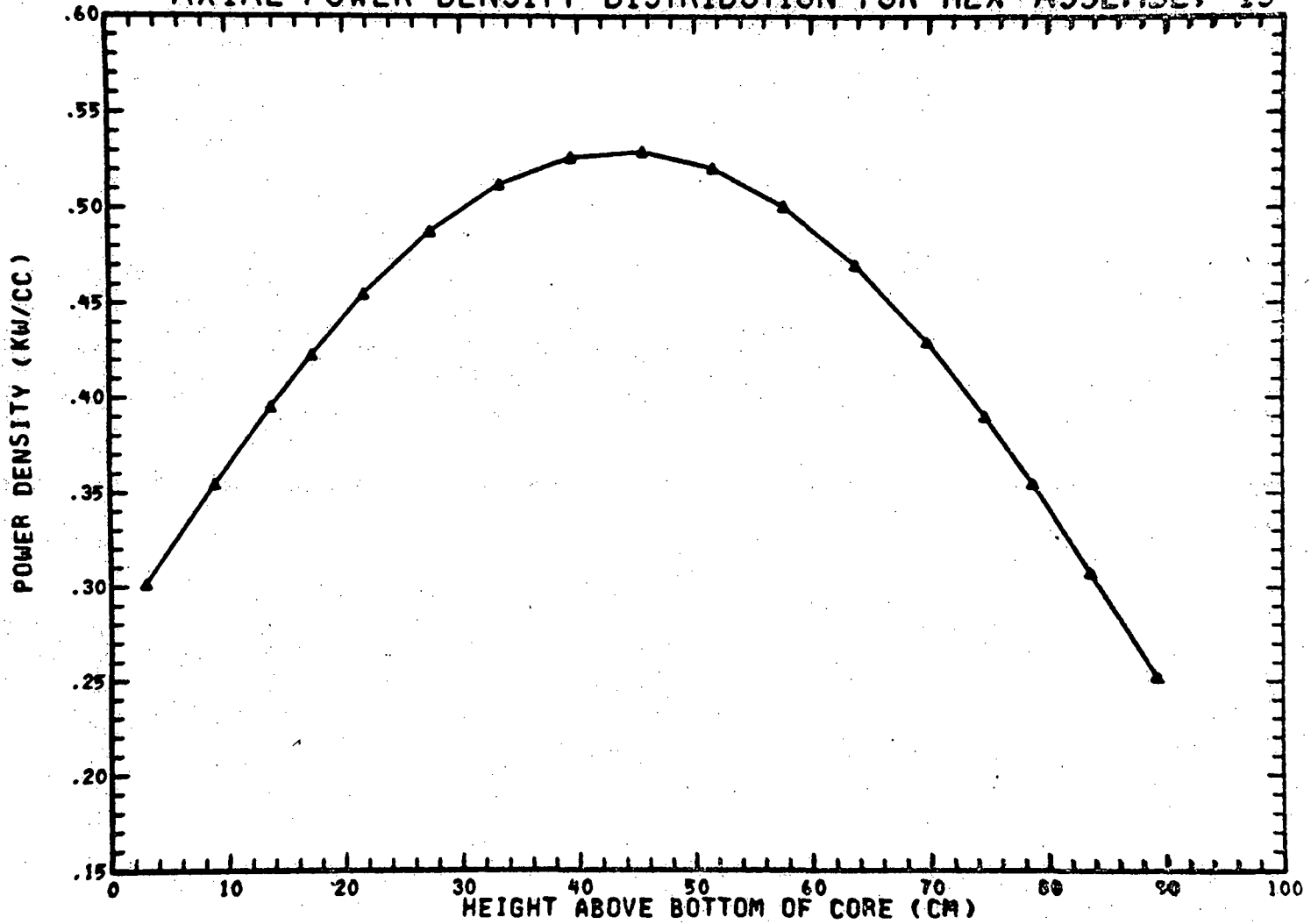
Q001.488-53

Amend. 60
Feb. 1981

FIGURE Q001.488-53

(END OF EQUILIBRIUM CYCLE)

AXIAL POWER DENSITY DISTRIBUTION FOR HEX ASSEMBLY 19



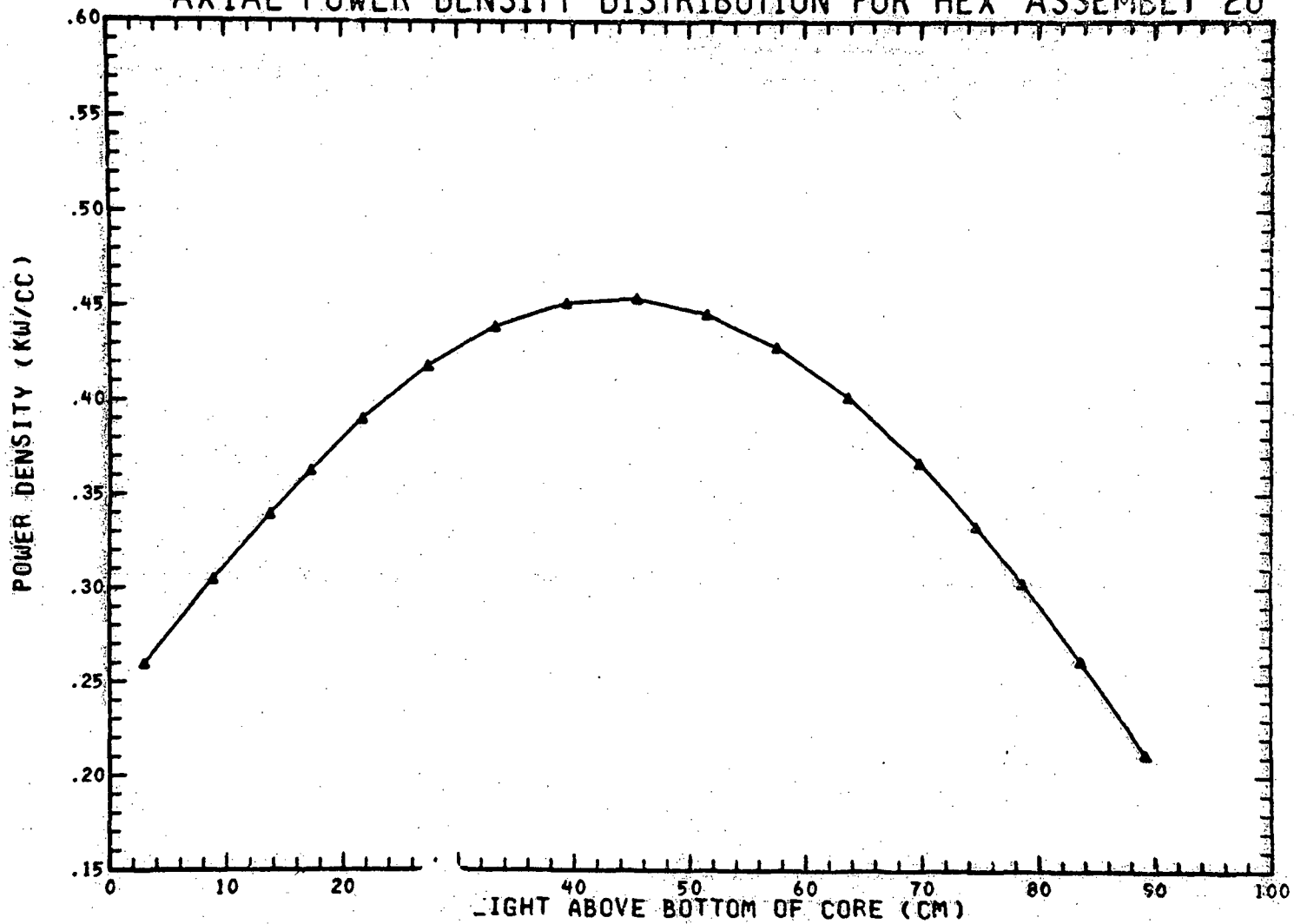
Q001.488-54

Amend. 60
Feb. 1981

TOTAL POWER FOR THIS ASSEMBLY= .5053E+01 MEGAWATTS

(END OF EQUILIBRIUM CYCLE)

AXIAL POWER DENSITY DISTRIBUTION FOR HEX ASSEMBLY 20



TOTAL POWER FOR THIS ASSEMBLY = .4329E+01 MEGAWATTS

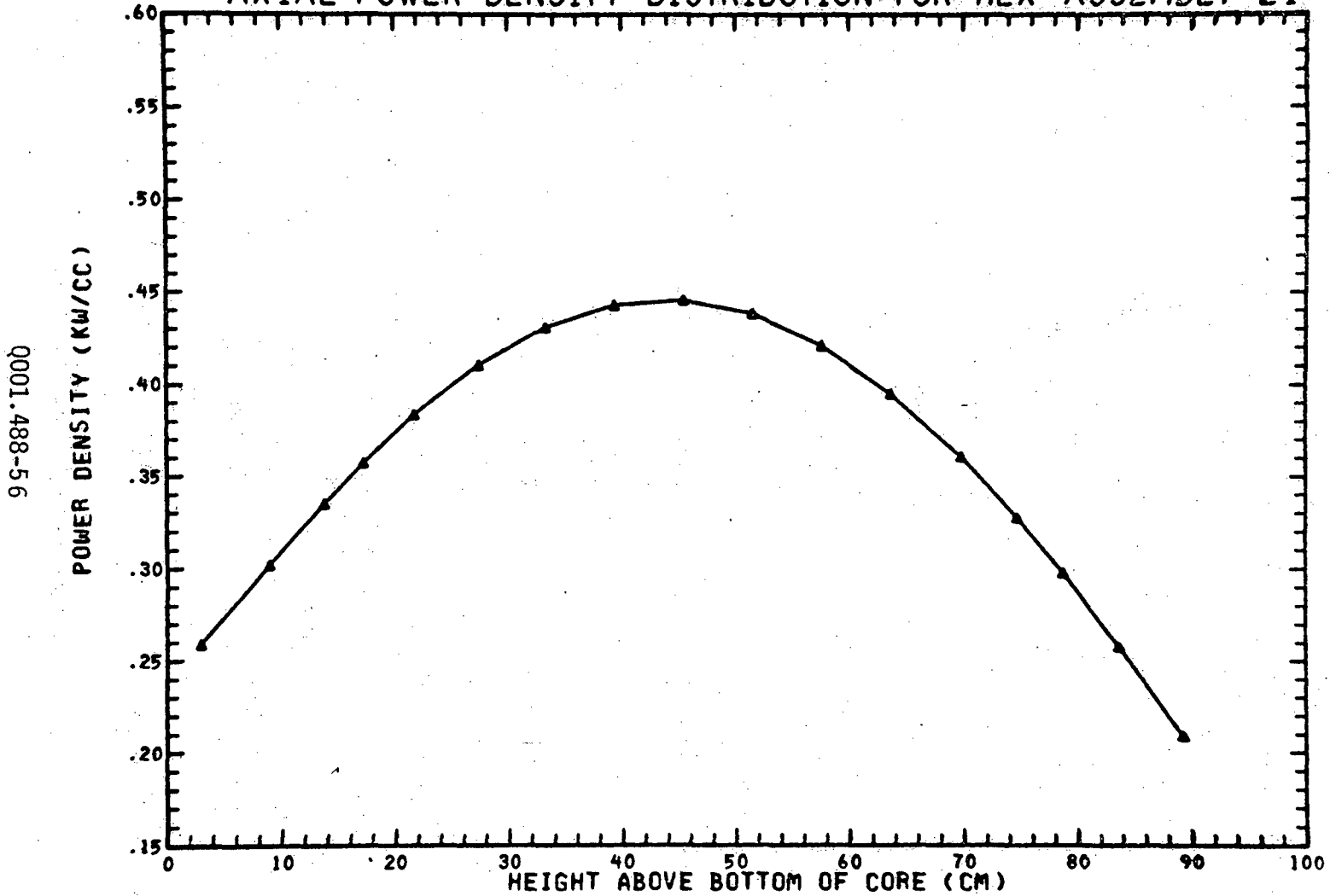
Q001.488-55

Amend. 60
Feb. 1981

FIGURE Q001.488-5 5

(END OF EQUILIBRIUM CYCLE)

AXIAL POWER DENSITY DISTRIBUTION FOR HEX ASSEMBLY 21



Q001.488-5 6

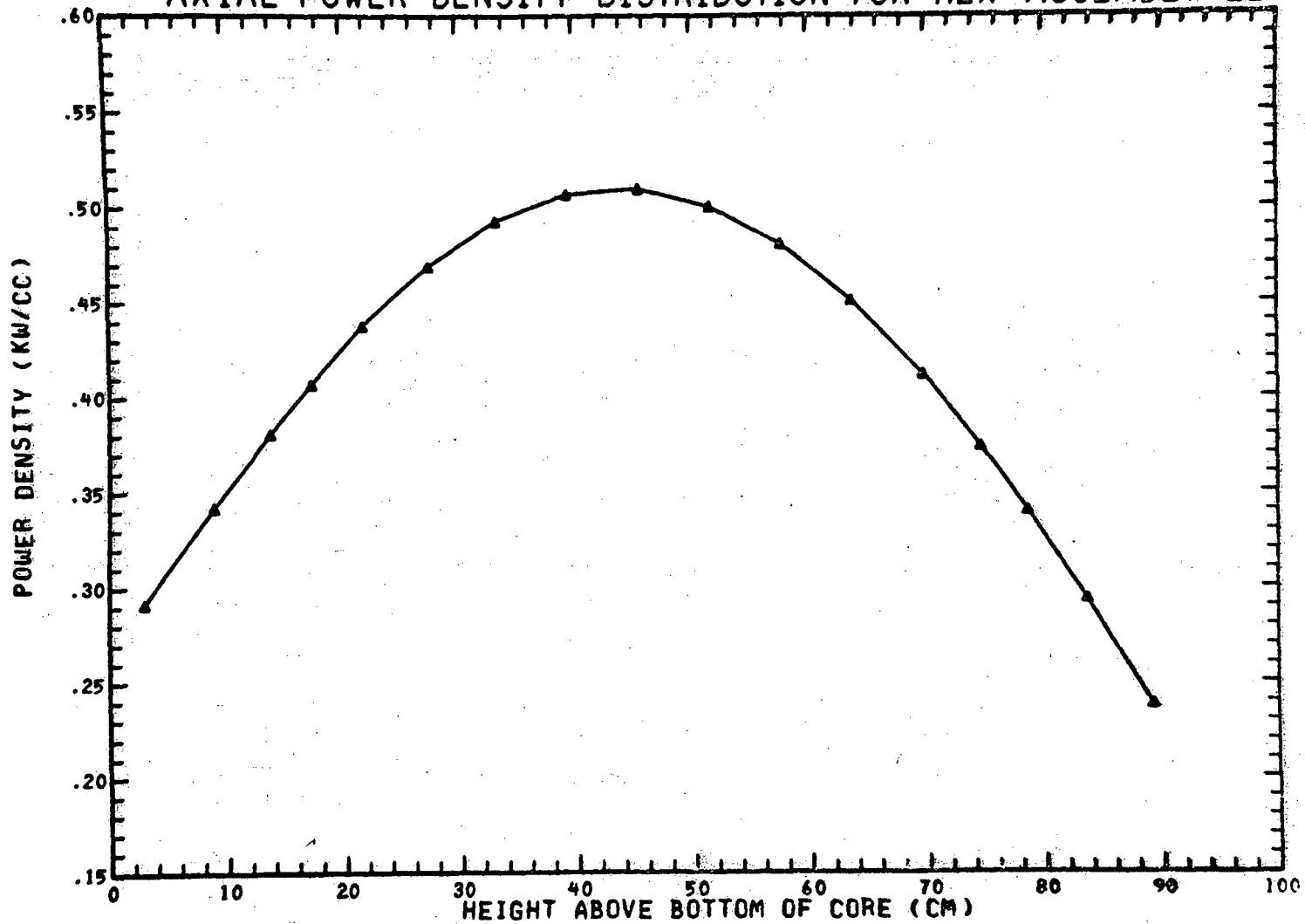
Amend. 60
Feb. 1981

TOTAL POWER FOR THIS ASSEMBLY= .4260E+01 MEGAWATTS

FIGURE Q001.488-56

(END OF EQUILIBRIUM CYCLE)

AXIAL POWER DENSITY DISTRIBUTION FOR HEX ASSEMBLY 22



TOTAL POWER FOR THIS ASSEMBLY = .4857E+01 MEGAWATTS

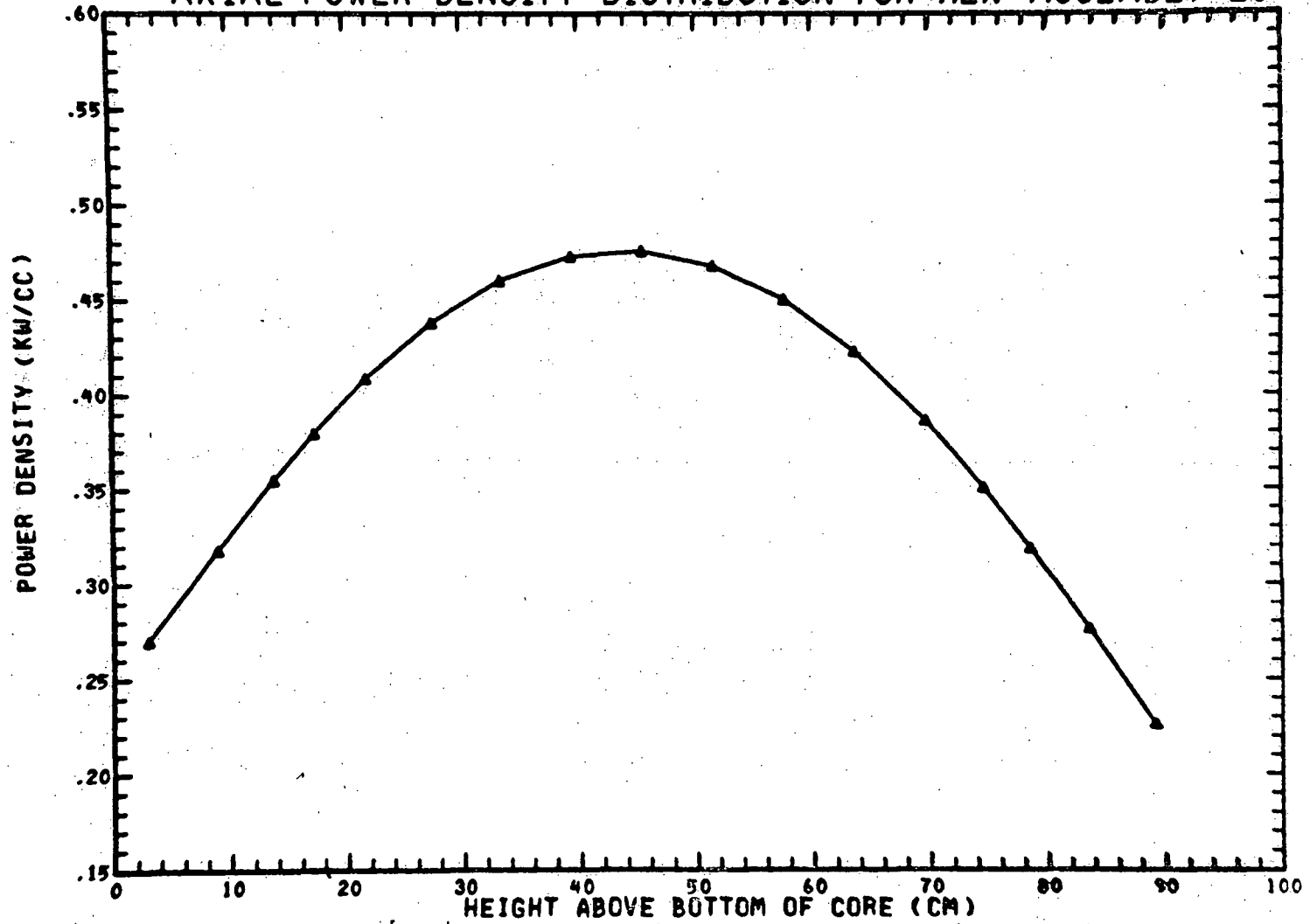
Q001.488-57

Amend. 60
Feb. 1981

FIGURE Q001.488-57

(END OF EQUILIBRIUM CYCLE)

AXIAL POWER DENSITY DISTRIBUTION FOR HEX ASSEMBLY 23



TOTAL POWER FOR THIS ASSEMBLY= .4541E+01 MEGAWATTS

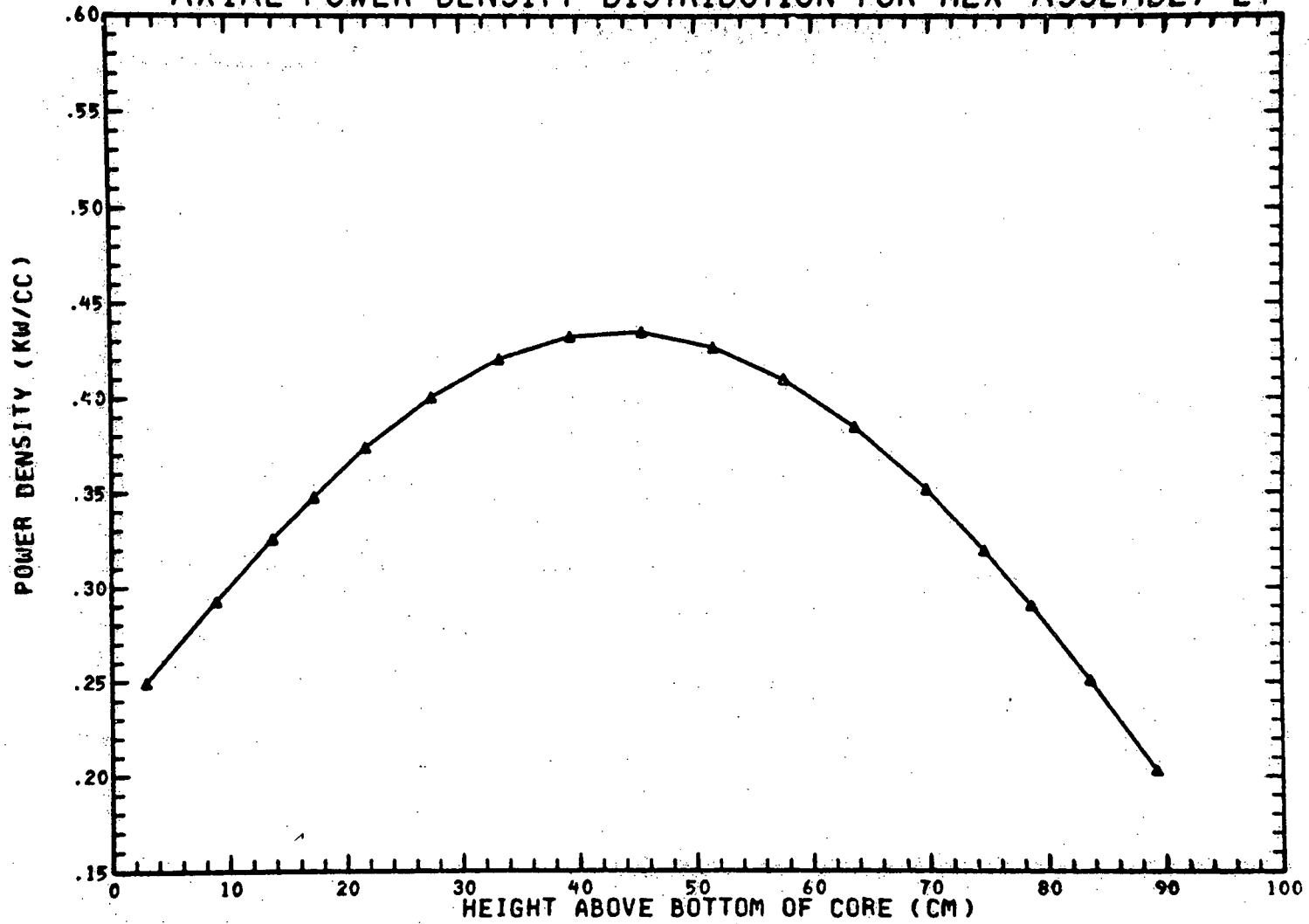
Q001.488-58

Amend. 60
Feb. 1981

FIGURE Q001.488-5 8

(END OF EQUILIBRIUM CYCLE)

AXIAL POWER DENSITY DISTRIBUTION FOR HEX ASSEMBLY 24



TOTAL POWER FOR THIS ASSEMBLY= .4146E+01 MEGAWATTS

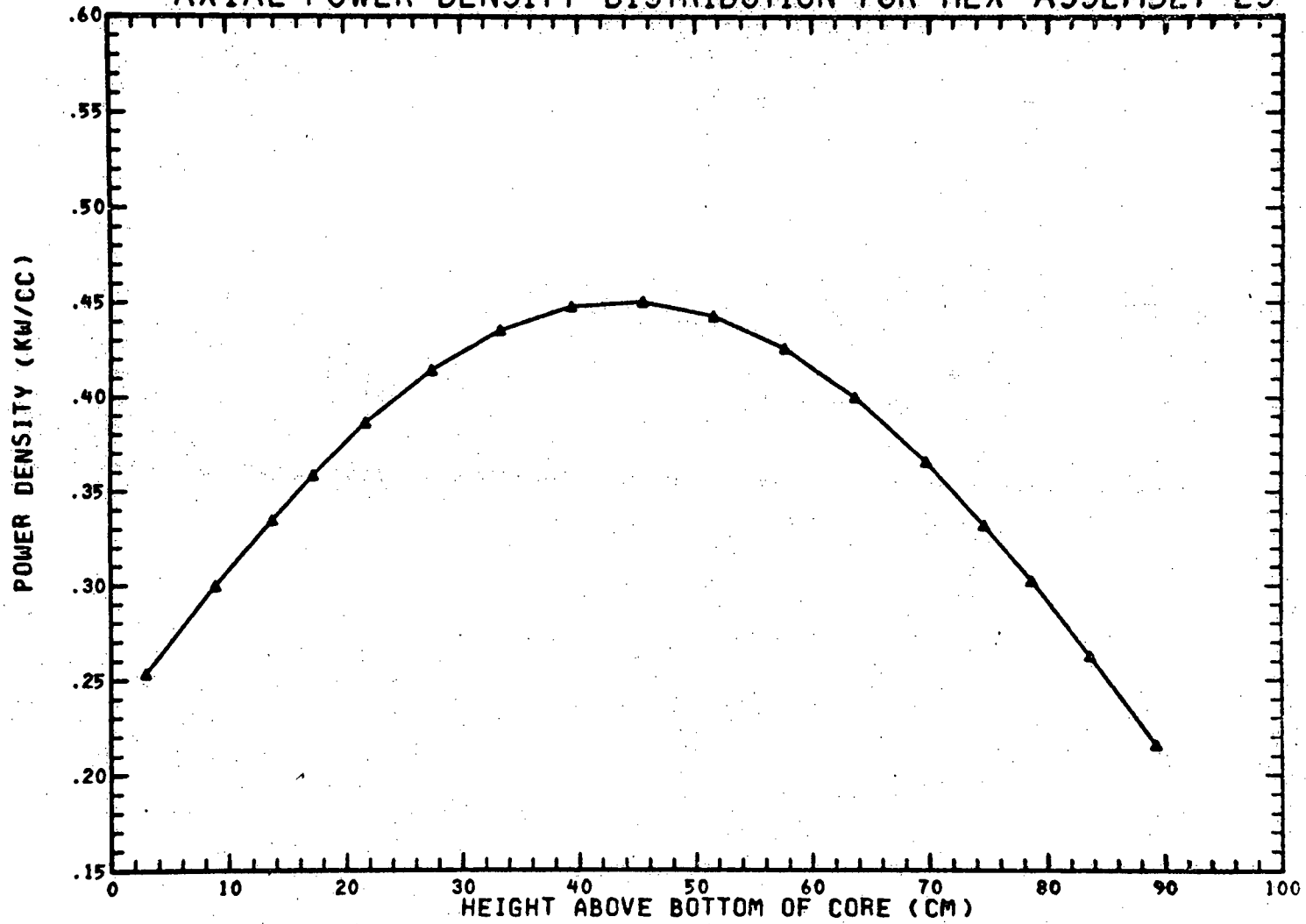
Q001.488-59

Amend. 60
Feb. 1981

FIGURE Q001.488-59

(END OF EQUILIBRIUM CYCLE)

AXIAL POWER DENSITY DISTRIBUTION FOR HEX ASSEMBLY 25

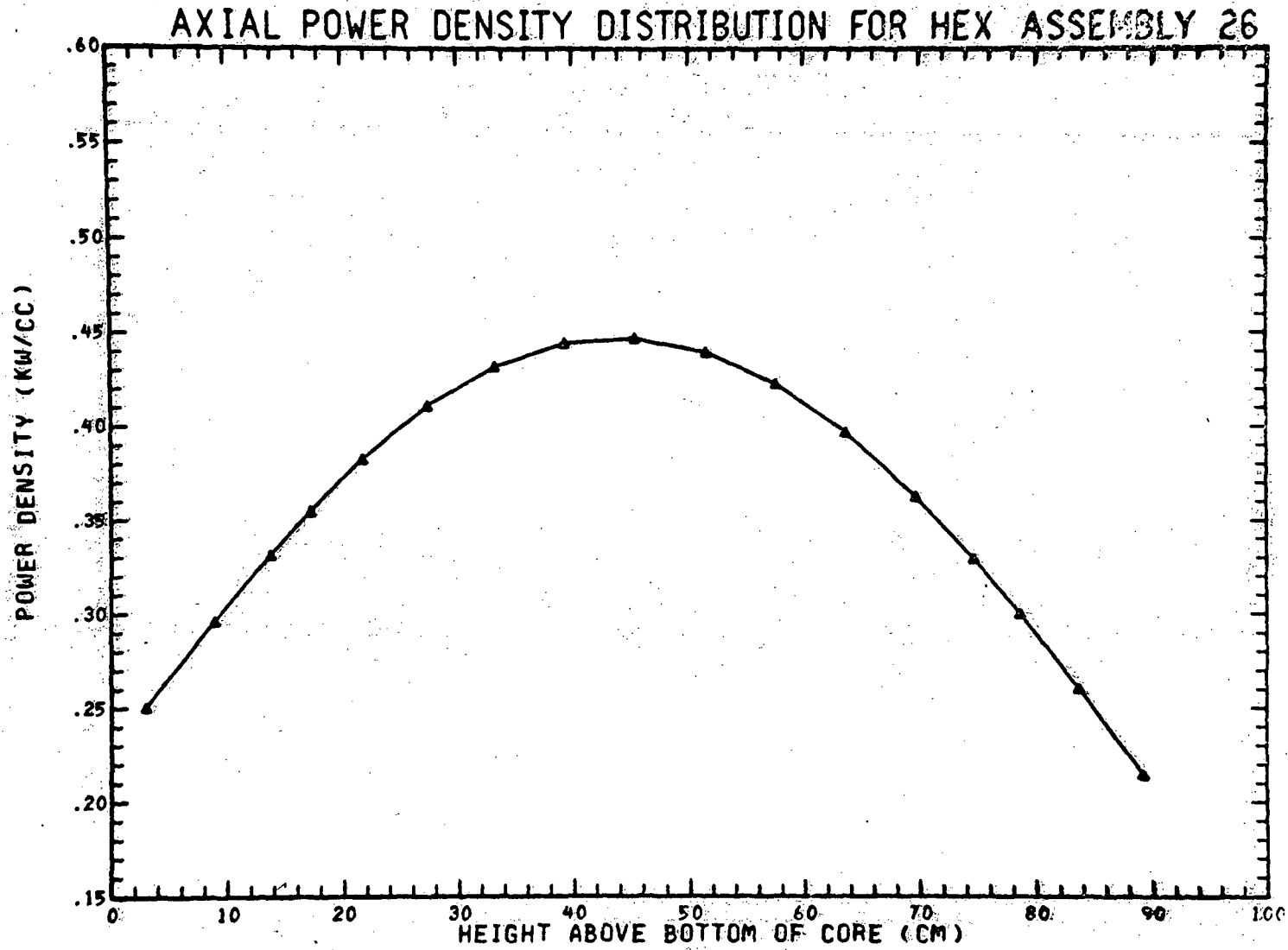


TOTAL POWER FOR THIS ASSEMBLY= .4300E+01 MEGAWATTS

Q001.488-60

Amend. 60
Feb. 1981

FIGURE Q001.488-60
(END OF EQUILIBRIUM CYCLE)



TOTAL POWER FOR THIS ASSEMBLY = .4263E+01 MEGAWATTS

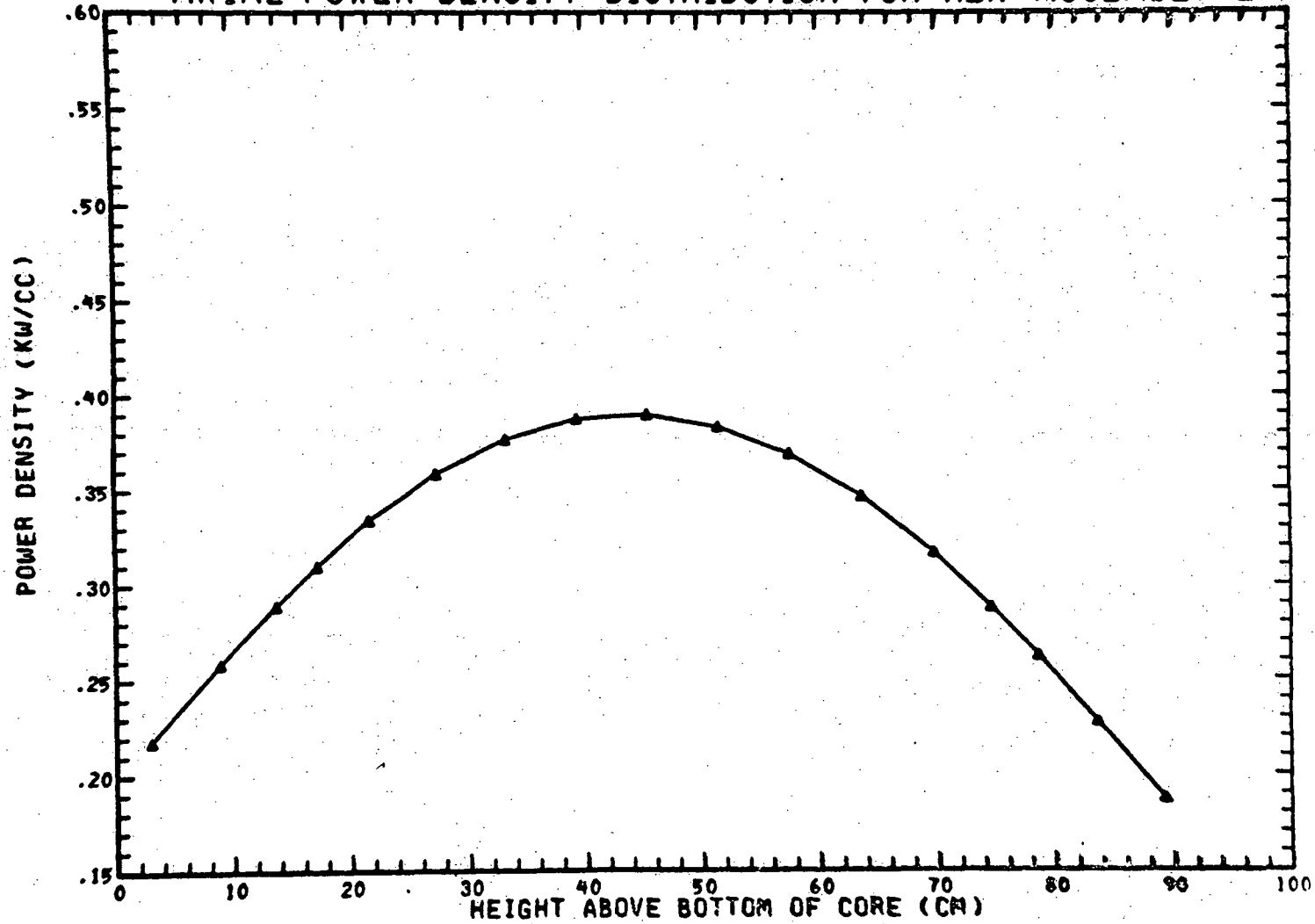
Q001.488-61

Amend. 60
Feb. 1981

FIGURE Q001.488.61

(END OF EQUILIBRIUM CYCLE)

AXIAL POWER DENSITY DISTRIBUTION FOR HEX ASSEMBLY 27



TOTAL POWER FOR THIS ASSEMBLY= .3718E+01 MEGAWATTS

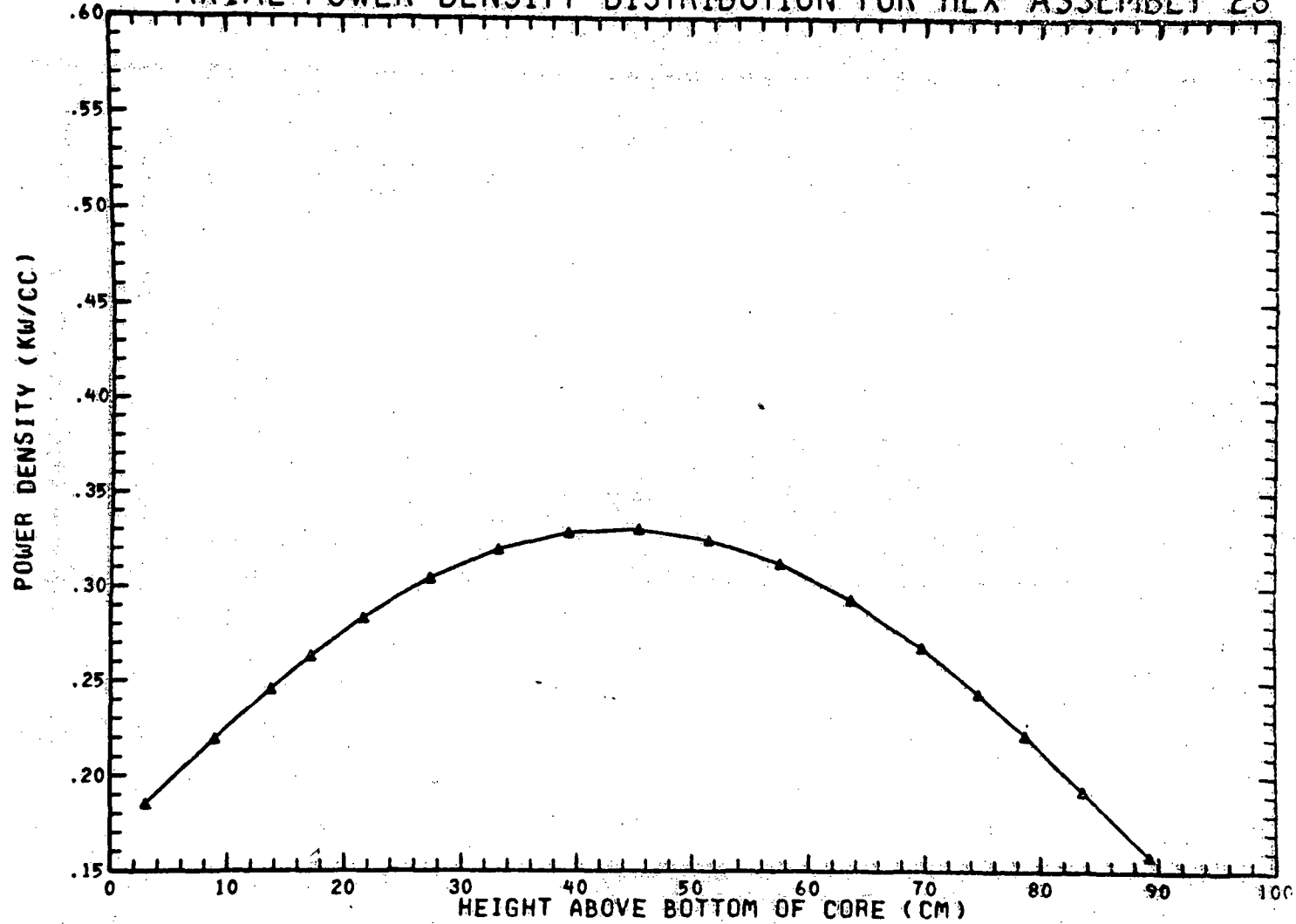
Q001.488-62

Amend. 60
Feb. 1981

FIGURE Q001.488-62

(END OF EQUILIBRIUM CYCLE)

AXIAL POWER DENSITY DISTRIBUTION FOR HEX ASSEMBLY 28



TOTAL POWER FOR THIS ASSEMBLY= .3156E+01 MEGAWATTS

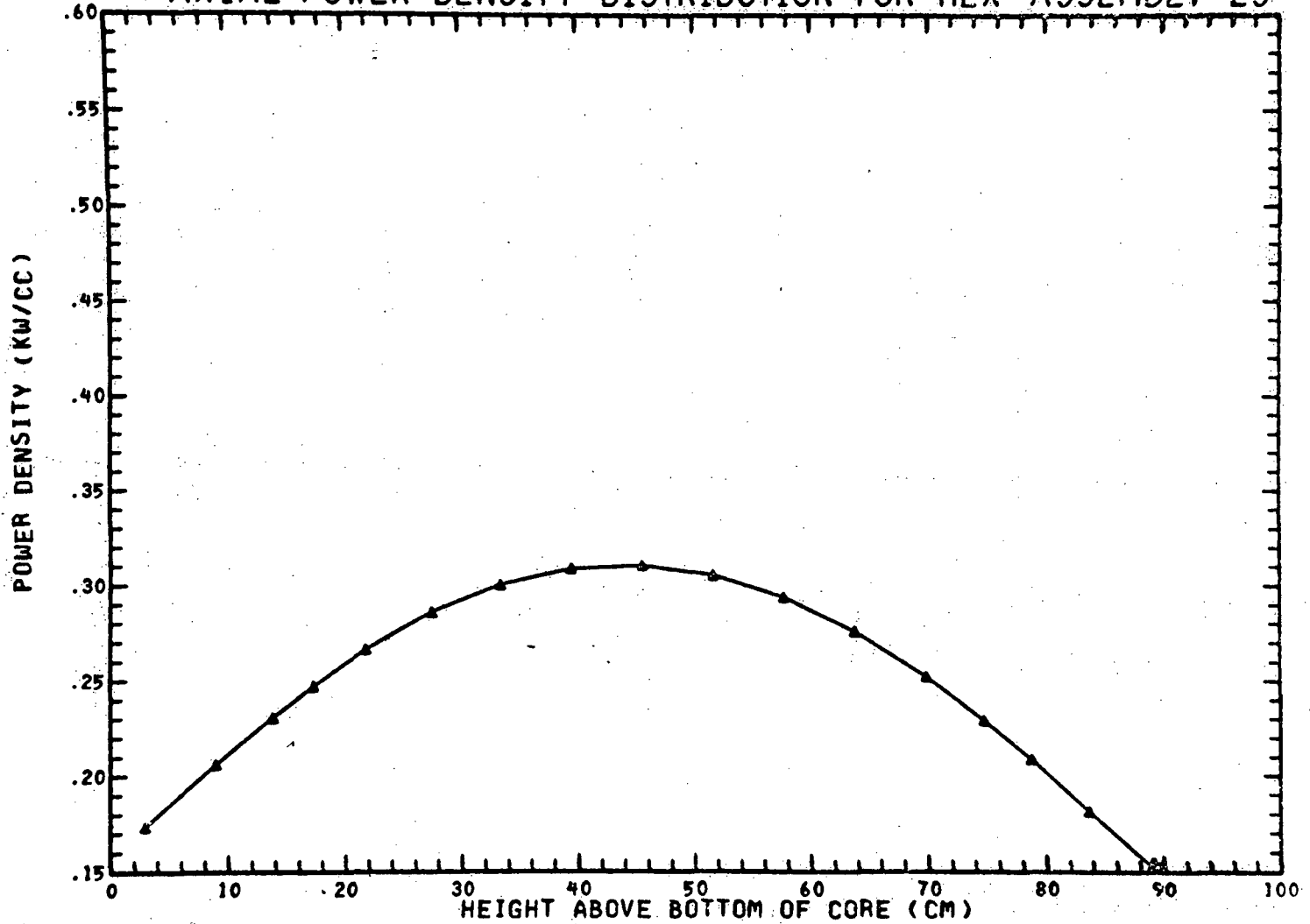
Q001.488-63

Amend. 60
Feb. 1981

FIGURE Q001.488-63

(END OF EQUILIBRIUM CYCLE)

AXIAL POWER DENSITY DISTRIBUTION FOR HEX ASSEMBLY 29



TOTAL POWER FOR THIS ASSEMBLY= .2962E+01 MEGAWATTS

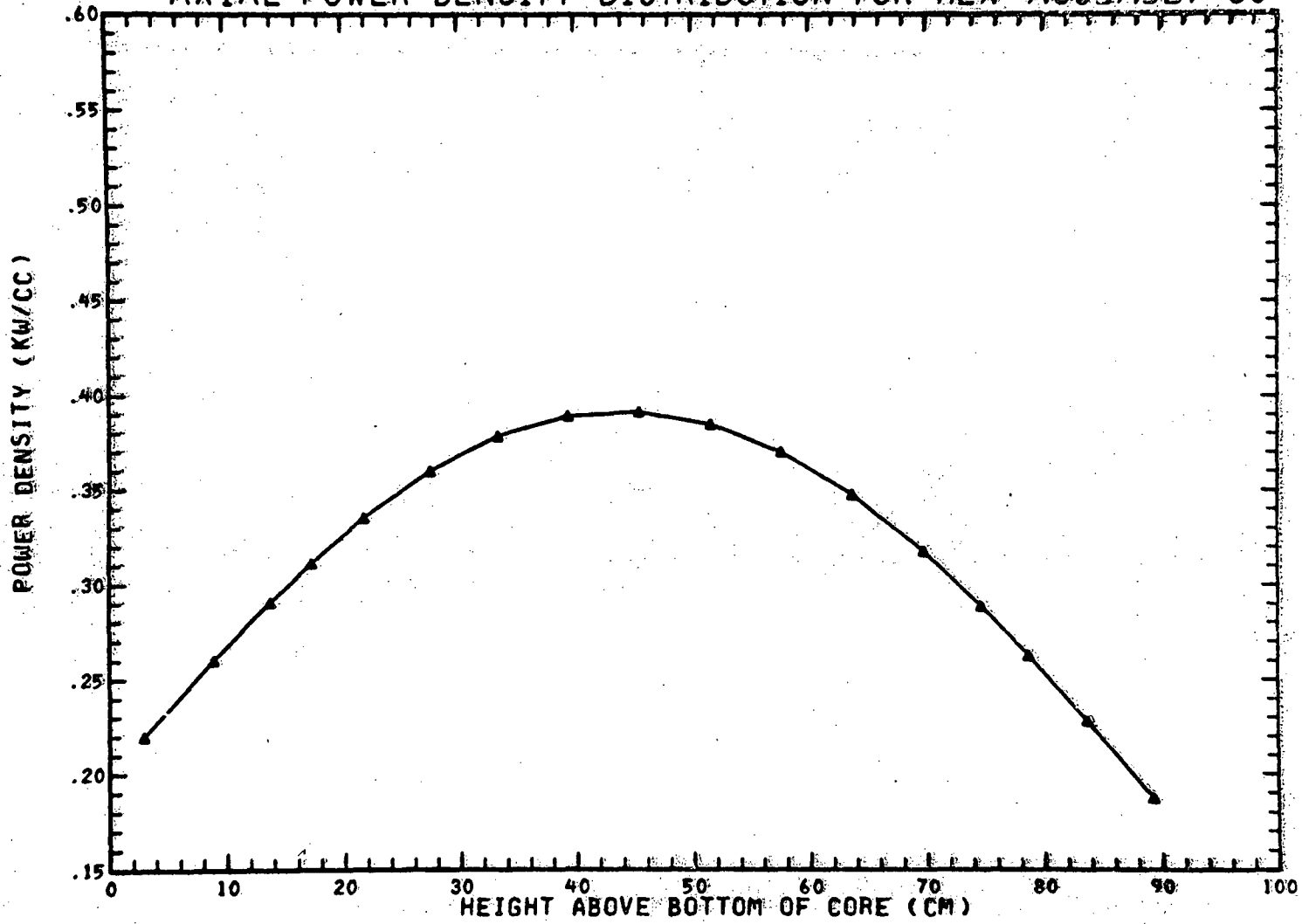
Q001.488-64

Amend. 60
Feb. 1981

FIGURE 0001.488-64

(END OF EQUILIBRIUM CYCLE)

AXIAL POWER DENSITY DISTRIBUTION FOR HEX ASSEMBLY 30



TOTAL POWER FOR THIS ASSEMBLY= .3734E+01 MEGAWATTS

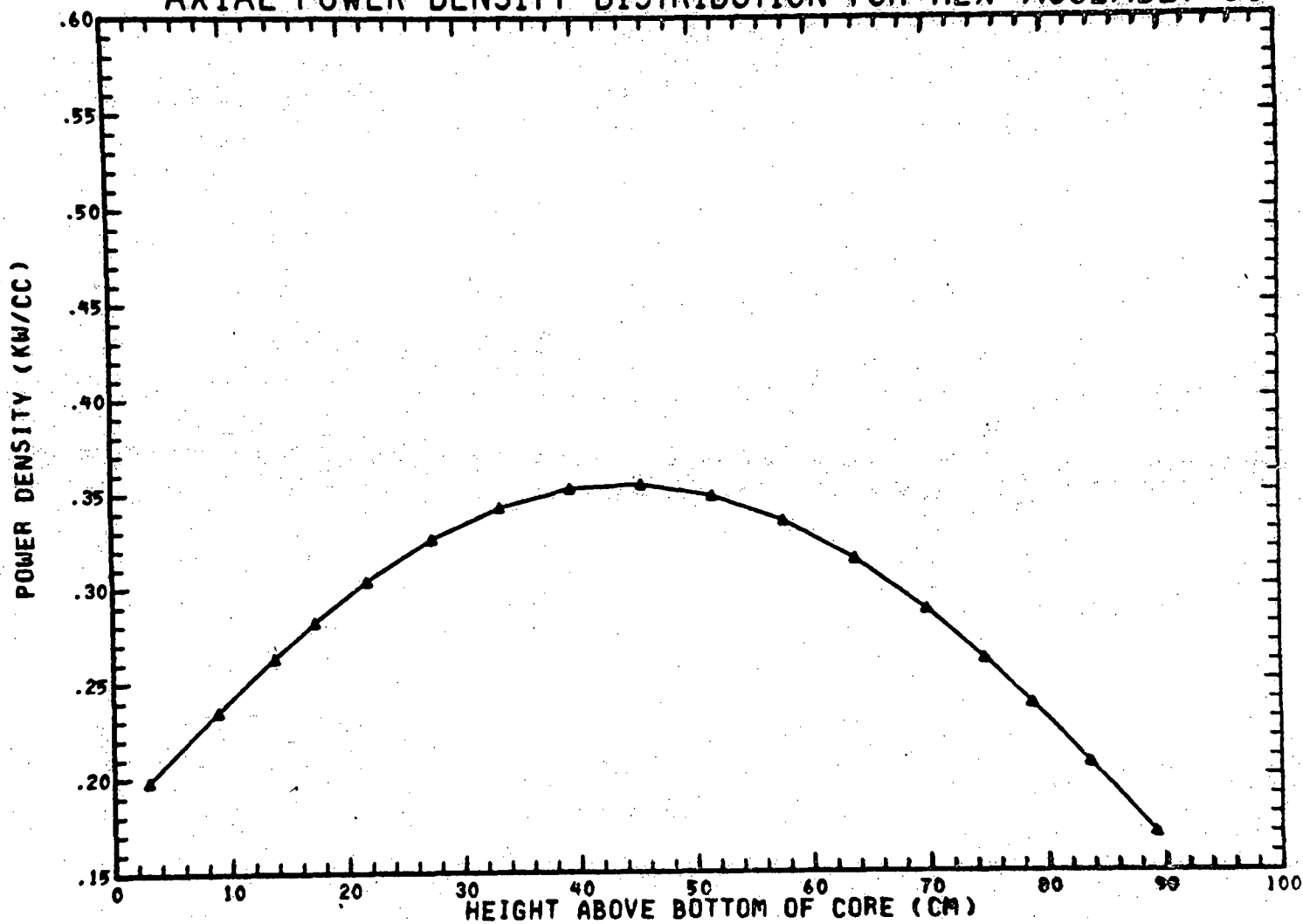
0001.488-65

Amend. 60
Feb. 1981

FIGURE Q001.488-65

(END OF EQUILIBRIUM CYCLE)

AXIAL POWER DENSITY DISTRIBUTION FOR HEX ASSEMBLY 31



TOTAL POWER FOR THIS ASSEMBLY = .3377E+01 MEGAWATTS

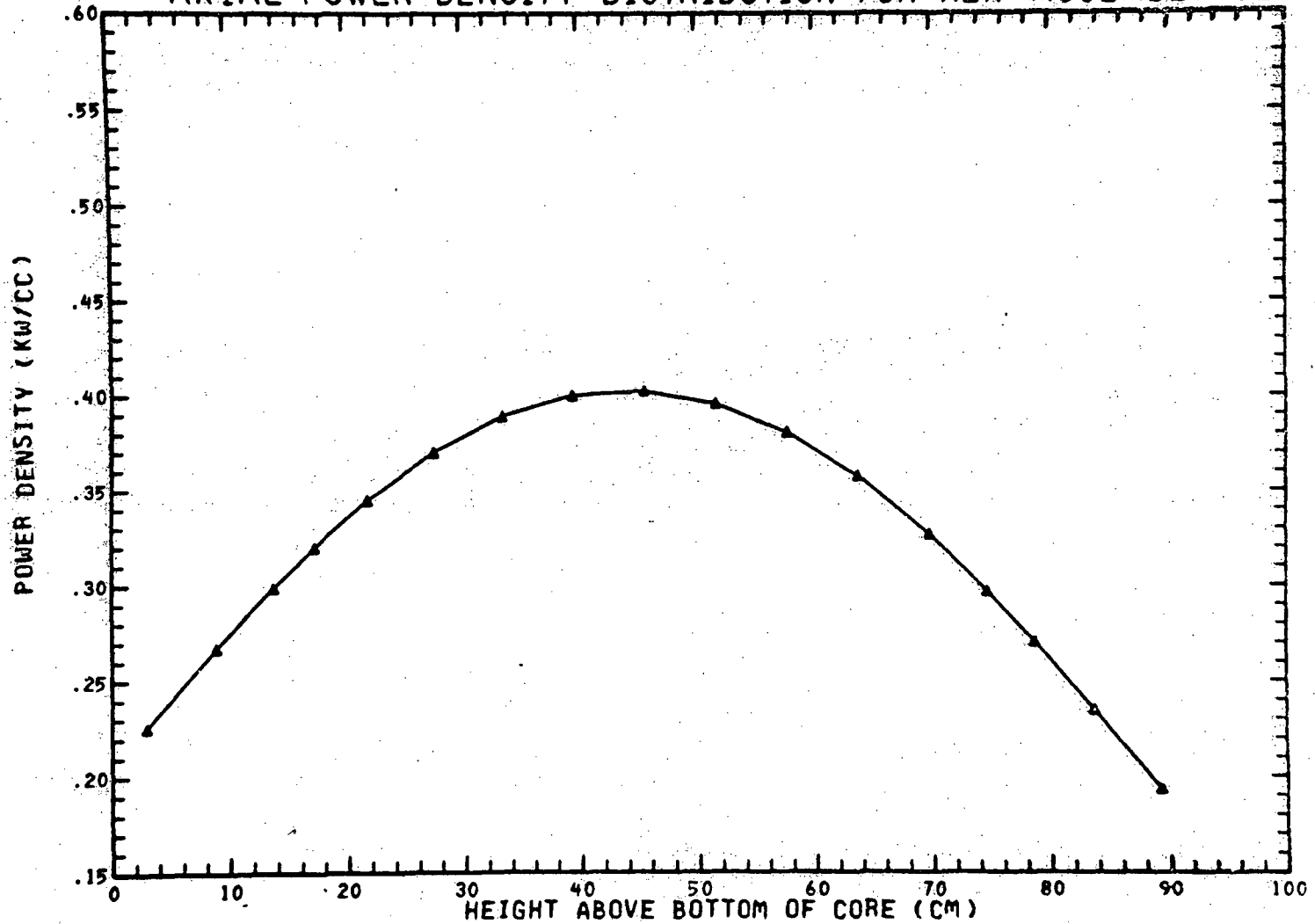
Q001.488-66

Amend. 60
Feb. 1981

FIGURE Q001.488-66

(END OF EQUILIBRIUM CYCLE)

AXIAL POWER DENSITY DISTRIBUTION FOR HEX ASSEMBLY 32



TOTAL POWER FOR THIS ASSEMBLY= .3840E+01 MEGAWATTS

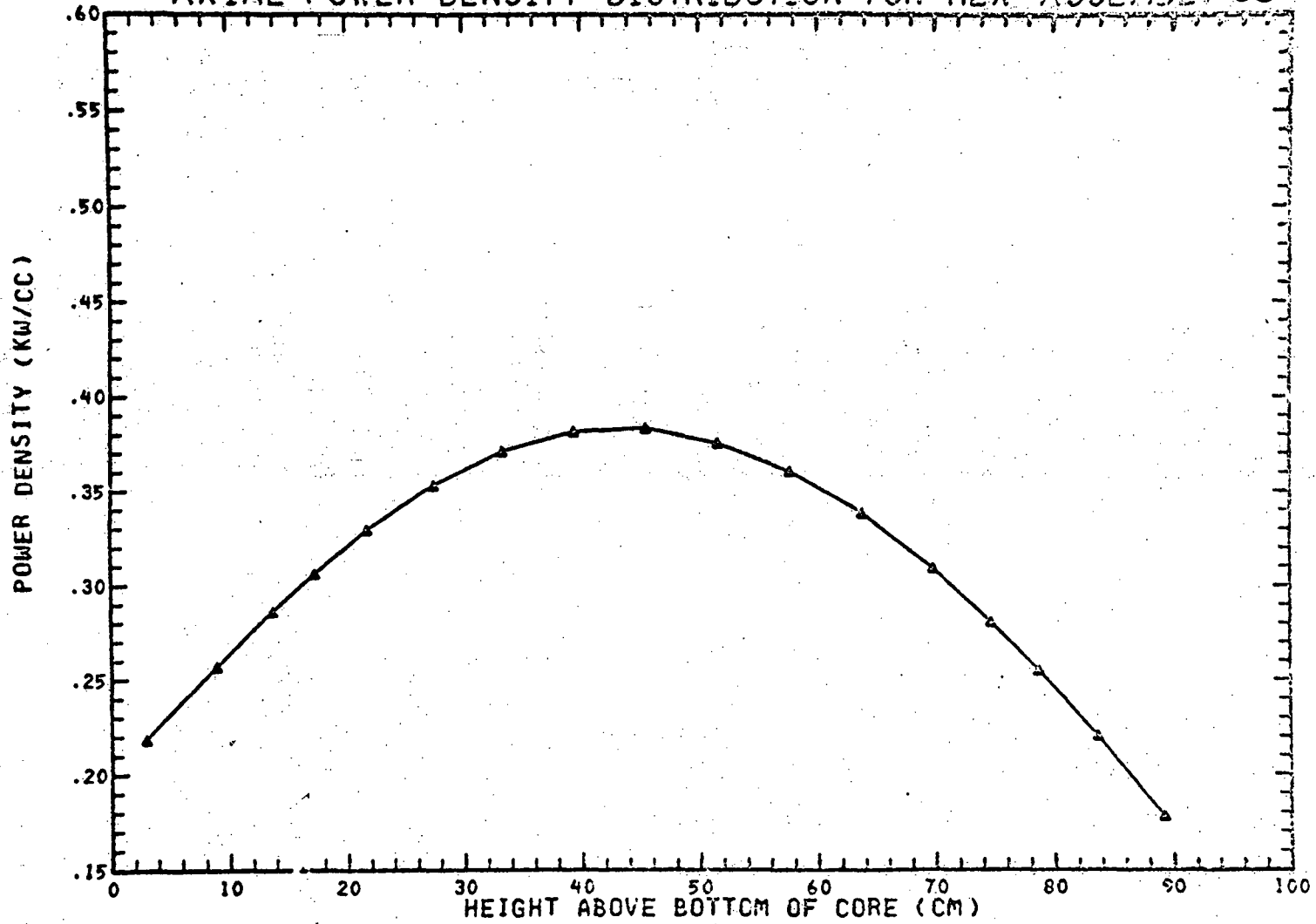
Q001.488-67

Amend. 60
Feb. 1981

FIGURE Q001.488-67

(END OF EQUILIBRIUM CYCLE)

AXIAL POWER DENSITY DISTRIBUTION FOR HEX ASSEMBLY 68



TOTAL POWER FOR THIS ASSEMBLY= .3649E+01 MEGAWATTS

Q001.488-68

Amend. 60
Feb. 1981

FIGURE Q001.488-68

DESCRIPTION OF AXIAL PLANES

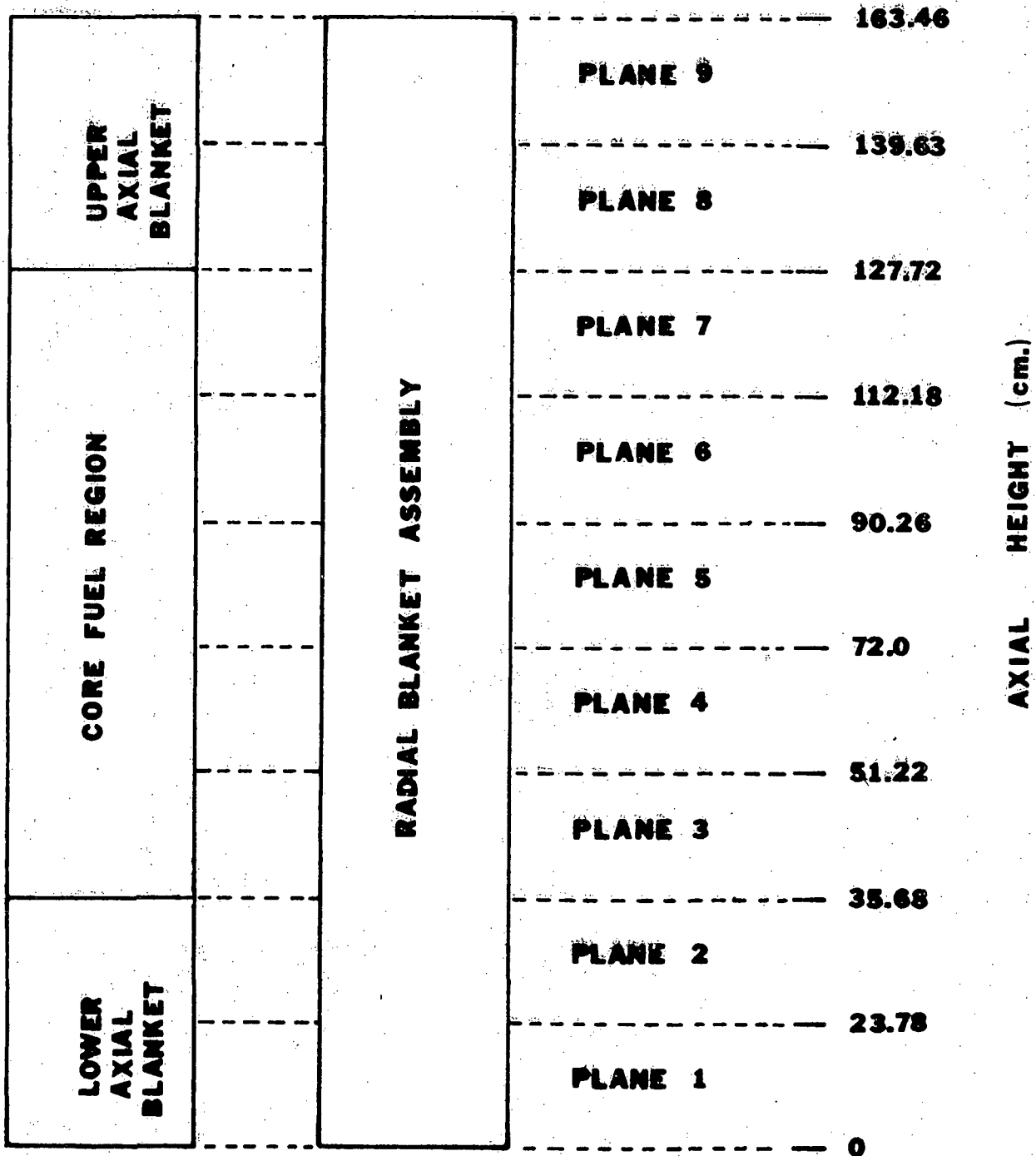
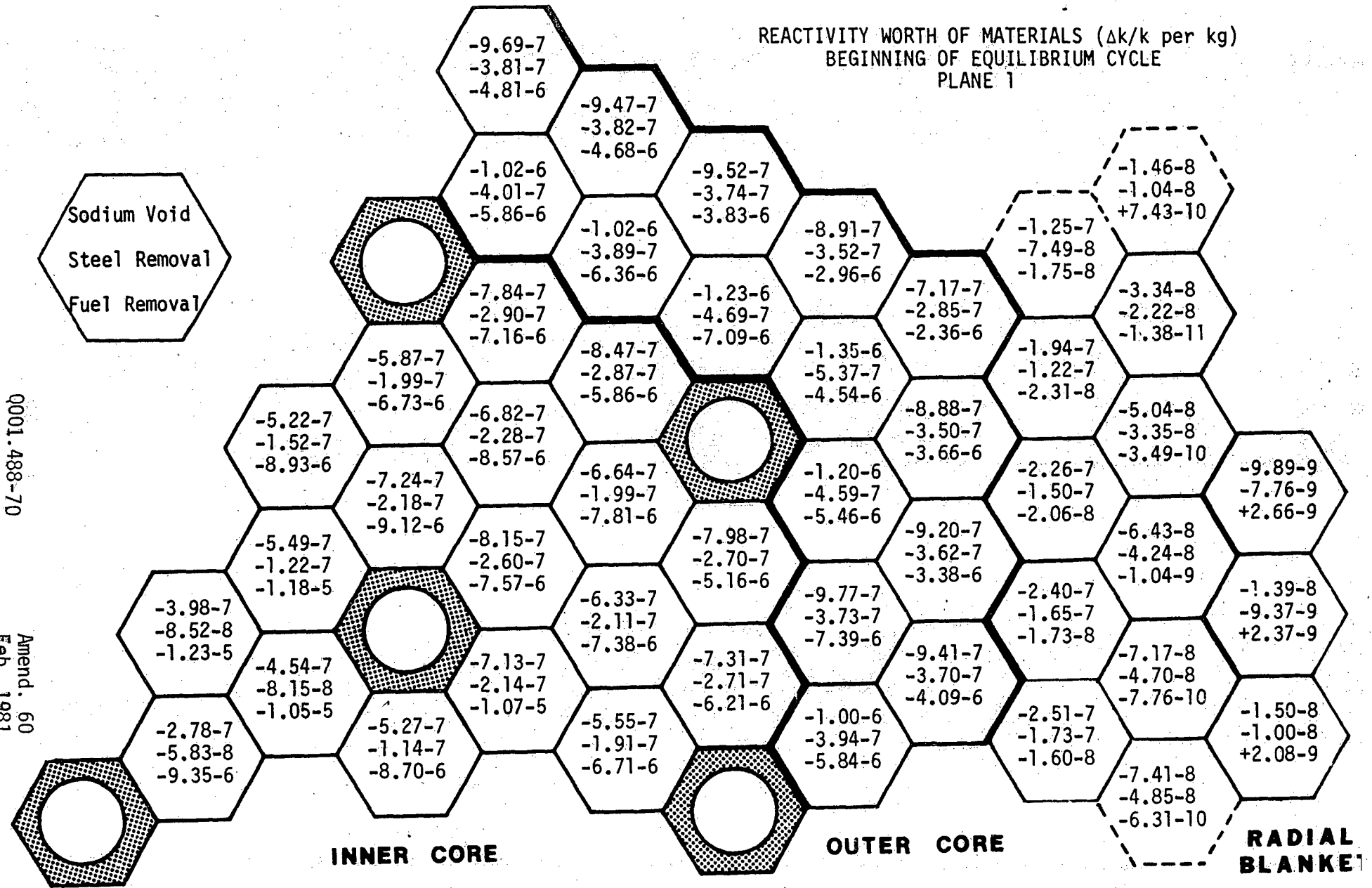


FIGURE Q001.488-69

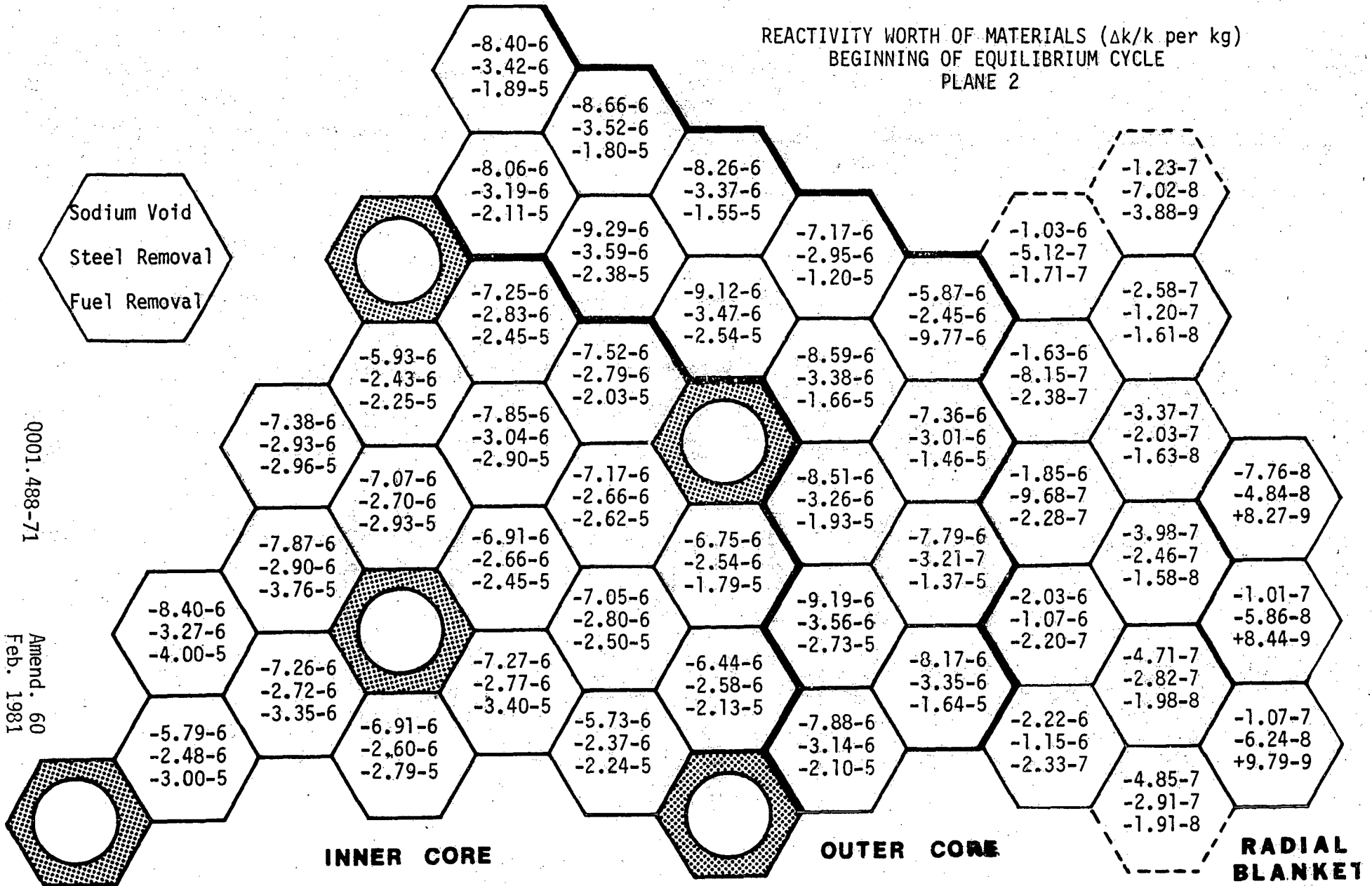
REACTIVITY WORTH OF MATERIALS ($\Delta k/k$ per kg)
 BEGINNING OF EQUILIBRIUM CYCLE
 PLANE 1



Q001.488-70
 Amend. 60
 Feb. 1981

FIGURE Q001.488-70

REACTIVITY WORTH OF MATERIALS ($\Delta k/k$ per kg)
 BEGINNING OF EQUILIBRIUM CYCLE
 PLANE 2

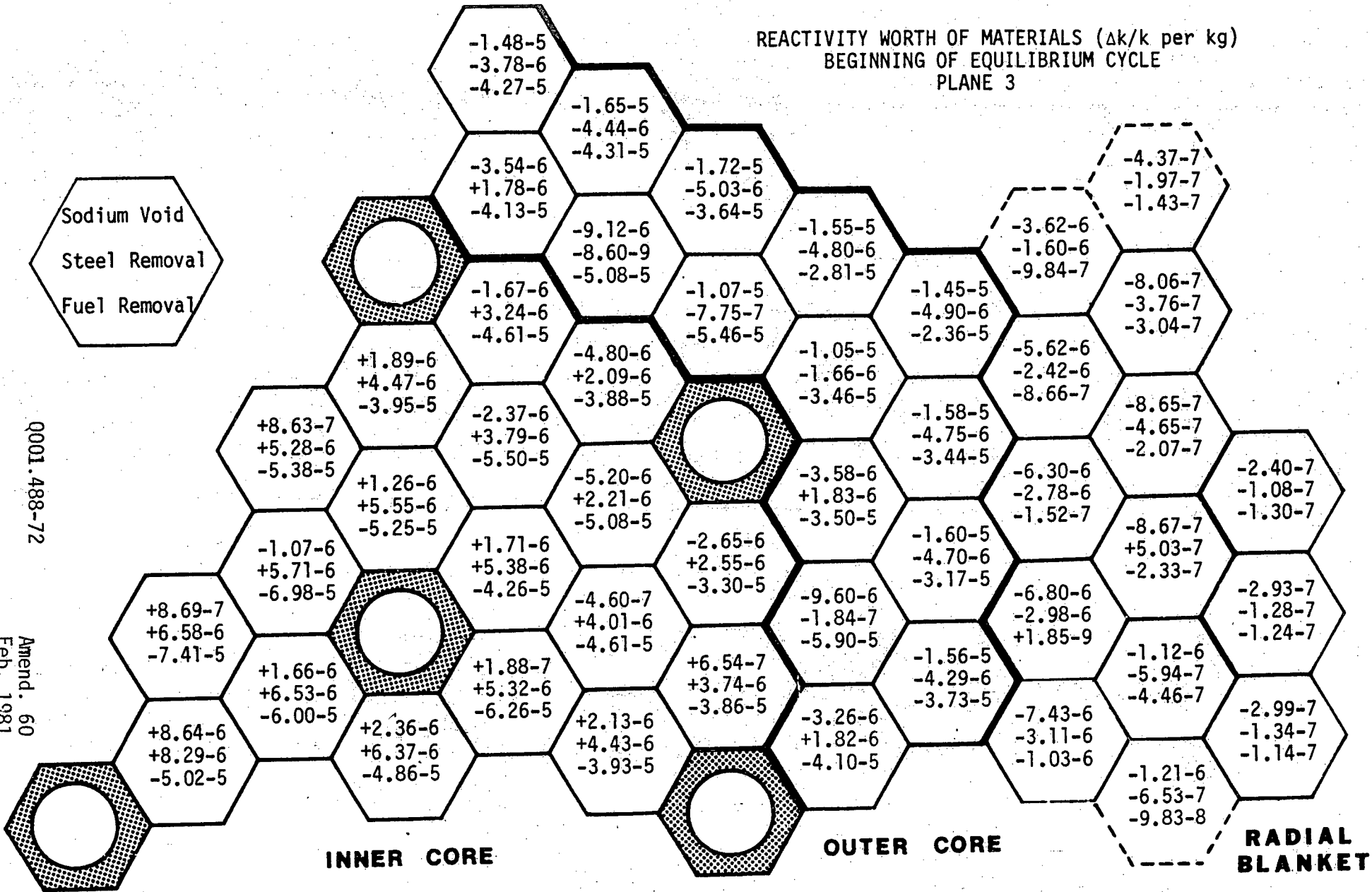


Q001.488-71

Amend. 60
 Feb. 1981

FIGURE Q001.488-71

REACTIVITY WORTH OF MATERIALS ($\Delta k/k$ per kg)
 BEGINNING OF EQUILIBRIUM CYCLE
 PLANE 3



Q001.488-72

Amend. 60
 Feb. 1981

FIGURE Q001.488-73

REACTIVITY WORTH OF MATERIALS ($\Delta k/k$ per kg)
 BEGINNING OF EQUILIBRIUM CYCLE
 PLANE 5

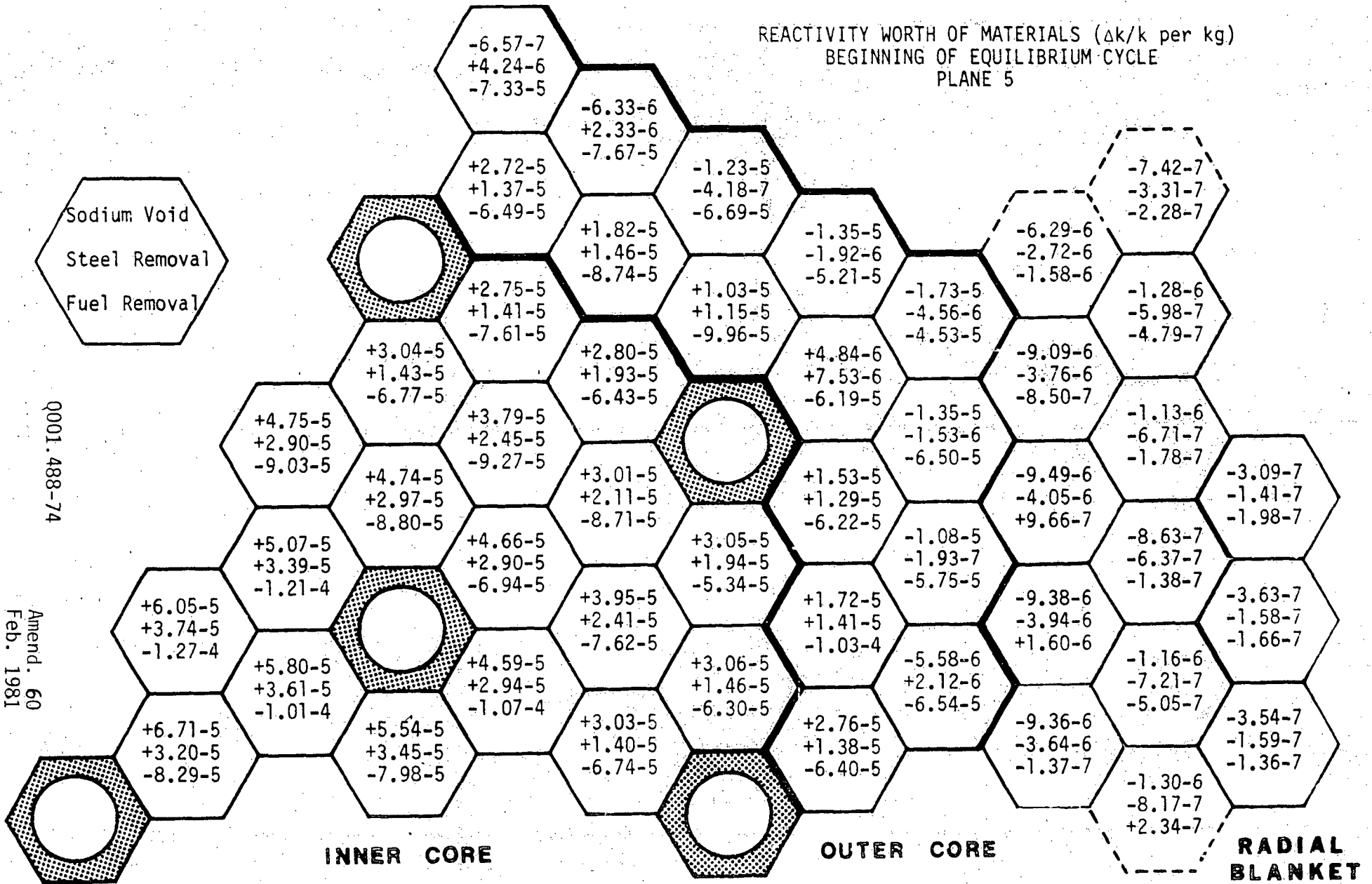


FIGURE Q001.488-74

REACTIVITY WORTH OF MATERIALS ($\Delta k/k$ per kg)
 BEGINNING OF EQUILIBRIUM CYCLE
 PLANE 6

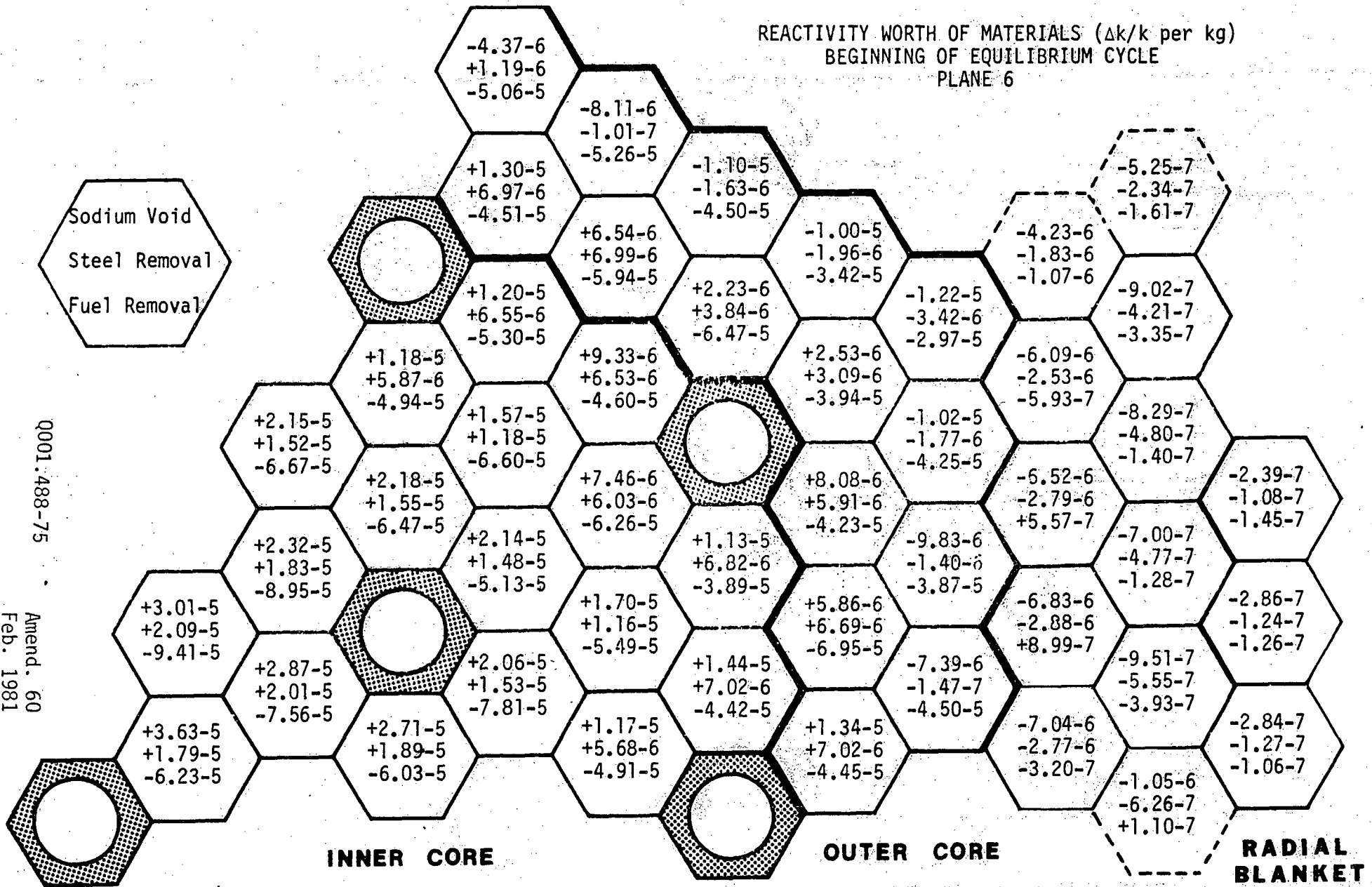
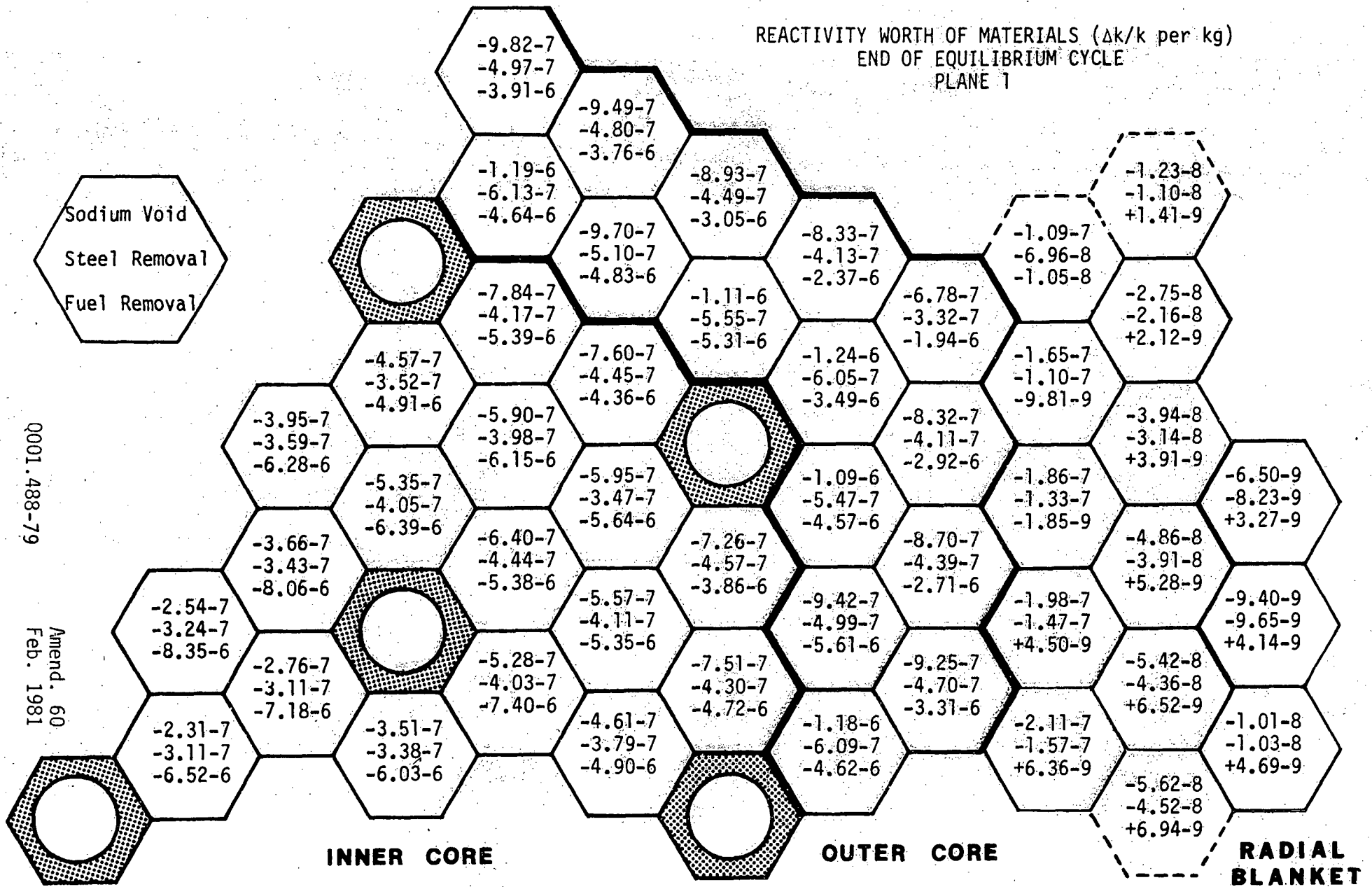


FIGURE Q001.488-78

REACTIVITY WORTH OF MATERIALS ($\Delta k/k$ per kg)
 END OF EQUILIBRIUM CYCLE
 PLANE 1

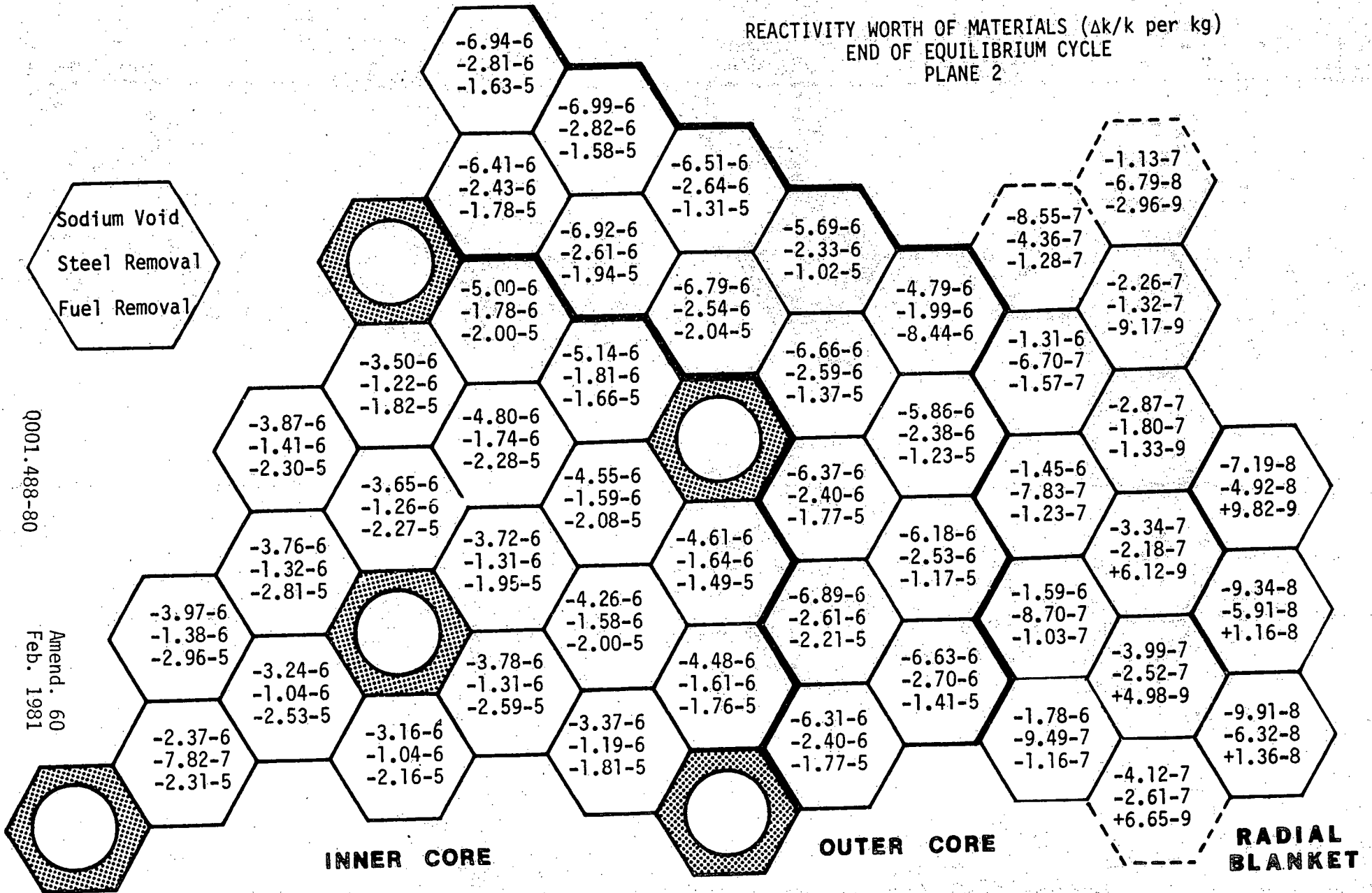


Q001.488-79

Amend. 60
 Feb. 1981

FIGURE Q001.488-79

REACTIVITY WORTH OF MATERIALS ($\Delta k/k$ per kg)
 END OF EQUILIBRIUM CYCLE
 PLANE 2



Q001.488-80

Amend. 60
 Feb. 1981

FIGURE 0001.488-80

REACTIVITY WORTH OF MATERIALS ($\Delta k/k$ per kg)
 END OF EQUILIBRIUM CYCLE
 PLANE 3

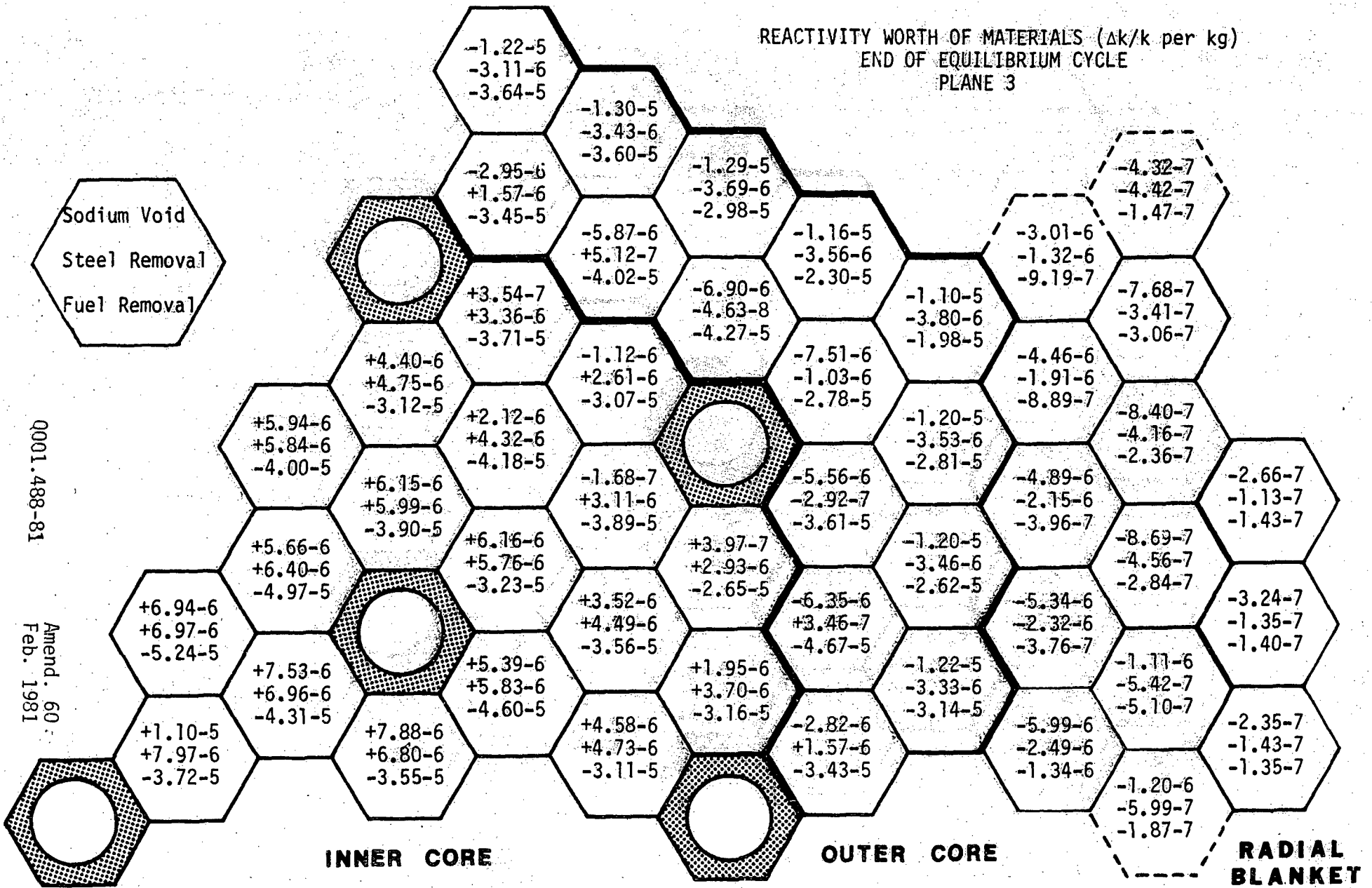


FIGURE Q0011.488-82

REACTIVITY WORTH OF MATERIALS ($\Delta k/k$ per kg)
END OF EQUILIBRIUM CYCLE
PLANE 5

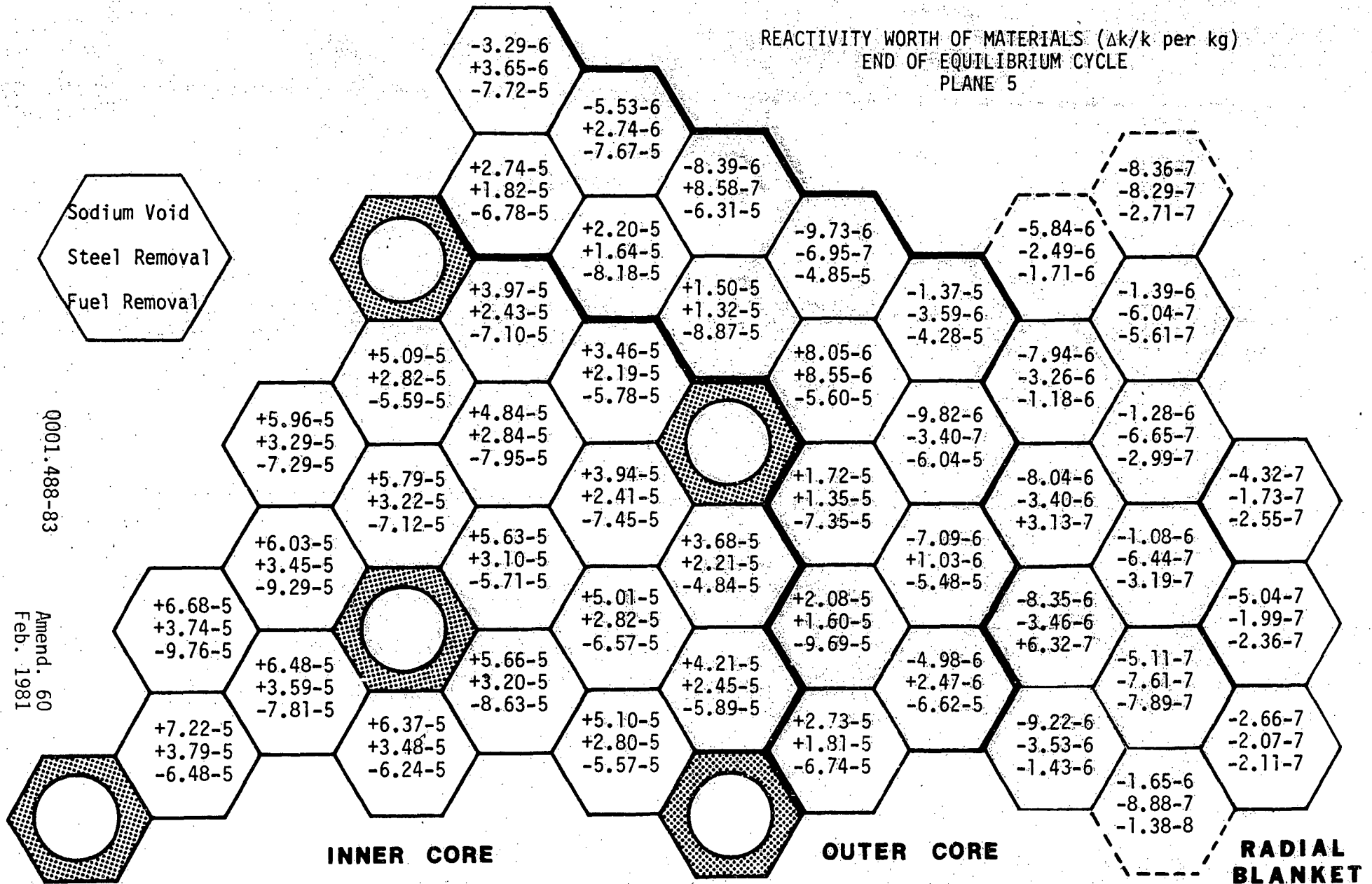


FIGURE Q001.488-84

REACTIVITY WORTH OF MATERIALS ($\Delta k/k$ per kg)
END OF EQUILIBRIUM CYCLE
PLANE 7

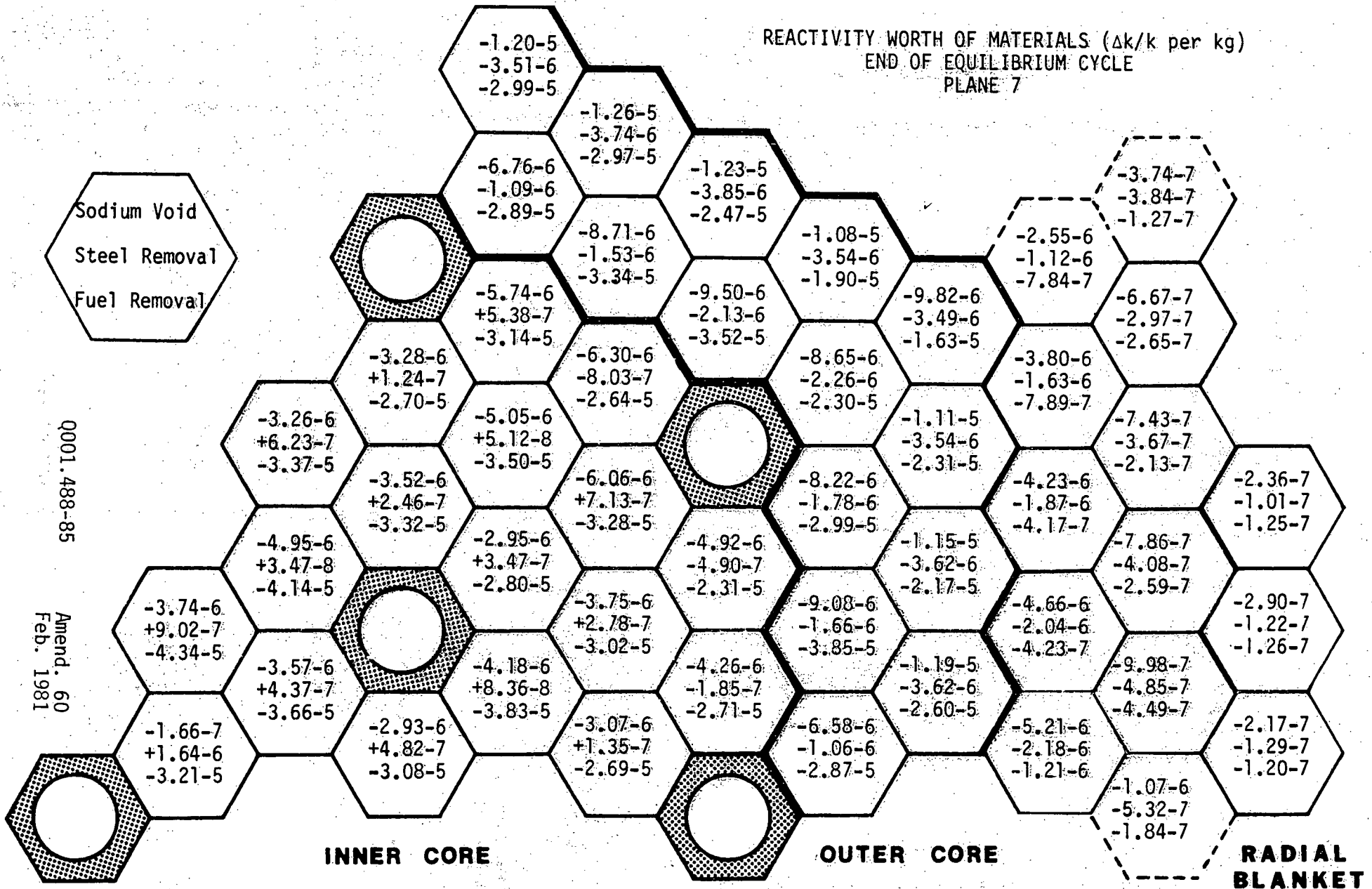


FIGURE Q001.488-85

REACTIVITY WORTH OF MATERIALS ($\Delta k/k$ per kg)
 END OF EQUILIBRIUM CYCLE
 PLANE 8

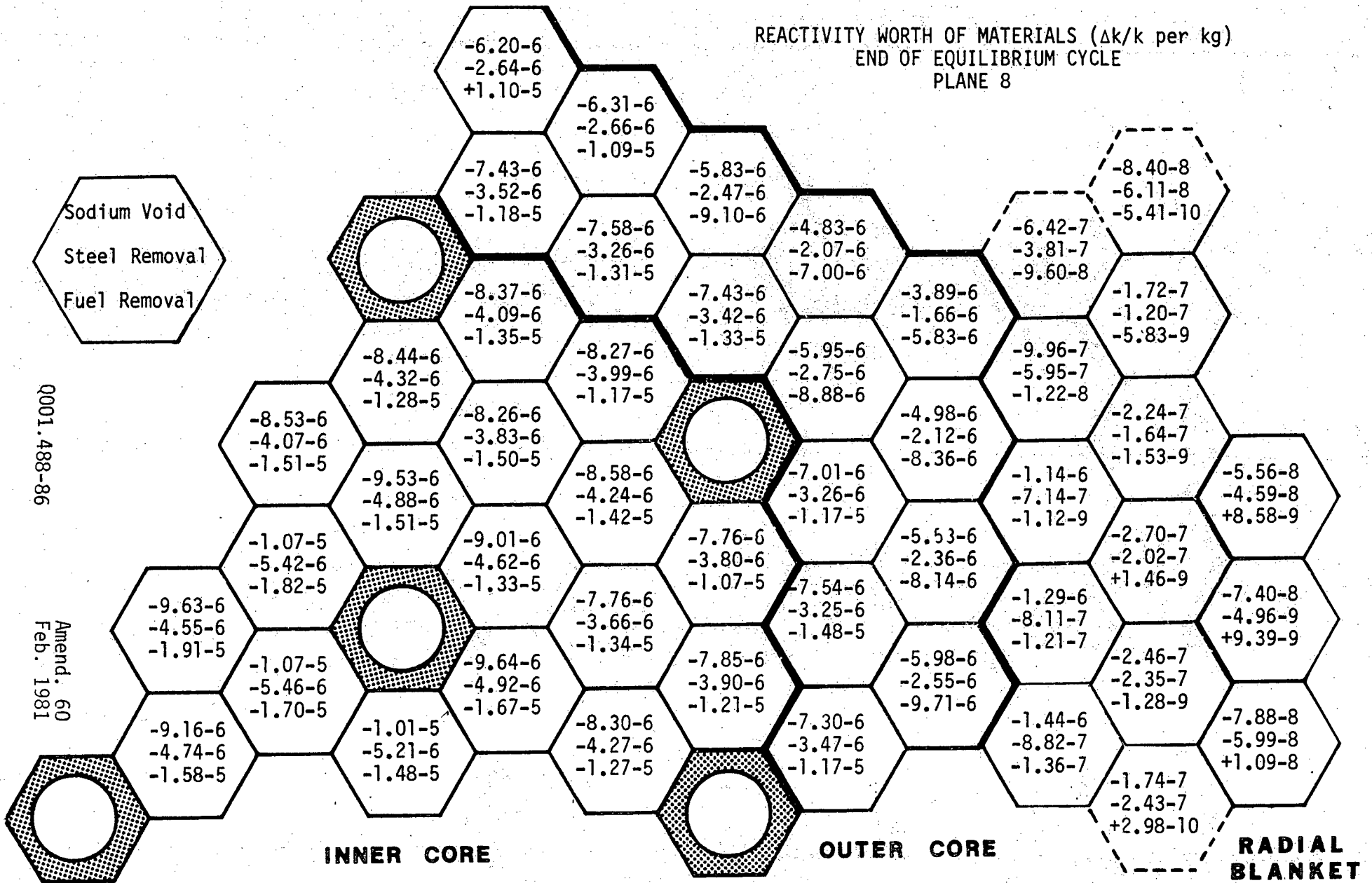
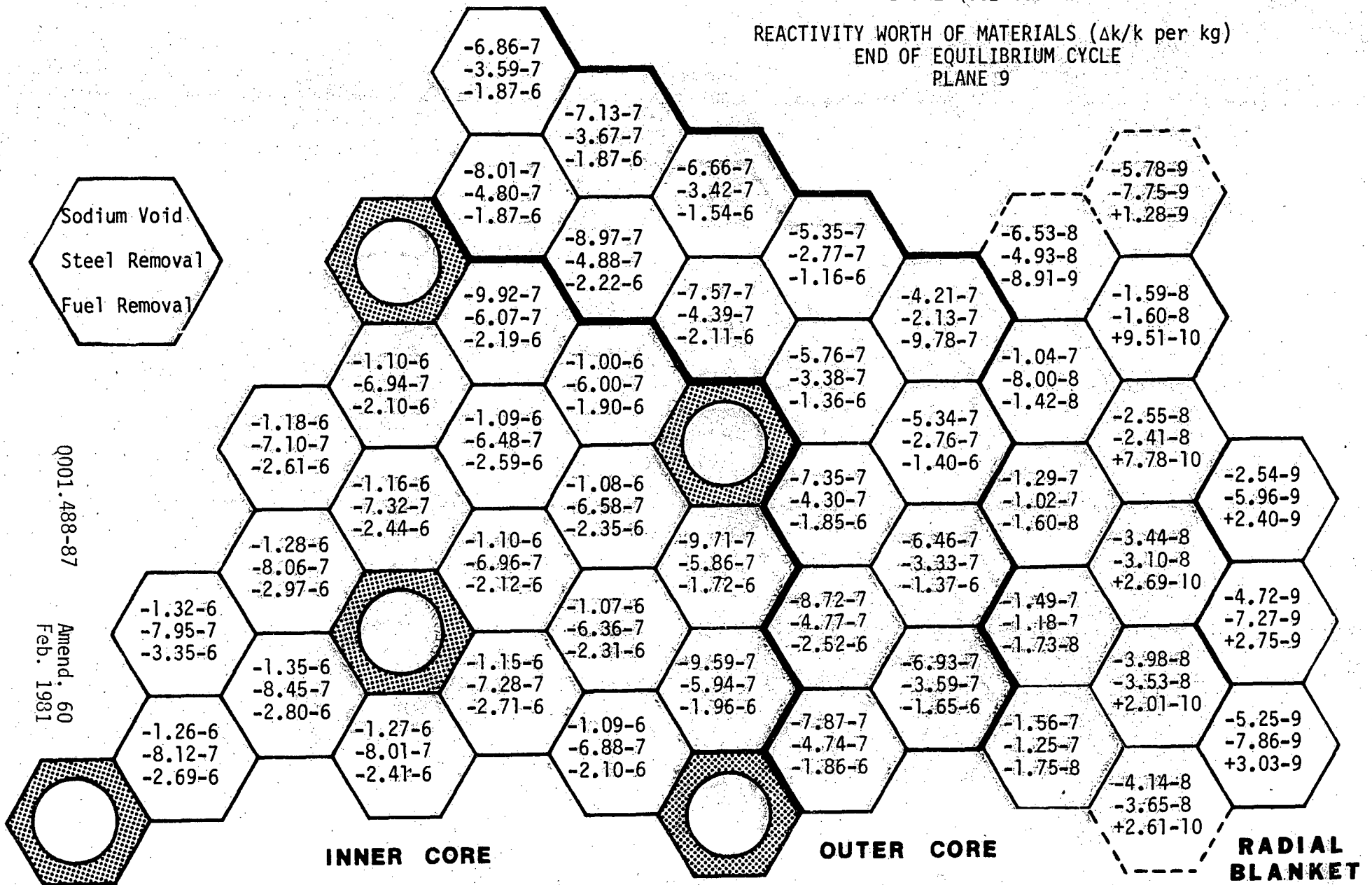


FIGURE Q001.488-86

REACTIVITY WORTH OF MATERIALS ($\Delta k/k$ per kg)
 END OF EQUILIBRIUM CYCLE
 PLANE 9



Question 001.489 (F6.2.4.1.1)

The experimental basis in support of the fuel motion models (SLUMPY and SASFCI) used in the SAS calculation should be described. In view of the importance of fuel motion in assessing the complete sequence of the accident scenario, justify your use of these models; also provide a description of the R&D program, including schedules, to provide for further information in this area.

Response:*

| 60

The conceptual formulation of the SLUMPY and SAS/FCI models took place in 1972. At that time only limited information was available on oxide fuel motion under transient conditions. This information was mainly available from TREAT transient capsule tests and the preliminary HEDL out-of-pile experiments on small fuel samples. Qualitatively, this information suggested a strong effect from entrained fission gas as irradiated solid fuel approached the melting point and absorbed the heat of fusion. Hence, the SLUMPY parametric treatment of fuel relocation was based on the conceptual idea that motion begins when fission gas has caused pin fragmentation and disruption in a voided coolant channel. Likewise, SAS/FCI was based on the concept of pin failure due to internal pressures generated as fission gas was released from melting fuel. This model was parametrically implemented into the SAS2A code using the then existing FCI technology with the logical extensions needed for whole core accident analysis.

These models were used for the Project's HCDA analysis because they are the best of the models that have been integrated into whole core accident analysis codes. Since both SLUMPY and SAS/FCI are parametric in nature, they allow simulation of some of the phenomenological effects observed in recent experiments. For example, the heat transfer coefficient between fuel and coolant can be varied by orders-of-magnitude in SAS/FCI, and the amount of fission gas available to disperse fuel in SLUMPY is user-controlled. Further, additional numerical and physical model improvements have been made in both SLUMPY and SAS/FCI which allow them to better account for information gained in later experiments. For example, a stable method of treating slow slumping in quasi-solid fresh fuel was implemented in SLUMPY, and a FRAS-correlated algorithm for release of fission gas to grain boundaries was inserted into the pin cavity model in SAS/FCI. | 60

SLUMPY calculations have been done on various TREAT tests. The SLUMPY input used to fit these tests is generally consistent with that used in the CRBR analyses. In the L2 and R4 tests, SLUMPY can simulate the slow slumping that was observed. In the L3 and L4 tests, all fission gas was calculated to have been released before fuel motion due to the radial heat sink, and both experimental data and SLUMPY calculations suggest eruptions from stainless steel vapor pressures. In the F1 test, high-power irradiated fuel melted at constant power with a nuclear heated wall; CRBR type SLUMPY assumptions predicted the slow slumping which occurred. In the L5 test, GETR-irradiated fuel was melted with a power burst timed after voiding had occurred such that peak fuel temperatures were around the fuel melting point; both SLUMPY and the experimental evidence predict fuel motion away from the core midplane.

*Note that Appendix F has been withdrawn. The text, upon which the question was based, can now be found in Section 3.2 of Reference 15, PSAR Section 1.6. | 60

SAS/FCI has not been used to actually calculate experiments. Rather, the approach taken has been to calculate experiments with PLUTO, and then compare SAS/FCI and PLUTO phenomenological predictions. This is summarized in the response to Question 001.470. 60 124

In conclusion, use of the SLUMPY, SAS/FCI and PLUTO models in CRBRP HCDA analyses have provided the best predictions of fuel motion currently available to calculate the energetic consequences of hypothetical loss-of-flow and transient overpower events. The Project is currently assessing the need for additional out of pile experiments to characterize the effects of fission gas release on SLUMPY predicted fuel motion and identifying the additional code development requirements.

Question 001.490 (F6.2.5.2.2)

On page F6.2-101 reference is made to certain experiments addressing the question of pressure driven recompaction. Provide the reference or references describing the experiments as well as an analysis and interpretation of their relation to pressure driven recompaction.

Response:

The reference discussing the experiments relating to the question of pressure driven recompaction is ANL/RAS-76-4, "Upper Plenum Injection Tests No. 1 and No. 2," by R. E. Henry et al. Further information is provided in the response to Question 001.496.

Q001.490-1

Amend. 20
May 1976

Question 001.491 (F6.2.4.1 , F6.2.4.2)

The case when coolant has been left in low power channels at the end of the initiating phase calculations should be considered explicitly. The situation to be addressed is that rapid increase of the core power will lead to rapid voiding and large and rapid reactivity insertion. Under such conditions clad failure of an uncertain rip length and fuel ejection into the coolant channel will occur, where liquid or vapor coolant flow will be present. The above circumstances, combined with the possibility of partial or total plug formation, could conceivably lead into pin-to-pin or subassembly-to-subassembly autocatalytic events. Address this scenario and discuss the basis for the limiting 15 cm rip length. Provide a description including the status and schedule of your R&D program related to the above questions.

Response:*

Those cases in the BOEC analysis in Reference 15, PSAR Section 1.6 which treat the effects of phenomenological uncertainties (Section 7.2.2) lead to situation where pins fail in low-power, sodium filled channels when the power is high, the cladding hot and weak, and the reactivity is close to prompt critical. Under these conditions rapid reactivity insertions resulted, both because of axial fuel motion to the (midplane-centered) failure locations, and because of the subsequent rapid sodium voiding due to fuel-coolant interactions. While it is true that the rip length is uncertain, it is expected to be large because the cladding is hot and weak at the time of failure, and the loading mechanism provides high pressure. Hot and weak cladding means that midwall cladding temperatures of 950°C-1000°C exist over a long length, from the area of the axial core midplane to the upper regions of the core. A choice of 15 cm for the rip length is considered conservative because it is considered to be less than the true rip would be. By centering such a rip at the core midplane (where the burst-pressure criterion predicts it to be) positive reactivity from fuel motion within pins to the failure location is predicted. When cases considered to be more realistic were run with larger rip lengths (e.g. 30 cm), the fuel motion reactivity was very quickly negative, thus leading to permanent shutdown without a super-prompt critical burst.

Formation of plugs or blockages following large-scale fuel ejection (in a large-rip-length situation) seems unlikely to cause difficulties such as pin-to-pin or subassembly-to-subassembly autocatalytic events. Since a large portion of the core has already been voided, the most likely path to termination is via core meltdown and a subsequent transition phase. Reactivity effects of reentry of molten fuel into the central regions of the core will be small, if such events occur at all. Reactivity effects of blockage melting are treated in sections 10 and 11 of Reference 15, PSAR Section 1.6. From these, it can be concluded

*Note that Appendix F has been withdrawn. The text, upon which the question was based, can now be found in Section 7 of Reference 15, PSAR Section 1.6.

that, in order for severe autocatalytic events to occur, (30 \$/sec at prompt critical or greater) a significant amount of fuel must reenter coherently and rapidly (e.g., 20 cm slugs dropping under gravity, simultaneously and coherently in 36 high-worth subassemblies). Such events are considered highly unlikely, and would not lead to consequences as serious as those that would result from direct disassemblies predicted for cases of small rip length.

An R&D program has been proposed to address the LOF-driven TOP question. It calls for a) out-of-pile tests to study the effects of fission gas and molten fuel upon cladding loading and their roles in pin failure, mechanical loading tests to determine initial rip sizes, and tension tests to study rip propagation, and b) updated modeling within the SAS code system to obtain updated treatment of fuel motion, cladding failure, and sodium voiding under LOF-driven TOP conditions. Details of this program are provided in Appendix A of Ref. 10a, PSAR Section 1.6.

60 | 27

The schedule of this proposed program is geared toward resolution of the subject areas of uncertainty by the time of FSAR submittal.

Question 001.492 (F6.2.4.2.1)

The relatively large pressure spikes in the lower plenum from FCI voiding of the lower power channels, have not been taken into account for the base case clad motion. Even if it is argued that the pressure drop conditions correspond to the static head, the above pressure spikes appear at a time when large amounts of cladding are molten.

Discuss the possibility of significant clad motion due to lower plenum pressurization from subassembly FCI voiding and provide the basis for the discussion.

Response:

The CRBRP Project has consolidated all considerations given Hypothetical Core Disruptive Accidents into report CRBRP-3 (References 10a and 10b, PSAR Section 1.6) and its associated references; consequently, PSAR Appendices D and F have been withdrawn in Amendments 24 and 60 respectively. The response to this question is now found in Section 7.2.1 of Reference 15, PSAR Section 1.6.

Question 001.493 (F6.2.4.1, F6.2.4.1.2.3)

Provide, in your parametric evaluation, the justification for the choice of 50% reduction of the axial expansion reactivity feedback. Provide any available experimental verification of the values currently used.

Response:**

| 60

Sections F6.2.4.1 and F6.2.4.1.2.3 related to the beginning of equilibrium cycle (BOEC), loss-of-flow (LOF) base case and the no axial expansion parametric analysis case, respectively. For the base case LOF analysis no reduction in axial expansion feedback was made.

For the reactivity insertion accident (TOP) analyses a reduction of 50% in the calculated, free axial expansion reactivity feedback was made. The justification for a reduction in axial expansion reactivity feedback is provided in the following paragraphs.

| 60

| 60

The justification for a reduction in axial expansion feedback is based on expected fuel-cladding mechanical interaction due to the inherent fuel-clad heating sequence of TOP events. Fuel heating experiments are available to provide guidance for engineering judgement in this area.

Mixed oxide fuel columns (~10 inch length) which are near prototypic (Reference Q001.493-1) and prototypic (Reference Q001.493-2) of CRBRP have been irradiated in-pile with real time measurements of axial expansion during power changes. From these GE and ORNL experiments, it was observed that when prior fuel-cladding interaction did not exist (up to 20 GWD/T), the fuel pin demonstrated approximately uniform and reproducible transient expansion behavior. After steady-state fuel-cladding gap closure (20 to 44 GWD/T) the transient relative expansion of fuel and cladding became erratic, but absolute fuel column expansion was always measured. The key point is that fuel column axial expansion did occur even under conditions of prior gap closure. The magnitude of the effect was characterized as "always less than the value computed from fuel center temperature and out-of-pile isothermal expansion data", (Reference Q001.493-1) or, as "controlled by temperature changes in the outer one-seventh of the FTR dished pellet" (Reference Q001.493-2)*. Out-of-pile comparisons on cracked and uncracked UO₂ fuel pellet specimen expansion during heating transients (1 1/4 inch long, 97% theoretical density axial load of 27 psi) were done at Argonne National Laboratory and led to a conclusion that the two fuel specimens expanded in the same manner. Additionally, the magnitude of the expansion was correlated to the calculated fuel center temperature increase via an isothermal coefficient of $1.1 \times 10^{-5}/^{\circ}\text{C}$.

| 60

* The GE and ANL experiment employed non-dished pellets.

**Note that Appendix F has been withdrawn.

| 60

Imposed reductions in calculated axial expansion feedback, however, are treated as an invariant, core wide multiplier within the SAS code.

With respect to the characterizations above, the CRBRP model, which is based upon a radial mass average fuel temperature, is generally consistent during TOP events.

The 50% reduction in core wide fuel axial expansion reactivity feedback employed in the CRBRP TOP analyses recognizes modeling restraints, potential fuel-clad interference, first principles, and the experimental knowledge currently available.

References:

- Q001.493-1: Cantely, Hull and Craig, "Axial Expansion of Mixed-Oxide Fuel Measured In Pile", General Electric Co., July 1971 (GEAP 10403).
- Q001.493-2: Pitts, Fleisher, and Senn, "Fuel-Cladding Mechanical Interaction and Gas Pressure Buildup in a Shortened FTR-Type Fuel Pin", Oak Ridge National Laboratory, June 1973, (ORNL-4875).

Question 001.494 (F6.2, F6.2.3.2.6)

From the R5 experimental reference material in TREAT you have concluded that CLAZAS overestimates the reactivity feedback. This conclusion was essentially drawn from the interpretation of the post test radiographs of the clad motion, due to the fact that substantial cladding blockages were formed at the bottom of the fuel column. However, this fact alone could be interpreted as indicative of substantial upward clad motion at the beginning, plug formation and subsequent draining. The conditions in the upper part of the core may not favor core freezing as in the R5 experiments. Discuss what additional evidence is there which leads to your current interpretation of the R5 experiments and eventually lead to the conclusion of the CLAZAS overestimation of the clad upward motion. In view of the importance of clad motion to the energetic outcome of the LOF accident a better basis for the base case assumptions used in your analysis is needed. Therefore, provide an updated account of the cladding relocation experiments, already performed, as well as those planned for the future. In addition, provide all essential information necessary for the quantitative assessment of these experiments as well as certain qualitative features (i.e., flow regimes) where available.

Response:*

60

The TREAT R-5 test has been used as a basis for comparison of SAS with CLAZAS sodium voiding and clad relocation models (Ref. Q001.494-1). In addition, a more recently developed clad motion analysis (Ref. Q001.494-2) has also been compared with the same R-5 test. One finds generally good agreement between the two independent calculations in terms of the calculated time lapse between the onset of sodium boiling and the onset of clad motion (2.49 sec. in Ref. Q001.494-1 and 2.2 sec. in Ref. Q001.494-2) and the calculated time lapse between the onset of clad motion and clad blockage formation in the upper reflector region of the pin (0.4 sec. in Ref. Q001.494-1 and 0.55 sec. in Ref. Q001.494-2). Following the upper blockage formation, both analyses proceed to calculate clad draining with eventual solidification and accumulation of a large blockage in the lower reflector region. In fact, one can infer from the general qualitative and quantitative good agreement between independent analytical approaches that CLAZAS by itself can provide an adequate one-dimensional description of clad motion. The basis for the assessment that CLAZAS can overestimate the rate of upward clad relocation and hence overestimate the reactivity feedback when applied to the CRBRP is only partially based upon the R-5 posttest radiographs.

There are three potential mechanisms through which the current SAS with CLAZAS formulation can overestimate the rate and extent of upward clad motion. They are (1) by overestimating the extent of clad penetration into the axial blanket or reflector region before plug formation, (2) by overestimation of the vapor source strength, and (3) by limitations in the ability of one-dimensional model to account for potential two-dimensional effects on clad motion.

60

*Note that Appendix F has been withdrawn. The text, upon which the question was based, can now be found in Section 7.1 of Reference 15, PSAR Section 1.6.

60

The overestimate of the extent of clad penetration into the upper reflector as determined from R-5 posttest radiographs was recognized in Reference Q001.494-1. From page 30 of Ref. Q001.494-1 "large upper blockages are to a certain degree a consequence of the SAS axial node structure and the segment formalism of CLAZAS. It generally takes two or three relatively long axial nodes to overlap so that a blockage forms. Analytical cladding motion could be modified to allow for shorter upper blockages." Such an improved analytical formulation of the clad solidification process was included in Ref. Q001.494-2 and did indeed give results in much closer agreement with posttest R-5 examination. (See the discussion on pages 30-31 of Ref. Q001.494-2).

A second potential cause for an overestimate of the rate of upward cladding relocation which is related to the strength of the vapor streaming source was also noticed in the R-5 experiment - SAS/CLAZAS comparison. It was found that significant surges of clad motion were being calculated (Fig. 44 of Ref. Q001.494-1 illustrates the phenomena) as a result of the sodium reentry formulation in SAS. Other characteristics of the behavior of the reentry model such as inlet pressure and flow oscillations were not confirmed by experiment. Figure 15 of Ref. Q001.494-1 illustrates the rather good agreement between calculated and experimentally observed inlet flow oscillations during the sodium voiding time interval (≈ 14.5 sec. to ≈ 17.7 sec.) which includes some initial clad melting. However, as the clad overheats to near melting temperatures near the bottom of the fuel pin, the current assumptions in SAS regarding vapor bubble formation and liquid film behavior can give rise to substantial overprediction of surges in channel inlet pressure and the resulting sodium vapor flow velocity. Note the sudden change in calculated frequency and amplitude of inlet flow oscillations in Fig. 15 of Ref. Q001.494-1 which set in about 18.8 sec. and beyond. Here it is important to note that the R-5 test was designed and executed to simulate the FFTF loss-of-flow accident conditions. This case differs from the CRBRP loss-of-flow case in two important aspects. The first is that for CRBRP, clad melting occurs at pin power levels substantially in excess of nominal power, because of sodium voiding reactivity feedback. This causes clad overheating and melting to proceed along the length of the fuel pin much faster than for the FFTF case. This allows the potential for the above-mentioned difficulty with the sodium reentry model to set in earlier. The second aspect is related to the longer thermal response time of the CRBRP axial blanket as compared to the inconel reflector of the FFTF pin. Clad blockage formation in the former can be delayed such that coupled with the overprediction of surges in the sodium reentry model, large upward clad relocation velocities could be calculated. These model refinements, discussed in Reference Q001.494-3, overcome the previous over conservatism in the sodium re-entry model.

The third and perhaps most important cause for overestimate of early clad relocation effects is related to the inability of a one-dimensional formalism to account for parallel channel or two-dimensional characteristics of the behavior of sodium vapor and molten clad in a subassembly with a radial temperature or radial power skew or both. These effects have been described

in Ref. Q001.494-4. Very simply, in a one-dimensional model or single channel experiment, the molten clad at any axial location is influenced by a vapor velocity characteristic of the total gas flow through the channel. In a two-dimensional model or in a test section with radial nonuniformity in clad melting at a given axial location, the gas or vapor can be partially diverted from flowing over molten clad with a characteristic high friction factor into an increased flow over unmolten clad at the same axial location. This reduces the effective drag or shear force on the molten clad. As noted in Ref. Q001.494-4 in the early stages of clad melting, a clear case cannot be made for either upward relocation or draining. This coupled with the fact that depending upon the cases considered the onset of fuel motion occurs very close to the onset of clad motion, leads to a "best estimate" that the actual behavior of the clad in a CRBRP loss-of-flow analysis is closer to the assumption of zero clad relocation than that which would be calculated on the basis of the current one-dimensional clad relocation model with an unimproved sodium reentry formalism. It should also be noted that two-dimensional effects would tend to become less significant under conditions in which the power level and core pressure drop are significantly higher than conditions typical of the early voiding and clad melting in the CRBRP loss-of-flow analysis.

However, with regard to clad motion itself, the out-of-pile simulation experiments are continuing. See Ref. Q001.494-5 for a discussion of the observations of the simulated clad motion in a ten-pin pie-shaped test section. In these experiments carried out in a transparent apparatus, the gas velocity was varied parametrically. High-speed photography illustrated the representative flow regimes and simulated clad behavior. Two-dimensional behavior was clearly illustrated for a gas throughput velocity in the range of the flooding velocity for an equivalent single channel. These conditions simulate the reactor conditions cited in Fauske's discussion previously referenced. These experiments will be extended to a 28-pin pie-shaped test section. (Note the 10-pin and 28-pin pie-shaped test sections simulate 60° sectors of a 37- and a 127-pin hexagonal test bundle, respectively). The principal observations in these tests will be high-speed photography of "clad" behavior under parametric variations in gas velocity. The concern over fission gas effects on clad motion will be addressed in the forthcoming in-pile test R-8. End-of-life fission-gas pressure will be simulated in a 7-pin loss-of-flow transient. Information on transient clad relocation in this test must be inferred from axial thermocouples. An attempt to monitor steel motion with the TREAT Hodoscope Instrumentation will also be made.

In summary:

- (1) Posttest radiographs of the R-5's test are only partially responsible for the interruption that CLAZAS overestimate the extent of upward clad relocation and hence reactivity feedback in the CRBRP analysis.
- (2) Comparison of SAS with Tests R-4 and R-5 revealed aspects of the combined SAS/CLAZAS formalism which were responsible for potential overestimate in upward clad relocation. These have been verified in independent analysis and are currently being updated in SAS.

60

- (3) TREAT Test R-5 by itself is not directly related to the CRBRP loss-of-flow analysis because of the difference in power level and resulting time scale at the onset of clad motion and differences in blanket and reflector regions of the FFTF and CRBRP pins.
- (4) Current model limitations related to clad solidification, sodium reentry, and inability to directly consider two-dimensional effects along with supporting laboratory simulation experiments lead to the engineering assessment that the nominal early clad behavior in the loss-of-flow analysis should be much closer to the assumption of net zero clad motion as opposed to the motion associated with the one-dimensional SAS/CLAZAS.
- (5) A supporting experiment program is ongoing and continuing model improvements are being developed.
- (6) Most important, at higher power levels, the characteristics of the combined clad and fuel motions are more important than details of the clad dynamics alone.

References:

- Q001.494-1: G. Hoppner, "SAS3A Analysis of R. Series Experiments", ANL/RAS 74-14, August 1974.
- Q001.494-2: M. Ishii, W. L. Chen and M. A. Grolmes, "One-Dimensional Clad Relocation Model for Fast Reactor Loss-of-Flow Accidents", ANL/RAS 75-28, August 1975.
- Q001.494-3: L. Semenza and H. U. Wider, "Reactor Development Program", Argonne National Laboratory, 1976 (ANL-RDP-49).
- Q001.494-4: H. K. Fauske, "Some Comments on Cladding and Early Fuel Relocation in LMFBR Core Disruption Accidents", Trans. Am. Nuc. Soc. 21, (1975).
- Q001.494-5: ANL-RDP-33, Reactor Development Physics Progress Report, pp. 7.1 - 7.2.

Question 001.495 (F6.2.5.2.1, F6.2.5.2.2)

In the discussion of the potential for steel blockages, reference 68 was used to advance the argument that such blockages will not be formed. However, we find it difficult to establish the same conclusion from the material presented in reference 68. Steel blockages will also critically affect fuel dispersion as it is recognized in F6.2.5.2.1. With respect to blockage formation and fuel dispersal, provide a justification for clad sloshing and assess quantitatively the role of the fission gas as it may apply to the plug formation. Refer to recent experiments with thermite and provide pertinent references as they may support or conflict with the assumption that steel blockages will not be formed. Provide references and the experimental basis from using stimulant materials referred to in page F6.2-46 for the conduction model and its applicability to the reactor geometry.

Response:*

The phenomenon of clad slashing is described in detail in Reference Q001.495-2. The justification of this phenomenon is based on experiments simulating reactor materials using Woods metal as described in Reference Q001.495-5.

The role of fission gas as it may apply to plug formation is described in Section 10.2.1 of Reference 15, PSAR Section 1.6.

The following paragraphs provide further information regarding experimental observation of fuel-steel blockages.

Experiments with molten uranium dioxide (Reference Q001.495-1) have been performed primarily to investigate the possible influence of sodium as a vapor source of recompact molten fuel when the fluidized fuel-steel mixture is ejected out of the core during the transition phase. The results indicated that the reaction products froze in the test bundle, although these tests were not performed primarily to assess fuel-steel plug formation.

The results of recent experiments to assess fuel freezing, reported in Reference Q001.495-2 indicate that the formation of a complete fuel-steel blockage is likely to occur during the transition phase.

The formation of subassembly blockages due to the transient freezing of molten fuel-steel ejected into the axial blanket regions early in the transition phase is best described by the Bulk Freezing Model, which is discussed in detail in Reference Q001.495-2. Assuming complete core plugging due to early clad and/or fuel relocation the analyses provided earlier in this section indicated

*Note that Appendix F has been withdrawn. The text, upon which the question was based, can now be found in Section 10 of Reference 15, PSAR Section 1.6.

that the blockages would open up due to meltout and the fuel-steel mixture would be ejected into the sodium outside the core, resulting in subcriticality. As described below, the transition phase energetics are not sensitive to the details of freezing and plugging. The result is the same whether complete or incomplete plugging is assumed. Only the time sequence to reaching a permanent subcritical fuel configuration will change. With incomplete plugging, this condition will be reached a few seconds after major core disruption, while in the case of complete plugging this condition is achieved in several tens of seconds. This difference in time does not appear to be crucial, since fuel dispersal and boilup are likely to occur down to and even below 1% of nominal power.

The experimental basis for the Conduction Model referred to in Section 10.2.2.3 of Reference 15, PSAR Section 1.6 and its applicability to CRBRP safety analysis are described in Reference Q001.495-2. The Conduction Model considers a stable frozen layer forming at the wall. Freezing begins at the wall and the frozen layer grows as long as the heat flux to the wall exceeds that from the bulk liquid to the frozen layer. The heat flux to the wall is controlled by conduction through the frozen layer. However, fuel freezing experiments in a seven-pin subassembly structures (Q001.495-3) results in considerably smaller fuel penetration distances into the upper plenum than are predicted by the conduction model of fuel freezing. Therefore, the conduction model theory does not explain fuel freezing under the conditions that existed in these experiments.

The results of a series of small-scale out-of-pile fuel freezing experiments (Ref. Q001.495-4) conducted to investigate the condition under which the Bulk Freezing and the Conduction Model are applicable indicated that at low steel structure temperatures the formation of a continuous and thin frozen fuel film was indeed a limiting mechanism to the freezing process. However, at test section temperatures more characteristic of the steel temperatures following a hypothetical loss-of-flow accident ($\sim 900^{\circ}\text{C}$), significant ablation and entrainment of the stainless steel occurred, which indicates that the freezing behavior is closely represented by the Bulk Freezing Model.

It therefore appears that the formation of fuel-steel blockages in the upper and lower core structure due to the ejection of the molten-fuel steel mixture into the axial blanket regions is best described by the steel ablation controlled Bulk Freezing Model. In situations of interest where the fuel velocity will be too low for crust breakup, the fuel freezing predictions may be based on the conduction model. This is the usual case of interest in post-accident heat removal analysis.

References:

- Q001.495-1: R. E. Henry, et al., "Upper Plenum Injection Tests, No. 1 and No. 2, "Argonne National Laboratory, April 1976 (ANL/RAS 76-4). 60

References: (Continued)

- Q001.495-2: M. Epstein, et al., "Transient Freezing of a Flowing Ceramic Fuel in a Steel Channel", Argonne National Laboratory, March 1976, (ANL/RAS 76-3).
- Q001.495-3: R. N. Ostensen, et al., "Fuel Flow and Freezing in the Upper Subassembly Structure Following an LMFBR Disassembly", Trans Am Nuc. Soc. 18, pp. 214-215 (1974).
- Q001.495-4: R. E. Henry, et al., "Fuel Freezing Tests", Trans Am Nuc. Soc., June 23, 1976.
- Q001.495-5: R. E. Henry, et al., "Woods Metal Cladding Relocation Experiments", Argonne National Laboratory, May 1978 (ANL/RAS 77-37).

60

Question 001.496 (F6.2.5.2.3)

In the discussion of the transition phase recriticality, recompaction due to pressure from FCI from fuel discharged to the upper plenum is addressed with reference to undocumented experiments (upper plenum experiments). Provide the experimental basis and appropriate documentation and discussion, as applicable, for the upper plenum experiments. Also with reference to the benign behavior of the fuel discharging into the sodium pool as deduced from the thermite and simulant materials test, reference 6, discuss the applicability and elaborate on the conclusions. In particular, discuss the impact of the possibly low pressure (a few atmospheres) in the core region during the discharge.

Response:*

| 60

The question of pressure-driven fuel compaction by fuel-coolant interaction can be conveniently discussed in terms of two generic geometric configurations (see Figure Q001.496-1). In the first case disrupted fuel material may be ejected into yet-intact fuel-pin stubs containing liquid sodium and/or liquid-sodium films, whereby a thermal interaction could be depicted leading to reversal of the fuel motion and subsequent compaction. Prototypic experiments (Reference Q001.496-1) using the thermite method to simulate reactor conditions have demonstrated that the freezing and ablation processes (Reference Q001.496-2) between the molten mixture and the relatively cold pin structure is controlling the fuel motion and not the thermal interactions. No significant differences could be discerned in tests with and without sodium.

In the second case, following structural melting and formation of escape paths, the disrupted core material is ejected directly into the liquid-sodium plenum, as a result of the blowdown process. The pressure in the pool prior to formation of escape paths is likely to be at least several atmospheres. In this case sustained pressure generation above that generated in the core region due to internal heat generation is not expected, since 1) the contact temperature between the ejected mixture and the liquid sodium is estimated to be below the spontaneous nucleation temperature - experiments with simulant materials have demonstrated if this threshold condition is not satisfied, sustained pressure generation above ambient pressure as a result of mixing a hot and cold fluid is not developed (see Reference Q001.496-3), 2) even if this threshold should be exceeded, experiments with simulant materials have demonstrated that flashing of the hot fluid during blowdown largely prevents sustained pressure generation above that controlling the blowdown process (see Reference Q001.496-3) and 3) even if sustained pressure generation should occur, it would be reduced considerably by the time it is seen coherently by the core fuel mass. This is because the first escape paths to be formed is likely to be a small fraction of the core cross-sectional area - an escape area equivalent to ten subassemblies only would allow a major fraction of the core fuel to be discharged in ~ 1 sec for an overpressure corresponding to several atmospheres, an insufficient time to substantially increase the escaped path during blowdown.

| 60

| 60

*Note that Appendix F has been withdrawn. The text, upon which the question was based, can now be found in Section 10 of Reference 15, PSAR Section 1.6.

| 60

Amend. 60
Feb. 1981

References

- Q001.496-1 R. E. Henry, et. al., "Upper Plenum Injection Tests No. 1 and No. 2", Argonne National Laboratory, February 1976, (ANL/RAS 76-4).
- Q001.496-2 M. Epstein, et. al., "Transient Freezing of a Flowing Ceramic Fuel in a Steel Channel", Argonne National Laboratory, March 1976, (ANL/RAS 76-3).
- Q001.496-3 R. E. Henry, et al., "Large-Scale Vapor Explosions", Proc. Fast Reactor Safety Meeting, April 2-4, 1974, Beverly Hills, CA, USAEC Report CONF-740401-P2 (1974).

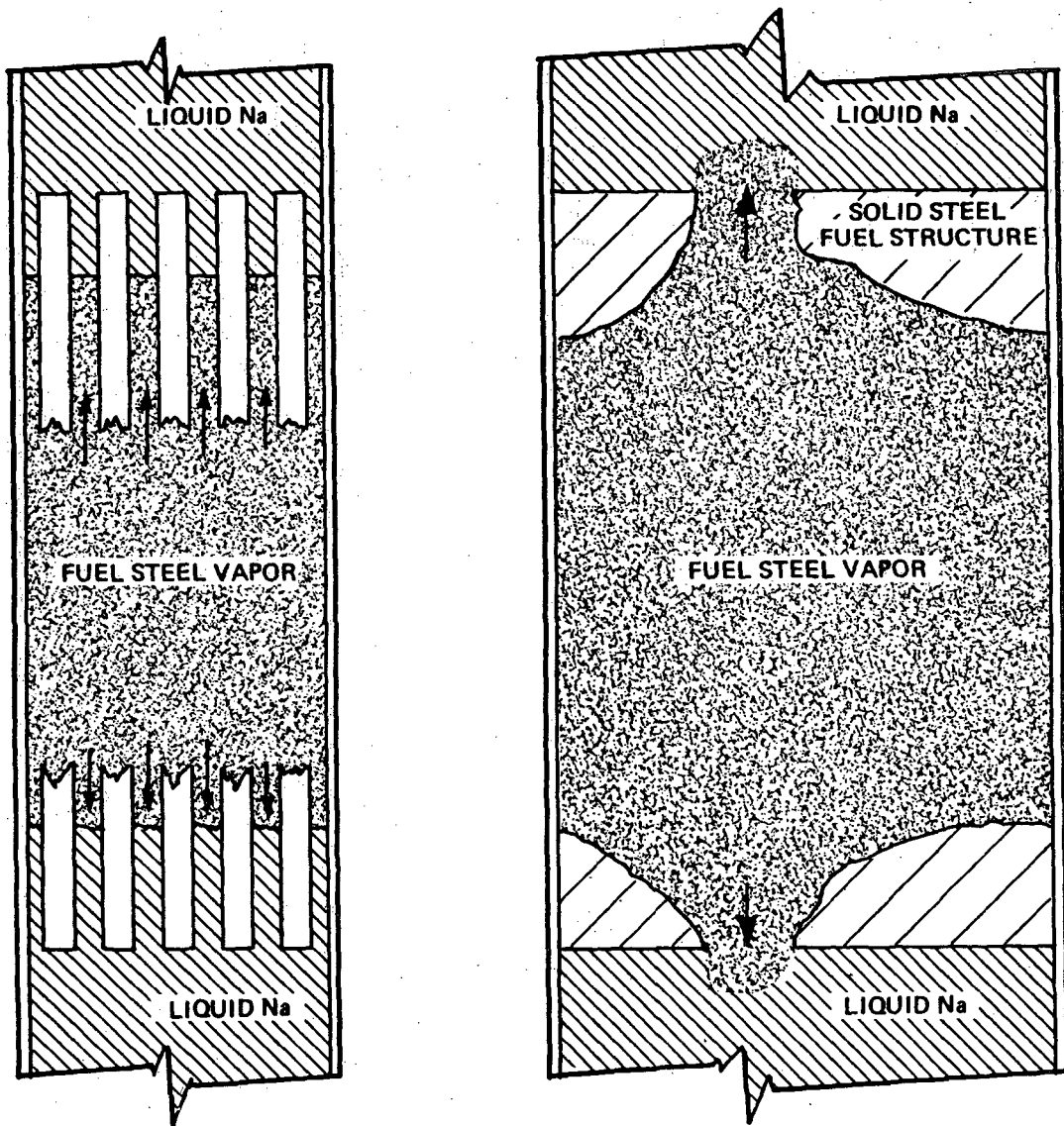


Figure 001.496-1. ILLUSTRATION OF GEOMETRIC CONFIGURATIONS OF INTEREST IN ASSESSING THE POTENTIAL FOR PRESSURE-DRIVEN RECOMPACTION OF DISRUPTED FUEL

Question 001.497 (F6.2.6.1 and F6.2.6.2.1)

In view of the current state of technology, with tools and data still being in the state where substantial improvements can be anticipated, there may be a tendency to place too much emphasis on future developments in assessing the adequacy of design margins. Due consideration must be given to present uncertainties and design capabilities should be compatible with present understanding. For example, disassembly calculations results will depend on the results of the initiating phase calculation and the equation of state for the disassembly phase. For the initiating phase, four major parameters have been identified which are subject to significant uncertainties, i.e., fuel axial expansion, clad motion, fuel motion and voiding rate due to FCI. For the disassembly phase perhaps the single most important source of uncertainty is the equation of state, especially for temperatures and pressures close to the critical point of fuel vapor. In the recriticality area the uncertainties exist due to the deficiencies in current analytical tools or experimental data to account for extensive fuel motion. For example, a 30 \$/sec recriticality rate at an initial power level of 21 times normal power, leads to 99 MW-sec (Table F6.2-24). If the design level is 101 MW-sec the available margin cannot be regarded as ample unless strong argument can be raised against such a ramp rate. In view of the above comments discuss your conclusion that the design has ample margin in light of factors such as noted above and the general uncertainties related to predictions of disassembly work potential.

Response:*

60

The question identifies a six items or areas of uncertainty in the CRBRP CDA analysis which introduce concern about the adequacy of the Structural Design Basis. These are (1) fuel axial expansion, (2) clad motion, (3) fuel motion due to FIC, (4) voiding rate due to FCI, (5) fuel equation of state for disassembly calculations, and (6) extensive fuel motion during transition phase. Each of these concerns has been discussed in answer to more detailed NRC questions. Specifically, item (1) was discussed in answer to 001.493, item (2) in Section 4.4.2.2 of Ref. 10a, PSAR Section 1.6; and in answer to 001.494, item (3) Section 4.4.2.2 of Reference 10a, PSAR Section 1.6, and in answer to 001.489 and 001.491, item (4) Section 4.4.2.2 of Ref. 10a, PSAR Section 1.6, and in answer to 001.491, item (5) in answer to 001.485, and item (6) in answer to 001.496. Therefore, only the last part of the question will be discussed herein, that is, our conclusion that design has ample margin. We would first like to point out however, that the 30 \$/sec. recriticality from an initial power level of 21 times normal power leads to 80 MW-sec. not 99 MW-sec. as stated in the question. The 99 MW corresponds to an initial power level of 2.1 times normal.

60

The approach we have used in characterizing the margins in our analysis was presented to the NRC at the meeting of February 3, 1976 on the subject of CDA Energetics. The approach identifies five probability categories, with

*Note that Appendix F has been withdrawn. The text, upon which the question was based, can now be found in Section 11.2 of Reference 15, PSAR Section 1.6.

60

Question 001.498 (F6.2.6.1 and F6.2.6.5)

In the disassembly calculations, the average temperature was used to characterize the work potential. However, the work potential increases in an exponential fashion with temperature; therefore, the temperature distribution should be taken into account explicitly in calculating the work. The temperature distribution should be consistently reported (in all cases). If the work calculation is based on the average core temperature, the omission of the temperature distribution should be justified.

Response:

The CRBRP Project has consolidated all considerations given Hypothetical Core Disruptive Accidents into report CRBRP-3 (References 10a and 10b, PSAR Section 1.6) and its associated references; consequently, PSAR Appendices D and F have been withdrawn in Amendments 24 and 60 respectively. The response to this question is now found in Section 4.5.2 of Reference 10a, PSAR Section 1.6.

60

Question 001.499 (F6.2)

The experimental base should be identified clearly and care taken to distinguish between arguments based on experimental grounds or analytical grounds or first principles. Provide in a summary form or table the correspondence between the important physical phenomena treated and the pertinent experimental data. Emphasize the completeness and applicability of the summary.

Response:

The CRBRP Project has consolidated all considerations given Hypothetical Core Disruptive Accidents into report CRBRP-3 (References 10a and 10b, PSAR Section 1.6) and its associated references; consequently, PSAR Appendices D and F have been withdrawn in Amendments 24 and 60 respectively. The response to this question is now found in Section 3 of Reference 15, PSAR Section 1.6.

60

Question 001.500 (F6.4.1.1):

The particle size distribution for fuel and steel fragments are based on the ANL M-series tests. These tests involved interaction of molten materials with liquid sodium. However, for some CDA sequences, namely, the transition phase regime of the LOF accident, it is expected that two-phase vapor/liquid core materials will be ejected into the sodium pool. For this case no experimental results have been cited for the particle size distribution.

- a) Provide the justification for using particle size distributions from liquid/liquid materials interaction tests (ANL M-series) to represent the size distribution resulting from interaction of two-phase fuel materials with sodium.
- b) Provide estimates of the depth of a thermally stable bed as a function of the particle size distribution.
- c) Provide a discussion and description of any proposed R&D programs that will yield the necessary information relative to Items (a) and (b) above.

Response:

The information requested is provided in the response to question 001.683. |

Question 001.501 (F6.4.1.1.2)

Catton and Dhir (Reference: Post-Accident Heat Removal for LMFBRs, UCLA-ENG-7593, dated October, 1975) report predictions for stable debris depths, based on theoretical and experimental treatments, that are at variance with the ANL data, generally being much shallower. They found factors such as trapped vapor and wall interference played an important role in fixing the dryout heat flux for a given bed depth. The expressions developed to predict the maximum stable depth were intended to encompass these interfering factors with a conservative choice of an empirical constant. Discuss how this section makes allowances for these considerations.

Response:

The factors considered by Catton and Dhir in Reference Q001.501-1 are not considered to alter the evaluation presented in CRBRP 3, Vol. 2 (Reference 10b of Section 1.6) for the following reasons:

- a) Trapped vapor: The particulate beds postulated in the CRBRP are formed by the settling of particles through several feet of sodium. The gases present in the system (fission gases released from the fuel pin at the time of breach or from the fuel at the time of fuel melting would separate from the particles due to turbulence) are buoyant and would rise to the sodium surface rather than being entrapped by the falling particles. A discussion of the effects of sodium vapor generation within the debris bed is provided in Reference Q001.501-2.

This is a different situation than that considered in the UCLA experiments in which a dry solid material and a liquid are placed in a small container, trapping vapor already present in the system.

- b) Wall effects: Catton and Dhir's experiments were conducted in a small (4.7 cm diameter) beaker and wall effects could be expected to have an important influence on their results. The surface area of settled debris in the CRBRP is orders of magnitude greater than the surface area of the beaker, and wall effects would be expected to have little influence on the bed dryout heat fluxes.
- c) Bed depth comparisons with ANL data

Catton and Dhir have developed a correlation for a deep debris bed, i.e., a height greater than 5 cm, by using a correlation factor which describes a line running through the lower three points of their data.

Q001.501-1

Amend. 62
Nov. 1981

For the power levels used in the analysis, 2 to 3%, Catton and Dhir's correlation predicts bed depths of 0.7 to 1.4 cm. Depths of this magnitude have a heat transfer mechanism different from that of deep beds, primarily because the vapor channels extend the full depth of the bed, and a comparison with ANL data (Reference Q001.501-2) should be made on the basis of a shallow bed correlation.

The assessments of debris bed behavior and their bases are provided in Appendix G.1 of CRBRP-3, Volume 2 (Reference 10b of PSAR Section 1.6).

References

- Q001.501-1. I. Catton and V. Dhir, "Post-Accident Heat Removal for LMFBRs", UCLA-ENG-7593, November 1975.
- Q001.501-2. L. Baker, Jr., et. al., "Post-Accident Heat Removal Technology," ANL/RAS 74-12, July 1974.

Question 001.502 (F6.4.1.2)

Expand Section F6.4.1.2 to provide the distribution of debris between the internal reactor vessel structures and the primary heat transport system for a spectrum of CDA's ranging from highly energetic to benign ones, including scenarios that lead to the transition phase.

Response:

The analyses questioned above have been superseded by those currently presented in Section 3.1.1 and Appendix I of CRBRP-3, Volume 2 (Reference 10b of PSAR Section 1.6).

Q001.502-1

Amend. 62
Nov. 1981

Question 001.503 (F6.4.1.2)

For the particle settlement analysis presented in this section, describe and discuss the experimental evidence, if any, that supports this analysis.

Response:

The information requested is provided in the response to question 001.688. |

Q001.503-1

Amend. 62
Nov. 1981

Question 001.504 (F6.4.1.2)

Provide the basis (including accident energetics) of the estimate that 58% of the debris is expected to enter the Primary Heat Transport System (PHTS). In addition, provide information on the consequences of such an occurrence, including consideration of the final destination of the debris in the PHTS and settling and dryout of debris leading to failures of PHTS components.

Response:

The analyses questioned above have been superseded by those currently presented in Section 3.1.1 and Appendix I of CRBRP-3, Volume 2 (Reference 10b of PSAR Section 1.6).

Question 001.505 (F6.4.1.3)

Melt-through of the lower reactor vessel head is predicted to occur in not less than 1600 seconds. However, non-uniformities in the steel melting could result in significantly earlier penetrations. The melting irregularities may develop due to the lighter, molten steel bubbling up through the more dense UO₂ at preferred locations. This bubble spacing would be established by a Taylor-type instability. If the bubble release points were to remain spatially stationary, the heat flux through a thinner molten layer between these points would be higher than the average value predicted by a uniformly advancing melt front. Since the thermal load on the Ex-Vessel Core Catcher (EVCC) and the External Cooling System (ECS) is strongly dependent upon the time required for a melting attack to breach the reactor and guard vessels, provide an assessment of the impact that earlier arrival of molten material would have on the performance of the EVCC and ECS.

Response:

The information requested, as applicable to the TMBDB design, is addressed in the response to question 001.633.

Question 001.506 (F6.4.1.3.1)

Provide complete details on your calculation of time to melt through the lower heads of the reactor and guard vessels. These details should include the decay heat level and sodium temperature versus time, individual masses of core debris and steel components being melted, criteria for vessel penetration, and all relevant assumptions.

Response:

The information requested can be found in CRBRP-3, Volume 2 (Reference 10b of Section 1.6), Appendix B.

Q001.506-1

Amend. 62
Nov. 1981

Question 001.507 (F6.4.1.4)

Clarify how debris beds in a dry environment on the thermal baffle can radiate to the cavity EVCC external cooling system.

Response:

With the deletion of the Parallel Design in Amendment 24 this question is no longer applicable as the features upon which the question is based are no longer a part of the design.

Q001.507-1

Amend. 62
Nov. 1981

Question 001.508 (F6.4.2)

Provide the basis for not requiring OHRS to be operational following a CDA.

Response:

The objective of the Direct Heat Removal Service, DHRS, (formerly the OHRS) is specified in Section 5.6.2.1.1 as preventing loss of in-place coolable geometry of the core following reactor shutdown in the event of simultaneous failure of the normal shutdown heat removal systems. A hypothetical CDA, by definition, goes beyond the point of maintaining in-place coolable core geometry. As such, no credit has been taken for either the normal shutdown system or for the DHRS capability in the TMBDB analysis.

Question 001.509 (F6.4.2)

For the case of extensive reactor vessel flow blockages resulting in temperatures exceeding 1230°F, and subsequent failure of the reactor and guard vessels, provide the basis for assuming that core debris will not be introduced on any other portion of the reactor cavity except the EVCC.

Response:

With the deletion of the Parallel Design in Amendment 24 this question is no longer relevant as the EVCC is no longer a part of the design.

Q001.509-1

Amend. 62
Nov. 1981

Question 001.510 (F6.4.3.2)

Provide the technical justification for not considering the heat load associated with the decay of radioactive nuclides in the reactor steel structures due to neutron captures.

Response:

The activation of reactor steel structures is confined primarily to the stainless steel concentrated in the core, blanket and near-core shielding regions. The associated decay power at shutdown from this activation is on the order of 112 kw. This is negligible when compared to the fuel and blanket decay heat loads from Table C.1-3 of CRBRP-3, Volume 2 (Reference 10b of PSAR Section 1.6).

Question 001.511 (F6.4.3.4):

Provide a discussion of the consideration that has been given to precluding thermal stress induced cracking in the sacrificial bed because of sudden contact with hot molten core debris.

Response:

With the deletion of the Parallel Design in Amendment 24 this question is no longer relevant as the features upon which the question is based are no longer a part of the design.

Q001,511-1

Amend. 62
Nov. 1981

Question 001.512 (F6.4.3.5):

In view of the uncertainties of solubility rate and heat transfer from molten fuel pools in sacrificial beds, provide the following information:

- a) Provide estimates of the uncertainties and design margins associated with the final pool configuration and the thermal load distribution to the EVC system.
- b) In determining the capabilities of the EVCC and ECS, provide a discussion of the consideration that has been given to possible non-uniformities in sodium temperatures and molten pool heat fluxes.
- c) Because of the potentially significant effect on heat transfer and penetration into the sacrificial bed, provide a discussion of the consideration that has been given to solid UO₂ and/or stainless steel crust formation on the molten fuel in the core catcher.
- d) Provide a description and discussion of any proposed R&D programs that will yield the appropriate information relative to Items (a), (b) and (c) above.

Response:

With the deletion of the Parallel Design in Amendment 24 this question is no longer applicable as the features upon which the question is based are no longer a part of the design.

Question 001.513 (6.2.6.1.3 Yellow)

Provide additional details on how the margin seals on the closure head plug risers prevent sodium or core debris egress into the sealed head access area following a CDA.

Response:

The sealed HAA is not part of the present design. Also, the CDA is now only considered as a hypothetical event beyond the design base. The margin seals must meet the SMBDB sodium and gas leakage requirements given in Section 5.3.2 of CRBRP-3, Volume 1 (Reference 10a of PSAR Section 1.6). Details on the margin seals are given in PSAR Section 5.2.4.4. Tests in support of the margin seal design are discussed in Section 5.4.1.5 of CRBRP-3, Volume 1.

Q001.513-1

Amend. 62
Nov. 1981

Question 001.514 (6.2.6.1.3 Yellow)

Provide additional details on how the structural integrity of the sealed head access area concrete is assured considering the additional heat load introduced following a CDA.

Response:

In Amendment 24 to the PSAR, the Project withdrew the Parallel Design from further consideration by the NRC staff. This question requests additional design information on a specific feature of the Parallel Design. Therefore, the question is no longer relevant.

Q001.514-1

Amend. 62
Nov. 1981

Question 001.515 (6.2.7.2 Yellow)

Provide the thermo-physical properties of the magnesia powder relative to the initial impact of UO_2 on the core debris receptacle. Include in your response a discussion to address the possibility and consequences that the 5 inch thick layer of MgO powder may be flushed away by the impingement of a hot, dense liquid stream, thereby diminishing resistance to thermal shock.

Response:

With the deletion of the Parallel Design in Amendment 24 this question is no longer applicable as the features upon which the question is based are no longer a part of the design.

Q001.515-1

Amend. 62
Nov. 1981

Question 001.516 (6.2.7.2 Yellow)

Figure F6.4-11 shows significantly greater temperature gradients at the centerline of the sacrificial bed than along the side walls. In view of this, provide a discussion of the consideration that has been given in your design to accommodating local hot spot effects, such as varying either cooling coil spacing or NaK flow rate.

Response:

With the deletion of the Parallel Design in Amendment 24 this question is no longer applicable as the features upon which the question is based are no longer a part of the design.

Question 001.517 (6.2.7.2 Yellow)

Provide the technical justification that the 35 feet height for the cooling system annulus is adequate to maintain structural integrity of the reactor cavity structures and concrete following a CDA.

Response:

With the deletion of the Parallel Design in Amendment 24 this question is no longer applicable as the features upon which the question is based are no longer a part of the design.

Q001.517-1

Amend. 62
Nov. 1981

Question 001.518 (6.2.7.2 Yellow)

Provide a discussion of the consideration that has been given to cooling the reactor guard vessel support structure, including whether conduction from hot sodium along the steel structure could result in localized hot spot areas of concern as to structural adequacy.

Response:

After penetration, no cooling of the guard vessel support structure is necessary since the guard vessel serves no function in the TMBDB scenario. The heating of the support structure could be expected to cause sagging of the guard vessel until it comes to rest on the outlet nozzles of the reactor vessel.

Question 001.519 (6.2.7.2 Yellow)

Provide additional details on the structural support of the various Ex-Vessel Core Catcher (EVCC) components, including the impact loads that are being considered. Provide the impact loads that are being used in the design of the EVCC, including a discussion of the consequences of reactor and guard vessel impact.

Response:

With the deletion of the Parallel Design in Amendment 24 this question is no longer relevant as the features upon which the question is based are no longer a part of the design.

Question 001.520 (6.2.7.2 Yellow)

Provide a discussion of the impurity content and control, especially moisture for the magnesia sacrificial bed, including the consequences of such impurities on materials interactions following introduction of core debris. Provide a description of the instruments, systems and measures to be employed to monitor impurity levels in the magnesia bed.

Response:

With the deletion of the Parallel Design in Amendment 24 this question is no longer relevant as the features upon which the question is based are no longer a part of the design.

Question 001.521 (6.2.7.2 Yellow)

Provide additional details on the type and thermo-physical properties of the graphite material that will be used to fill the cooling system annulus.

Response:

With the deletion of the Parallel Design in Amendment 24 this question is no longer relevant as the features upon which the question is based are no longer a part of the design.

Question 001.522 (6.2.7.2 Yellow)

Since significant adverse materials interactions have been observed to take place between sodium and silica-containing materials, justify the use of silica-alumina firebrick insulation in the area behind the steel liner.

Response:

With the deletion of the Parallel Design in Amendment 24 this question is no longer applicable as the features upon which the question is based are no longer a part of the design.

Question 001.523 (6.2.7.3.1 Yellow)

Provide a discussion of the consequences of sodium absorption in the sacrificial bed on the molten pool heat transfer, including the impact of sodium vapor generation on the structural integrity of the sacrificial bed and reactor cavity.

Response:

With the deletion of the Parallel Design in Amendment 24 this question is no longer applicable as the features upon which the question is based are no longer a part of the design.

Question 001.524 (6.2.7.3.1 Yellow):

The assumption appears to have been made that the sodium pool above the molten core debris is at uniform temperature and that any sodium vapor, created by local boiling, will be condensed, precluding any increase in the reactor cavity pressure. Natural convection may result in an upswelling plume of hot sodium in the center of the sodium pool above the EVCC and hot core debris. The vapor pressure of the hot sodium surface near the center of the pool could influence the extent of overpressure in the reactor cavity. Consider this in your evaluation and provide an assessment of the consequences; the capability of the reactor cavity design to cope with these consequences, including overpressures must be addressed.

Response:

The EVCC is not part of the current design. The information requested, as applicable to the TMBDB analysis, is addressed in the response to question 001.617.

Question 001.525 (6.2.7.3.1 Yellow):

There does not appear to be adequate design margin for the sacrificial bed depth in view of the uncertainties associated with solubility rate of bed material into the molten core debris, and variations in heat flux distribution over the pool boundary. Justify that conservative solubility and heat transfer rates were used in calculating final pool size, including a description and discussion of applicable R&D programs. In addition, provide a discussion of the sensitivity of the molten pool termination point to variations in solubility and heat transfer rates.

Response:

With the deletion of the Parallel Design in Amendment 24 this question is no longer applicable as the features upon which the question is based are no longer a part of the design.

Question 001.526 (6.2.7.3.2 Yellow)

Since maintenance is intended to be performed on one of the ECS cooling loops during reactor operation, provide the technical justification to demonstrate that, in the event of a single failure in the operating loop, sufficient time is available for restoration of one of the cooling loops to service before either sodium or reactor cavity structural temperatures reach unacceptable levels following a CDA.

Response:

With the deletion of the Parallel Design in Amendment 24 this question is no longer applicable as the features upon which the question is based are no longer a part of the design.

Question 001.527 (6.2.7.3.2 Yellow)

Confirm whether both ECS cooling systems can be operated simultaneously in the event of unanticipated higher heat loads.

Response:

With the deletion of the Parallel Design in Amendment 24 this question is no longer applicable as the features upon which the question is based are no longer a part of the design.

Question 001.528 (6.2.7.3.1 Yellow)

Provide the estimated ECS NaK coolant activity levels following a CDA and an assessment of the radiological consequences of any NaK spills, leakage or other release in the DHX building.

Response:

With the deletion of the Parallel Design in Amendment 24 this question is no longer applicable as the features upon which the question is based are no longer a part of the design.

Question 001.529 (6.2.7.3.2 Yellow)

Provide the sequence of operator actions and corresponding times to manually activate the ECS in the event of a CDA. In addition, provide a discussion of the necessary instrumentation that will be provided to assist the operator in determining the actions to be taken. Address the potential for and consequences of incomplete or inadequate operator action.

Response:

In Amendment 24 to the PSAR, the Project withdrew the Parallel Design from further consideration by NRC staff. This question requests additional information pertinent to a specific feature of the Parallel Design. Accordingly, the question is no longer directly applicable. However, the operator actions associated with the TMBDB features are discussed in Section 2.3 of CRBRP-3, Volume 2 (Reference 10b of PSAR Section 1.6). Instrumentation requirements are provided in Section 2.1.2.12 of the reference.

Question 001.530 (6.2.6.1.2, 5.2.1.3 Yellow)

In view of the uncertainties associated with sealed head access (SHAA) head margin seal performance during a CDA, provide an upper bound estimate of the quantity of sodium that can be ejected into the SHAA before nitrogen inerting becomes a necessity. Justify on a conservative basis that ejection of the above amount of sodium is precluded by head margin seal design.

Response:

With the deletion of the Parallel Design in Amendment 24 this question is no longer applicable as the features upon which the question is based are no longer a part of the design. See the response to question 001.513 for a discussion of potential head leakage.

Question 001.531 (3A.1.3 Yellow)

Since the primary sodium overflow and make-up line penetrations are extensions of the reactor cavity and part of the inner containment boundary, provide the basis for the differences in design pressures as listed in Table 3A.1-3.

Response:

With the deletion of the Parallel Design in Amendment 24 this question is no longer applicable as the inner containment boundary is no longer a part of the design.

Question 001.532 (9.13.2.2 Yellow)

For the EVCC cooling system cells in the Reactor Containment Building which contain an air atmosphere, provide the technical justification that structural integrity of these cells and independence of cooling loops will not be compromised in the event of a NaK spray fire on the side walls and ceiling, or in the event of a NaK spill onto a catch pan where the nitrogen flooding system fails to operate.

Response:

In Amendment 24 to the PSAR, the Project withdrew the Parallel Design from future consideration by the NRC staff. This question requests additional design information on a specific feature of the Parallel Design. Accordingly, the question is no longer applicable.

Question 001.533 (11.3.2.6 Yellow)

Since leakages through the reactor head seals and buffered seals represent the principal constituents of the total off-site radioactive release, provide the basis for not processing the SHAA atmosphere through the Cell Atmosphere Processing System (CAPS) in order to satisfy as low as is reasonably achievable release criteria.

Response:

With the deletion of the Parallel Design in Amendment 24 this question is no longer applicable as the features upon which the question is based are no longer a part of the design.

Question 001.534 (F6.4.3.5, 6.2.7.2, 8.3.1.1)

The capacity (2000 gpm) for each of the two EM pumps in the Ex-Vessel Core Catcher Cooling System appears to be beyond the current state of the art. Since these pumps will be required to operate for an extended period of time for decay heat removal, provide a description and discussion of the experience and/or R&D program that exists for EM pumps of this capacity.

Response:

With the deletion of the Parallel Design in Amendment 24 this question is no longer applicable as the features upon which the question is based are no longer a part of the design.

Question 001.535 (6.2.7.3.1 Yellow):

Jahn and Reineke (Reference: Paper NC2.8, International Heat Transfer Conference, Tokyo, 1974) have shown that a wide variation exists in the heat transfer coefficient along the submerged surface of a volumetrically heated liquid pool held within cylindrical cavity. This result indicates the possibility of the reactor vessel being initially penetrated by molten UO_2 at a point on the vessel sidewall near the surface of the UO_2 pool, and not at the midpoint of the lower dome. Similar possibilities exist for the reactor guard vessel penetration. Provide a discussion of the capability of the EVCC to cope with introduction of core debris in an asymmetric manner, including thermal, structural, and criticality considerations. Include a discussion of the dependence of molten pool growth on the initial core debris distribution in the sacrificial bed. Furthermore, provide a description and discussion of the R&D program proposed to resolve this question.

Response:

With the deletion of the Parallel Design in Amendment 24, the EVCC is no longer a part of the design. Response to this question, as applicable to the TMBDB analysis, is provided in the response to question 001.617.

Question 001.536 (6.2.7.3.1 Yellow)

If the sodium pool is deep enough to submerge a portion of the cylindrical guard vessel support skirt, two isolated ullage regions could be created above the sodium pool in the bottom of the reactor cavity. If this occurs the vapor pressure associated with higher temperature sodium near the center of the pool would cause the surface to move downward within the support skirt while raising the level in the annular region outside the skirt. Discuss the effect that the uneven sodium level would have on the reactor cavity and ECS. In addition, confirm whether or not openings through the guard vessel support skirt would be provided to eliminate the potential sodium level unevenness.

Response:

With the deletion of the Parallel Design in Amendment 24, the ECS is no longer part of the design. The effect of unevenness of sodium pool level within the reactor cavity has little effect on the reactor cavity. The sodium level outside the guard vessel skirt would be raised less than one foot from the complete expansion of gases entrapped to fill the area in question to the level of the bottom of the guard vessel. Once the gas has expanded to push the sodium level below the elevation of the ruptured area of the guard vessel, the entrapped gas would escape into the reactor cavity between the reactor vessel and guard vessel. The guard vessel support skirt includes openings as indicated in Section 2.1.2.3 of CRBRP-3, Volume 2 (Reference 10b of PSAR Section 1.6).

Question 001.537 (F5.3.3)

Describe the clearances between each of the head-mounted components and the overhead structures associated with sealing the head access area.

Response:

This question requests clarification of information which is no longer a part of the current documentation. The Project has since consolidated all considerations given Hypothetical Core Disruptive Accidents into report CRBRP-3 (References 10a and 10b, PSAR Section 1.6) and its associated references; consequently, PSAR Appendices D and F have been withdrawn in Amendments 24 and 60 respectively. The CRBRP does not have a sealed head access area.

60

Question 001.538 (F5.4, F6.3)

In Chapter F5.4, the pressures in selected zones in the REXCO calculation are displayed (Figure F5.4-2 through Figure F5.4-30). Discuss how these pressures were translated into the forces, loads and displacements shown in Figure F6.3-12 through Figure F6.3-26.

Response:

This question requests clarification of information which is no longer a part of the current documentation. The Project has since consolidated all considerations given Hypothetical Core Disruptive Accidents into report CRBRP-3 (References 10a and 10b, PSAR Section 1.6) and its associated references; consequently, PSAR Appendices D and F have been withdrawn in Amendments 24 and 60 respectively. A discussion of the use of REXCO calculations is provided in Section 5 of Reference 10a, PSAR Section 1.6.

Question 001.539 (F6.3.2.3)

Provide curves of the energy partition as a function of time between the vessel, core barrel, core support structure, the rotating plugs, the vessel holddown bolts, support ledge and sodium slug as derived from the REXCO calculations. Tabulate the % total strain, maximum deflection and permanent elongation for each major structural member.

Response: *

| 60

The energy partition curves as a function of time are presented in Figure Q001.539-1 and Figure Q001.539-2. Figure Q001.539-1 contains the energy curves of axial positive kinetic energy (sodium slug), core barrel strain energy, vessel strain energy, head kinetic energy (rotating plugs) and total head energy. Since the rotating plugs are modeled as a rigid body in REXCO analysis, the difference between the total head energy and head kinetic energy will be the strain energy of vessel holddown bolts. The support ledge is modeled as a rigid foundation in REXCO, therefore there is no strain energy associated with it. The core support is modelled as a flat thick plate. The energy curve associated with this model is not provided here because the model is not considered as representative to provide the strain energy of the support. (The purpose of the model is to reflect a conservative load on the core support.) Figure Q001.539-2 is an enlarged version of head kinetic energy and total head energy.

As explained in the REXCO reactor vessel modeling, see Section 5.1.1.3 of Ref. 10a, PSAR Section 1.6, the axial deformation and strain are not representative of REXCO output. A separate structural dynamics study of the reactor vessel system based on REXCO predicted loads is more appropriate and is provided in Section 5.4.1 of Reference 10a, PSAR Section 1.6. The circumferential maximum strain and radial maximum displacement are presented as follows: | 60

Core barrel strain	6.22%
Vessel strain	6.05%
Core barrel deflection	12.09 cm (4.76 in.)
Vessel deflection	18.85 cm (7.42 in.)

*Note that Appendix F has been withdrawn. The text, upon which the question was based, can now be found in Section 5 of Reference 10a, PSAR Section 1.6. | 60

ENERGY PARTITION OF DEMO F

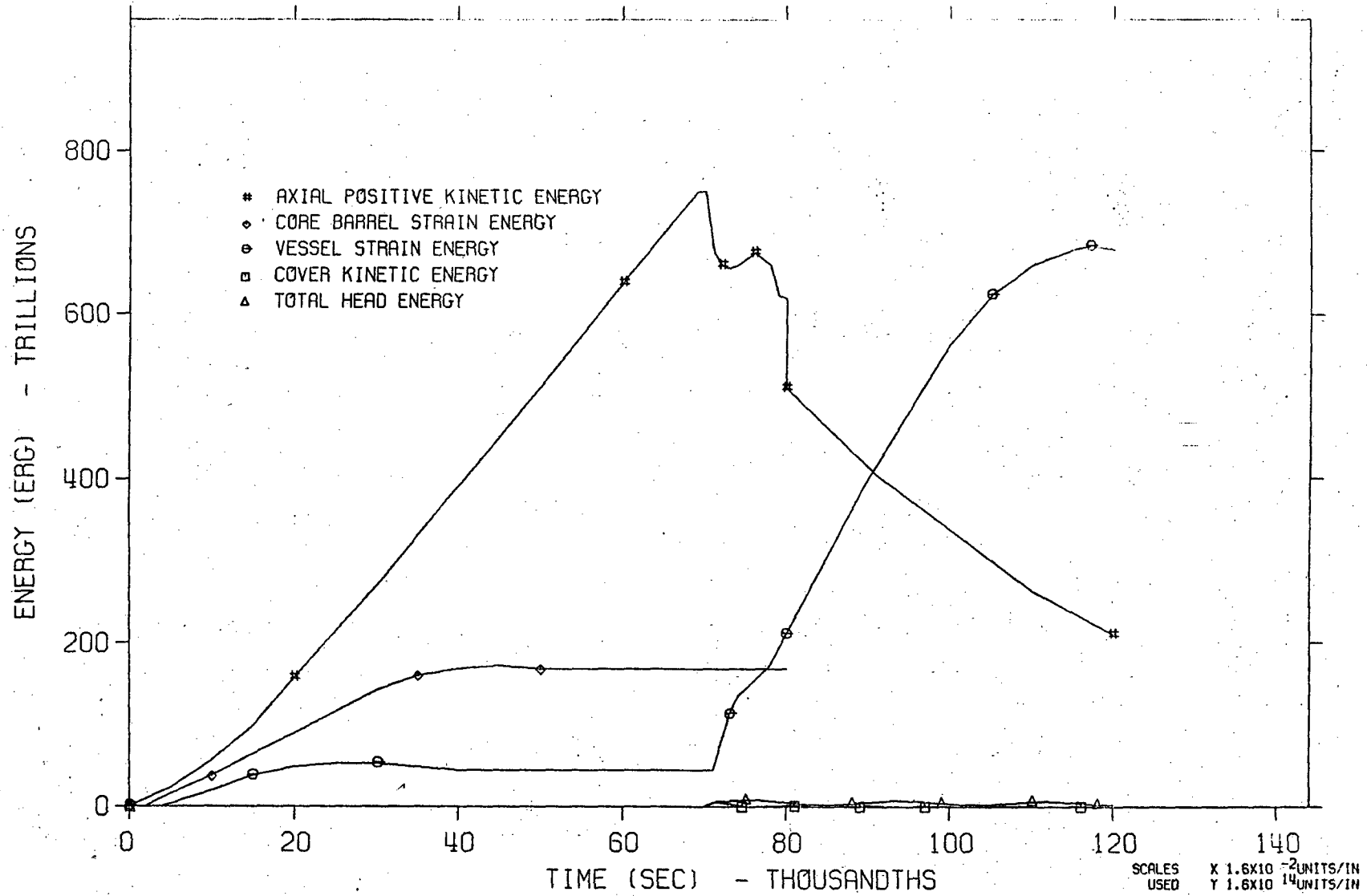


Figure Q001.539-1

Q001.539 - 2

Q001.539-3

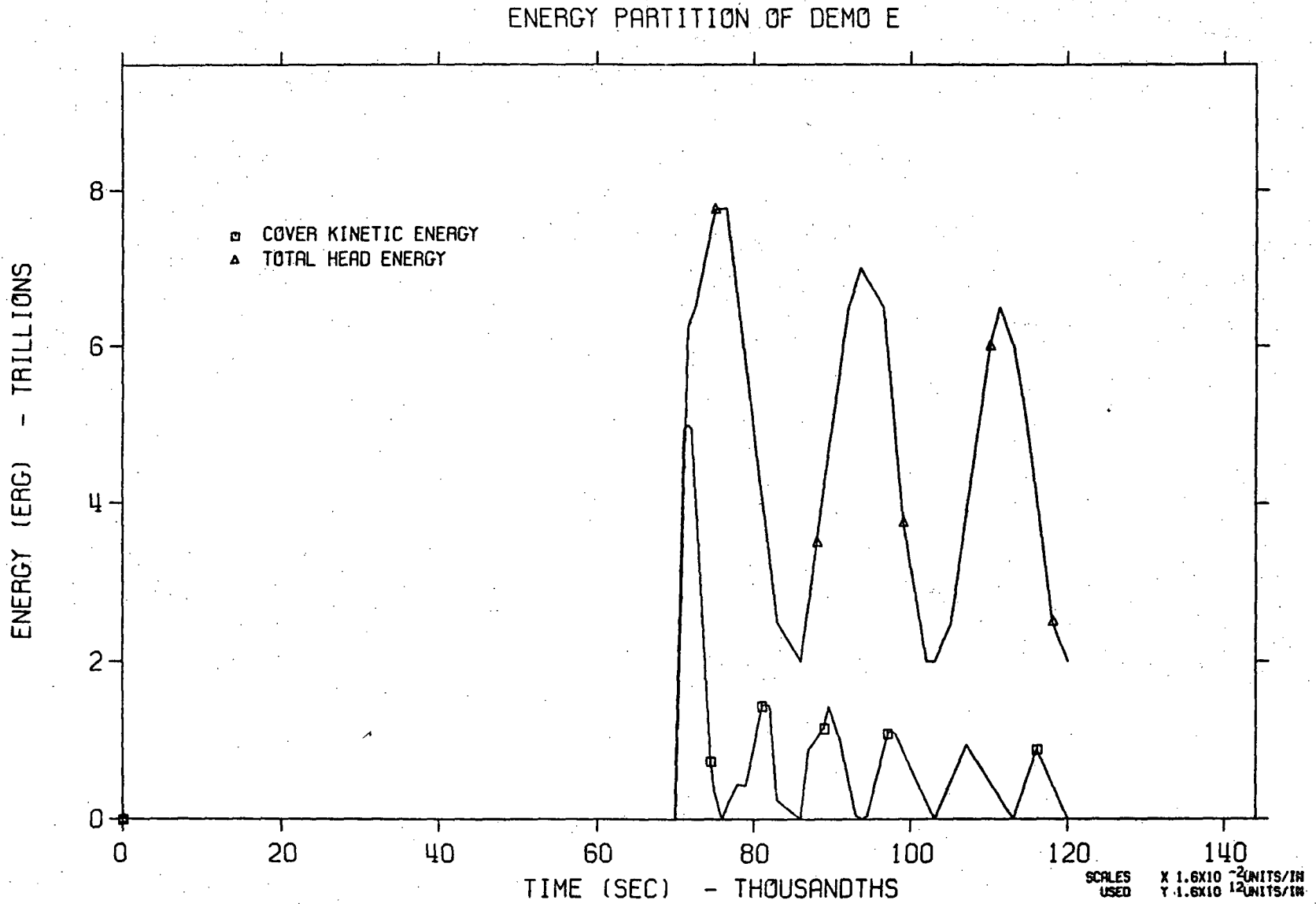


Figure Q001.539-2

Question 001.540 (F6.3.1)

Provide an estimate of the limiting accident in terms of energetics which the CRBR can be expected to withstand. In other words, determine the most energetic CDA that could be accommodated by the CRBR design before either the ledge fails or the primary containment boundary is breached in the head area.

State sequentially the order in which components in the head region fail and the energy level at which they fail.

Response:*

| 60

The specification of an energetics level at which components fail is not meaningful because the available work energy if a pressurized region is allowed to expand to atmospheric pressure is not directly correlated to the mechanical loads on components. The expansion to the point of sodium slug impact with the head is a more appropriate measure of energetics since the system does not normally permit this full expansion. This emphasizes the energy released during the early part of the expansion, which has the greatest potential for damaging the system. The shape of the pressure-volume curve is also important in determining component dynamic loads. Two different p-v curves could result in the same work energy if expanded to one atmosphere and yet result in completely different component loads, with the possibility that each could result in limiting loads in different components.

| 60

Because of this difficulty in defining energetics in a unique manner, the capability of the design was assessed by evaluating the following four different energetic conditions:

Case 1 (SDB)

The Structural Design Basis (SDB) is discussed in Section 5 of Ref. 10a, PSAR Section 1.6. This is based on fuel vapor expansion from a core having a non-uniform temperature distribution and an average temperature of 4800°K. The structural requirements are consistent with the loads derived from this condition. If expanded to one atmosphere, the available work energy would be 661 MJ.

| 60

Case 2

A higher level energetics case similar to Case 1 but having a non-uniform temperature distribution that results in an average temperature of 5000°K. If expanded to one atmosphere, the available work energy would be 858 MJ.

| 35

Case 3

A pressure-volume curve derived from considerations of an energetic molten fuel-coolant interaction, even though such interactions are not considered to be a realistic possibility. If expanded to one atmosphere, the available work energy would be 307 MJ.

| 35

*Note that Appendix F has been withdrawn. The text, upon which the question was based, can now be found in Section 5 of Reference 10a, PSAR Section 1.6.

| 60

Case 4

A pressure-volume curve based on fuel vapor expansion from an initial uniform temperature of 5200°K. If expanded to one atmosphere, the available work energy would be 1324 MJ.

40

The work energy values in the above four cases should only be considered as convenient labels for the cases rather than as a measure of the severity of the events. Table Q001.540-1 summarizes the principal characteristics of these four cases. Figure Q001.540-1 provides the p-v curves for all four cases. Cases 1 and 2 are considered to be more representative of the potential loading conditions which result in a pessimistic treatment of phenomena (divergent from experimental data) associated with hypothesized energetic core disruptive accidents than cases 3 and 4. This is due to the fact that Case 3 hypothesizes sodium vapor as the working fluid, which is contrary to experimental evidence and Case 4 hypothesizes a uniform temperature distribution, which is arbitrary.

The structural assessment of these cases used loads derived from REXCO-HEP and applied to a recent one-dimensional model of the reactor head and vessel. For Case 1, a three-dimensional dynamic inelastic ANSYS calculation had previously been performed and verified the adequacy of the one dimensional approximation. An important input to the recent 1-D calculations was experimental results from static loading tests on a scale-model section of the head plugs and shear rings. These tests indicated greater head structural capability than previously predicted with analysis. The margin of safety in all cases was based on a strain allowable of 70% of the strain at the plastic instability load, except for the concrete vessel support ledge where the allowable load was taken to be the design requirement of 50 million pounds. The analyses addressed the structural integrity of the components and did not assess leakage; i.e. the emphasis in this assessment is placed on avoiding gross mechanical failure of the components. The calculational details are provided in the Addendum to this response. The results are summarized in Table Q001.540-2.

60

40

Based on this assessment, along with previous studies and engineering judgment, the following conclusions on the energetics capability are reached:

40

- In the region of the head, the components expected to reach failure criteria first are certain head mounted components, such as the upper internals structure jacking mechanism, the dip seal maintenance ports or the CRDM seismic support bolts. Although these components do not meet a highly conservative criterion based on elastic analyses, it is likely that these can be shown to meet the intent of the Code (i.e. 70% of strain at the plastic instability load). This is illustrated in the case of the CRDM nozzles, where Table Q001.540-2 shows a substantial margin of safety on the basis of this strain criterion (which is more appropriate for an impulse type loading) for all loadings evaluated, even though the application of the highly conservative stress criterion (i.e. 70% of stress of the plastic instability load) would indicate a negative margin. This provides confidence that the head mounted components will meet the strain criterion for the Structural Design Basis loads. Meeting the intent of the Code for the Structural Design Basis loads (Case 1) should provide inherent margins to failure to accommodate somewhat higher loads such as those described in Case 2.
- The reactor vessel head including the shear rings and riser bolts has margin to accommodate all of the loads analyzed, with a substantial margin to failure.
- The vessel support ledge loads are not very sensitive to the HCDA loads | 60 because of yielding in the head bolting system and the vessel. Therefore the ledge design load is not exceeded in any of the cases analyzed. Furthermore, using the design requirement of 50 million pounds as the "allowable" is conservative since gross failure would not be expected at 50 million pounds.

In summary, it is not meaningful to specify an energy level at which components fail. First, the severity of mechanical loadings do not directly correlate to total energy release. Second, the energy distribution, which varies from case to case is critical in determining the load-history seen by a particular component. For these reasons, the approach employed here was to examine a range of different pressure-volume expansions as a source of loadings, and from these to identify the components which appeared to be the most limiting in the system. At present, limiting components appear to be the jacking mechanisms, the dip seal maintenance ports and the CRDM seismic support bolts. The design provides margins so that failure (as defined by exceeding the specified strain criteria) would not be predicted for a range of postulated conditions involving both different energetics and different shaped p-v curves as typified by the analyses of Cases 2,3 and 4.

40

Table Q001.540-3 tabulates the P-V curves used as input to the REXCO-HEP calculations for cases 1 through 4.

34

The Addendum to Response Q001.540 has been provided in support of the preceding response.

60

TABLE Q001.540-1

35

CHARACTERISTICS OF ENERGETICS CASES ANALYZED

	<u>Case 1</u> (SDB)	<u>Case 2</u>	<u>Case 3</u>	<u>Case 4</u>	
Working Fluid	Fuel Vapor	Fuel Vapor	Sodium Vapor	Fuel Vapor	
Fuel Temperature (°K)	4800	5000	----	5200	
Temperature Distribution	Non-Uniform	Non-Uniform	----	Uniform	35
Initial Core Pressure (Atmos)	273	313	202	151	
Work Energy in Expansion to Slug Impact (MJ)	101	155	100	170	35
Sodium Slug Kinetic Energy (MJ)	75	96	41	96	
Work Energy if Expanded to 1 Atmos (MJ)	661	858	301	1324	
Work Energy if Expanded to Dynamic Equilibrium (MJ)	141	221	130.9	350	
Average Core Pressure at Dynamic Equilibrium (psi)	303	312	276	399	35

Q001.540-5

Amend. 35
Feb. 1977

TABLE Q001.540-2

MARGINS OF SAFETY* for HCDA LOADINGS

Component		Case 1 (SDB)	Case 2	Case 3	Case 4
Shear Rings	SRP	27.20*	25.12	28.03	27.48
	IRP	8.70	7.33	8.23	8.42
	LRP	9.03	7.52	8.58	7.91
Riser Bolts	SRP	19.00	15.67	24.92	29.43
	IRP	19.00	15.67	24.92	29.43
	LRP	6.81	5.48	10.78	16.50
Vessel Flange Bolts		21.63	7.25	10.16	11.42
Vessel Wall (Stretching)		44.95	40.35	20.72	22.36
Concrete Ledge	Downward	0.165	0.160	0.132	0.154
	Upward	0.518	0.078	0.078	0.078
Seismic Support Bolts		0.84	0.54	1.39	1.91
CRDM Nozzle Extension		8.17	6.63	10.89	13.50

$$* \text{ Margin of Safety} = \frac{\text{Allowable Value}}{\text{Calculated Value}} - 1$$

(In the evaluations, the allowable value for the concrete ledge was the 50×10^6 lbs. requirement. For all other components, the allowable value was 70% of the strain or comparable deformation at which the respective plastic instability load occurred. See the Addendum to Response Q001.540. 160
23 justification of this criterion).

TABLE Q001. 540-3

PRESSURE-VOLUME RELATIONSHIPS

Case 1		Case 2		Case 3		Case 4	
Pressure (bars)	Volume (meters ³)						
273.	2.558	312.8	2.56	204.4	2.14	150.5	2.558
203.	2.6179	272.5	2.67	101.4	6.43	138.	3.837
147.3	2.878	203.	2.95	91.24	7.14	120.	5.6276
103.8	3.595	147.3	3.6	81.1	7.99	100.2	8.134
86.09	4.309	124.2	4.19	70.96	9.04	88.3	10.74
70.77	5.415	103.8	5.1	60.82	10.38	76.2	14.069
57.6	7.228	86.1	6.47	50.68	12.20	64.1	18.647
46.47	10.098	70.8	8.56	40.55	14.84	56.6	23.022
37.08	14.748	57.6	11.83	30.41	19.22	46.5	30.696
29.25	22.01	46.5	16.66	20.27	28.33	39.07	38.67
22.8	33.13	37.08	23.76	10.13	54.89	32.0	51.16
17.55	49.54	29.25	33.86	9.12	60.68	26.8	63.95
13.32	75.38	22.8	49.0	8.11	67.95	22.53	78.42
9.96	115.26	17.55	71.7	7.09	77.16	16.3	115.11
		13.3	105.4	6.08	89.38	12.6	153.48
		9.96	156.	5.06	106.21	8.8	230.22
				4.05	131.04	6.094	344.56
				3.04	171.39	0.7048	3166.8
					248.52		
					459.15		

Q001.540-6a

Amend. 34
Feb. 1977

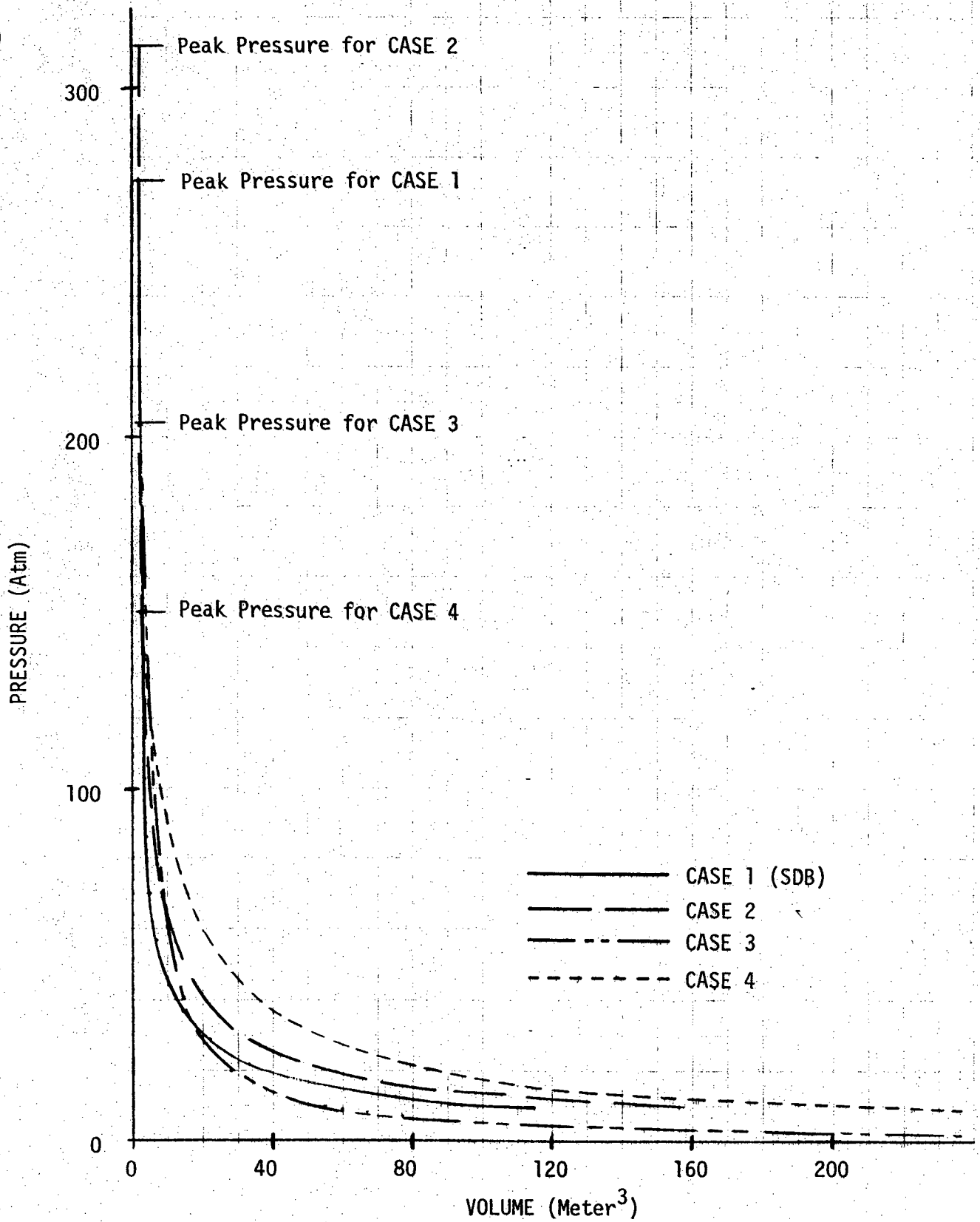


FIGURE Q001.540-1

Pressure-Volume Relationships for
Energetics Cases Analyzed

Q001.540-7

Amend. 21
June 1976

ADDENDUM

TO RESPONSE Q001.540

ANALYSES OF THE CRBRP

CLOSURE HEAD RESPONSE

TO VARIOUS HCDA ENERGETICS

Amend. 60
Feb. 1981

TABLE OF CONTENTS

1.0	INTRODUCTION	1
1.1	Criteria Used in Determining Margin of Safety	3
2.0	SUMMARY.	4
3.0	SHEAR RINGS, FLANGE BOLTS, AND LEDGE	6
3.1	Method of Analysis	6
3.2	Assumptions.	6
3.3	Model.	8
3.4	Dynamic Properties	8
3.4.1	Plugs	8
3.4.1.1	Masses	8
3.4.1.2	Flexibilities and Damping	8
3.4.1.3	Bearings	10
3.4.2	Shear Rings	11
3.4.2.1	Force-Deflection	11
3.4.2.2	Impact Damping	14
3.4.2.3	Gaps	15
3.4.3	Vessel Flange	15
3.4.3.1	Mass	15
3.4.3.2	Bolts	15
3.4.4	Vessel.	20
3.4.4.1	Mass	20
3.4.4.2	Wall	20
3.4.5	Concrete Ledge	24
3.5	Loading Conditions	25
3.5.1	Case 1 - Structural Design Basis (SDB)	26
3.5.2	Case 2.	26
3.5.3	Case 3 - Fuel Coolant Interaction (FCI) Loading	26
3.5.4	Case 4.	43
3.6	Analysis and Results	43
3.6.1	Gravity	43
3.6.2	Case 1 - Structural Design Basis (SDB)	51

TABLE OF CONTENTS (continued)

3.6.3 Case 2	57
3.6.4 Case 3	62
3.6.5 Case 4	67
3.6.6 Summary and Conclusions	72
3.7 Structural Criteria	75
3.8 Margin of Safety	77
4.0 CRDM, RISERS, AND SEISMIC SUPPORT	78
4.1 Analysis and Results	78
4.2 Margins of Safety	80
APPENDIX A - MINIMUM POSSIBLE SHEAR RING YIELD FORCES	A-1
APPENDIX B - CRBRP SHEAR RING TEST RESULTS	B-1

ACRONYMS AND SYMBOLS

SDB	Structural Design Basis
CRDM	Control Rod Drive Mechanism
LRP	Large Rotating Plug
1D	One-Dimensional
PI (or P_I)	Plastic Instability
SRP	Small Rotating Plug
IRP	Intermediate Rotating Plug
3D	Three-Dimensional
K (or k)	Elastic Stiffness
Fy (or FY)	Yield Force
UIS	Upper Internals Structure
STIF 21	Mass Element in ANSYS
STIF 40	Combination Element in ANSYS
C	Damping
ϕ (or D)	Diameter
G	Gap or Gravity Acceleration
E	Young's Modulus
UNC	Unified National Coarse
σ_y	Yield Stress
ω_n	Resonant Frequency
ζ	Fraction
ϵ	Strain
σ_L	Stress at Low Strain Rate
σ_H	Stress at High Strain Rate
σ_A	Mean Stress

ACRONYMS AND SYMBOLS

CSP	Core Support Plate
FCI	Fuel Coolant Interaction
MS (or M.S.)	Margin of Safety
PEL	Proportional Elastic Limit
PD	Plastic Deformation

1.0 INTRODUCTION

This report presents the results of a series of analyses designed to determine the limiting Hypothetical Core Disruptive Accident (HCDA) which will not breach the closure head and reactor vessel. A complete analysis to determine this level would require parametric analysis of a series of non-linear 3-D problems and even this may not result in meaningful conclusions since the correlation between energetics and structural response is so low. The analysis presented in

this report is designed to provide engineering intuition as to the adequacy of the closure head and reactor vessel for the Structural Design Basis (SDB) and to give qualitative estimates of the structural response at higher energetics. The SDB is based on a pressure-time history curve as derived by ANL/GE for fuel vapor expansion from a core having a non-uniform temperature distribution and an average fuel temperature of 4800°K. The structural requirements in Appendix F are consistent with the Loads derived from the SDB. If expanded to one atmosphere, the available work energy would be 661 MJ. Three dimensional non-linear analyses of the above mentioned components have been performed with the resultant pressure time history. The use of previous force-deflection data for the shear rings resulted in the prediction of negative margins for the shear rings while other head mounted components had significant positive margins. It was anticipated that increasing the shear ring capability so as not to have negative margins would result in lessening the margin for the other components because their margins resulted from the shear rings acting as dampers to lessen the loads on the other components. To support this analysis, experiments were carried out using a unit circumferential width of 1/10 scale of a large rotating plug (LRP) shear ring prototypic cross section dimensions. See Appendices B & C. A symmetrical loading direction (classical double shear) was used. Accordingly, in-plane plug diametrical flexibilities

and respective failure modes are not reflected in these results. The use of the data from the experiments resulted in showing positive margin for all closure head components as well as the concrete support ledge and reactor vessel for the Structural Design Bases loadings. These results must be taken cautiously, however, because no one single test can be considered as fully conclusive in such analysis. Furthermore, although the criteria applied comply with the intent of ASME Code criteria, they do not actually meet the criteria as explained in Section 1.1.

Three other cases were analyzed using the force deflection data derived from the experiments. Case 2 was a fuel vapor temperature scale up of Case 1, the SDB, to an average fuel temperature of 5000°K. The resultant energy, expanded to one atmosphere, would be 881 MJ. The shape of the PV curve is comparable to the shape of the PV curve for the SDB but is scaled-up in pressure through the period of expansion. Case 3 corresponds to a molten fuel coolant interaction. The energetics of this curve correspond to 300 MJ when expanded to one atmosphere. Although the energetics of this reaction are considerably lower, the change in the shape of the diametrical loading results in this being a more severe loading on some components than that derived from either SDB or Case 2. Case 4, the last one investigated, is derived from a model of fuel vapor expansion for a 5200°K uniform temperature. When expanded to one atmosphere, this case corresponds to an energy of 1324 MJ. Although the energy in Case 4 is significantly greater than that in the other cases, the loadings developed on the various components are significantly less, except the concrete ledge loads which are the same. Case 4 thus shows larger margins than any of the other three cases.

Several other groundrules were used in the analysis. These are:

- This analysis was based only on simple representations of CRBRP features. Analyses performed were 1-Dimensional. 3-Dimensional analyses were not performed. However, previous 3-D analyses on the SDB were extended, as required.
- The time-history loadings included upward acting head loads and downward acting core support loads for all four energetics.
- For components not directly included in the 1D model of the shear rings, flange bolts, and ledge, such as CRDM, seismic support and riser bolts, previous SDB and Case 3 analyses results were extended to Case 2 and Case 4 by loading comparisons.

1.1 Criteria Used in Determining Margin of Safety

In the margin of safety evaluations, the allowable value for the concrete ledge was the 50×10^6 lbs. requirement. For all other components, the allowable value was 70% of strain or comparable deformation at which the respective plastic instability load occurs. The interpretation of an acceptable strain or deformation allowable is in accordance with the intent of the ASME Code Faulted Condition Plastic Instability (PI) load (F-1321.1 e and F-1321.3 b) and the 70% of the plastic instability load allowable (F-1324.4). The strain or deformation allowables based on 70% of respective values at the plastic instability load are justified because the brief duration of the HCDA loads dynamically places the evaluations in what is normally considered a secondary classification of strain or deformation common to the classical long term loadings. A primary classification characterized by long term loads and using 70% of the plastic instability load is not applicable due to the brief duration of HCDA loads. In essence, HCDA loads with

magnitudes equal to component yield forces in respective elastic-perfectly plastic representations do not impair structural integrity providing the time duration of the HCDA loads is small so as to prevent a significant accumulation of plastic deformations. The structural criteria are summarized in Table 1.1-1.

2.0 SUMMARY

The CRBRP response results for all cases show positive margin of safety. Structural criteria, with the exception of limiting load differences, were based on 70% of the strain in which instability in material force deflection occurs. The components and the calculated allowable response values and the margin of safety are summarized in Table 2.0-1. (Refer also to Section 3.6.6, page 72, for further summary information on the analysis.)

As can be seen from the table, there is an implied margin of safety for all cases. These are based on limited experimental data and on an interpretation of the ASME Code intent rather than strict application of Code rules. Nevertheless, the results are encouraging in that the components analyzed can withstand the SDB and a range of other energetics, all of which are improbable progression paths of an accident too remote for inclusion in the Design Basis. The forthcoming 1/10 scale CRBRP model tests at SRI will provide meaningful data regarding the HCDA response of the CRBRP. The results of these tests and the detailed three dimensional analysis will identify further margin, if any, to withstand more severe postulated events. These preliminary analyses show that the CRBRP components analyzed can withstand the SDB loadings with some margin which accounts for the relative simplicity of the analyses. Further, the comparisons presented indicate that these components can accommodate effects of postulated events based on different P-V relationships than that of the

SDB. Therefore, the component loading requirements defined, provide for a spectrum of pessimistic analyses of postulated HCDA's. The indicated margins do not infer that these components can easily withstand energetic events considerably more severe than the SDB. Rather, these margins provide the prudent difference which is desirable at this stage of the analysis.

Table 1.1-1

HCDA STRUCTURAL CRITERIA

COMPONENT	MATERIAL	CRITERION	COMMENTS AND REFERENCE
SHEAR RINGS AND PLUGS	SA-540 AND SA-508	TOTAL DEFORMATION $\delta \leq 1.75 \text{ in.}$	SHEAR RING DESIGN
VESSEL FLANGE BOLTS	SA-540	TOTAL DEFORMATION $\delta \leq 4.2 \text{ in.}$	BOLT LENGTH 60 in. $\epsilon_u = 0.10$
VESSEL WALL	SA-304-SS	TOTAL DEFORMATION $\delta \leq 64.1 \text{ in.}$	VESSEL LENGTH 482 in. $\epsilon_u = 0.19$
CONCRETE LEDGE LOAD	CONCRETE	TOTAL FORCE $F \leq 50 \times 10^6 \text{ lb.}$	DESIGN REQUIREMENTS SPECIFIED AS ALLOWABLE

Amend. 60
Feb. 1981

Table 2.0-1

HCDA MARGINS OF SAFETY
REFERENCE CRBRP DESIGN

COMPONENT		CALCULATED VALUE	ALLOWABLE VALUE	LIMITING CASE	MARGIN* OF SAFETY
SHEAR RINGS	SRP	0.067 in.	1.75 in.	Case 2	25.12
	IRP	0.210 in.	1.75 in.	Case 2	7.33
	LRP	0.205 in.	1.75 in.	Case 2	7.52
VESSEL FLANGE BOLTS		0.509 in.	4.20 in.	Case 2	7.25
VESSEL WALL (STRETCHING)		2.951 in.	64.1 in	Case 3	20.72
CONCRETE LEDGE (DOWNWARD)		44.14x10 ⁶ lb.	50x10 ⁶ lb.	Case 3	0.132
CONCRETE LEDGE (UPWARD)		46.37x10 ⁶ lb.	50x10 ⁶ lb.	Case 2,3,4	0.078
CRDM NOZZLE EXTENSION		0.0173 in/in	0.132 in/in	Case 2	6.63
RISER BOLTS	SRP	0.0042 in/in	0.07 in/in	Case 2	15.67
	IRP	0.0042 in/in	0.07 in/in	Case 2	15.67
	LRP	0.0108 in/in	0.07 in/in	Case 2	5.48
SEISMIC SUPPORT BOLTS		0.0456 in/in	0.07 in/in	Case 2	0.54

* Margin of Safety = $\frac{\text{ALLOWABLE VALUE}}{\text{CALCULATED VALUE}} - 1$

5

Amend. 60
Feb. 1981

3.0 SHEAR RINGS, FLANGE BOLTS, AND LEDGE

The evaluation of the CRBRP in relation to the limiting HCDA for the shear rings, vessel flange bolts, and ledge is presented in this section. The energetics considered are the four cases described in the introduction. The respective response analysis, methods, assumptions, model, dynamic properties, loading conditions, analysis results, and energetic level correlations are described for the shear rings, vessel flange bolts, and ledge. Structural criteria are presented and margins of safety computed in relation to response/energetic correlations from which a limiting energetic is estimated. Similar estimates of a limiting energetic for head mounted components (CRDM, seismic support, and risers) are assessed in Section 4.0 of this report.

3.1 Method of Analysis

The method of analysis directed to the limiting HCDA for the shear rings, flange bolts, and ledge is a 1D representation employing the ANSYS computer program (ANSYS "L", April 1976) to determine the necessary response parameters (deformations and loads) for the specified energetics. Respective criteria are presented from which margins of safety are quantified and an estimate of a limiting HCDA made.

3.2 Assumptions

The assumptions made in the 1D analyses are summarized as follows.

- **Translational Motion...**The 1D analysis implicitly assumed only translational motion. Rotational motion was not considered.
- **Plugs...**The SRP was considered rigid. The IRP and LRP were considered linear elastic with respective flexibilities selected to provide the first and second resonant frequencies found in earlier 3D analysis of the SDB. Further, the IRP and LRP were considered damped (2% structural).

- Shear rings...The SRP, IRP, and LRP shear rings were represented with elastic-perfectly plastic force-deflection characteristics including local plug deformations adjacent to the respective shear ring. Elastic stiffness (K) and yield force (Fy) values used in the previous SDB analysis were assessed to provide minimum possible values. In order to more properly define the force deflection characteristics of the shear rings, an experimental test of the LRP shear rings (1/10 scale) was conducted. The test plan and results (Appendices B & C) were extended to the SRP and IRP shear rings. Impact damping (20% structural) in combination with a nominal shear ring gap (1/8 in) was selected for all SRP, IRP, and LRP shear rings.
- Bearings...The SRP, IRP, and LRP bearings were included in the 1D analysis so as to provide support for deadweight as gravity was included in the solution runs. A bearing clearance (gap = 1×10^{-6} in) and damping (20% structural) including riser stiffnesses was assumed.
- Vessel Flange Bolts...The vessel flange bolts were represented with elastic-perfectly plastic force deflection behavior. Flange bolt pre-load was not considered. A flange to bolt clearance (gap = 1×10^{-6} in) and damping (2% structural) was considered in the analysis.
- Concrete Ledge...The concrete ledge was assumed fixed in the 1D analyses. A linear elastic stiffness was assumed. Flange to concrete surface damping was taken as 20% structural and a respective gap (1×10^{-6} in) was assumed.
- Vessel Wall...The vessel wall characteristics in the axial direction (stretching) was represented with elastic-perfectly plastic properties. Damping (2% structural) was assumed.

- Crush Tubes...The crush tubes located between the plugs and shielding were neglected in the 1D analysis based on the results obtained in prior analysis. The rigidly secured shielding configuration was analyzed.
- Other Components...CRDM, UIS, seismic support, and riser features, except as included in the supporting plug masses, were neglected in the analysis.

3.3 Model

The 1D ANSYS representation of the rigidly secured shielding CRBRP head configuration including the SRP, IRP, and LRP with respective shear rings, in combination with the vessel flange, concrete ledge, vessel flange bolts, vessel wall and core support plate is illustrated in Figure 3.3-1. Specifics of the dynamic properties used in the response analyses of various energetics are described as follows.

3.4 Dynamic Properties

3.4.1 Plugs

3.4.1.1 Masses

The SRP, IRP, and LRP were modeled with ANSYS (STIF 21) mass elements. The LRP, IRP, and SRP including the suspended component masses are designated by node points 2, 3, and 4 with numerical values of 1229, 1232, and 158.9 lb-sec²/in respectively.

3.4.1.2 Flexibilities and Damping

The SRP was considered rigid in the analysis. The IRP and LRP were assigned flexibilities corresponding to the first and second resonant frequencies found in the 3D modal analysis. Respective stiffnesses (K_1 , K_2) were

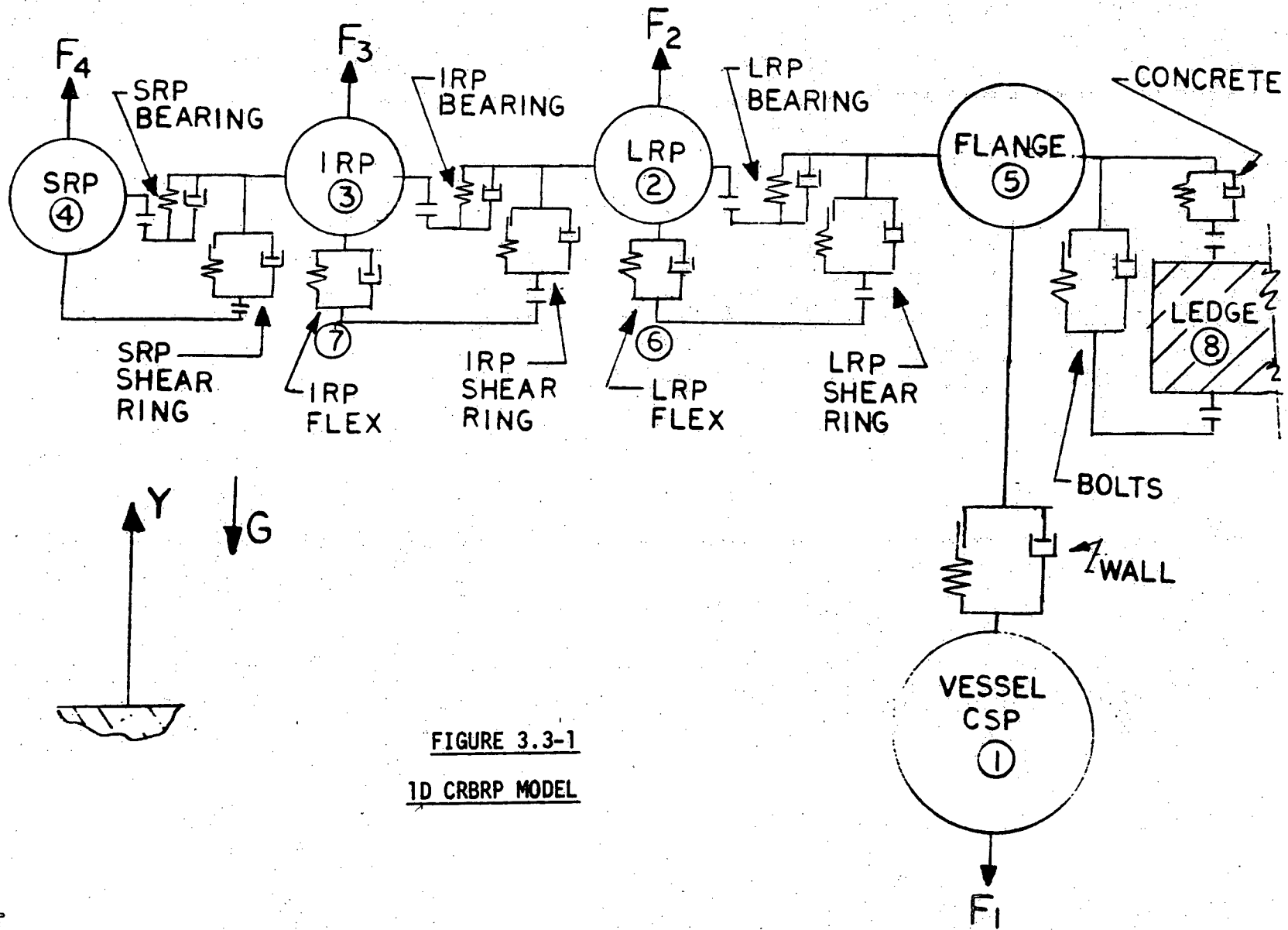


FIGURE 3.3-1
1D CRBRP MODEL

49.76×10^6 lb/in. Structural (2%) damping (C_1, C_2) values were 16,672 lb-sec/in. Both plug stiffness (K) and Damping (C) were represented with ANSYS (STIF 40) combination elements without gaps and with infinite yield forces.

3.4.1.3 Bearings

The SRP, IRP, and LRP bearings were included in the analysis to permit gravity to be included in the solutions. The risers were considered in series with the bearings as their relative flexibility dominates overall suspension stiffness. The SRP, IRP, and LRP riser stiffnesses were selected as 4.56, 15.35, 18.36 $\times 10^6$ lb/in from prior analysis. The bearings and risers were modeled with ANSYS (STIF 40) combination elements. The bearing clearance was represented by an arbitrarily gap (1×10^{-6} in). The risers were considered linear elastic with an infinite yield force. Damping was selected to correspond to a 20% structural value. Numerical values of damping were based on simple single degree of freedom oscillator relations.

SRP Bearing Damping

$$C = 2\zeta M \sqrt{\frac{K}{M}}$$

$$C = 2(.2)(158.9) \sqrt{\frac{4.56 \times 10^6}{158.9}}$$

$$C = 10767 \text{ lb-sec/in}$$

IRP Bearing Damping

$$C = 2\zeta M \sqrt{\frac{K}{M}}$$

$$C = 2(.2)(1232) \sqrt{\frac{15.35 \times 10^6}{1232}}$$

$$C = 55006. \text{ lb-sec/in}$$

LRP Bearing Damping

$$C = 2\zeta M \sqrt{\frac{K}{M}}$$

$$C = 2(.2)(1229) \sqrt{\frac{18.36 \times 10^6}{1229}}$$

$$C = 60118 \text{ lb-sec/in.}$$

3.4.2 Shear Rings

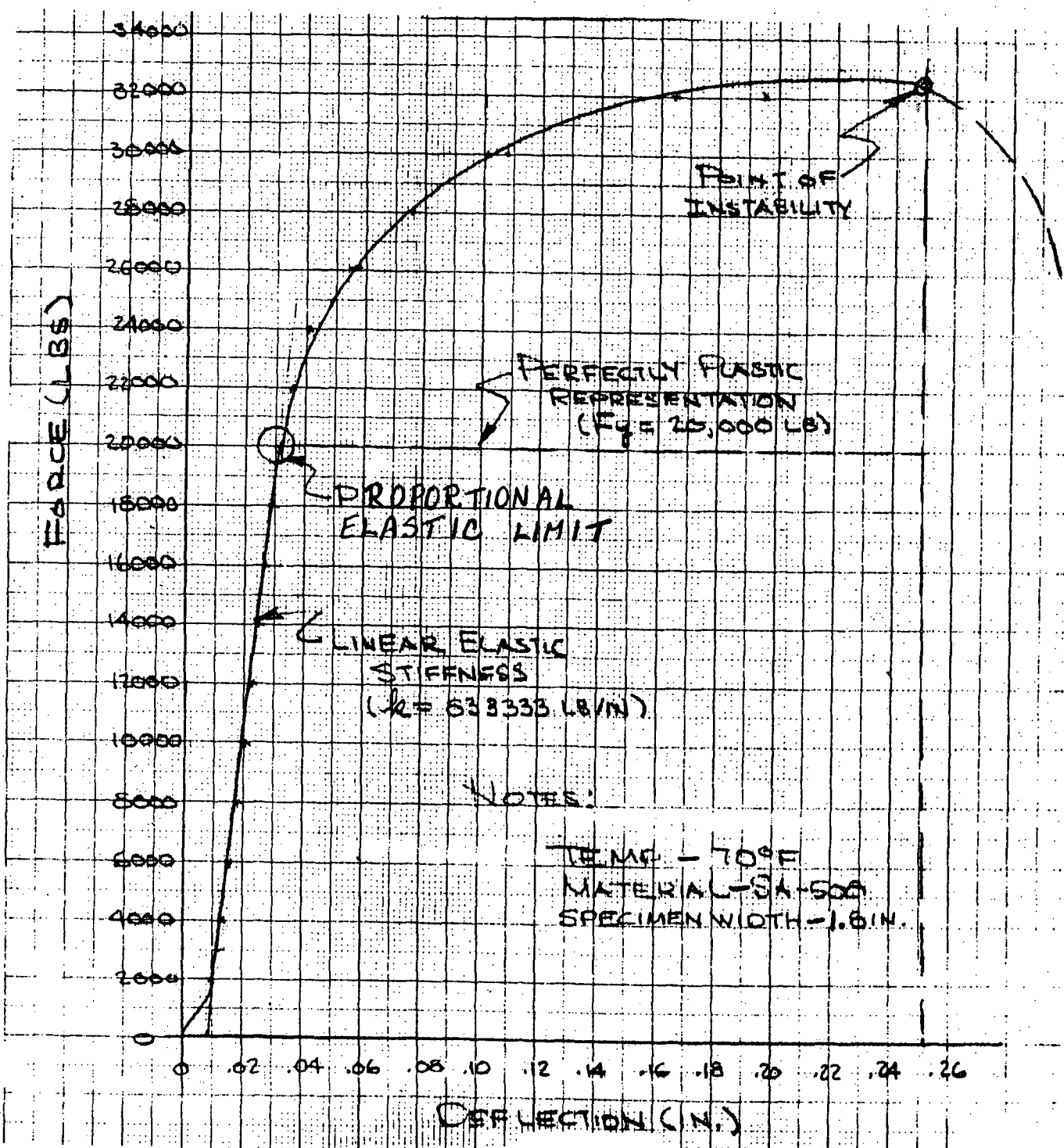
3.4.2.1 Force-Deflection

Previous 1D analysis of the CRBRP closure head assumed that the shear rings and locally adjacent plug ledges deformed in an elastic-perfectly plastic manner. The elastic stiffnesses (K) and yield forces (Fy) for the full circumferential periphery of the SRP, IRP, and LRP were (K, Fy) ~ (411 x 10⁶ lb/in, 7.13 x 10⁶ lb); (1075 x 10⁶ lb/in, 22.02 x 10⁶ lb); and (1552 x 10⁶ lb/in, 35.59 x 10⁶ lb) respectively.

Recent experimental tests (Appendix B) were directed to the force-deflection characteristics of a 1/10 scale model of the LRP, LRP shear ring, and vessel flange. Increases in yield strength with prototypic dynamic strain rate and decreases in yield strength with prototypic operating temperature for the plug material (SA-508) were considered essentially self compensating relative to 1/10 scale testing conditions. Accordingly, only geometric scaling of 1/10 scale test results to prototypic values was required. A plot of Test No. 2 LRP shear ring force-deflection data is presented in Figure 3.4.2-1.

In order to most conveniently represent the 1/10 scale data, an elastic-perfectly plastic representation is desirable. A very conservative representation would correspond to a yield force (Fy = 20,000 lbs) and an elastic stiffness (k = 833,333 lb/in). This approach would provide conservative plastic deformations for the LRP shear ring. A total effective width (W = 1.8 in) was used in the 1/10 scale LRM shear ring test. The prototype diameter (D) of the SRP, IRP, and LRP shear rings are 70, 175, 270 in. respectively. Accordingly, the SRP prototype yield force (FY)_{SRP} is by similarity.

FIGURE 3.4.2-1
LRP SHEAR RING
1/10 SCALE
FORCE-DEFLECTION DATA



$$(FY)_{SRP} = \frac{10\pi D Fy}{W}$$

$$(FY)_{SRP} = \frac{10\pi(70)(20,000)}{1.8}$$

$$(FY)_{SRP} = 24.43 \times 10^6 \text{ lbs.}$$

The prototype yield force for the IRP shear ring $(FY)_{IRP}$ and the LRP shear ring $(FY)_{LRP}$

$$(FY)_{IRP} = 61.09 \times 10^6 \text{ lbs.}$$

$$(FY)_{LRP} = 94.24 \times 10^6 \text{ lbs.}$$

The prototype SRP, IRP, and LRP shear ring stiffnesses (K) are as follows.

$$(K)_{SRP} = k\pi D/W$$

$$(K)_{SRP} = (833,333)\pi(70)/1.8$$

$$(K)_{SRP} = 101.81 \times 10^6 \text{ lb/in}$$

Similarly:

$$(K)_{IRP} = 254.53 \times 10^6 \text{ lb/in.} \quad \text{and}$$

$$(K)_{LRP} = 392.70 \times 10^6 \text{ lb/in.}$$

The representation of the prototype SRP, IRP, and LRP shear ring yield forces (FY) and linear elastic stiffnesses (K) is made with ANSYS (STIF 40) elements. Corresponding damping (C) and gap values are described as follows.

3.4.2.2 Impact Damping

The damping (C) associated with SRP, IRP, and LRP shear ring impact is based on 20% critical for a 0.5 coefficient of restitution. The damping (C) for the individual plugs is based on the response of single degree of freedom oscillators.

SRP Shear Ring

$$C = 2\zeta M \sqrt{K/M}$$

$$C = 2(.2)(158.9) \sqrt{\frac{101.81 \times 10^6}{158.9}}$$

$$C = 50,876 \text{ lb-sec/in.}$$

Similarly for the IRP and LRP shear rings

$$C_{IRP} = 223,993 \text{ lb-sec/in.}$$

$$C_{LRP} = 277,886 \text{ lb-sec/in.}$$

The damping values selected as based on a single degree of freedom oscillator are conservative as higher frequencies occur during multiple impact

3.4.2.3 Gaps

A shear ring gap of 1/8 in. was used in the analysis for the SRP, IRP, and LRP, corresponding to the latest design.

3.4.3 Vessel Flange

3.4.3.1 Mass

The vessel flange mass, as designated by Node 5, was represented with an ANSYS (STIF 21) mass element. The weight of the vessel flange was taken as 257,802 lb, or a mass of 667.38 lb-sec²/in.

3.4.3.2 Bolts

The vessel flange bolts are specified as 72 - 2 3/4 in. diameter x 60 in. long on a 310 in. diameter bolt circle. Bolt material is SA-193, Grade B7 (ASTM 4140) steel. In this analysis, the following dynamic properties were selected.

The vessel flange bolts were represented in an elastic-perfectly plastic manner with ANSYS (STIF 40) combination elements. The linear elastic stiffness (K), yield force (FY), damping (C), and gaps (G) used in the analysis are described as follows.

The elastic stiffness (K) for the total 72 bolts.

$$K = 72 A E/L$$

The Young's modulus of ASTM 4140 at 400°F is given ($E = 30 \times 10^6$ lb/in) in Figure 3.4.3-1. The tensile area of 2 3/4 - 4 UNC threads ($A = 4.93$ in²). For a length ($L = 60$ in.), the elastic stiffness (K)

$$K = 72(4.93)(30 \times 10^6)/60$$

$$K = 177.48 \times 10^6 \text{ lb/in}$$

The total yield force (FY) for all 72 bolts

$$FY = 72 A \sigma_Y$$

The minimum yield stress ($\sigma_{Y, \min}$) of ASTM 4140 at 400°F is 95,000 psi. (Tempering Temp. = 1215°F) as given in Figure 3.4.3-1. For average yield stress ($\sigma_{Y,A}$),

$$\sigma_{Y,A} = 1.25 \sigma_{Y, \min}$$

$$\sigma_{Y,A} = 1.25(95,000)$$

$$\sigma_{Y,A} = 118,750 \text{ psi}$$

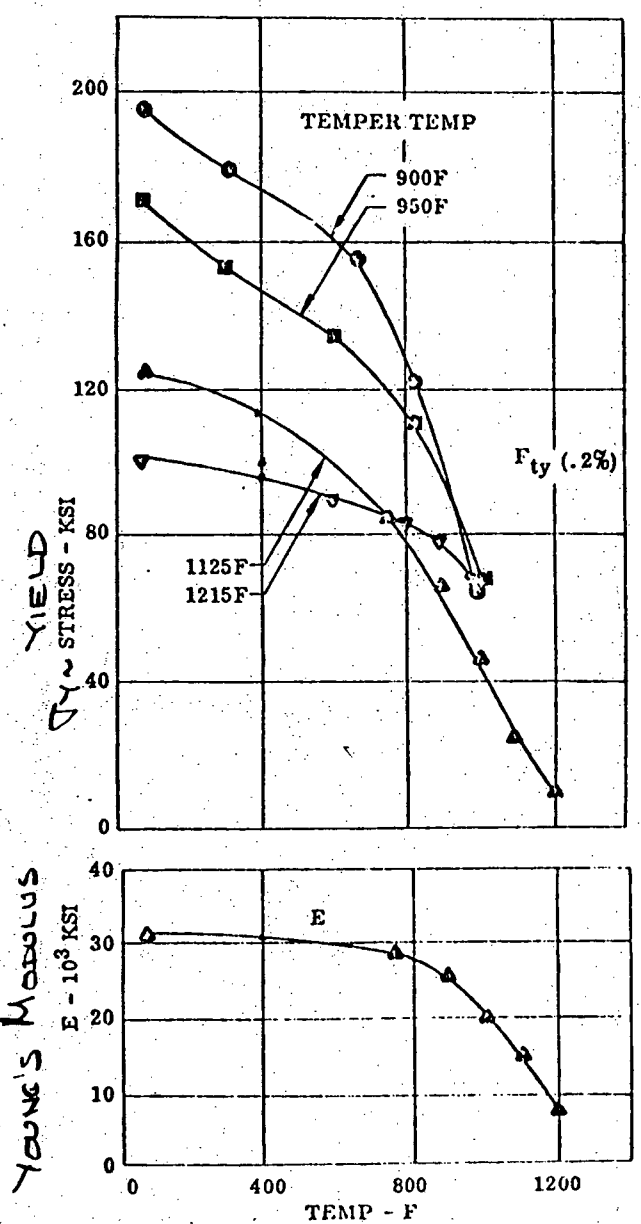
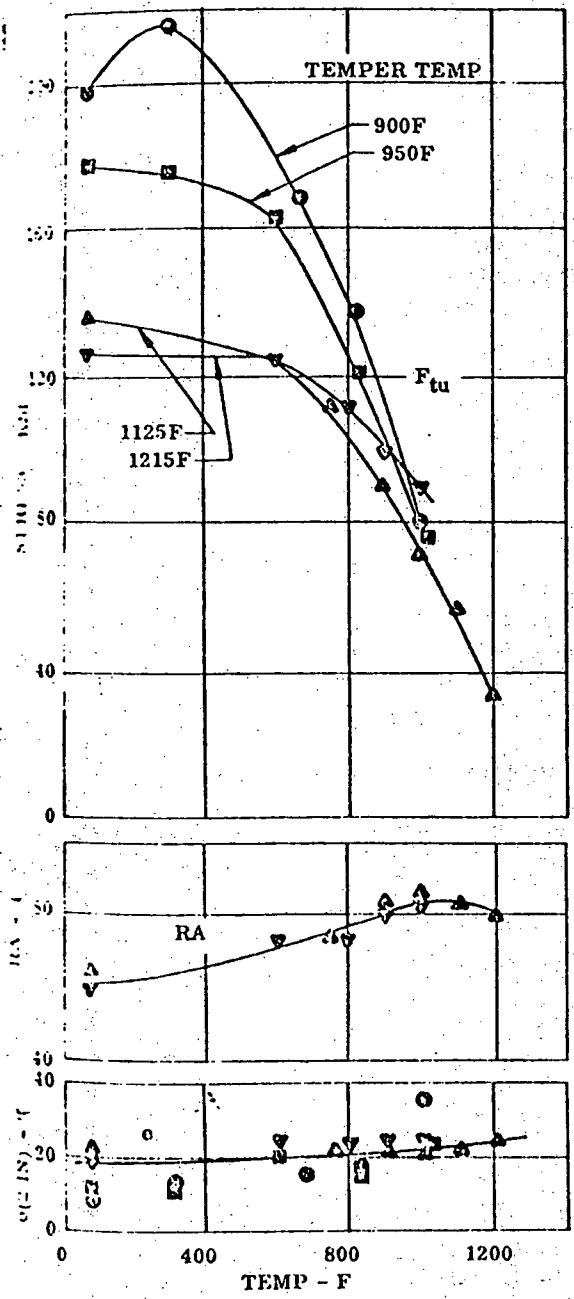
The effect of dynamic strain rate in increasing the yield strength of ASTM 4340 steel is presented in Figure 3.4.3-2. It can be seen that increase in yield strength is not significant, and at most a 10% increase at strain rates of 10 in/in/sec occurs. Because of similarity in general alloy content, the effect of dynamic strain rate of 4140 can be expected to be similar to that of 4340. Accordingly, the yield strength (σ_Y) of 4140 with strain

TENSILE (TEMPERATURE EFFECTS)

**4140
STEEL**

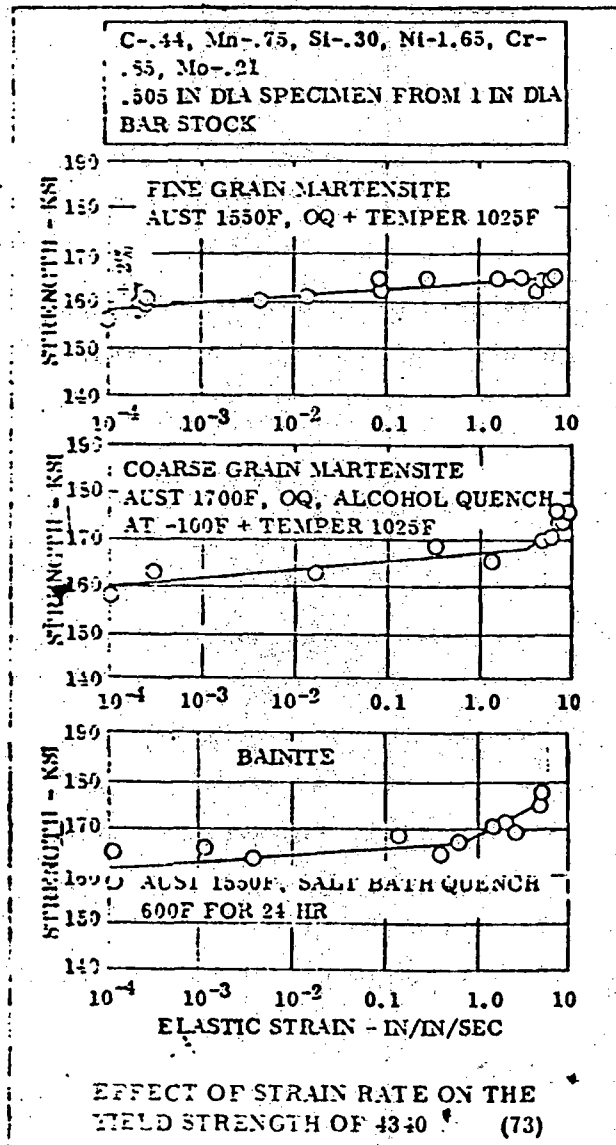
SAE 4140		
○ BAR	C-.40, Mn-.90, Si-.30, Cr-.95, Mo-.20	1550F, OQ + TEMPER 900F
□		1550F, OQ + TEMPER 950F
▲ ROLLED 3/4 IN BAR	C-.40, Mn-.60, P-.017, S-.025, Si-.25, Cr-.92, Mo-.18	1525F, OQ + TEMPER 1125F
▼ ROLLED	C-.39, Mn-.80, P-.031, S-.026, Si-.26, Cr-.97 Ni-.20 Mo-.72	NORM 1650F, OQ 1575F, + TEMPER 2 HR 1215F

FIGURE 3.4.3-1



EFFECT OF TEST TEMPERATURE ON TENSILE PROPERTIES (37)

FIGURE 3.4.3-2



rate effects:

$$\sigma_Y \approx 1.10 \sigma_{Y,A}$$

$$\sigma_Y = 1.10(118,750)$$

$$\sigma_Y = 130,625 \text{ psi}$$

The total yield force (FY)

$$FY = 72(4.93)(130.625)$$

$$FY = 46.37 \times 10^6 \text{ lb}$$

The vessel flange bolt configuration provides a total yield force less than 50×10^6 lb. which implicitly assures that the upward ledge load limit will be satisfied.

The damping (C) of the vessel flange bolts selected for analysis was based on 2% structural. Considering the entire vessel mass (M) acting upward on the vessel flange bolt stiffness (K), the resonant frequency (ω_n) is as follows.

$$\omega_n = \sqrt{\frac{K}{M}}$$

$$\omega_n = \sqrt{\frac{177.48 \times 10^6 (386)}{3.5 \times 10^6}}$$

$$\omega_n = 139.91 \text{ rad/sec.}$$

The vessel flange bolt damping (C) in relation to the fraction (ζ) and mass (M) is as follows:

$$C = 2\zeta M \omega_n$$

$$C = 2(.02)\left(\frac{3.5 \times 10^6}{386}\right)(139.91)$$

$$C = 50,742 \text{ lb-sec/in.}$$

The vessel flange to bolt clearance was selected arbitrarily small (gap = 1×10^{-6} in) in the analysis.

3.4.4 Vessel

3.4.4.1 Mass

The vessel mass was represented with an ANSYS (STIF 21) mass element, as designated Node 1. The weight of the vessel including the vessel wall, core, core barrel and support plate, and contained sodium was taken as 2.23×10^6 lbs, or a mass of $5780 \text{ lb-sec}^2/\text{in.}$

3.4.4.2 Wall

The vessel wall was represented with an ANSYS (STIF 40) combination element through elastic-perfectly plastic properties including an elastic stiffness (K), yield force (FY), and damping (C). The gap (G) is not relevant to the vessel wall.

The vessel wall considered in the analysis was simplified to a cylinder (243 in. ID x 2.38 in. wall x 482 in. long). Material was considered to be 304 SS @ 775°F. The Young's modulus at 775°F is $E = 23.7 \times 10^6$ psi, from the Nuclear Systems Materials Handbook, Property Code 2111 (Rev. 2). Accordingly, the elastic stiffness (K),

$$K = A E/L$$

$$K = \frac{\pi(245.38)(2.38)(23.7 \times 10^6)}{482}$$

$$K = 90.21 \times 10^6 \text{ lb/in.}$$

In order to establish the perfectly plastic yield force (FY) for the vessel wall in the longitudinal direction, the effect of dynamic strain-rate on stress-strain properties must be considered.

The effect of strain rate on the average true stress-strain behavior of Type 304 SS, annealed is given in the Nuclear Systems Materials Handbook, Property Code 2301 (Rev. 0).

$$\sigma = K_1 \epsilon^{n_1} + e^{(K_2 + n_2 \epsilon)}$$

For 800°F,

$$n_1 = 0.508 - 0.013 \text{ LOG } \dot{\epsilon}$$

$$K_1 = 164,220 + 1930 \text{ LOG } \dot{\epsilon}$$

$$n_2 = -50.45 - 4.28 \text{ LOG } \dot{\epsilon}$$

$$K_2 = 9.583 + 0.063 \text{ LOG } \dot{\epsilon}$$

At low strain rates ($\dot{\epsilon} = 1 \times 10^{-5}$ /sec),

$$n_1 = 0.573$$

$$K_1 = 154,570$$

$$n_2 = -29.05$$

$$K_2 = 9.268$$

Thus,

$$\sigma_L = 154570 \epsilon^{0.573} + e^{(9.268 - 29.05 \epsilon)}$$

At high strain rates ($\dot{\epsilon} = 10$ /sec),

$$n_1 = 0.495$$

$$K_1 = 166,150$$

$$n_2 = -54.73$$

$$K_2 = 0.646$$

Thus,

$$\sigma_H = 166150 \epsilon^{0.495} + e^{(9.646 - 54.73 \epsilon)}$$

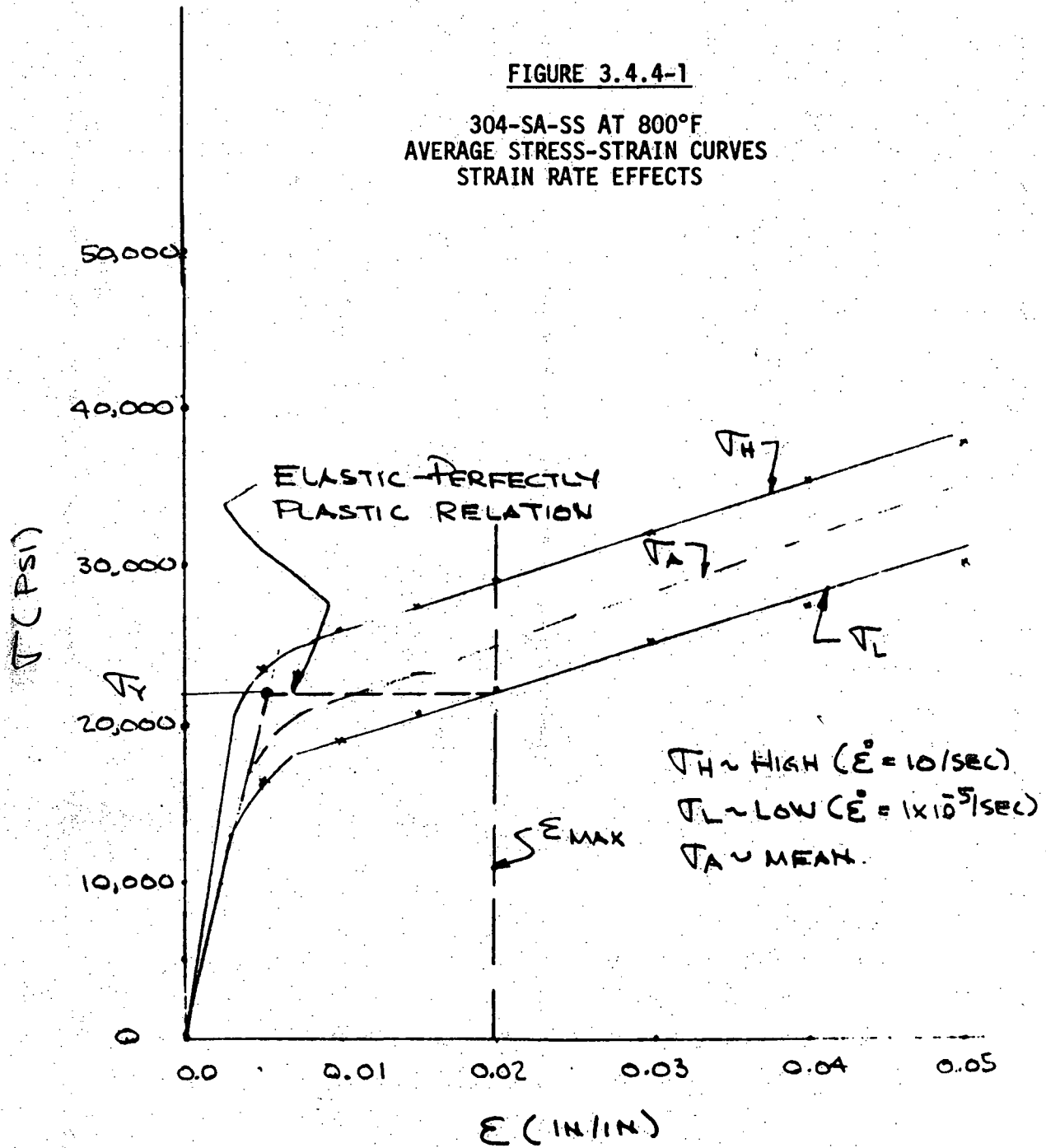
The stress-strain data for low and high strain rates (σ_L , σ_H) as a function of strain is computed in Table 3.4.4-1.

Table 3.4.4-1
304-SA-SS STRAIN RATE

STRAIN (ϵ)	STRESS (PSI)	
	σ_L	σ_H
0.005	16,577	23,811
0.010	18,959	25,937
0.015	20,778	27,577
0.020	22,349	29,131
0.030	25,153	32,277
0.040	27,752	35,499
0.050	30,250	38,713
0.100	41,896	53,214
0.150	52,258	64,967
0.200	61,494	74,905
0.250	69,853	83,652

The maximum longitudinal strain expected in the vessel wall ($\epsilon_{max} = 0.02$), over the full vessel length, (482 in) would produce 9.64 in. of axial motion. The high and low (σ_H , σ_L) stress-strain relations with an elastic-perfectly plastic representation of a mean (σ_A) stress-strain curve is presented in Figure 3.4.4-1.

FIGURE 3.4.4-1
 304-SA-SS AT 800°F
 AVERAGE STRESS-STRAIN CURVES
 STRAIN RATE EFFECTS



Based on the mean (σ_A) curve for strains not exceeding ($\epsilon_{\max} = 0.02$). The perfectly plastic yield approximation is $\sigma_Y = 22,000$ psi. Accordingly, the corresponding total vessel yield force (FY) is,

$$FY = \pi(245.38)(2.38)(22,000)$$

$$FY = 40.36 \times 10^6 \text{ lbs.}$$

The total vessel wall yield force implicitly limits the downward ledge force to less than 50×10^6 lb provided total strains are less than 2%.

The damping (C) of the vessel wall selected for analysis was based on (2% structural). Considering the entire core support plate mass (M) acting on the vessel stiffness (K), the resonant frequency (ω_n) is as follows.

$$\omega_n = \sqrt{\frac{K}{M}}$$

$$\omega_n = \sqrt{\frac{90.21 \times 10^6 (386)}{2.23 \times 10^6}}$$

$$\omega_n = 124.96 \text{ rad/sec}$$

The vessel wall damping (C) in relation to the fraction (ζ) and mass (M) is as follows.

$$C = 2\zeta M \omega_n$$

$$C = 2(.02) \left(\frac{2.23 \times 10^6}{386} \right) (124.96)$$

$$C = 28,876 \text{ lb-sec/in.}$$

3.4.5 Concrete Ledge

The concrete ledge, designated by Node 8 in the 1D model, was assumed fixed in the analysis. The ledge elastic stiffness (K), damping (C), and flange to concrete clearance gap (G) were modeled with ANSYS (STIF 40) combination elements. An infinite perfectly plastic yield force (FY) was assumed.

The linear-elastic stiffness (K) of the concrete ledge in compression was taken as

$$K = 1089 \times 10^6 \text{ lb/in.}$$

The flange to concrete damping (C) was based on 20% structural damping with the entire vessel mass (M) supported on the ledge stiffness (K). The respective resonant frequency (ω_n) and damping (C) are as follows.

$$\begin{aligned}\omega_n &= \sqrt{\frac{K}{M}} \\ \omega_n &= \sqrt{\frac{1089 \times 10^6 (386)}{3.5 \times 10^6}} \\ \omega_n &= 346.56 \text{ rad/sec}\end{aligned}$$

Thus,

$$\begin{aligned}C &= 2\zeta M \omega_n \\ C &= 2(0.2) \left(\frac{3.5 \times 10^6}{386} \right) (346.56) \\ C &= 1256935 \text{ lb-sec/in}\end{aligned}$$

3.5 Loading Conditions

Four loading conditions were considered in the analysis. Case 1 was the Structural Design Basis (SDB). Case 2 is a higher temperature version of Case 1. Case 3 corresponds to a fuel-coolant interaction case, and Case 4 is an arbitrary higher temperature but uniform temperature use. For each of the loading conditions, only the upward acting head loads and downward acting core support plate loads were considered. Other loadings are not of relevance to the concept of a limiting HCDA energetic in relation to the structural integrity of the shear rings, vessel flange bolts, and ledge.

As specified in the ANL/GE/REXCO energetic response results, the total head load alone is given. In order to obtain individual loads for the SRP, IRP, and LRP, the fraction of plug to total head area was used. For the SRP, IRP, and LRP, the fractions of the total head load were taken as 0.05979, 0.384161, and 0.55608 respectively. The total CSP load was taken directly.

3.5.1 Case 1 - Structural Design Basis (SDB)

The SDB loading time-history corresponding to the 661 MW-sec HCDA in terms of the total upward head force and total downward CSP force is given in Figures 3.5.1-1 and -2.

The numerical representation of the data over the full ~ 120 ms is presented in Table 3.5.1-1.

3.5.2 Case 2

The Case 2 loading time-history in terms of the total upward head force and total downward CSP force is given in Figures 3.3.2-1 and -2.

The numerical representation of the data over the full ~ 120 ms is presented in Table 3.5.2-1.

3.5.3 Case 3 - Fuel Coolant Interaction (FCI) Loading

The Case 3 time-history corresponding to a hypothetical FCI is given in Figures 3.5.3-1 and -2.

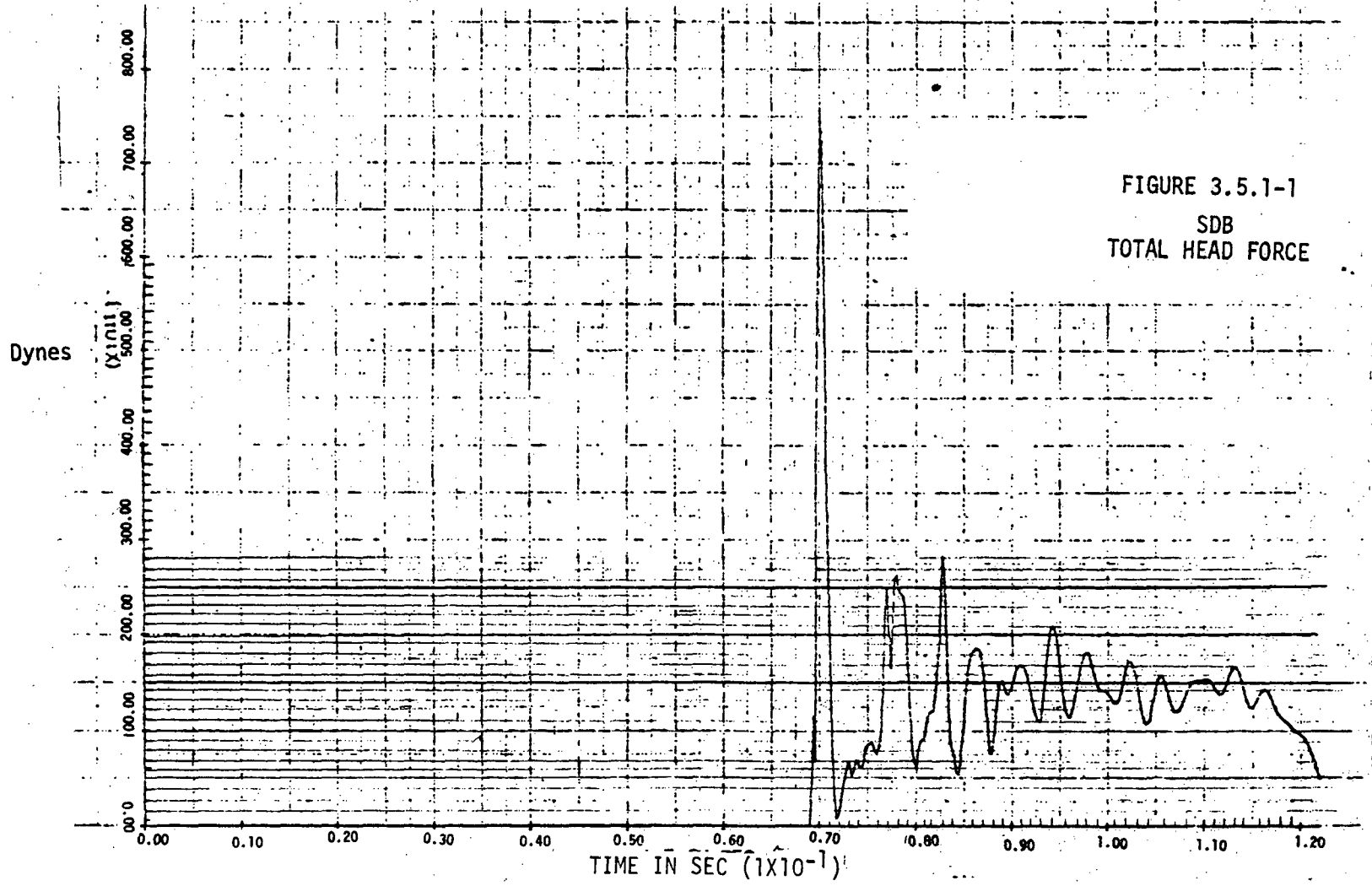
The numerical representation of the data over the full ~ 120 ms is presented in Table 3.5.3-1.

3.5.4 Case 4

The Case 4 loading time-history in terms of the total upward head force and total downward CSP force is given in Figures 3.5.4-1 and -2.

The numerical representation of the data over the full ~ 120 ms is presented in Table 3.5.4-1.

FIGURE 3.5.1-1
SDB
TOTAL HEAD FORCE



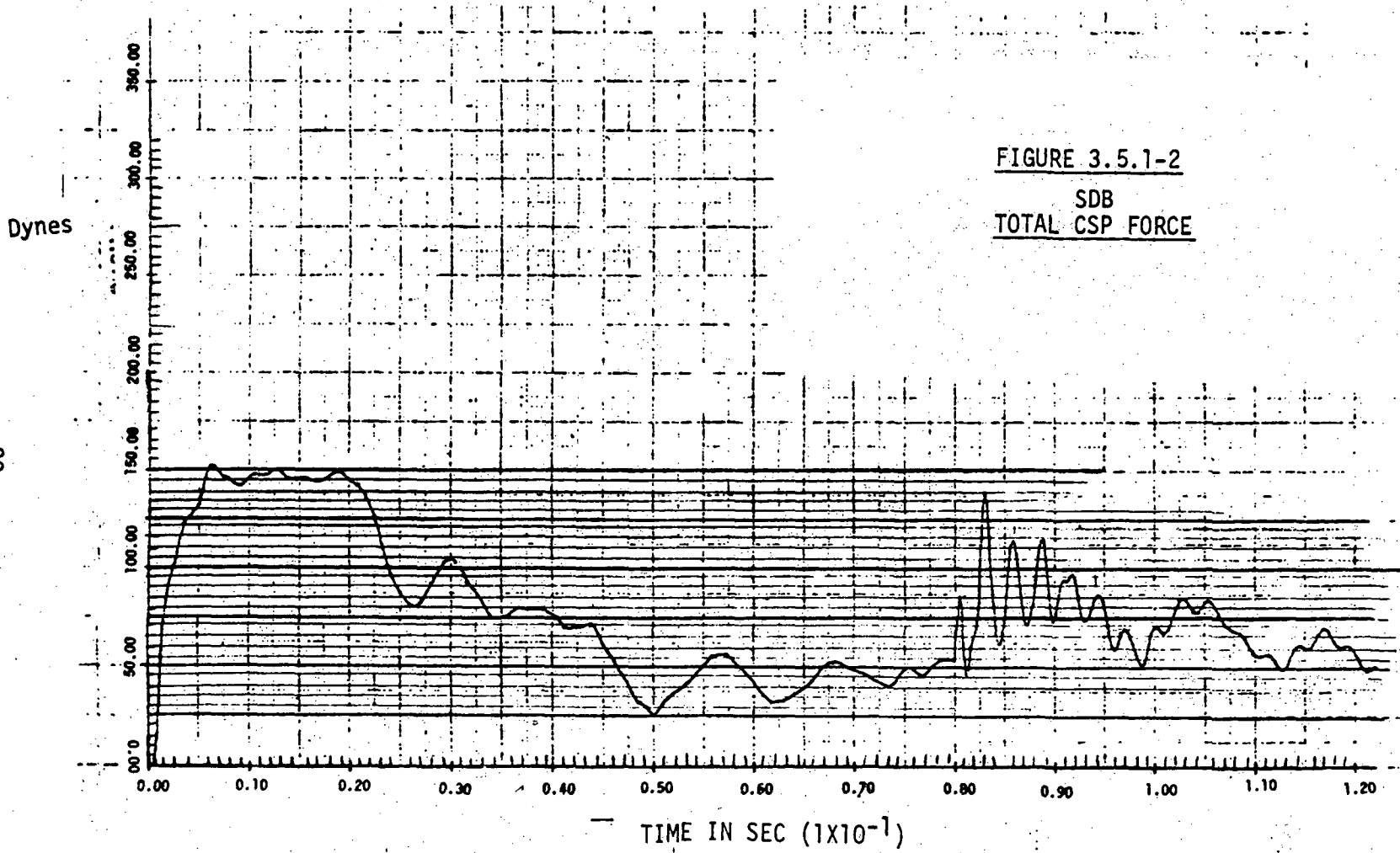


FIGURE 3.5.1-2
SDB
TOTAL CSP FORCE

TABLE 3.5.1-1
SDB LOADING TIME-HISTORY

TIME (SEC)	FH	LRP	IRP	SRP	CSP	
	DYNFS X10 ¹¹	LBS X10 ⁶	LBS X10 ⁶	LBS X10 ⁶	DYNFS X10 ¹¹	LBS X10 ⁶
0.000	0.0	0.0	0.0	0.0	0.0	0.0
0.004	↑	↑	↑	↑	120	26.98
0.005	↑	↑	↑	↑	125	28.10
0.007	↑	↑	↑	↑	150	33.72
0.009	↑	↑	↑	↑	145	32.60
0.011	↑	↑	↑	↑	150	33.72
0.012	↑	↑	↑	↑	150	33.72
0.027	↑	↑	↑	↑	180	40.46
0.030	↑	↑	↑	↑	105	23.60
0.034	↑	↑	↑	↑	75	16.86
0.036	↑	↑	↑	↑	80	17.98
0.041	↑	↑	↑	↑	70	15.74
0.044	↑	↑	↑	↑	70	15.74
0.050	↑	↑	↑	↑	25	5.62
0.057	↑	↑	↑	↑	55	12.36
0.062	↓	↓	↓	↓	35	7.87
0.068	0.0	0.0	0.0	0.0	55	12.36
0.070	750	93.75	64.76	10.08	40	8.99
0.071	0.0	0.0	0.0	0.0	45	10.12
0.072	70	8.75	6.05	0.94	45	10.12
0.073	50	6.25	4.32	0.67	45	10.12
0.075	90	11.25	7.77	1.21	45	10.12
0.076	80	10.00	6.91	1.08	45	10.12
0.077	250	31.25	21.59	3.36	45	10.12
0.078	265	33.13	22.88	3.56	50	11.24
0.080	60	7.50	5.18	0.81	55	12.36
0.083	280	35.00	24.18	3.76	165	37.09
0.085	55	6.87	4.75	0.74	65	14.61
0.086	185	23.13	15.98	2.49	115	25.85
0.088	80	10.00	6.91	1.08	75	16.86
0.091	170	21.25	14.68	2.28	115	25.85
0.093	110	13.75	9.50	1.48	75	16.86

CONTINUED

Table 3.5.1-1
SDB LOADING TIME-HISTORY
 (continued)

TIME (SEC)	FH	LRP	IRP	SRP	CSP	
	DYNES X10 ¹¹	LBS X10 ⁶	LBS X10 ⁶	LBS X10 ⁶	DYNES X10 ¹¹	LBS X10 ⁶
0.094	210	26.25	18.14	2.82	85	19.11
0.096	115	14.37	9.93	1.54	60	13.49
0.098	180	22.50	15.54	2.42	50	11.24
0.101	130	16.25	11.23	1.75	65	14.61
0.103	170	21.25	14.68	2.28	85	19.11
0.104	110	13.75	9.50	1.48	80	17.98
0.106	160	20.00	13.82	2.15	85	19.11
0.107	120	15.00	10.36	1.61	70	15.74
0.110	150	18.75	12.95	2.02	55	12.36
0.112	140	17.50	12.09	1.88	50	11.24
0.113	170	21.25	14.68	2.26	50	11.24
0.115	120	15.00	10.36	1.61	70	15.74
0.117	140	17.50	12.09	1.88	60	13.49

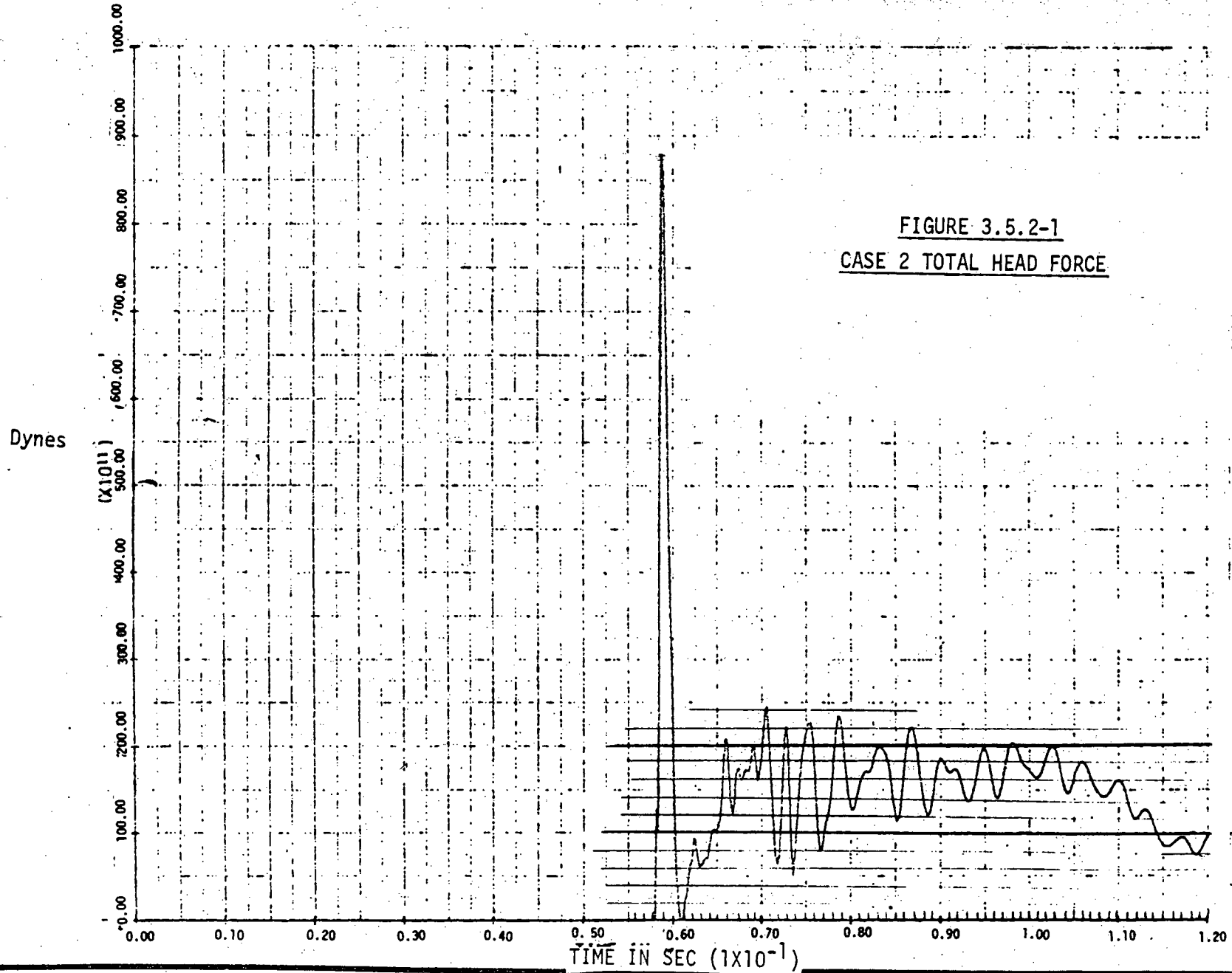


FIGURE 3.5.2-1
CASE 2 TOTAL HEAD FORCE

FIGURE 3.5.2-2
CASE 2 TOTAL CSP FORCE

Dynes

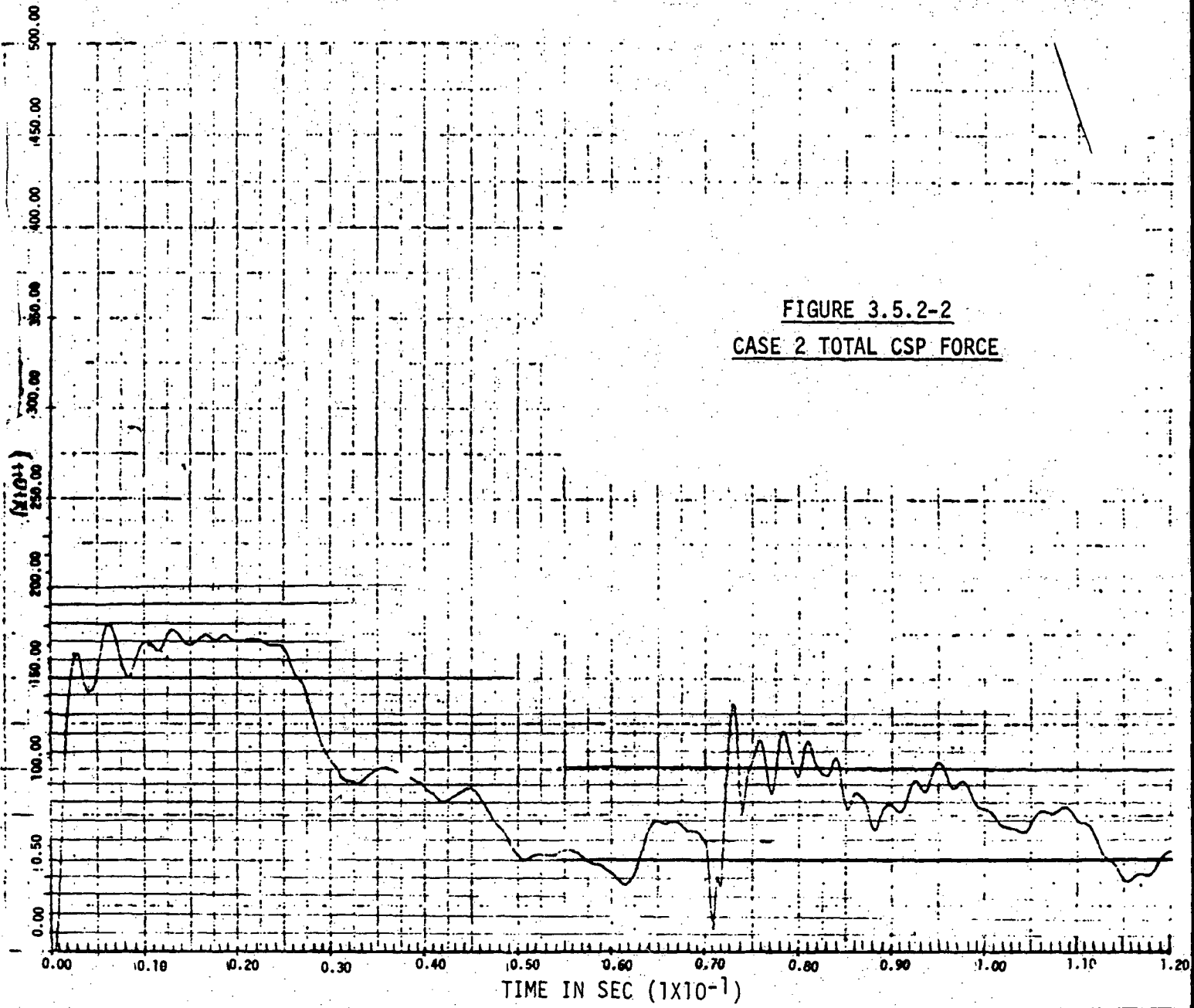


TABLE 3.5.2-1

CASE 2 LOADING TIME-HISTORY

TIME (SEC)	F _H	L _{RP}	I _{RP}	S _{RP}	C _{SP}	
	DYNES X10 ¹¹	LBS X10 ⁶	LBS X10 ⁶	LBS X10 ⁶	DYNES X10 ¹¹	LBS X10 ⁶
0.000	0.0	0.0	0.0	0.0	0.0	0.0
0.002	↑	↑	↑	↑	165	37.09
0.004	↑	↑	↑	↑	140	31.47
0.006	↑	↑	↑	↑	160	40.46
0.008	↑	↑	↑	↑	150	33.72
0.010	↑	↑	↑	↑	170	38.22
0.012	↑	↑	↑	↑	165	37.09
0.014	↑	↑	↑	↑	175	39.34
0.016	↑	↑	↑	↑	170	36.22
0.018	↑	↑	↑	↑	175	39.34
0.026	↑	↑	↑	↑	170	36.22
0.032	↑	↑	↑	↑	95	21.36
0.034	↑	↑	↑	↑	90	20.23
0.036	↑	↑	↑	↑	100	22.48
0.042	↑	↑	↑	↑	80	17.98
0.044	↑	↑	↑	↑	90	20.23
0.050	↓	↓	↓	↓	50	11.24
0.058	0.0	0.0	0.0	0.0	50	11.24
0.060	890	111.26	76.86	11.96	40	8.99
0.062	40	5.00	3.45	0.54	35	7.67
0.064	80	10.00	6.90	1.08	60	13.49
0.066	210	26.25	18.13	2.62	70	15.74
0.070	160	22.50	15.54	2.42	60	13.49
0.072	70	8.75	6.05	0.94	135	30.35
0.074	225	28.12	19.43	3.02	75	16.86
0.076	80	10.00	6.91	1.08	115	25.85
0.078	230	28.75	19.66	3.09	120	26.98
0.080	130	16.25	11.23	1.75	95	21.36
0.084	200	25.00	17.27	2.69	105	23.60
0.088	150	15.75	12.95	2.02	65	14.61
0.090	160	22.50	15.54	2.42	80	17.98
0.094	200	25.00	17.27	2.69	85	19.11
0.096	140	17.50	12.09	1.86	100	22.48

CONTINUED

TABLE 3.5.2-1
CASE 2 LOADING TIME-HISTORY
 (continued)

TIME (SEC)	FH	LRP	IRP	SRP	CSP	
	DYNES X10 ¹¹	LBS X10 ⁶	LBS X10 ⁶	LBS X10 ⁶	DYNES X10 ¹¹	LBS X10 ⁶
0.098	200	25.00	17.27	2.69	90	20.23
0.100	160	20.00	13.82	2.15	60	17.98
0.102	200	25.00	17.27	2.69	70	15.74
0.106	170	21.25	14.68	2.28	75	16.66
0.110	160	20.00	13.82	2.15	60	17.98
0.112	120	15.00	10.36	1.61	70	15.74
0.116	90	11.25	7.77	1.21	40	0.99
0.118	100	12.50	8.64	1.34	45	10.12
0.120	100	12.50	8.64	1.34	55	12.36

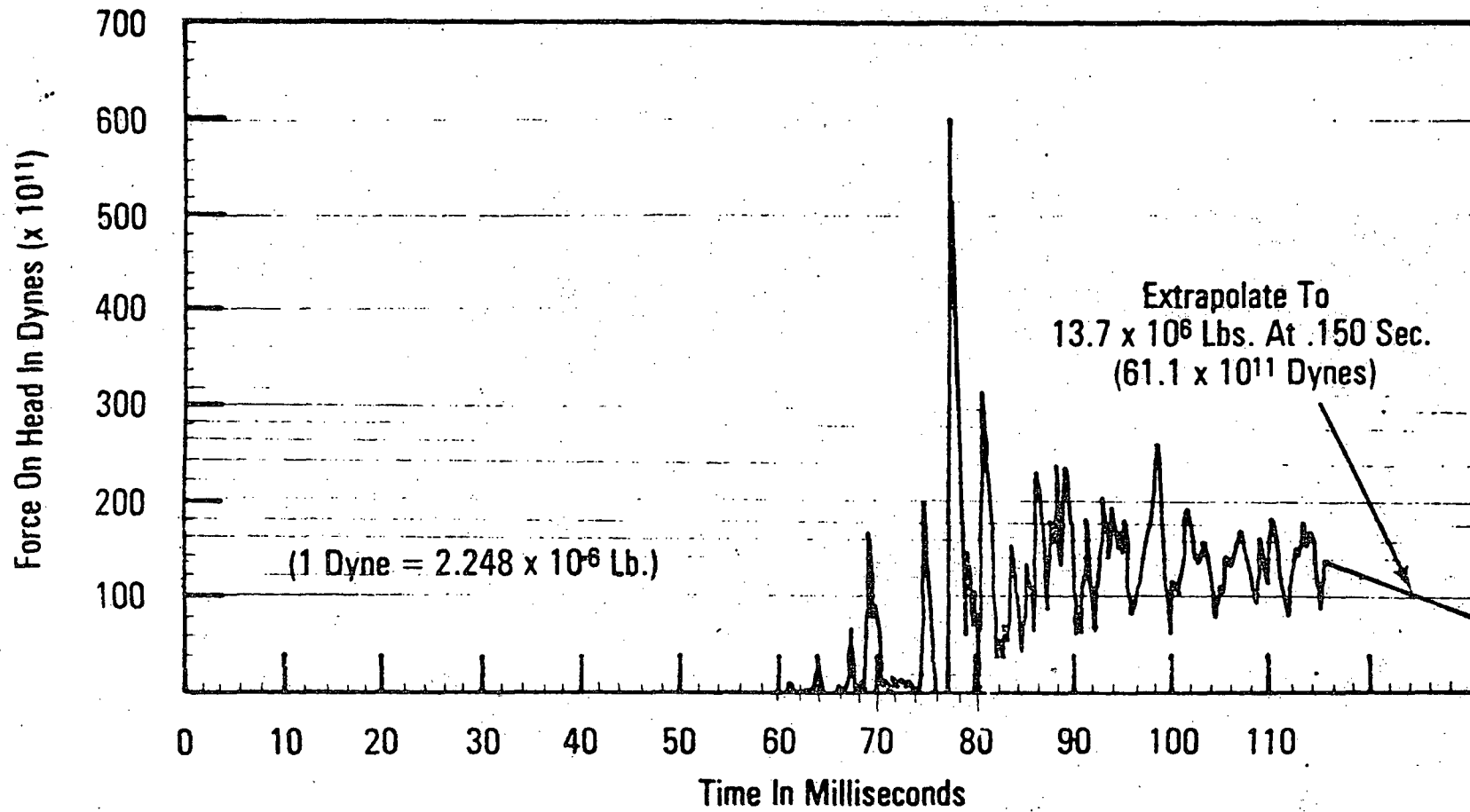


FIGURE 3.5.3-1
CASE 3 TOTAL HEAD FORCE

Force On Top Of Core Support Structure
In Dynes ($\times 10^{11}$)

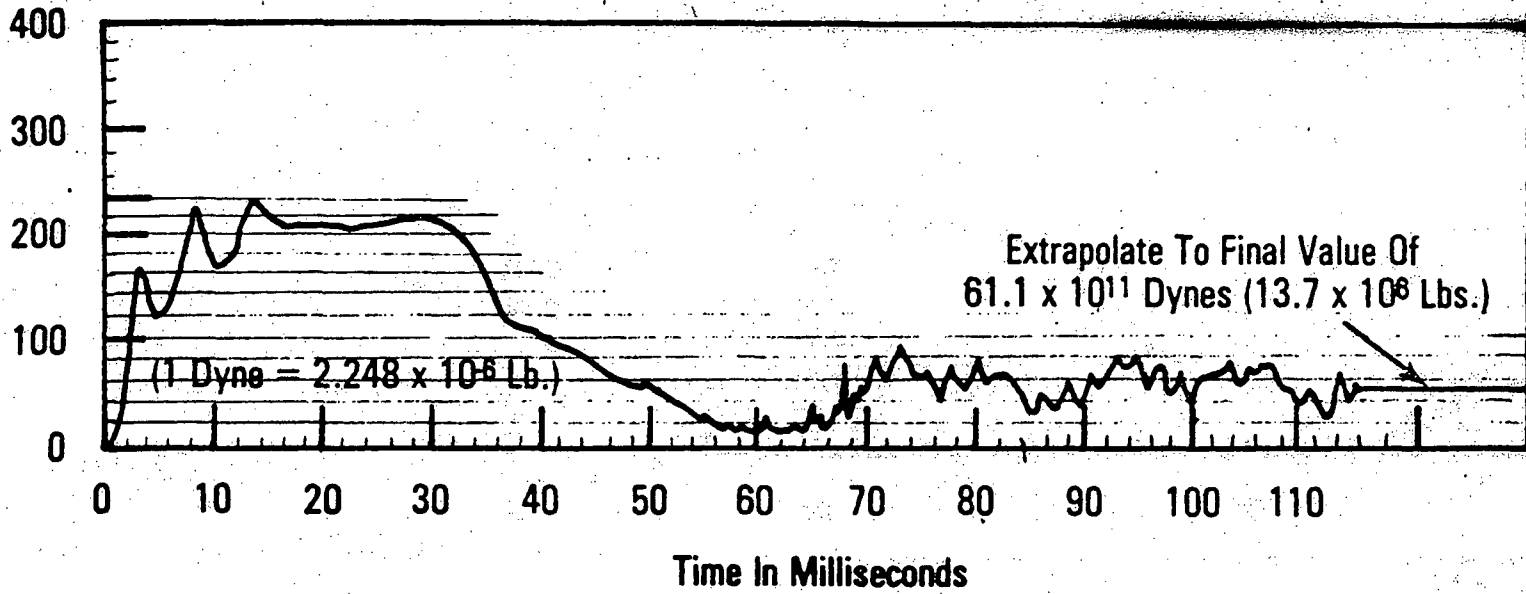


FIGURE 3.5.3-2

CASE 3 TOTAL CSP FORCE

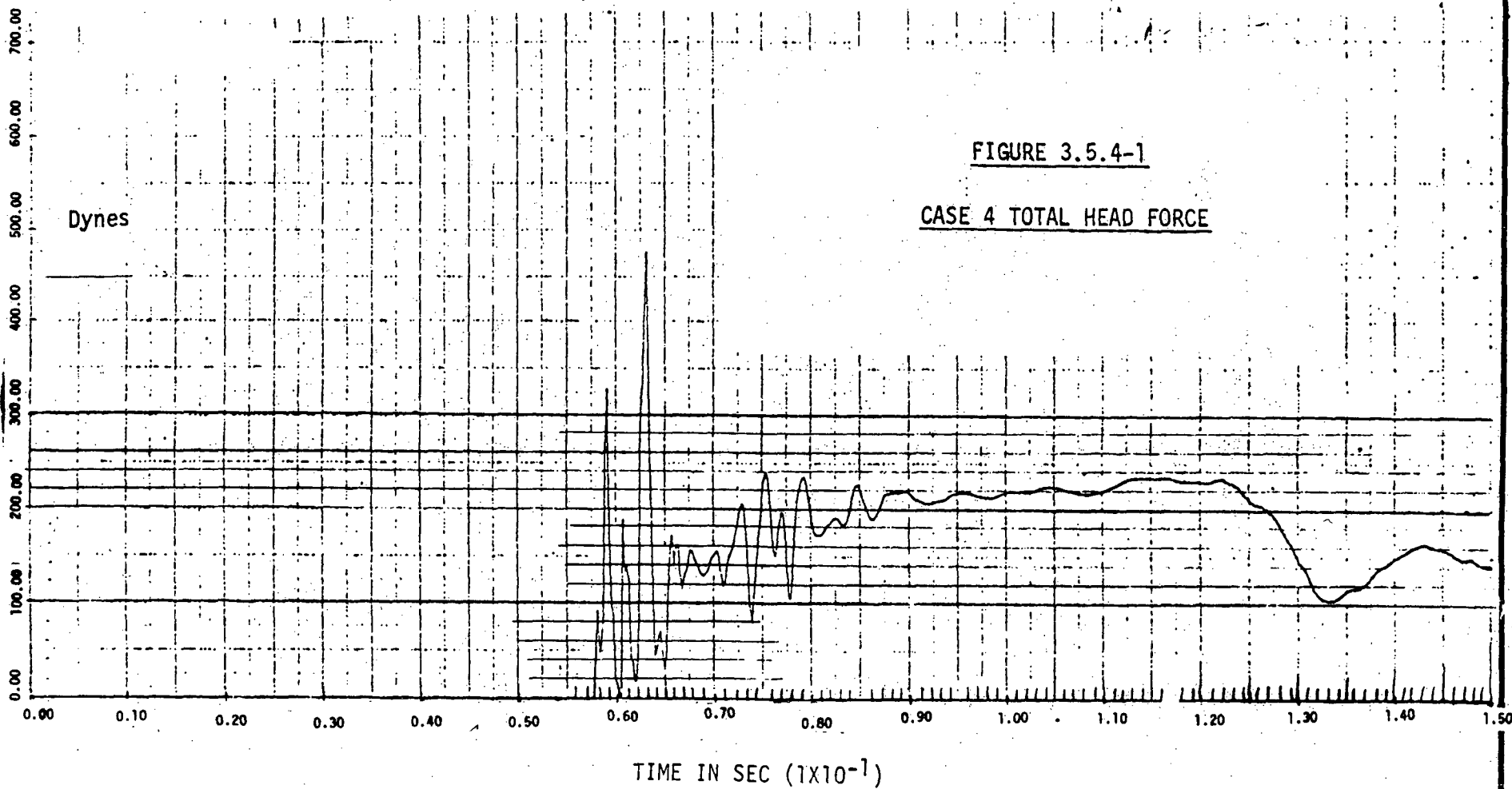
Table 3.5.3-1
CASE 3 LOADING TIME-HISTORY

TIME (SEC)	F _H	LRP	IRP	SRP	CSP	
	DYNES x 10 ¹¹	LBS x 10 ⁶	LBS x 10 ⁶	LBS x 10 ⁶	DYNES x 10 ¹¹	LBS x 10 ⁶
0.000	0.0	0.0	0.0	0.0	0.0	0.0
0.004	↑	↑	↑	↑	160	35.87
0.006	↑	↑	↑	↑	120	26.98
0.008	↑	↑	↑	↑	230	51.70
0.010	↑	↑	↑	↑	170	38.22
0.014	↑	↑	↑	↑	240	53.95
0.016	↑	↑	↑	↑	210	47.21
0.024	↑	↑	↑	↑	210	47.21
0.030	↑	↑	↑	↑	220	49.46
0.036	↑	↑	↑	↑	110	24.73
0.050	↑	↑	↑	↑	60	13.49
0.056	↓	↓	↓	↓	20	4.50
0.058	0.0	0.0	0.0	0.0	25	5.62
0.060	5	0.63	0.43	0.07	30	6.74
0.061	10	1.25	0.86	0.13	35	7.87
0.062	0.0	0.00	0.00	0.00	33	7.42
0.064	40	5.00	3.45	0.54	35	7.87
0.065	0.0	0.00	0.00	0.00	40	8.99
0.067	70	8.75	6.05	0.94	70	15.74
0.068	10	1.25	0.86	0.13	30	6.74
0.069	170	21.25	14.66	2.28	40	8.99
0.072	20	2.50	1.72	0.26	60	13.49
0.075	200	25.00	17.27	2.69	90	20.23
0.076	0.0	0.00	0.00	0.00	40	8.99
0.077	600	75.00	51.82	8.06	70	15.74
0.079	60	7.50	5.18	0.81	80	17.98
0.080	320	40.00	27.64	4.30	80	17.98
0.082	40	5.00	3.45	0.54	60	13.49
0.084	150	18.75	12.95	2.02	40	8.99
0.085	45	5.63	3.89	0.60	30	6.74
0.086	230	28.75	19.86	3.09	40	8.99
0.087	90	11.25	7.77	1.21	30	6.74
0.089	240	30.00	20.73	3.23	60	13.49

CONTINUED

Table 3.5.3-1
CASE 3 LOADING TIME-HISTORY
(continued)

TIME (SEC)	F _H	LRP	IRP	SRP	CSP	
	DYNES X10 ¹¹	LBS X10 ⁶	LBS X10 ⁶	LBS X10 ⁶	DYNES X10 ¹¹	LBS X10 ⁶
0.090	60	7.50	5.18	0.81	40	8.90
0.091	180	22.50	15.54	2.42	60	13.49
0.092	70	8.75	6.05	0.94	50	11.24
0.093	200	25.00	17.27	2.69	60	17.98
0.094	140	17.50	12.09	1.68	70	15.74
0.095	180	22.50	15.54	2.42	60	17.98
0.096	80	10.00	6.91	1.08	45	10.12
0.098	260	32.50	22.45	3.49	50	11.24
0.100	60	7.50	5.18	0.81	40	8.90
0.102	200	25.00	17.27	2.69	60	13.49
0.104	80	10.00	6.91	1.08	60	17.98
0.107	170	21.25	14.68	2.28	70	15.74
0.109	90	11.25	7.77	1.21	50	11.24
0.110	180	22.50	15.54	2.42	40	8.90
0.112	80	10.00	6.91	1.08	30	6.74
0.114	180	22.50	15.54	2.42	60	13.49
0.115	90	11.25	7.77	1.21	40	8.90
0.116	140	17.50	12.09	1.68	50	11.24



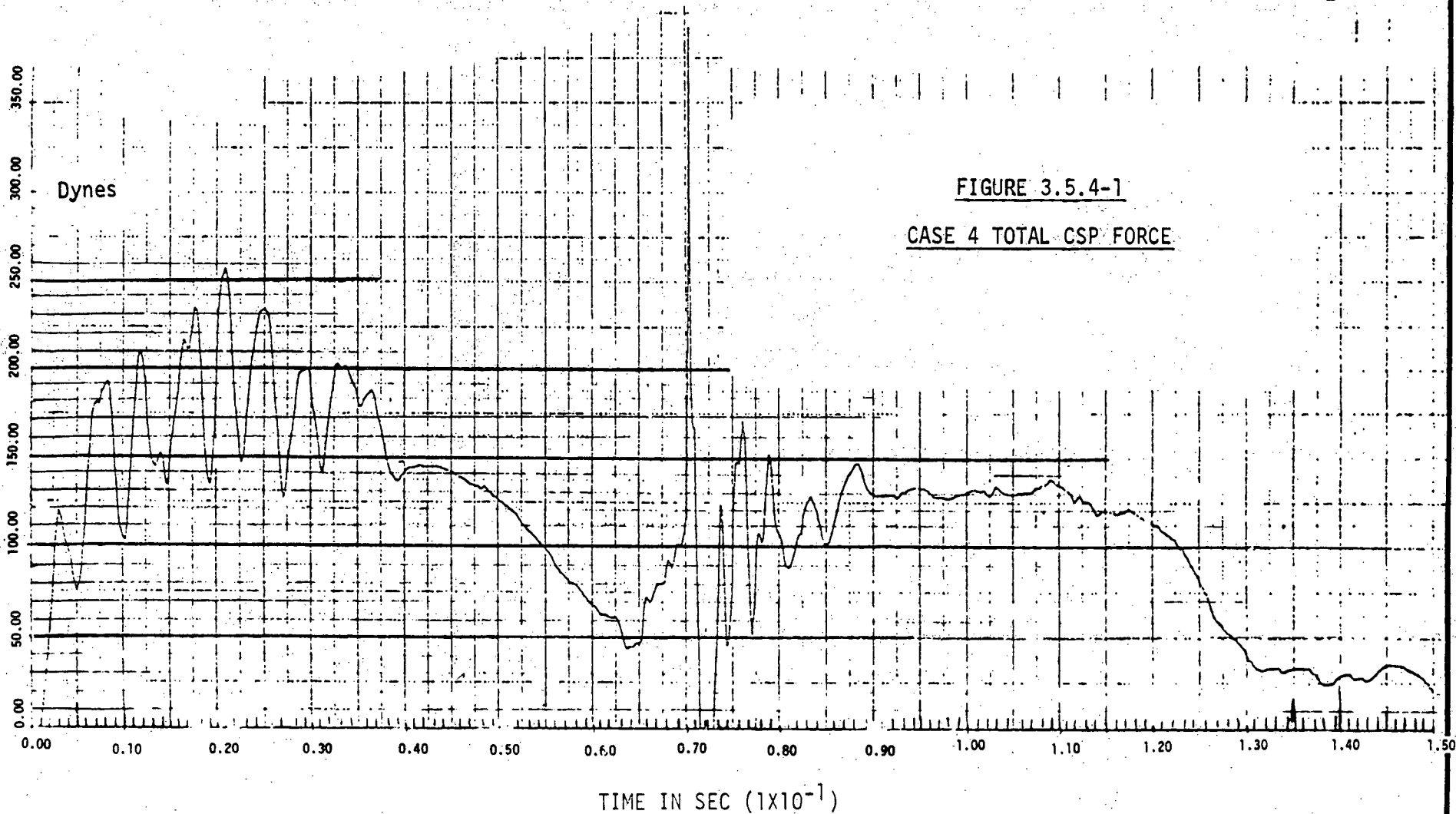


FIGURE 3.5.4-1
CASE 4 TOTAL CSP FORCE

TABLE 3.5.4-1

CASE 4 LOADING TIME-HISTORY

TIME (SEC)	F _H	LRP	IRP	SRP	CSP	
	DYNES X 10 ¹¹	LBS X 10 ⁶	LBS X 10 ⁶	LBS X 10 ⁶	DYNES X 10 ¹¹	LBS X 10 ⁶
0.000	0.0	0.0	0.0	0.0	0.0	0.0
0.004	↑	↑	↑	↑	120	26.98
0.006	↑	↑	↑	↑	75	16.86
0.008	↑	↑	↑	↑	190	42.71
0.010	↑	↑	↑	↑	105	23.06
0.012	↑	↑	↑	↑	210	47.21
0.014	↑	↑	↑	↑	150	33.72
0.016	↑	↑	↑	↑	230	51.70
0.018	↑	↑	↑	↑	135	30.35
0.020	↑	↑	↑	↑	255	57.32
0.022	↑	↑	↑	↑	150	33.72
0.024	↑	↑	↑	↑	230	51.70
0.026	↑	↑	↑	↑	125	25.10
0.030	↑	↑	↑	↑	200	45.00
0.032	↑	↑	↑	↑	140	31.47
0.034	↑	↑	↑	↑	200	45.00
0.036	↑	↑	↑	↑	185	41.59
0.040	↑	↑	↑	↑	135	30.35
0.042	↑	↑	↑	↑	145	32.60
0.048	0.0	0.0	0.0	0.0	130	29.22
0.056	90	11.25	7.77	1.21	90	20.23
0.058	50	6.25	4.32	0.67	80	17.98
0.060	330	41.25	28.50	4.44	70	15.74
0.062	20	2.50	1.73	0.27	60	13.49
0.064	480	60.00	41.45	6.45	45	10.12
0.066	70	8.75	6.05	0.94	65	14.61
0.068	160	20.00	13.82	2.15	100	22.48
0.070	150	18.75	12.95	2.02	380	85.42
0.072	200	25.00	17.27	2.69	120	26.98
0.074	80	10.00	6.91	1.08	90	20.23
0.076	200	25.00	17.27	2.69	160	35.97
0.078	110	13.75	9.50	1.48	50	11.24
0.080	230	28.75	19.86	3.09	150	33.72

TABLE 3.5.4-1

CASE 4 LOADING TIME-HISTORY
(continued)

TIME (SEC)	FH	LRP	IRP	SRP	CEP	
	DYNES X10 ¹¹	LBS X10 ⁶	LBS X10 ⁶	LBS X10 ⁶	DYNES X10 ¹¹	LBS X10 ⁶
0.082	180	22.50	15.54	2.42	90	26.23
0.084	220	27.50	18.99	2.96	130	29.22
0.086	190	23.75	16.41	2.55	100	22.48
0.088	220	27.50	18.99	2.96	150	33.72
0.090	220	27.50	18.99	2.96	130	29.23
0.110	225	28.13	19.43	3.02	140	31.47
0.120	230	28.75	19.86	3.09	120	26.98
0.126	210	26.25	18.14	2.82	60	13.49
0.132	100	12.50	8.64	1.34	35	7.87
0.142	160	20.00	13.82	2.15	30	6.74
0.150	140	17.50	12.09	1.88	20	4.50

3.6 Analysis and Results

The ANSYS derivation of the 1D CRBRP response to the HCDA energetics was arranged to include gravity (deadweight) in the respective solutions. This was accomplished by slowly imposing gravity in the model and permitting time (1 sec.) for the corresponding vibrations to be attenuated by structural damping within the system. With the ANSYS restart option, the four cases were individually started after the (1 sec.) of the gravity solution. Descriptions of the analysis and results are as follows.

3.6.1 Gravity

The ANSYS gravity solution for the 1D CRBRP model was obtained by slowly imposing gravity (386 in/sec^2) in 6 analysis load steps and permitting time (1 second) for system damping to attenuate free vibrations. The analysis load steps, iterations, gravity, and time specifications are presented in Table 3.6.1-1.

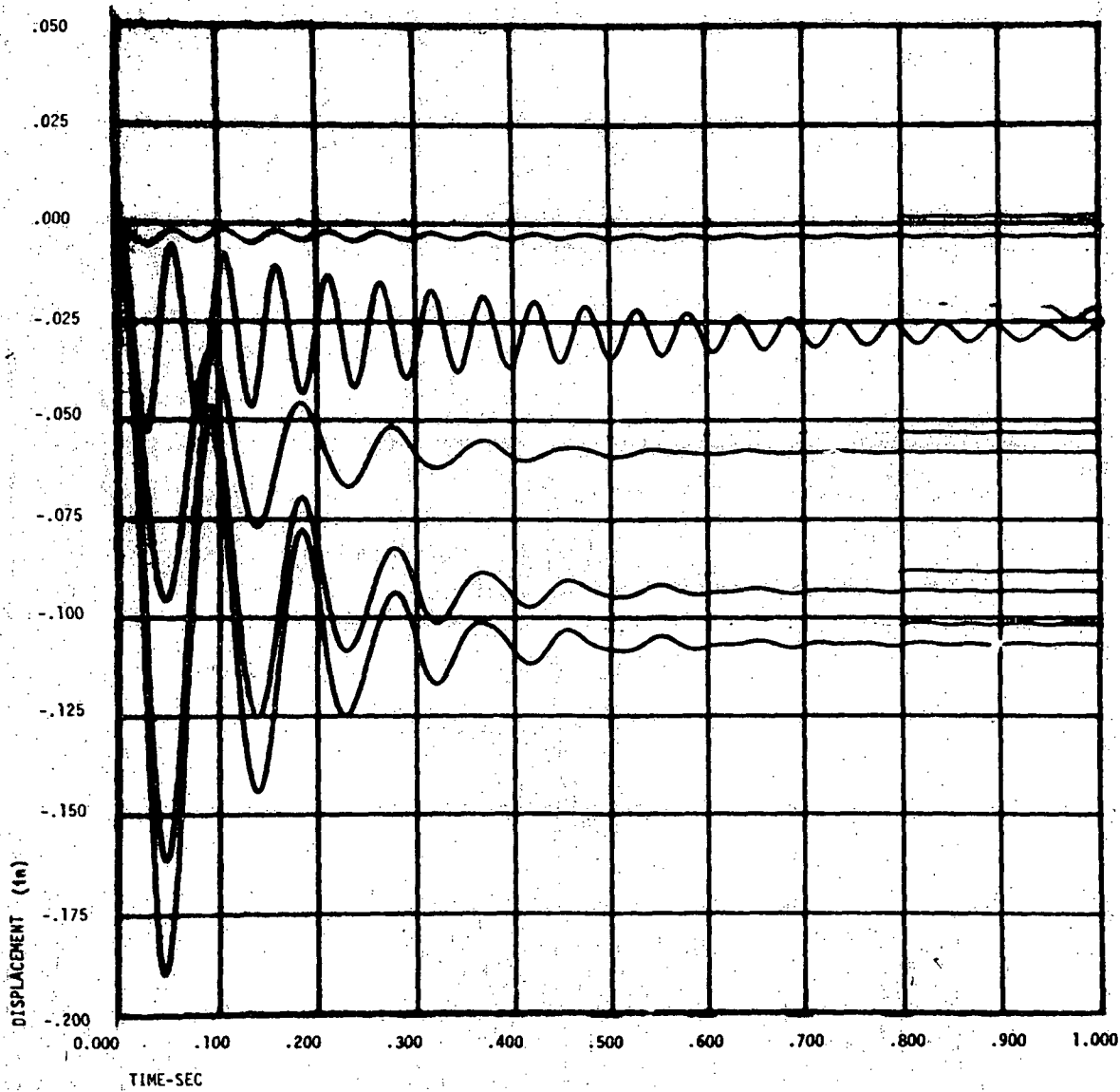
Table 3.6.1-1
Gravity Solution

Load Step	Iterations	G (in/sec ²)	Time (sec)
1	1	0.0	0.0
2	1	0.0	0.001
3	800	386	0.801
4	300	386	0.951
5	200	386	0.991
6	90	386	1.000

The gravity deflections for the experimental shear ring properties including the SRP, IRP, LRP, vessel flange, and vessel CSP are illustrated in Figure 3.6.1-1. Corresponding velocities and accelerations are illustrated in Figures 3.6.1-2 and -3 respectively. The gravity solution is completely elastic without plastic shear ring, vessel wall, and flange bolt deformations.

The concrete ledge load under gravity is illustrated in Figure 3.6.1-4. The load in the vessel wall is illustrated in Figure 3.6.1-5. The gravity load on the SRP, IRP, and LRP bearings and risers is illustrated in Figure 3.6.1-6.

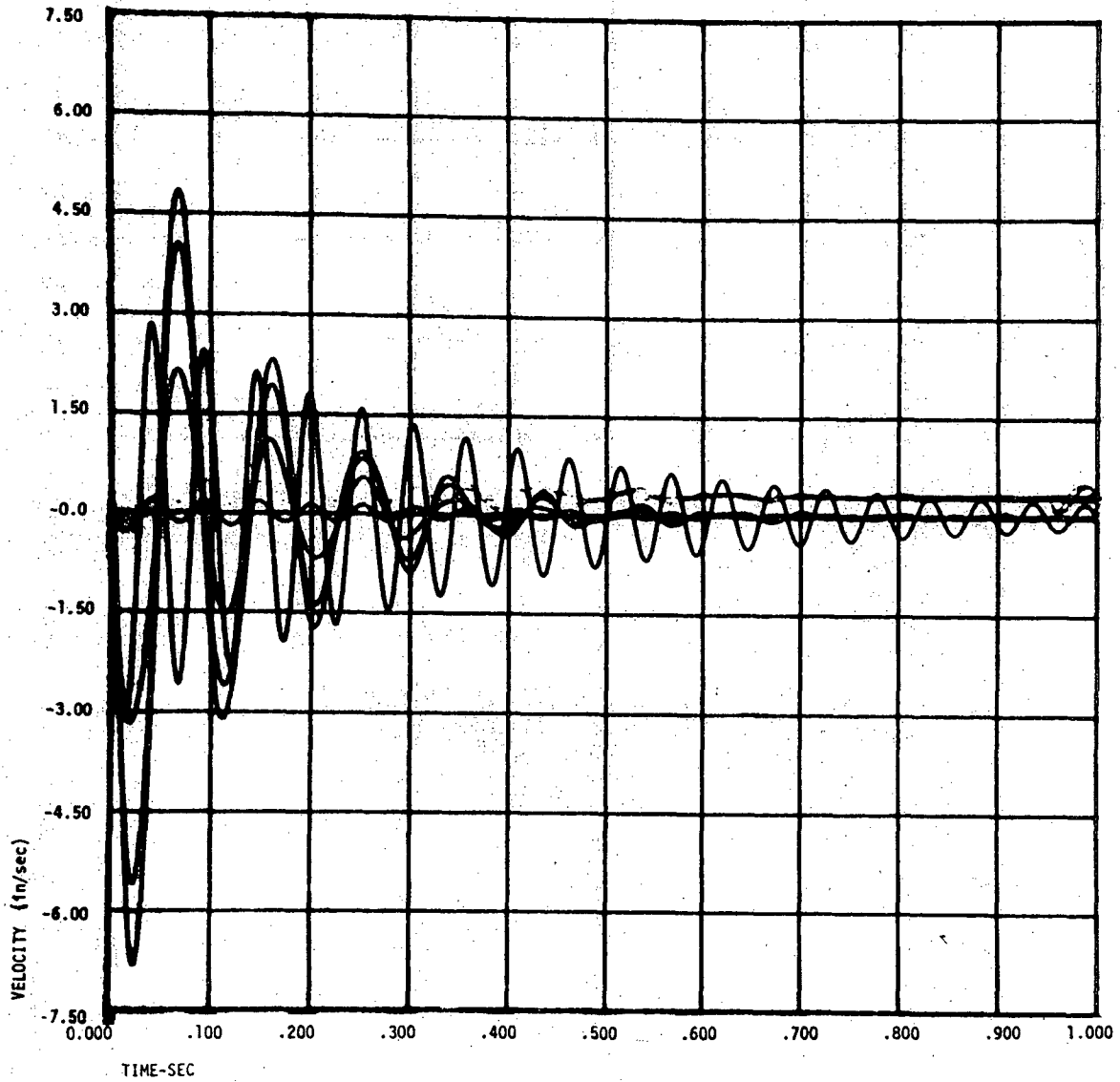
A review of the CRBRP gravity deflections and loads shows that the free vibrations associated with the method of solution are essentially attenuated to 1G values by system damping after 1 second. Accordingly, the responses as obtained by performing ANSYS restarts from the gravity solution do not sacrifice any accuracy and are an acceptable method of including gravity in the respective HCDA response.



CRBRP... LOADING HCDA ENERGETIC ANALYSIS ... GRAVITY SOLUTION

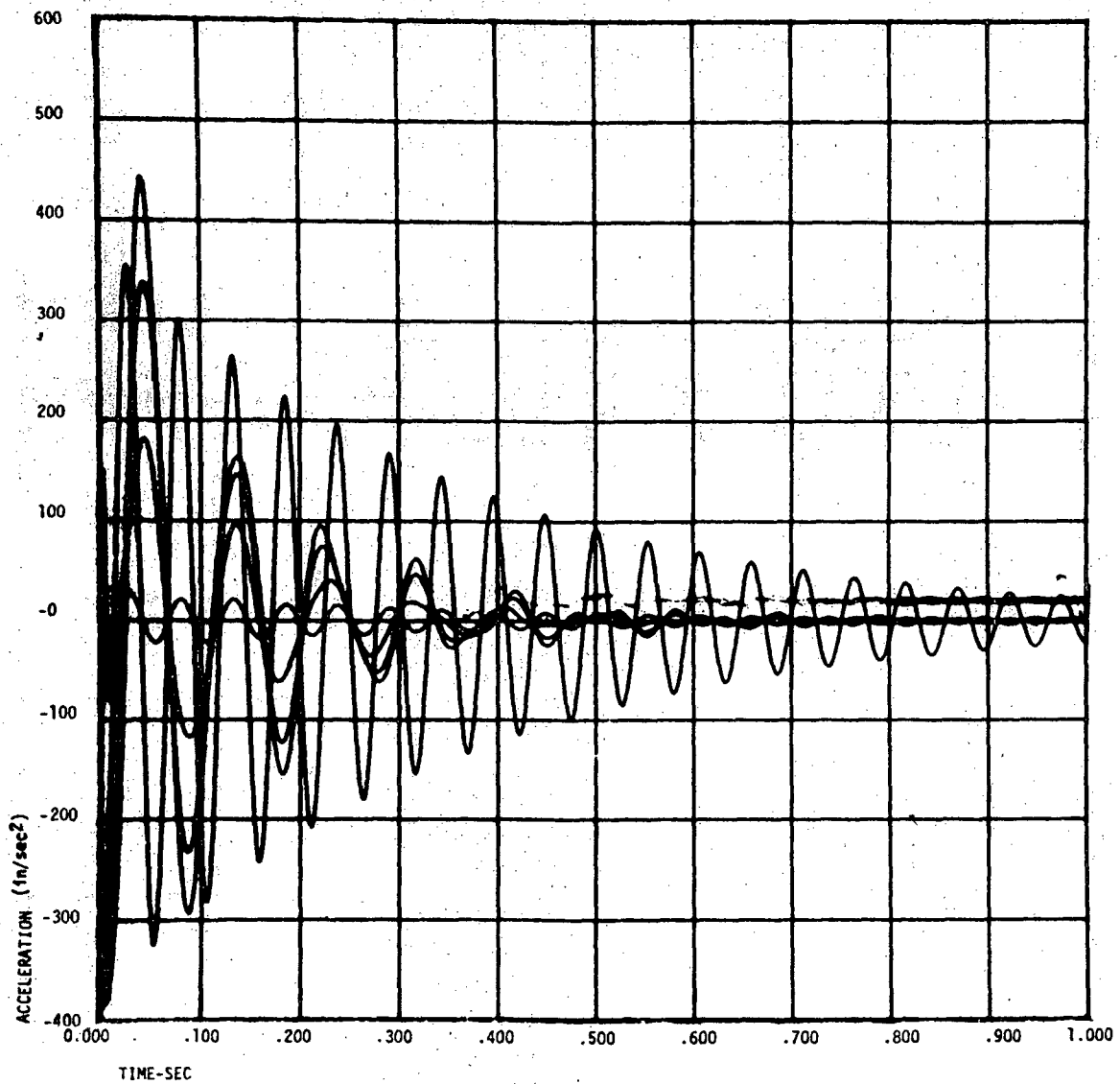
FIGURE 3.6.1-1

EXPERIMENTAL SHEAR RING PROPERTIES
GRAVITY SOLUTION
PLUG AND VESSEL
DISPLACEMENTS



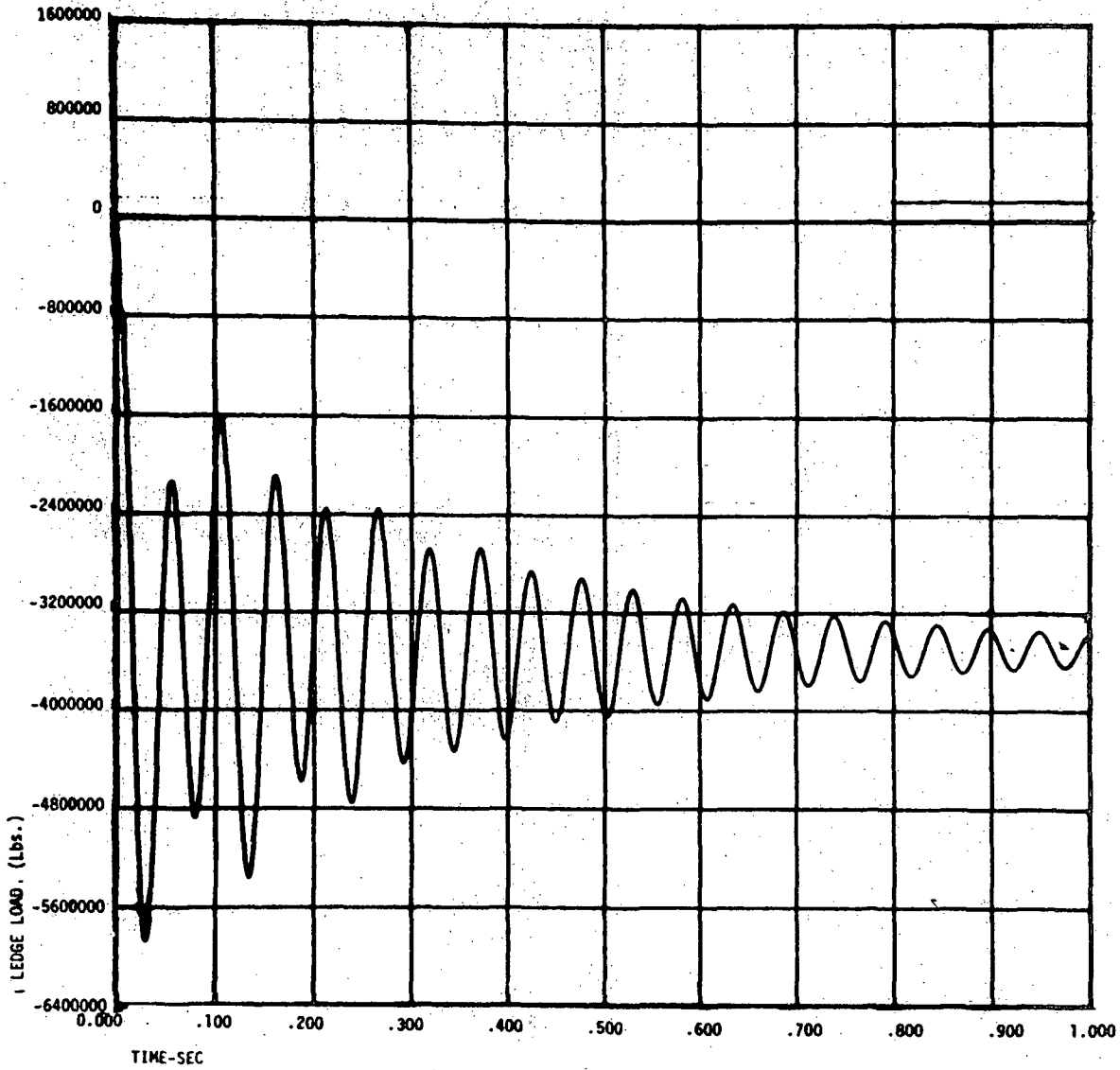
CRBRP... LOADING HCDA ENERGETIC ANALYSIS ... GRAVITY SOLUTION

FIGURE 3.6.1-2
EXPERIMENTAL SHEAR RING PROPERTIES
GRAVITY SOLUTION
PLUG AND VESSEL
VELOCITIES



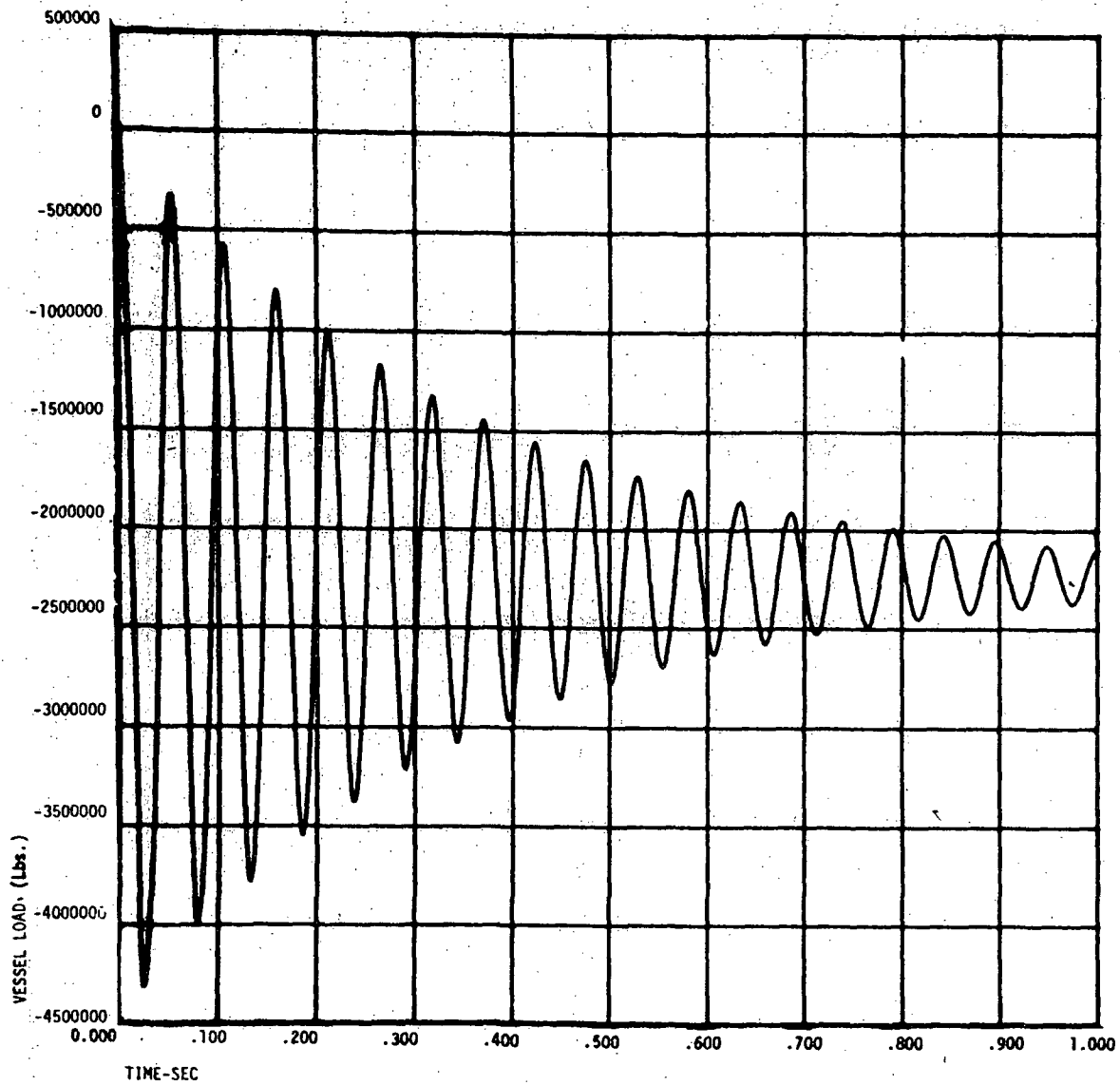
CRBRP... LOADING HCDA ENERGETIC ANALYSIS ... GRAVITY SOLUTION

FIGURE 3.6.1-3
EXPERIMENTAL SHEAR RING PROPERTIES
GRAVITY SOLUTION
PLUG AND VESSEL
ACCELERATIONS



CRBRP... LOADING MCDA ENERGETIC ANALYSIS ... GRAVITY SOLUTION

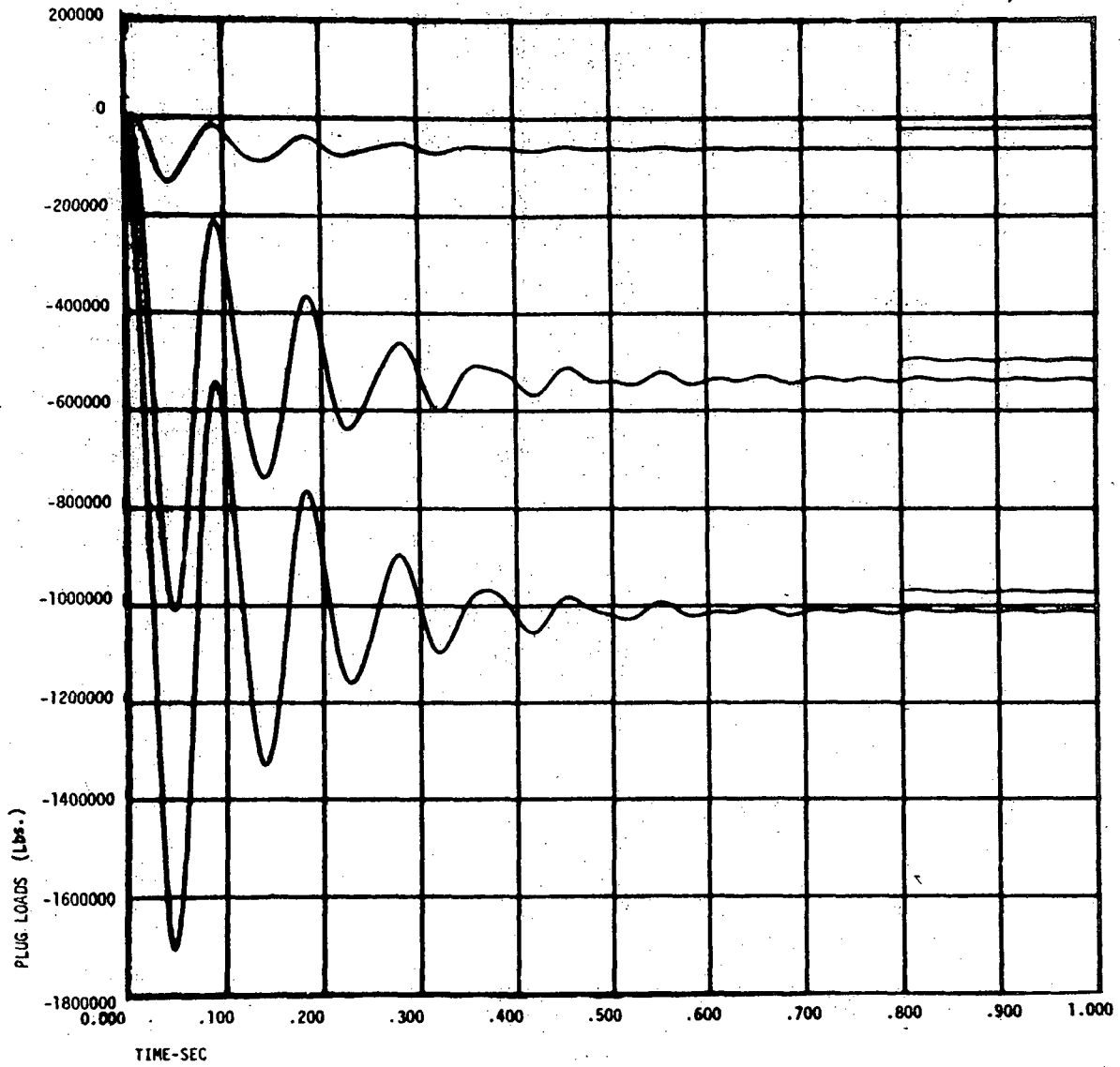
FIGURE 3.6.1-4
EXPERIMENTAL SHEAR RING PROPERTIES
GRAVITY SOLUTION
CONCRETE AND BOLT LEDGE LOAD



CRBRP... LOADING MCDA ENERGETIC ANALYSIS ... GRAVITY SOLUTION

FIGURE 3.6.1-5

EXPERIMENTAL SHEAR RING PROPERTIES
GRAVITY SOLUTION
VESSEL LOAD



CRBRP... LOADING HCDA ENERGETIC ANALYSIS ... GRAVITY SOLUTION

FIGURE 3.6.1-6
EXPERIMENTAL SHEAR RING PROPERTIES
GRAVITY SOLUTION
PLUG BEARING LOADS

3.6.2 Case 1 - Structural Design Basis (SDB)

The 1D CRBRP response to the SDB energetic was derived with the ANSYS program by restarting the gravity solution at time ($t = 1$ second). The SDB energetic force time-history data (Table 3.5.1-1) was advanced in time (1 second) and arranged in 45 analysis load steps with a total of 1170 iterations to span the duration (0.1160 sec). The SRP, IRP, and LRP forces were applied to model mass nodes 4, 3, and 2 in the upward direction. The CSP force was applied in the downward direction at mass Node 1. Gravity (386 in/sec^2) was maintained throughout the response.

The absolute SDB displacements of the SRP, IRP, LRP, flange, and CSP are illustrated in Figure 3.6.2-1.

The SDB energetic response showed that the SRP, IRP, and LRP shear ring deformations were linear elastic. Respective forces are illustrated in Figure 3.6.2-2.

The SDB response in terms of downward acting concrete ledge loads and upward acting vessel flange bolt force is illustrated in Figure 3.6.2-3.

Both downward concrete ledge force and upward vessel flange bolt forces were processed as negative values. The downward concrete ledge force alone occurs from 1 to 1.06 seconds while the upward bolt force alone occurs after 1.06 seconds.

The SDB accelerations of the SRP, IRP, LRP, flange, and CSP are illustrated in Figure 3.6.2-4.

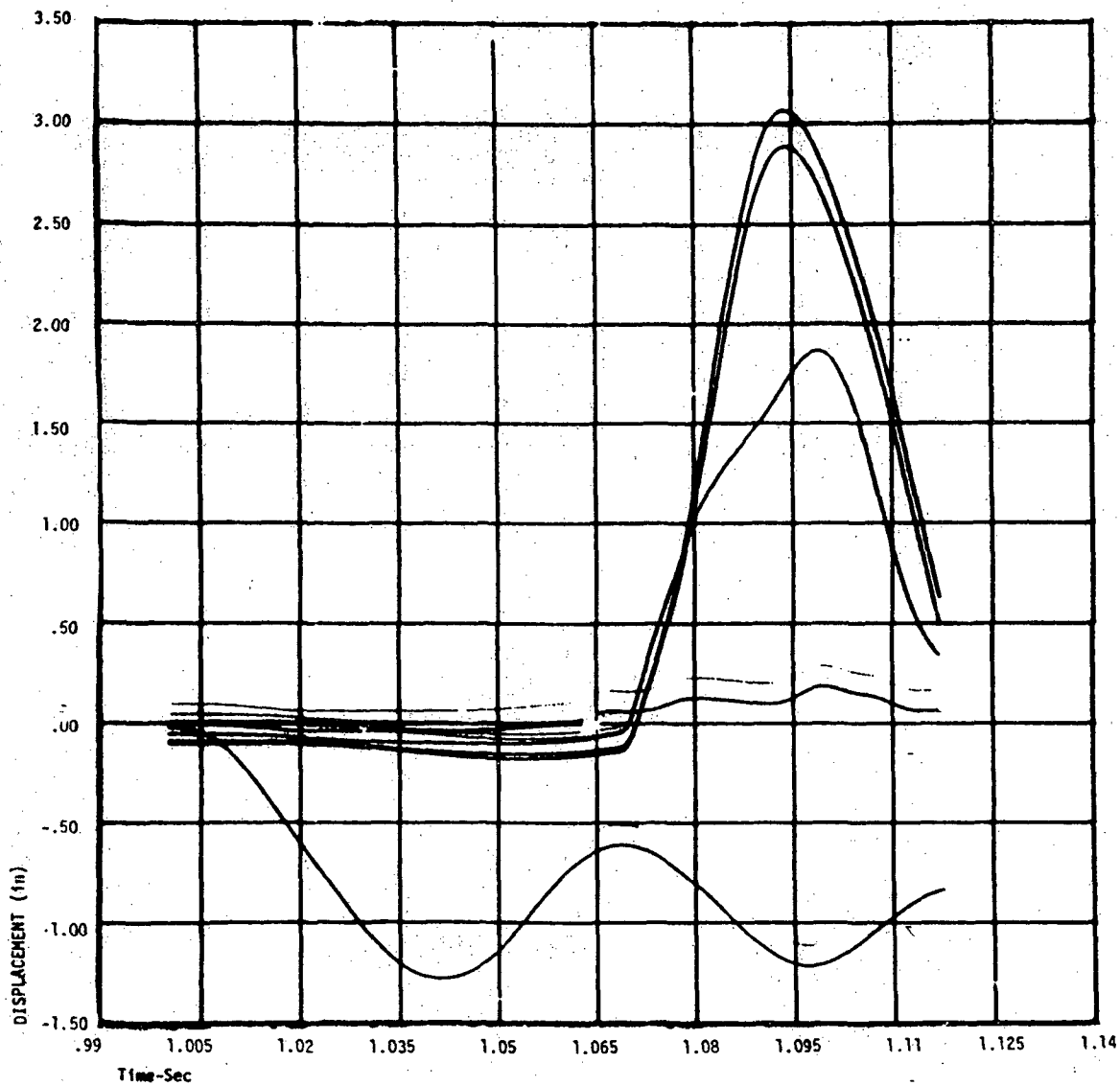


FIGURE 3.6.2-1
SDB ENERGETIC
EXPERIMENTAL SHEAR RING PROPERTIES
ABSOLUTE DISPLACEMENTS

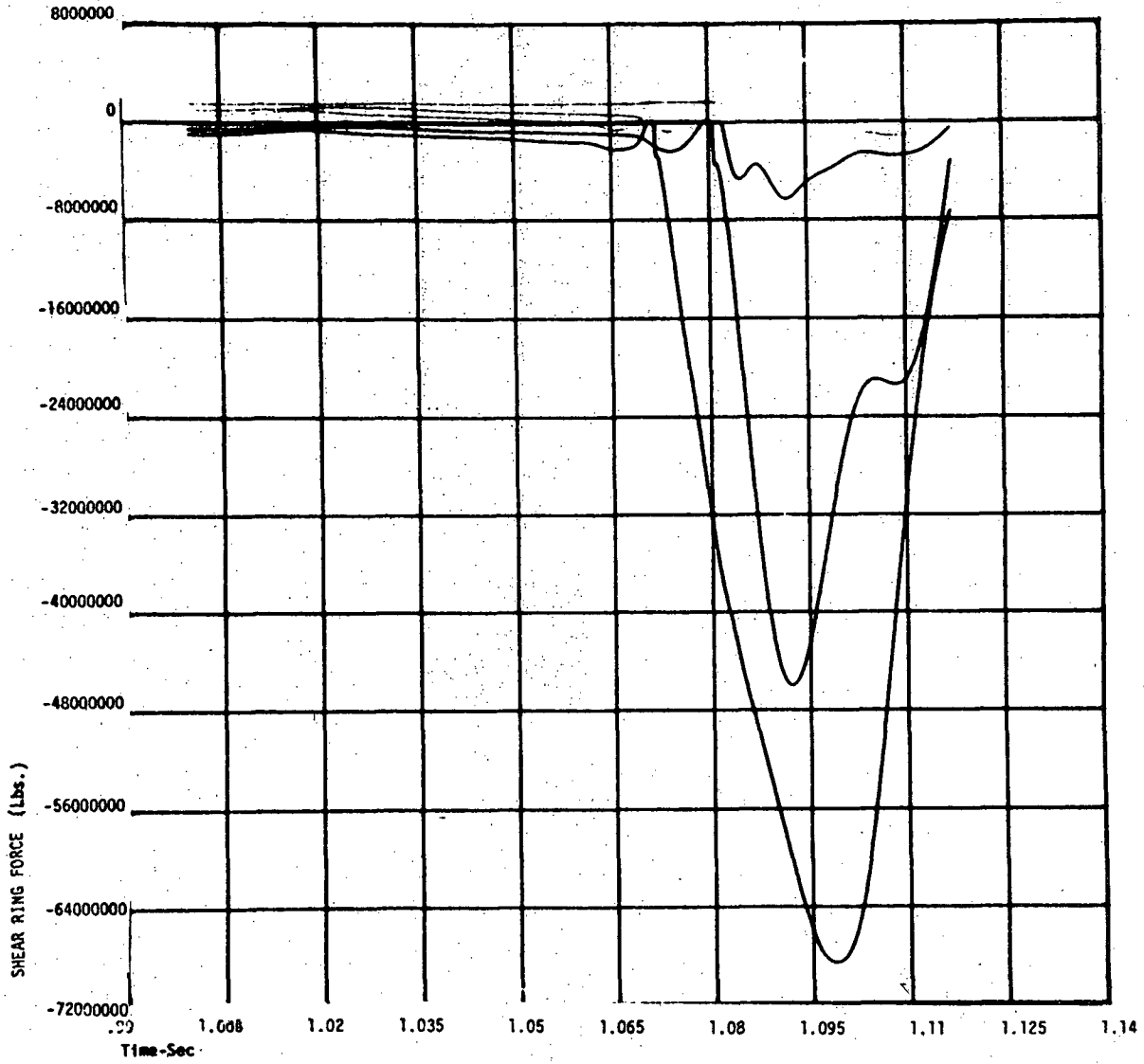


FIGURE 3.6.2-2
SDB ENERGETIC
EXPERIMENTAL SHEAR RING PROPERTIES
SHEAR RING FORCES

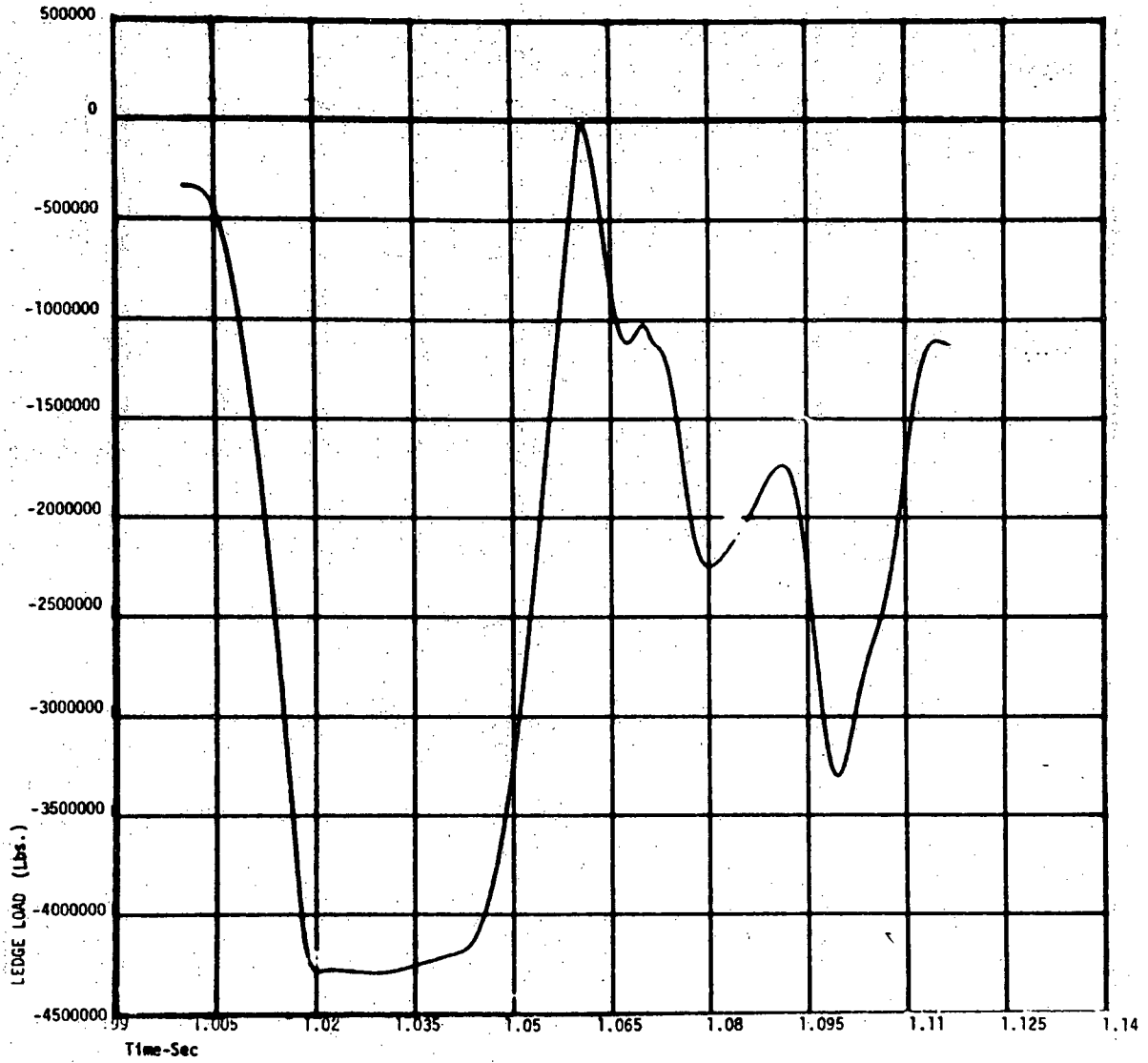


FIGURE 3.6.2-3
SDB ENERGETIC
EXPERIMENTAL SHEAR RING PROPERTIES
CONCRETE LEDGE AND BOLT FORCE

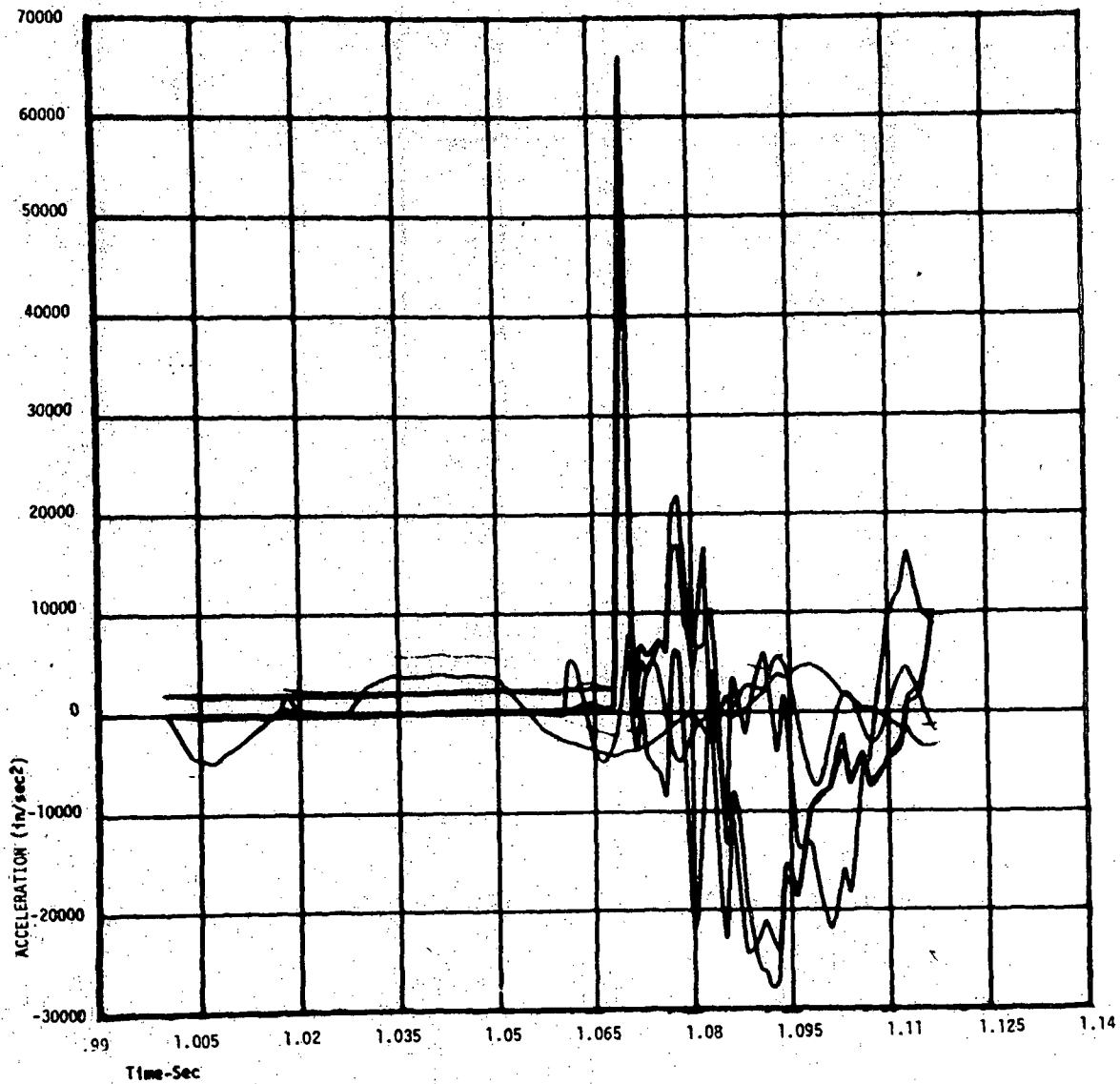


FIGURE 3.6.2-4
SDB ENERGETIC
EXPERIMENTAL SHEAR RING PROPERTIES
ACCELERATIONS

3.6.3 Case 2

The 1D CRBRP response to the Case 2 energetics was derived with the ANSYS program by restarting the gravity solution at time ($t = 1$ second). The Case 2 energetic force time-history data (Table 3.5.2-1) was advanced in time (1 second) and arranged in 42 analysis load steps with a total of 1200 iterations. Integration time step, plug and CSP forces, and gravity procedures were identical to those described for Case 1.

The absolute Case 2 displacements of the SRP, IRP, LRP, flange, and CSP are illustrated in Figure 3.6.3-1.

The Case 2 energetic response showed that the SRP, IRP, and LRP shear ring deformations were linear elastic. Respective forces are illustrated in Figure 3.6.3-2.

The Case 2 response in terms of downward acting concrete ledge loads and upward acting vessel flange bolt forces is illustrated in Figure 3.6.3-3.

The Case 2 accelerations of the SRP, IRP, LRP, flange, and CSP are illustrated in Figure 3.6.3-4.

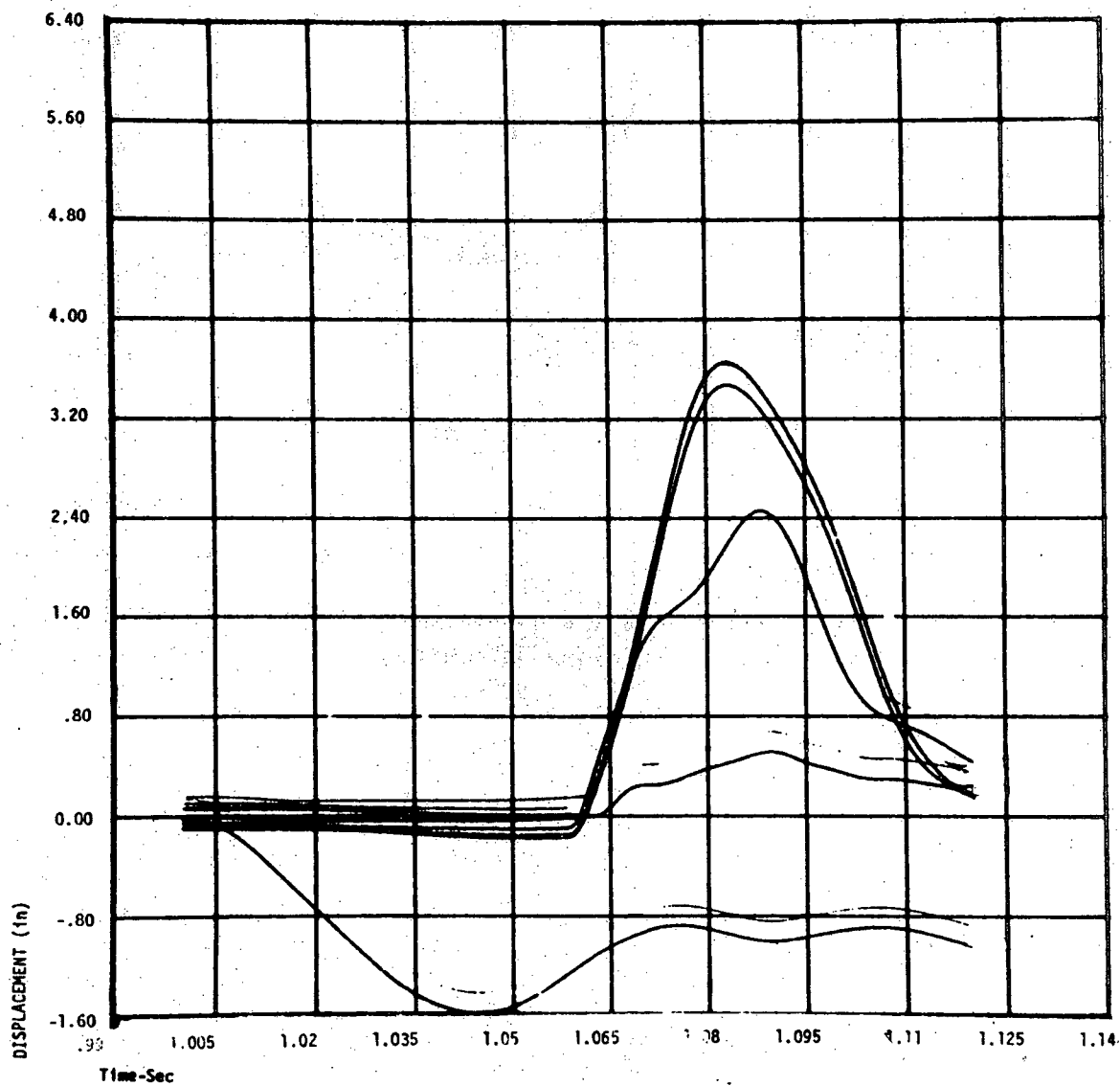


FIGURE 3.6.3-1
CASE 2 ENERGETIC
EXPERIMENTAL SHEAR RING PROPERTIES
ABSOLUTE DISPLACEMENTS

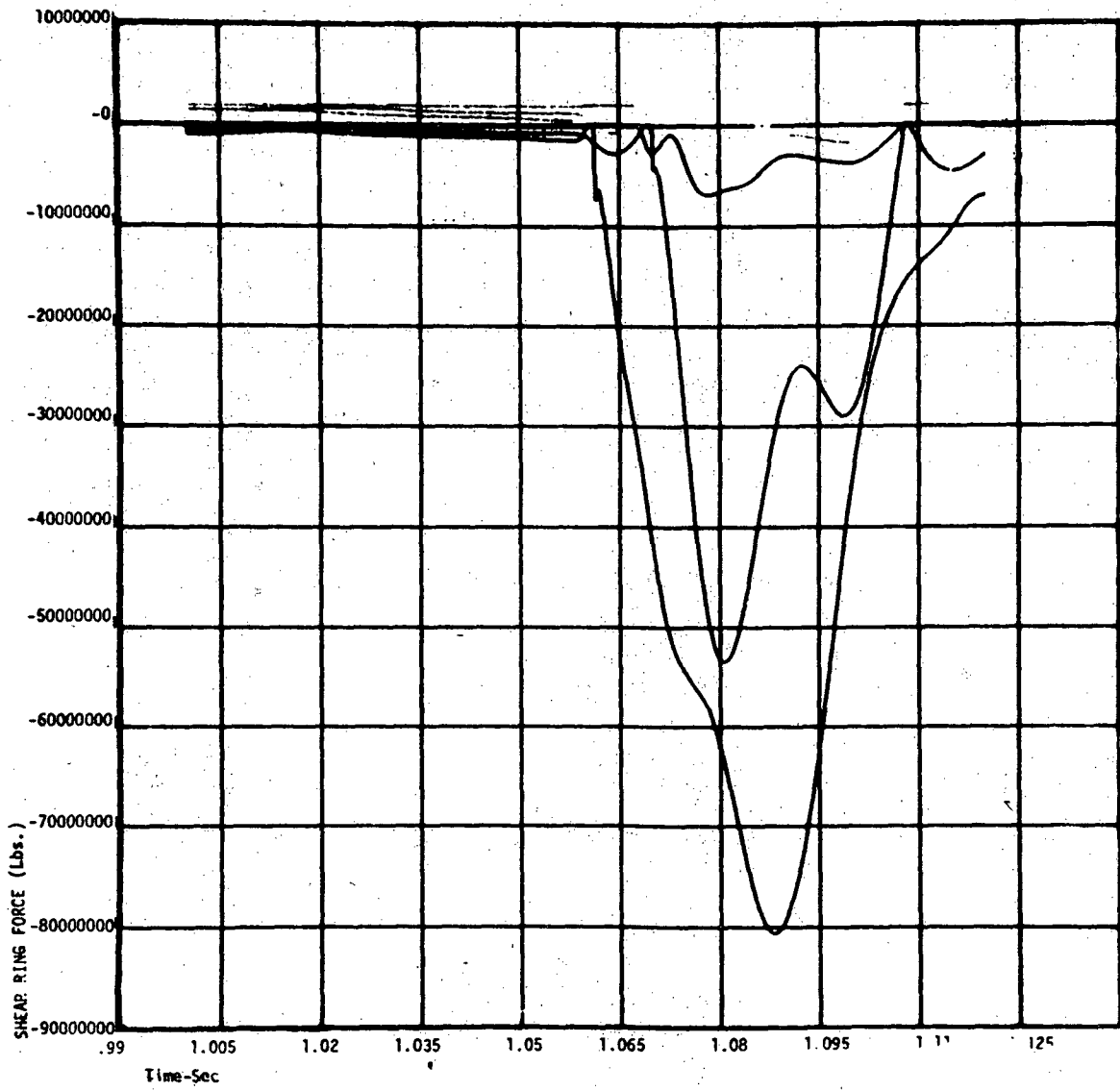


FIGURE 3.6.3-2
CASE 2 ENERGETIC
EXPERIMENTAL SHEAR RING PROPERTIES
SHEAR RING FORCES

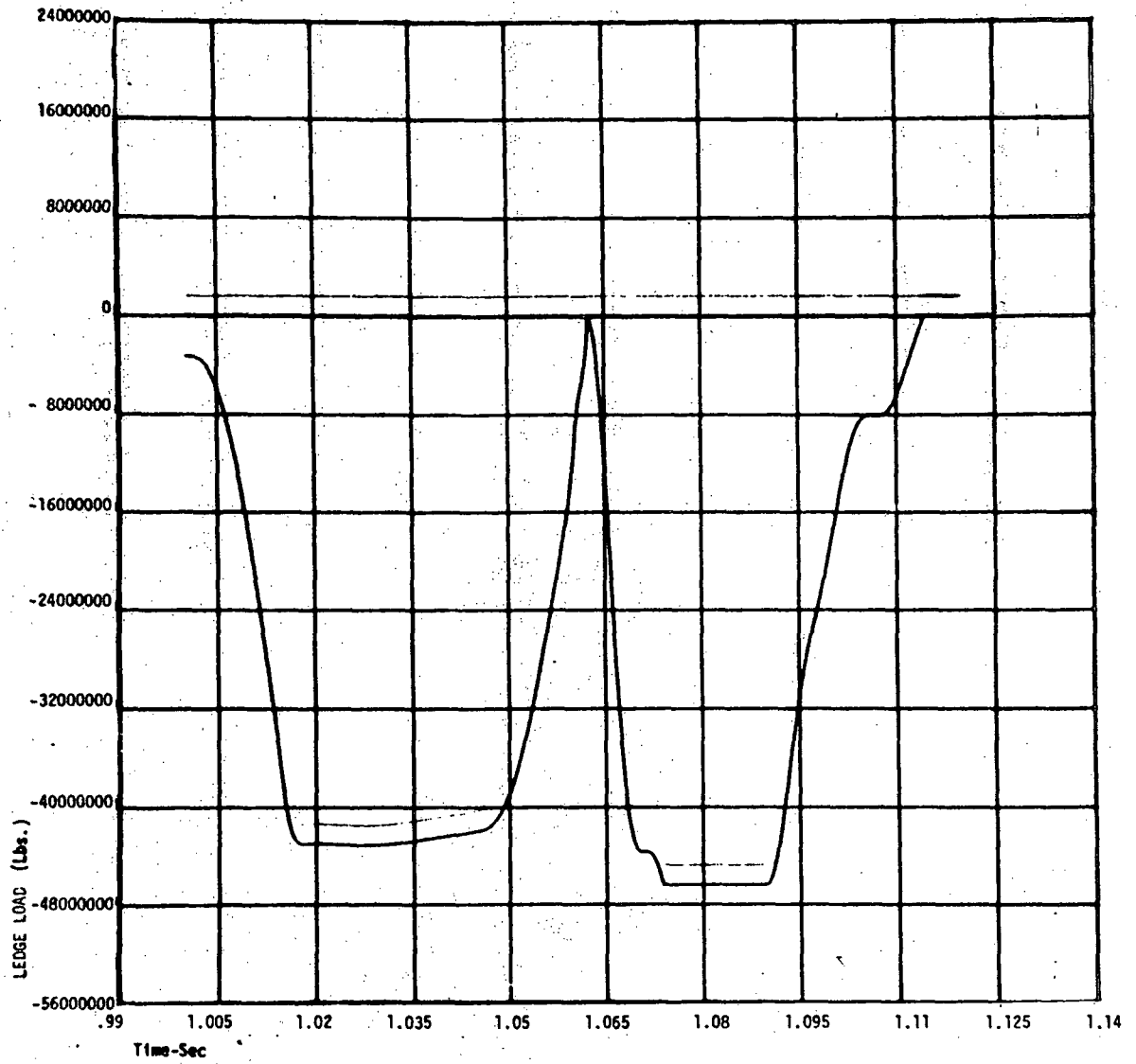


FIGURE 3.6.3-3
CASE 2 ENERGETIC
EXPERIMENTAL SHEAR RING PROPERTIES
CONCRETE LEDGE AND BOLT FORCE

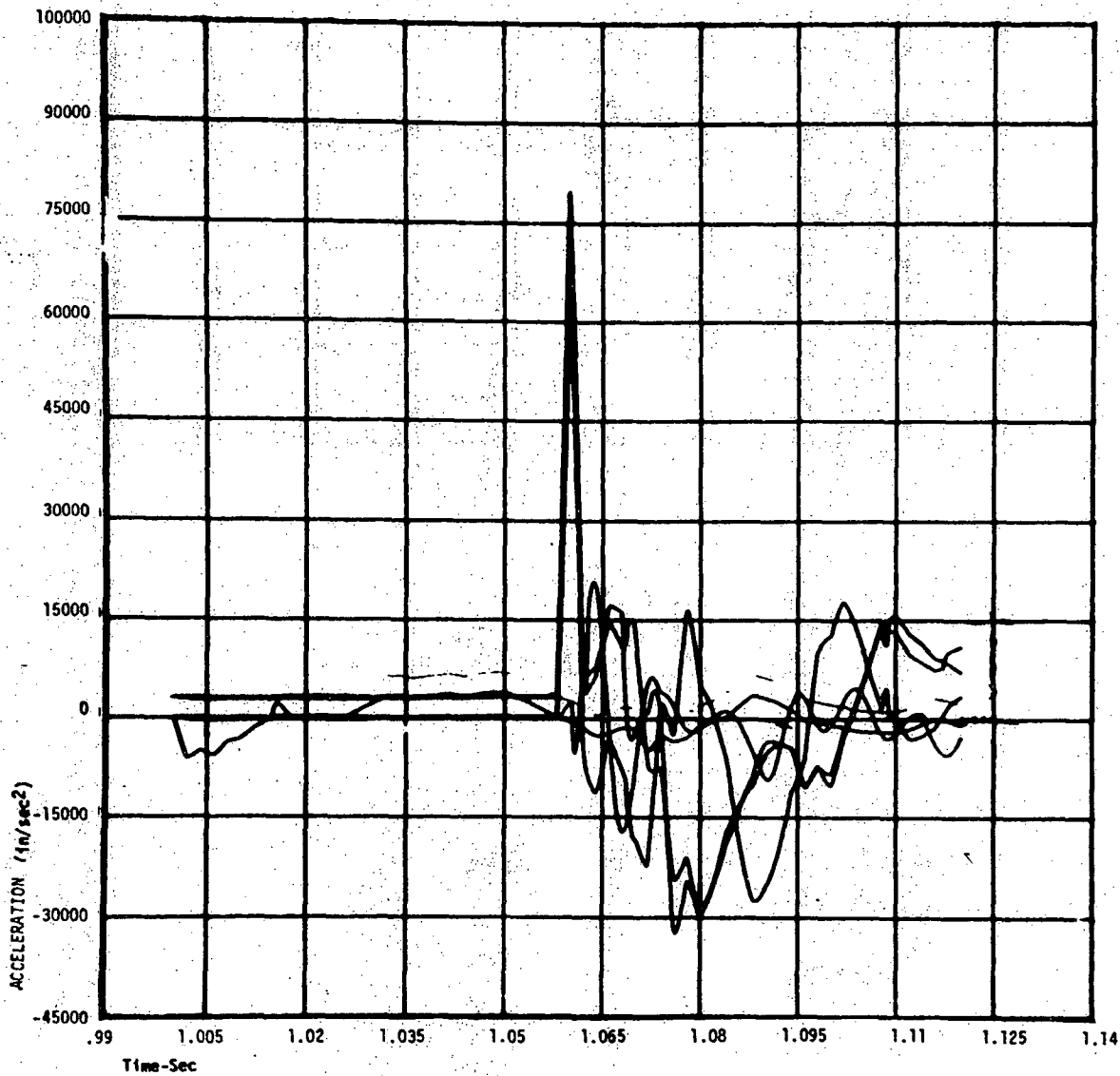


FIGURE 3.6.3-4
CASE 2 ENERGETIC
EXPERIMENTAL SHEAR RING PROPERTIES
ACCELERATIONS

3.6.4 Case 3

The 1D CRBRP response to the Case 3 energetics was derived with the ANSYS program by restarting the gravity solution at time $t = 1$ second. The Case 3 energetic force time-history data (Table 3.5.3-1) was advanced in time (1 second) and arranged in 51 analysis load steps. For an integration timestep ($\Delta t = 0.0001$ sec), a total of 1160 iterations was used. Integration time step, plug and CSP forces, and gravity procedures were identical to those described for Case 1.

The absolute Case 3 displacements for SRP, IRP, LRP, flange, and CSP are illustrated in Figure 3.6.4-1.

The Case 3 energetic response showed that the SRP, IRP, and LRP shear ring deformations are linear elastic without plasticity for the experimental shear ring properties. The SRP, IRP, and LRP shear ring forces during Case 3 energetic are less than respective yield forces. Respective forces are illustrated in Figure 3.6.4-2.

The Case 3 response in terms of downward acting concrete ledge force and upward acting vessel flange bolt force is illustrated in Figure 3.6.4-3.

The Case 3 accelerations of the SRP, IRP, LRP, flange, and vessel are illustrated in Figure 3.6.4-4.

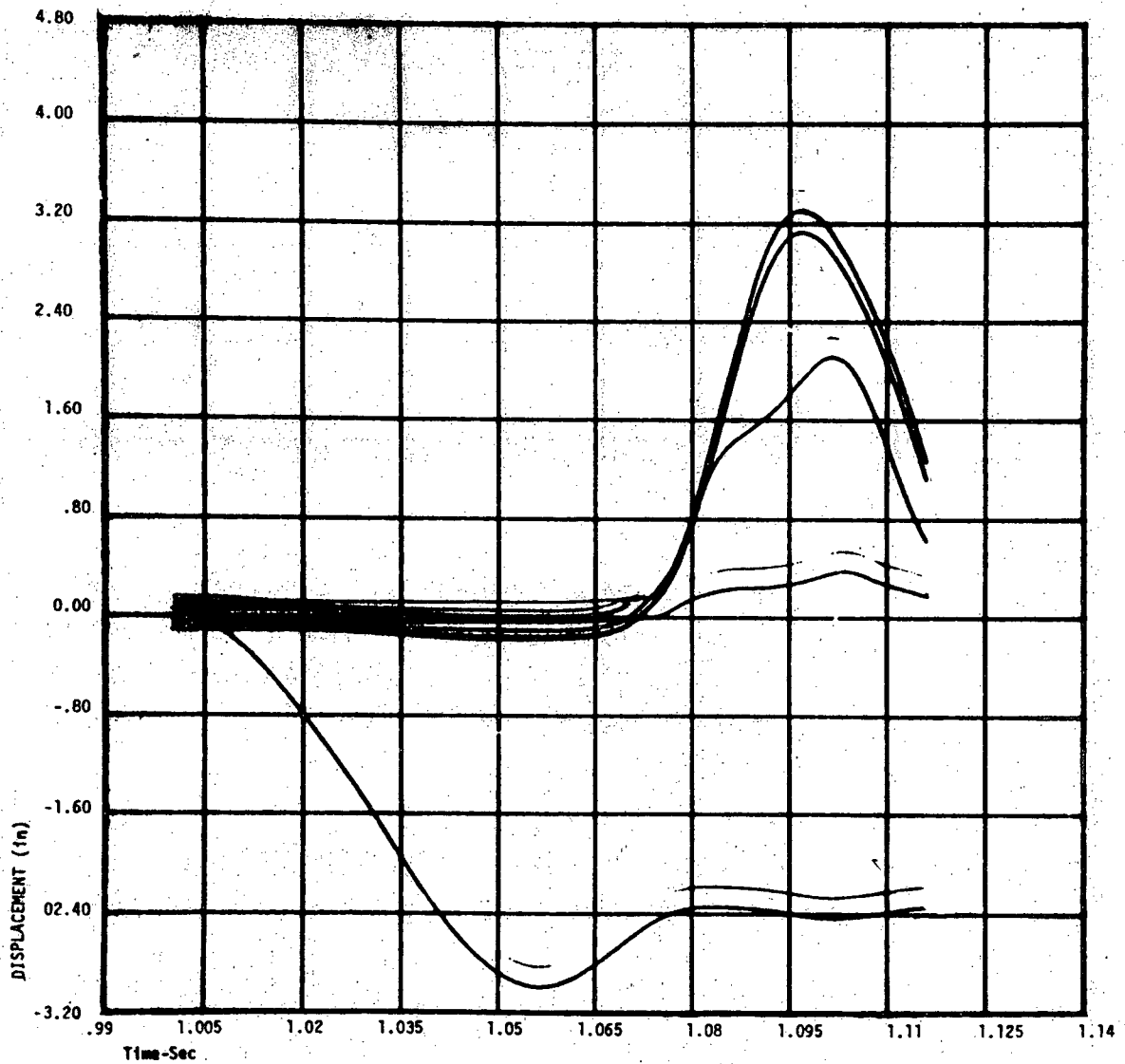


FIGURE 3.6.4-1
CASE 3 ENERGETIC
EXPERIMENTAL SHEAR RING PROPERTIES
ABSOLUTE DISPLACEMENTS

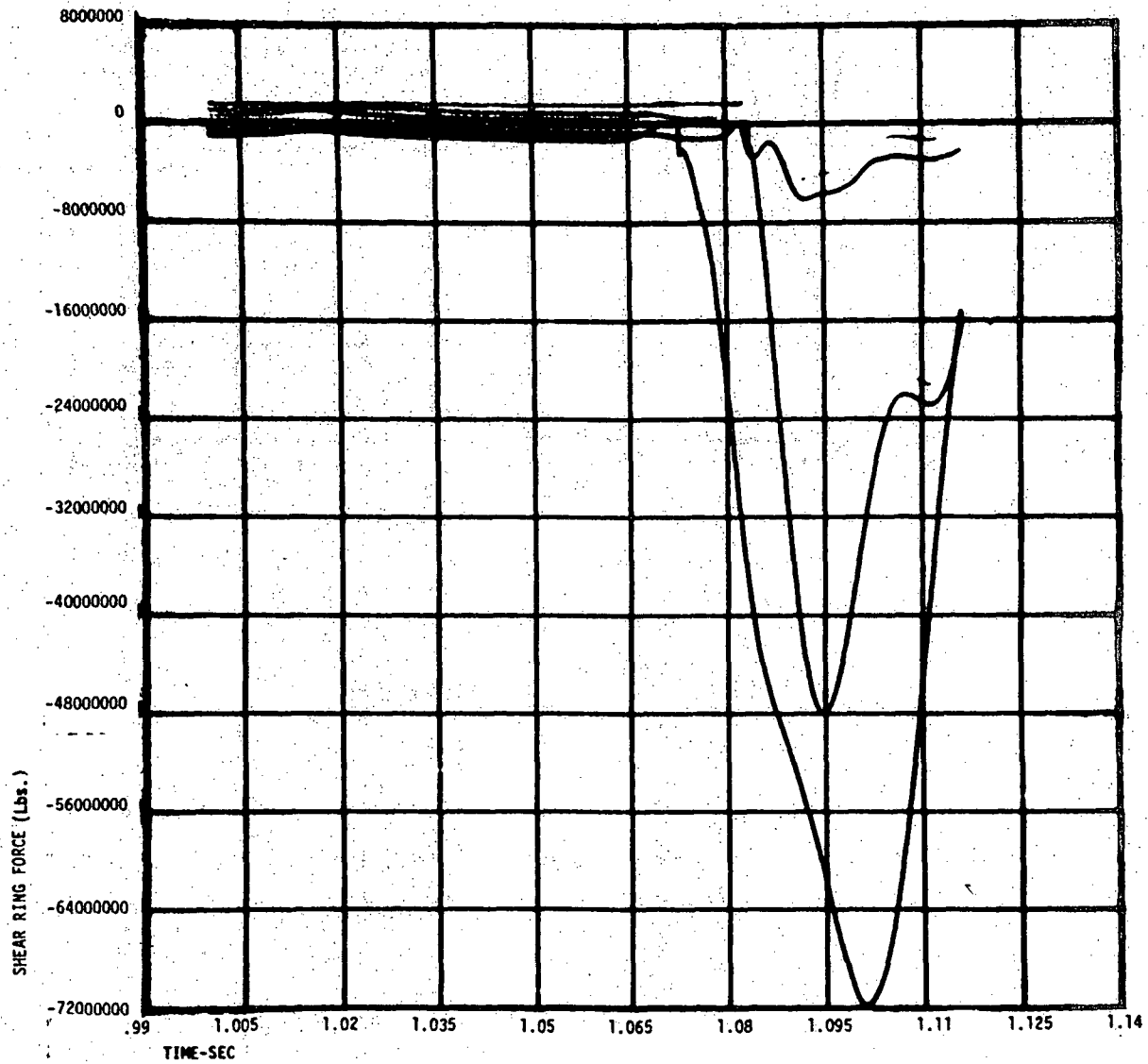


FIGURE 3.6.4-2
CASE 3 ENERGETIC
EXPERIMENTAL SHEAR RING PROPERTIES
SHEAR RING FORCES

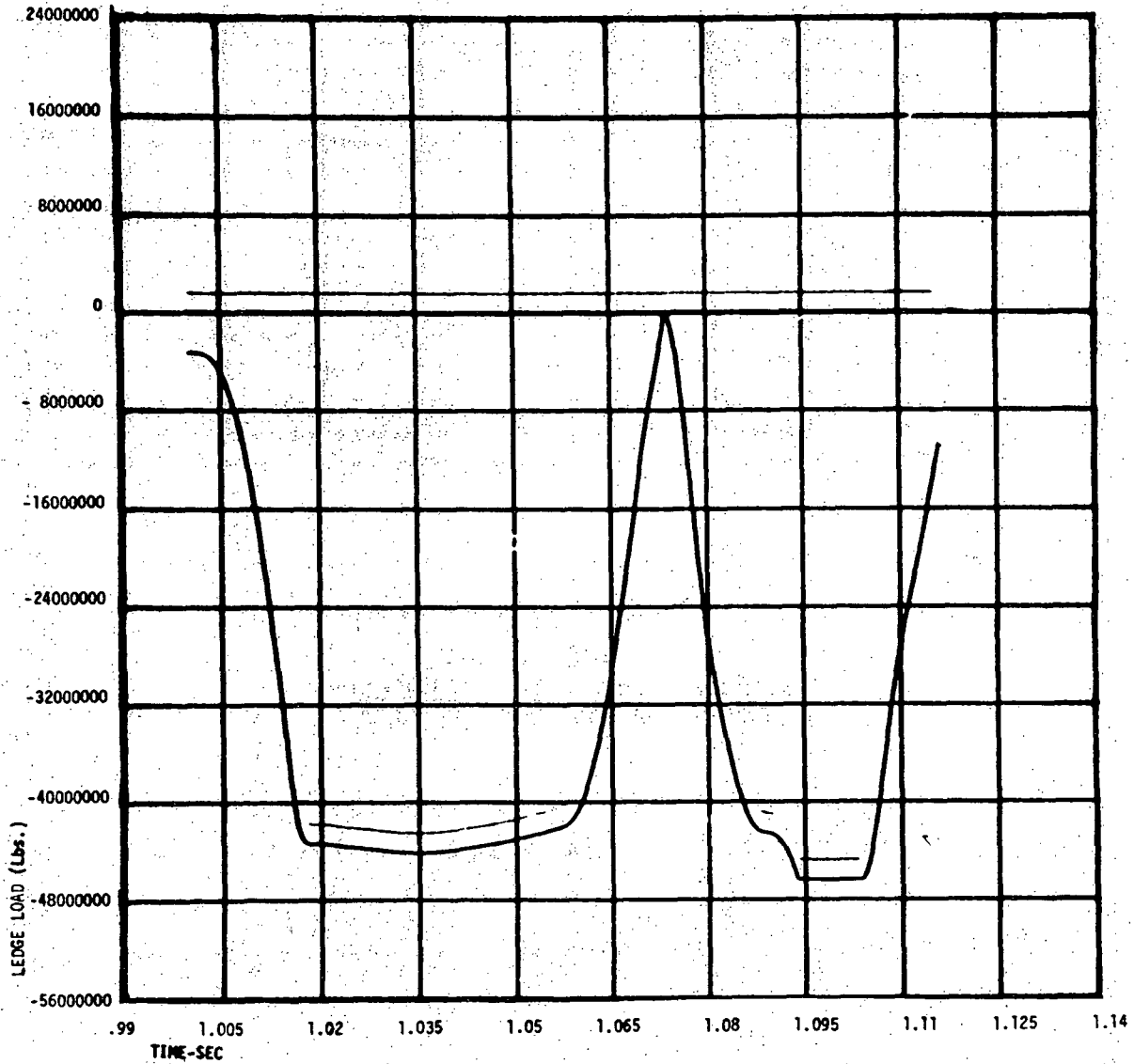


FIGURE 3.6.4-3
CASE 3 ENERGETIC
EXPERIMENTAL SHEAR RING PROPERTIES
CONCRETE LEDGE AND BOLT FORCE

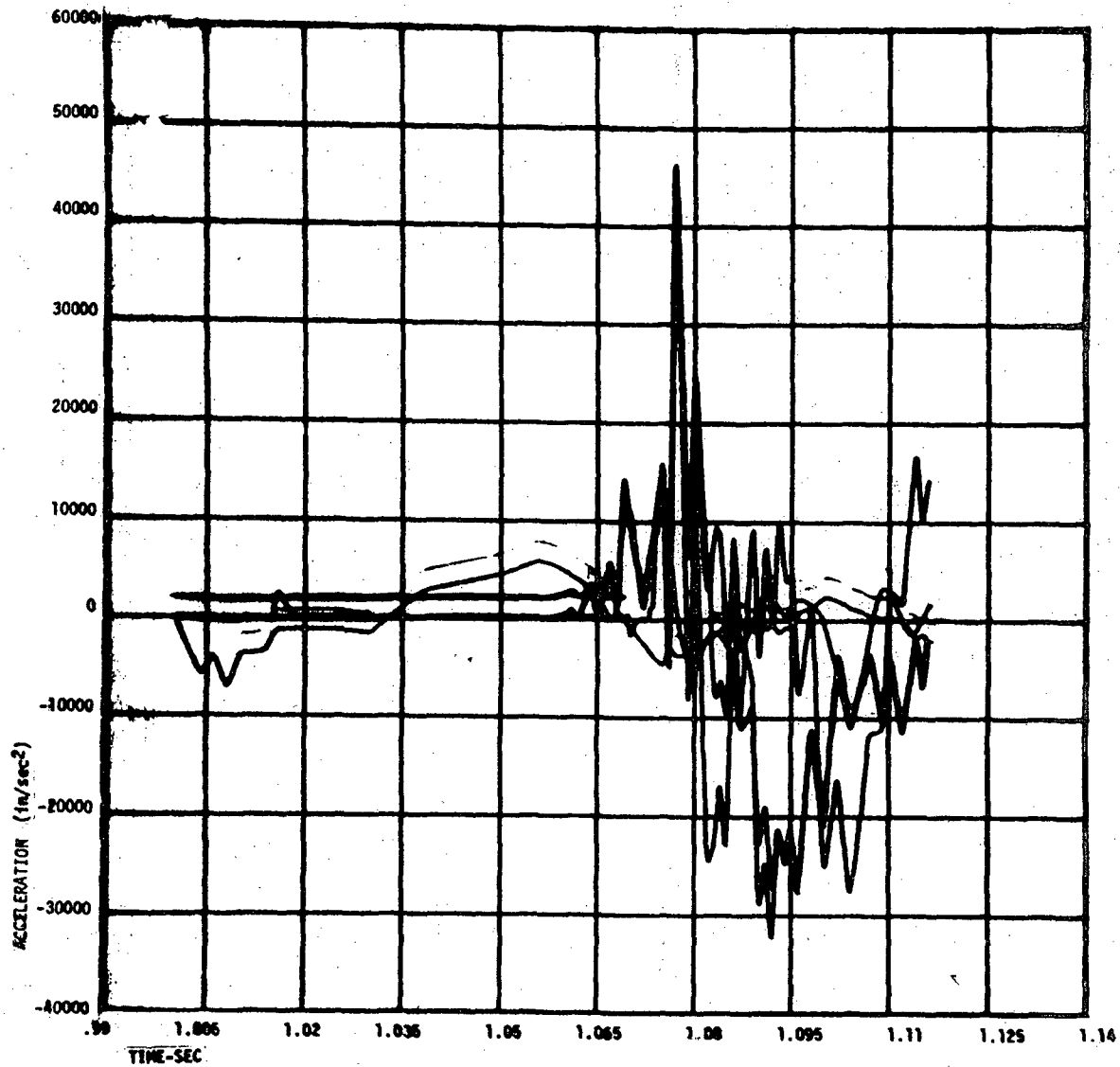


FIGURE 3.6.4-4
CASE 3 ENERGETIC
EXPERIMENTAL SHEAR RING PROPERTIES
ACCELERATIONS

3.6.5 Case 4

The 1D CRBRP response to the Case 4 energetics was derived with the ANSYS program by restarting the gravity solution at time ($t = 1$ second). The Case 4 energetic force time-history data (Table 3.5.4-1) was advanced in time (1 second) and arranged in 44 analysis load steps with a total of 1500 iterations. Integration time step, plug and CSP forces, and gravity procedures were identical to those described for Case 1.

The absolute Case 4 displacements of the SRP, IRP, LRP, flange and CSP are illustrated in Figure 3.6.5-1.

The Case 4 energetic response showed that the SRP, IRP, and LRP shear ring deformations were linear elastic. Respective forces are illustrated in Figure 3.6.5-2.

The Case 4 response in terms of downward acting concrete ledge load and upward acting vessel flange bolt forces is illustrated in Figure 3.6.5-3.

The Case 4 accelerations of the SRP, IRP, LRP, flange, and CSP are illustrated in Figure 3.6.5-4.

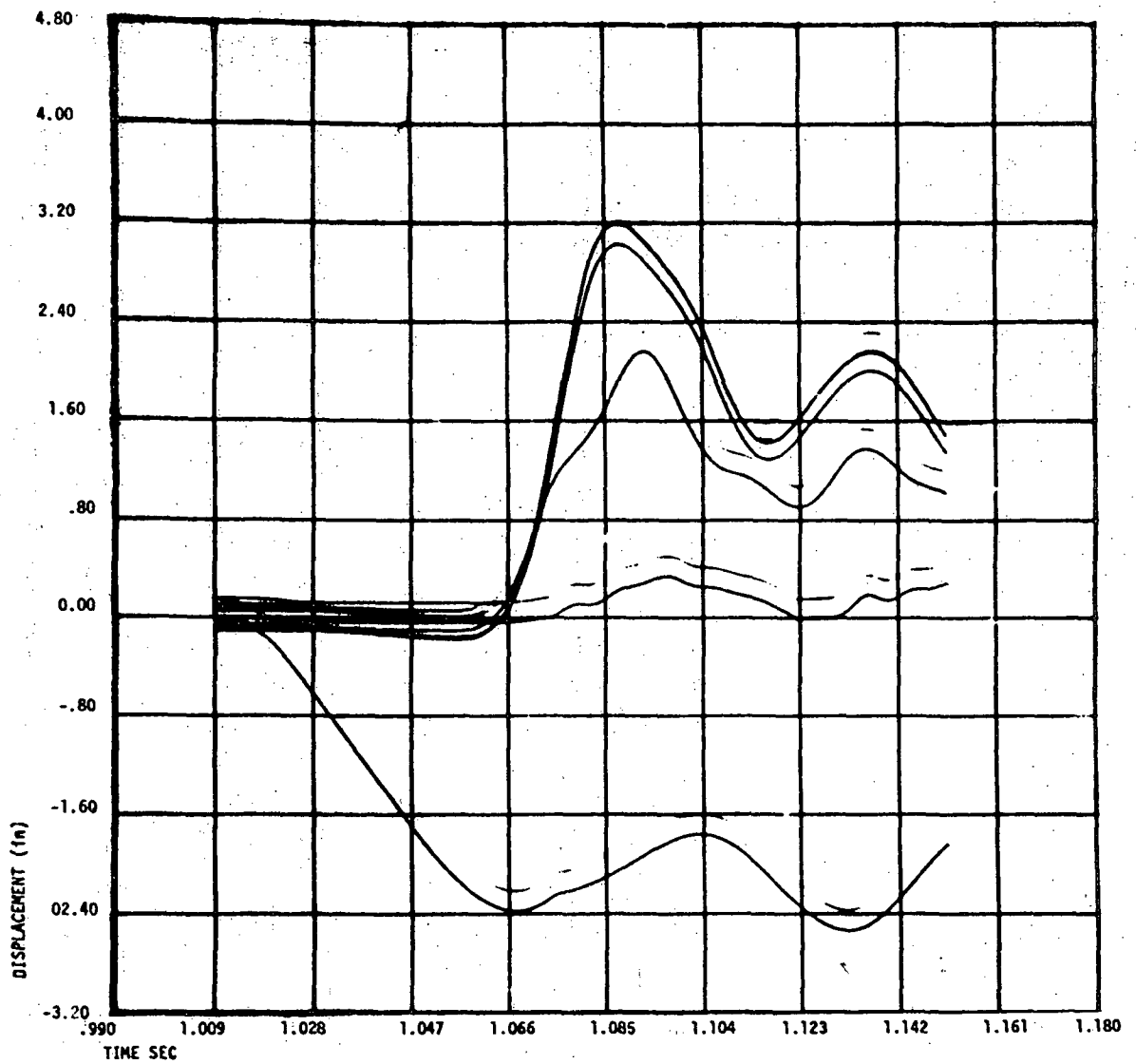


FIGURE 3.6.5-1
CASE 4 ENERGETIC
EXPERIMENTAL SHEAR RING PROPERTIES
ABSOLUTE DISPLACEMENTS

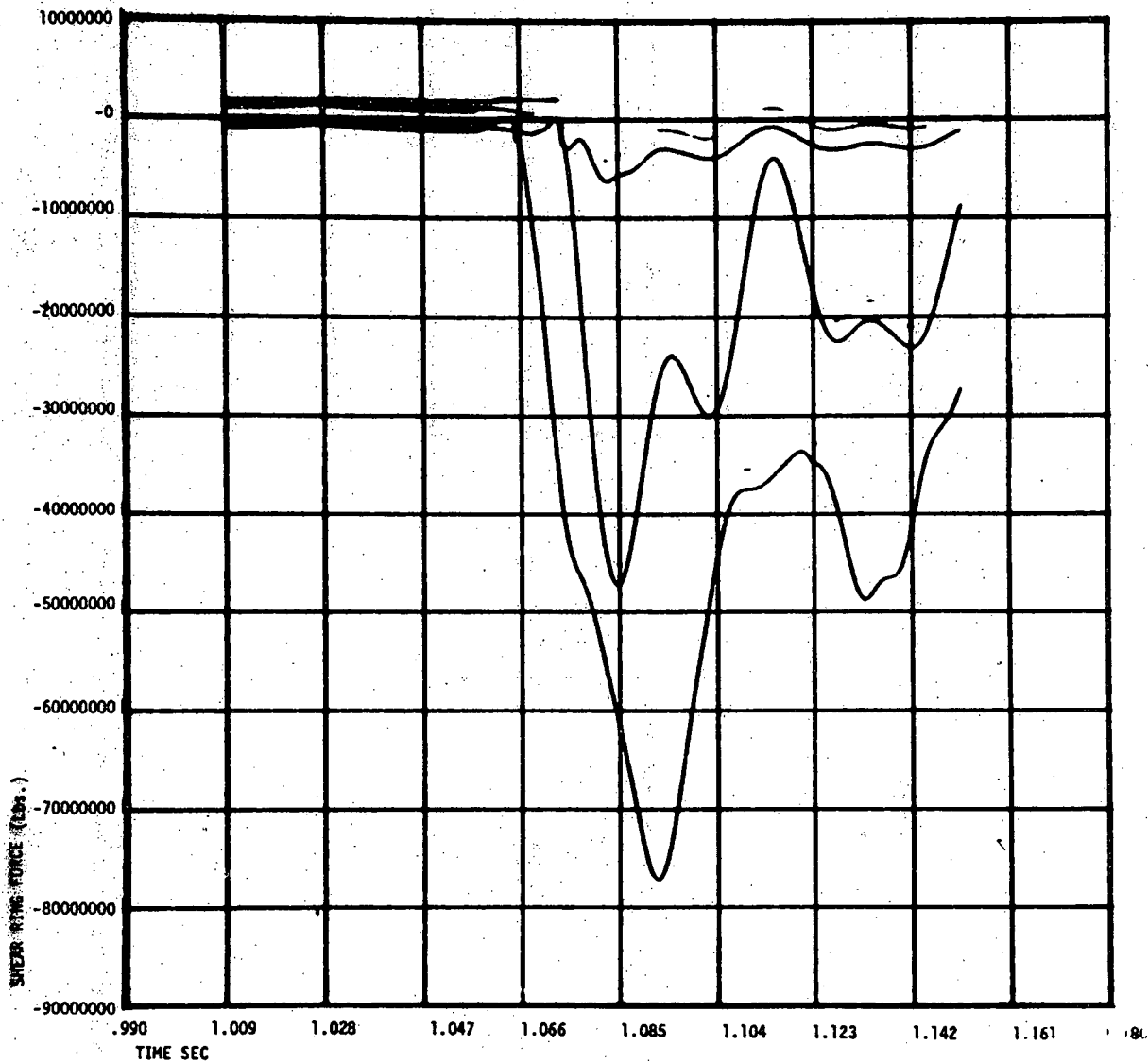


FIGURE 3.6.5-2
CASE 4 ENERGETIC
EXPERIMENTAL SHEAR RING PROPERTIES
SHEAR RING FORCES

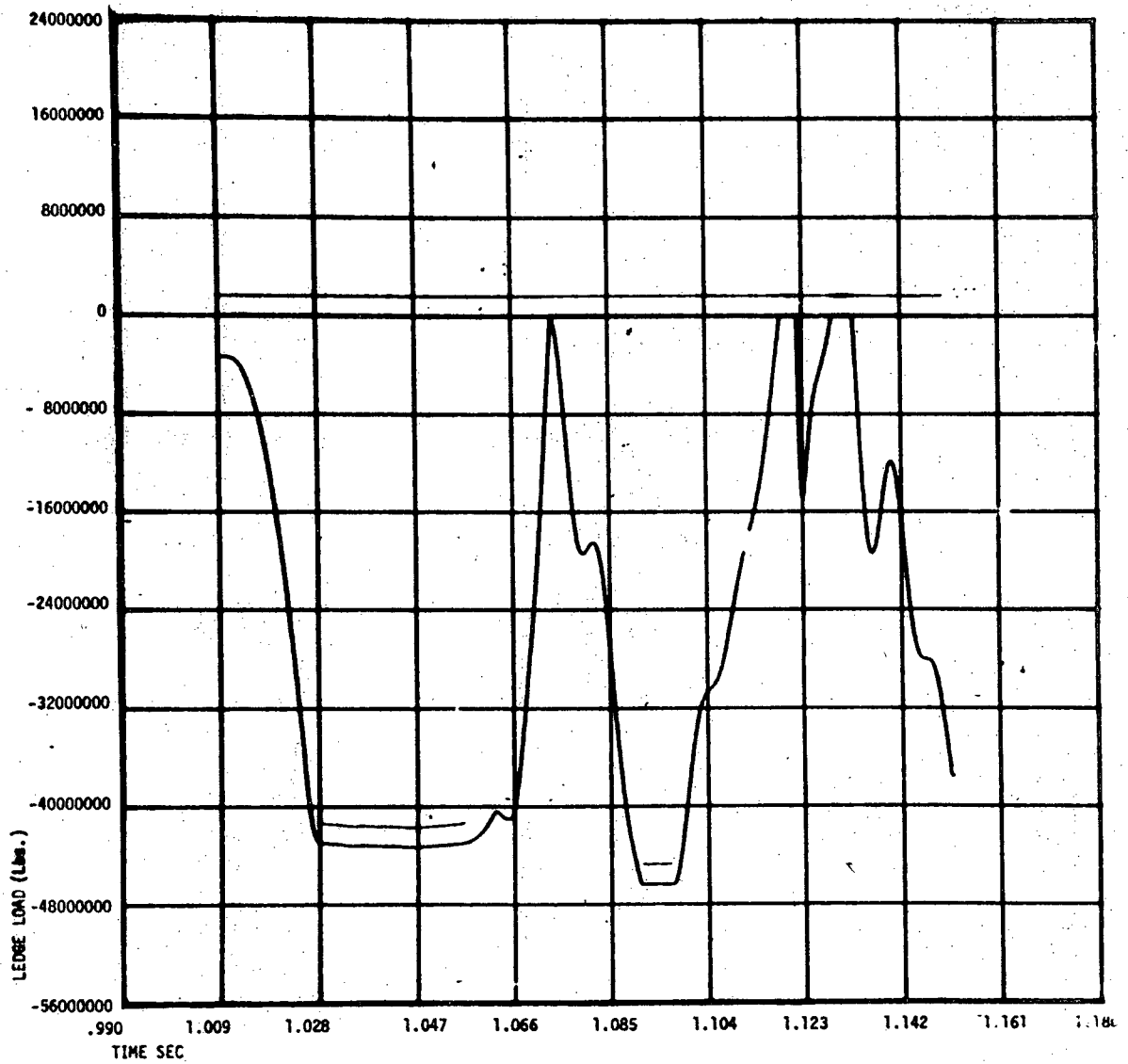


FIGURE 3.6.5-3
CASE 4 ENERGETIC
EXPERIMENTAL SHEAR RING PROPERTIES
CONCRETE LEDGE AND BOLT FORCE

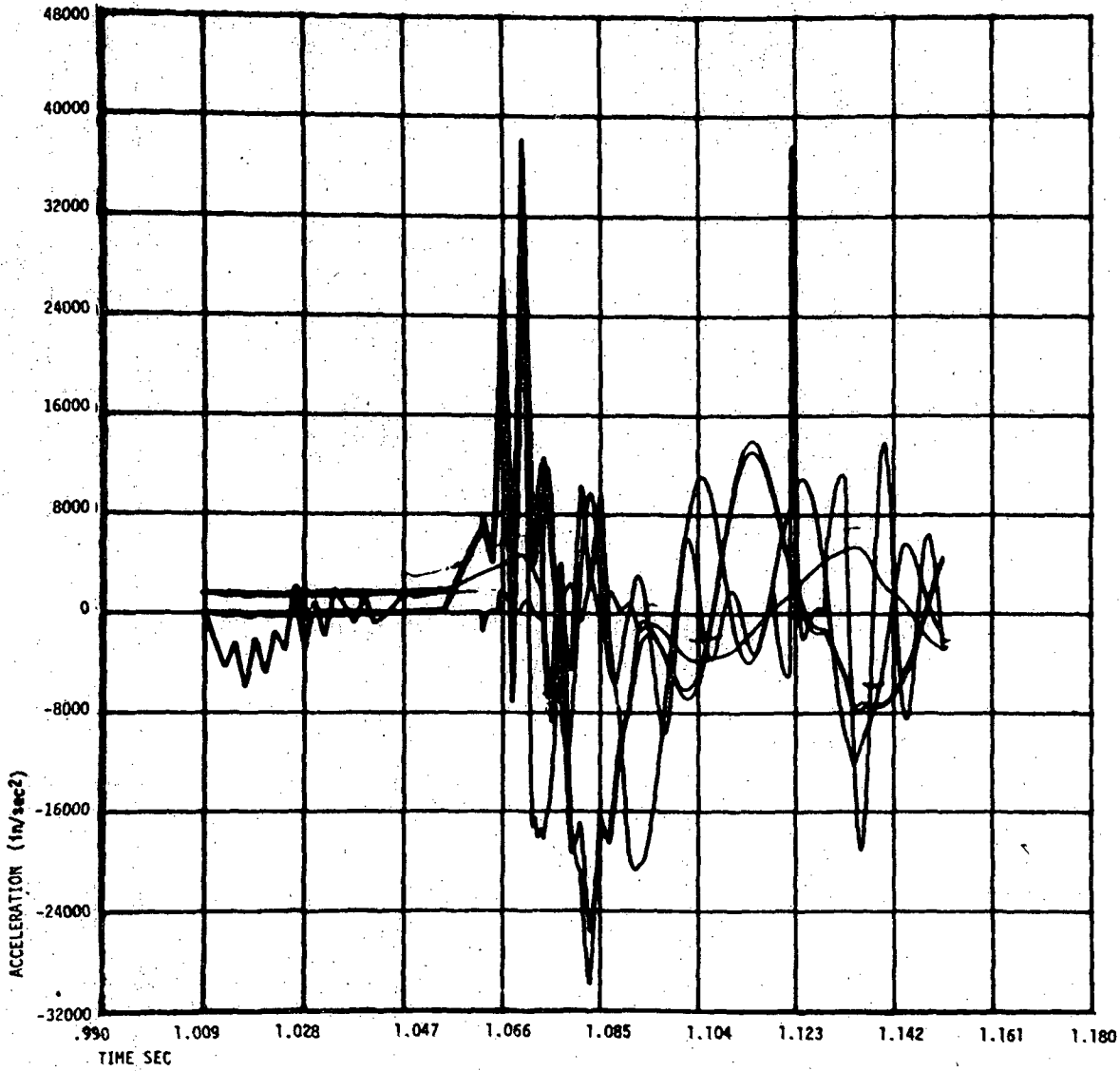


FIGURE 3.6.5-4
CASE 4 ENERGETIC
EXPERIMENTAL SHEAR RING PROPERTIES
ACCELERATIONS

3.6.6 Summary and Conclusions

The 1D CRBRP response to HCDA energetics for the experimental shear ring properties in terms of peak accelerations, peak forces, and plastic deformations are summarized in Tables 3.6.6-1, -2, and -3 respectively.

Conclusions based on the HCDA energetic response results are as follows.

Peak accelerations increase from Case 1 to Case 2 energetics. Case 3 has the lowest acceleration. However, the Case 4 peak accelerations are less than any other values although the energy in Case 4 is the largest of all. This is so, because the peak accelerations are, in all cases, mass limited. Accordingly, the energetic time-histories with the greatest peak forces also produce the greatest peak accelerations. The peak forces in the Case 1, 2, 3 & 4 time histories in terms of total head force are 750, 890, 600 and 480×10^{11} dynes respectively. Thus, peak Case 4 accelerations are minimum for the HCDA energetics analyzed.

Peak forces for the HCDA energetics reflect the peak acceleration response in the case of the SRP, IRP, and LRP shear rings. For the vessel flange bolts, only in the SDB energetic do the bolts remain elastic. The vessel wall yield force was reached in all HCDA energetics. Downward concrete ledge loads were essentially the same and less than 50×10^6 lbs for all energetics.

Plastic deformations of the SRP, IRP, and LRP shear rings were not accumulated in any of the HCDA energetics analyzed. This is so, because the experimental shear ring yield forces are greater than the SRP, IRP, and LRP forces in the HCDA energetic time-histories. The Case 3 energetic is most severe in terms of vessel wall stretching even though the total energy release in Case 3 is the lowest of all cases considered.

Table 3.6-1
EXPERIMENTAL SHEAR RING PROPERTIES
PEAK ACCELERATIONS (G)

CRBRP COMPONENT	HCDA ENERGETIC			
	CASE 1	CASE 2	CASE 3	CASE 4
SRP	152	182	120	99
IRP	131	157	101	83
LRP	171	206	119	74
VESSEL FLANGE	20	54	28	28
CSP	11	12	12	23

Table 3.6-2
EXPERIMENTAL SHEAR RING PROPERTIES
PEAK FORCES ($\sim 10^6$ LBS)

CRBRP COMPONENT	HCDA ENERGETIC			
	CASE 1	CASE 2	CASE 3	CASE 4
SRP SHEAR RING	6.32	6.82	6.14	6.26
IRP SHEAR RING	45.94	53.43	47.90	47.28
LRP SHEAR RING	68.50	80.58	71.70	77.07
FLANGE BOLTS	32.94	46.37	46.37	46.37
VESSEL WALL	40.36	40.36	40.36	40.36
CONCRETE LEDGE	42.90	43.10	44.14	43.33

Table 3.6-3
EXPERIMENTAL SHEAR RING PROPERTIES
 PLASTIC DEFORMATIONS (~ in.)

CRBRP COMPONENT	HCDA ENERGETIC			
	CASE 1	CASE 2	CASE 3	CASE 4
SRP SHEAR RING	0.0	0.0	0.0	0.0
IRP SHEAR RING	0.0	0.0	0.0	0.0
LRP SHEAR RING	0.0	0.0	0.0	0.0
FLANGE BOLTS	0.0	0.248	0.115	0.077
VESSEL WALL	0.948	1.103	2.504	2.296

3.7 Structural Criteria

The structural criteria are presented and discussed in Section 1.1.

3.8 Margins of Safety

The resulting margins of safety are included in Table 2.0-1.

4.0 CRDM, RISERS, AND SEISMIC SUPPORT

The evaluation of the CRBRP in relation to the limiting HCDA for the CRDM, risers, and seismic support is presented in this section. The energetics considered are the four cases previously described. The method of analysis employs only comparison of the SDB energetic response used in previous HCDA analysis with the SDB and other three cases responses derived with the 1D CRBRP model presented in this report. As the CRDM, risers, and seismic support are head mounted components, the peak plug accelerations as derived with the 1D CRBRP model are used to provide the basis of comparison from which judgements are made as to the results that could be expected for the various energetics. Structural criteria are presented and margins of safety computed.

4.1 Analysis and Results

Previous structural evaluation of the CRDM, risers, and seismic support were based on the 3D closure head response to the SDB energetic. The 3D closure head model assumed minimum possible shear ring yield forces and higher linear elastic stiffnesses than those found in the recent experimental tests. The 1D CRBRP model response for minimum possible shear ring yield forces and the linear elastic shear ring stiffnesses used in the previous 3D closure head analysis are presented in Appendix A of this report. A review of the SRP, IRP, and LRP peak accelerations shows that the Case 2 energetic is more severe than the other energetics. The ratio of the peak Case 2 accelerations to the peak SDB accelerations for the SRP, IRP, and LRP are derived from Table A.3-1. The ratio (R) for the SRP,

$$R_{SRP} = \frac{(A_{SRP})_{Case\ 2}}{(A_{SRP})_{Case\ 1}}$$

$$R_{SRP} = \frac{182}{152} = 1.20$$

Similarly, for the IRP and LRP

$$R_{IRP} = \frac{157}{131} = 1.20$$

$$R_{LRP} = \frac{206}{171} = 1.20$$

It is of interest to note that the peak plug accelerations for the 1D response with the experimental shear ring properties (Section 3.0) are virtually identical to those for minimum possible shear ring yield forces (Appendix A). This is so, as the peak plug accelerations are mass limited and occur prior to shear ring impact.

The approach taken in extending the previous SDB response results to the more severe Case 2 energetic is to linearly increase the relevant structural response parameter by a 1.20 factor. As a first approximation, this approach is justifiable as the shape and duration of the acceleration content is not significantly different between the four cases in terms of SRP, IRP, and LRP motions. The relevant response parameter for the CRDM is the peak strain in the nozzle extension. For the SRP, IRP, and LRP risers, the relevant response parameters are the strains in the bolts which secure the risers to the respective plugs. In the case of the seismic support, the strains in the bolts that secure the seismic support to the IRP are of interest. The Case 2 response as an upper bound to all cases is presented in Table 4.1-1.

Table 4.1-1

Case 2 Energetic
Scaled Response Results

COMPONENT		Case 2 STRAIN (in/in)	SDB STRAIN (in/in)
CRDM NOZZLE EXTENSION		0.0173	0.0144
RISER BOLTS	SRP	0.0042	0.0035
	IRP	0.0042	0.0035
	LRP	0.0106	0.009
SEISMIC SUPPORT BOLTS		0.0456	0.038

4.2 Margins of Safety

The HCDA Margins of Safety for the CRDM, riser bolts, and seismic support bolts are based on 70% of the available strain at the point of tensile instability on the conventional stress-strain curve of the respective materials. For the CRDM nozzle extension (SA-304-SS), the allowable strain is $0.7(0.19) = 0.132$ in/in. In the case of the riser and seismic support bolts (SA-540), the allowable strain is $0.7(.1) = 0.07$ in/in. The Case 2 energetic, as an upper bound to all HCDA energetics, is used to establish the margins of safety (MS) summarized in Table 4.2-1.

Table 4.2-1

HCDA MARGINS OF SAFETY

COMPONENT		CALCULATED CASE 2 STRAIN	ALLOWABLE STRAIN	M.S.*
CRDM NOZZLE EXTENTION		0.0173	0.132	6.63
RISER BOLTS	SRP	0.0042	0.07	15.67
	IRP	0.0042	0.07	15.67
	LRP	0.0108	0.07	5.48
SEISMIC SUPPORT BOLTS		0.0456	0.07	0.54

$$* MS = \frac{\text{ALLOWABLE STRAIN}}{\text{CALCULATED STRAIN}} - 1$$

APPENDIX A

MINIMUM POSSIBLE SHEAR RING YIELD FORCES

A.1 INTRODUCTION AND PURPOSE

A.2 ANALYSIS AND RESULTS

A.2.1 GRAVITY

A.2.2 CASE 1 - SDB

A.2.3 CASE 2

A.2.4 CASE 3

A.2.5 CASE 4

A.3 SUMMARY AND CONCLUSIONS

A.1 INTRODUCTION AND PURPOSE

The 1D CRBRP closure head response analysis and results for the various energetics for minimum possible shear ring yield properties is presented in this appendix. The minimum possible SRP, IRP, and LRP Shear Ring Yield Forces are 7.13×10^6 , 22.02×10^6 , and 35.59×10^6 lbs. Respective stiffnesses and damping are (411; 1075; and 1552×10^6 lb/in) and (47,575; 175,80; and 270,210 LB-SEC IN). The shear ring gaps considered in the analysis are 1/8 in. nominal. Otherwise, the method of analysis, assumptions, model, dynamic properties, and loading conditions are identical to those described in the body of this report. The results provide a basis for extending previous HCDA results for SDB and Case 3 to Cases 2 and 4.

A.2 ANALYSIS AND RESULTS

A.2.1 GRAVITY

The gravity response is required to provide the initial conditions for the dynamic response of the various energetics. The gravity solution was derived with the ANSYS program using the Non-Linear Transient Analysis (Type 4) option. The solution was obtained using the exact same procedure for load steps and cumulative iterations described in Section 3.6.1 of this report.

The gravity deflections of the vessel (CSP), LRP, IRP, SRP, and vessel flange are illustrated in Figure A.2.1-1. Corresponding velocities and accelerations are illustrated in Figure A.2-2 and -3 despectively. The gravity solution is completely elastic without plastic shear ring, vessel wall, and vessel flange bolt deformations.

The concrete ledge load under gravity is illustrated in Figure A.2.1-4. The load in the vessel wall under gravity is illustrated in Figure A.2.1-5. The gravity load on the SRP, IRP, and LRP bearings is illustrated in Figure A.2.1-6.

A review of the CRBRP gravity deflections and loads shows that the free vibrations associated with the method of solution are essentially attenuated to 1G values by system damping after 1 second. Accordingly, the responses as obtained by performing ANSYS restarts do not sacrifice any accuracy and are an acceptable method of including gravity in the respective HCDA response.

A.2.2 CASE 1 - SDB

The 1D CRBRP response to the SDB energetic was derived with the ANSYS program by restarting from the gravity solution at time ($t = 1$ second).

The absolute displacements of the SRP, IRP, LRP, Flange, and CSP are illustrated in Figure A.2.2-1.

The SRP, IRP, and LRP shear ring plastic deformations are illustrated in Figure A.2.2-2. Respective forces are illustrated in Figure A.2.2-3.

The downward acting concrete ledge force and upward acting vessel flange bolt force are illustrated in Figure A.2.2-4.

The accelerations of the SRP, IRP, LRP, Flange, and CSP are illustrated in Figure A.2.2-5.

A.2.3 CASE 2

The 1D CRBRP response to the Case 2 energetic was derived with the ANSYS Program using the same procedure described for the SDB energetic.

The absolute displacements of the SRP, IRP, LRP, Flange and CSP are illustrated in Figure A.2.3-1.

The SRP, IRP, and LRP shear ring, plastic deformations are illustrated in Figure A.2.3-2. Respective forces are illustrated in Figure A.2.3-3.

The downward acting concrete ledge force and upward acting vessel flange bolt forces are illustrated in Figure A.2.3-4.

The accelerations of the SRP, IRP, LRP, Flange, and CSP are illustrated in Figure A.2.3-5.

A.2.4 CASE 3

The ID CRBRP response to the Case 3 energetic was derived with the ANSYS program using the same procedure described for the SDB energetic.

The absolute displacements of the SRR, LRP, IRP, Flange, and CSP are illustrated in Figure A.2.4-1.

The SRP, IRP, and LRP shear ring plastic deformations are illustrated in Figure A.2.4-2. Respective forces are illustrated in Figure A.2.4-3.

The downward acting concrete ledge force and upward acting vessel flange bolt forces are illustrated in Figure A.2.4-4.

The accelerations of the SRP, IRP, LRP, Flange, and CSP are illustrated in Figure A.2.4-5.

A.2.5 Case 4

The 1D CRBRP response to the Case 4 energetic was derived with the ANSYS program using the same procedure described for the SDB energetic. Case 4 energetic solution for minimum possible shear ring yield forces was obtained in computer run WMTVOMN. Microfiche are documented.

The absolute displacements of the SRP, IRP, LRP, flange, and CSP are illustrated in Figure A.2.5-1.

The SRP, IRP, and LRP shear ring plastic deformations are illustrated in Figure A.2.5-2. Respective forces are illustrated in Figure A.2.5-3.

The downward acting concrete ledge force and upward acting vessel flange bolt forces are illustrated in Figure A.2.5-4.

The accelerations of the SRP, IRP, LRP, flange, and CSP are illustrated in Figure A.2.4-5.

A.3 SUMMARY AND CONCLUSIONS

The 1D CRBRP response to the various HCDA energetics in terms of peak accelerations, peak forces, and total accumulated plastic deformations is presented in Tables A.3-1, -2, and -3.

A review of the acceleration results indicates that the most severe HCDA is the Case 2 energetic. The trend shows a general increase in severity from Case 3 to SDB to Case 2. However, the Case 4 is less severe than any other, even though Case 4 has the highest energy. This is so, as the peak accelerations are all mass limited (positive) and the peak head forces in the respective time histories increase from Case 3 (600×10^{11} dynes), SDB (750×10^{11} dynes), and Case 2 (890×10^{11} dynes). On the other hand, the peak head force for Case 4 (480×10^{11} dynes) is the least of all energetics.

The peak force results also show that the Case 2 energetic is more severe than the other energetics for the same reasons described for the peak accelerations.

The plastic shear ring deformations, however, show that the Case 4 energetic is most severe even though peak accelerations and forces are less severe than for the other energetics. This is so, as the force content in the Case 4 head force time history is generally greater than the minimum possible shear ring yield forces for the greater portion of the HCDA duration, thus, permitting more time for plastic deformations to accumulate.

Table A.3-1

MINIMUM POSSIBLE SHEAR RING YIELD FORCES
PEAK ACCELERATIONS (G)

COMPONENT	SDB	CASE 2	CASE 3	CASE 4
SRP	152	182	120	99
IRP	131	157	101	82
LRP	171	206	117	72
VESSEL FLANGE	20	57	29	27
CSP	11	13	12	23

Table A.3-2

MINIMUM POSSIBLE SHEAR RING YIELD FORCES
PEAK FORCES (10⁶ lbs)

COMPONENT	SDB	CASE 2	CASE 3	CASE 4
SRP SHEAR RING	7.13	7.13	7.13	7.13
IRP SHEAR RING	22.02	22.02	22.02	22.02
LRP SHEAR RING	35.59	35.59	35.59	35.59
FLANGE BOLTS	23.74	46.37	40.84	42.88
VESSEL WALL	40.36	40.36	40.36	40.36
CONCRETE LEDGE	42.90	43.03	44.14	43.33

Table A.3-3

MINIMUM POSSIBLE SHEAR RING YIELD FORCES
PLASTIC DEFORMATIONS (in.)

COMPONENT	SDB	CASE 2	CASE 3	CASE 4
SRP SHEAR RING	0.003	0.009	0.003	0.002
IRP SHEAR RING	0.609	0.899	0.650	0.667
LRP SHEAR RING	1.009	1.911	1.180	3.378
FLANGE BOLTS	0.0	0.007	0.0	0.0
VESSEL WALL	0.827	1.103	2.504	1.967

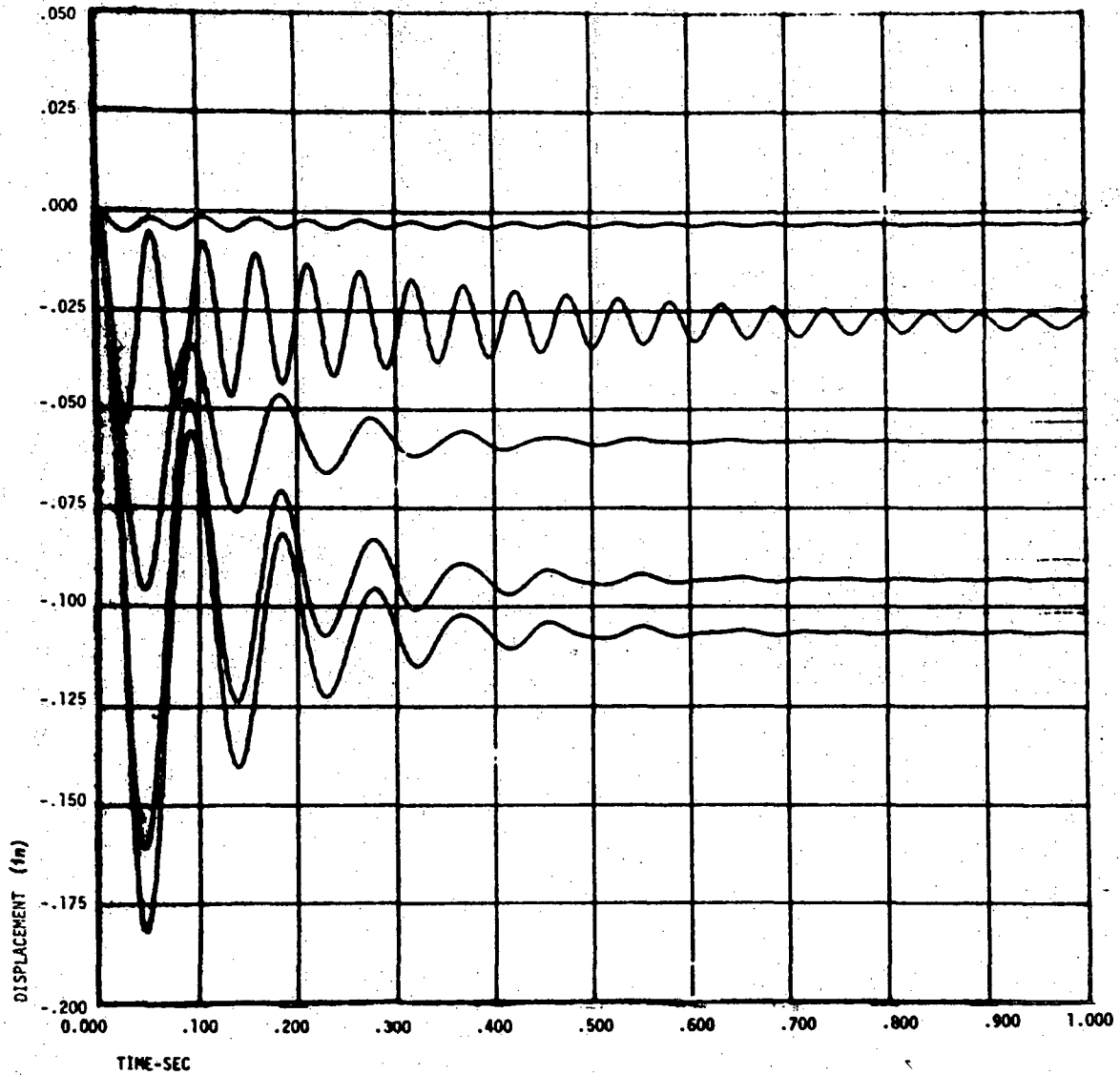


FIGURE A.2.1-1
MINIMUM POSSIBLE SHEAR RING YIELD FORCES
GRAVITY SOLUTION
PLUG AND VESSEL
DISPLACEMENTS

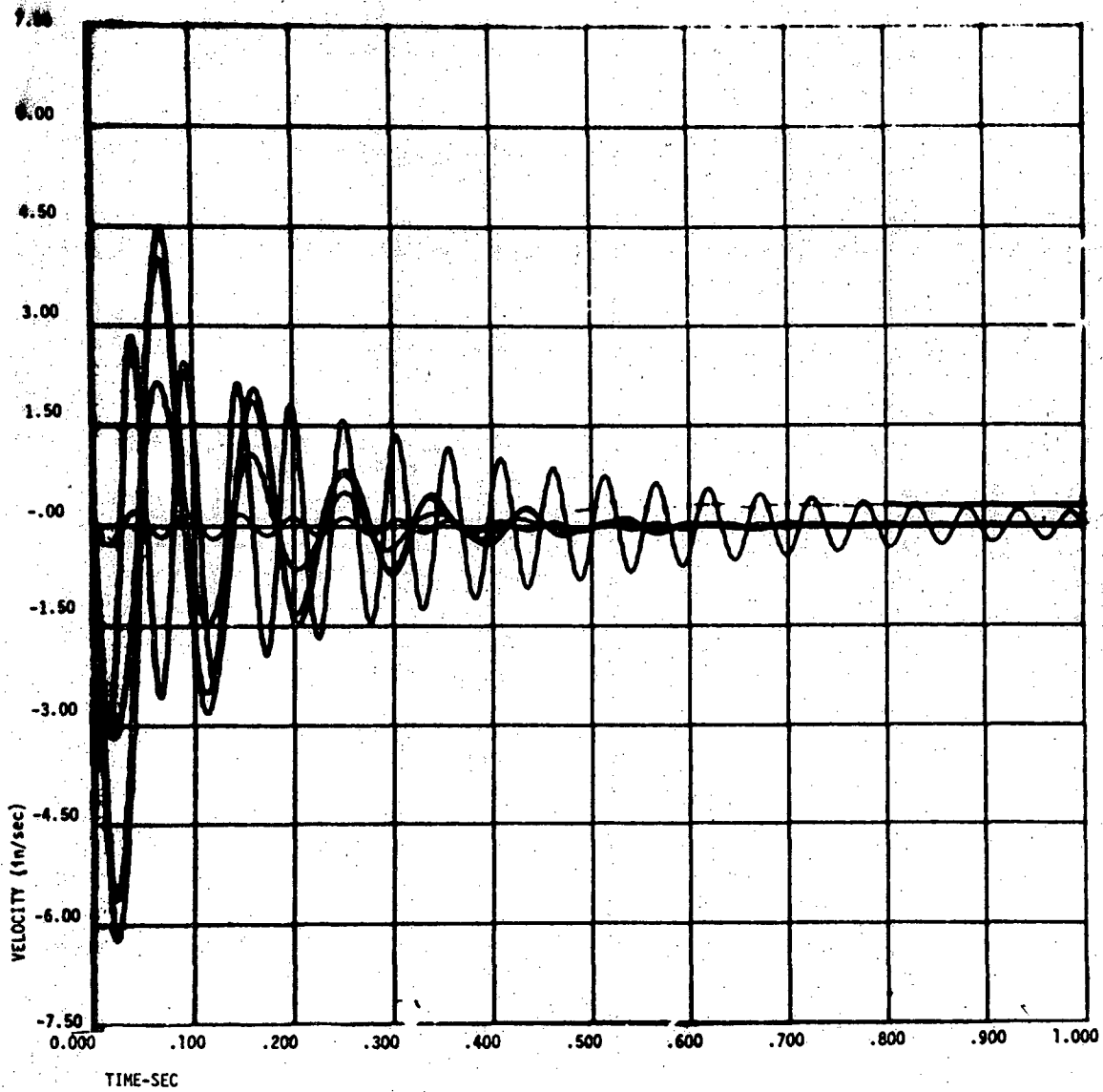


FIGURE A.2.1-2
MINIMUM POSSIBLE SHEAR RING YIELD FORCES
GRAVITY SOLUTION
PLUG AND VESSEL
VELOCITIES

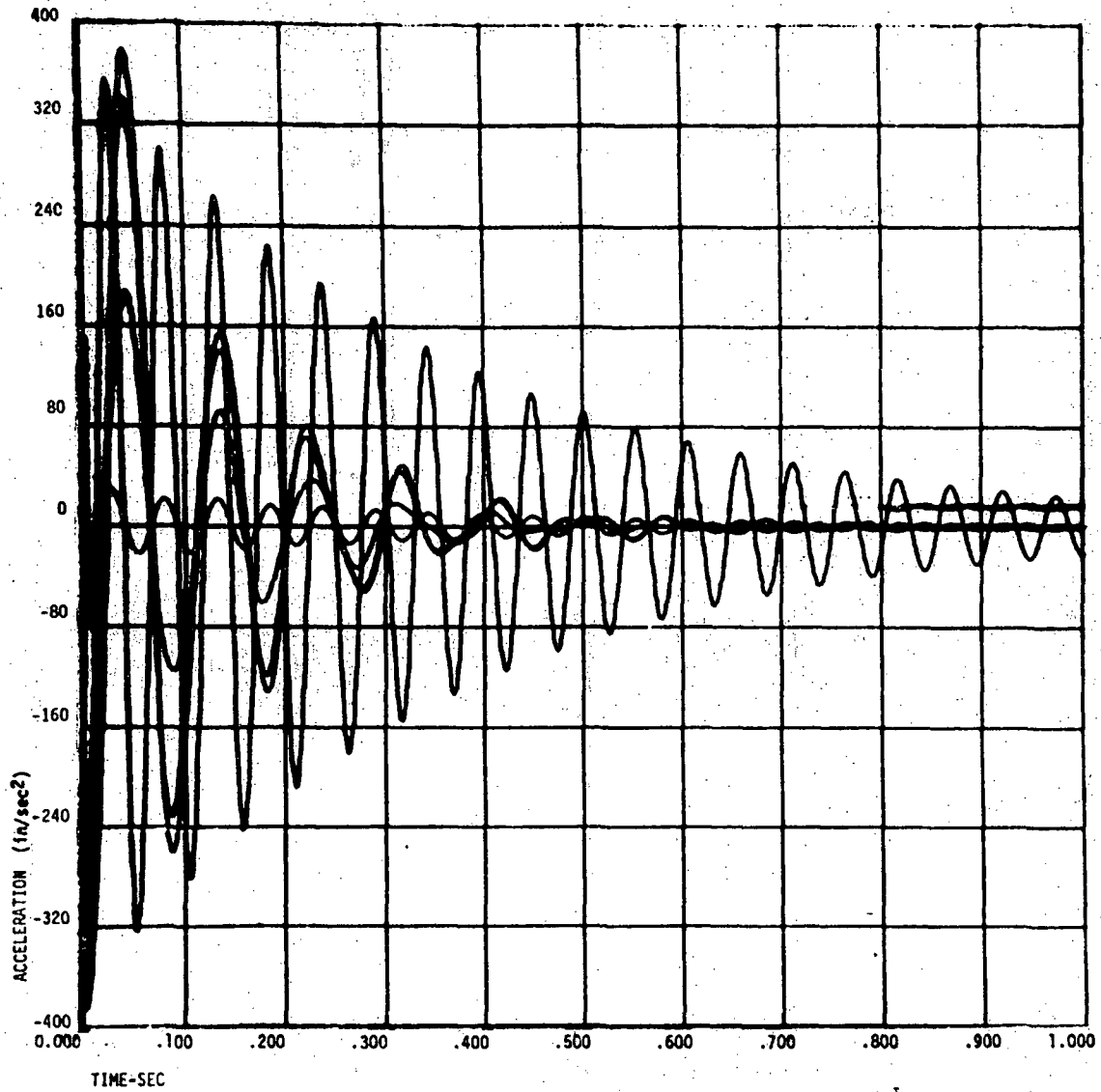


FIGURE A.2.1-3
MINIMUM POSSIBLE SHEAR RING YIELD FORCES
GRAVITY SOLUTION
PLUG AND VESSEL
ACCELERATIONS

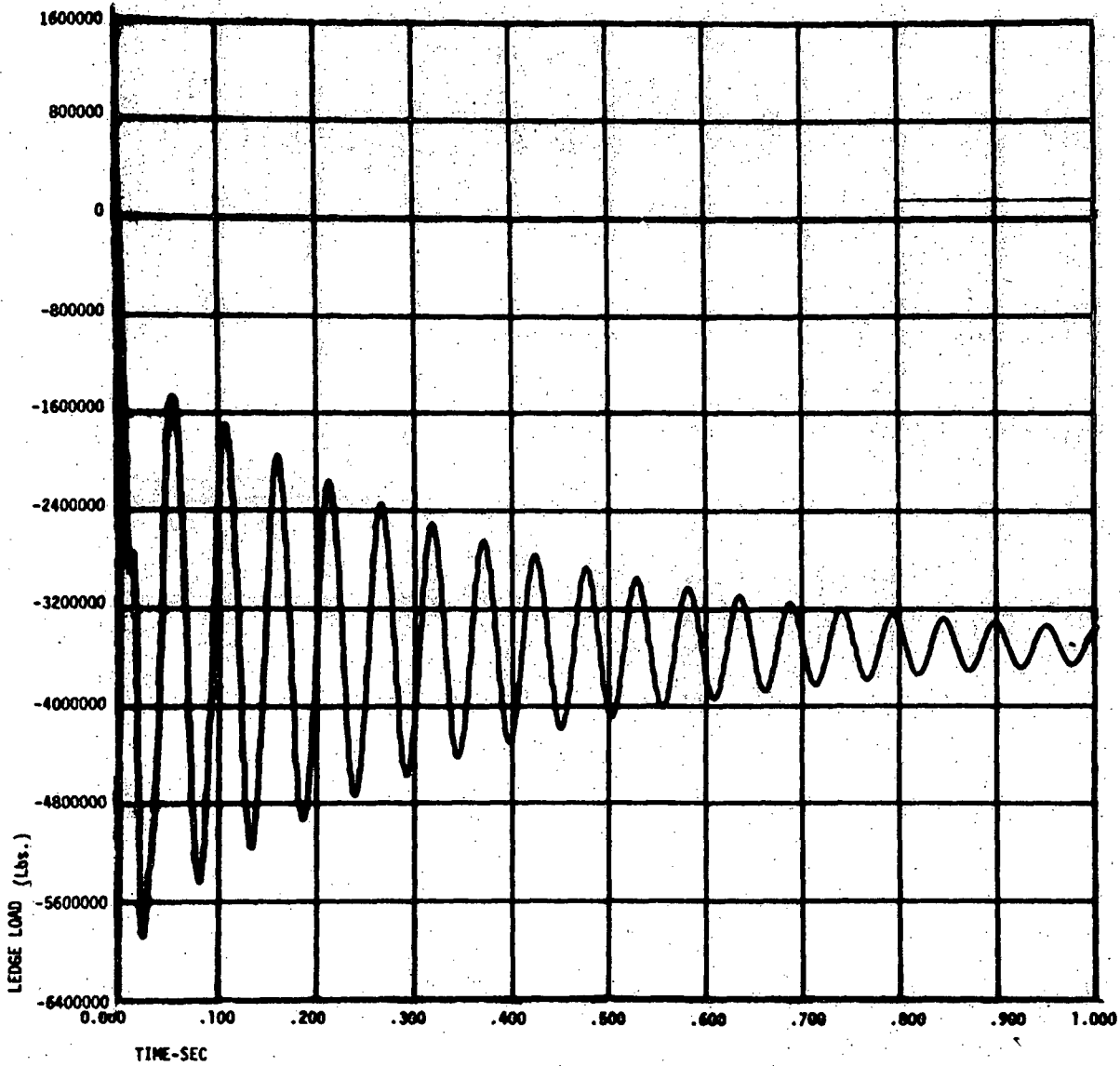


FIGURE A.2.1-4
MINIMUM POSSIBLE SHEAR RING YIELD FORCES
GRAVITY SOLUTION
CONCRETE AND BOLT LEDGE LOAD

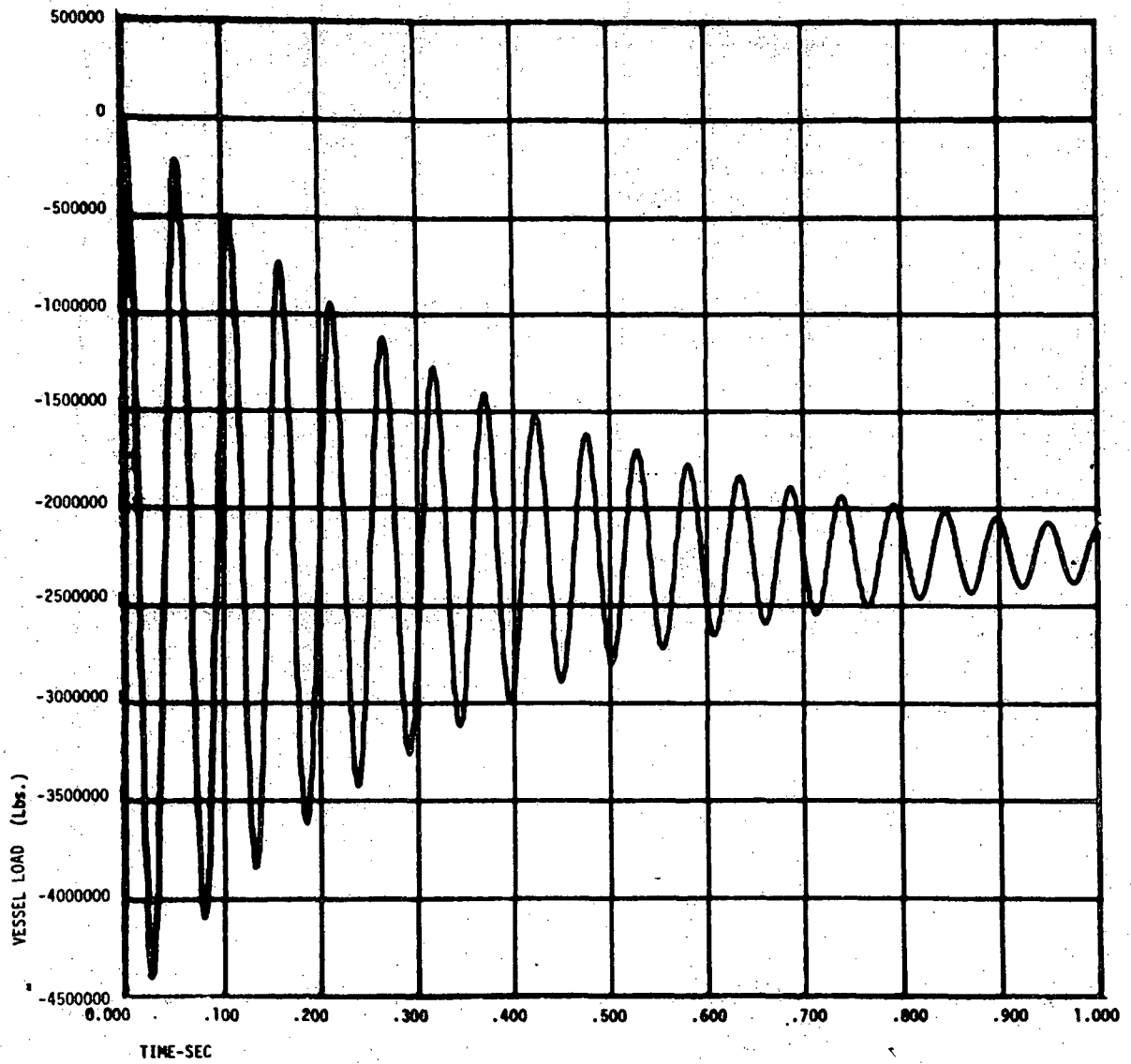


FIGURE A.2.1-5
MINIMUM POSSIBLE SHEAR RING YIELD FORCES
GRAVITY SOLUTION
VESSEL LOAD

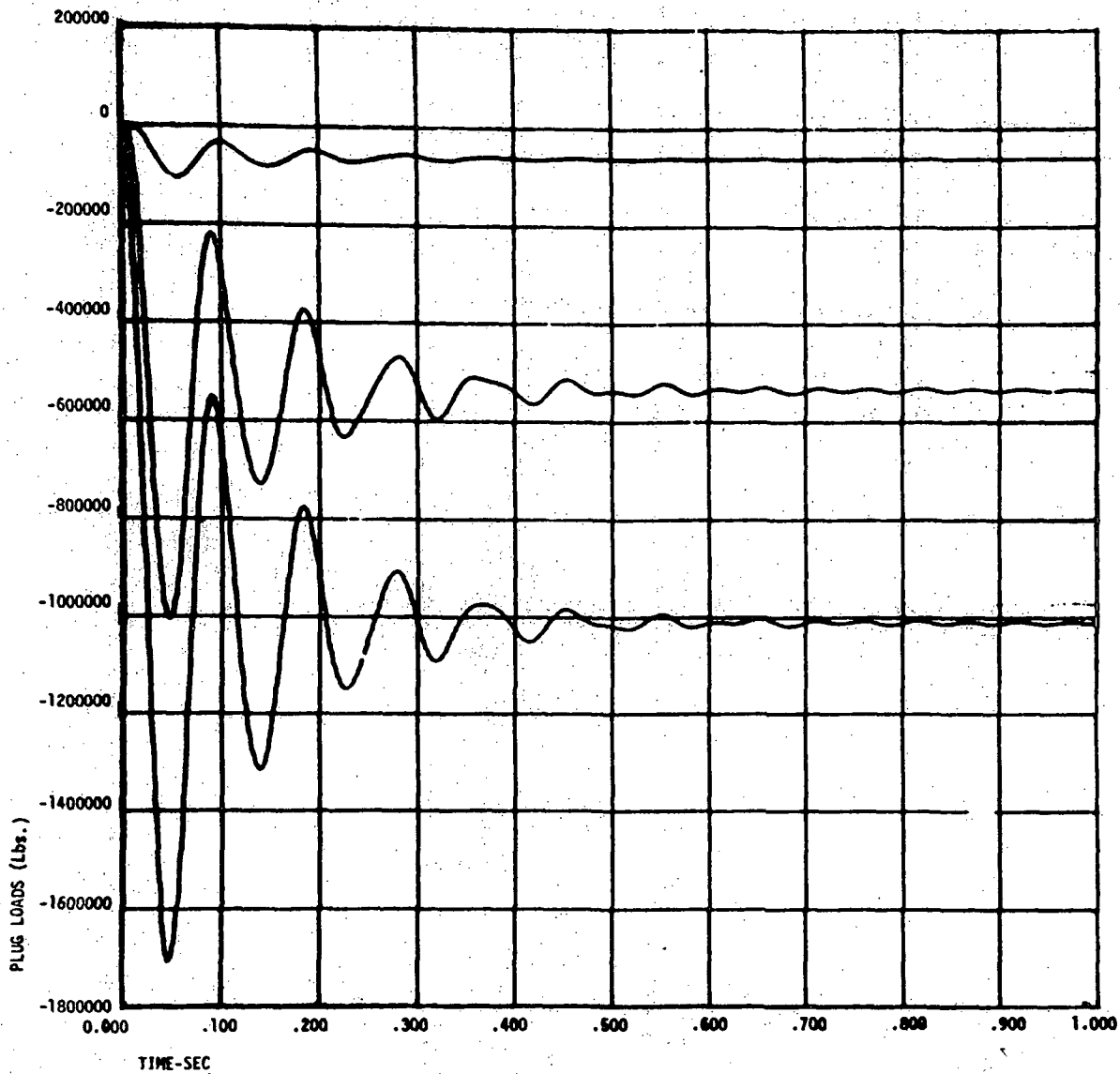


FIGURE A.2.1-6
MINIMUM POSSIBLE SHEAR RING YIELD FORCES
GRAVITY SOLUTION
PLUG BEARING LOADS

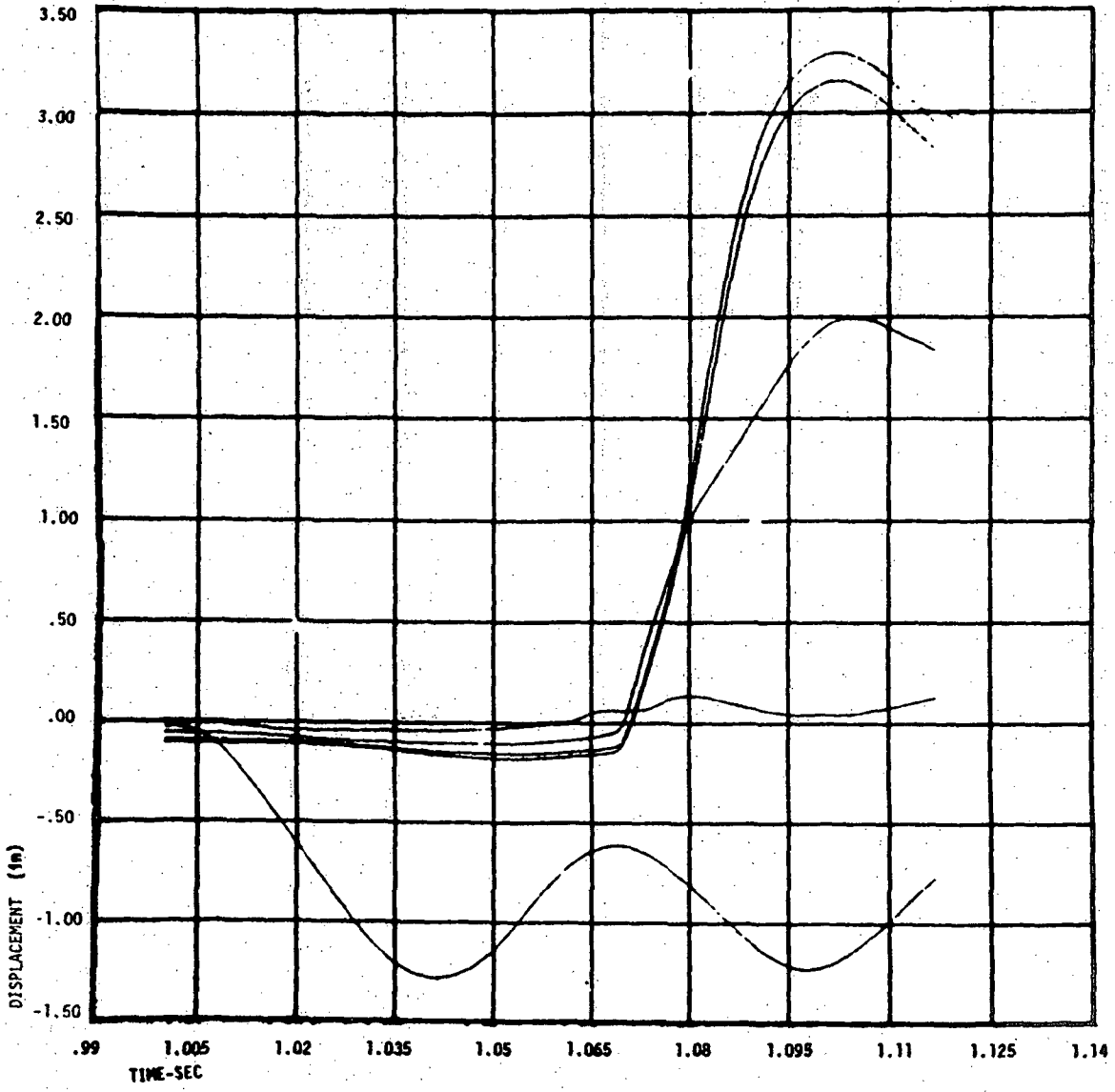


FIGURE A.2.2-1
SDB ENERGETIC
MINIMUM POSSIBLE SHEAR RING YIELD FORCES
ABSOLUTE DISPLACEMENTS

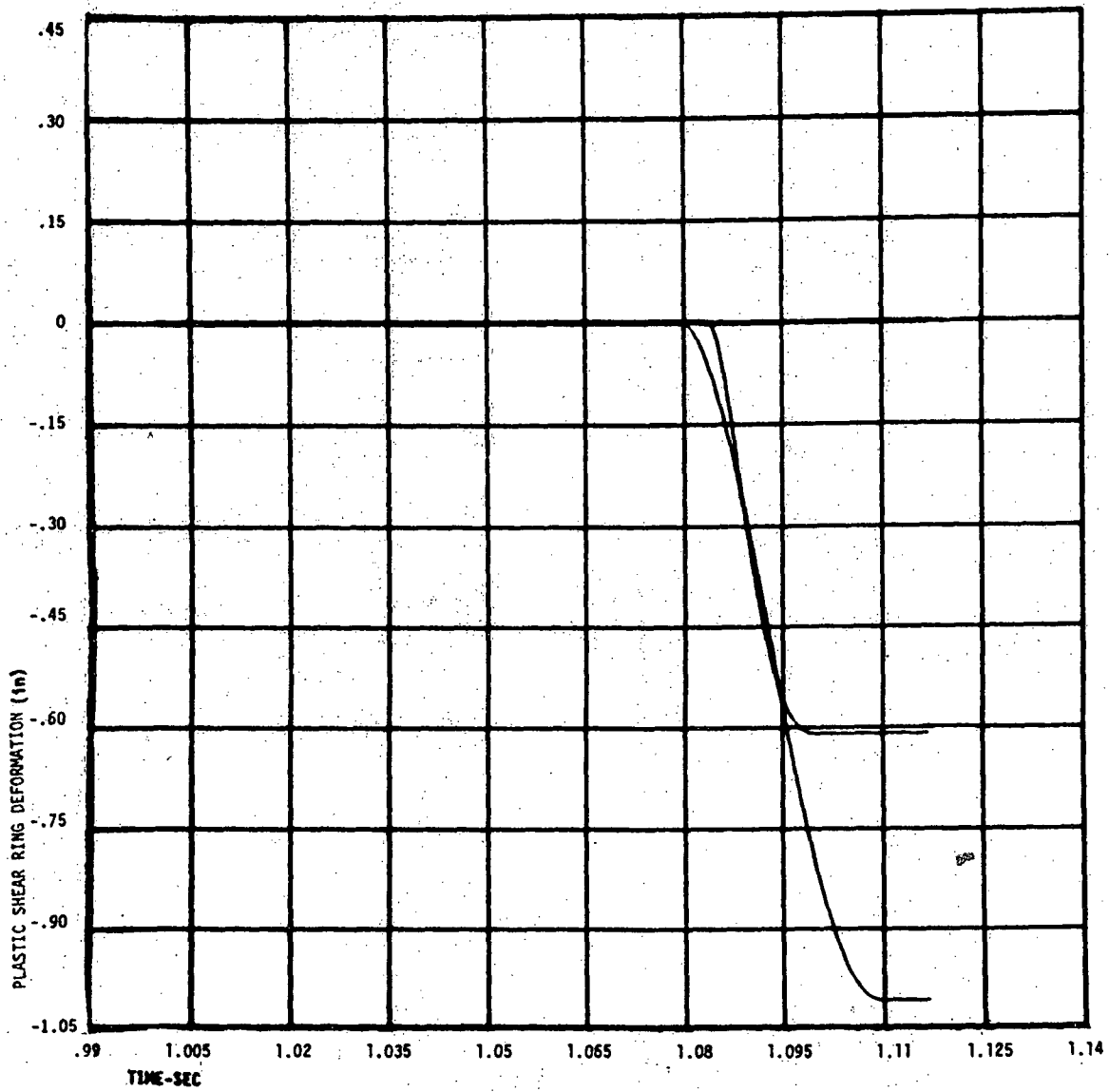


FIGURE A.2.2-2
SDB ENERGETIC
MINIMUM POSSIBLE SHEAR RING YIELD FORCES
PLASTIC SHEAR RING DEFORMATIONS

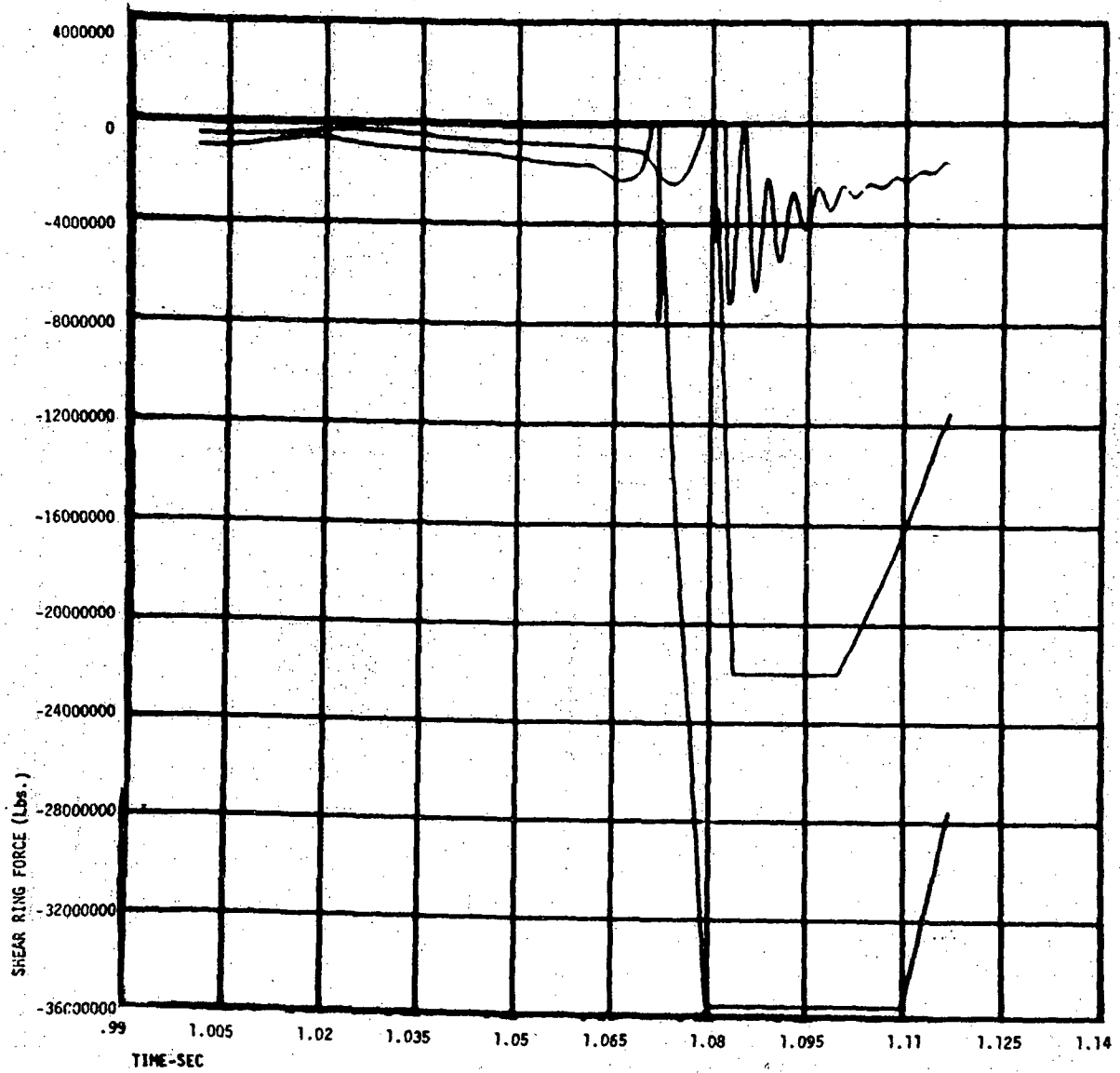


FIGURE A.2.2-3
SDB ENERGETIC
MINIMUM POSSIBLE SHEAR RING YIELD FORCES
SHEAR RING FORCES

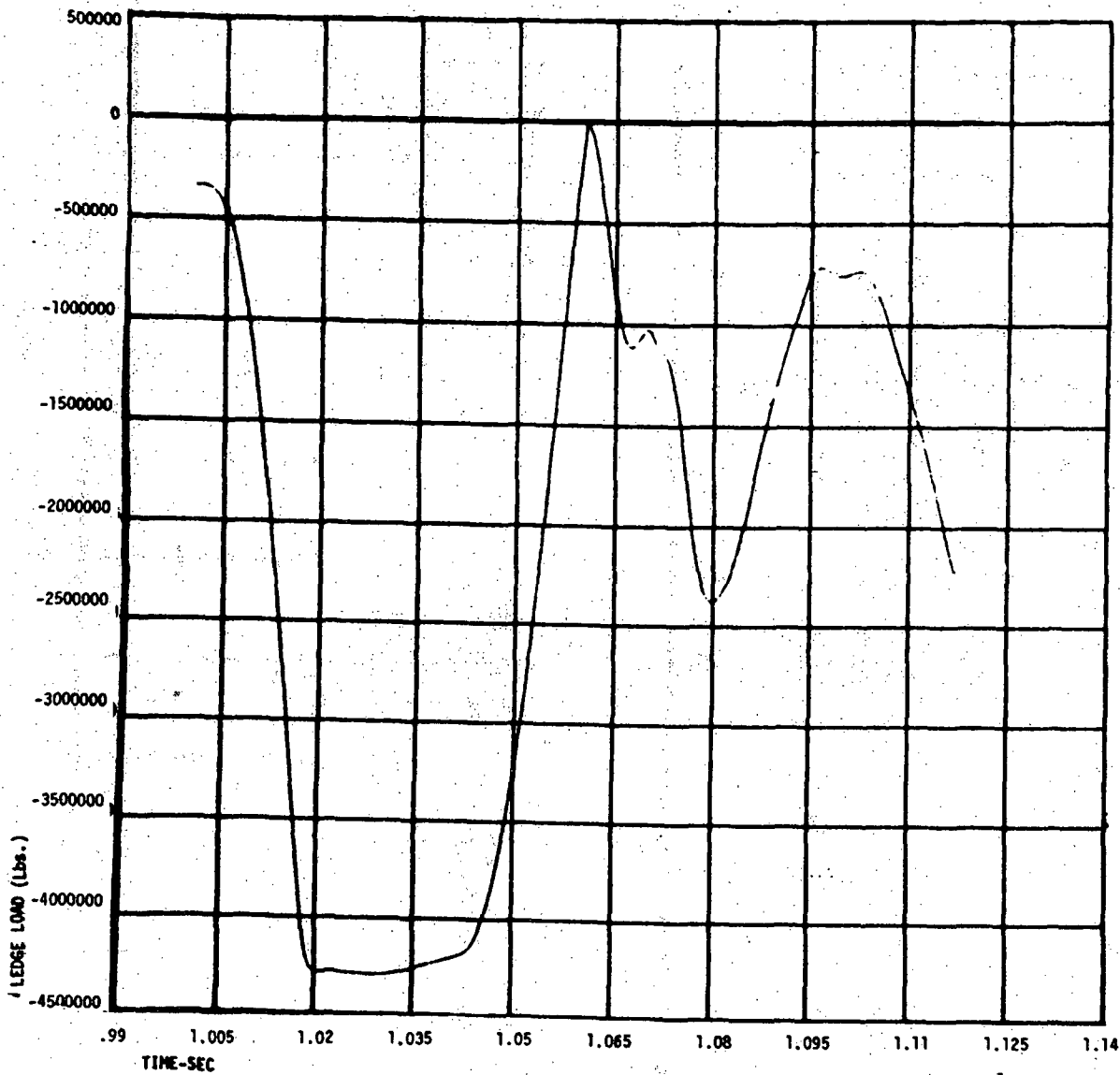


FIGURE A.2.2-4
SDB ENERGETIC
MINIMUM POSSIBLE SHEAR RING YIELD FORCES
CONCRETE LEDGE AND BOLT FORCES

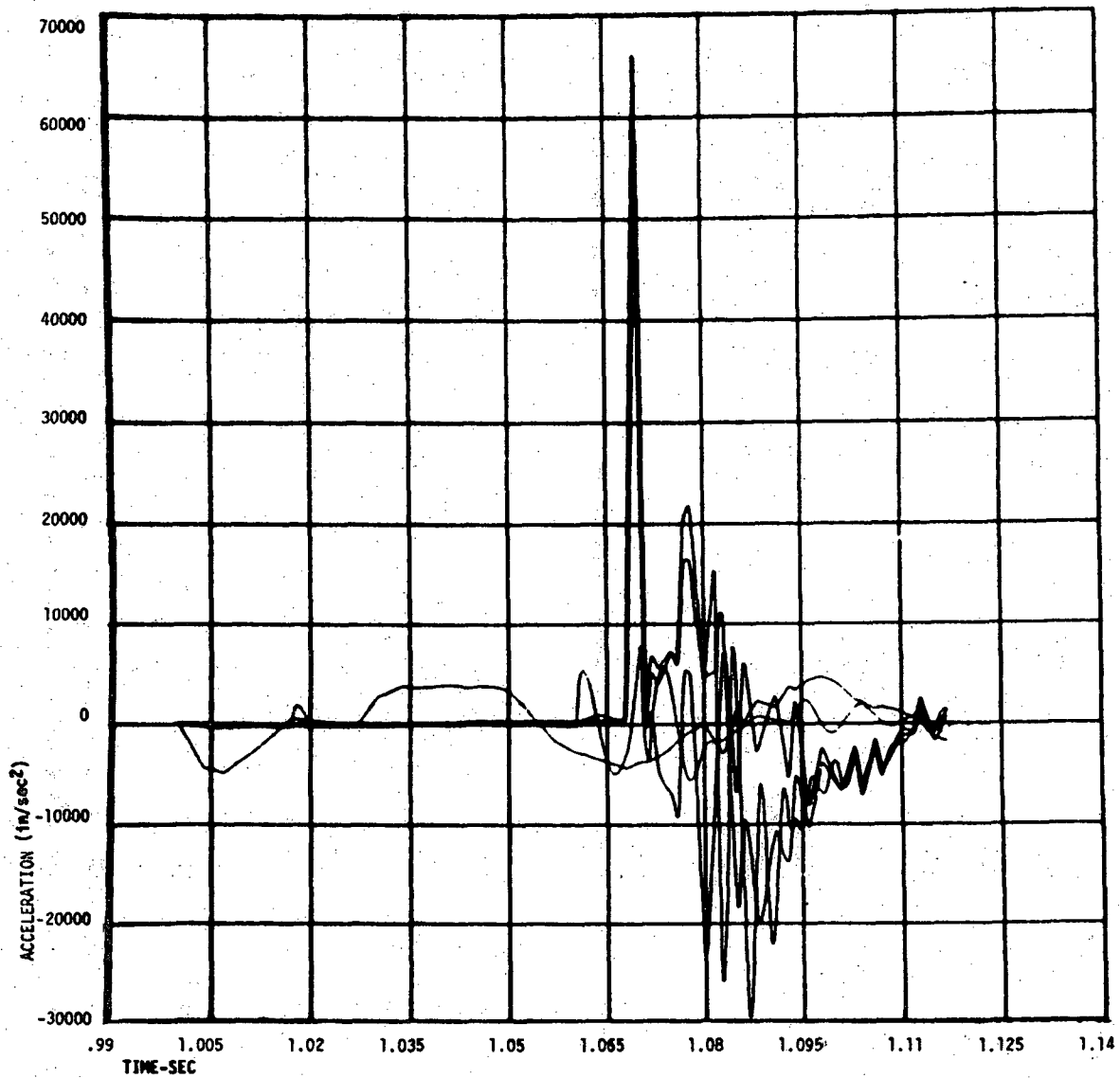


FIGURE A.2.2-5
SDB ENERGETIC
MINIMUM POSSIBLE SHEAR RING YIELD FORCES
ACCELERATIONS

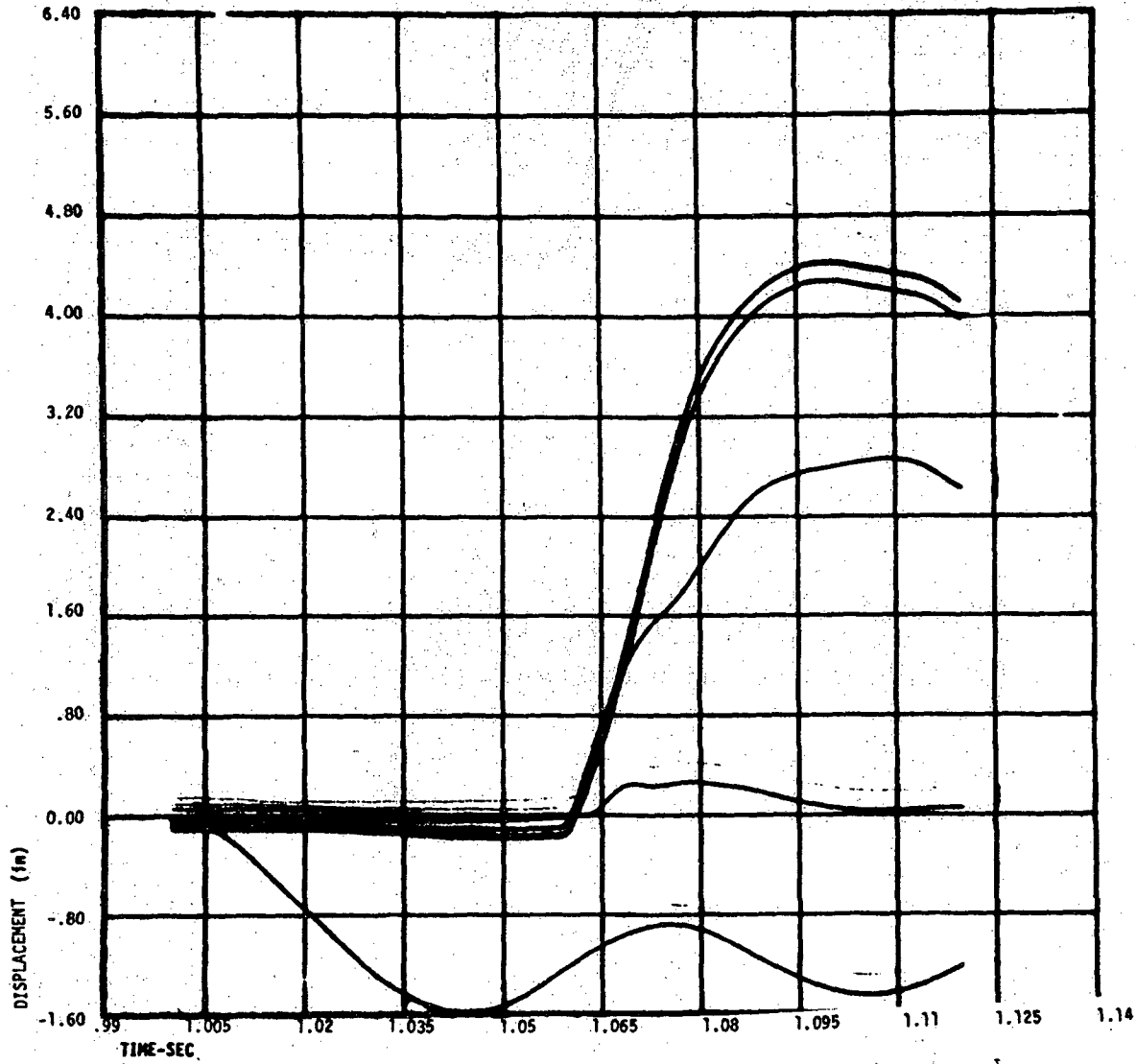


FIGURE A.2.3-1
CASE 2 ENERGETIC
MINIMUM POSSIBLE SHEAR RING YIELD FORCES
ABSOLUTE DISPLACEMENTS

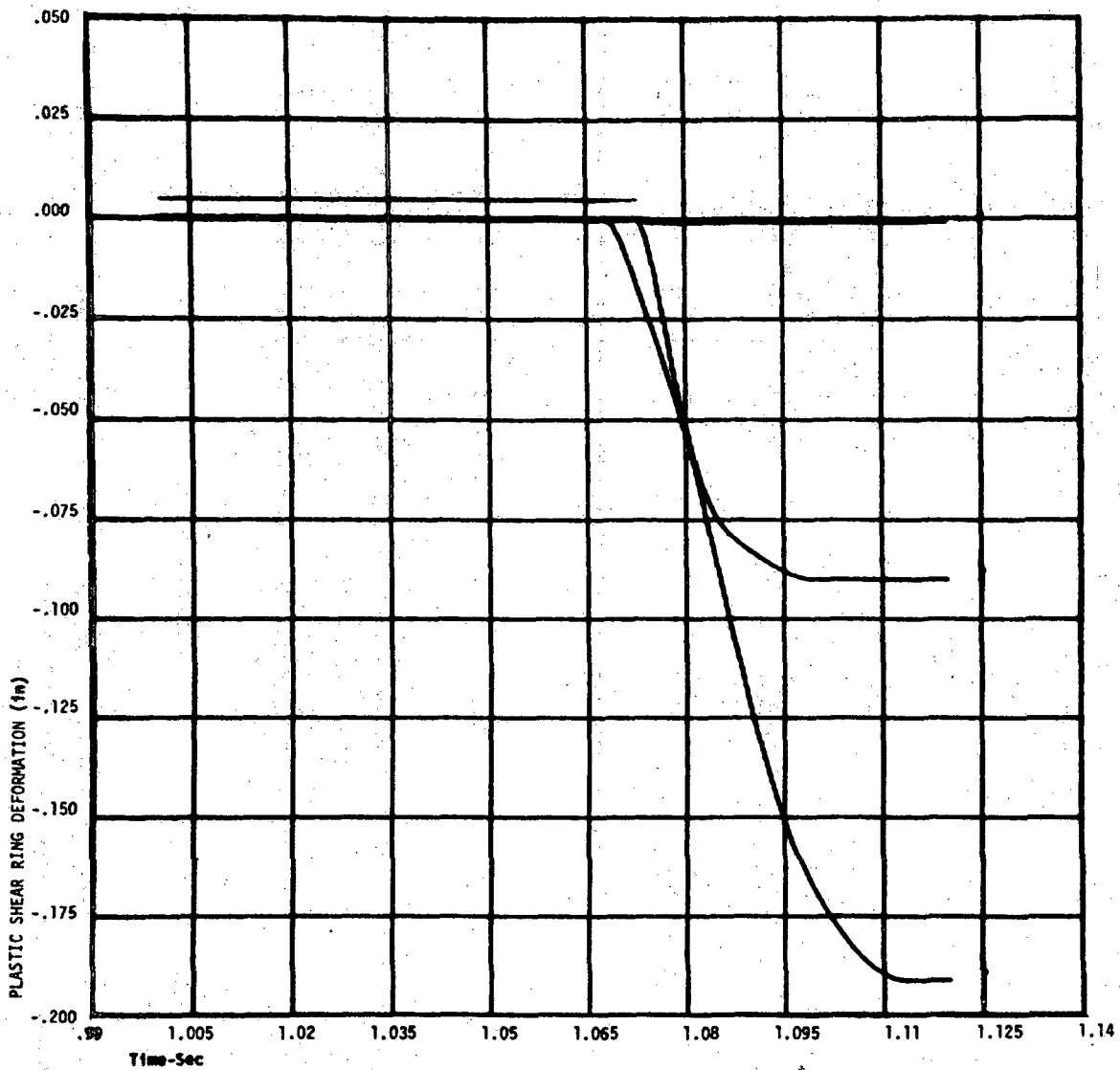


FIGURE A.2.3-2
CASE 2 ENERGETIC
MINIMUM POSSIBLE SHEAR RING YIELD FORCES
PLASTIC SHEAR RING DEFORMATIONS

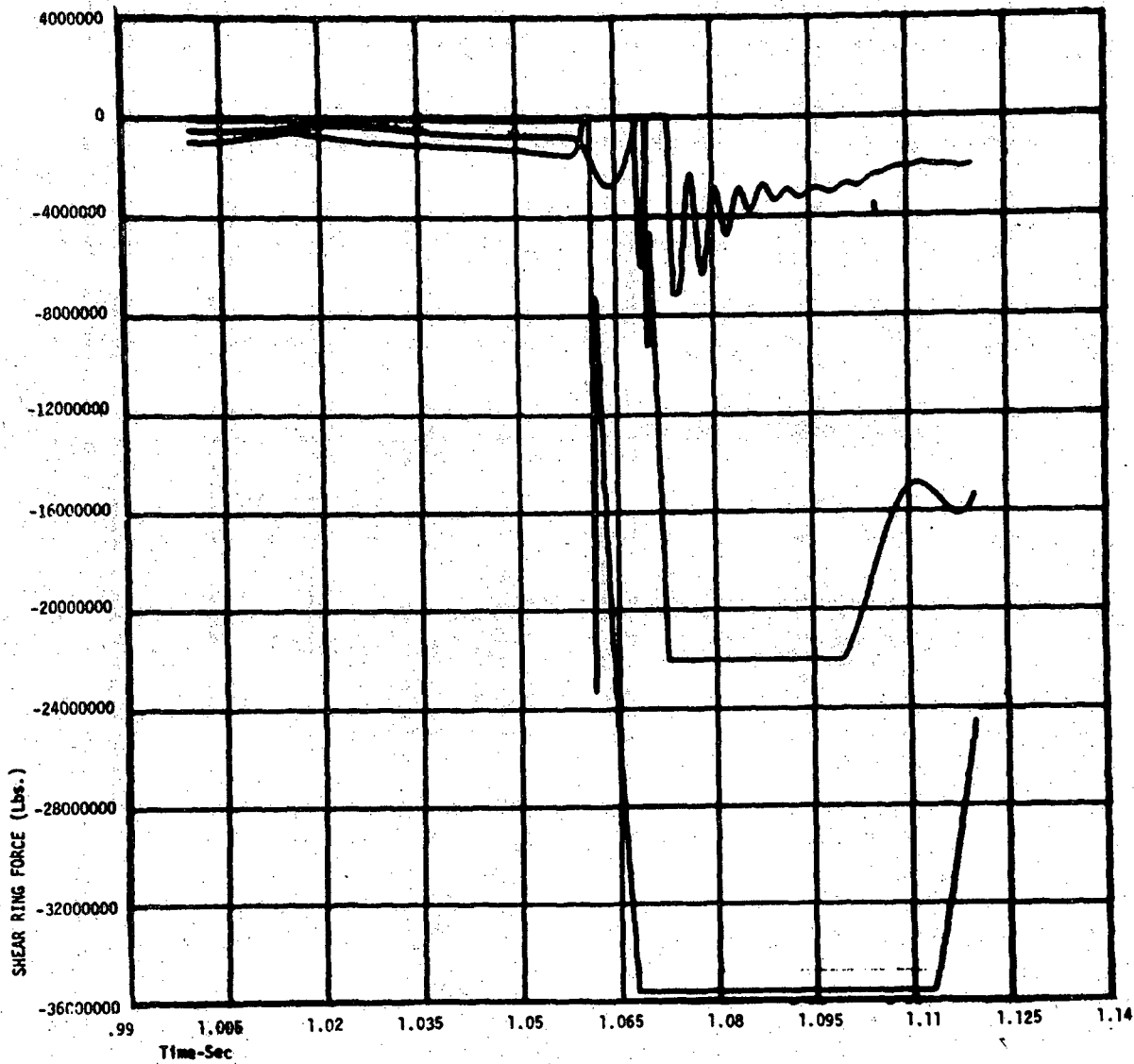


FIGURE A.2.4-3
CASE 2 ENERGETIC
MINIMUM POSSIBLE SHEAR RING YIELD FORCES
SHEAR RING FORCES

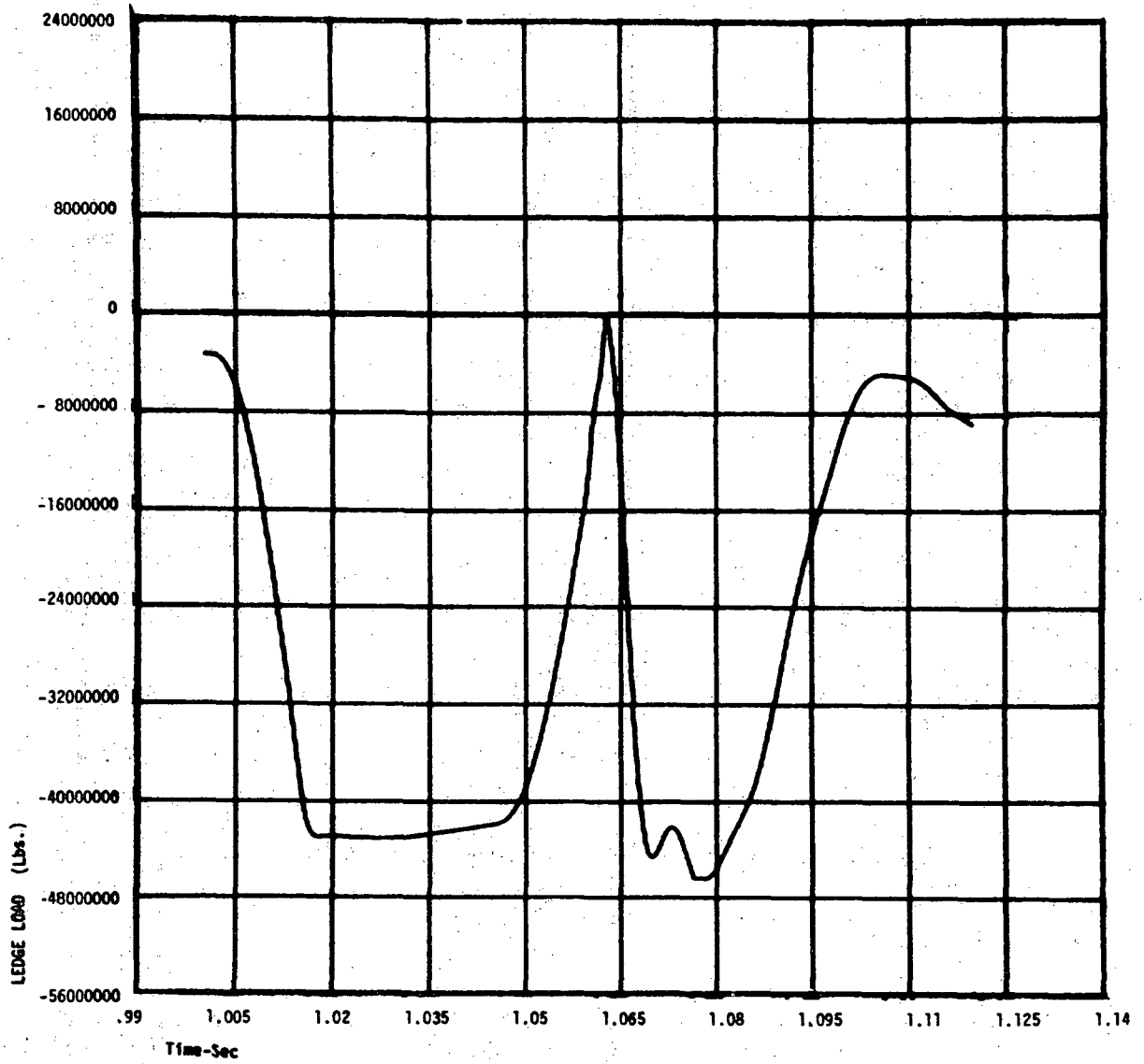


FIGURE A.2.3-4
CASE 2 ENERGETIC
MINIMUM POSSIBLE SHEAR RING YIELD FORCES
CONCRETE LEDGE AND BOLT FORCES

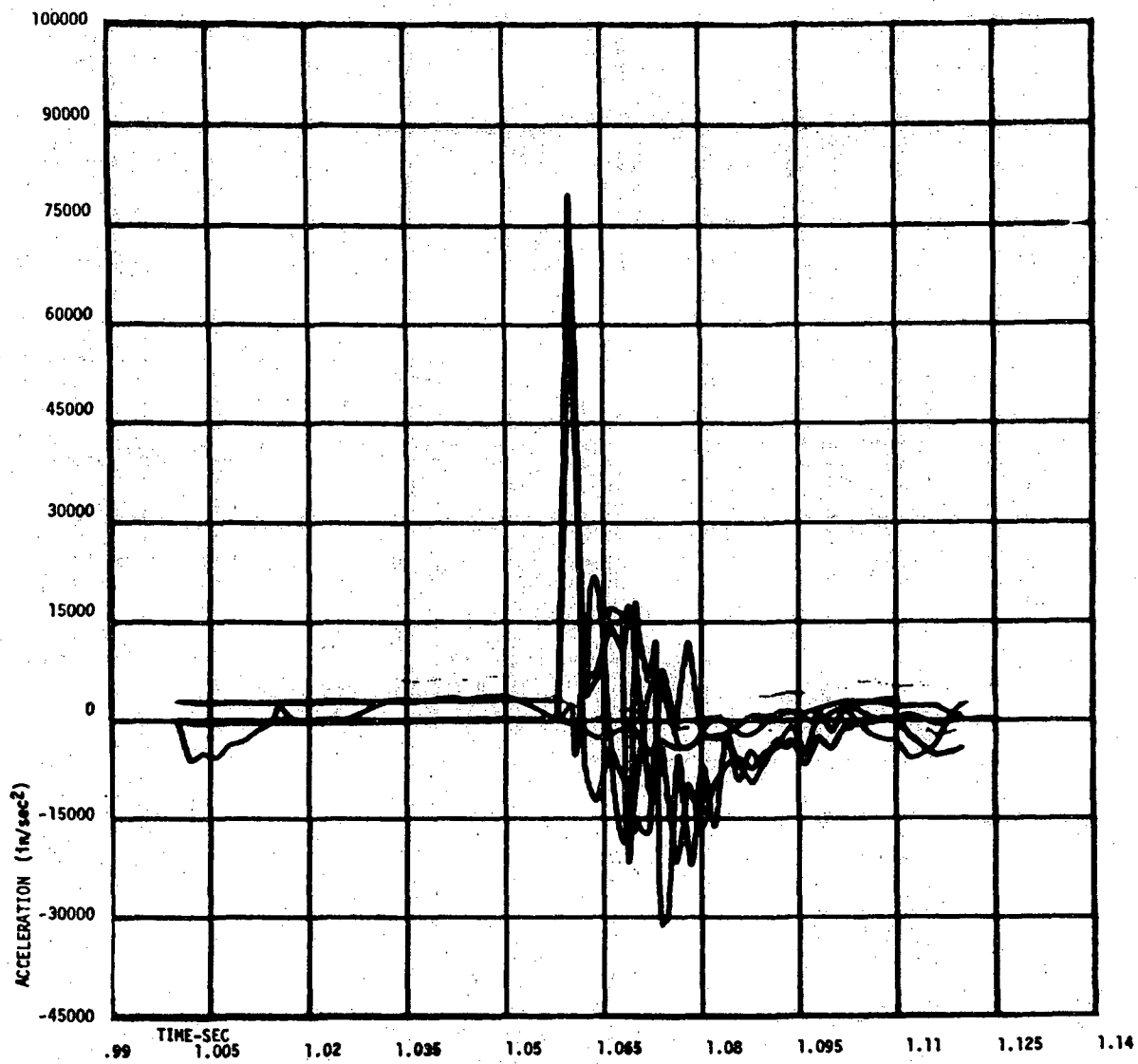


FIGURE A.2.3-5
CASE 2 ENERGETIC
MINIMUM POSSIBLE SHEAR RING YIELD FORCES
ACCELERATIONS

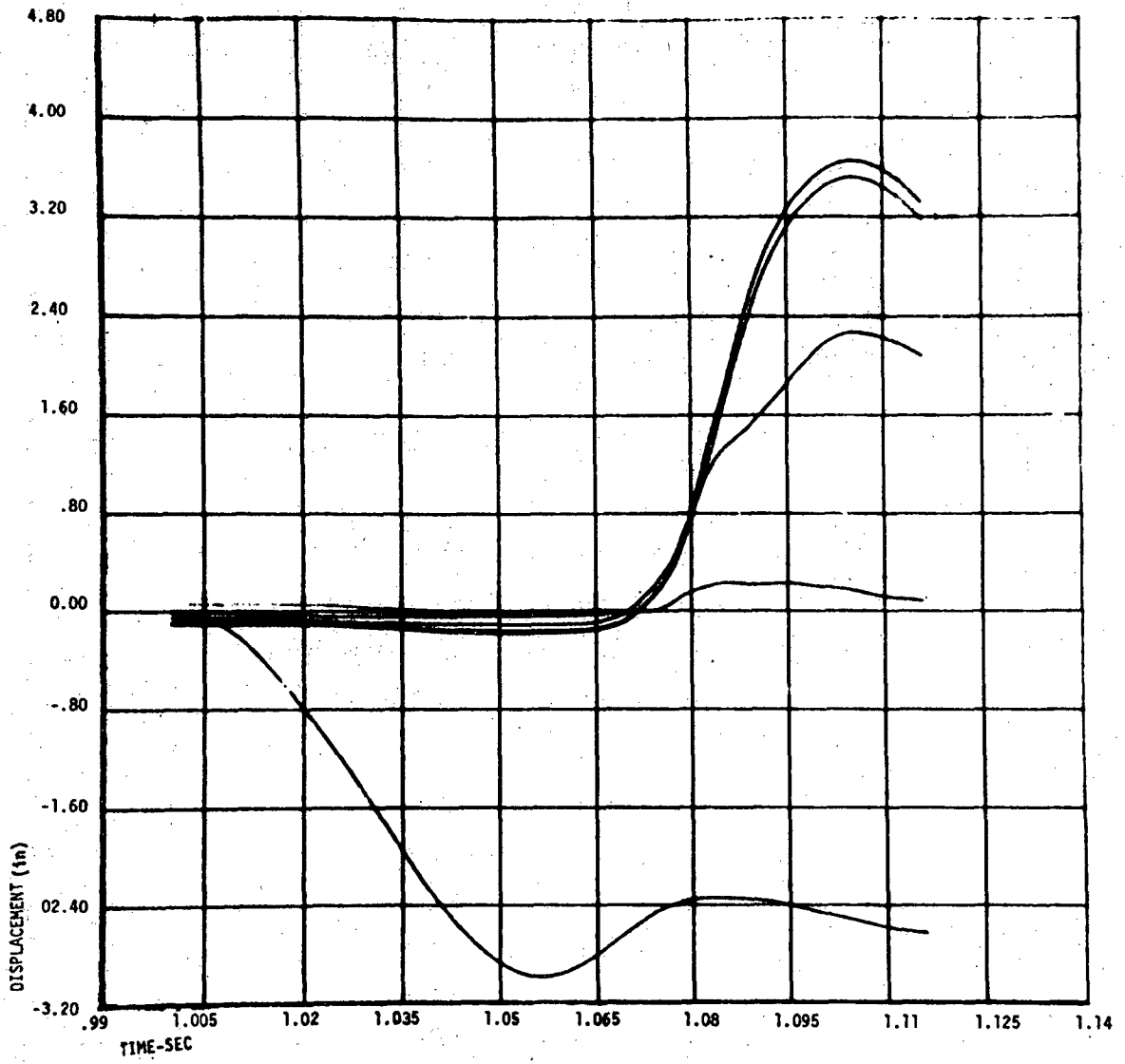


FIGURE A.2.4-1
CASE 3 ENERGETIC
MINIMUM POSSIBLE SHEAR RING YIELD FORCES
ABSOLUTE DISPLACEMENTS

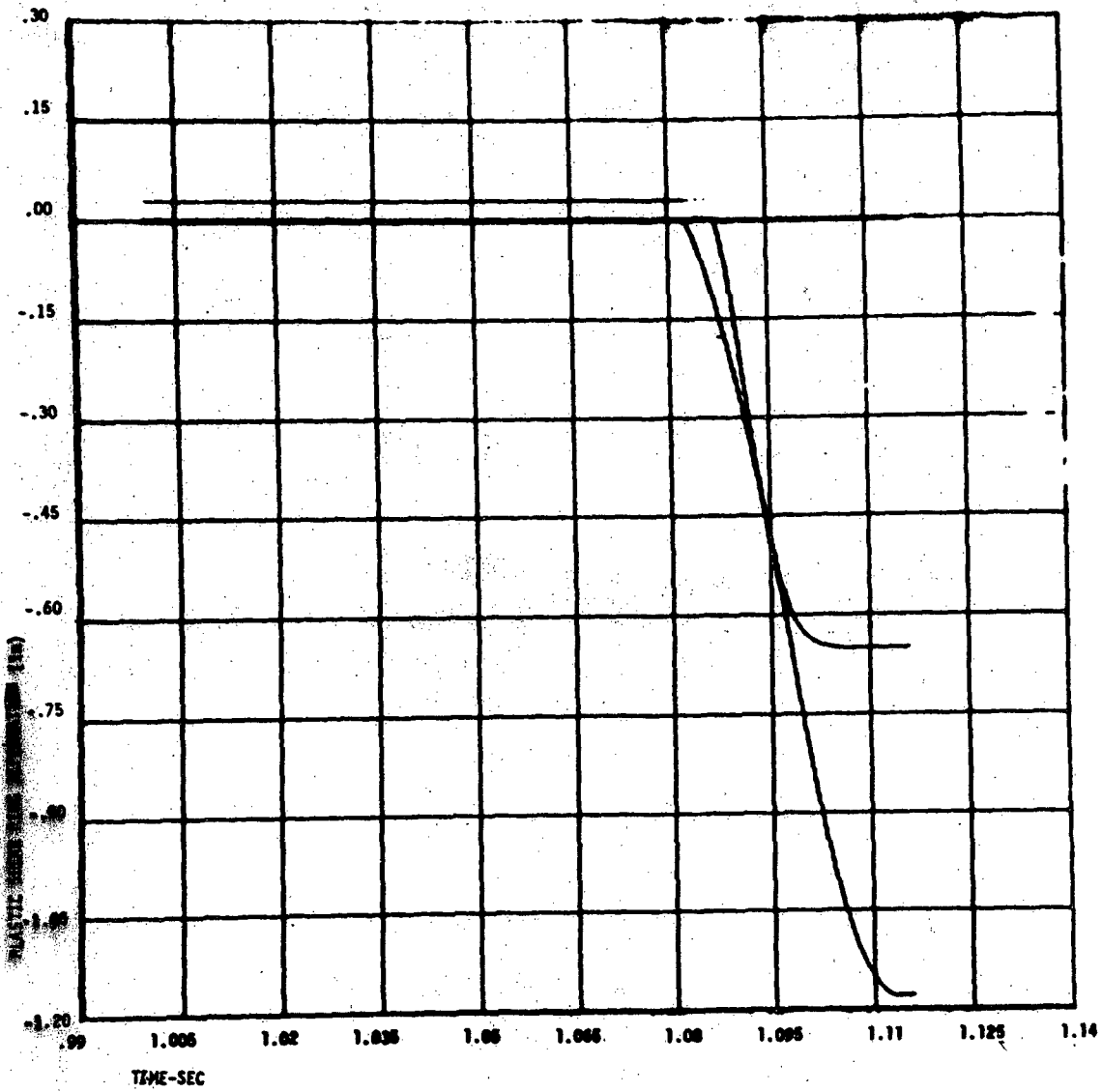


FIGURE A.2.4-2
CASE 3 ENERGETIC
MINIMUM POSSIBLE SHEAR RING YIELD FORCES
PLASTIC SHEAR RING DEFORMATIONS

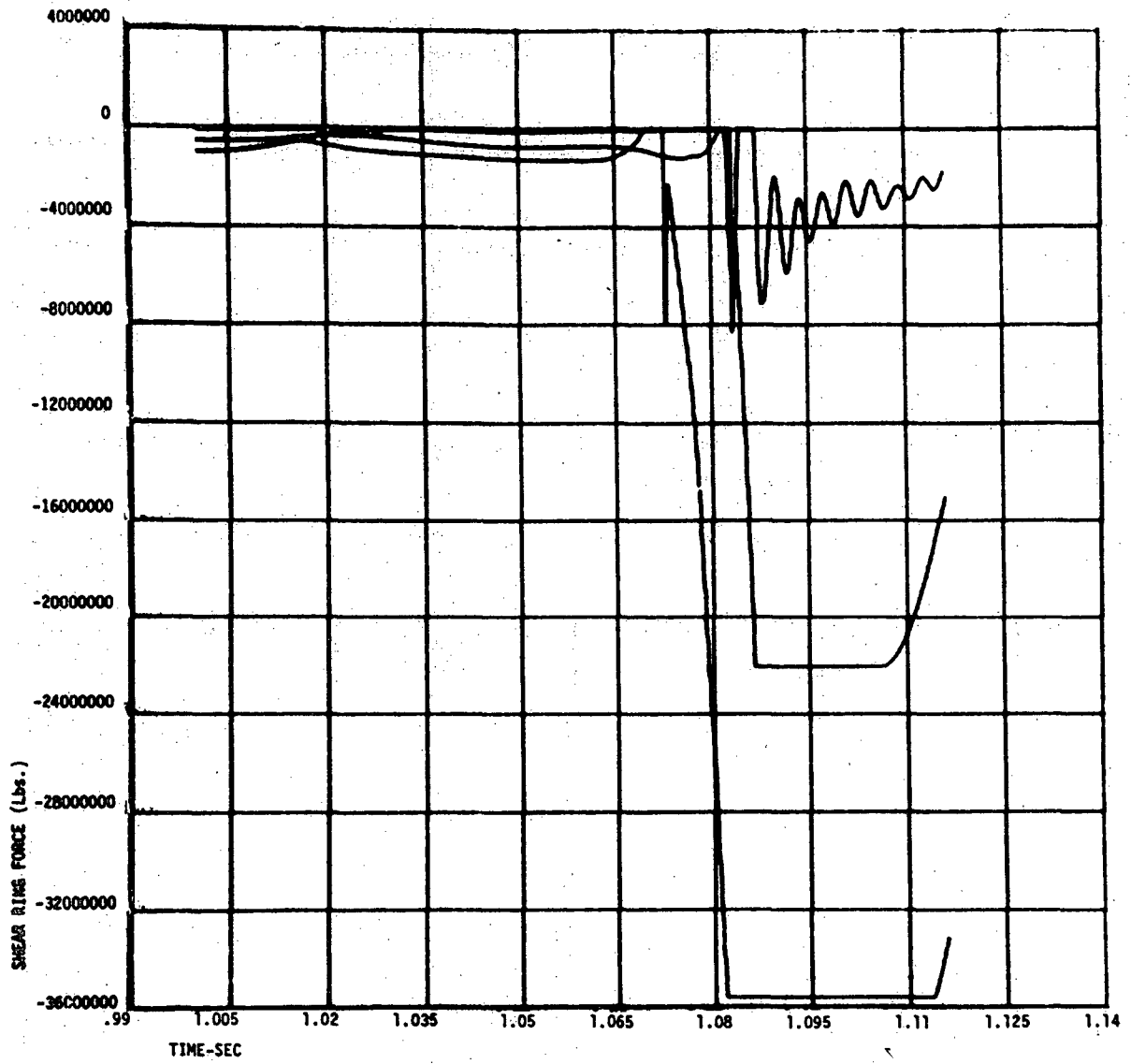


FIGURE A.2.4-3
CASE 3 ENERGETIC
MINIMUM POSSIBLE SHEAR RING YIELD FORCES
SNEAR RING FORCES

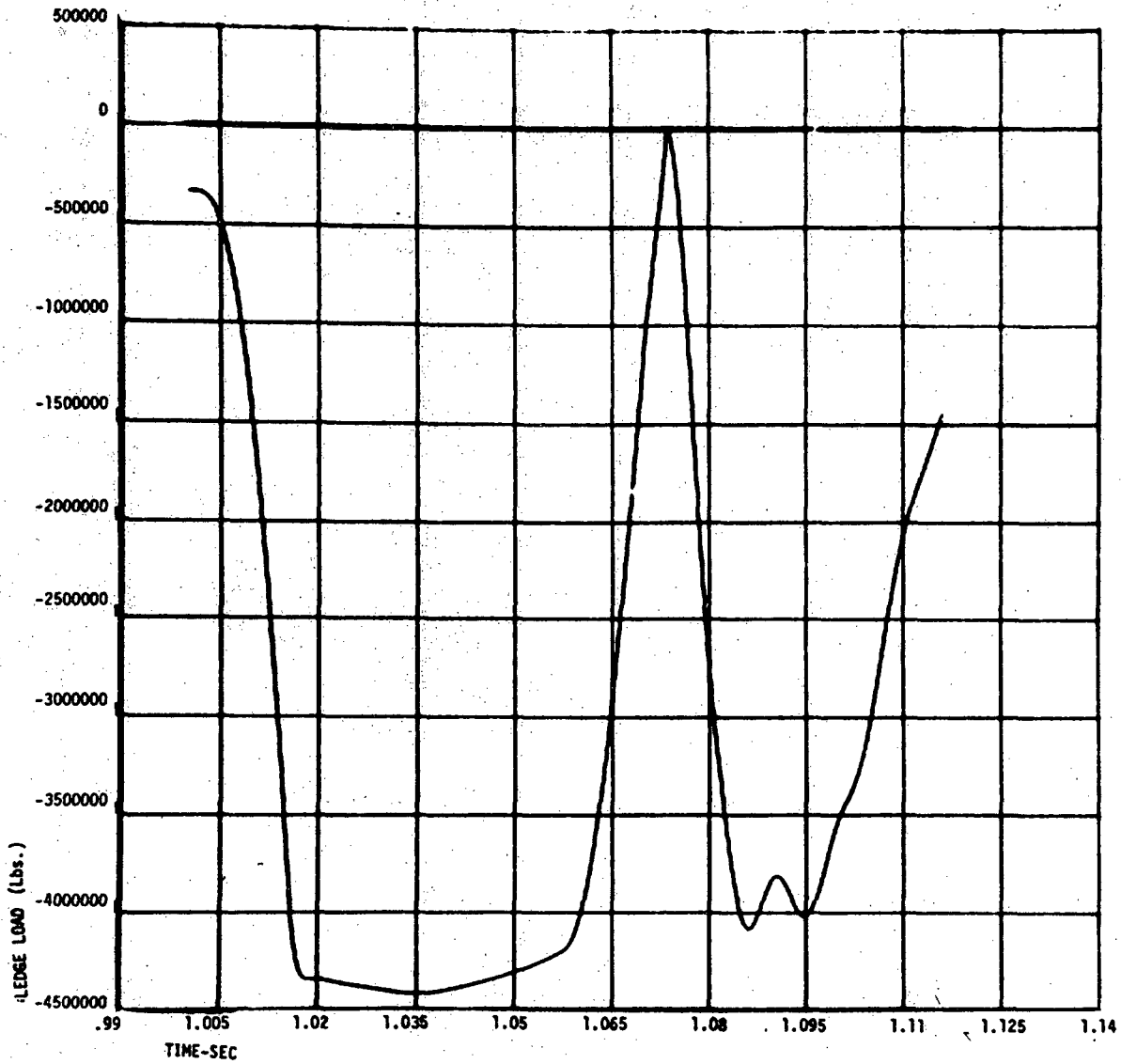


FIGURE A.2.4-4
CASE 3 ENERGETIC
MINIMUM POSSIBLE SHEAR RING YIELD FORCES
CONCRETE LEDGE AND BOLT FORCE

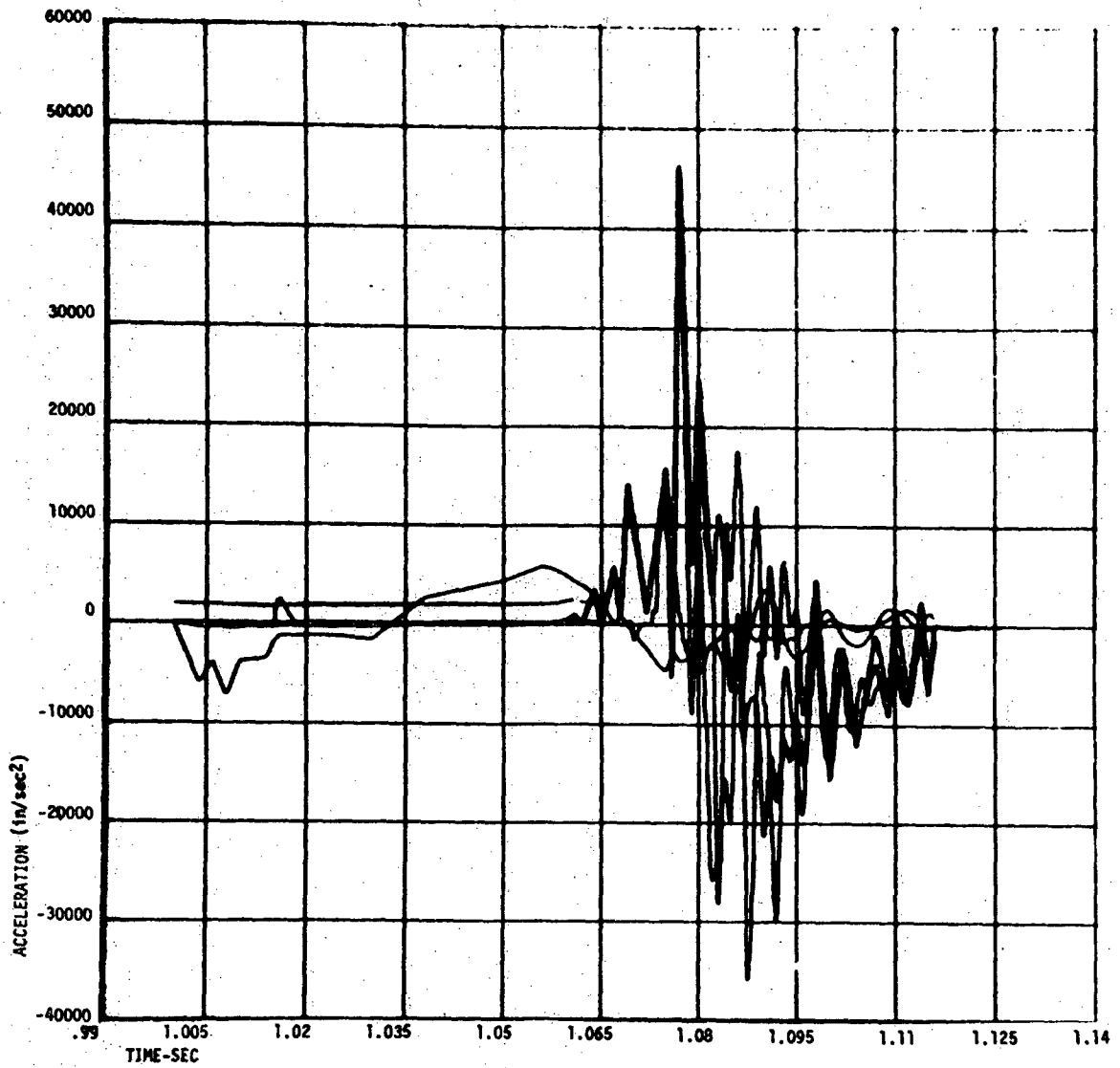


FIGURE A.2.4-5
CASE 3 ENERGETIC
MINIMUM POSSIBLE SHEAR RING YIELD FORCES
ACCELERATIONS

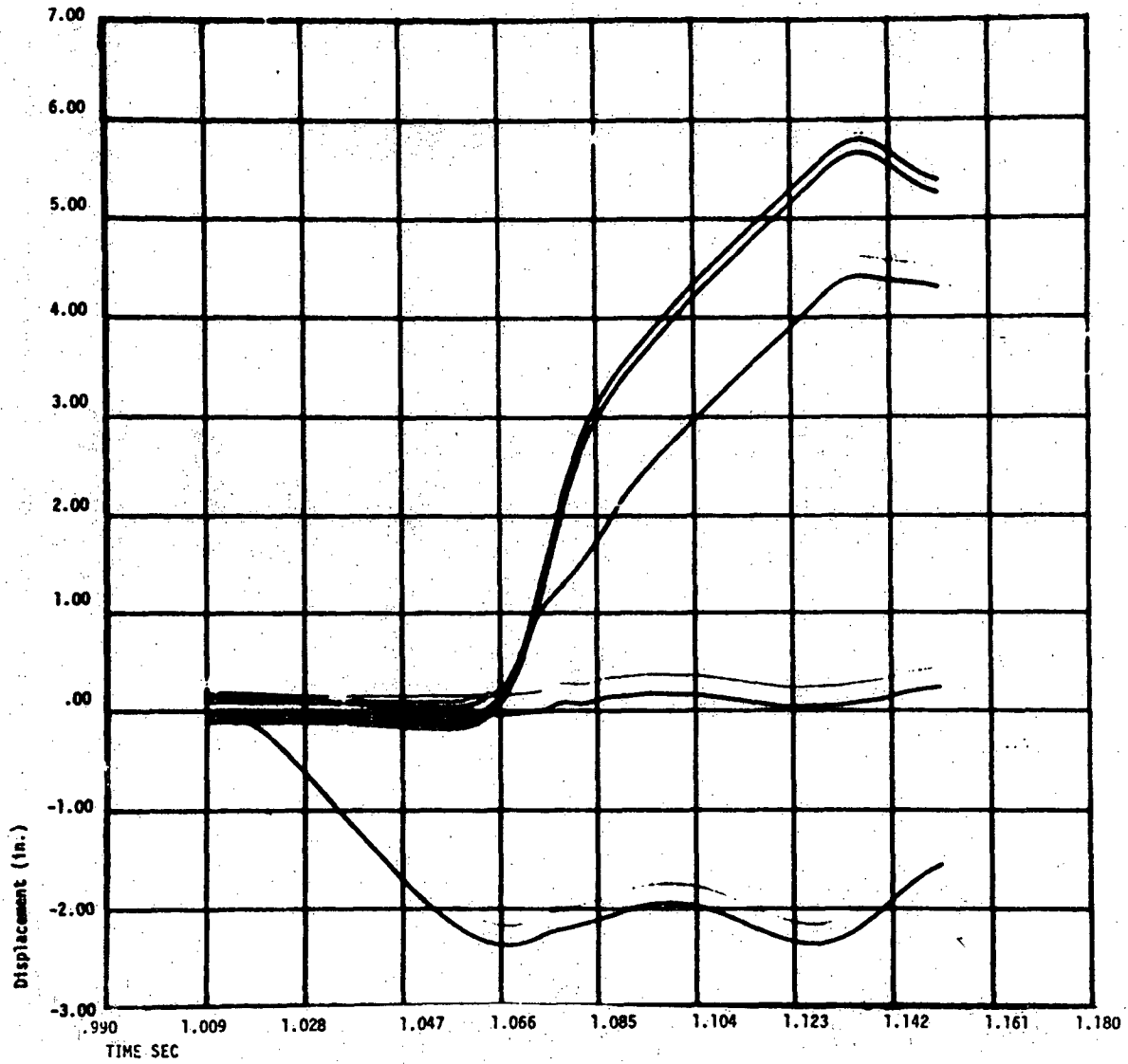


FIGURE A.2.5-1

CASE 4 ENERGETIC
MINIMUM POSSIBLE SHEAR RING YIELD FORCES
ABSOLUTE DISPLACEMENTS

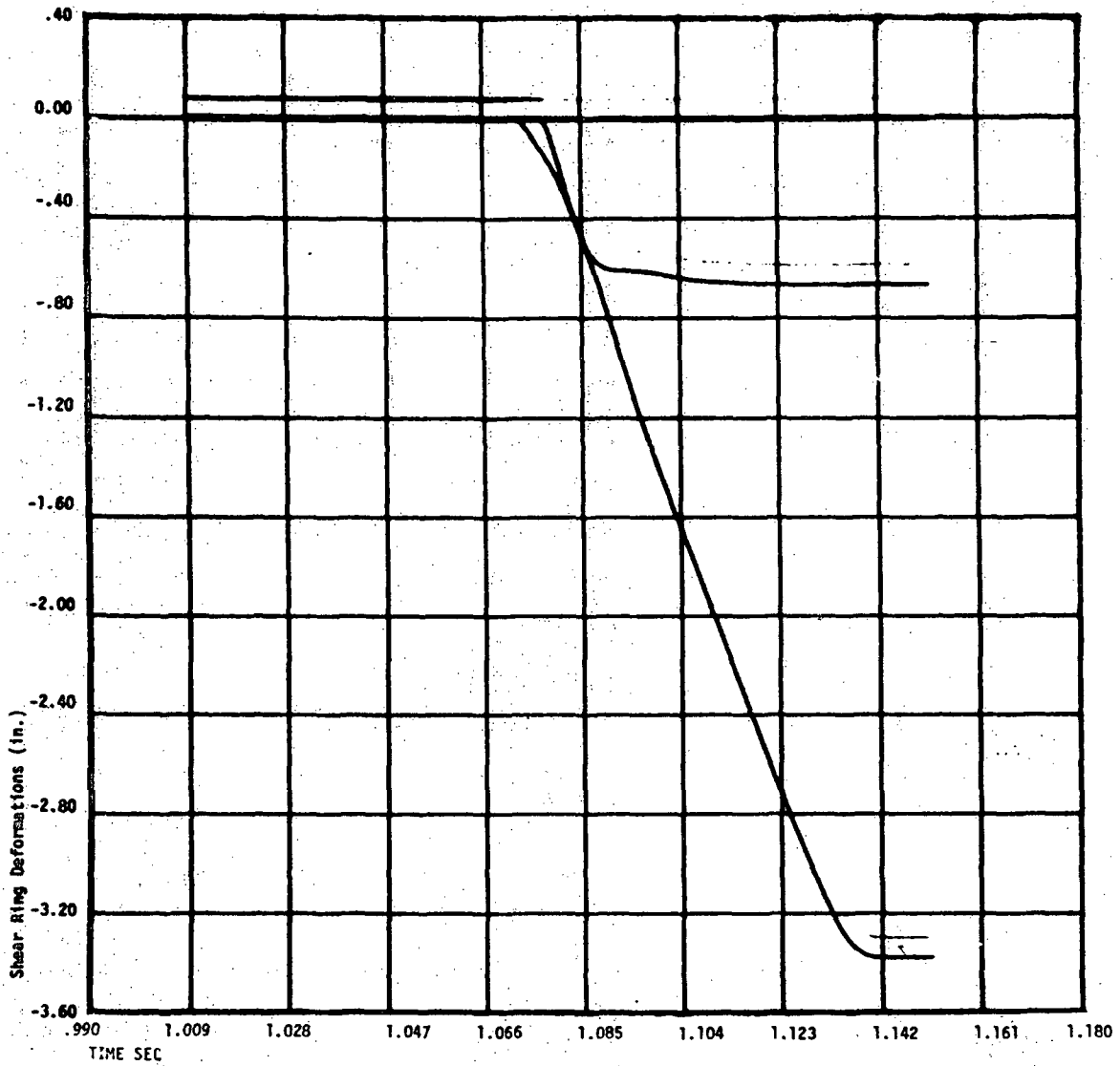


FIGURE A.2.5-2
CASE 4 ENERGETIC
MINIMUM POSSIBLE SHEAR RING YIELD FORCES
PLASTIC SHEAR RING DEFORMATIONS

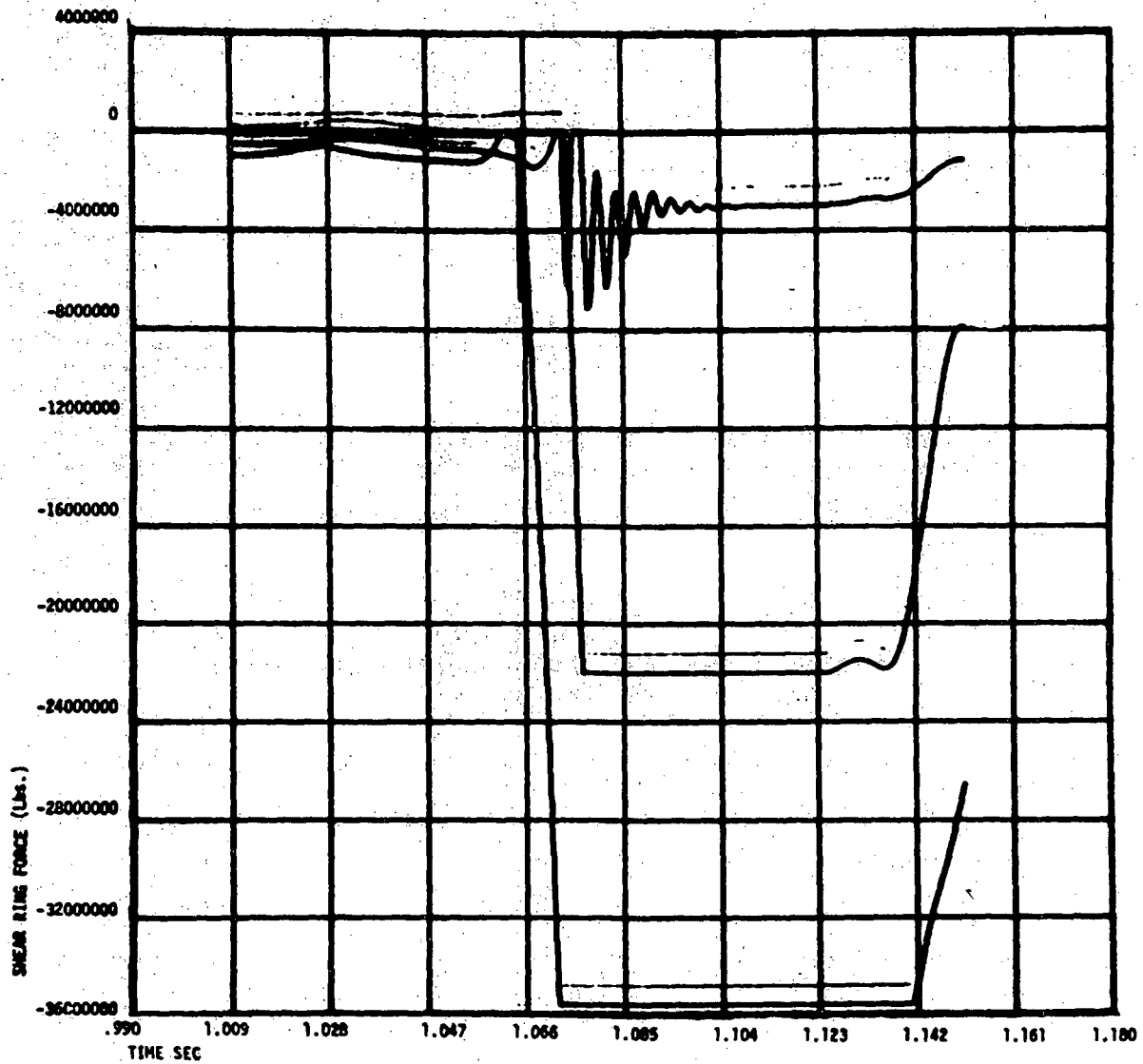


FIGURE A.2.5-3
CASE 4 ENERGETIC
MINIMUM POSSIBLE SHEAR RING YIELD FORCES
SHEAR RING FORCES

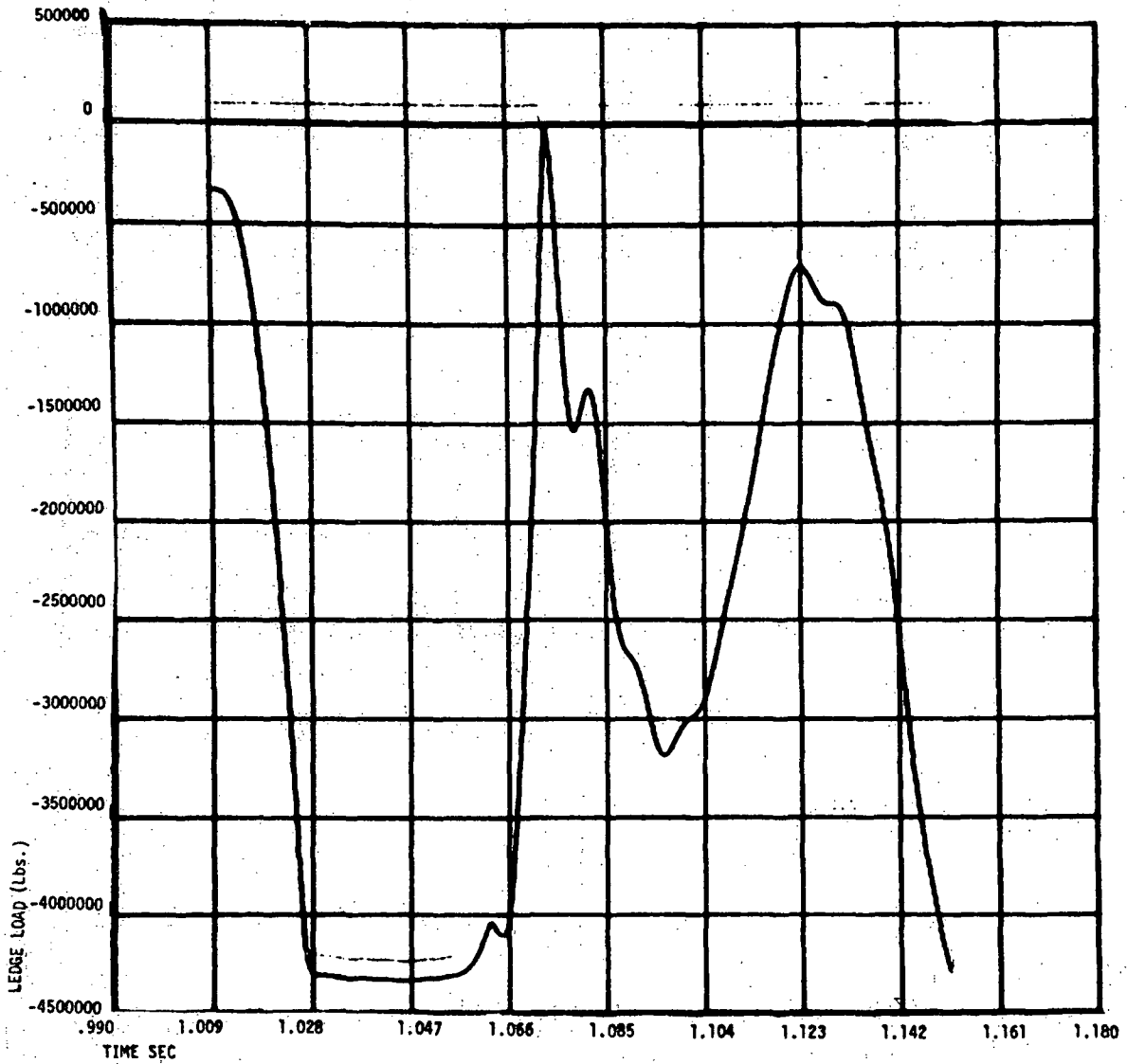


FIGURE A.2.5-4

CASE 4 ENERGETIC
MINIMUM POSSIBLE SHEAR RING YIELD FORCES
CONCRETE LEDGE AND BOLT FORCES

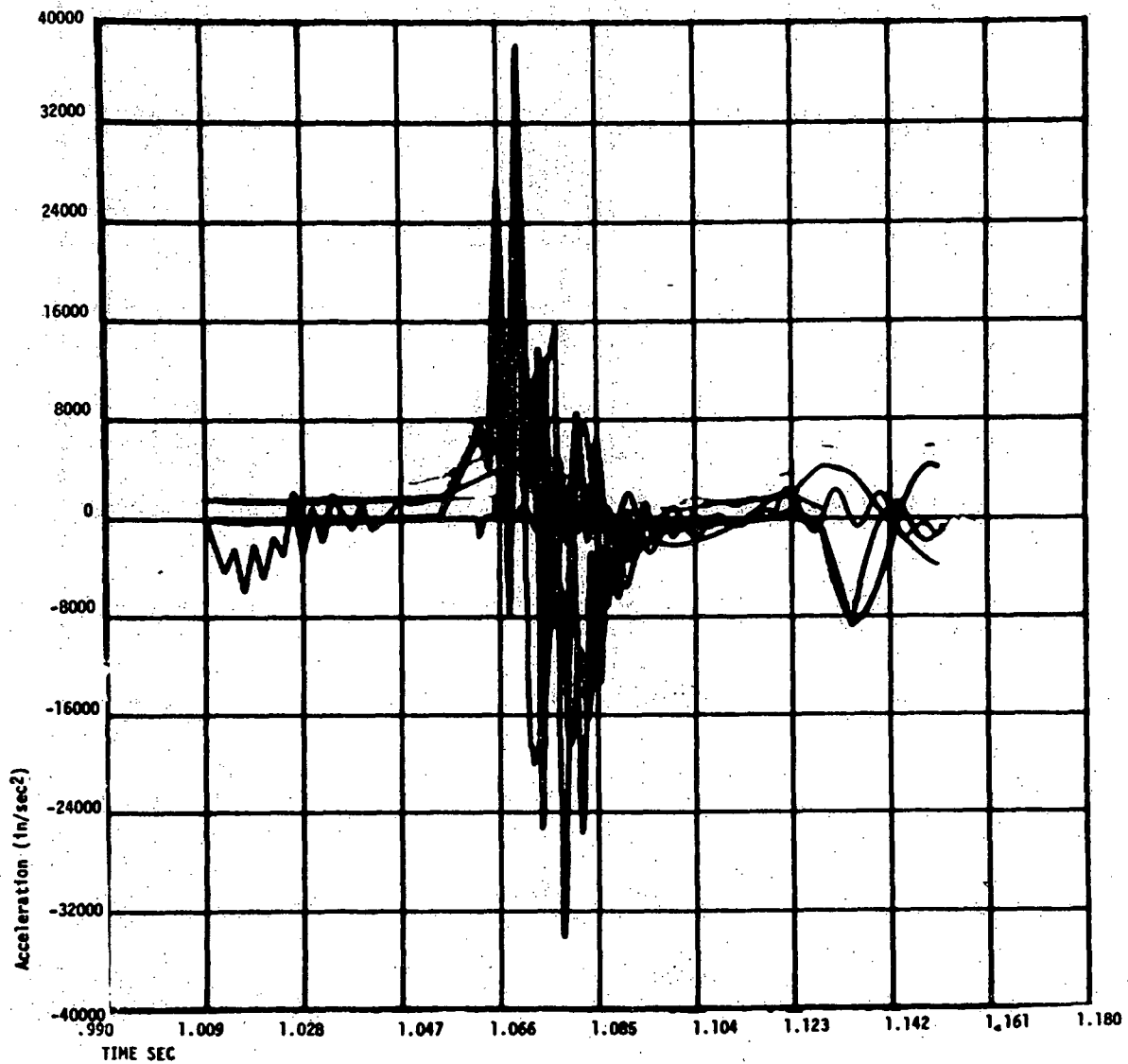


FIGURE A.2.5-5
 CASE 4 ENERGETIC
MINIMUM POSSIBLE SHEAR RING YIELD FORCES
ACCELERATIONS

APPENDIX B

CRBRP Shear Ring Test Results

- ● Introduction
- ● ● Test No. 1
- ● ● Test No. 2
- ● ● Test No. 3

B.1 INTRODUCTION

B.1.1 PURPOSE OF TEST

Reference CRBRP Design features SRP, IRP, and LRP shear rings to assure structural integrity of the primary boundary formed by the Closure Head in relation to the postulated Hypothetical Core Disruptive Accident (HCDA). Recently, NRC has requested the Project to provide an estimate of the limiting HCDA energetic which the Reference CRBRP Design, and particularly the Closure Head, can safely withstand. In order to provide an estimate of a limiting HCDA energetic in the Closure Head region, the behavior of the shear rings in terms of force-deflection characteristics is required for subsequent dynamic Closure Head response analyses at various HCDA energetic levels. Further, the plastic instability load and deformation in the shear ring force-deflection characteristics, which is described by unbounded deformation, is required to establish an acceptable HCDA structural criterion. Analytical derivations of shear ring force-deflection characteristics and the respective point of instability which include the large deformations inherent with the concept of a limiting HCDA energetic are implicitly complex, and even if performed are not likely to be reliable. Accordingly, an experimental approach which is direct and relatively simple was selected to provide the force-deflection behavior and plastic instability load and deformation for the CRBRP shear rings.

Prototype CRBRP Closure Head size does not permit practical full scale testing. In relation to conventional testing machines, specimens of unit width were selected with depth features which are exact 1/10 scale replicas of the prototypic LRP shear ring, LRP, and vessel flange.

B.1.2 TEST SET-UP

The scale model LRP shear ring test set-up is illustrated in W assembly drawing 1456F73. Details of specimens and fixtures are presented in W drawing 1185E14. Copies of both drawings are provided as Figures B.1.1-1 and 2.

The LRP scale model shear ring test includes a fixture (Item 1) bolted to the top plate of the testing machine. Bolted to the fixture are two (2) symmetrically arranged specimens of the vessel flange, designated as Plug 1 (Item 2). The LRP shear ring, represented by the shear bar (Item 5), is loosely inserted in the grooves formed in the respective Plug 1. The LRP, represented by Plug 2 (Item 3), is bolted to two (2) plates (Items 2 and 8), which in turn, rest on the bottom plate of the testing machine. Apertures are provided in the fixture (Item 1) to permit visual observation and/or photographic recording of the local deformation behavior.

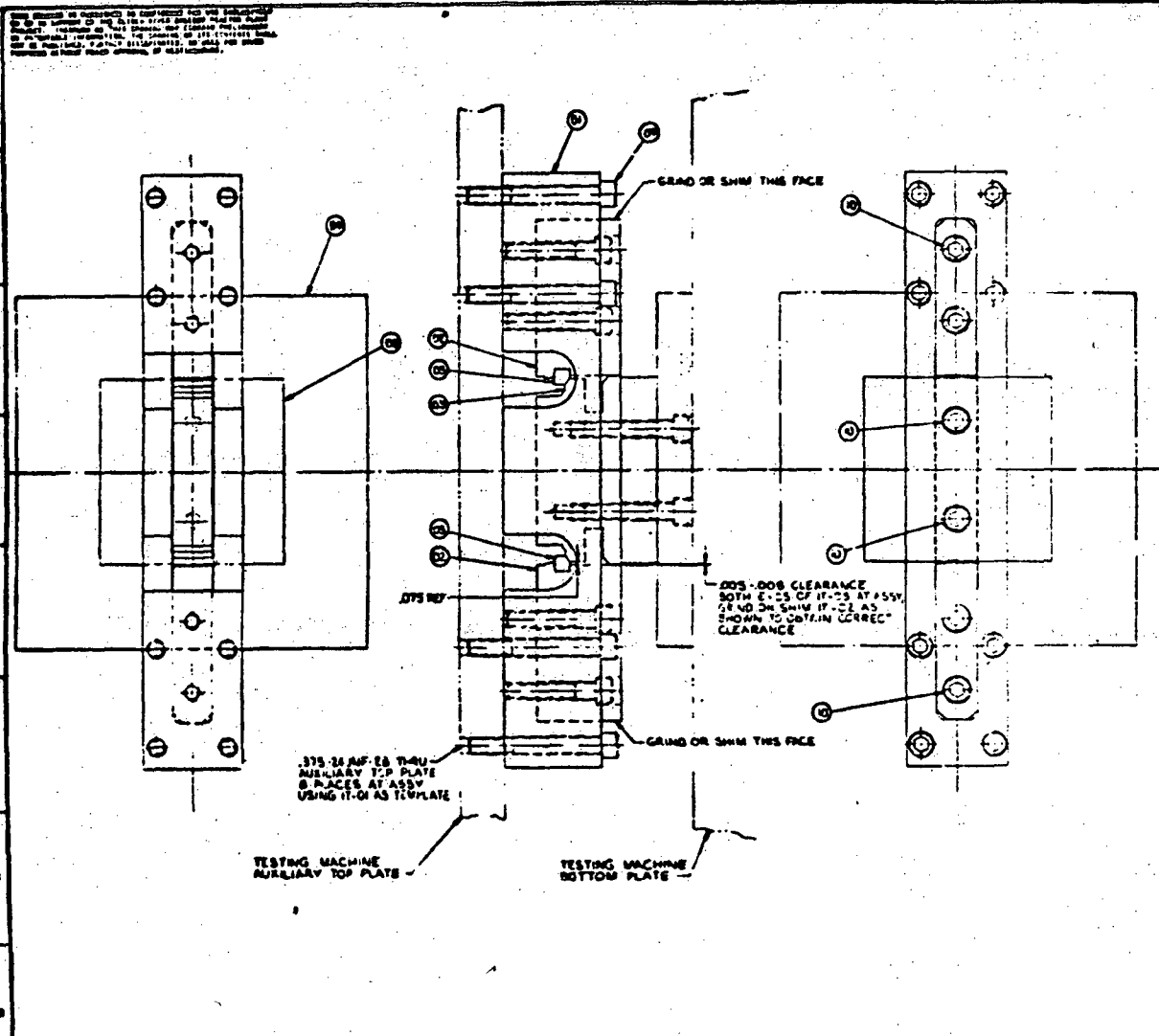
A Baldwin Universal Testing Machine, SN-68-255 with a maximum capacity of 60,000 lbs. was used. Available load ranges are (1) Low < 1200 lb, \pm 5 lb accuracy, (2) Medium < 20,000 lbs, \pm 10 lb accuracy, and (3) High < 60,000 lbs, \pm 50 lb accuracy. The high range was used in the test.

A total of four (4) Starret Dial Indicators with a range of 1/2 inch and \pm 0.0010 inch accuracy were used.

Three (3) tests designated as Test No. 1, 2, and 3 were performed. Test No. 1 was performed on low carbon steel specimens to de-bug set-up, equipment, and procedures. Tests No. 2 and 3 were performed on SA-508 specimens with material traceable to the prototype CRBRP Closure Head IRP.

Test 1 data, in terms of specimen loading, was taken on an intermittent-hold basis. Test 2 and Test 3 data acquisition was similar to Test 1 except as modified to improve test results. In the intermittent-hold loading of the specimens, the load was slowly increased in approximate 500 lb. increments by manually adjusting the Baldwin Test Machine and observing the load cell readout. At each of the loading increments, the load was held briefly to permit dial indicators to be manually read and recorded. Photographs were taken at selected load increments depending on the relevance of the deformation. As loading approached the plastic instability a rapid increase in deformation occurred. The operator manually reduced the applied force as best possible to obtain maximum force-deflection data at the point of instability.

THIS DRAWING IS UNCLASSIFIED AND IS NOT TO BE RELEASED TO THE PUBLIC UNLESS IT IS DETERMINED THAT IT IS NECESSARY TO DO SO IN THE INTERESTS OF NATIONAL DEFENSE. IT IS THE POLICY OF THE DEPARTMENT OF DEFENSE TO MAKE AVAILABLE TO THE PUBLIC INFORMATION THAT DOES NOT RELATE TO NATIONAL DEFENSE. IT IS THE POLICY OF THE DEPARTMENT OF DEFENSE TO MAKE AVAILABLE TO THE PUBLIC INFORMATION THAT DOES NOT RELATE TO NATIONAL DEFENSE.



BILL OF MATERIAL			
ITEM NO.	NAME DESCRIPTION	QTY REQD	REF. DRAWING
01	01 001 001 PLATE	SEE 4-1	
02	02 001 002 PLUG	SEE 4-1	
03	03 001 003 PLUG	SEE 4-1	
04	04 001 004 PLATE	SEE 4-1	
05	05 001 005 SHEAR BAR	SEE 4-1	
06	06 001 006 PLUG	SEE 4-1	
07	07 001 007 PLUG	SEE 4-1	
08	08 001 008 SPACER PLATE	SEE 4-1	
09	09 001 009 WASH COIL	SEE 4-1	
10	10 001 010 WASH COIL	SEE 4-1	
11	11 001 011 WASH COIL	SEE 4-1	

NOTES:
 ① USED IN PLACE OF ITEMS 02 AND 03 FOR INITIAL SET-UP OF TESTING.
 ② TORQUE ITEMS 09 TO 11 TO 30 FT LBS.

Figure B.1.1-1

Amend. 60
 Feb. 1981

DATE	BY	APPROVED	REVISION
			1456F73

B.2 SCALE SPECIMEN RESULTS

B.2.1 Test No. 1

Test No. 1 was performed on low carbon steel specimens. The purpose of the test was to de-bug set-up, equipment, and procedures. Accordingly, traceability of the low carbon steel material and development Q.A. verification of equipment calibration and data recording procedures was not required or established.

B.2.1.1 Data

Test No. 1 loading was increased until the plastic instability load was reached. The equipment originally planned for the scale specimen tests included a Satec Deflectometer which would automatically record the deflection during the test. In the course of Test No. 1, it was found that the maximum test deflections were approximately 3/8 inch. As the Satec deflectometer range (0.10 inch) was not adequate to cover the test data, automatic recording of deflection was not obtained. The larger than expected deflections also caused the range on Dial Indicator No. 2 to be exceeded. Only Dial Indicator No. 1 readings were valid and accurate over the full range of test data. Dial Indicators No. 3 and 4 which measured lateral motion of the bottom test fixture showed motion only at the plastic instability and respective readings were not recorded. Force readings recorded from visual observation of the Baldwin Universal Testing Machine dial gauge were easily obtained. Manual adjustments of the testing machine required to achieve desired force levels, even during rapid changes at the plastic instability load, were not found to be difficult.

B.2.1.2 Force-Deflection Curves

The 1/10 scale LRP shear ring force-deflection curve for low-carbon steel, based on Dial Indicator No. 1 readings, is illustrated in Figure B.2.1-1.

Features of the low carbon steel specimens force-deflection curve relevant to subsequent structural behavior are the linear elastic stiffness (K),

proportional elastic limit (PEL), and plastic instability load (P_I) and deformation (PD). Numerical values for low carbon steel are as follows.

$$K = 0.5 \times 10^6 \text{ LB/in}$$

$$\text{PEL} = 11,000 \text{ LBS.}$$

$$\text{PD} = 0.400 \text{ inch.}$$

$$P_I = 22,500 \text{ LBS.}$$

B.2.1.3 Photographs

Photographs of the 1/10 scale low carbon steel specimens were taken at selected force levels throughout Test No. 1. Two (2) rolls of film were used. The first roll included 20 frames which covered force levels from no load to 20,800 lbs. The second roll included 4 frames which covered the 22,000 to 22,500 lb. range at the point of instability. As the frames on the second roll were lost during developing, a post test photograph was taken to document final deformation shape.

Test No. 1 photographs of the specimens at no load (200 lbs.) and the PEL (11,000 lbs.) are presented in Figures B.2.1-2 and -3 respectively. The photograph of post Test No. 1 deformation shape of the specimens is presented in Figure B.2.1-4.

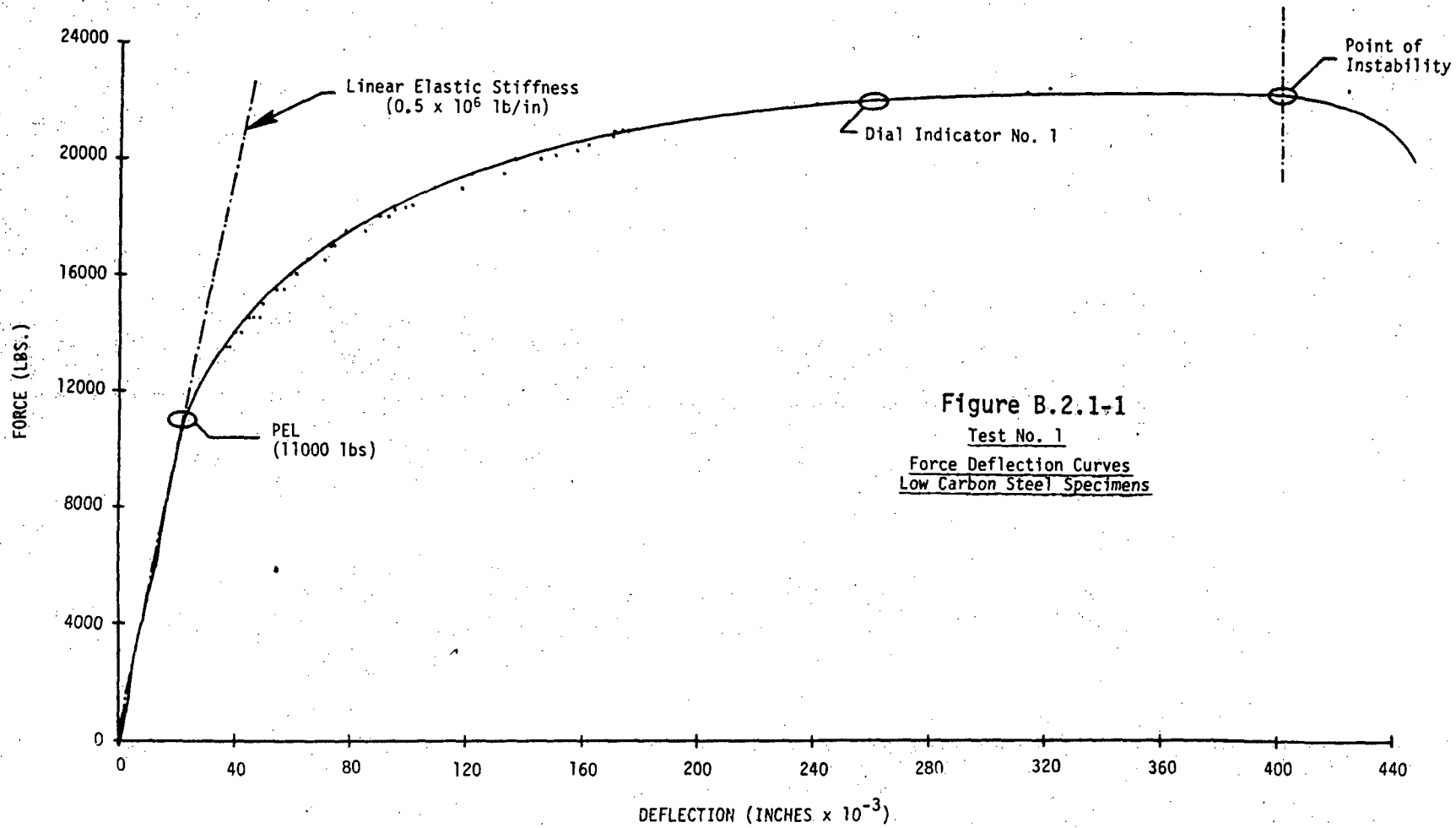


Figure B.2.1-1
 Test No. 1
 Force Deflection Curves
 Low Carbon Steel Specimens

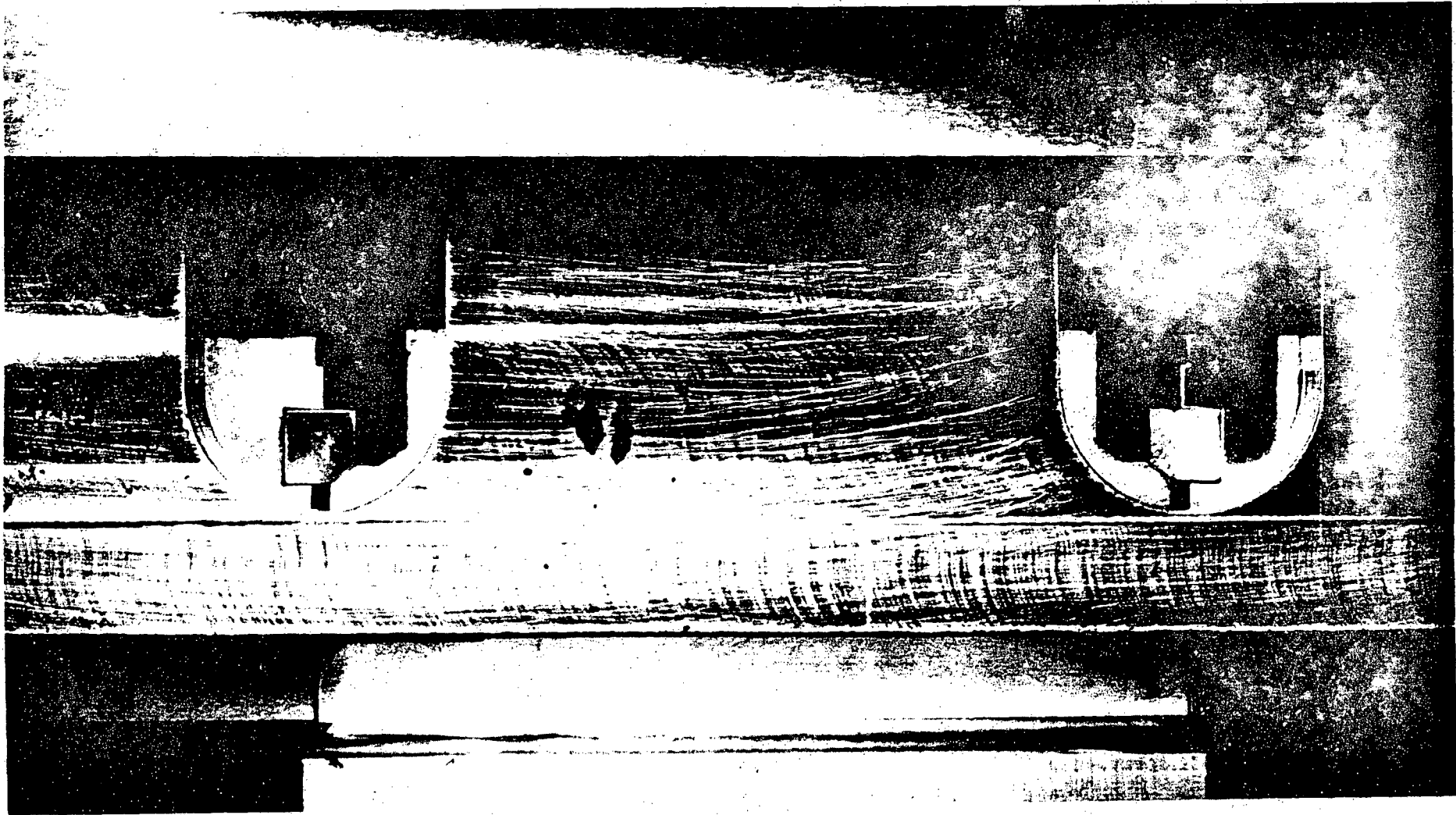
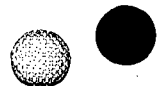


Figure B.2.1-2
Test No. 1
No Load



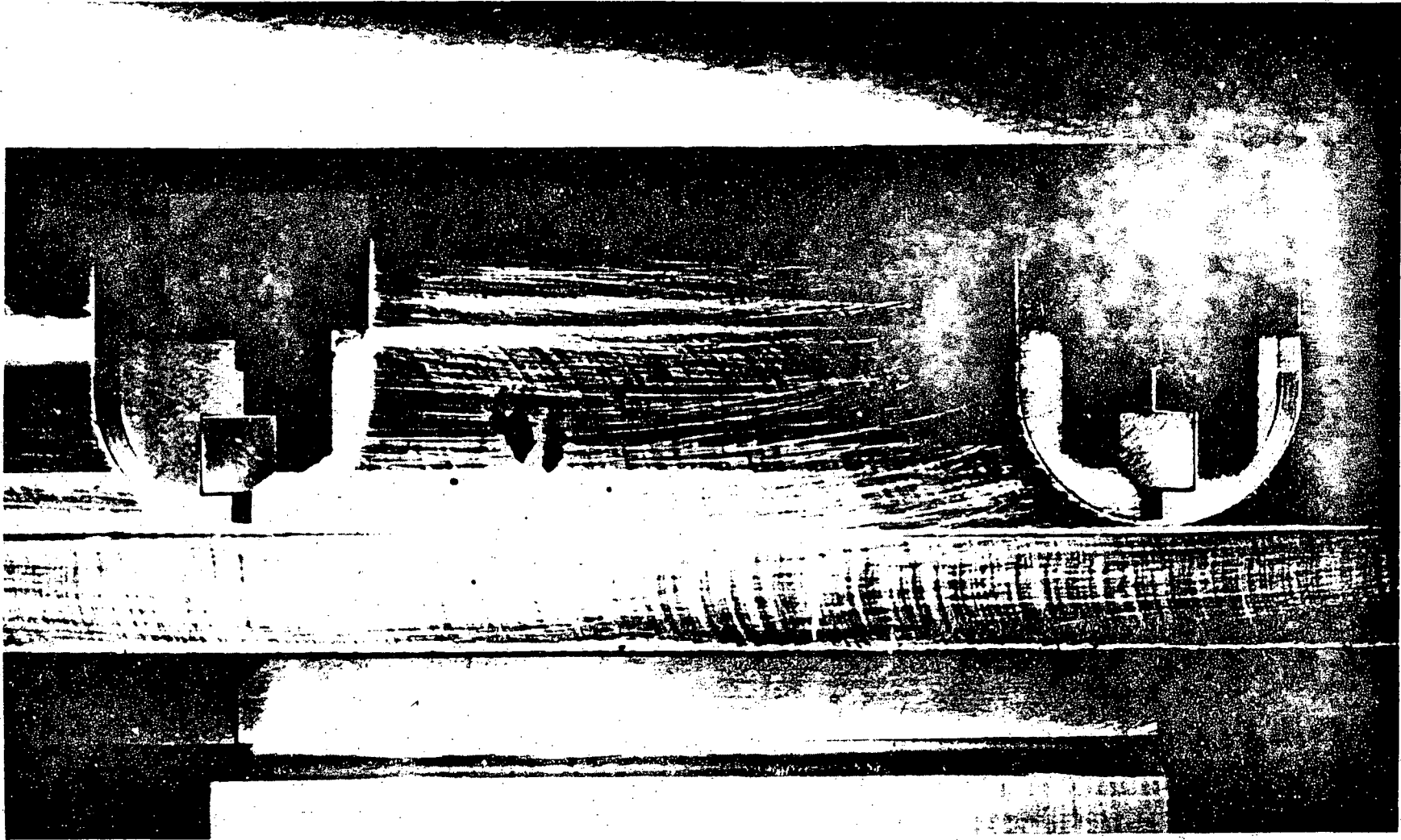


Figure B.2.1-3
Test No. 1
PEL

B-7

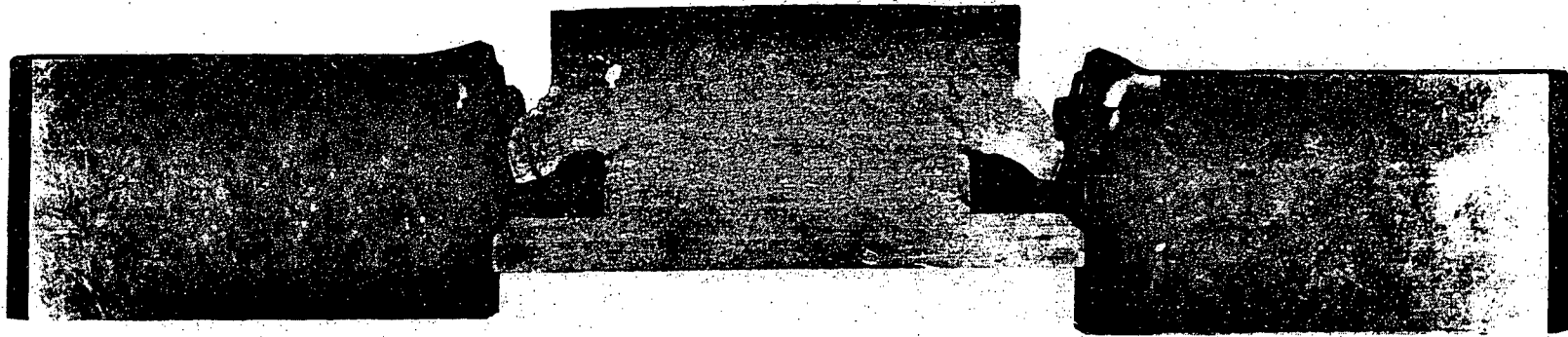
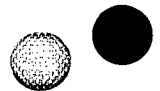
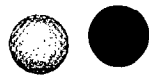


Figure B.2.1-4
Test No. 1
Final Deformation Shape



B.2.2 Test No. 2

Test No. 2 was performed on SA-508 material traceable to the prototype CRBRP Closure Head IRP. Development Q.A. verification of equipment calibration and data recording procedures was required and established.

B.2.2.1 Data

Test No. 2 loading was increased until the plastic instability load was reached. Dial Indicators alone were used to measure deflections. Data acquisition proceeded without difficulty throughout the test. Dial Indicator No. 1 measured total deflection between the top and bottom plates of the Baldwin Universal Testing Machine. Dial Indicator No. 2 measured the deflection between the top of the vessel flange and bottom plate of the testing machine. Dial Indicators No. 3 and 4 measured lateral motion of the top fixture and bottom fixture relative to the bottom plate of the testing machine. The Test No. 2 data with cognizant Development Q.A. and Materials Test Engineer signatures is presented in Appendix B.

B.2.2.2 Force-Deflection Curves

The 1/10 scale LRP shear ring force-deflection curves for SA-508, based on Dial Indicator No. 1 and No. 2 readings, is illustrated in Figure C.2.2-1.

Features of the SA-508 specimens force deflection curve were based on Dial Indicator No. 1 readings. The respective linear elastic stiffness (K), proportional elastic limit (PEL), and plastic instability load (P_I) and deformation (PD) are as follows.

$$K = 0.833 \times 10^6 \text{ LB/in}$$

$$\text{PEL} = 20,000 \text{ LBS.}$$

$$\text{PD} = 0.250 \text{ in.}$$

$$P_I = 32,500 \text{ LBS.}$$

B.2.2.3 Photographs

Photographs of the 1/10 scale SA-508 specimens were taken at selected force levels throughout Test No. 2. Three (3) rolls of film were used. The first

roll included 15 frames which covered force levels from an initial load of 80 LBS to 23,000 LBS. The second roll included 8 frames which covered the range from 24,000 to 29,500 LBS. The third roll included 4 frames over the 30,000 to 32,700 LB force range.

Photographs of the Test No. 2 specimens at no load (80 lbs.), PEL (20,000 lbs.), and P_I load (32,500 lbs.) are presented in Figures B.2.2-2 through -4 respectively. The photographs of the front and back of the Test No. 2 set-up after full loading is presented in Figures B.2.2-5 and -6 respectively.

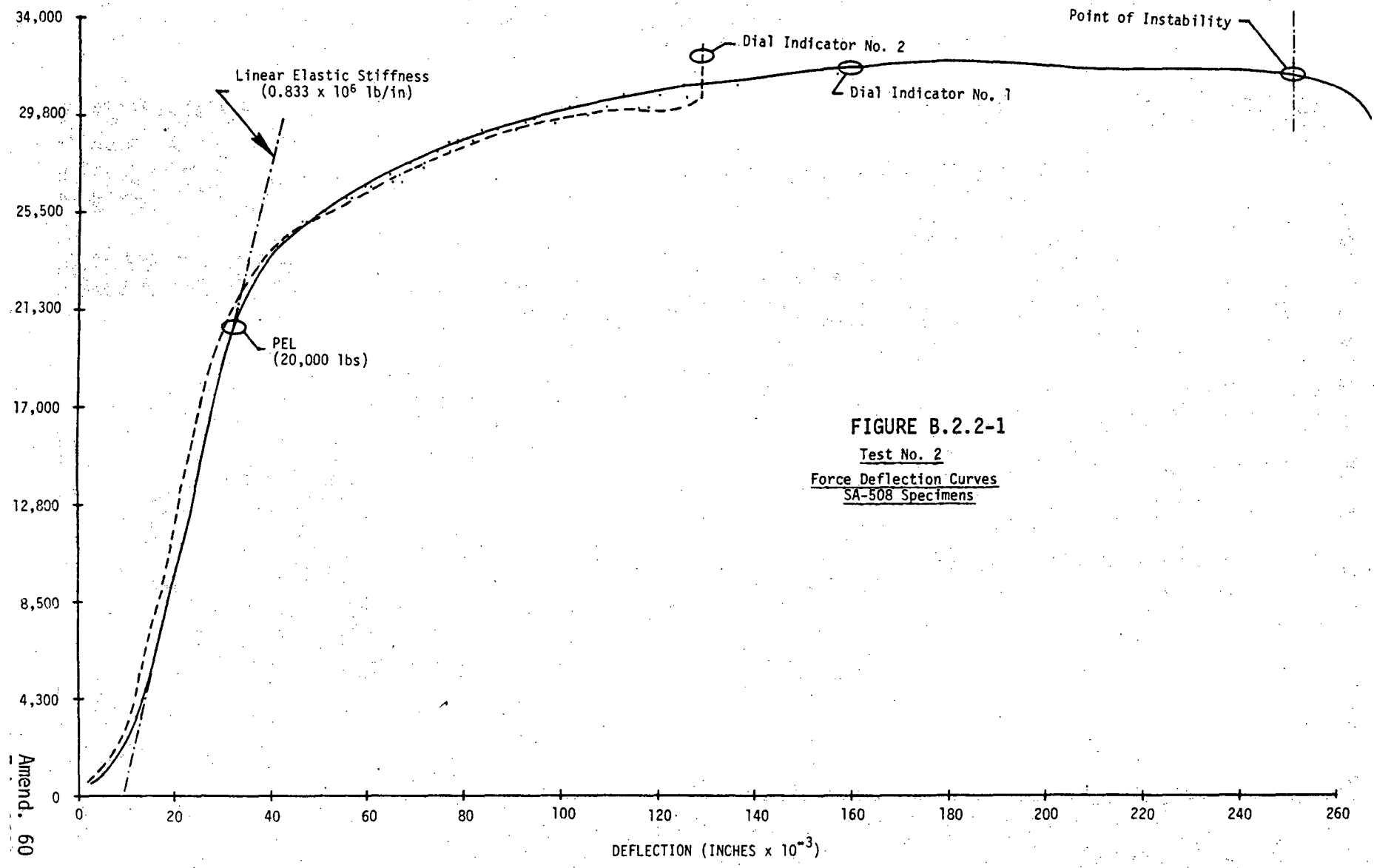


FIGURE B.2.2-1
 Test No. 2
 Force Deflection Curves
 SA-508 Specimens

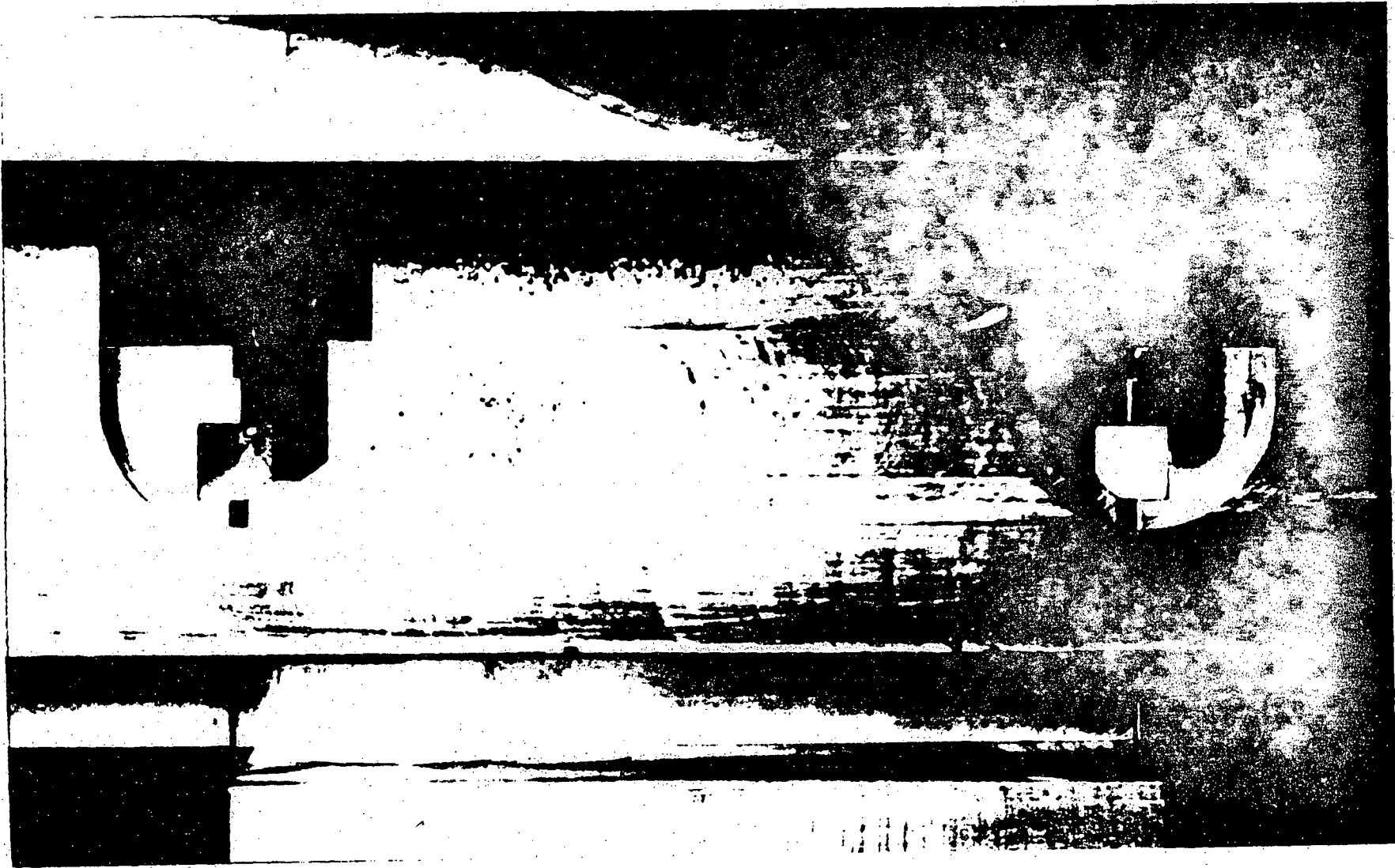
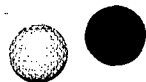


Figure B.2.2-2
Test No. 2
No Load



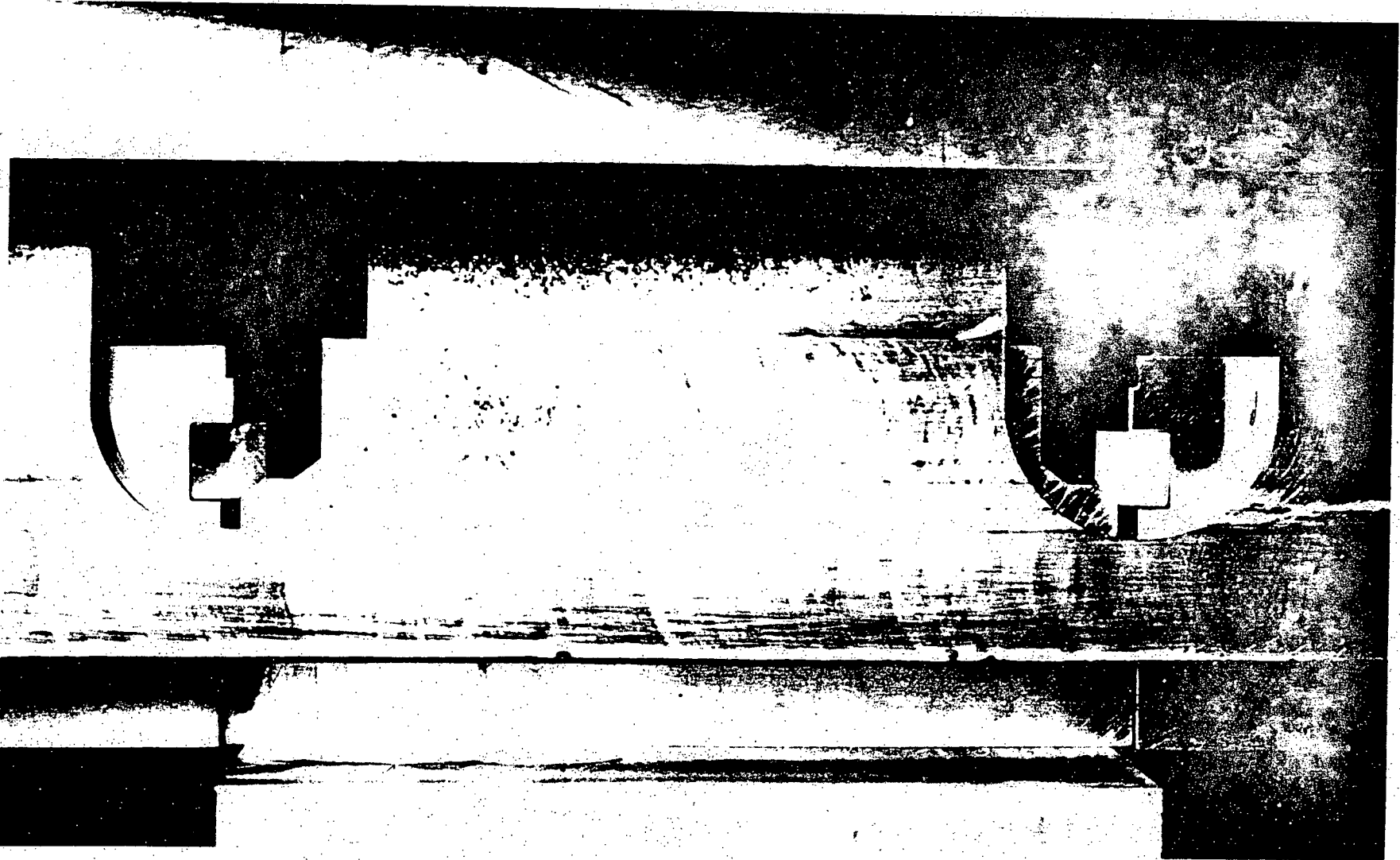


Figure B.2.2-3
Test No. 2
PEL

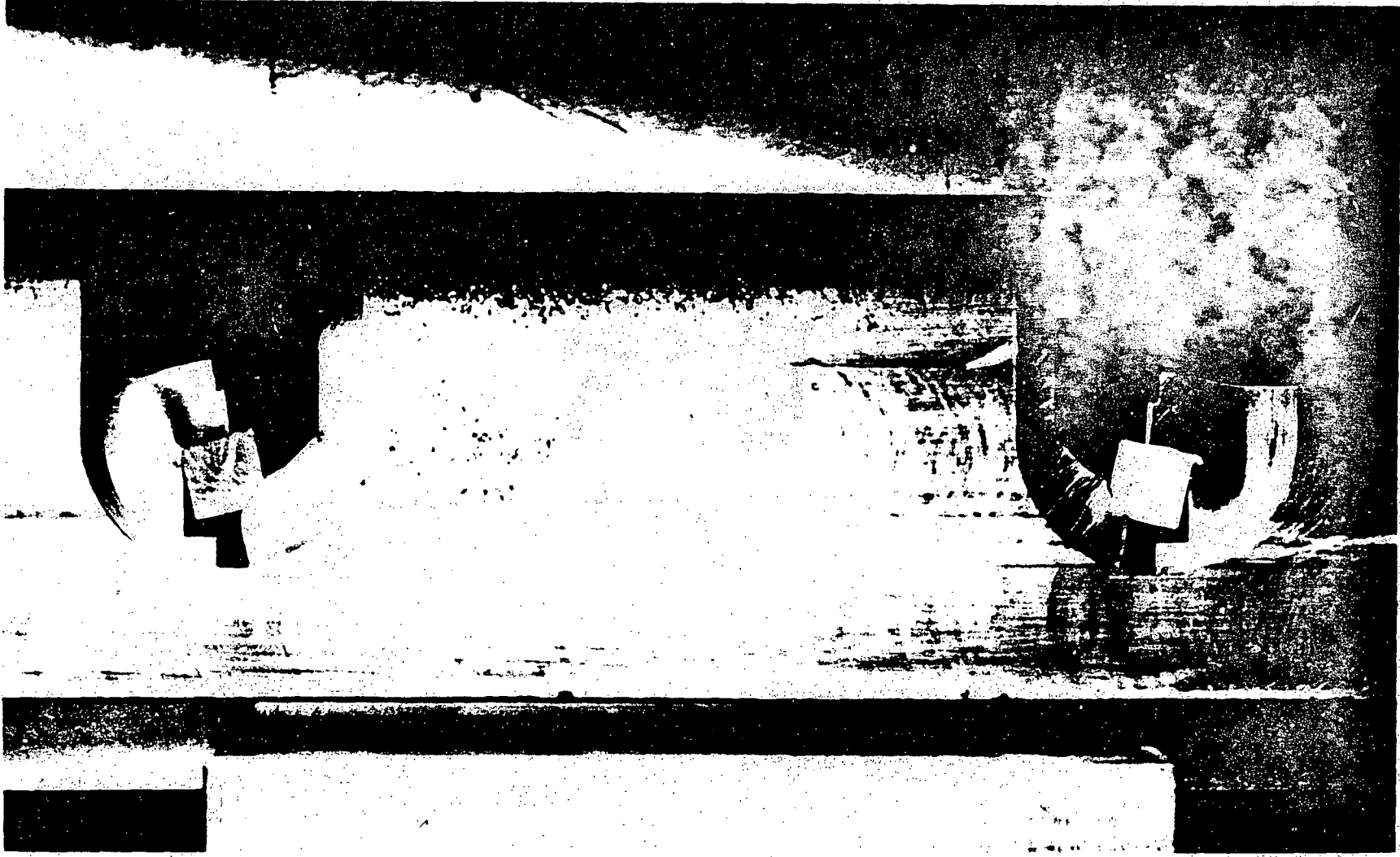
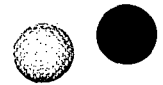
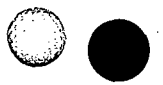


Figure B.2.2-4
Test No. 2
PI

R-1A

Amend. 60



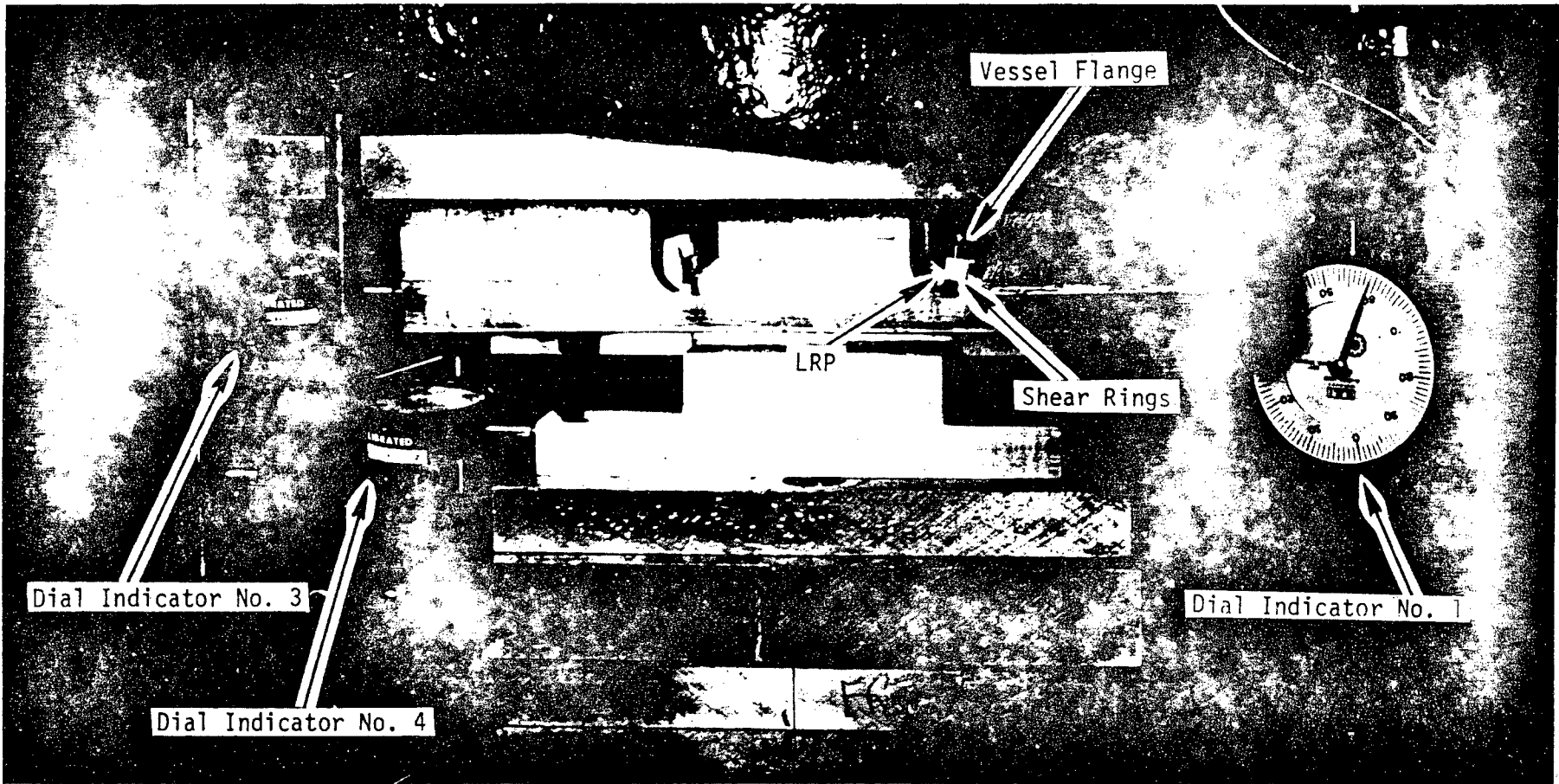


Figure B.2.2-5
Test No. 2
Test Set-Up - Front

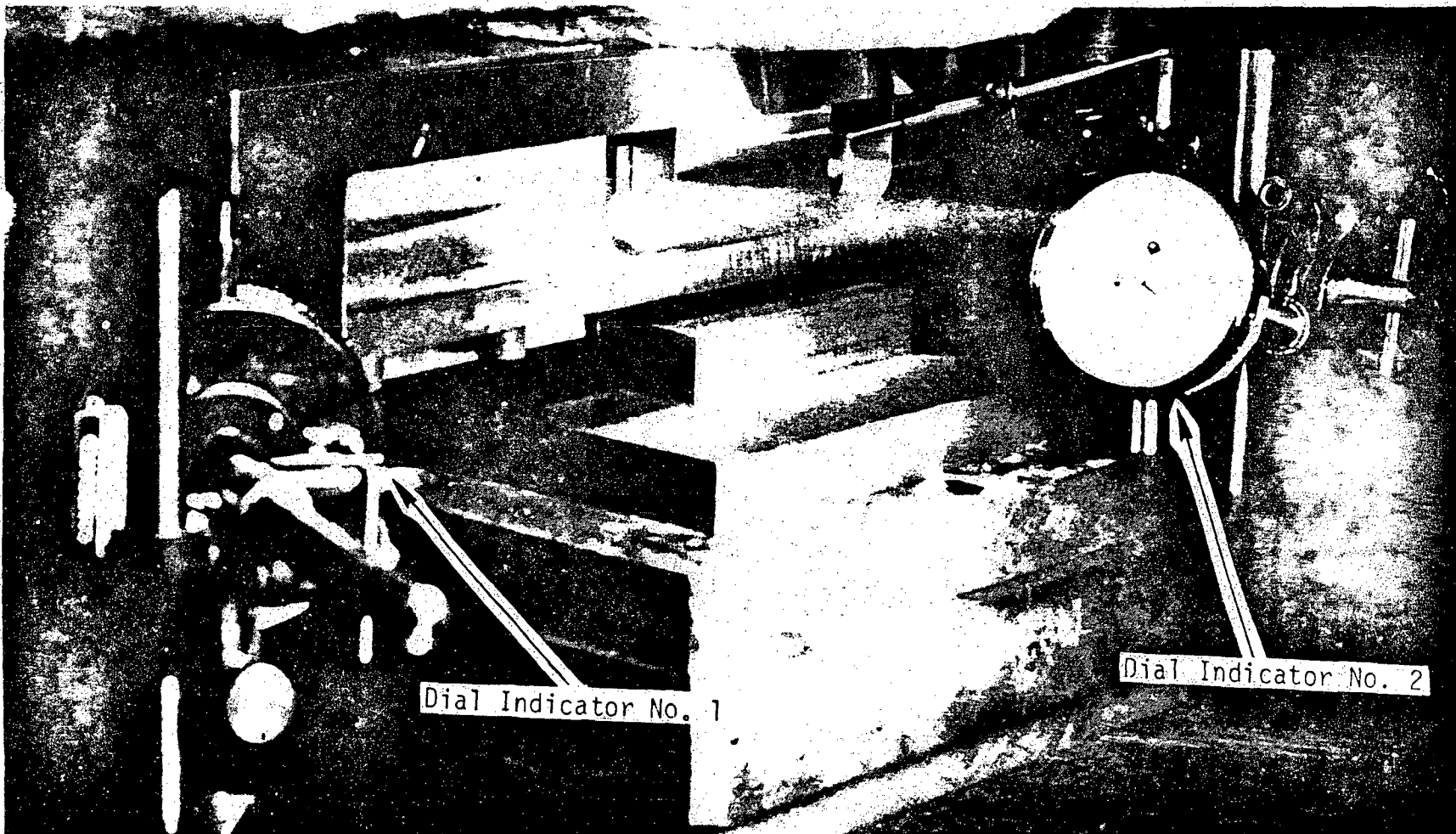


Figure B2.2-6
Test No. 2
Test Set-Up - Back

B.2.3 Test No. 3

Test No. 3 was performed on SA-508 material traceable to the Prototype CRBRP Closure Head IRP. Development Q.A. verification of equipment calibration and data recording procedures was required and established.

B.2.3.1 Data

Test No. 3 loading covered the range only to the PEL (20,000 lbs.) found in Test No. 2. Two (2) cycles of loading and unloading were made to establish linearity and hysteresis effects.

The Test No. 3 equipment utilized a total of six (6) Dial Indicators. No. 1, 2, 3, and 4 were the same in terms of identification and position as used in Test No. 2. Dial Indicators No. 5 and 6 were arranged to measure the rotation of the shear ring. In order to permit shear ring rotational measurements, one (1) shear bar was drilled and tapped to accommodate a right angled lever arm. In this arrangement, Dial Indicator No. 5 measured the combined translation of the shear bar and lever arm rotation while Dial Indicator No. 6 measured shear bar translation alone. Optical comparator readings were made before and after Test No. 3 to determine the residual plastic distortion in the test specimens after successive loadings and un-loadings over the PEL range.

During the first cycle of loading, Dial Indicator No. 6 was found to be improperly adjusted and deflection readings were considered invalid. Proper adjustment of Dial Indicator No. 6 was made before the start of the second loading cycle. Dial Indicator 1 through 5 readings are valid for both loading cycles.

B.2.3.2 Force Deflection Curves

The 1/10 scale LRP shear ring force-deflection curves for the first and second loading cycles, based on Dial Indicator No. 1 and No. 2 readings, are illustrated in Figure B.2.3-1. Dial Indicator No. 3 and 4 readings did

not vary significantly during Test No. 3. The rotation of the shear ring during the second loading cycle is illustrated in Figure B.2.3-3.

Features of the SA-508 specimens force deflection curve are the linear elastic stiffnesses (K) and proportional elastic limit (PEL). For the first and second loading cycles, the PEL was approximately 20,000 lbs. Linear elastic stiffnesses (K) during the loading portion were found to increase from the first to second cycle with approximate values of 1.16 and 1.42×10^6 Lb/in respectively.

B.2.3.3 Photographs

Photographs were taken at selected force levels throughout the first loading cycle of Test No. 3. One (1) roll of film was used which included 16 frames to cover the loading from 200 to 20,000 lbs. and unloading to 20 lbs.

Test No. 3 photographs during the first loading cycle at no load (200 lbs.) and the PEL (20,000 lbs.) are presented in Figures B.2.3-3 and -4 respectively. Photographs of the front and back of the Test No. 3 set-up after the second loading cycle are presented in Figures B.2.3-5 and -6 respectively.

FIGURE B.2.3-1
Test No. 3
Force-Deflection Curves
SA-508 Specimens

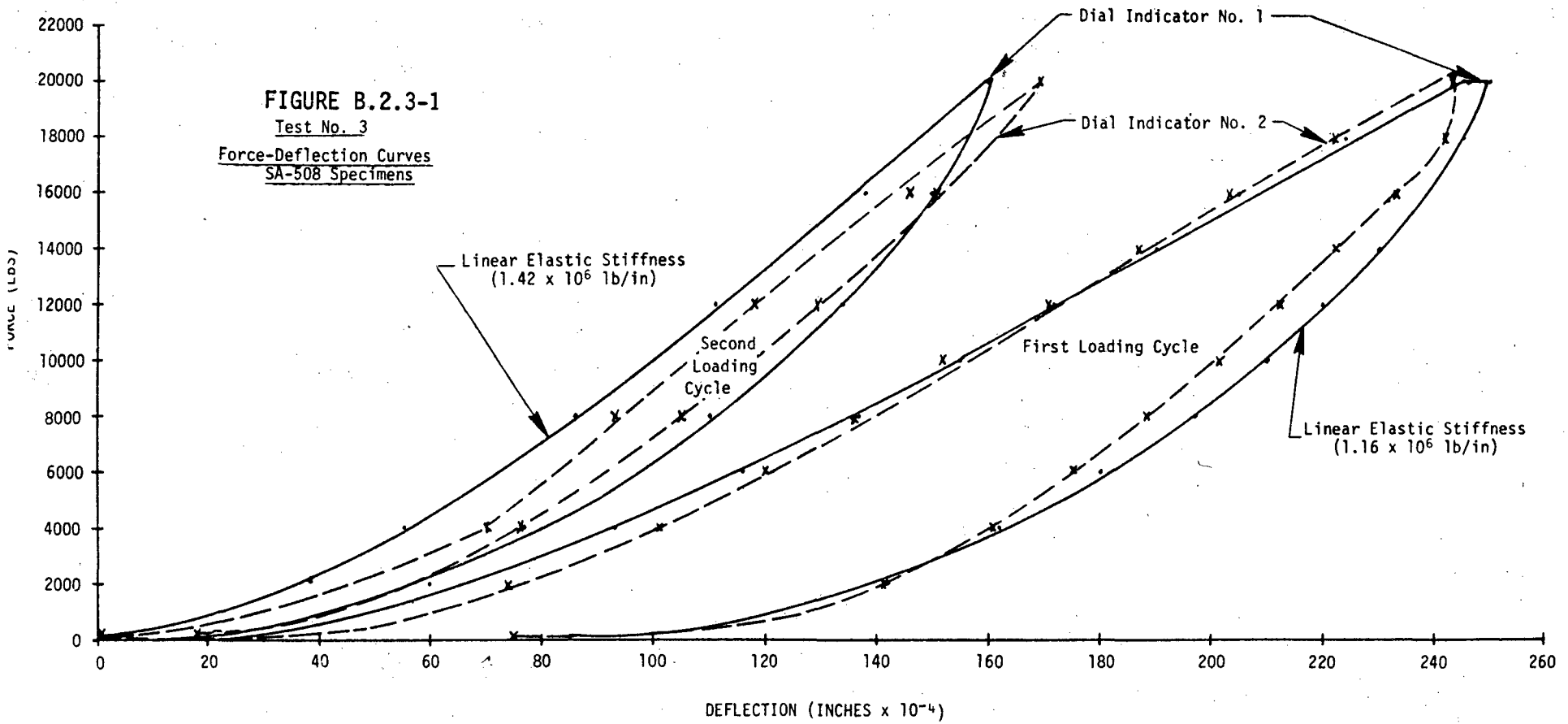
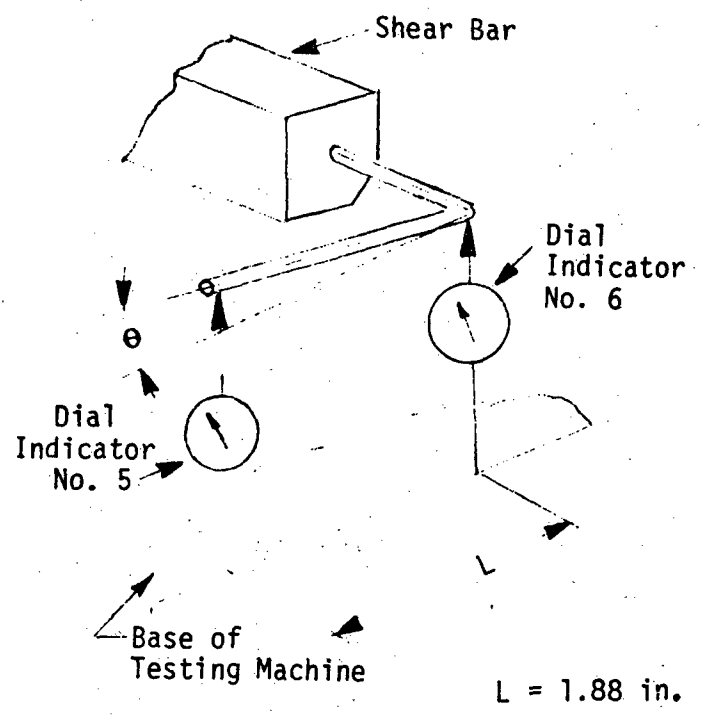
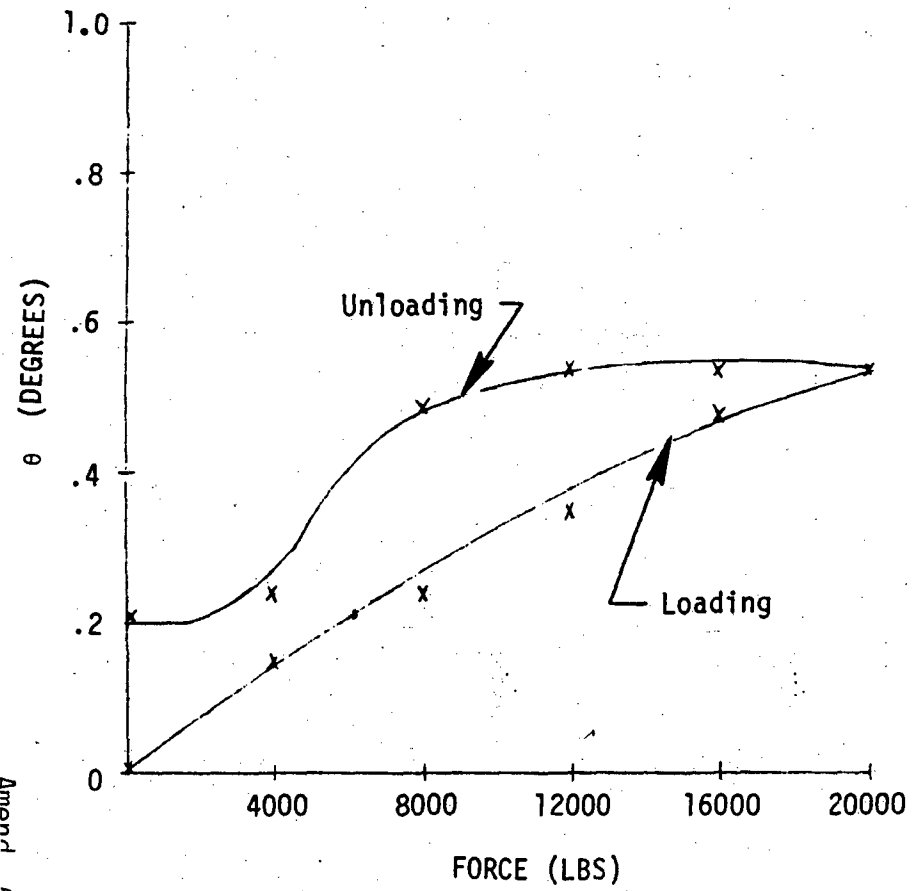
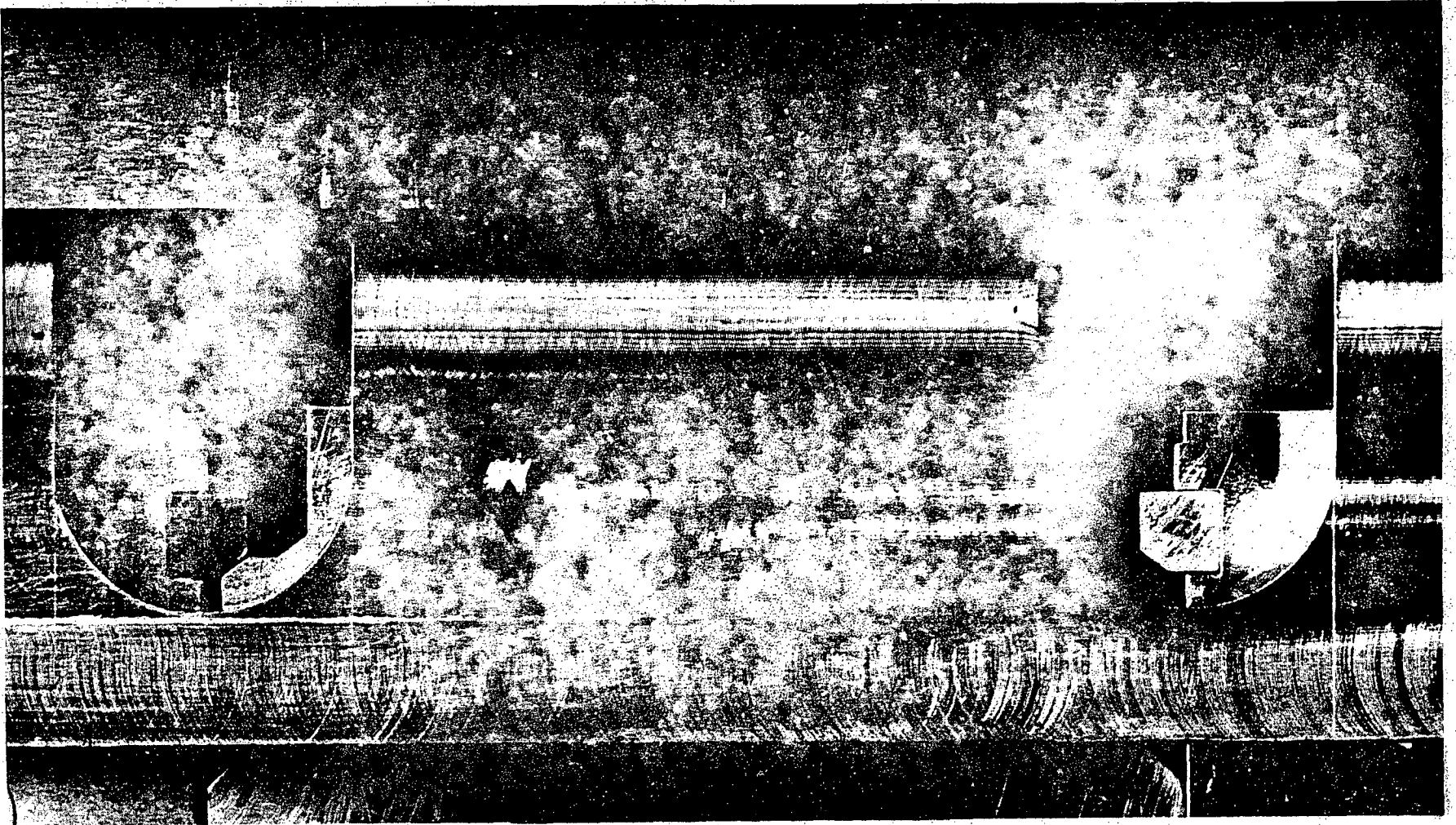


FIGURE B.2.3-2
Test No. 3
Shear Ring Rotation
Second Loading Cycle



B-21



FigureB. 2.3-3
Test No. 3
No Load

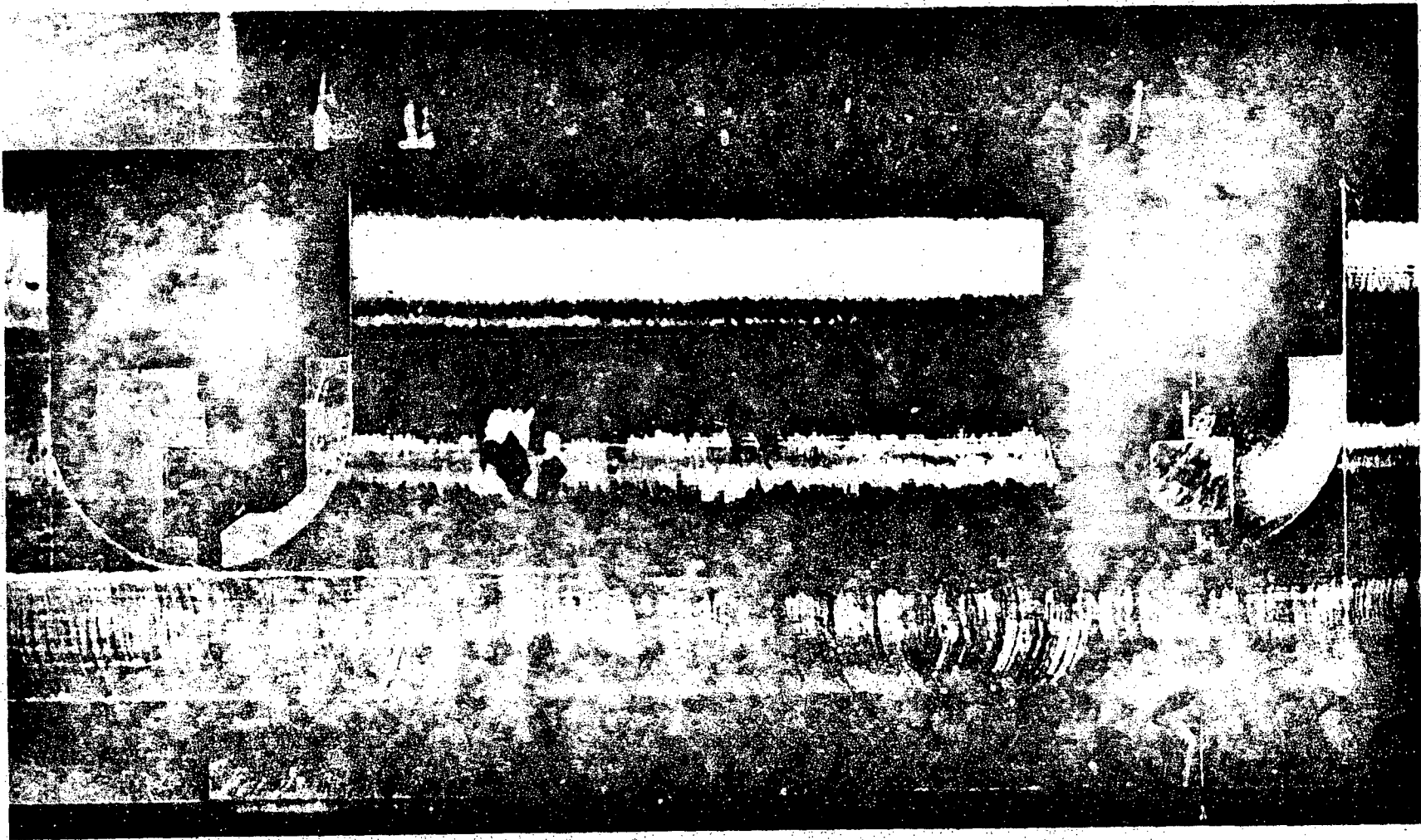
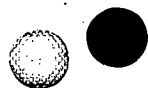


Figure B.2.3-4
Test No. 3
PEL



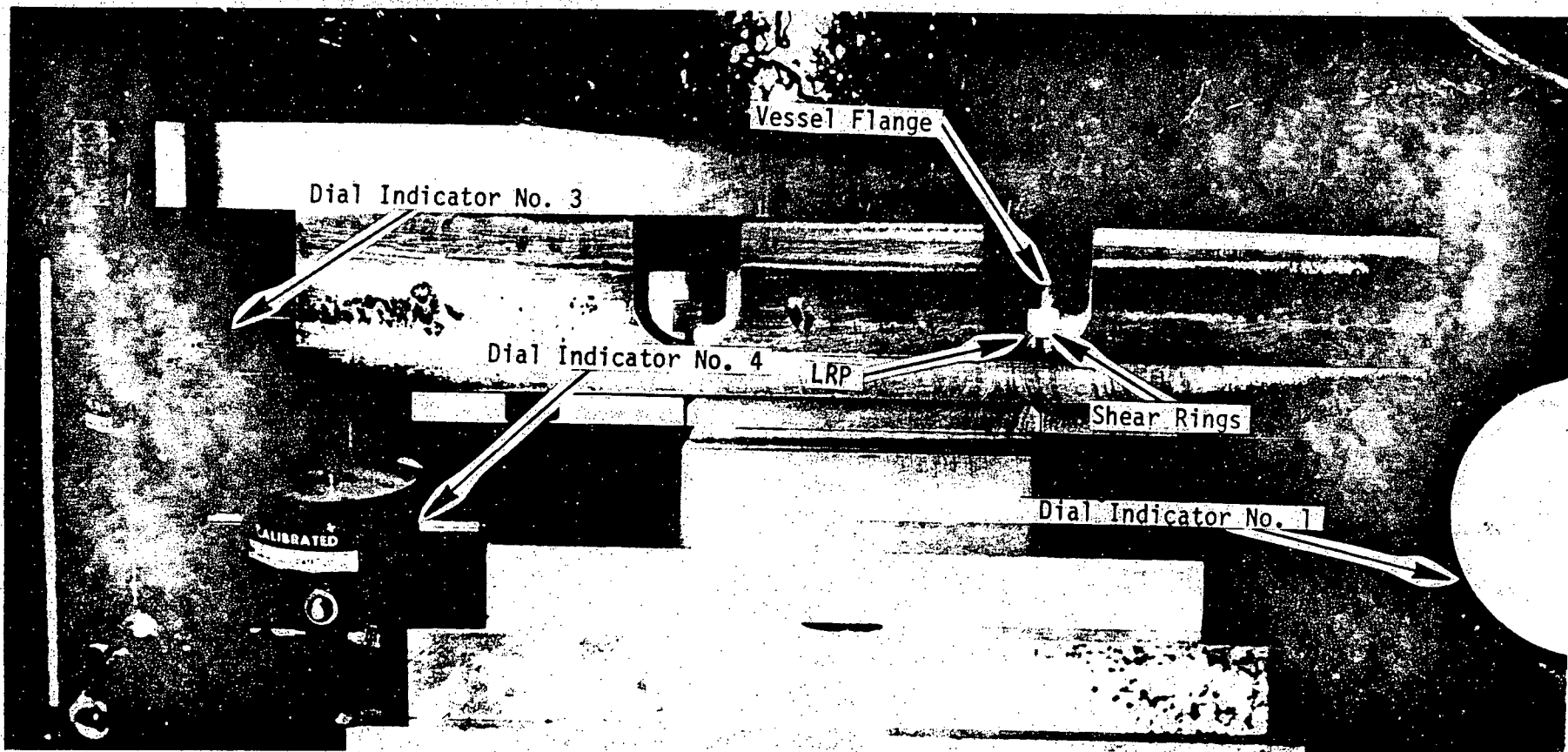


Figure B.2.3-5
Test No. 3
Test Set-Up - Front

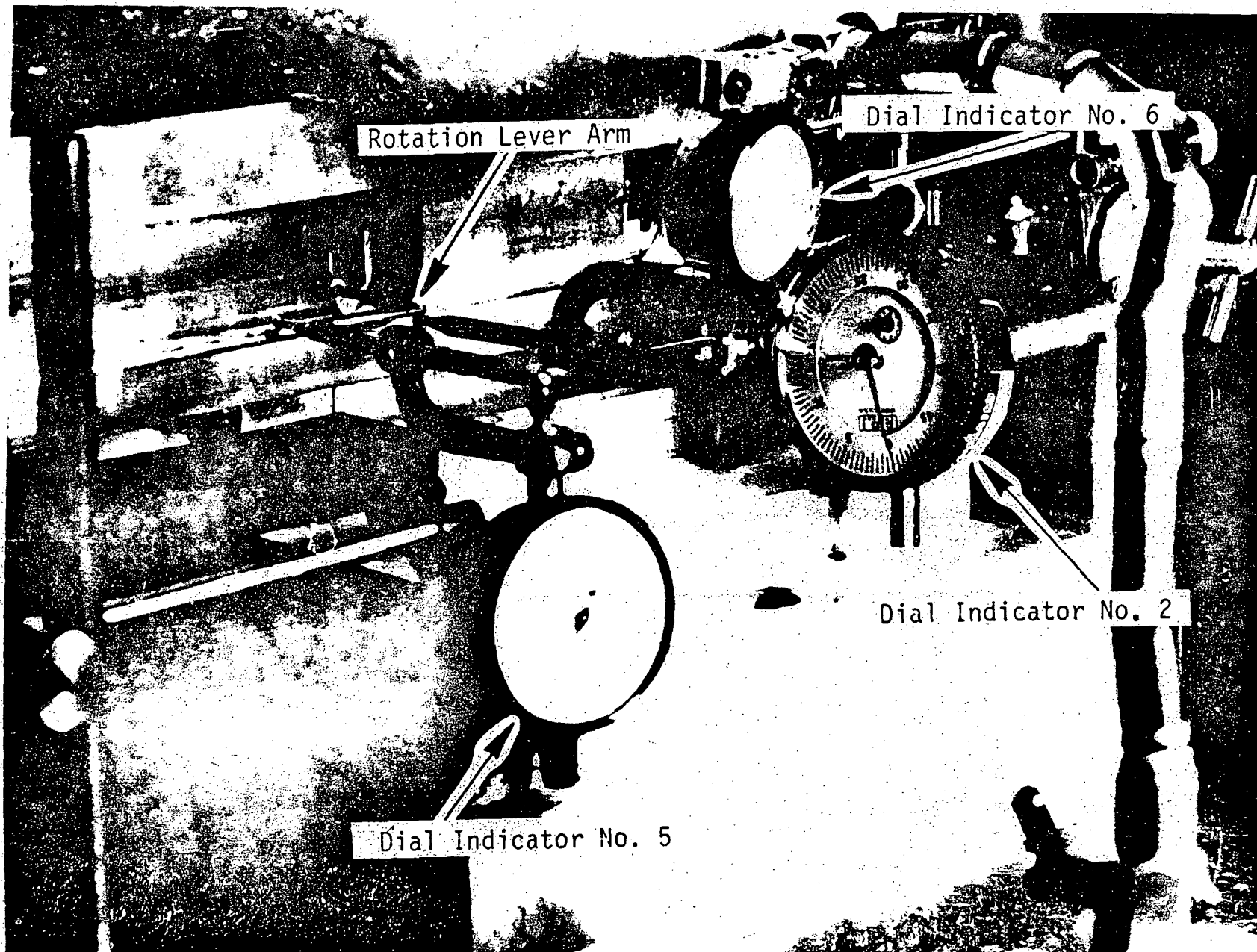


Figure B.2.3-6
Test No. 3
Test Set-Up - Back

Question 001.541 (F6.3.2.3)

Discuss in a quantitative manner the effect of the shield plates, the vortex suppressor plate and crush tubes on the sodium slug impact forces transmitted to the head. Discuss how the CDA analysis presented accounts for the presence of these members.

Response:

The CRBRP Project has consolidated all considerations given Hypothetical Core Disruptive Accidents into report CRBRP-3 (References 10a and 10b, PSAR Section 1.6) and its associated references; consequently, PSAR Appendices D and F have been withdrawn in Amendments 24 and 60 respectively. The response to this question is now found in Section 5.4 of Reference 10a and 14, PSAR Section 1.6.

60 | 61

Question 001.542

Provide an estimate of the additional distortion of the core barrel and mid-reactor vessel wall, and the additional loading of the Core Support Structure when the resistance of the Upper Internals Structure (UIS) to the core vapor expansion is taken into account. Describe how the UIS is included in the REXCO calculations.

Response:

In the REXCO model used to generate the Structural Design Basis loads, the Upper Internals Structure (UIS) was omitted. However, the REXCO model has been adapted since to include the UIS as an inertial mass. While this model does not include the structural resistance of the UIS, a qualitative assessment of the addition of this resistance has been made based on UIS structural analysis and the new REXCO model.

60

In addition to the Structural Design Basis calculation, the four additional REXCO cases listed below were run:

- Case 1 Structural Design Basis Case (no UIS)
- Case 2 Distributed UIS model. The mass of the UIS and its associated sodium are smeared over the REXCO zones in which the UIS is located (See Figure Q001.542-1)
- Case 3 Concentrated UIS model. The mass of the UIS and its associated sodium are smeared over the first two REXCO zones above the core region (See Figure Q001.542-2)
- Case 4 Concentrated UIS model. This has the same specifications as Case 3 except that the density of the two UIS zones is increased ten times.
- Case 5 Concentrated UIS model. This has the same specifications as Case 3 except that the density of the two UIS zones is increased one hundred times.

Figures Q001.542-3 through Q001.542-5 compare the responses generated by the above calculations. Figure Q001.542-3 shows the sensitivity of pressure under the UIS when its effective (inertial) stiffness is increased. It can be seen that the peak pressure more than doubles from Case 1 (the Structural Design Basis case) to Case 5 (the 100X density case). Figure Q001.542-4 shows the associated UIS displacements under such pressure loadings. As expected, the greater the UIS mass, the less upward displacement is observed. Figure Q001.542-5 shows the resulting pressure loads experienced by the core support structure for these cases (Case 4

is not plotted for clarity). As can be seen, the core support structure load is virtually insensitive to the configuration of the UIS. This insensitivity can be explained through the fact that, with such a rapid transient, (tens of milliseconds) the vapor bubble effectively decouples the response of the upper and lower regions of the core. As the UIS resistance is increased, the pressure under this structure increases, but only locally. This fact is reflected in Figure Q001.542-6, where the core barrel strains for Case 3 and Case 5 are compared. As the UIS resistance increases, the strain in the top of the core barrel increases, but the peak that occurs near the bottom of the core barrel remains unchanged. Table Q001.542-1 summarizes pertinent data from the five cases described above. From this table, the insensitivity of the peak loads on the core support structure, the core barrel and vessel wall to UIS resistance can clearly be seen.

The above discussion has been limited to a UIS whose resistance is purely inertial. However, the UIS pressure in Case 5 was seen to be double that of the Structural Design Basis Case (Case 1). It was shown that the UIS column load resulting from the Structural Design Basis case (851,000 lbs) was well in excess of the minimum allowable column buckling load (320,000 lbs). Hence column buckling would be expected at loads below those seen in Case 5. The resulting pressure reduction will thus limit additional loads on such structures as the core support structure and the core barrel.

In summary, it has been shown that introduction of a UIS structure has virtually no effect on the loads seen at the core support plate and mid reactor vessel wall. While distortion of the upper core barrel does occur as a result of introducing a UIS, the peak distortions, which occur at the bottom of the core barrel, remain unchanged.

| 60

TABLE Q001.542-1
EFFECTS OF UIS REPRESENTATIONS ON PERTINENT LOADINGS

Output Parameter	No UIS	Distributed UIS	Concentrated UIS		
	Case 1 (Structural Design Basis)	Case 2 Normal UIS Density	Case 3 Normal UIS Density	Case 4 10X UIS Density	Case 5 100X UIS Density
Peak Pressure Under UIS Structure (psi)	628	696	766	1156	1288
Net Force on Core Support Structure (10^7 lb.)	3.24	3.25	3.24	3.26	3.24
Peak Pressure in Lower Core Barrel (psi)	1192	1187	1189	1213	1204
Peak Pressure on Vessel at Core Centerline (psi)	426	425	426	429	431

Q001.542-3

Amend. 22
June 1976

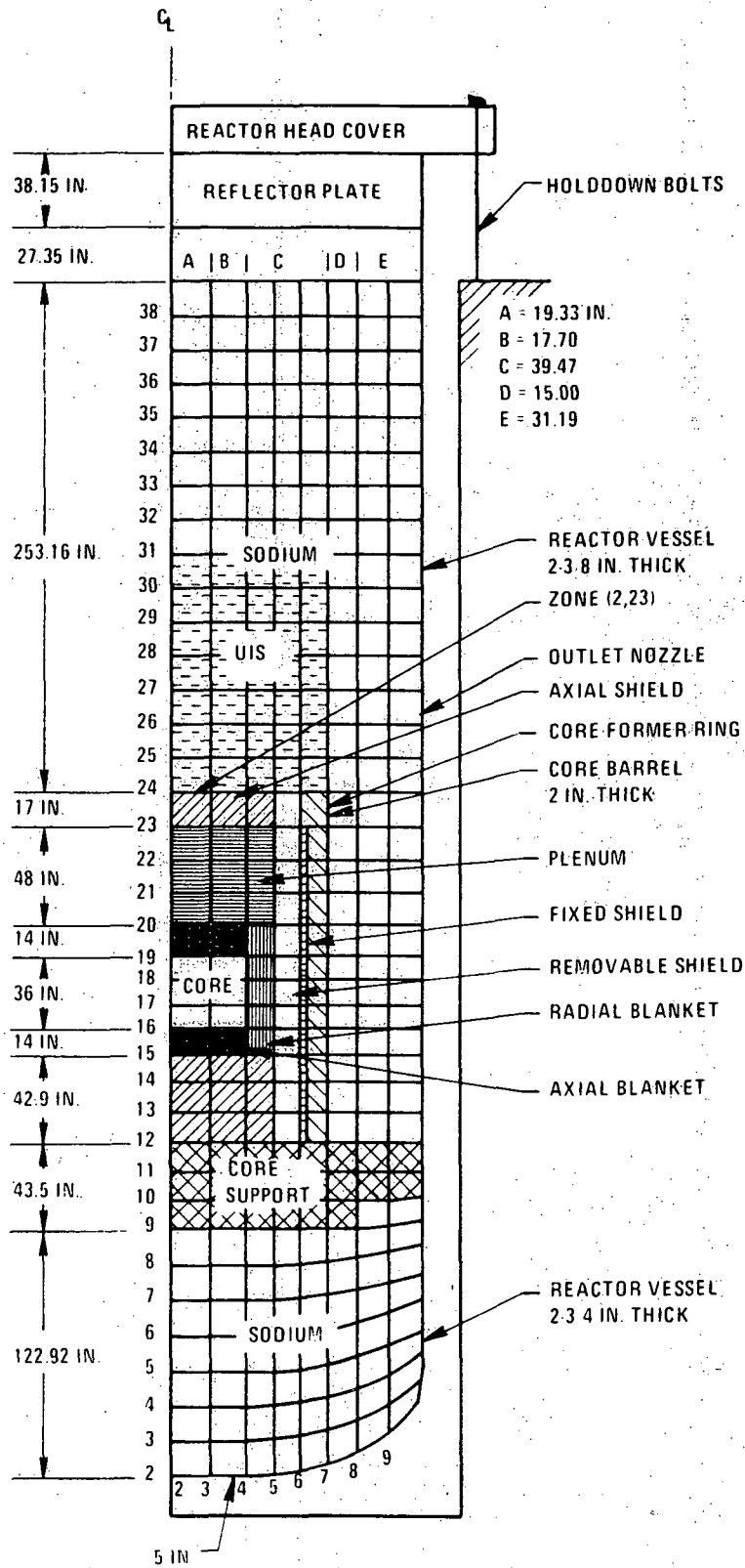


Figure Q001.542-1 REXCO Model With Distributed UIS

7683-183

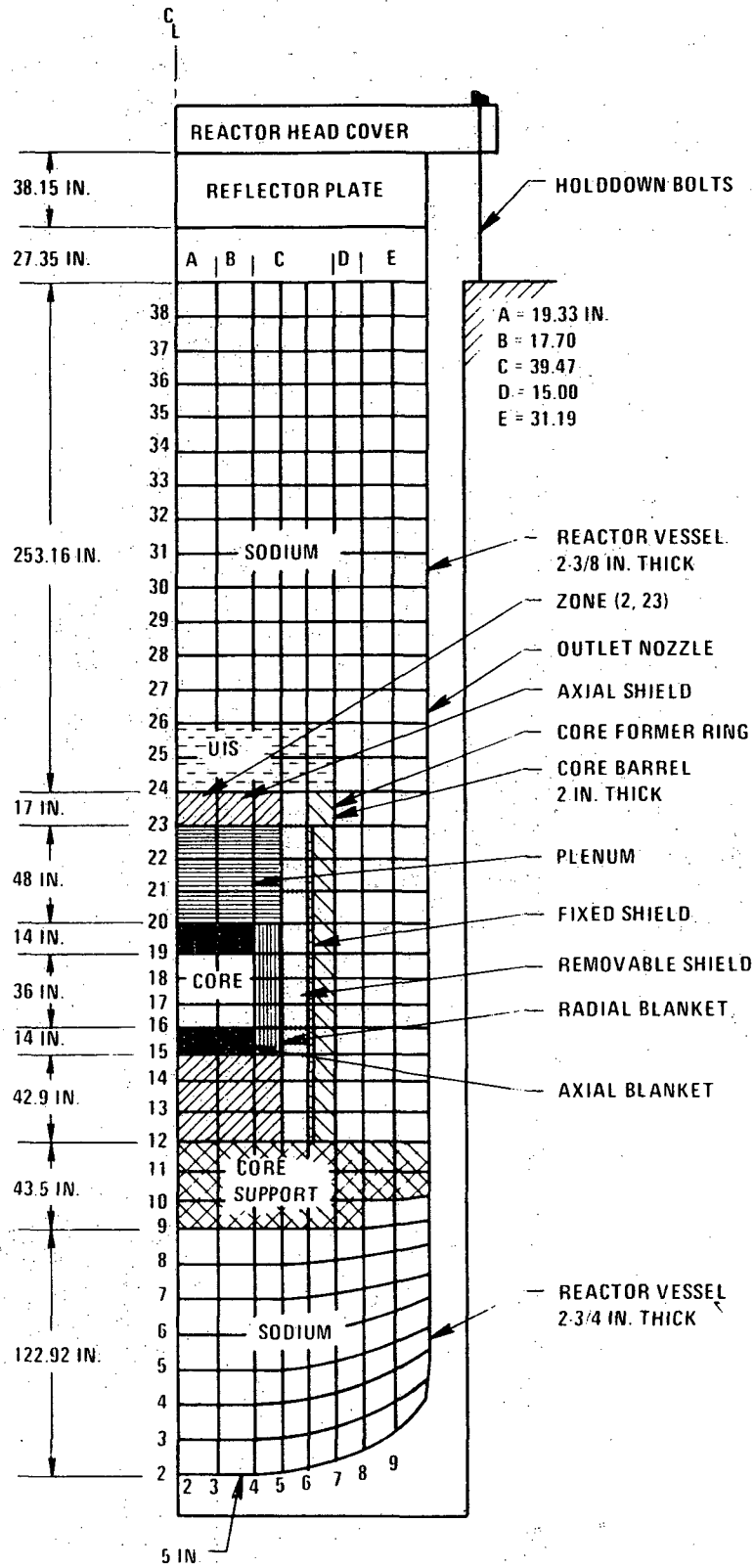


Figure Q001.542-2 REXCO Model With Concentrated UIS

7683-184

Q001.542- 5

Amend. 22
June 1976

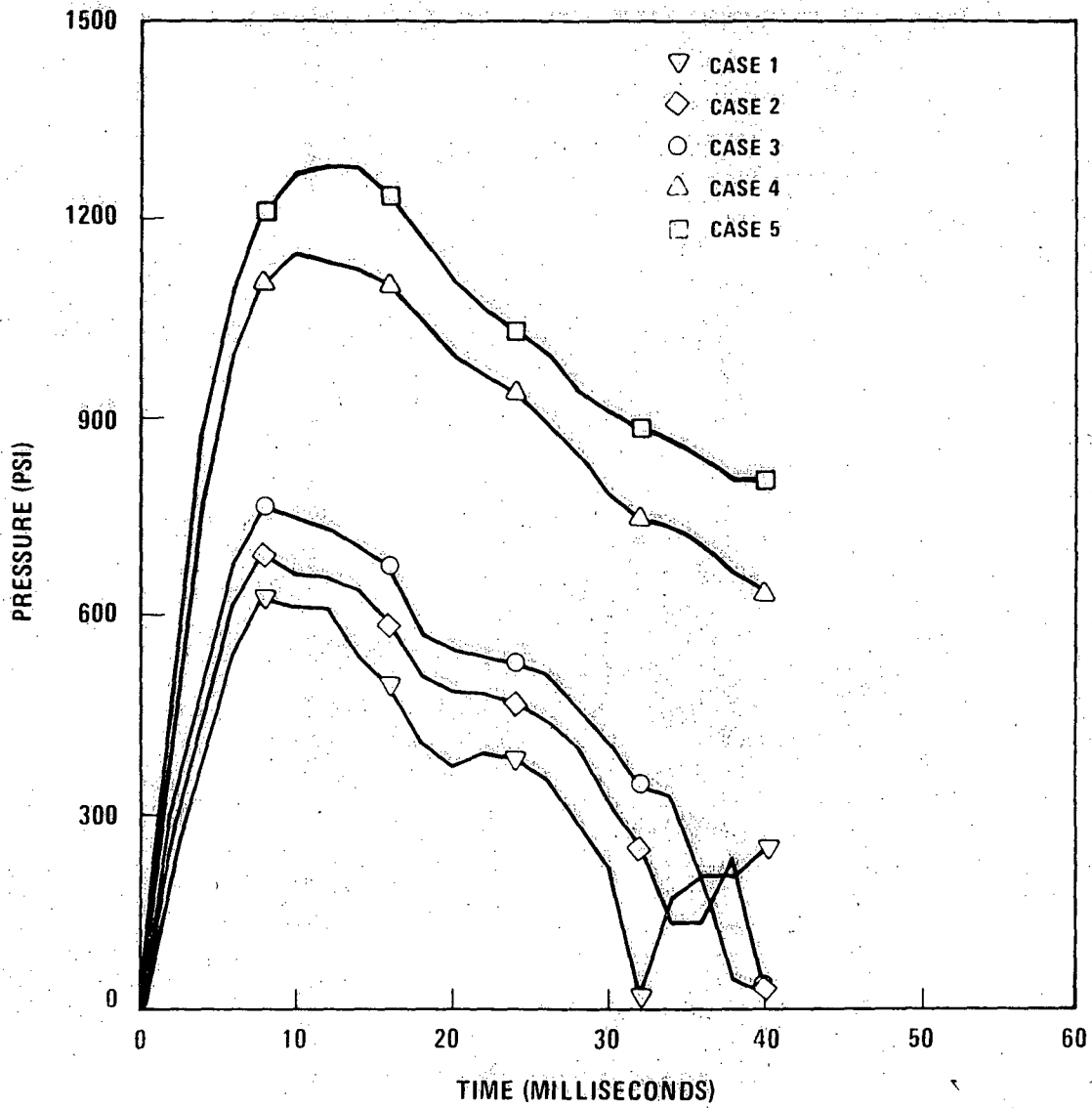


Figure Q001.542-3. Pressure Histories Under UIS

8680-2

Q001.542-6

Amend. 22
June 1976

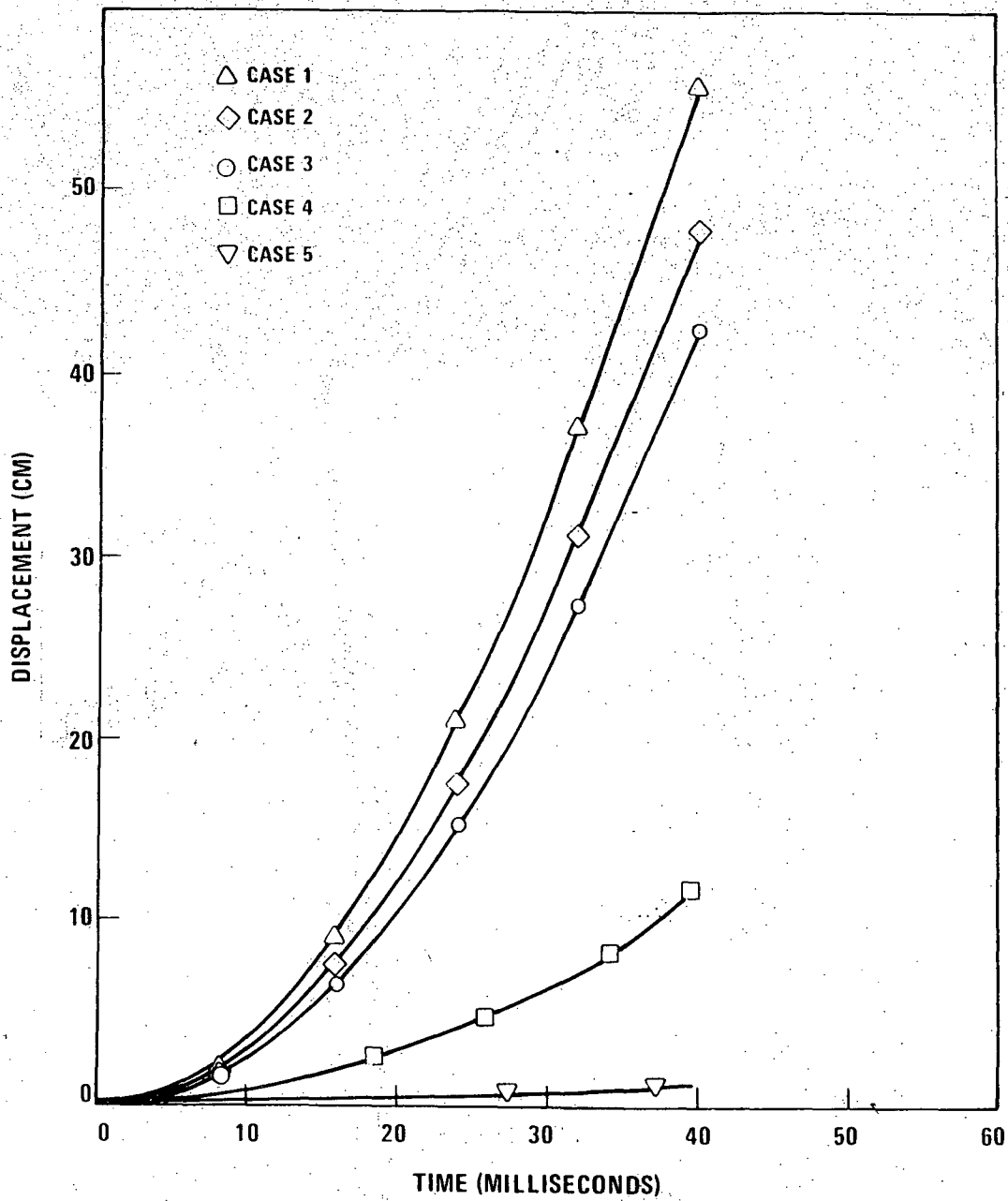


Figure Q001.542-4. Displacements Of Underside Of UIS

8680-3

Q001.542-7

Amend. 22
June 1976

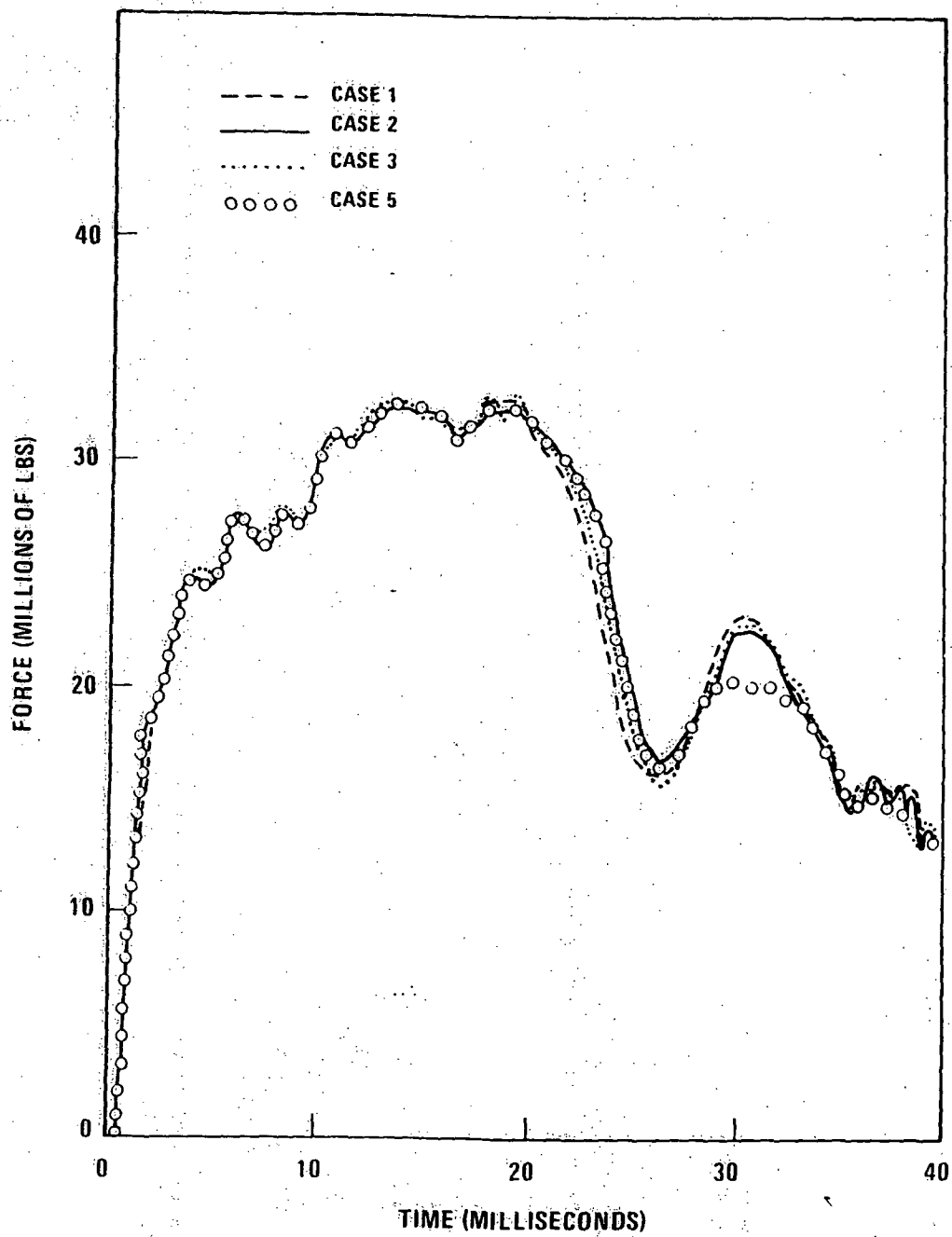


Figure Q001.542-5. Load Histories On Core Support Plate

8680-4

Q001.542-8

Amend. 22
June 1976

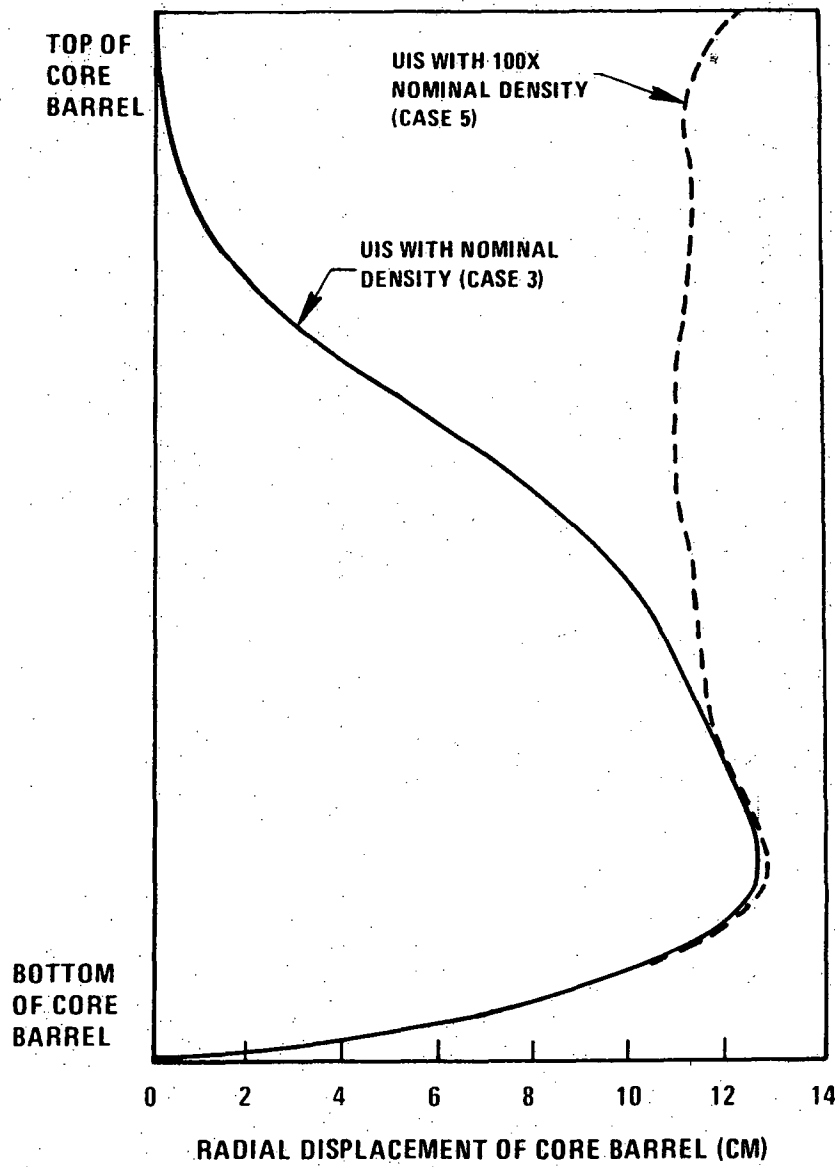


Figure Q001.542-6. Radial Displacement Of Core Barrel For Concentrated UIS Models

8680-1

Q001.542-9

Amend. 1976

Question 001.543 (F6.3.2.2)

Identify which version of REXCO-HEP was used for the CDA analysis presented in Appendix F. The input listed in Section D6.5 and the description of REXCO-HEP in Appendix A (see Section F6.3.2.2) are for a version of REXCO-HEP older than the version documented in Reference (1) of Section F6.3.

Response:

This question requests clarification of information which is no longer a part of the current documentation. The Project has since consolidated all considerations given Hypothetical Core Disruptive Accidents into report CRBRP-3 (References 10a and 10b, PSAR Section 1.6) and its associated references; consequently, PSAR Appendices D and F have been withdrawn in Amendments 24 and 60 respectively. The formal documentation of the REXCO-HEP used in HCDA analysis is contained in "REXCO-HEP: A Two-dimensional Computer Code for Calculating the Primary System Response in Fast Reactors" by Y. W. Chang and J. Gvildys, ANL-75-19, June 1975.

Question 001.544 (F6.3.2.3)

The closure head moves independently of the reactor vessel in the REXCO computer model. Section F6.3.2.3 states that the "mass of the head has been increase to better reflect the restraint afforded by the suspended vessel and holdown bolts". Provide the mass of the head and head-mounted components. Discuss what amount the mass was increased and indicate how the amount of the increase in mass was determined.

Response:*

160

In the current reactor system design (See PSAR Section 5.2) and the REXCO model (Section 5.1, Reference 10a, PSAR Section 1.6), the reactor vessel and its contents are suspended from a ledge. The closure head is mounted on the vessel flange. In calculating the sodium slug upward force, it was thought necessary to increase the mass of the head, so that the head upward acceleration and its effects on the sodium slug force calculation would be properly modeled. |47 |60

In a static sense, the total mass of the reactor vessel system would be added. However, during a core disruptive accident, the whole reactor vessel system behaves as a vertical spring, able to vibrate up or down. There is no clear definition as to the amount of additional mass that should be added to the head. To resolve this difficulty, a sensitivity study of the sodium slug upward force with different head masses was performed.

The cases studied ranged from one case in which the head was modeled with the head plus head-mounted components mass (1.26×10^6) to the other extreme case in which the head was modeled with the mass of the complete reactor system (3.97×10^6 lb). The sodium slug impact energy for the larger mass (3.97×10^6 lb) was less than 1% greater than the impact energy for the mass of the head plus head mounted components (1.26×10^6 lb.). The smaller mass (head plus head mounted components) was used in the REXCO model for Structural Margin Beyond the Design Basis (SMBDB) analysis because of the insensitivity of the results to the mass, and because of the non-conservatism of the larger mass model with regard to the load on the holdown bolt system. |47 |47

*Note that Appendix F has been withdrawn. The text, upon which the question is based, can now be found in Section 5.1 of Reference 10a, PSAR Section 1.6. |60

Question 001.545 (F6.3.2.3)

The Core Support Structure is represented by an overly-strong structure in the REXCO model of the CRBR (compare Figures 4.2-51 and F5.4-1). It is our opinion that the core support cone can and should be modeled as a REXCO thin vessel. This will obviate the need for much of the improvising described in Section F6.3.2.3 to obtain realistic pressure pulses in the inlet plenum. Discuss the modification to the REXCO model suggested and discuss why it would not be appropriate to provide a new calculation of the inlet plenum pressure history in accordance with the above suggestion.

Response: *

| 60

The Core Support Structure consists of a thick cone and a thick perforated plate. During the initial stages of a core disruptive accident, the pressure is predicted to build up very rapidly in the inlet plenum as compressive fluid transmits pressure through the coolant flow passages. Later, after the pressure in the inlet plenum and the pressure on the core support plate reached equilibrium, further pressure increases may be caused by the inlet plenum volume reduction due to core support plate deflection.

Based on the above discussion, one of the major weaknesses in the REXCO model modifications suggested in this question is that a thin vessel core support is incapable of simulating the rapid pressure rise due to direct fluid communication through the porosity of core support plate. Also there is no assurance that a thin core support structure will provide a conservative estimate of the further pressure increase due to core support vibration. Therefore we do not agree with the suggested model modification as a substitute for the approach used in Section 5.1.1.3 of Reference 10a, PSAR Section 1.6.

| 60

Section 5.1.1.3 includes an explanation of the approach used in modeling the core support structure.

| 60

*Note that Appendix F has been withdrawn. The text, upon which the question has been based, can now be found in Section 5.1 of Reference 10a, PSAR Section 1.6.

| 60

Question 001.546 (F6.3.4.1, F6.3.4.2)

Apparently the force time displacements from REXCO were input to ANSYS to determine dynamic structural responses for the head, vessel, core support, holddown bolts and concrete ledge. It is not clear from the discussion provided how this was done. REXCO itself has some built-in capability for determining structural response. Amplify your discussion on how the synthesis of these two codes was accomplished without invalidating either computation. Both analyses used common structural members which accumulate strain according to definitive equations built into the respective codes. Describe your computational methods in the utilization of the REXCO output.

Response:

A generally recognized technique for determining the structural adequacy of a complex system is to perform a dynamic analysis on the overall structure and use the derived system loads (pressures, displacements etc.) as boundary conditions when detailed component analysis is made.

In the analysis performed here, these system loads were generated using the REXCO code and selectively applied as external boundary conditions to each component when the component's response was evaluated using the ANSYS code (see Appendix A). The fact that REXCO determines the gross structural response of the reactor system while generating system loads in no way invalidates the application of these loads to the component analyses. In either the system or component analysis, the component will experience identical body forces and hence, within the modelling capability of the codes, will respond in the same manner.

The ANSYS calculation will however, result in finer resolution of the stress field and hence allow more detailed evaluations of the structure to be made. For example, the REXCO modelling of the core support structure and the vessel head are somewhat approximate (although these approximations are such as to lead to conservative loads on these components). More detailed models are thus necessary to make more detailed assessments of the component integrity.

Question 001.547 (F6.3.2.4)

Discuss why the net load on the concrete ledge in Figure F6.3-22 does not return to zero when the system has reached dynamic equilibrium at 120 msec (cf. Section F6.3.2.4). Define the meaning of the net load. Discuss the causes of the maxima and minima responses shown in Figure F6.3-22.

Response:

This question requests clarification of information which is no longer a part of the current documentation. The Project has since consolidated all considerations given Hypothetical Core Disruptive Accidents into report CRBRP-3 (References 10a and 10b, PSAR Section 1.6) and its associated references; consequently, PSAR Appendices D and F have been withdrawn in Amendments 24 and 60 respectively.

Question 001.548 (F6.3.4.2)

Figure F6.3-22 shows that the maximum ledge load (48 million lbs.) calculated by the ANSYS code is very close to the ultimate strength of the concrete ledge (50 million lbs.) for the 661 MW-sec CDA. Provide the input parameters and loading functions for the ANSYS models depicted in Figure 6.3-11 and Figure 6.3-31 and discuss how these values were chosen. Describe how gravity was included in the ANSYS calculation and its importance in the solution.

Response:*

60

It should be noted that 50 million lbs. is the design requirement ledge load for SMBDB; it is not the ultimate strength as stated in the question. The predicted ledge load from the analysis referred to in the question is near the 50 million lb. design requirement. The ANSYS models, input parameters and load functions relevant to the vessel support ledge force are as follows:

The ANSYS model used in the derivation of the vessel support ledge force was an axisymmetric representation of the reactor vessel. The loading function $F(t)$ input to the axisymmetric reactor vessel model was derived with a 1D representation of the closure head. The total upward loading function $F(t)$ acting on the vessel flange as processed from the 1D head response was used to determine the maximum upward force on the ledge. The total downward acting pressure $P(t)$, acting on the core support plate was taken from the REXCO analysis, which included inertial effects of fluid masses inside the vessel. Both anchor bolts and vessel support ledge restraint to upward and downward acting loading functions assumed linear elastic force-deflection behavior. Gravity was not included in the axisymmetric reactor vessel model as HCDA head forces and core support pressures are much greater than the respective weights over the 120 milli-second duration considered in the analysis.

60

*Note that Appendix F has been withdrawn.

60

Question 001.549 (F6.3.4.1)

Provide the time dependent CDA loading on the Upper Internals Structure.

Response:

The CRBRP Project has consolidated all considerations given Hypothetical Core Disruptive Accidents into report CRBRP-3 (References 10a and 10b, PSAR Section 1.6) and its associated references; consequently, PSAR Appendices D and F have been withdrawn in Amendments 24 and 60 respectively. The response to this question is now found in Figure 5-19 of Reference 10a, PSAR Section 1.6.

60

Question 001.550 (F6.3.4.2)

Provide an assessment of the maximum stresses in the transition joints between the Inconel 600, the Stainless Steel Vessel and Vessel Flange. Discuss whether there is a potential problem with these welds being able to withstand the CDA near the end of the plant life due to material degradation effects in the weld or heat affected zones.

Response: *

The service environment and temperature of the transition region of the reactor vessel will not degrade its performance. PSAR Section 5.2.6 has been expanded to discuss the transition region.

While concerns have been expressed and failures noted in a recent survey (Ref. Q001.550-1) of dissimilar metal transition joints, they have been associated with substantially more severe service conditions than those associated with the joints in question. Thermal cycling between room temperature and 1000 to 1200°F has typically been utilized to evaluate the performance of dissimilar metal joints. This cycle is extremely severe in comparison to the temperature cycle between 400 and 465°F for less than 160 1000 cycles to which the vessel transition joint (ferritic to Inconel 600) will be subjected. It has also been suggested by several studies that in the presence of an oxidizing environment a mechanical notch will form at the interface between weld metal (nickel alloy) and ferritic base metal because of differences in oxidation resistance at high (<1000°F) temperatures. The vessel transition weld will not be subjected to high temperatures (1000°F and up) nor to a highly oxidizing environment. 160

The pressure vessel nozzle safe end transition joint utilized in PWR plants consists of an overlay of Inconel 182 (coated stick version of Inconel 82) on SA 508 class 2 nozzle forgings for subsequent joining to Type 304 stainless pipe. This joint is about 30" in diameter, 3" thick and operates at approximately 600°F. Performance experience with this joint has not indicated the occurrence of any problems related to material degradation in service.

Such factors as microfissuring of the weld filler metal and the presence of oxide inclusions cannot be overlooked in performing these transition welds. These concerns have been overcome through the introduction of improved weld filler metal compositions, recognition and control of base metal dilution effects on the filler metal, welding process qualifications with related inspections, and monitoring of welding and inspection techniques.

The generally accepted method of making transition welds between austenitic stainless and ferritic steels for service under substantially more severe conditions than those imposed on the transition joints in this vessel is to use nickel-base filler metals. Large numbers of such welds are in service in petrochemical plants and fossil as well as conventional nuclear power plants with apparently satisfactory results.

*Note that Appendix F has been withdrawn. The text, upon which the question was based, can now be found in Section 5 of Reference 10a, PSAR Section 1.6. 160

Based on these considerations, it is expected that there will be no appreciable material degradation over the plant life in the transition joint region. All preliminary analyses show that both stresses and strains in the transition area satisfy the SMBDB criteria (stress and strain) defined in reference 10a, PSAR Section 1.6. Therefore, the SMBDB criteria will be satisfied in the transition joint region at the end of plant life.

60 | 61

References:

- Q001.550-1: J. F. King, "Behavior and Properties of Welded Transition Joints Between Austenite Stainless and Ferrite Steels - A Literature Review", ORNL-TM-5163, November 1975.

Question 001.551 (F6.5.1.1)

Provide gap widths, annular radii, and effective K-loss factors (ignoring elastomer seals) for the possible leak paths of significance identified in section F6.5.1.1 for the closure head and head-mounted components.

Response:

This question requests clarification of information which is no longer a part of the current documentation. The Project has since consolidated all considerations given Hypothetical Core Disruptive Accidents into report CRBRP-3 (References 10a and 10b, PSAR Section 1.6) and its associated references; consequently, PSAR Appendices D and F have been withdrawn in Amendments 24 and 60 respectively. The question requested information concerning a source term for a seal head access area that is no longer a part of the CRBRP design.

Question 001.552 (F7.1.3.1.1)

If a very low design margin exists in the lower core support structure and the strain hardening characteristics have to be included to claim positive margin, then embrittlement due to irradiation damage should also be included. The problem should be evaluated for near the end of life condition to include all degradation processes not normally included in ASME Code allowables for the core support structure before claiming a positive design margin. Re-evaluate your design and discuss the effect this factor would have on your conclusions.

Response:

This question requests clarification of information which is no longer a part of the current documentation. The Project has since consolidated all considerations given Hypothetical Core Disruptive Accidents into report CRBRP-3 (References 10a and 10b, PSAR Section 1.6) and its associated references; consequently, PSAR Appendices D and F have been withdrawn in Amendments 24 and 60 respectively. Assessments of Structural Margins Beyond the Design Base for the core support structure is provided in Section 5 of Reference 10a, PSAR Section 1.6.

60

Question 001.553 (F7.2.4)

Provide, as a supplement to Table F7.2-2, the force displacement data and initial pre-stress loads for the concrete ledge bolts and their material properties.

Response:

This question requests clarification of information which is no longer a part of the current documentation. The Project has since consolidated all considerations given Hypothetical Core Disruptive Accidents into report CRBRP-3 (References 10a and 10b, PSAR Section 1.6) and its associated references; consequently, PSAR Appendices D and F have been withdrawn in Amendments 24 and 60 respectively. An assessment of Structural Margins Beyond the Design Base of the reactor vessel support ledge is provided in Section 5 of Reference 10a, PSAR Section 1.6.

60

Question 001.554 (F7.2.5)

Describe and discuss the interaction of the shear rings, risers, riser bolting and support bearing during a CDA. Provide details of the arrangement of shear rings, shear ring keepers and their material properties. Discuss the response of the bearing and retention in its seat during a CDA. Indicate at what load the shear ring keepers can be displaced. Discuss the possibility and the effect of non-uniform loading in the shear rings and non-uniform deformation which may result in tilting of the plug and, the subsequent potential for the plug not to reseat and seal.

Response:

The CRBRP Project has consolidated all considerations given Hypothetical Core Disruptive Accidents into report CRBRP-3 (References 10a and 10b, PSAR Section 1.6) and its associated references; consequently, PSAR Appendices D and F have been withdrawn in Amendments 24 and 60 respectively. The response to this question is now found in Reference 11, PSAR Section 1.6.

| 32

| 60 | 61

Question 001.555 (F1.5.2.9 Part II)

Considering the differences between the FFTF and the CRBR designs, as well as the differences in the mechanical source term, describe how you plan to verify the response of the upper portion of the CRBRP reactor structure experimentally. Describe and discuss any planned experimental program and its schedule to address this matter.

Response:

The CRBRP Project has consolidated all considerations given Hypothetical Core Disruptive Accidents into report CRBRP-3 (References 10a and 10b, PSAR Section 1.6) and its associated references; consequently, PSAR Appendices D and F have been withdrawn in Amendments 24 and 60 respectively. The response to this question is now found in Section 5.4.2.4 of Reference 10a and 14, PSAR Section 1.6.

60 | 61

Question 001.556 (Appendix F, Part II, 6.2.3)

Since our review is not completed, the need for a containment clean up system has been neither dismissed nor established. However, if core vapor was ejected through the head into the HAA compartment and it could not contain the resultant pressure then the RCB could potentially be pressurized. Other than designing the HAA for a high pressure, describe and discuss the possible means for protecting the RCB in such an event.

Response:

A containment cleanup (vent, purge and filter) system is being added to the CRBRP design to provide additional containment margins as discussed in Reference 10b of PSAR Section 1.6.

| 60

Question 001.557 (6.2.6.1.1, yellow)

The following two PSAR statements may not be compatible if subsequent CDA review results are different from those currently in the PSAR. Clarify your intent for the sealed HAA requirements if different CDA consequences result. "The sealed HAA shall be capable of accommodating the maximum pressure and temperature caused by the effects of a CDA." "The sealed HAA shall be designed for 15 psig pressure and 400°F temperature."

Response:

This question requests clarification of information which is no longer a part of the current documentation. The Project has since consolidated all considerations given Hypothetical Core Disruptive Accidents into report CRBRP-3 (References 10a and 10b, PSAR Section 1.6) and its associated references; consequently, PSAR Appendices D and F have been withdrawn in Amendments 24 and 60 respectively. The CRBRP no longer has a sealed head access area.

60

Question 001.558 (6.2.7.2 Part II)

Several 4" vents are provided behind the cavity liner which vent into the RCB in the event of a meltdown. Indicate the rate of pressure rise in the RCB due to such venting and the time it will take to reach 10 psig.

Response:

In the present configuration the Reactor Cavity floor liner is vented to the Reactor Containment Building (RCB) and the wall liner is vented to Cell 105, which is connected to the RCB. In addition, the Reactor Cavity atmosphere is vented to the RCB via a planned vent path actuated by rupture disks which would open shortly after Reactor Vessel penetration due to heat up and pressurization of the Reactor Cavity atmosphere. After a liner section is predicted to fail, the area behind the failed section is assumed to vent into the Reactor Cavity. The TMBDB scenario has been analyzed with these release paths in CRBRP-3, Volume 2 (Reference 10b of PSAR Section 1.6). In the base case, the RCB reaches 10 psig in approximately 20 hours. (A short term pressure transient due to hydrogen burning exceeds 10 psig at approximately 10 hours).

Question 001.559 (F7.1.2.1.1)

Appendix F of the ASME Code is written for LWRs operating mostly in the elastic regime. In CRBR the thermally hot portion of the system is subjected to loadings which accumulate strain inelastically. Justify using LWR faulted criteria for evaluation of the thermally hot portions of CRBR during the CDA and discuss the rationale for why more conservative criteria for this evaluation should not be used in the safety assessment. Regulatory Guide 1.87, "Guidance for Construction of Class 1 Components in Elevated - Temperature Reactors (Revision 1, June 1975)" also addresses this issue. Revise your PSAR to address the positions of this Regulatory Guide.

Response:

This question requests clarification of information which is no longer a part of the current documentation. The Project has since consolidated all considerations given Hypothetical Core Disruptive Accidents into report CRBRP-3 (References 10a and 10b, PSAR Section 1.6) and its associated references; consequently, PSAR Appendices D and F have been withdrawn in Amendments 24 and 60 respectively. The core support plate, in considerations for accidents beyond the design base, is not required to meet ASME requirements. An assessment of Structural Margins Beyond the Design Base is provided in Chapter 5 of Reference 10a, PSAR Section 1.6.

Question 001.560 (F7.1.3.12)

Provide a figure showing the CRDM shield and seismic support structural arrangement giving critical dimensions.

Response:

The CRDM shield and seismic support, shown in Figure Q001.560-1, consists of a three-inch thick, hexagonal shaped cylinder which is bolted to the IRP and encircles both the Primary and Secondary CRDM/CRDs. A three-inch thick support plate with openings and clamps for the CRDM extension nozzles is mounted on top of the cylinder to provide horizontal restraint.

60

SHIELD AND SEISMIC SUPPORT

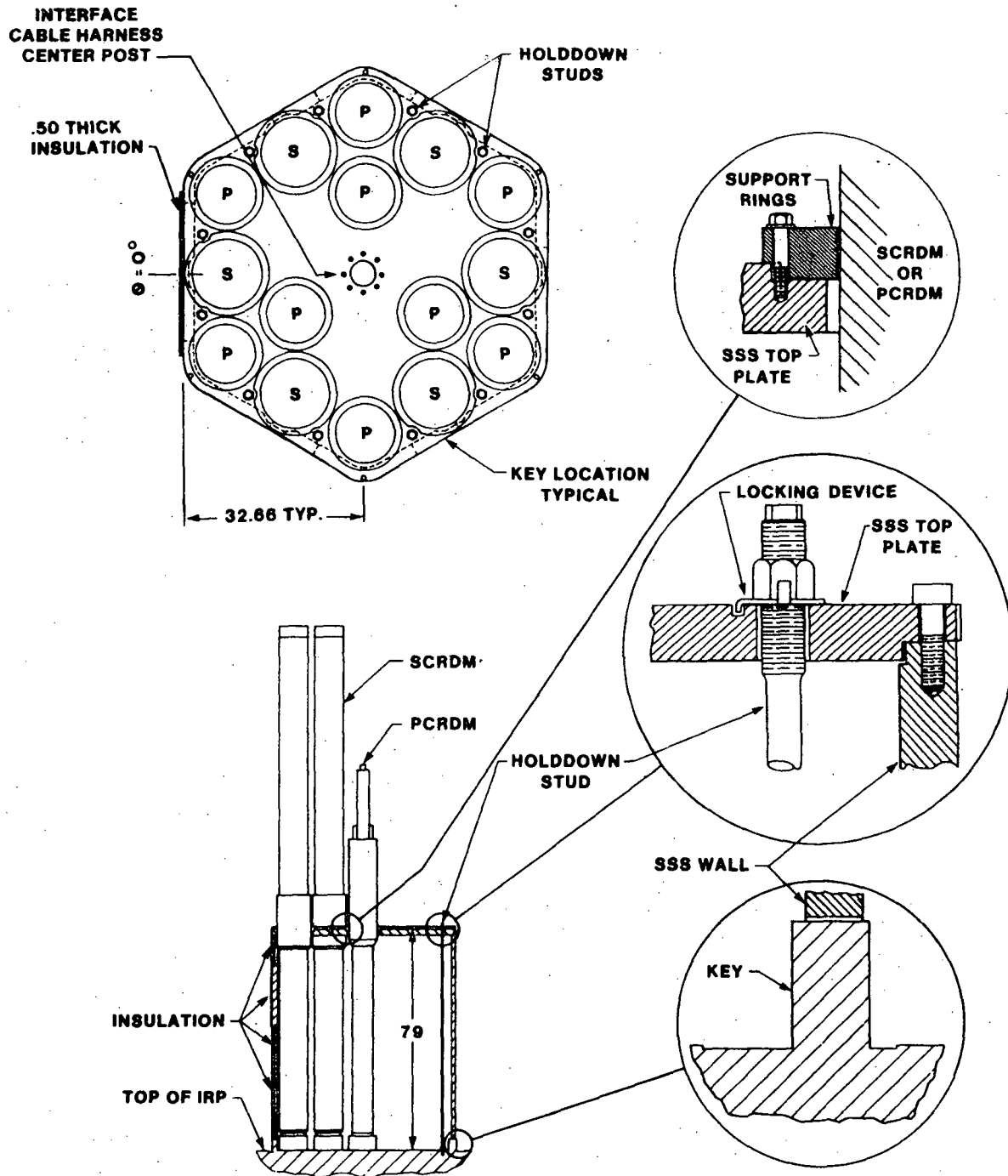


Figure Q001.560-1. Shield and Seismic Support Schematic

Question 001.561 (F7.1.3.15)

Amplify your discussion regarding the dip seal maintenance ports in the head. Provide an illustration showing the outer cylinder in the head. The dip seal maintenance ports appear to be holes in the head and the potential failure region is not understood. Discuss whether a failure in this region would provide a direct sodium path through the head.

Response

This question requests clarification of information which is no longer a part of the current documentation. The Project has since consolidated all considerations given Hypothetical Core Disruptive Accidents into report CRBRP-3 (References 10a and 10b, PSAR Section 1.6) and its associated references; consequently, PSAR Appendices D and F have been withdrawn in Amendments 24 and 60 respectively.

60

Question 001.562 (F7.1.3.6)

Since the horizontal baffle in the reactor is expected to slope inwards and downwards following a CDA, discuss how this will affect PAHR and secondary criticality potentials for reentry of ejected core debris. Discuss the potential for ejected core debris to be retained on the thermal baffles with a downward slope and provide your conclusions regarding the acceptability of this situation.

Response:

Due to the potentially large deflection of the horizontal baffle, its final slope cannot be precisely determined. Reference Q001.562-1 shows that debris beds (thicknesses less than the maximum thermally stable thickness) can be maintained on horizontal baffle surfaces which are tilted down less than 20° , the debris would slip off the baffle into the annulus between the core barrel and the vessel wall. Thus it would not fall back into the core region and contribute to a secondary criticality.

Since the debris would be distributed around the core barrel circumference, in the core barrel/vessel annulus there is no likelihood of attaining a critical configuration in the annulus. The debris may locally exceed the maximum thermally stable thickness and melt through the core support cone into the lower reactor plenum.

Therefore, it is concluded that a residual downward slope on the horizontal baffle will not result in any criticality consequences and with respect to PAHR the deflection either has no effect on the particulate bed on the baffle (for less than about 20°) or the debris would move downwards (for slopes greater than 20°) towards the lower reactor plenum where it would be retained.

Reference:

Q001.562-1 L. Baker, Jr., et al, "Post Accident Heat Removal in Fast Reactors," ANL/RAS 75-44, November, 1975.

Question 001,563 (F7.1.3)

Provide the design criteria on the holddown configuration for all head-mounted components. Include information on the number of bolts, the minimum cross-sectional area of the bolts, the force-displacement data for the bolts, and their initial pre-stress load. For each component, discuss the load and acceleration which will cause holddown to fail.

Response:*

| 60

The requested information will be included in Reference 10a, PSAR Section 1.6, Section 5.4, when it becomes available.

| 60

*Note that Appendix F has been withdrawn. The text, upon which the question was based, can now be found in Section 5.4 of Reference 10a, PSAR Section 1.6.

| 60

Question 001.564 (F7.2.2)

The reactor outlet nozzles are currently predicted to fail (Table F7.2-1), and it is implied that structural adequacy can be resolved by structural modifications confirmed by finite element techniques. Discuss what progress has been made towards the resolution of this problem area including to what extent the proposed finite element techniques have been verified.

Response:

This question requests clarification of information which is no longer a part of the current documentation. The Project has since consolidated all considerations given Hypothetical Core Disruptive Accidents into report CRBRP-3 (References 10a and 10b, PSAR Section 1.6) and its associated references; consequently, PSAR Appendices D and F have been withdrawn in Amendments 24 and 60 respectively. A discussion of structural margins of the reactor outlet nozzles is provided in Chapter 5 of Reference 10a, PSAR Section 1.6.

60

Question 001.565 (E4.3 Yellow)

Based on our review of LWR pipe break analyses, the staff believes that there is a spectrum of leaks smaller than a double ended rupture which can result in serious consequences that need to be evaluated. A design basis leak rationale appears to be missing in the PSAR. A systematic approach to provide the equivalent of LWR inservice inspection to assure that the safety margins incorporated in the design are retained throughout plant life also appears to be missing. Leak detectors are an after-the-fact device and do not provide this assurance. Justify your position for the omission of these important considerations in your safety approach.

Response

In the context of the Parallel Design for which a PHTS rupture is a design basis event it is certainly appropriate to consider a spectrum of leaks smaller than a double ended rupture. Figure E.3-1 has already demonstrated that the worst location for a break is at the RV inlet nozzle. Accordingly, analyses have been conducted, using the DEMO Code, Rev. 4 of the consequences of breaks of different sizes at this location. The results of these analyses, in which the same basic assumptions were made as for the earlier analyses, are presented in new Figures E.3-1A and E.3-1B. It will be noted that the double ended rupture does indeed represent the worst case.

Although not called a 'design basis leak rationale', a rationale for selection of an Extremely Unlikely Event leak for the reference design is given in Section 15.6. The full rationale for exclusion of large breaks from the Reference Design, including considerations such as in-service inspection and leak detection, is presented in the Clinch River Breeder Reactor Plant Primary Pipe Integrity Status Report, December 1975.

Question 001.566 (FII 1.5.2.8.5)

Specify what, at this time, would limit the design of the enclosure of the HAA and indicate if there are temperature limits on the seals, concrete, or pressures from the reaction products. Discuss the current limits on the design pressure, in terms of structural accommodation for higher pressures.

Response:

With the deletion of the Parallel Design in Amendment 24 this question is no longer relevant as the features upon which the question is based are no longer a part of the design.

Question 001.567 (1.5.2.8.5)

In the proposed simulated water tests of the margin shear rings and elastomer seals, indicate if the dynamic impact on an eccentrically loaded plug will be simulated. Elaborate on these tests and discuss why they are not required for the reference design as well as the parallel design.

Response:

In Amendment 18 to the PSAR, the Project indicated its intent to withdraw the Parallel Design from further consideration by the NRC Staff. This question requests information which is also pertinent to the Reference Design, as amended by PSAR Amendment 18 and will be responded to in that context.

The proposed simulated water tests are intended to test the effectiveness of the margin seal only, not the elastomer seals or margin shear rings. As designed the margin seals do not carry any of the plug loads, impact, eccentric or otherwise. Because of this it is not necessary to include these loads in the test. The dynamic conditions to be simulated in the test are:

- (1) Axial relative motion between two risers. This motion could be uniform or eccentric in the reactor and the test would be a valid simulation.
- (2) Forces on the margin seal due to gas and sodium being forced up the annulus between risers.

Question 001.580(RSP)

The staff has reviewed the proposed CRBRP systems for decay heat removal and finds that the proposed designs do not completely satisfy CRBRP Design Criteria 26 (Heat Transport System Design) and 35 (Reactor Residual Heat Extraction Systems). Furthermore, no credit can be given to natural convection as a diverse means of removing plant sensible and decay heat following reactor shutdown until sufficient analytical and experimental bases are developed. Based upon a preliminary evaluation of the CRBRP natural circulation verification plan, it is the staff opinion that, in general, the plan appears to identify those outstanding issues and concerns that need to be addressed. However, the plan is based solely on analytical techniques which in most instances have neither been completed nor scheduled for completion in the near future. The staff will continue its review of the natural circulation verification plan to assure that sufficient analyses and verification testing will be conducted. Additional information regarding those analyses and tests will be requested in the near future. However, since the projected schedule for these results is outside the time frame of the CP review, the staff cannot prejudge or predict the results of the analyses or tests. The staff encourages the project to pursue those activities necessary to demonstrate natural circulation capability; however, in order to resolve the issue at this stage of review, it is the staff position that forced circulation must be provided for all modes of decay heat removal. Accordingly, the following positions have been developed

- (1) Following reactor shutdown from all plant conditions, including those associated with postulated accident events, the decay heat removal train (i.e., PHTS, IHTS, SGS and SGAHRS) must be capable of assuring forced convection flow from the reactor to the heat sink assuming a single failure. Provide in the PSAR a design which has motive and control power to assure that for onsite electric power system operation (assuming offsite power is not available) the safety function can be performed.
- (2) Consistent with the staff's position on auxiliary feedwater system motive and control power diversity requirements (Branch Technical Position 10-1 provided 6/5/75) during short term cooling (e.g., steam venting), a diverse means of assuring forced convection flow must be provided for the entire heat removal train (i.e., PHTS, IHTS, SGS and SGAHRS). Such diversity should be assured for a nominal time period of two hours following reactor shutdown, and assuming the loss of onsite AC power and offsite power supplies.
- (3) The DHRS must retain its functional capability in the event of a postulated accident in the normal heat rejection paths. For example, the DHRS must be capable of accommodating a design basis PHTS leak. It should be recognized that the staff is currently developing its position on the CRBRP design basis leak. Nonetheless, it is the staff position that DHRS, or an equivalent system, must be capable of removing decay heat assuming the existence of the minimum sodium level in the reactor that would result from a design basis leak.

- (4) As stated above, the DHRS must be designed to accommodate a postulated accident in the normal heat rejection paths and a concurrent single failure of a PHTS pony motor. For two-loop operation (i.e., one loop out of service) the present design is not acceptable since a postulated pipe leak in an operating loop and a single failure of the remaining pony motor results in the complete loss of cooling capability, either through a normal heat removal path or through DHRS. If two-loop operation is contemplated, as it is stated in the PSAR, it is the staff position that the DHRS be capable of providing forced convection flow through the core assuming no pony motor flow and the existence of the minimum sodium level in the reactor that would result from a design basis leak.
- (5) Because the current DHRS inlet and discharge connections are both in the upper plenum, we are concerned about the potential for thermal short circuiting under low flow conditions. Provide the experimental basis (in sodium) to demonstrate adequate heat removal capacity under the various conditions required for DHRS operation, considering the potential for flow maldistribution and thermal short circuiting. This concern should be addressed consistent with the system changes resulting from conformance with items (3) and (4), as noted above.

Response

Natural circulation is a simple and proven technique for removing decay heat in a number of reactor types. Use of natural circulation for CRBRP is highly advantageous from a safety standpoint. The Project has completed a significant amount of analysis to demonstrate that natural circulation flow rates are more than adequate for decay heat removal. In areas where there are questions remaining, the Project has committed to address them by additional analyses or by testing. (Reference "Verification of Natural Circulation in Clinch River Breeder Reactor - A Plan ", transmitted to NRC June 21, 1976.) The Project intends to continue efforts in the area based on the judgment that natural circulation is an important safety feature and that proper recognition of this capability will be granted. However, as part of the on-going design evolution, the Project has evaluated the addition of a third safety grade power supply and, as a result, has decided to add a 250 V DC battery to power the sodium pump pony motors and protected air cooled condenser fans in one heat transport system loop. This change does not add diverse or safety grade power supplies to the Steam Generator System or to the steam side of the Protected Air Cooled Condenser. The project believes that natural circulation in the water/steam systems has a sound technical basis which has been demonstrated for previous reactor types.

The staff has developed five positions which expand this finding and the responses are provided below for each position.

Position: (1) Following reactor shutdown from all plant conditions, including those associated with postulated accident events, the decay heat removal train (i.e., PHTS, IHTS, SGS and SGAHRS) must be capable of assuring forced convection flow from the reactor to the heat sink assuming a single failure. Provide in the PSAR a design which has motive and control power to assure that for onsite electric power system operation (assuming offsite power is not available) the safety function can be performed.

Response: This position represents an expansion of the requirements of CRBRP Design Criteria 26 and 35. This position is not consistent with previous water reactor licensing practices. Other reactor plants which have been licensed rely on natural circulation because it is inherently more reliable. However, due to the developmental nature of several CRBRP systems, the Project has evaluated the addition of a third safety grade power supply and, as a result, has decided to add a 250 V DC battery to power the sodium pump pony motors and protected air cooled condenser fans in one heat transport system loop. This change does not add diverse or safety grade power supplies to the Steam Generator System or to the steam side of the Protected Air Cooled Condenser. The Project believes that natural circulation in the water systems has a sound technical basis which has been demonstrated for previous reactor types.

Position: (2) Consistent with the staff's position on auxiliary feed-water system motive and control power diversity requirements (Branch Technical Position 10-1 provided 6/5/75) during short term cooling (e.g., steam venting), a diverse means of assuring forced convection flow must be provided for the entire heat removal train (i.e., PHTS, IHTS, SGS and SGAHRS). Such diversity should be assured for nominal time period of two hours following reactor shutdown, and assuming the loss of on-site AC power and off-site power supplies.

Response: Letter, SL:1750, A.R. Buhl to R.S. Boyd, "Decay Heat Removal Issues," 10/15/76, documents the Project's commitment to add a diverse safety grade power supply to the sodium pump pony motors and PACC fans in one HTS loop. Details of this "diverse safety grade power supply" are provided in Section 8.3.1.

Position: (3) The DHRS must retain its functional capability in the event of a postulated accident in the normal heat rejection paths. For example, the DHRS must be capable of accommodating a design basis PHTS leak. It should be recognized that the staff is currently developing its position on the CRBRP design basis leak. Nonetheless, it is the staff position that DHRS, or an equivalent system, must be capable of removing decay heat assuming the existence of the minimum sodium level in the reactor that would result from a design basis leak.

Response: The CRBRP shutdown heat removal systems are capable of accommodating all design basis events identified for the Plant. (See PSAR Section 5.6) This includes accommodation of the PHTS design basis leak, although the DHRS would not be utilized to mitigate that event. Postulated design basis leaks in the PHTS are accommodated by the use of SCAMRS.

The NRC position broadens the design bases which have been previously established by the CRBRP design criteria. The staff position has been carefully evaluated. This evaluation has confirmed the judgment that the CRBRP design criteria provide a proper definition of the CRBRP design bases. As a result, the Project is not planning design modifications in response to this position. It is requested that the staff reevaluate this position in light of the above discussion.

Position: (4) As stated above, the DHRS must be designed to accommodate a postulated accident in the normal heat rejection paths and a concurrent single failure of a PHTS pony motor. For two-loop operation (i.e., one loop out of service) the present design is not acceptable since a postulated pipe leak in an operating loop and a single failure of the remaining pony motor results in the complete loss of cooling capability, either through a normal heat removal path or through DHRS. If two-loop operation is contemplated, as it is stated in the PSAR, it is the staff position that the DHRS be capable of providing forced convection flow through the core assuming no pony motor flow and the existence of the minimum sodium level in the reactor that would result from a design basis leak.

Response: For two-loop operation (i.e., one loop out of service), a postulated piping leak in one of two operating loops followed by a single failure of a pony motor can be accommodated by natural circulation in the loop with the failed motor. Because two loop operating restrictions are to be addressed during the FSAR stage of the license application and because the Project intends to adequately verify the natural circulation capability prior to submission of the FSAR, no design modifications are contemplated. If natural circulation is not adequately verified at FSAR/Operating License stage, the Project will modify its planned operational mode to delete two loop operation, or take other appropriate steps to resolve this issue.

Position: (5) Because the current DHRS inlet and discharge connections are both in the upper plenum, we are concerned about the potential for thermal short circuiting under low flow conditions. Provide the experimental basis (in sodium) to demonstrate adequate heat removal capacity under the various conditions required for DHRS operation, considering the potential for flow maldistribution and thermal short circuiting. This concern should be addressed consistent with the system changes resulting from conformance with items (3) and (4), as noted above.

Response: As discussed in response to parts (3) and (4), system changes to conform with (3) and (4) above will not be addressed.

The adequacy of the geometric locations of the DHRS make-up and overflow nozzles has been demonstrated in a 1/21 scale Outlet Plenum Feature Model (OPFM) test using water as the working fluid. The results, obtained for simulated prototype DHRS operating conditions, show that five to six percent of the make-up flow will appear in the overflow line, that is short circuit directly from the make-up nozzle to the overflow nozzle. These results confirm the conservatism of the design assumption used in sizing the DHRS capacity since an allowance of twenty percent flow short circuiting was used in design. Further testing is planned in the 0.248 scale Integral Reactor Flow Model (IRFM) to provide additional confirmation of these test results.

The justification for doing water testing, in the 1/21 scale OPFM test and the future 0.248 scale IRFM test, in lieu of doing sodium testing, is based on the knowledge of similitude relationships. Specifically, information is available to demonstrate that in many thermal-hydraulic tests it is possible to use scale models and fluids that are related to the parameters of interest through dimensionless groupings. These relationships, or dimensionless groupings, include fluid forces pertinent to the upper plenum flow field during operation of DHRS. The fluid forces include those of inertia, buoyancy and gravity. These forces can be expressed and related in terms of three dimensionless groups: the Reynolds Number, the Richardson Number, and the Froude Number. The definitions are as follows:

$$N_{Re} = \frac{\rho DV}{\mu}$$

$$N_{Ri} = \frac{gD\Delta\rho}{\rho V^2}$$

$$N_{Fr} = \frac{V^2}{gD}$$

where:

N_{Re} = The Reynolds Number, a ratio of inertia-to-viscous forces
 N_{Ri} = The Richardson Number, a ratio of bouyancy-to-inertia forces
 N_{Fr} = The Froude Number, a ratio of inertia-to-gravitational forces

V = Fluid velocity

D = Characteristic dimension

μ = Fluid viscosity

$\Delta\rho$ = Difference in density between the two fluid streams (make-up, of cold fluid, and outlet plenum inflo , or hot fluid)

ρ = Fluid density

g = Gravitational acceleration

An examination of these three ratios shows two are independent since the Froude Number is included in the Richardson Number. Therefore, an equality of the Reynolds Number and Richardson Number in the model and prototype results in dynamic similarity and flow patterns occurring in the prototype during DHRS operation will be duplicated in the model. Experience has shown that for Reynolds Number in the turbulent flow range, generally greater than 10,000, the fluid behavior becomes relatively independent of changes in the Reynolds Number, that is the ratio of inertia-to-viscous fluid forces. Consequently, an inequality in the Reynolds Number between model and prototype does not introduce significant error in the flow patterns. For Reynolds Number below 10,000 it is conceivable that the flow pattern would be affected by an inequality but based on the parameters of significance during DHRS operation, bouyancy and inertia, it is judged that Richardson Number simulation provides a valid simulation.

The accuracy of scale modeling with water rather than sodium based on this concept is substantiated by information presented in Reference Q001.580-1. It is reported by Lorenz, Reference Q001.580-2 that model size effects are insignificant and that, for small scale models, water data conservatively predicts the transient response compared to sodium data. He also argues that for full scale plenum, the agreement between water and sodium transients will be even better. Therefore, the data obtained in the outlet plenum flow stratification studies should reasonably simulate full scale CRBRP sodium temperature responses in the outlet plenum.

The elevations of the overflow ports and nozzles applicable to the DHRS operation are as follows:

1. Thermal Liner Ports (1.25 in. dia.) -89.76 in. Elevation
2. Overflow Nozzle (8 in. dia.) -148. in. Elevation
3. Makeup Nozzle (4 in. dia.) -156. in. Elevation

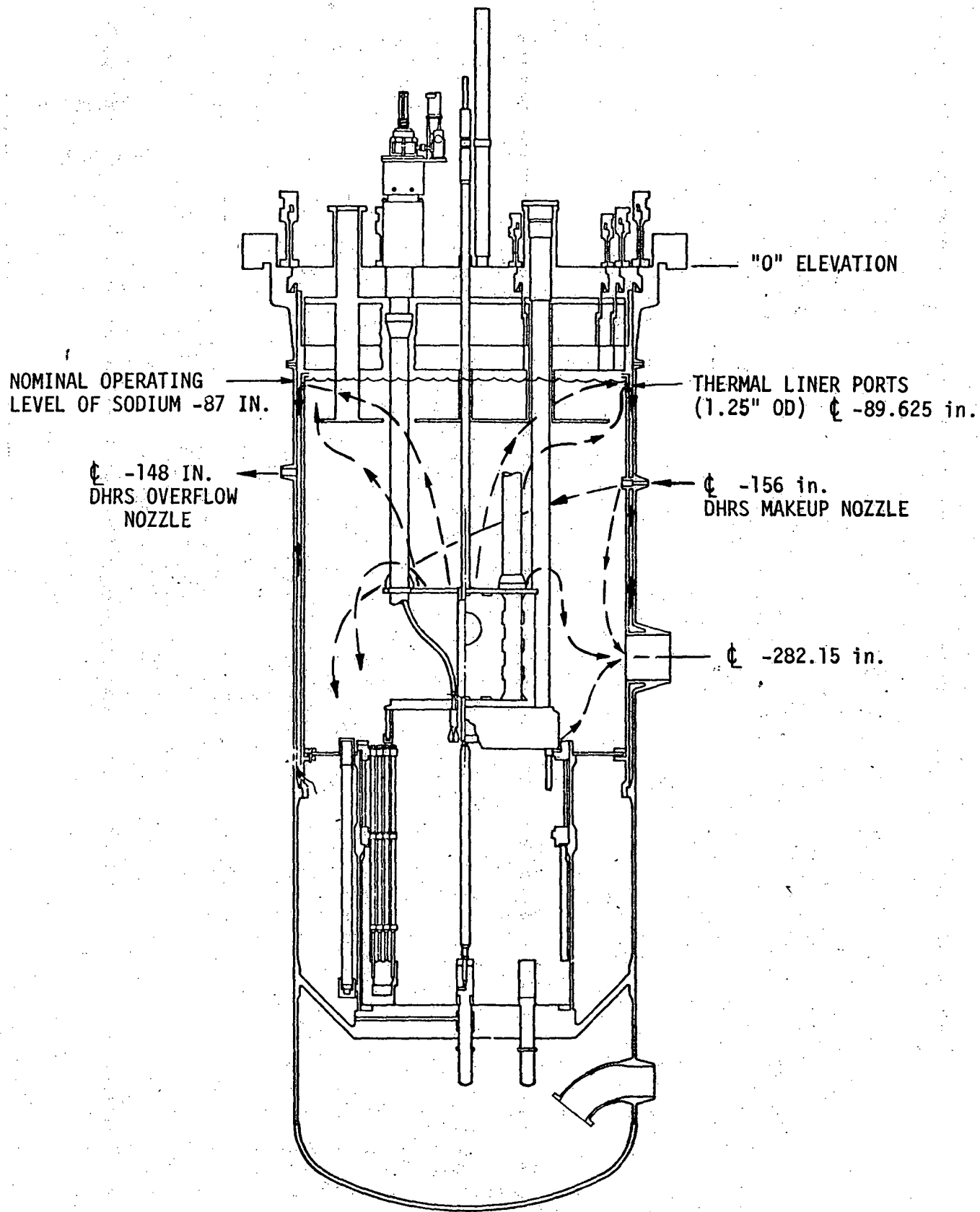
This is illustrated in Figure Q001.580-1 which also shows that the DHRS makeup nozzle penetrates both the reactor vessel and thermal liner walls with the flow entering into the outlet plenum. The DHRS overflow nozzle only penetrates the reactor vessel wall so that flow is obtained from both the reactor vessel outlet plenum sodium pool, through the thermal liner ports, and flow in the annulus between the thermal liner and the reactor vessel wall. Since buoyancy is the dominant flow characteristic in the outlet plenum, it is the hot sodium which rises and spills over the thermal liner/reactor vessel annulus and enters the DHRS overflow nozzle, Figure Q001.580-1. The upflow sodium coolant in the thermal liner annulus is at approximately the same temperature as the outlet plenum sodium coolant.

In Figure Q001.580-1, the general flow pattern is illustrated. The cold make-up sodium coolant enters the outlet plenum and falls to the lower region while mixing with the hot sodium pool coolant before exiting through the main coolant outlet pipes. The hot sodium coolant from the core rises through buoyancy and overflows into the thermal liner annulus; the thermal liner upflow, which is extremely low, absorbs heat conducted across the thermal liner and also enters the DHRS overflow nozzle.

These locations have been simulated in the 1/21 scale OPFM test with the DHRS operating conditions consisting of 7.5 to 10 percent loop flow and 400 to 540 GPM (gallons per minute) make-up flow. As noted previously, the short circuiting of the make-up flow ranged from five to six percent using the Richardson Number as a basis of similitude. Although these results are conservatively within the design allowance of twenty percent used in sizing the DHRS capacity, additional testing in the IRFM model will be used to obtain further confirmation of the adequacy of the DHRS.

References:

- Q001.580-1 E.H. Novendstern et.al., "Outlet Plenum Flow Stratification Studies for the Clinch River Breeder Reactor Plant." ASME 76-WA/HT-84, December 1976.
- Q001.580-2 J. J. Lorenz, et.al., "The Influence of Scale Size and Fluid Thermal Properties in Simulating LMFBR Outlet Plenum Behavior," ASME/AICHE Sixteenth National Heat Transfer Conference, June 1976.



DHR FLOW OPERATION
 FIGURE Q 001.580-1

Question 001,581 (6.2.1)

The staff has reviewed the CRBRP containment and inner cell system design bases and finds that the proposed designs do not completely satisfy CRBRP Design Criterion 41 (Containment Design Basis). The staff concludes that the applicant has not sufficiently justified the limitation of sodium fires to those discussed in the PSAR. The containment design basis, including the inner cell system, should envelope the pressures and temperatures resulting from consideration of a spectrum of sodium spray and pool fires coupled with sodium-concrete reactions in the event that part of the cell liner should fail. The primary or intermediate sodium releases should be based on considering a spectrum of postulated pipe breaks of different sizes, locations, and other properties sufficient to provide assurance that the entire spectrum of postulated sodium fire accidents is covered. The size of the pipe break in the reactor coolant system should extend from small breaks (i.e., those resulting in leaks near the threshold of detectability, about 125 gm/hr) up to and including a break equivalent in size to the double-ended rupture of (1) the largest pipe in the system, and (2) the hot leg pump discharge piping. For each location, various geometric pipe break configurations should be examined, including circumferential and longitudinal splits. Elevations of the pipe break should be considered which have the potential for (1) maximum cumulative sodium releases, consistent with the system hydraulic profile; and (2) maximum spray fire consequences, including influence of various sodium drop sizes. For each of the breaks considered, several assumptions regarding pump trip should be examined, namely: (1) Plant Protection System (PPS) pump trip, (2) operator initiated pump trip, and (3) no pump trip. Since the leak detectors are only alarms, for the operator initiated pump trip, you should assume no operator action for at least 10 to 20 minutes following any alarm. System pressure, pump inertia, fluid momentum and other relevant factors are to be included in the analysis. As indicated in PSAR Section 1.5.2.1, venting of the inner cell system may be proposed as a means to limit cell pressures, provided such pressure relief venting does not result in other unacceptable conditions, such as disabling of essential equipment.

Response:

The response to this question is presented in the format of a report entitled, "Analysis of Sodium Fires in the Reactor Containment Building Large Inerted Cells".

The report considers a wide range of leaks from less than 8 gpm to 33,500 gpm. Because the cell liners will be designed not to fail for the design basis leaks, the liners were assumed to be intact for the analysis. A margin evaluation, however, was performed for a limited liner failure (up to 50% of floor liner area) to demonstrate that liner leaks would not lead to unacceptable cell pressures or hydrogen concentration in containment.

The spectrum of PHTS piping leaks includes consideration of various plant shutdown actions. The shutdown actions considered are as follows: termination of the 8 gpm leak is by operator action after 30 to 40 minutes; termination of the Moderate Energy Fluid System Leak is conservatively considered to be by the plant protection system after approximately 5 minutes (the pump trip time for each case was chosen to envelope the maximum possible cell gas temperature and pressure); and the Evaluation Basis Leak is not terminated except by expulsion of all available sodium in the loop.

The conclusion of the report is that postulating a spectrum of spills far in excess of the plant Design Basis Leak, even when coupled with substantial cell liner failure, and failure of the pump to trip, does not result in unacceptable pressure, temperatures, or hydrogen concentrations in containment.

RESPONSE TO NRC QUESTION 001.581

ANALYSIS OF SODIUM FIRES IN THE
REACTOR CONTAINMENT BUILDING
LARGE INERTED CELLS

Q001.581-3.

Amend. 40
July 1977

TABLE OF CONTENTS

	<u>Page</u>
1.0 Introduction	Q001.581-8
2.0 Summary	Q001.581-10
2.1 Summary Results - Cell Liner Design Conditions	Q001.581-10
2.2 Summary Results - Evaluation with Cell Liner Failure	Q001.581-11
3.0 Detailed Analyses Description - Cell Liner Design Conditions	Q001.581-12
3.1 Primary Heat Transport System (PHTS Cell)	Q001.581-12
3.2 Reactor Cavity	Q001.581-14
3.3 Overflow and Primary Sodium Storage Tank Cell	Q001.581-15
4.0 Detailed Analyses Description - Evaluation with Cell Liner Failure	Q001.581-18
Tables	Q001.581-21
Figures	Q001.581-28

LIST OF TABLES

<u>Table No.</u>	<u>Table Title</u>
Q001.581-1	Summary Description of Piping Leaks Evaluated
Q001.581-2	Material Properties Used for the Spray-Sofire Analyses
Q001.581-3	Summary Results for Cell Liner Design Conditions
Q001.581-4	Summary Results for Partial Cell Liner Failure
Q001.581-5	Properties Used in the CACECO Analysis

LIST OF FIGURES

<u>Figure No.</u>	<u>Figure Title</u>
Q001.581-1	PHTS Cell - Gas Pressure and Temperature Design Basis Leak
Q001.581-2	PHTS Cell - Floor Transient Design Basis Leak
Q001.581-3	PHTS Cell - Non-Wetted Wall Transient Design Basis Leak
Q001.581-4	PHTS Cell - Spray Phase Transient Moderate Energy Fluid System Leak
Q001.581-5	PHTS Cell - Cell Gas Pressure Moderate Energy Fluid System Leak
Q001.581-6	PHTS Cell - Cell Gas Temperature Moderate Energy Fluid System Leak
Q001.581-7	PHTS Cell - Floor Transient Moderate Energy Fluid System Leak
Q001.581-8	PHTS Cell - Non-Wetted Wall Transient Moderate Energy Fluid System Leak
Q001.581-9	PHTS Cell - Spray Phase Transient Evaluation Basis Leak
Q001.581-10	PHTS Cell - Cell Gas Pressure Evaluation Basis Leak
Q001.581-11	PHTS Cell - Cell Gas Temperature Evaluation Basis Leak
Q001.581-12	PHTS Cell - Floor Transient Evaluation Basis Leak
Q001.581-13	PHTS Cell - Non-Wetted Wall Transient Evaluation Basis Leak
Q001.581-14	Reactor Cavity - Gas Pressure and Temperature Design Basis Leak
Q001.581-15	Reactor Cavity - Floor Transient Design Basis Leak
Q001.581-16	Reactor Cavity - Non-Wetted Wall Transient Design Basis Leak
Q001.581-17	Reactor Cavity - Spray Phase Transient Moderate Energy Fluid System Leak
Q001.581-18	Reactor Cavity - Gas Pressure Moderate Energy Fluid System Leak
Q001.581-19	Reactor Cavity - Gas Temperature Moderate Energy Fluid System Leak
Q001.581-20	Reactor Cavity - Floor Transient Moderate Energy Fluid System Leak
Q001.581-21	Reactor Cavity - Non-Wetted Wall Transient Moderate Energy Fluid System Leak

<u>Figure No.</u>	<u>Figure Title</u>
Q001.581-22	Reactor Cavity - Spray Phase Transient Evaluation Basis Leak
Q001.581-23	Reactor Cavity - Gas Pressure Evaluation Basis Leak
Q001.581-24	Reactor Cavity - Gas Temperature Evaluation Basis Leak
Q001.581-25	Reactor Cavity - Floor Transient Evaluation Basis Leak
Q001.581-26	Reactor Cavity - Non-Wetted Wall Transient Evaluation Basis Leak
Q001.581-27	Cell 102A - Cell Gas Pressure Design Basis Leak
Q001.581-28	Cell 102A - Cell Gas Temperature Design Basis Leak
Q001.581-29	Cell 102A - Floor Transient Design Basis Leak
Q001.581-30	Cell 102A - Non-Wetted Wall Transient Design Basis Leak
Q001.581-31	Cell 102A - Cell Gas Pressure
Q001.581-32	Cell 102A - Cell Gas Pressure Moderate Energy Fluid System Leak
Q001.581-33	Cell 102A - Cell Gas Temperature Moderate Energy Fluid System Leak
Q001.581-34	Cell 102A - Floor Transient Moderate Energy Fluid System Leak
Q001.581-35	Cell 102A - Non-Wetted Wall Transient Moderate Energy Fluid System Leak
Q001.581-36	Cell 102A - Spray Phase Transient Evaluation Basis Leak
Q001.581-37	Cell 102A - Cell Gas Pressure Evaluation Basis Leak
Q001.581-38	Cell 102A - Cell Gas Temperature Evaluation Basis Leak
Q001.581-39	Cell 102A - Floor Transient Evaluation Basis Leak
Q001.581-40	Cell 102A - Non-Wetted Wall Evaluation Basis Leak
Q001.581-41	PHTS Cell Pressure-Evaluation Basis Leak (25 Percent Failure)
Q001.581-42	PHTS Cell Temperature-Evaluation Basis Leak (25 Percent Failure)
Q001.581-43	RCB Hydrogen Concentration-Evaluation Basis Leak (25 Percent Failure)
Q001.581-44	PHTS Cell Pressure-Evaluation Basis Leak (50 Percent Failure)
Q001.581-45	PHTS Cell Temperature-Evaluation Basis Leak (50 Percent Liner Failure)
Q001.581-46	RCB Hydrogen Concentration-Evaluation Basis Leak (50 Percent Failure)

1.0 Introduction

Sodium Leaks from the Primary Heat Transport System (PHTS) piping into the Reactor Cavity and the PHTS Cells and from piping within the Overflow and Primary Sodium Storage Tank Cells have been analyzed. These cells constitute the major cells within the Reactor Containment Building (RCB) both with respect to the size of the cells and the volume of sodium contained in the equipment within the cells. All of these cells operate with an inerted atmosphere (nitrogen) with a maximum of two volume percent oxygen. A spectrum of leaks has been considered for the analysis.

Leaks as small as 100 gm/hr can be detected by the sodium leak detection system in 250 hours and are indicative only of the initiation of a potential breach of the piping. Such leaks are so small, however, that no significant sodium is lost from the affected system and the impact on the cell temperature and pressure and the cell liners is negligible.

The smallest leak rates considered in the analysis presented herein corresponds to the piping Design Basis Leaks (DBL) that have been established for CRBRP. The definition of these leaks is discussed in PSAR Section 3.8-B and represents a conservatively established limit for the leak rates that may be expected to occur in the piping systems within the RCB that contain primary coolant sodium. As shown in Table Q001.581-1 for the three cells considered here, the DBL leak rates are 8 gpm or less.

In order to assess the sensitivity of cell design parameters (pressures, temperatures, etc.) to leak rate and quantity, other leak rates were examined. A Moderate Energy Fluid Systems (MEFS) Leak has been defined which is equivalent to the leak size established in the NRC Standard Review Plan - Section 3.6.2. The leak size is defined as a circular opening with area equivalent to a rectangle which has dimensions of one-half the pipe diameter and one-half the pipe thickness. In addition, a still larger pipe break has been considered that results in a leak which approximates the maximum flow through the piping systems in the affected cells. This leak has been termed the Evaluation Basis Leak (EBL). In developing the spectrum of leaks considered, the operating characteristics of the plant were considered. The Design Basis Leak assumes that the leak detection system is functional and that operator actions will be taken to reduce and finally eliminate the source of the leak. The MEFS Leak scenario assumes that leaks in the primary piping which are large enough to reduce the sodium level in the reactor will activate the Plant Protection System (PPS) with resulting pump trip. However, the time of the trip is arbitrarily adjusted to maximize the resulting cell gas temperature and pressure. For the PHTS piping EBL leak it is conservatively assumed that the sodium leak rate is equal to the design sodium flow rate in the piping and that this flow rate is maintained until the maximum available system inventory is discharged through the break. No pump trip is therefore assumed. This is, of course, extremely conservative since the actual plant flow characteristics would tend to reduce the discharge rate

and the quantity of sodium released. Actually, for a leak of this magnitude, the protection system would detect the failure and shut down the pump within a few seconds. For leaks in the Overflow and Primary Sodium Storage Tank Cells, leak detection systems are assumed operable and operator action is assumed. Other conservative assumptions used in the analyses concerning leak rate and leak volume are noted below. It should be noted that the location of all PHTS leaks in the Reactor Cavity is assumed to be the cold leg. The cold leg leak was selected because cold leg pressure is significantly higher than that of the hot leg (~ 100 psig vs ~ 20 psig). Since the pipe leak geometrics are very close (an area within a factor of 2.5) for the hot and cold legs, leaks in the more highly pressurized cold leg result in significantly higher leak rates and thus higher cell atmosphere temperatures and pressures, even though the cold leg sodium temperature is lower.

Also, the duration of the EBL leaks are slightly different in the RC than in the PHTS Cell. The reason for this difference is that slightly more sodium can be discharged into the RC than the PHTS Cells because of the piping elevations, but the leak rate is assumed to be the same for both.

The EBL leak rate is not as high as might be postulated for a double ended rupture of the PHTS piping. However, as shown in the response to NRC Question 001.700, additional flow, if it were available, would not lead to higher cell pressurization.

In all cases, the elevation of the pipe break was chosen such that the maximum cumulative sodium release was considered. The maximum spray fire consequences were included by assuming that the entire discharge was completely converted into spray. This is, of course, unrealistically conservative for the larger leak sizes.

The effect of various geometric pipe break configurations has been included in the analyses which have been performed. The design basis leak considers a longitudinal crack in the pipe. The MEFS Leak assumes a circular hole in the pipe which has the same flow characteristics as a sharp-edged orifice. The EBL assumes that the break size has the same area as the original pipe. In all cases, it was assumed that the total discharge was converted into spray and the resulting droplets traveled through the entire height of the cell.

The analyses presented herein were performed to determine the transient temperatures and pressures imposed upon a PHTS cell, the Reactor Cavity and Cell 102A (In-Containment Primary Sodium Storage Tank Cell) for a spectrum of pipe leak sizes assuming the cell liners remain intact. To assess the consequences of a failed liner, a parametric study was also performed for the PHTS cell which assumed that portions of the liner system had failed. (The PHTS cell was chosen as a prototypic cell in which to demonstrate that the inerted lined cells in the containment have margin

to accommodate substantial failure of the liners.) A failure mode analysis of the liner system presented in the response to NRC Question 130.89 indicated that in the unlikely event of a liner failure, the extent of the failure would be very limited. Section 4 of this response presents an assessment of the consequences of a liner failure which includes the effects of sodium-concrete interaction.

The analyses were performed using three computer codes, SPRAY, SOFIRE and CACECO. For the conditions in which the liner was assumed to remain intact, SPRAY and SOFIRE were used to evaluate cell transients. For the evaluation assuming liner failure, all three codes were employed with the sodium-concrete-water reactions included in the CACECO analysis. The basic material properties included in the SPRAY and SOFIRE analyses are listed in Table Q001.581-2. The material properties for the CACECO code used in analyses of failed liners are presented in Table Q001.581-5.

Summary results of all the analyses are presented in Section 2. Detailed discussions of the analyses, on a cell-by-cell basis, are presented in Sections 3 and 4.

2.0 Summary

2.1 Summary Results - Cell Liner Design Conditions

Table Q001.581-4 presents the summary results of the analyses for the design conditions where cell liner integrity is maintained. For each cell and leak evaluated, the following peak transient values are itemized: gas pressure, gas temperature, liner temperature, floor structural concrete temperature and the non-wetted wall structural concrete temperature. The concrete temperatures provided in the table represent the temperatures in the first one-half inch of structural concrete behind the floor gravel aggregate and the wall insulating concrete. Note that the peak transient temperatures for the non-wetted wall structural concrete are not specified in absolute terms but rather as a temperature that this concrete will not exceed. This is necessary because it is not feasible to continue the SOFIRE analyses for the time the wall concrete passes through a peak temperature, as is the case for the floor concrete transient. However, by examining those transients in the insulating concrete which have passed through their peak temperature and are decreasing, it is possible to estimate a peak temperature value that the wall structural concrete will asymptotically approach and thus to specify a temperature it will not exceed over the entire course of the transient. This method was used to specify the bounding temperatures in Table Q001.581-4 for the wall structural concrete.

50 It should also be noted that the pressures in the reactor cavity quoted for the MEFS and the EBL will be limited by the pressure venting system that is being installed to accommodate the Thermal Margin Beyond the Design Base events. While provisions have been included for a venting system, the rupture disk burst pressure has not been selected. It is expected to

be in the range of 8-10 psig. The primary purpose of this study was to determine the potential pressures that may exist in these cells for a spectrum of postulated leaks. For this reason, use of the Reactor Cavity vent system or consideration of venting the PHTS cells or Cell 102A was not included in the evaluation.

It should be noted that the maximum pressures reached are less than the design pressures for the cells.

Three general observations based on the data summarized in Table Q001.581-4 follow:

- The transients associated with any of the DBLs are minor, both in terms of cell gas pressurization and in terms of structural concrete transients. Specifically, none of the DBLs result in a cell gas pressurization in excess of 1.1 psig. The structural concrete temperatures (floor and wall) do not exceed 120°F for any of the DBLs.
- For each of the cells considered, the MEFS Leaks result in peak gas pressures and temperatures approximately a factor of 2 less than the corresponding EBLs.
- For the PHTS Cell and the Reactor Cavity the structural concrete transients are essentially equivalent for either the MEFS or EBL. However, for Cell 102A, the EBL concrete structural transients are slightly (30°F-80°F) more severe than the MEFS concrete transients.

2.2 Summary Results - Evaluation with Cell Liner Failure

Cell Liners will prevent the interaction of sodium with the concrete cell structures in the event of all sodium spills. However, in response to NRC Question 130.89, a failure mode assessment was performed to determine a scenario that could lead to liner failure. Such a scenario was developed by assuming a series of very pessimistic conditions. The Failure Mode Evaluation results in the determination that the worst failure that can be postulated is a small crack in the liner floor, assumed to occur at or near a weld joint, which extends the entire length of the cell. The crack opening would not exceed approximately 0.25 inches in the PHTS Cell initially and would not appear until the pool of sodium began to cool down. For the conditions assumed in the response to NRC Question 130.89, the crack would not open for over an hour after the spill. During this time delay period, much of the water in the upper portion of the structural concrete will be released and vented through the liner venting system, thus reducing the amount of water available for reaction with the sodium pool following crack opening.

In order to accurately evaluate the effects of a liner failure, a very complex analysis would be required and probably a series of tests conducted to confirm the results. The sodium which leaks through the assumed liner crack would be contained in the aggregate. Since the aggregate is chemically inert to the sodium, it provides two major benefits. First, the aggregate will occupy approximately one-half the volume between the liner and the structural concrete. This will limit the amount of sodium that is available to react with the water released from the concrete. Since the liner failure is very small compared to the cell floor area, there will be little or no opportunity for fresh sodium to replace reacted sodium under the liner. Secondly, the aggregate will tend to hold the reaction products on the surface of the concrete, forming a partial barrier to further

sodium-concrete reaction. (This effect has been observed in the HEDL tests, as discussed in response to NRC Question 130.89.)

However, the effects described above are extremely difficult to evaluate analytically. For the analyses presented in Section 4.0, no credit is taken for these effects or the time delay to failure.

Parametric analyses of partial failures in the PHTS cell were done to demonstrate plant margin to accommodate the resulting cell atmosphere pressure and temperature and hydrogen concentration in the RCB. Two partial failures were considered for the EBL, 25 percent and 50 percent of the floor and submerged wall (Table 0001.581-3). In neither case was
40| intercell or cell to RCB venting assumed.

For the smaller failure, 25 percent of the liner failed, the cell pressure reaches a maximum during the spray phase, 24 psig. The maximum cell temperature, 1050°F, reaches a maximum at that time also. At the end of 50 hours, only negligible amounts of hydrogen are being produced and the RCB concentration is less than one percent.

Assuming 50 percent liner failure results in pressures which are only slightly higher than the spray phase, 29 psig. The maximum cell temperature occurs during the spray phase and is equal to 1050°F.

The cell atmosphere is assumed to leak from the cell to the RCB at a rate equivalent to 100 volume percent per day at 10 psid. At the end of 50 hours the RCB hydrogen concentration is 3.9 percent and at the end of 100 hours is 4.1 percent.

3.0 Detailed Analysis Description - Cell Liner Design Conditions

A discussion of the analyses and results for each cell and each pipe leak for the condition where liner integrity is maintained is presented in the following sub-sections.

3.1 Primary Heat Transport System (PHTS) Cell

Design Basis Leak

The PHTS Cell piping DBL is described in Table Q001.581-1. The total duration of the DBL is 390 minutes and the total sodium injected into the cell is 530 gallons; 45% of this sodium is injected during the first 30 minutes of the transient after which operator action can be assumed to trip the reactor and pumps. Over this period, all the sodium discharged was assumed to be injected in the form of a spray (0.18" droplets) at a temperature of 1015°F and in a manner such that the spray occupied one-third of the cell volume. The conservatism in these assumptions are discussed in PSAR Section 15.6.1. A SPRAY analysis of this leak was conducted for a time duration of 2130 seconds (36 minutes). The SPRAY analysis was terminated at approximately 36 minutes because the peak cell atmosphere transients, pressure and temperature, resulting from the spray phase are reached prior to this time. Specifically, the SPRAY analysis

indicates a peak cell pressure of 0.19 psig at 30 minutes. However, because of the relatively long duration and relatively low discharge rate of the DBL, the contribution of the sodium pool accumulated on the cell floor, which SPRAY does not consider, to the transient during this 30 minute interval needs to be considered.

The contribution of this pool was conservatively estimated based on a SOFIRE analysis. For the SOFIRE analysis, it was assumed that the entire sodium discharge (530 gallons) instantly forms a pool on the cell floor, rather than the actual pool formation mechanism which is a slow buildup over 6.5 hours. It was further assumed that the entire PHTS Cell oxygen content (2%) was available for reaction with this pool (i.e., oxygen-depletion during the spray injection was neglected). Based on these conditions, the SOFIRE analysis provides a conservative prediction of the rate of pool oxidation and the contribution of the pool to the cell pressure and temperature transients.

Figure Q001.581-1 presents the PHTS Cell atmosphere pressure and temperature transients. The pressure transient resulting from the spray phase is added to the conservatively defined pool pressure transient to provide the total PHTS Cell pressure transient. The long-term structural transients resulting from the DBL are presented in Figures Q001.581-2 and 3.

Moderate Energy Fluid System Leak

The total duration of the PHTS Cell MEFS Leak is 150 minutes and the total sodium injected into the cell is approximately 20,000 gallons; 20% of this sodium is injected in the first 4.5 minutes, after which the Plant Protection System can be assumed to have shutdown the plant. A SPRAY analysis of this leak was conducted for a time duration of approximately 14 minutes. Over this period, all the sodium injected was assumed to be in the form of a spray (0.18" droplets) at a temperature of 1015°F, and in a manner such that the spray occupied one-third of the cell volume. The SPRAY analysis was terminated at ~14 minutes because the peak cell atmosphere transients are reached prior to this time. Specifically, the peak cell pressure, 11 psig, occurs at 3.5 minutes, the end of the MEFS Leak maximum discharge rate (985 gpm).

To provide a conservative assessment of the longer-term transients, a SOFIRE analysis was conducted. The SOFIRE analysis assumed the entire sodium discharge (20,000 gallons) instantly forms a pool on the cell floor. The initial conditions for this SOFIRE analysis are taken as the peak pressure and temperature occurring during the spray-phase and the remaining oxygen concentration corresponding to this peak. This methodology is conservative in that the peak cell atmosphere transients are provided by the spray-phase analysis while the contribution of the pool to the long-term transients is conservatively estimated by assuming instantaneous pool formation, rather than the actual pool formation mechanism which involves a slow buildup over 2 hours, concurrent with the availability of all remaining oxygen. Actually, a portion of this remaining oxygen would continue to be depleted via interaction in the

cell atmosphere with sodium discharged after the peak is reached, but neglecting this and assuming only pool-oxygen reaction is conservative with regard to long-term structural transients and insignificant with regard to the cell atmosphere transients since the SPRAY analysis shows these transients to have already peaked.

Figure Q001.581-4 presents the results of the spray-phase transient analysis. As indicated, the peak cell pressure of 11 psig occurs at 3.5 minutes, corresponding to peak cell atmosphere temperature of 570°F. Figures Q001.581-5 through-8 present the longer-term cell transients based on the SOFIRE analysis.

Evaluation Basis Leak (EBL)

The PHTS Cell EBL is a spill of the total spillable volume in a loop (20,000 gallons). The spill rate is conservatively taken to be the normal loop flow rate of 33,500 gpm which yields a spill duration of 0.6 minutes.

The SPRAY analysis for this leak assumed that the entire discharge was in the form of 0.18" droplets at 1015°F and in a manner such that the spray occupied one-third of the cell volume. Figure Q001.581-9 presents the results of the spray-phase transient analysis. The peak cell atmosphere pressure and temperature of 23 psig and 1030°F, occur near the end of the sodium discharge and begin to decrease after the sodium discharge is complete. The entire PHTS Cell oxygen content is depleted by the end of the sodium discharge.

As discussed for the MEFS leak, the longer-term transients were evaluated with SOFIRE, with initial conditions corresponding to the peak spray-phase transient conditions. In this case, however, the oxygen concentration used for SOFIRE was zero, since all the oxygen is consumed during the spray. Figures Q001.581-10 through-13 present the longer-term cell transients based on the SOFIRE analysis.

The Evaluation Basis Leak (EBL) of the IHTS piping within a PHTS cell results in a maximum spill rate of 29900 gpm of 936°F sodium for a period of 30 seconds. When compared to the primary system EBL of 33,500 gpm of 1015° sodium for 35.5 seconds, it is noted that each of the above parameters for the primary system leak envelopes comparable parameters for the intermediate system. The analysis results presented for the primary system EBL therefore conservatively envelopes the intermediate system EBL in the PHTS cell.

50

3.2 Reactor Cavity

Design Basis Leak

The Reactor Cavity piping DBL is described in Table Q001.581-1. The total duration of the DBL is 410 minutes and the total sodium injected into the cavity is 390 gallons; 52% of this sodium is injected during the first 40 minutes of the transient after which operator action can be assumed to have tripped the reactor and pumps.

The basic method used to evaluate the transients resulting from this leak is identical to that described for the PHTS DBL. The only principal difference is that the Reactor Cavity DBL originates from a cold-leg piping fault so that the temperature of the injected sodium is taken

as 750°F, the peak cold-leg temperature.

Figure Q001.581-14 presents the Reactor Cavity atmosphere pressure and temperature transients. The structural transients resulting from the DBL are presented in Figures Q001.581-15 and -16.

Moderate Energy Fluid System Leak

The total duration of the Reactor Cavity MEFS Leak is 150 minutes and the total sodium injected into the cavity is approximately 20,000 gallons; 20% of this sodium is injected in the first 5 minutes after which it can be conservatively assumed that the Plant Protection System has shut-down the plant. The Reactor Cavity MEFS Leak originates from a cold-leg piping fault and the temperature of the sodium injected is specified as 750°F, the peak cold-leg sodium temperature. The same analysis procedure as described for the PHTS Cell MEFS Leak was used to evaluate this leak.

Figure Q001.581-17 presents the results of the spray-phase transient analysis. The peak Reactor Cavity atmosphere pressure and temperature, 9.8 psig and 560°F, occur at approximately 2.5 minutes. The pressure and temperature decline gradually out to 4 minutes, the end of the maximum MEFS Leak rate (880 gpm), and begin to decrease sharply at 5 minutes when the MEFS Leak rate decreases to 120 gpm. Figures Q001.581-18 through-21 present the long-term Reactor Cavity transients based on the SOFIRE analysis.

Evaluation Basis Leak

The Reactor Cavity EBL is a spill of the total spillable sodium in a loop (20,000 gallons). The spill rate is conservatively taken to be the normal loop flow rate of 33,500 gpm, which yields a spill duration of 0.6 minutes. The Reactor Cavity EBL originates from a hot-leg piping failure and the temperature of the sodium injected is taken as 1015°F, the maximum hot-leg sodium temperature. The same analysis procedure as described for the PHTS Cell EBL was used to evaluate this leak.

Figure Q001.581-22 presents the results of the spray-phase transient analysis. The peak Reactor Cavity atmosphere pressure and temperature, 21 psig and 1020°F, occur at approximately 15 seconds. The Reactor Cavity oxygen is also depleted at roughly 15 seconds. For the EBLs, which are essentially identical for both the Reactor Cavity and PHTS Cell, oxygen depletion occurs more rapidly in the Reactor Cavity principally because the Reactor Cavity free volume is only 50% as large as that of the PHTS Cell, so that oxygen available in the Reactor Cavity is roughly one-half that available in the PHTS Cell.

The longer-term Reactor Cavity transients, based on SOFIRE analysis, are provided in Figures Q001.581-23 through-26.

3.3 Overflow and Primary Sodium Storage Tank Cell

Design Basis Leak

The piping DBL for the Overflow and Primary Sodium Storage Tank Cell (Cell 102A) is defined as a 0.15 gpm leak (0.017 lbs/sec) for 990 minutes (16 hours) after which the leak would have been detected and pumps tripped by the Operator; followed by a 0.015 gpm leak for 410 minutes (6.9 hours). The assumptions regarding leak detection and Operator action are discussed in the response to Q040.4. The total sodium injected into the cell is 150 gallons.

| 41

Because of the extremely low discharge rate and the long discharge period, essentially this DBL is a weeping leak of roughly 0.6 cubic inches of sodium per second, it is not feasible to conduct a typical SPRAY/SOFIRE analysis of this leak. Therefore, to provide a conservative assessment of this event, a SOFIRE analysis was conducted assuming that the entire sodium discharge (150 gallons) instantly forms a pool on the cell floor, rather than the actual pool formation mechanism which is an extremely slow buildup over 23 hours. It was further assumed that the entire pool was initially at 830°F, the peak cell sodium temperature, whereas based on the actual discharge rate it is likely that the sodium accumulating slowly on the cell floor will solidify.

To insure that the assumption of instantaneous pool formation provides conservative transient results for this DBL, a SPRAY analysis was also conducted. For this SPRAY analysis, the initial discharge rate (0.15 gpm) was assumed to be injected in the form of a spray (0.18" droplets) at 830°F and in such a manner that one-third of the cell volume was occupied by the spray. This SPRAY analysis was conducted for a time duration of approximately 0.5 hours. At the termination of this SPRAY analysis the cell pressure was only 0.012 psig and the rate of pressurization was less than 3×10^{-6} psig/seconds. Extrapolating this rate out to 23 hours (the total DBL duration), which is conservative since it neglects the discharge reduction to 0.015 gpm at 16 hours, indicates a maximum cell pressurization due to the discharge of less than 0.3 psig. This estimated peak pressure is extremely conservative in that it ignores the reduction in flow rate to 0.015 gpm as well as the cell concrete heat sink effects, which SPRAY neglects, but which are important for this long duration leak. Since the SOFIRE results, presented below, envelop this conservative peak spray-phase pressure estimate, it is concluded that the assumption of instantaneous pool formation results in an adequate assessment of the transients resulting from this DBL.

The results of the SOFIRE analysis are presented in Figures Q001.581-27 through-30. As the Figures indicate, the peak cell pressure is only 0.39 psig and the peak cell atmosphere temperature is 140°F. Note also from Figure Q001.581-27 that the cell pressure goes negative at approximately 4.5 hours, and by 10 hours the pressure has decreased to -0.24 psig. This effect results directly from depletion of the cell oxygen via combustion. In the limit, depleting all the cell oxygen (2%) can result in a negative pressure of -0.29 psig, if the heat input to the cell atmosphere is not sufficient to compensate for this decrease in cell gas mass. Any in-leakage of air due to the negative pressure may result in additional pool fire combustion, but because of low sodium temperatures the effects would be insignificant compared to the initial sodium fire effects.

Because of the very small quantity of sodium associated with the Cell 102A DBL, the oxygen depletion effect is more controlling than the heat source associated with the DBL and consequently the cell pressure approaches -0.29 psig at 10 hours. This will have no adverse effect on the liner integrity, since liners are designed to withstand external pressure of 5 psid.

Moderate Energy Fluid System Leak

The total duration of the Cell 102A MEFS Leak is 400 minutes (6.7 hours) and the total sodium injected into the cell is 4400 gallons. 28% of this sodium is injected in the first 15 minutes after which the spill would be detected and the pumps tripped resulting in a lower spill rate (see Response Q040.4). The same analysis procedure as described for the PHTS Cell MEFS Leak was used to evaluate this leak. A SPRAY analysis was conducted for a time duration of approximately 0.5 hours. Over this period all the sodium injected was assumed to be in the form of a spray (0.18" droplets) at a temperature of 830°F and in a manner such that the spray occupied one-third of the cell volume. The SPRAY analysis was terminated at ~0.5 hours because the peak cell atmosphere transients resulting from the spray-phase are reached prior to this time. Specifically, the peak spray-phase cell pressure, 3.1 psig, occurs at 15 minutes, the end of the MEFS Leak maximum discharge rate (83 gpm).

As discussed previously for the PHTS Cell MEFS Leak, it was conservatively assumed that the entire sodium discharge (4400 gallons) instantly forms a pool on the cell floor with initial conditions corresponding to the peak spray-phase conditions, and a SOFIRE analysis was conducted based on this condition to provide a conservative assessment of the long-term cell transients.

Figure Q001.581-31 presents the results of the spray-phase transient analysis. As indicated, the peak cell pressure resulting from the spray-phase is 3.1 psig at 15 minutes, corresponding to a peak cell atmosphere temperature of 240°F. Figures Q001.581-32 through -35 present the longer-term cell transients based on the SOFIRE analysis. Note from Figures Q001.581-32 and -33 that the cell gas pressure and temperature initially increase from the peak spray-phase pressure and temperature used as initial conditions for the SOFIRE analysis. This phenomenon results because of the conservative assumption that the entire sodium discharge (4400 gallons) is available as a pool on the cell floor at 15 minutes, corresponding to the peak spray-phase conditions, whereas the actual pool formation mechanism is a buildup of the pool over 6.7 hours. Consequently, the peak pressure and temperature calculated in the spray-phase analysis are more representative of the actual peak transient conditions. This phenomenon occurs here but not for the PHTS Cell or Reactor Cavity MEFS Leaks because the sodium discharge rate (spray) for the Cell 102A MEFS Leak is relatively small in comparison to either the PHTS Cell or Cavity MEFS rate and consequently, the Cell 102A spray-phase discharge does not dominate the cell atmosphere transients as do the other MEFS Leaks. Notwithstanding the fact that the SOFIRE calculated peak pressure and temperature slightly over-

estimate the expected peak transient values, it is conservatively assumed that these represent the peak cell atmosphere transients because (1) they are not markedly different from the spray-phase values, the peak pressures differ by only 14% and the peak temperatures differ by only 10%, (2) they provide a conservative estimate of the peak transient conditions, and (3) adopting these values is consistent with the methodology used throughout these analyses with regard to coupling of SPRAY-SOFIRE.

Evaluation Basis Leak

The Cell 102A EBL is a 150 gpm leak for 15 minutes after which the leak would be detected and pump(s) tripped by operator action (see Response Q040.4), followed by a 15 gpm leak for 370 minutes. The total duration of the EBL is 380 minutes (6.4 hours) and the total sodium injected into the cell via this flow/time pattern is 7700 gallons. However, in Cell 102A the potential exists (after a PHTS loop has been drained to the in-containment Primary Sodium Storage Tank) for a larger total spill volume (24,000 gallons), although no spray-phase discharge would be associated with this larger spill.

Consistent with the analysis method used throughout this evaluation, a SPRAY analysis was performed for the initial discharge, and the total potential spill (24,000 gallons) was then assumed to instantly form a pool on the cell floor with initial conditions corresponding to the peak spray-phase conditions.

For the SPRAY analysis, the sodium discharge was assumed injected as a spray (0.18" droplets) at 830°F in a manner such that the spray occupied one-third of the cell volume. The SPRAY analysis was terminated at roughly 0.5 hours, since the peak spray-phase transient values occur prior to this time. Figure Q001.581-36 presents the results of the SPRAY analysis. The peak spray-phase pressure and temperature, 4.6 psig and 300°F, occur at 15 minutes, the end of the EBL maximum discharge rate of 150 gpm.

Figures Q001.581-37 through-40 present the long-term transients based on the SOFIRE analysis. Note from Figures Q001.581-37 and-38 that the longer-term cell atmosphere pressure and temperature exceed those associated with the spray-phase release. Specifically, the peak pressure and temperature are 7.1 psig and 410°F at 6 hours. These pressure and temperature transients are actually representative of the cell transients due to the pool and are not subject to analysis anomalies as discussed for the Cell 102A MEFS Leak. This is the case since the total spill (24,000 gallons) is relatively large and since the spray discharge does not significantly deplete the cell oxygen content, the contribution of this large pool to the cell atmosphere transient is more controlling than the spray-phase transient.

4.0 Detailed Analysis Description - Evaluation with Cell Liner Failure

The previous section (Section 3) evaluated the consequences of a spectrum

of sodium spill into several of the cells within the Reactor Containment Building on the basis that the cell liners will maintain their integrity and provide a barrier between the sodium and the concrete and the water vapor released from the concrete as it is heated. The cell liners are designed to provide this barrier. Additional analyses are presented below to show the effect of a non-mechanistic failure of the cell liner whereby a limited section of the liner fails and permits sodium contact with the concrete floor directly under the failed portion. Water vapor release from that portion of the concrete is assumed to react with the sodium pool. These analyses were performed for the EBL into the PHTS cell as a prototypic cell in which to demonstrate the margin in the plant inerted cell design. The results indicate that for limited failure of the PHTS cell liner (less than 50 percent of wetted surface failed) the consequences are not severe, i.e., the calculated pressure in the cell does not exceed the design pressure and the maximum hydrogen concentration in the RCB does not exceed 5 volume percent.

Evaluation Basis Leak

The PHTS cell EBL is a spill of the total volume of sodium in a loop (20,000 gallons). The spill rate is conservatively taken to be the normal loop flow rate of 33,500 gpm which yields a spill duration of 0.6 minutes.

The SPRAY analysis for this leak was discussed in Section 3.1 and the results of the spray phase transient are presented in Figure Q001.581-9. The peak cell pressure and temperatures occur near the end of the sodium discharge and begin to decrease after the discharge is complete. The entire PHTS cell oxygen content is depleted in 33 seconds.

The long term transient was analyzed with the CACECO code based on the oxygen burning rate defined by SPRAY as described above. In addition, the exothermic reactions due to sodium concrete and sodium water reaction have been considered.

Two partial failures were considered by assuming 25 and 50 percent of the floor and wall submerged under the pool fail upon contact with sodium. Water released from the failed section of the liner reacts with sodium and water released from the intact portion of the cell wall is vented to a non-vital area.

Assuming 25 percent liner failure results in a pressure which reaches a maximum of 24 psig during the spray phase. The maximum temperature in the cell (1050°F) is also reached at that very early time. The PHTS cell pressure and temperature for the EBL are presented in Figures Q001.581-41 and -42. At the end of 50 hours, the hydrogen concentration in the RCB is 0.91 percent (Figure Q001.581-43). The unreacted sodium remaining in the cell at that time (130,000 lbs) has cooled to 290°F and no significant increase in hydrogen is occurring.

Assuming 50 percent liner failure results in a maximum pressure of 29 psig which occurs at 0.30 hour (Figure Q001.581-44). The maximum cell temperature occurs at the end of the spray phase and reaches 1050°F (Figure Q001.581-45). At the end of 50 hours, 11,300 lbs of unreacted sodium remain in the cell at a temperature of 370°F.

The hydrogen released in the PHTS cell is assumed to leak to the RCB at a leak rate equivalent to 100 volume percent per day at 10 psid. The hydrogen concentration in the RCB at 50 hours is 3.9 percent and still increasing (Figure Q001.581-46). The total hydrogen mass in the PHTS cell and the RCB at that time is 1100 lbs. This corresponds to an equivalent concentration of 6 volume percent if all of the hydrogen were introduced into the RCB. At 100 hours the hydrogen concentration in the RCB is 4.1 percent and the total hydrogen mass in the PHTS cell and the RCB is 1200 lbs.

TABLE Q001.581-1

SUMMARY DESCRIPTION OF PIPING LEAKS EVALUATED

<u>Parameter</u>	<u>Design Basis Leak</u>	<u>Moderate Energy Fluid System Leak</u>	<u>Evaluation Basis Leak</u>
<u>PHTS Cell</u>			
Discharge	30 Min. @8 GPM 360 Min. @0.8 GPM	3.5 Min. @980 GPM 1.0 Min. @560 GPM 120 Min. @125 GPM 25 Min. @28.0 GPM	0.59 Min. @33,500 GPM
Duration	390 Minutes	147.7 Minutes	0.59 Minutes
Total Spill	530 Gallons	20000 Gallons	20000 Gallons
Na Temperature	1015°F	1015°F	1015°F
<u>Reactor Cavity</u>			
Discharge	40 Min. @5 GPM 370 Min. @0.5 GPM	4.0 Min. @880 GPM 1.0 Min. @550 GPM * 120 Min. @120 GPM 19 Min. @79 GPM	0.61 Min. @33,500 GPM
Duration	410 Minutes	150 Minutes	0.61 Minutes
Total Spill	390 Gallons	20,000 Gallons	20000 Gallons
Na Temperature	750°F	750°F	1015°F

* Intermediate flow for 1 minute represents pump coast down.

TABLE Q001.581-1 (Continued)
SUMMARY DESCRIPTION OF PIPING LEAKS EVALUATED

<u>Parameter</u>	<u>Design Basis Leak</u>	<u>Moderate Energy Fluid System Leak</u>	<u>Evaluation Basis Leak</u>
	<u>Cell 102A</u>		
Discharge	990 Min. @0.15 GPM 410 Min. @0.015 GPM	15 Min. @ 83 GPM 390 Min. @ 8.3 GPM	15 Min. @150 GPM 370 Min. @15 GPM
Duration	1400 Minutes	400 Minutes	380 Minutes
Total Spill	150 Gallons	4400 Gallons	24000 Gallons*
Na Temperature	830°F	830°F	830°F

*Sodium volume discharged via EBL discharge rate/time is 7700 gallons;
 24000 gallons is maximum potential spill volume and this larger volume
 is used to evaluate long-term cell transients associated with the sodium pool.

Q001.581-22

Amend. 40
 July 1977

TABLE Q001.581-2

MATERIAL PROPERTIES USED FOR THE SPRAY-SOFIRE ANALYSES

<u>Material</u>	<u>Denisty lb./ft.³</u>	<u>Thermal Conductivity Btu/hr.ft.²°F/ft.</u>	<u>Specific Heat Btu/lb.°F</u>
Steel	490	25	0.12
Liner Air Gap*	0.037	0.0135	0.6
Light Weight Insulating Concrete	65	0.07	0.25
Structural Dolomite Concrete	143	0.95	0.21
Floor Gravel Bed	30	0.16	0.25
Ambient Air	0.0709	0.0135	0.17**

* Air Gap properties based on saturated steam at 1 atm and 212°F

**Specific Heat at Constant Volume

TABLE Q001.581-3
SUMMARY RESULTS FOR PARTIAL CELL LINER FAILURE

Percentage of Submerged Liner Failure	25	50
Liner Area Failed, ft ²	470	950
Maximum Cell Pressure, psig	24	29
Maximum Cell Temperature, °F	1050	1050
RCB Hydrogen Concentration @ 50 hours, %	0.91	3.91
Na in Cell @ 50 hours, lbs.	130000	110000
Temperature of Na in Cell @ 50 hours, °F	290	370

Q001.581-24

Amend. 40
July 1977

TABLE Q001.581-4
SUMMARY RESULTS CELL LINER DESIGN CONDITION

Cell/Leak	Peak Transient Values				
	Gas Pressure Psig	Gas Temperature °F	Cell Liner Temperature Floor/Wall °F	Floor Structural Concrete Temperature °F	Wall Structural Concrete Temperature °F
<u>PHTS Cell</u>					
DBL	1.1	160	330/160	120	<110
MEFS	11	570	900/450	220	<150
EBL	23	1000	870/430	200	<150
<u>Reactor Cavity</u>					
DBL	0.7	180	290/150	120	<110
MEFS	9.8*	560	700/350	190	<140
EBL	21 *	1000	925/460	220	<150
<u>Cell 102A</u>					
DBL	0.39	140	240/130	110	<110
MEFS	3.6	270	700/240	150	<120
EBL	7.1	410	750/370	230	<150

* Does not consider a vent system operating.

TABLE Q001.581-5

PROPERTIES USED IN THE CACECO ANALYSISI. CRBRP LIMESTONE CONCRETE

Thermal Conductivity

<u>Temp, °F</u>	<u>K, Btu/hr-ft-°F</u>
0	1.0
200.	.98
1000.	.65
1600.	.55
2000.	.55

Heat Capacity
(Btu ft³ - °F)

<u>Temp, °F</u>	<u>ρCp contribution from water</u>	<u>ρCp without water</u>	<u>ρCp (total)</u>
0	0.0	28.7	28.7
32	0.0	28.7	28.7
212	0.0	28.7	28.7
392	3.75	28.7	32.45
572	8.12	28.7	36.82
752	13.11	28.7	41.82
932	14.37	28.7	43.07
1112	16.24	28.7	44.94
1292	9.68	28.7	38.38
1472	2.82	28.7	31.52
1652	0.0	28.7	28.7
2000	0.0	28.7	28.7

TABLE Q001.581-5 (Continued)

II. PROPERTIES OF INSULATING CONCRETE

Thermal Conductivity
 $k = 0.07 \text{ BTU/hr-ft-}^\circ\text{F}$

Heat Capacity

<u>Temp, °F</u>	<u>ρC_p contribution from water</u>	<u>ρC_p without water</u>	<u>ρC_p total</u>
0	0.0	14.4	14.4
32	0.0	14.4	14.4
212	0.0	14.4	14.4
392	3.75	14.4	18.15
572	8.12	14.4	22.52
752	13.11	14.4	27.51
932	14.37	14.4	28.77
1112	16.24	14.4	30.64
1292	9.68	14.4	24.08
1472	2.82	14.4	17.22
1652	0.0	14.4	14.4
2000	0.0	14.4	14.4

4" insulating concrete was used in the cell's roof and wall.

III. WATER VAPOR RELEASE FROM LIMESTONE CONCRETE AND INSULATING CONCRETE

<u>Temp, °F</u>	<u>Water Release lbs water ft³ of concrete</u>
0.	0.0
190.	0.0
275.	3.85
285.	5.78
420.	6.84
700.	7.51
800.	8.28
1500.	9.63
5000.	9.63

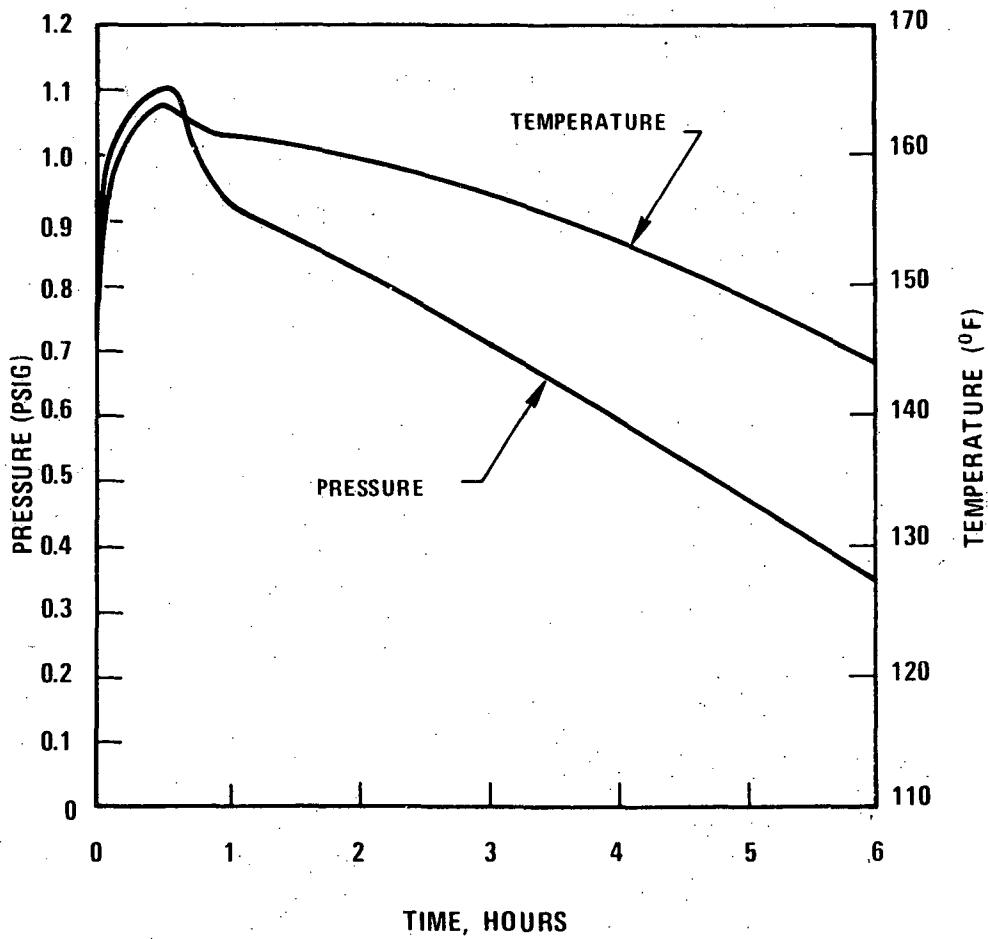


Figure Q001.581-1. PHTS Cell - Gas Pressure and Temperature Design Basis Leak

9653-5

Q001.581-28

Amend. 40
July 1977

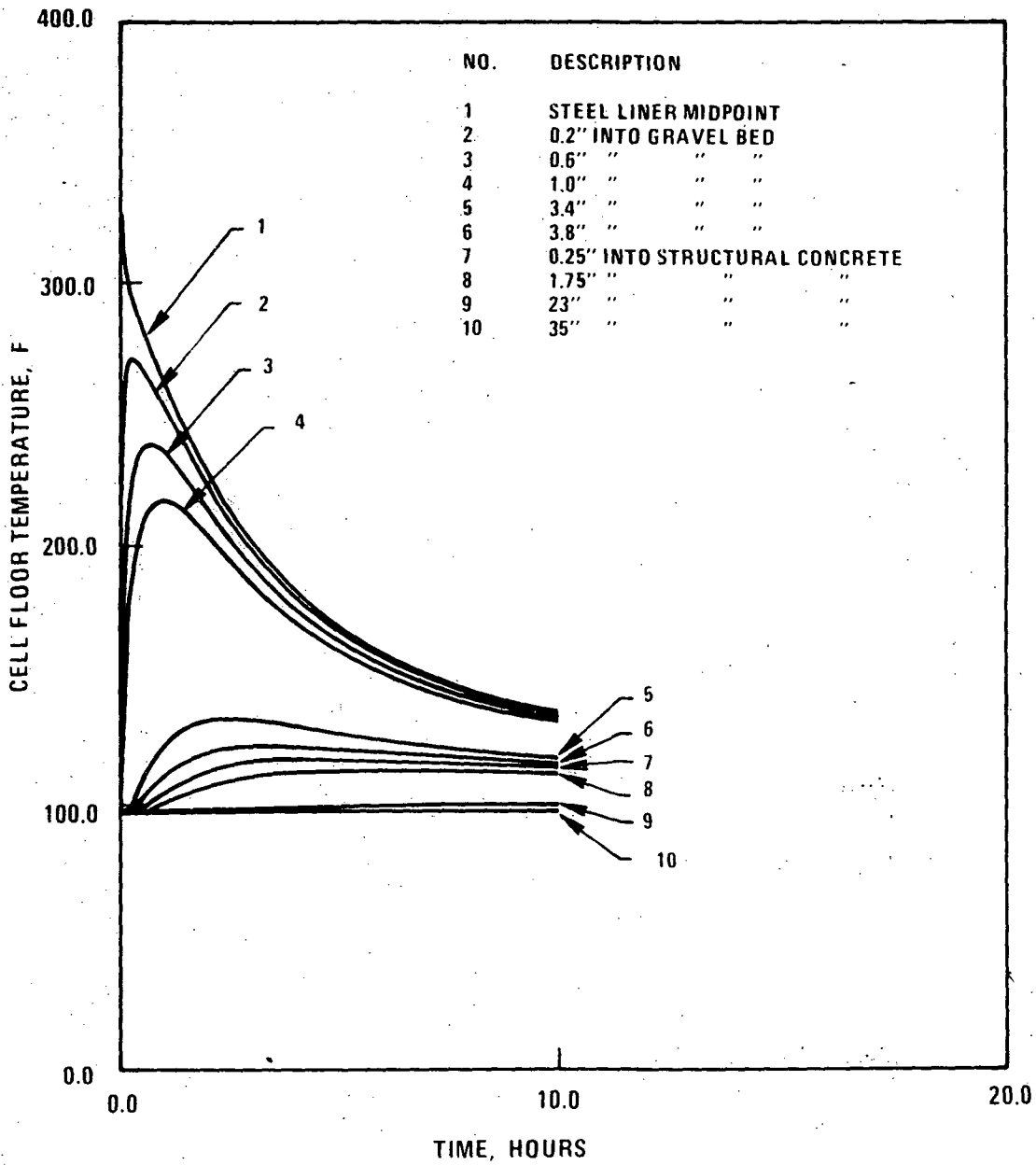


Figure Q001.581-2. PHTS Cell - Floor Transient Design Basis Leak

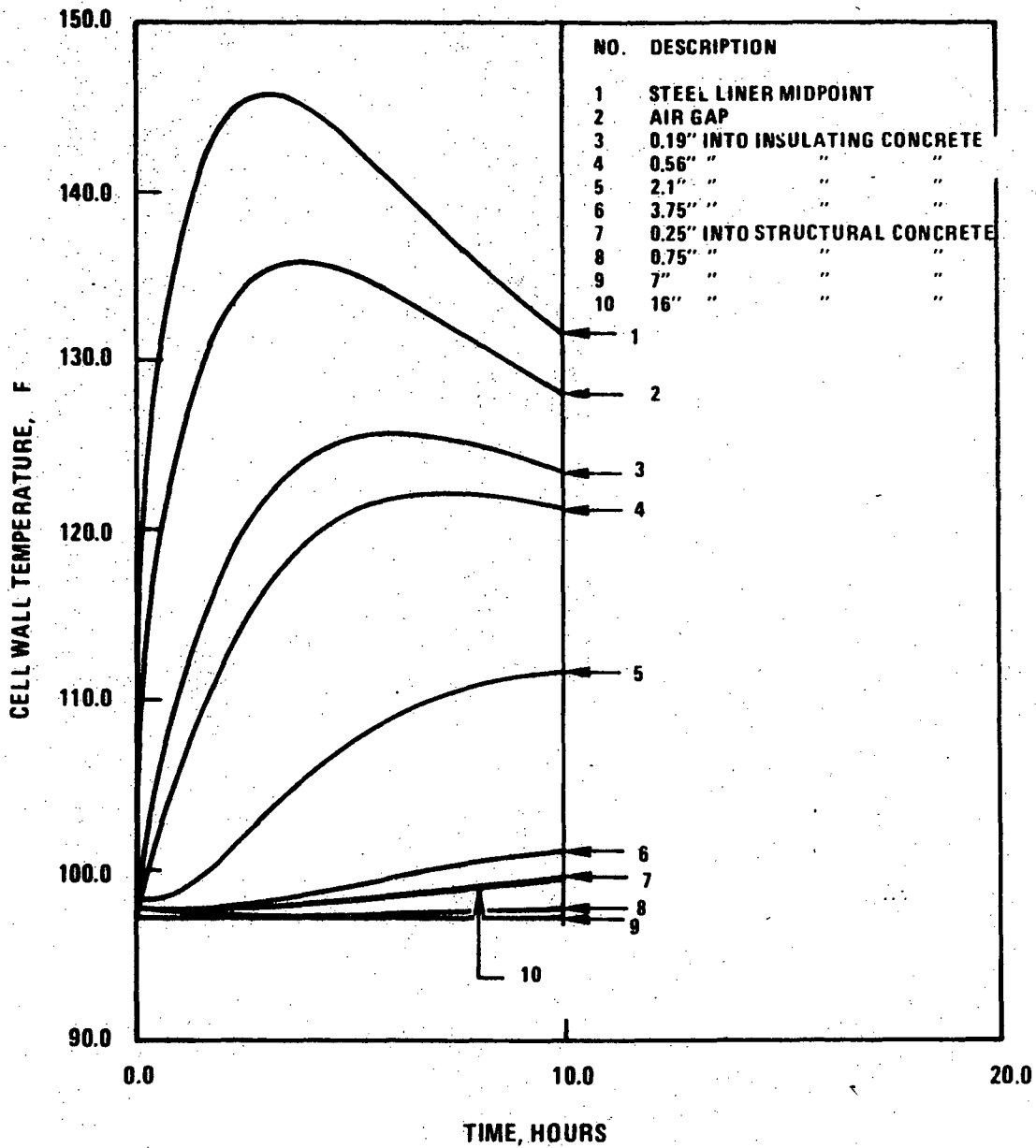


Figure Q001.581-3. PHTS Cell - Non-Wetted Wall Transient Design Basis Leak

96.5.3-24

Q001.581-30

Amend: 40
July 1977

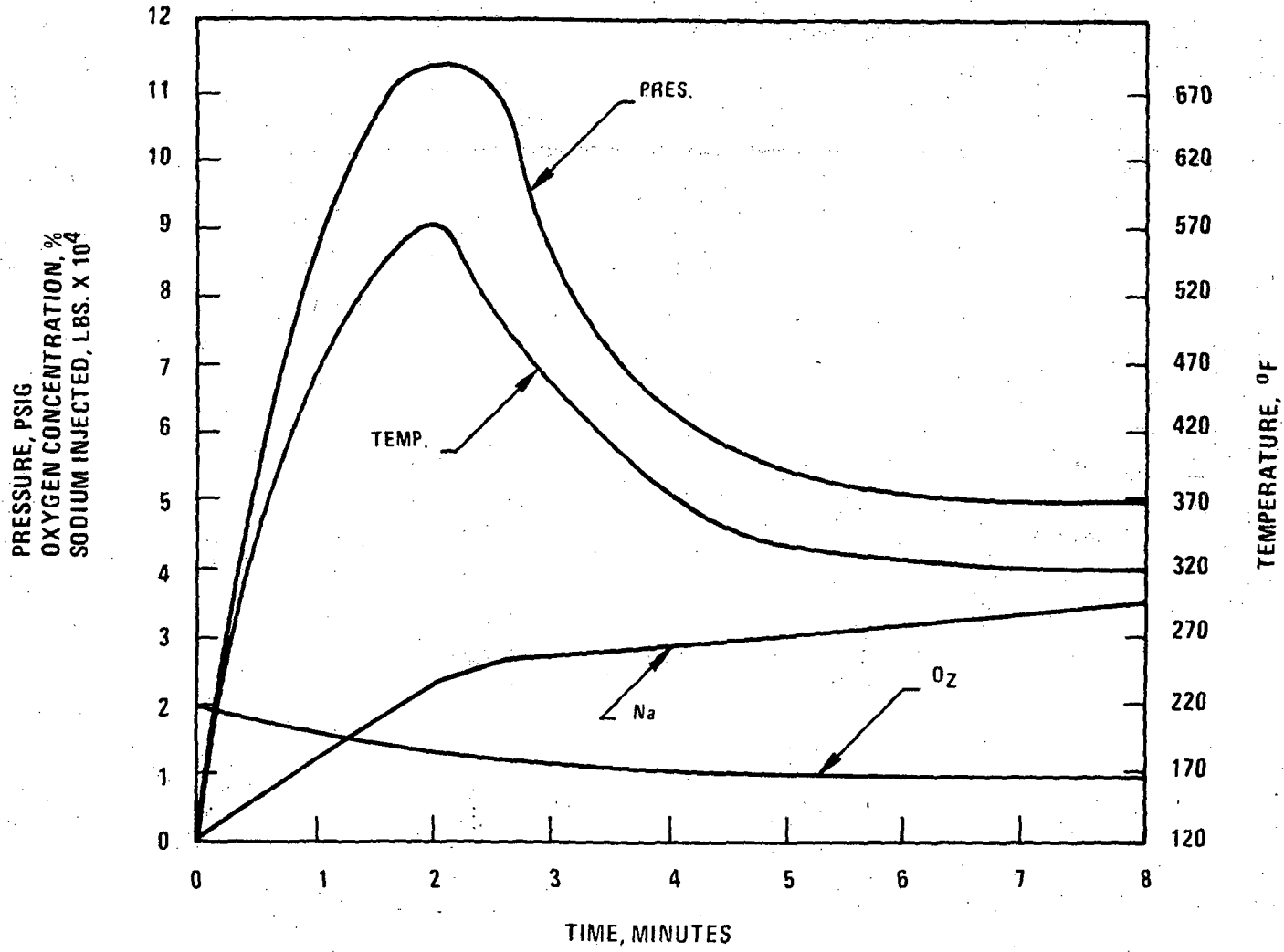


Figure Q001.581-4. PHTS Cell - Spray Phase Transient Moderate Energy Fluid System Leak

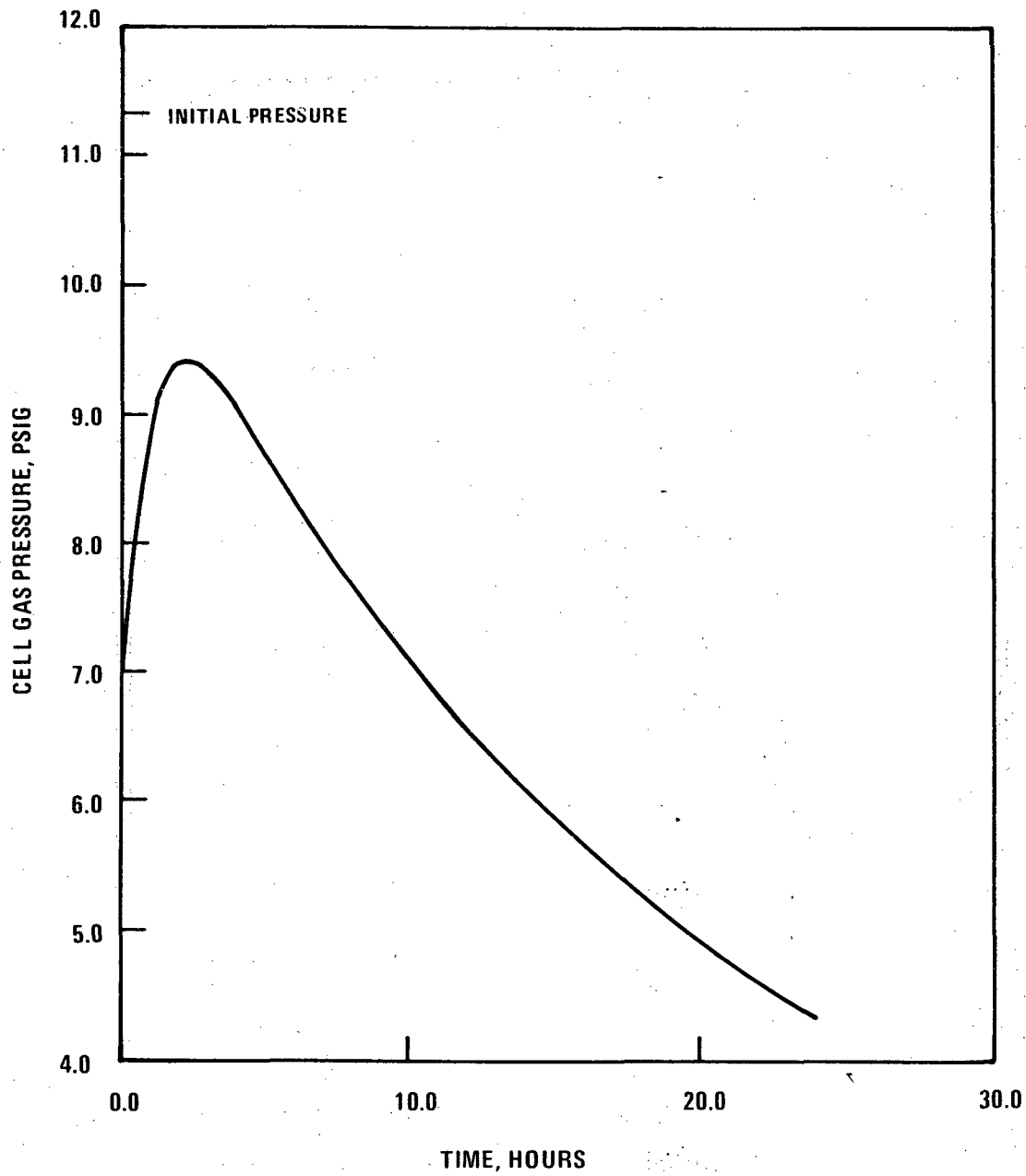


Figure Q001.581-5. PHTS Cell - Cell Gas Pressure Moderate Energy Fluid System Leak

9653-25

Q001.581-32

Amend. 40
July 1977

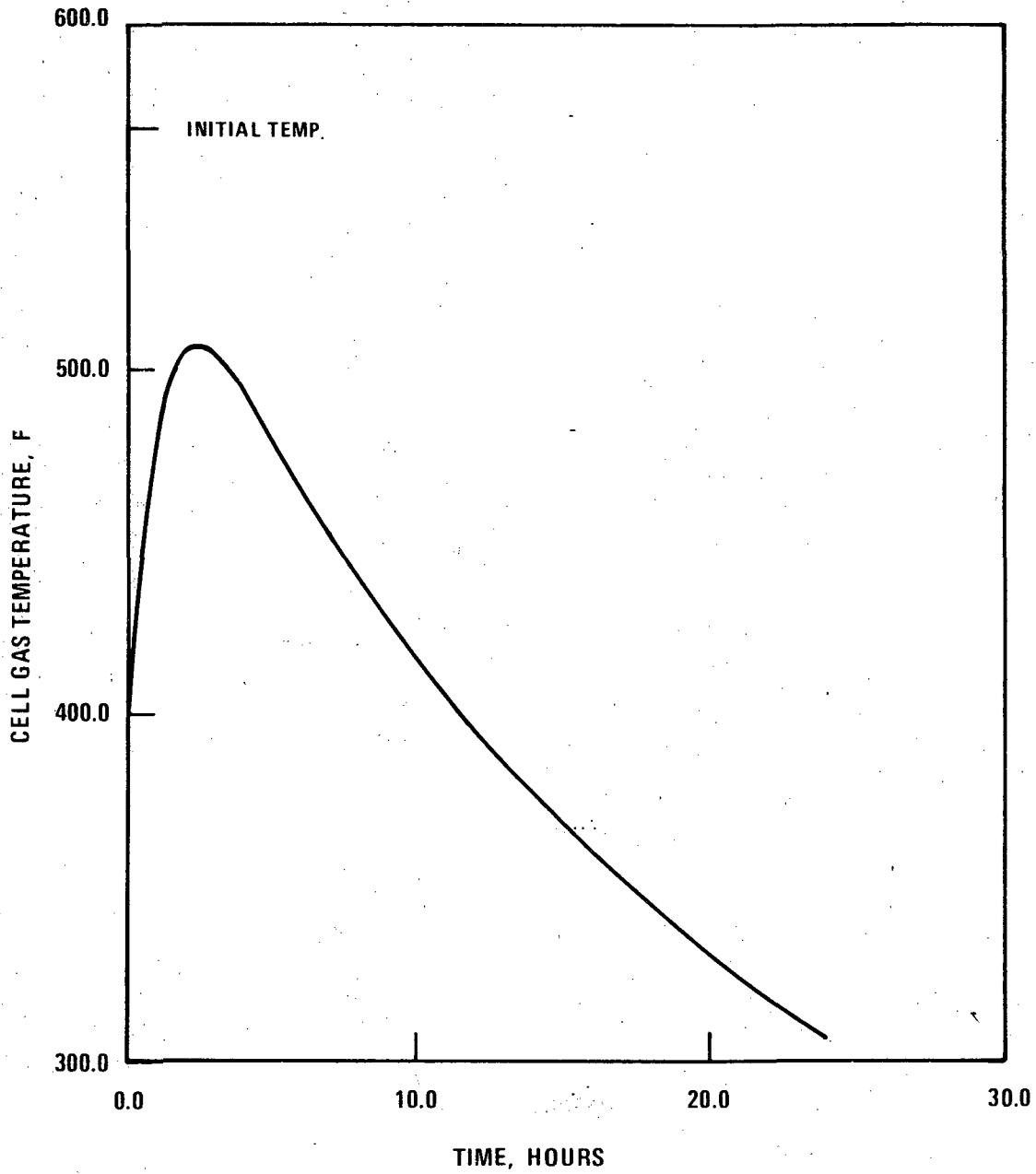


Figure Q001.581-6. PHTS Cell - Cell Gas Temperature Moderate Energy Fluid System Leak
9653-27

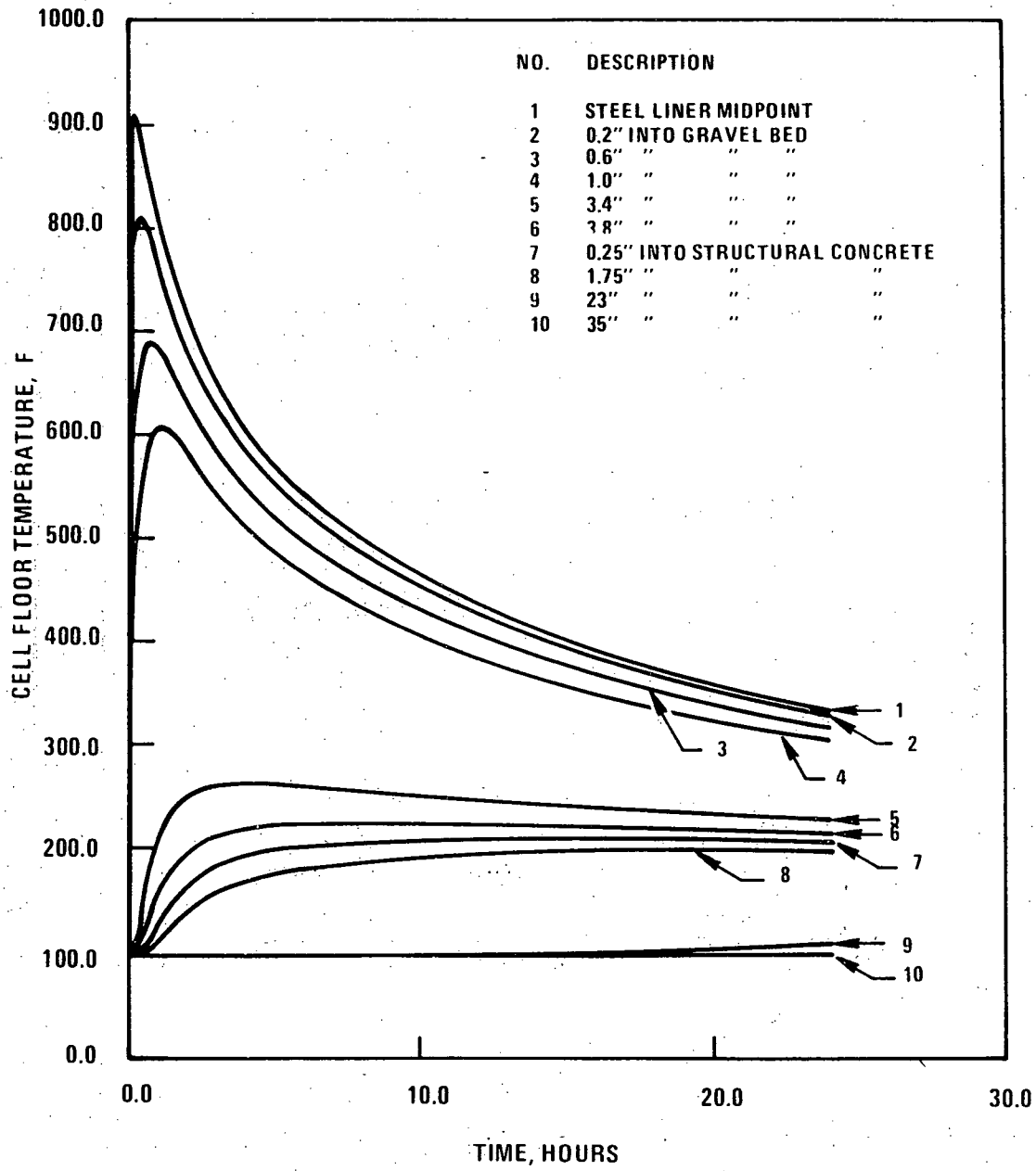


Figure Q001.581-7. PHTS Cell - Floor Transient Moderate Energy Fluid System Leak

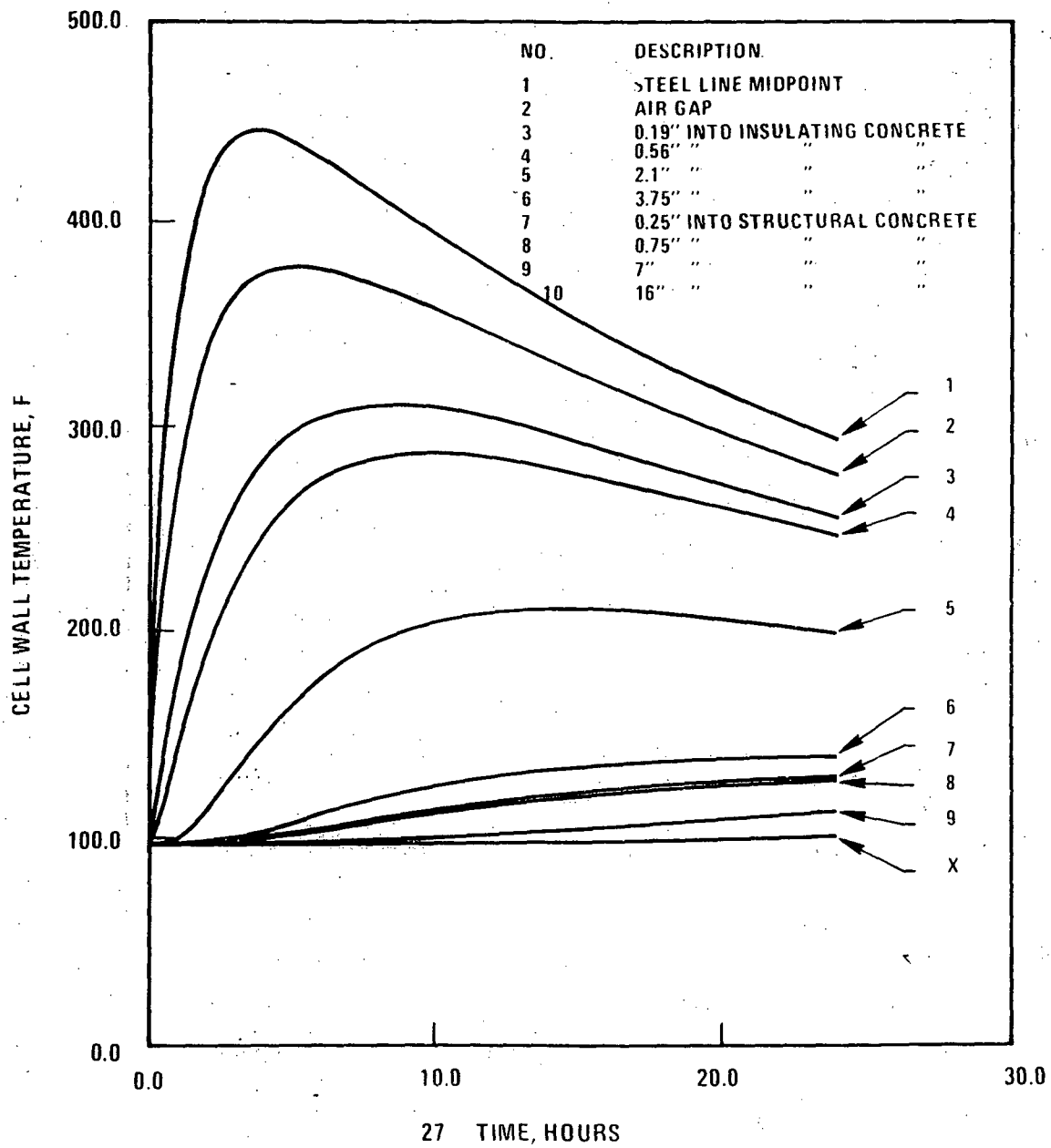


figure Q001.581-8. PHTS Cell - Non-Wetted Wall Transient Moderate Energy Fluid System Leak
9653-36

9653-13

Q001.581-36

Amend. 40
July 1977

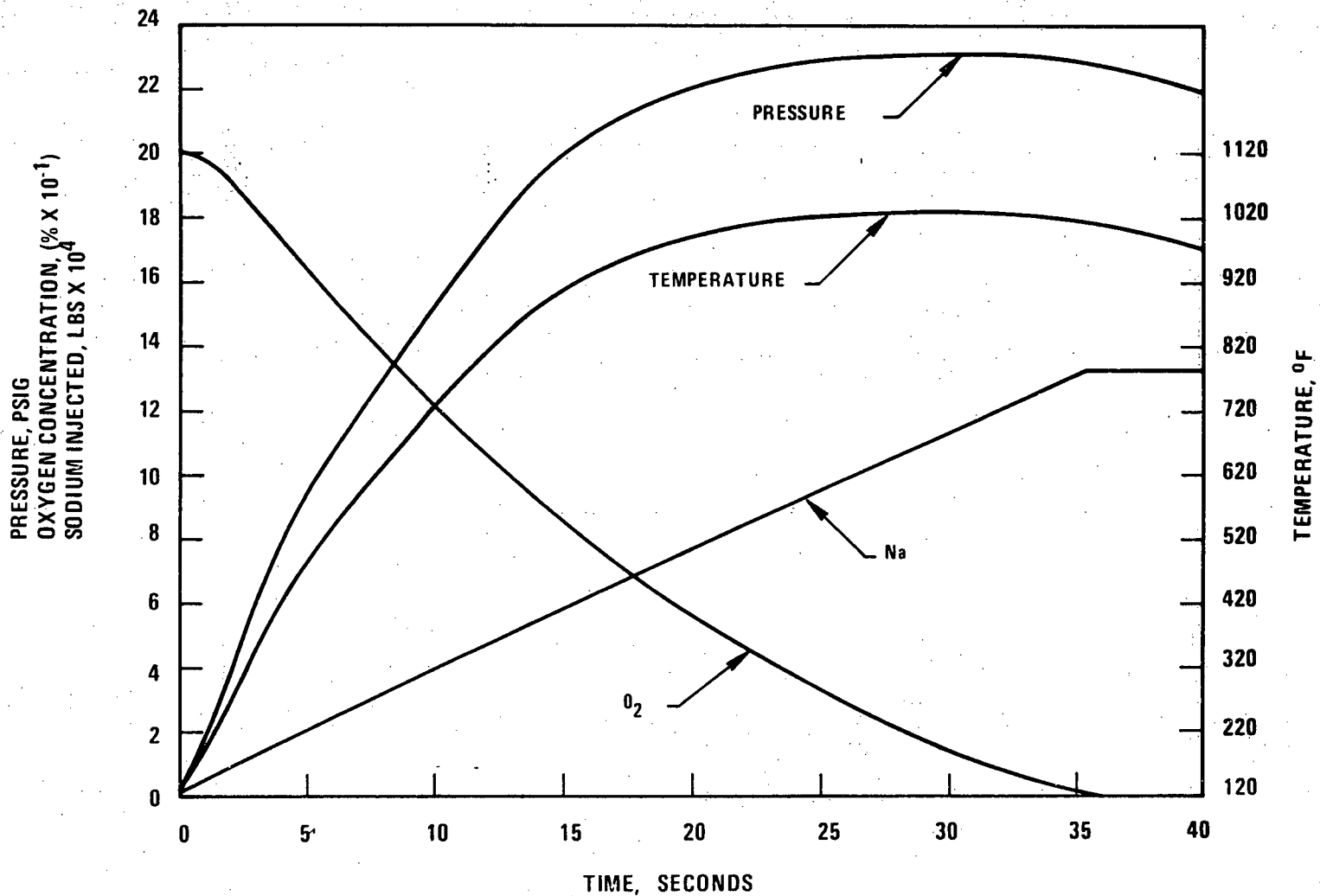


Figure Q001.581-9. PHTS Cell - Spray Phase Transient Evaluation Basis Leak

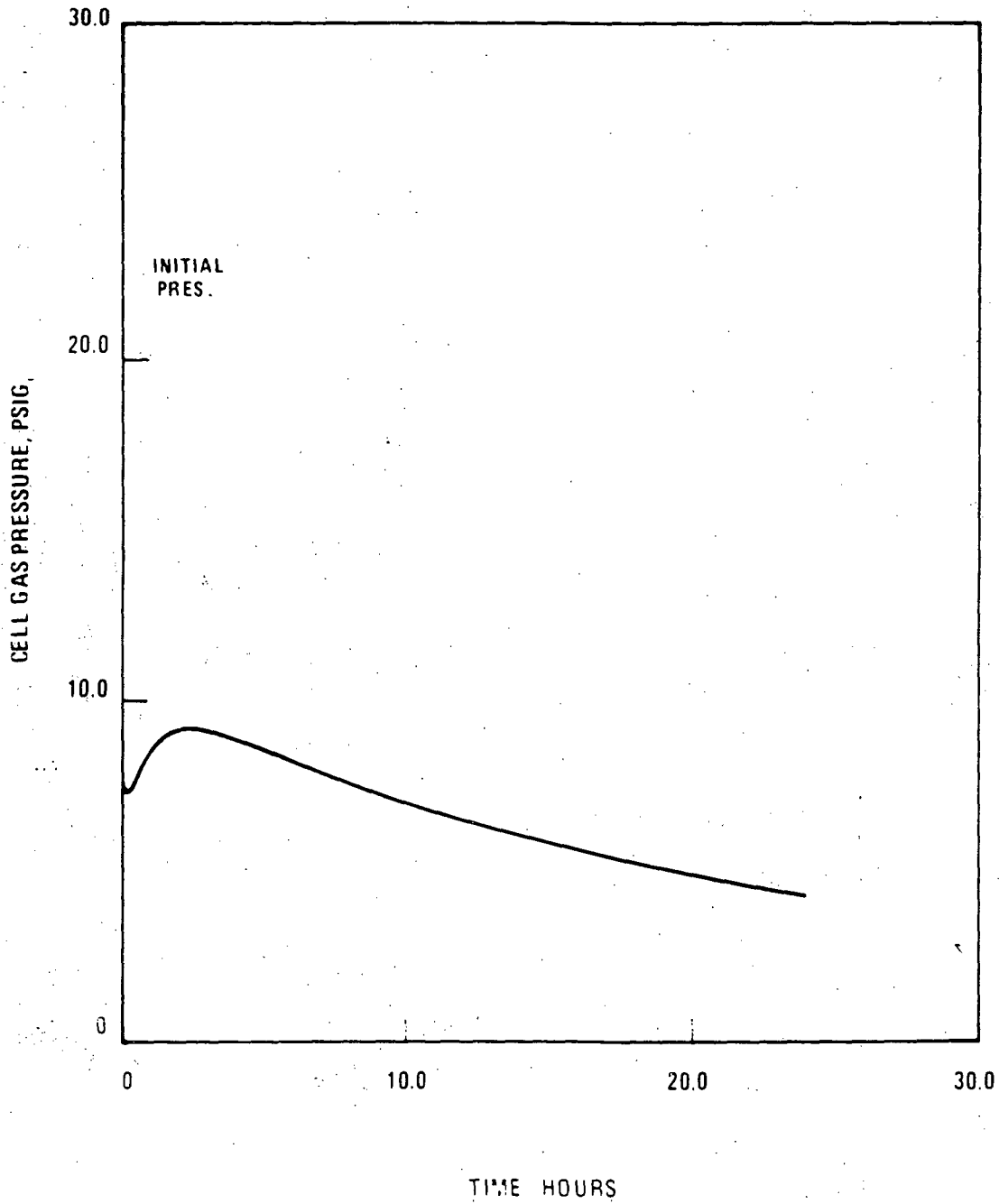


Figure Q001.581-10. PHTS Cell - Cell Gas Pressure Evaluation Basis Leak

Q001.581-37

Amend. 40

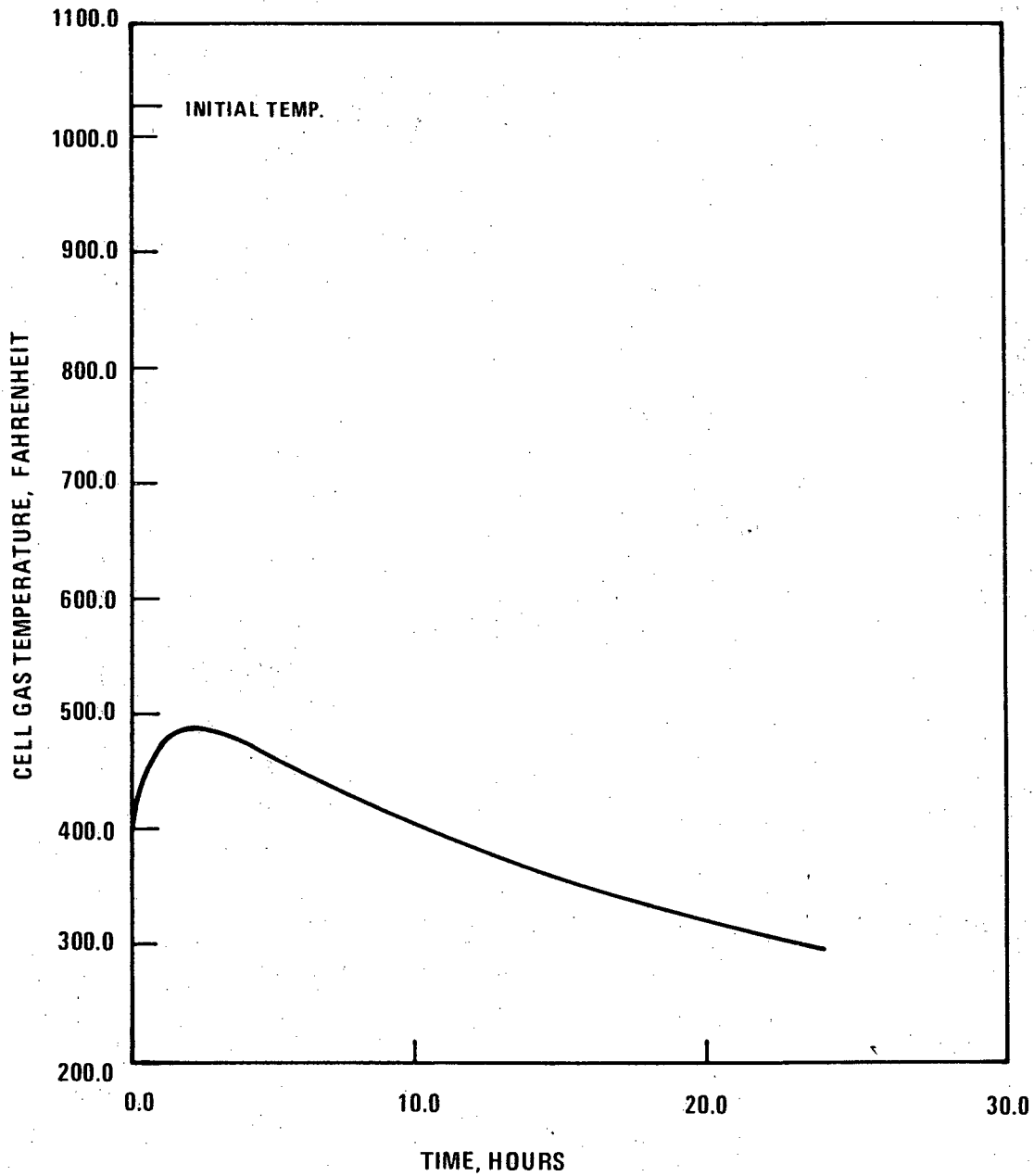


Figure Q001.581-11. PHTS Cell - Cell Gas Temperature Evaluation Basis Leak
9653-31

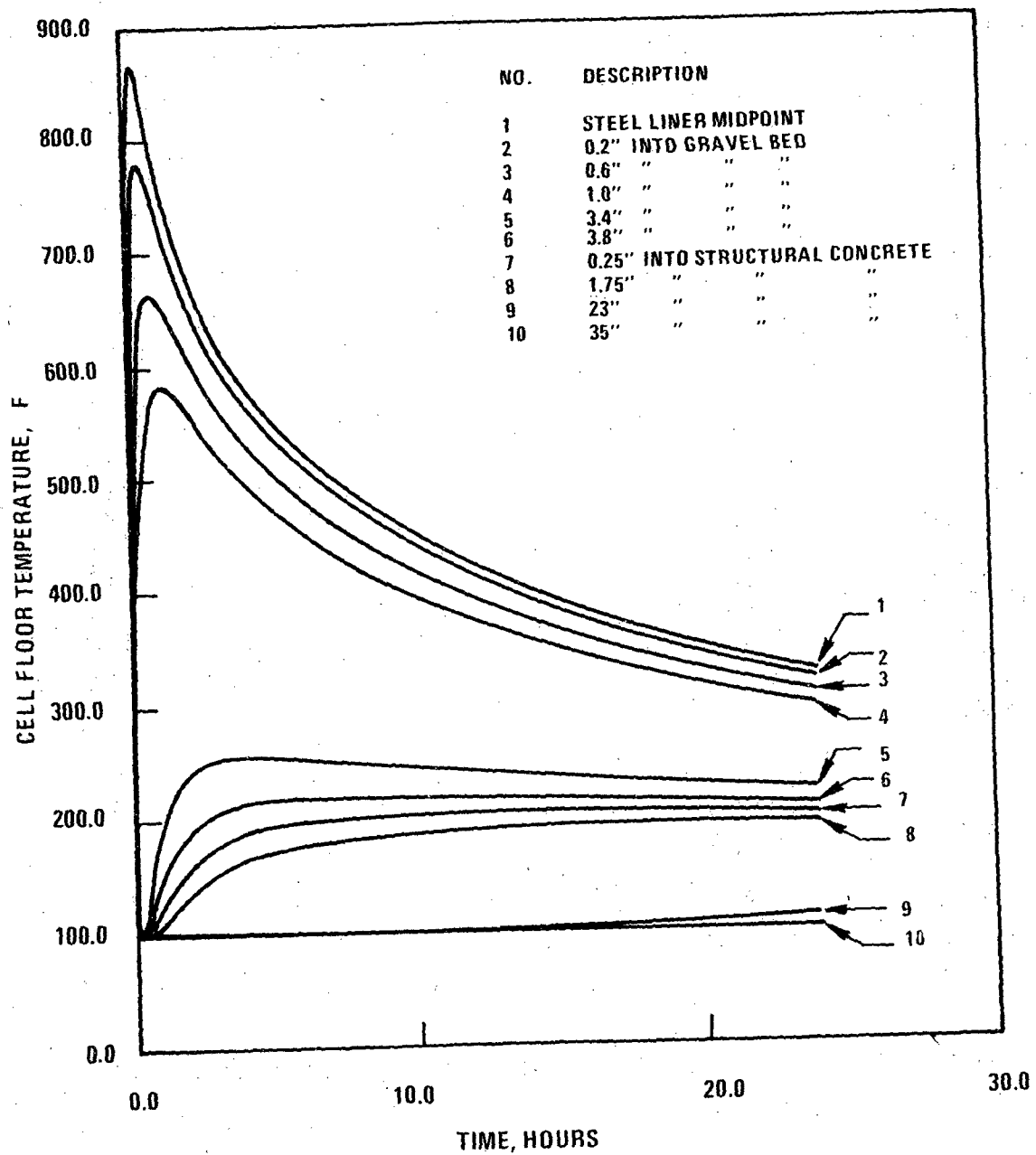


Figure Q001-581-12. PHTS Cell - Floor Transient Evaluation Basis Leak

9653-32

Q001.581-39

Amend. 40
July 1977

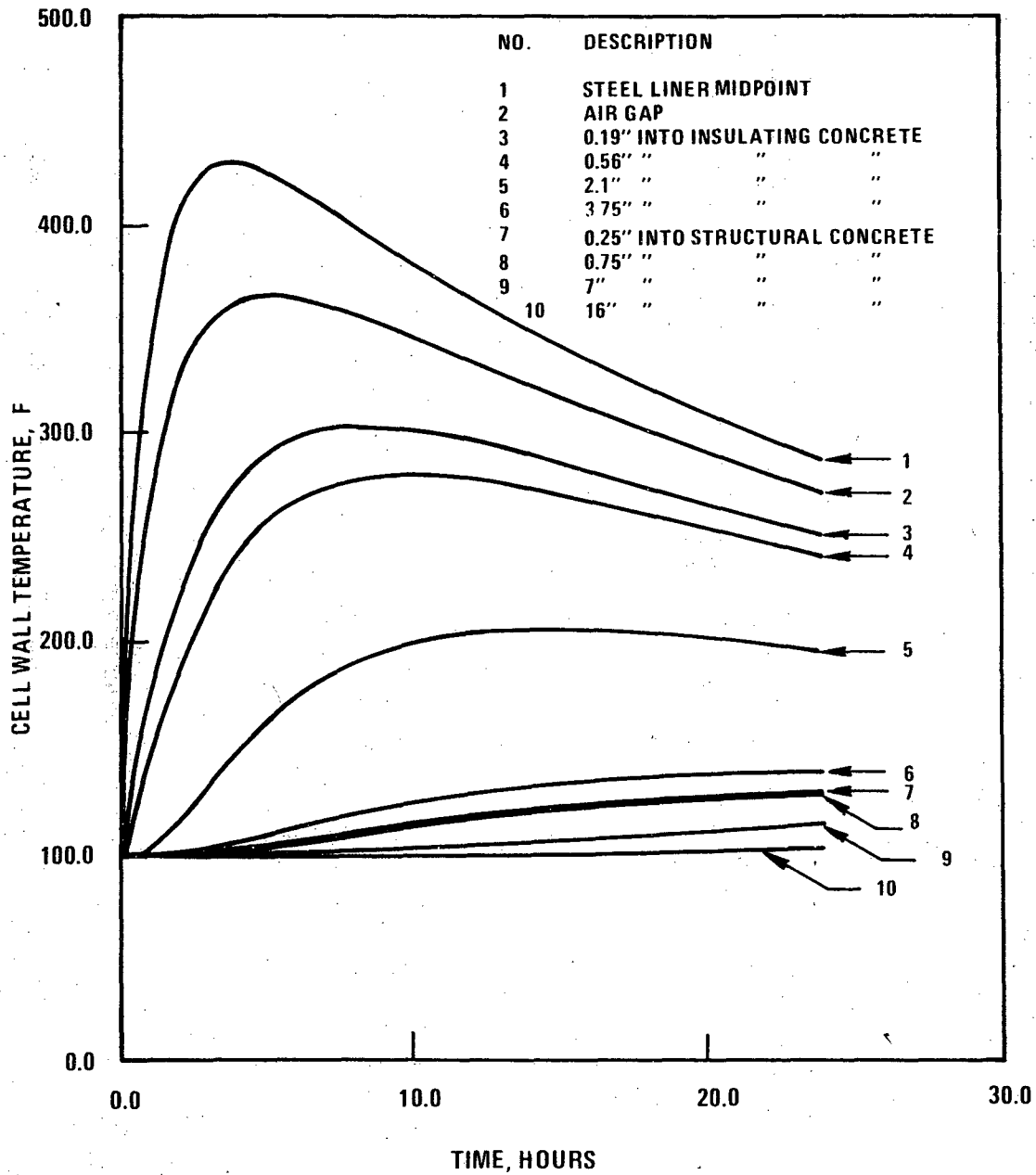


Figure Q001.581-13. PHTS Cell - Non-Wetted Wall Transient Evaluation Basis Leak 9653-33

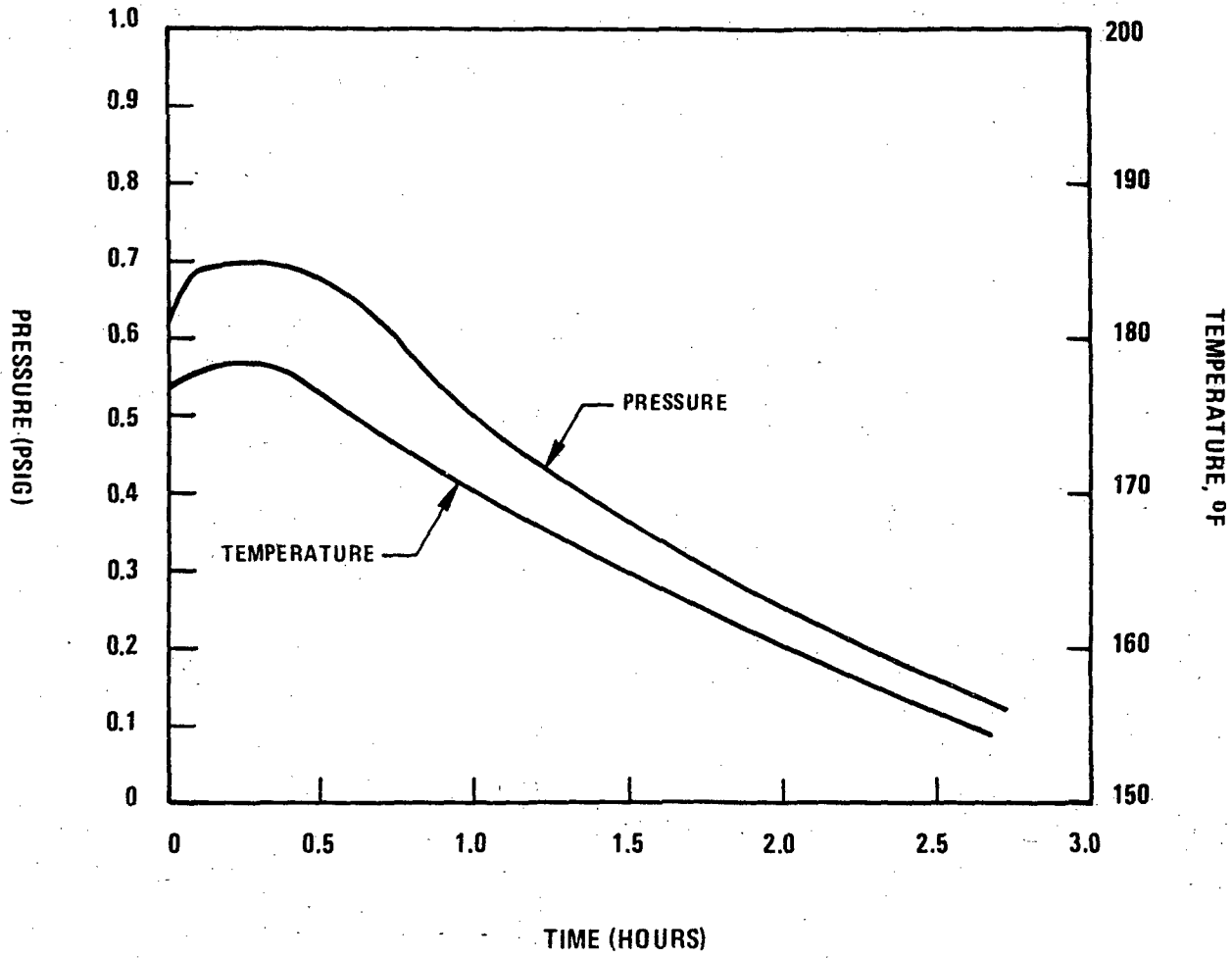


Figure Q001-581-14. Reactor Cavity - Gas Pressure and Temperature Design Basis Leak

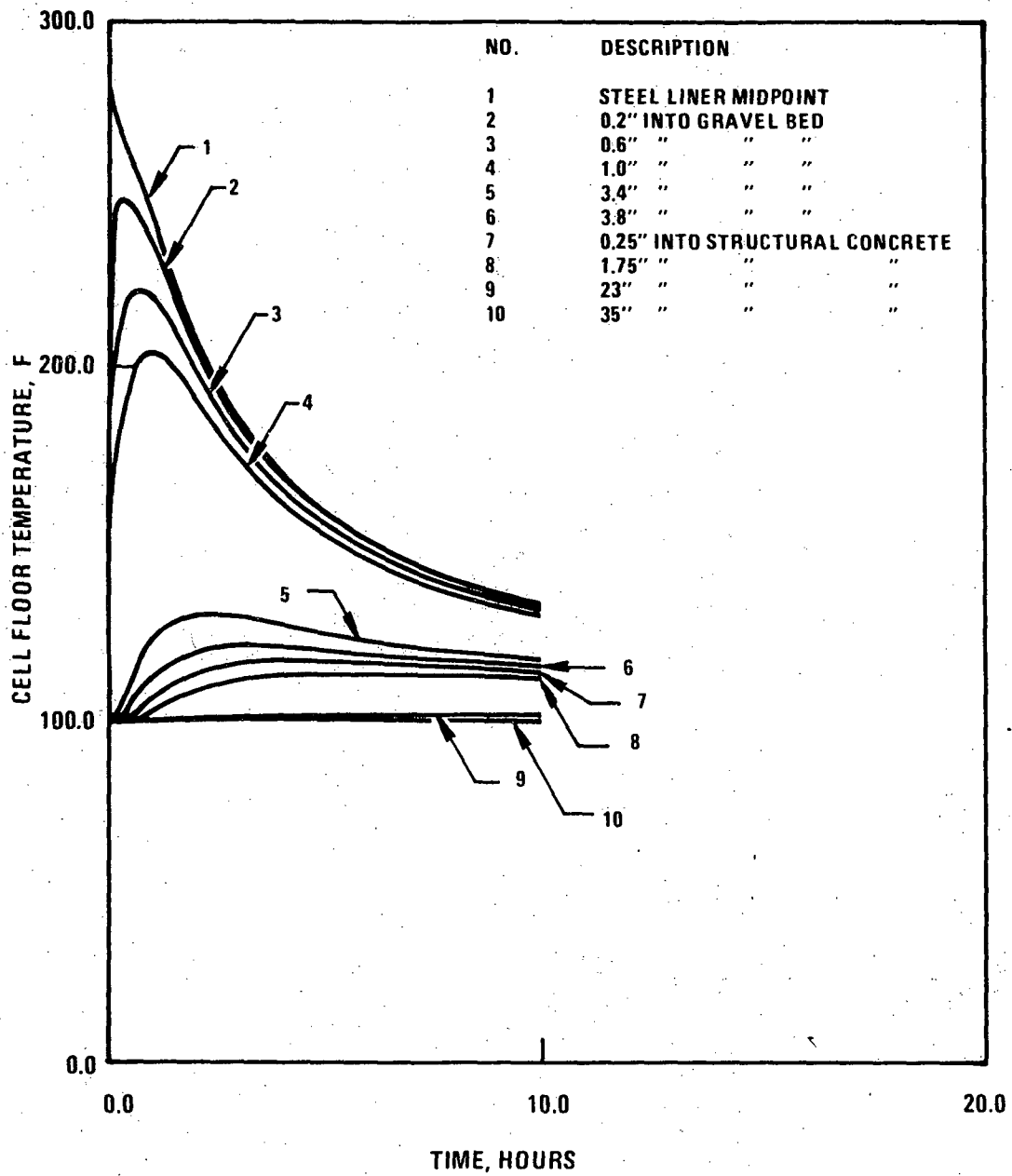


Figure Q001.581-15. Reactor Cavity - Floor Transient Design Basis Leak

9653-35

Q001.581-42

Amend. 40
July 1977

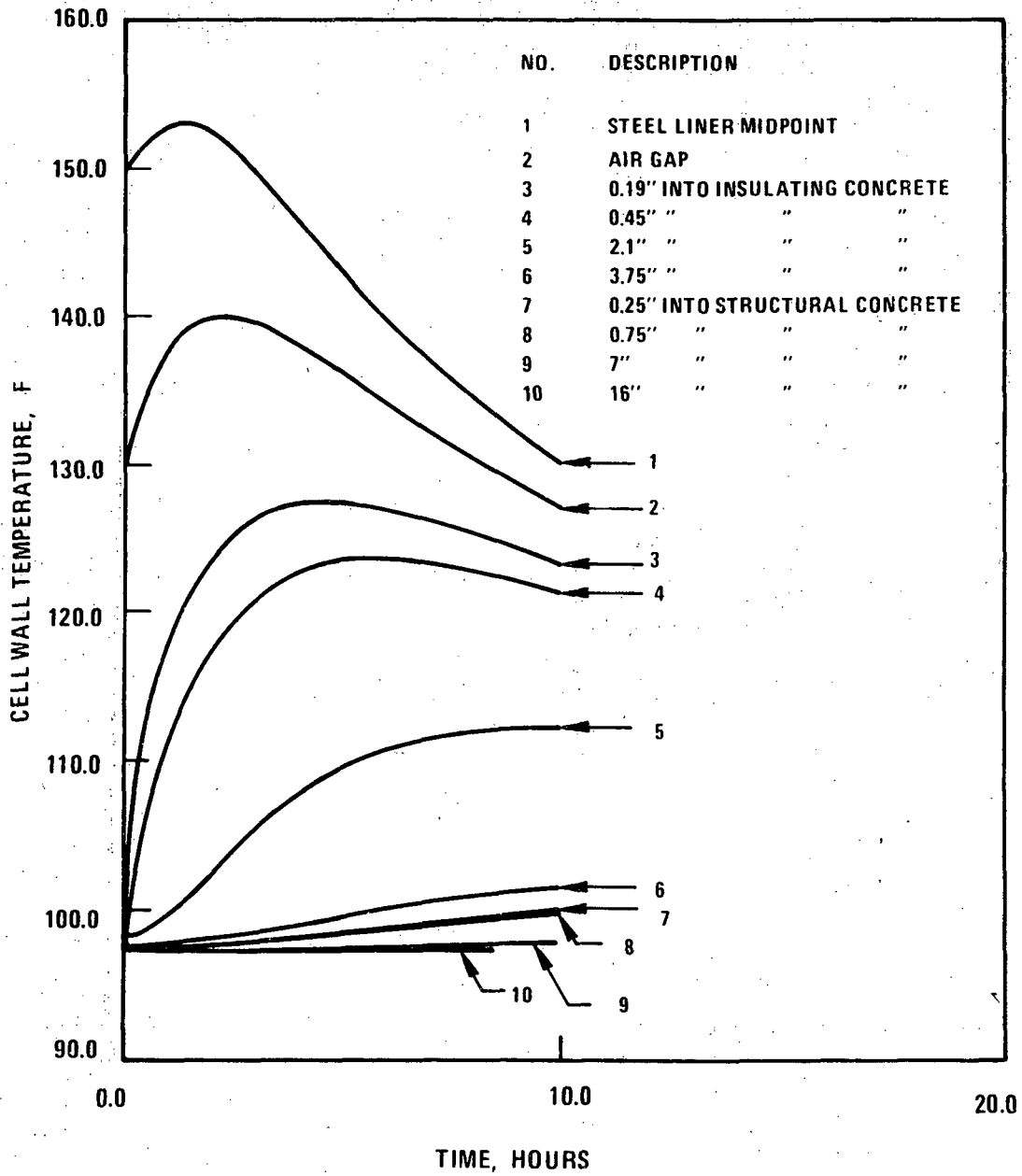


Figure Q001.581-16. Reactor Cavity - Non-Wetted Wall Transient Design Basis Leak

9653-38

Q001.581-43

Amend. 40
July 1977

9653-41

Q001.581-44

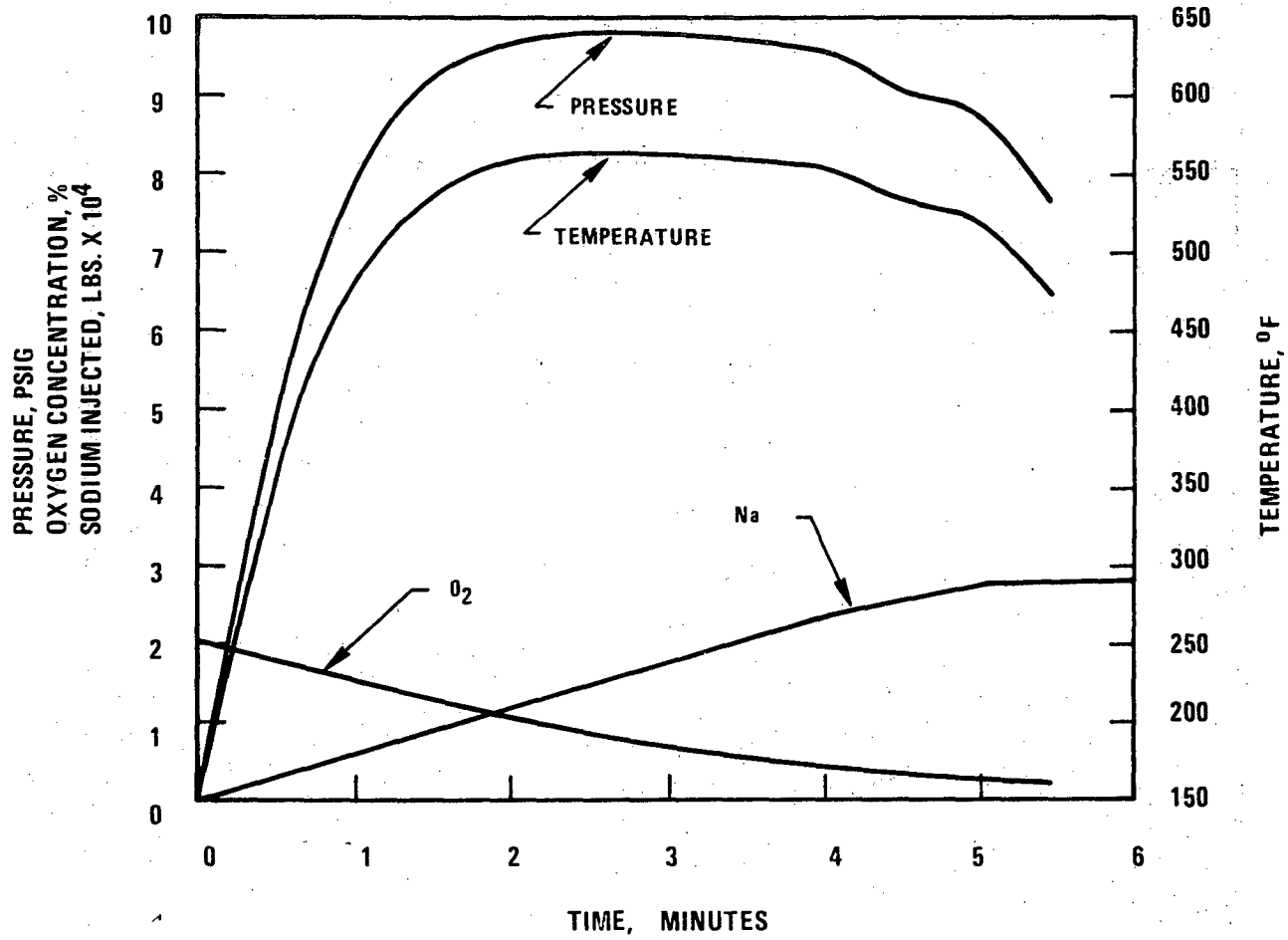


Figure Q001.581-17. Reactor Cavity - Spray Phase Transient Moderate Energy Fluid System Leak

Amend. 40
July 1977

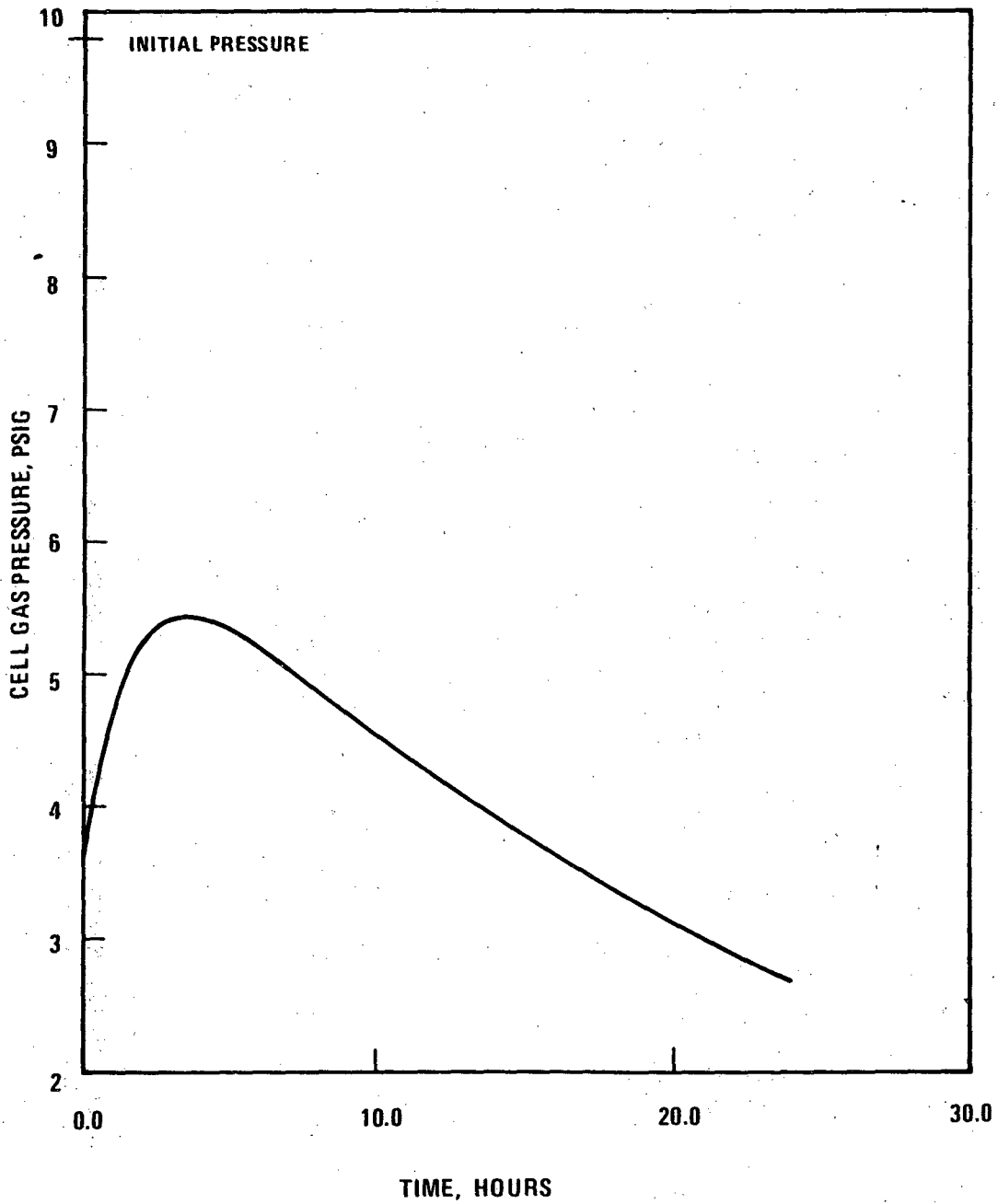


Figure Q001.581-18. Reactor Cavity - Gas Pressure Moderate Energy Fluid System Leak

9653-42

Q001.581-45

Amend. 40

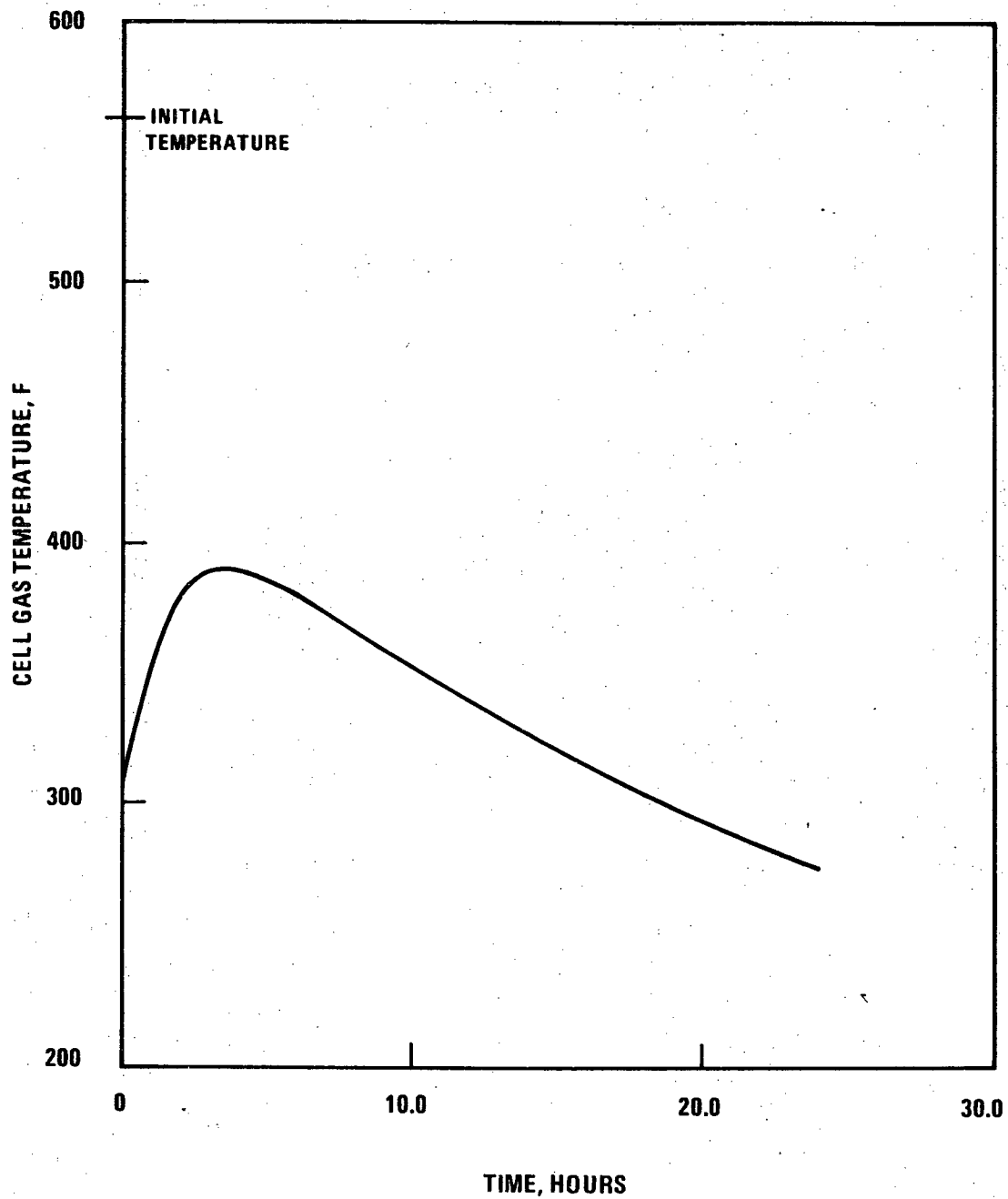


Figure Q001.581-19. Reactor Cavity - Gas Temperature Moderate Energy Fluid System Leak
9653-44

Q001.581-46

Amend. 40
1977

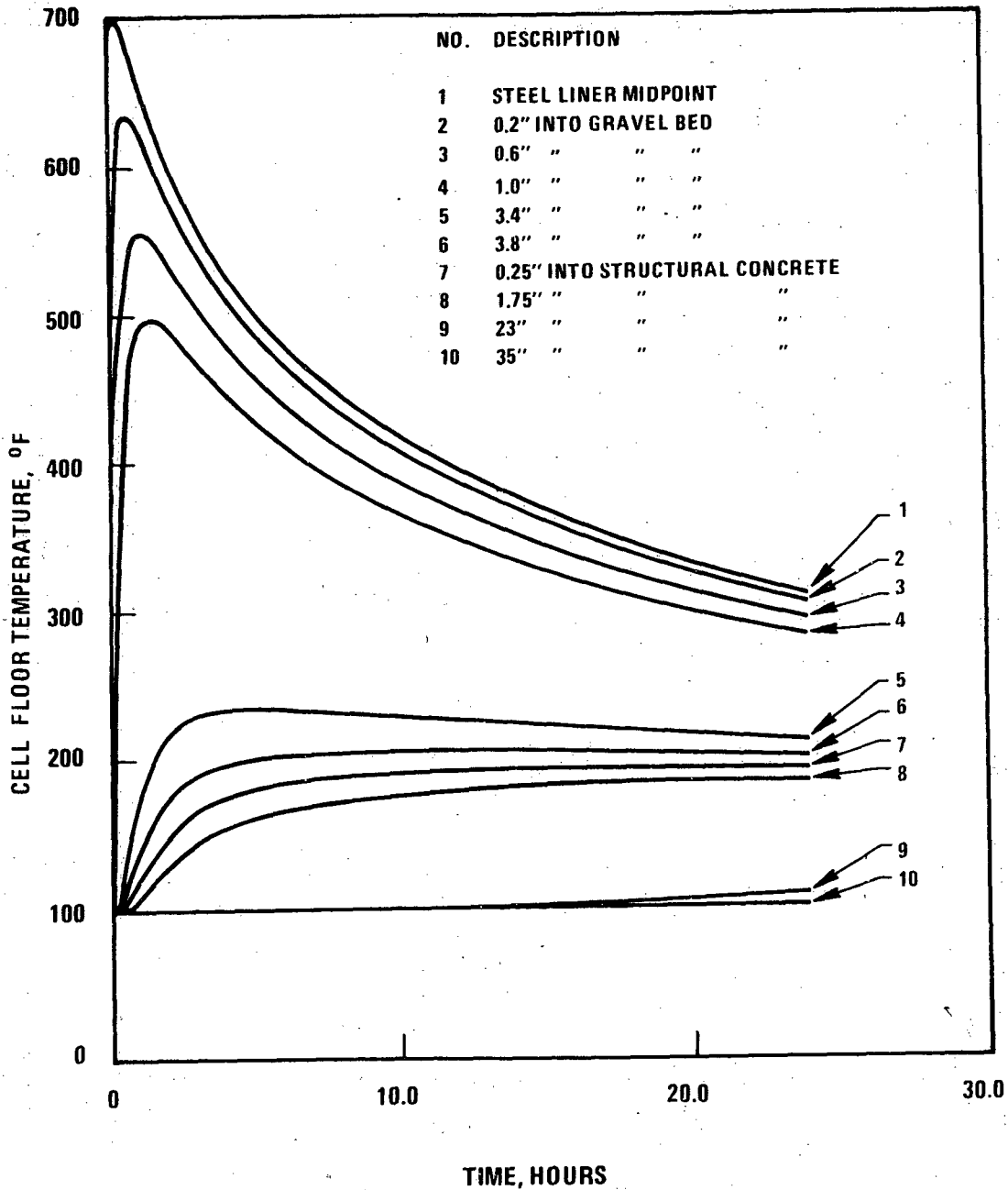


Figure Q001.581-20. Reactor Cavity - Floor Transient Moderate Energy Fluid System Leak
9653-46

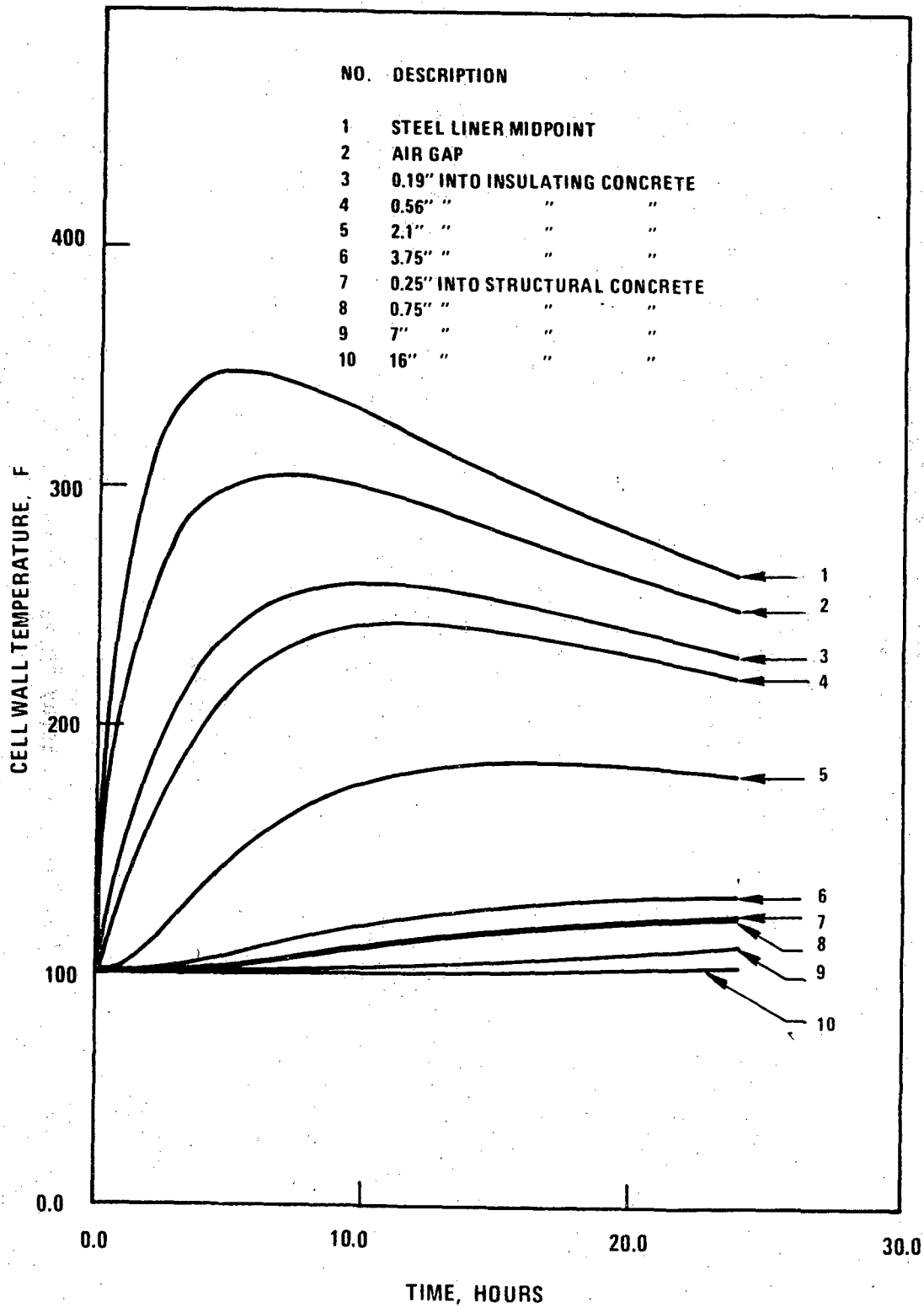


Figure Q001.581-21. Reactor Cavity - Non-Wetted Wall Transient Moderate Energy Fluid System Leak

9653-47

Q001.581-48

Amend. 40
July 1977

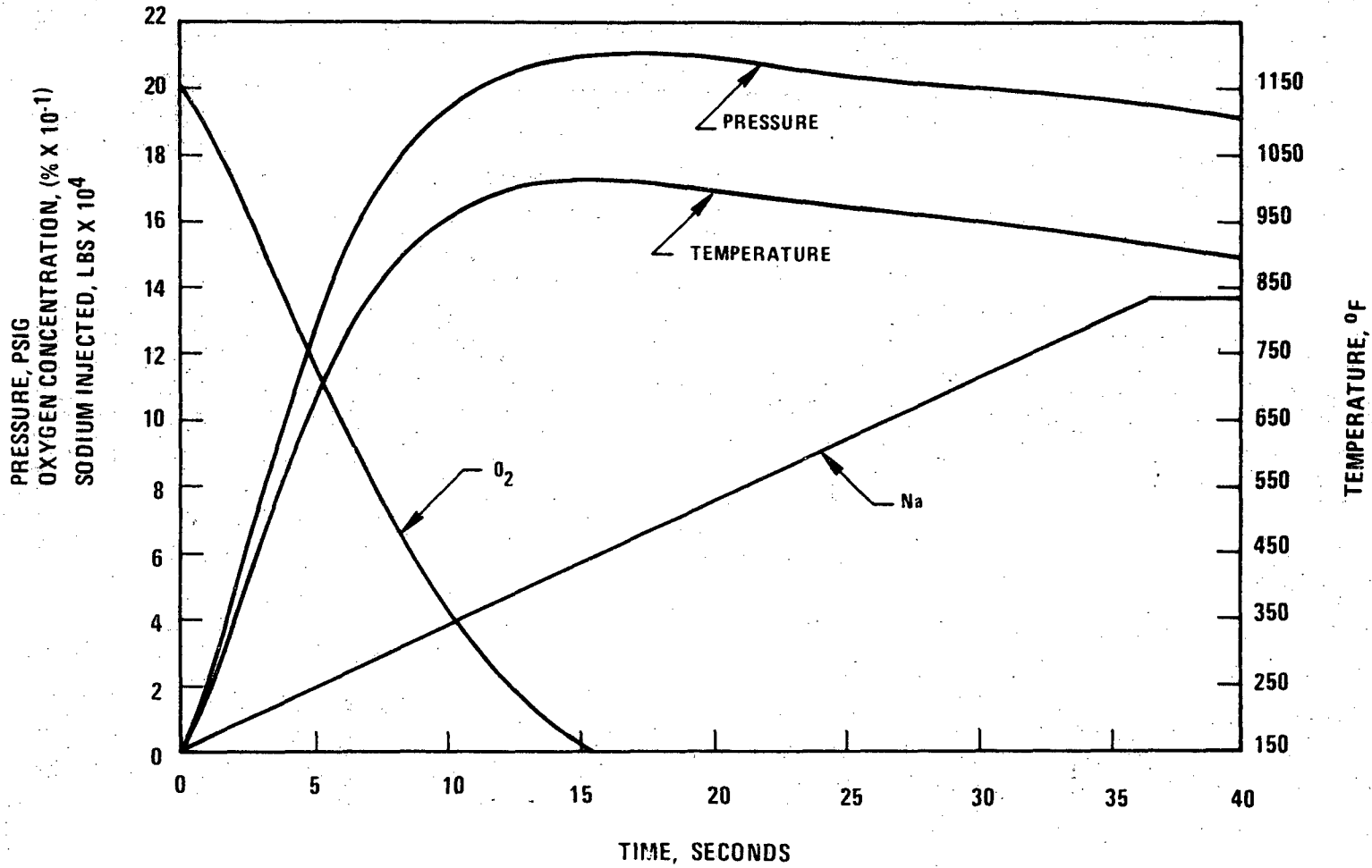


Figure Q001.581-22. Reactor Cavity - Spray Phase Transient Evaluation Basis Leak

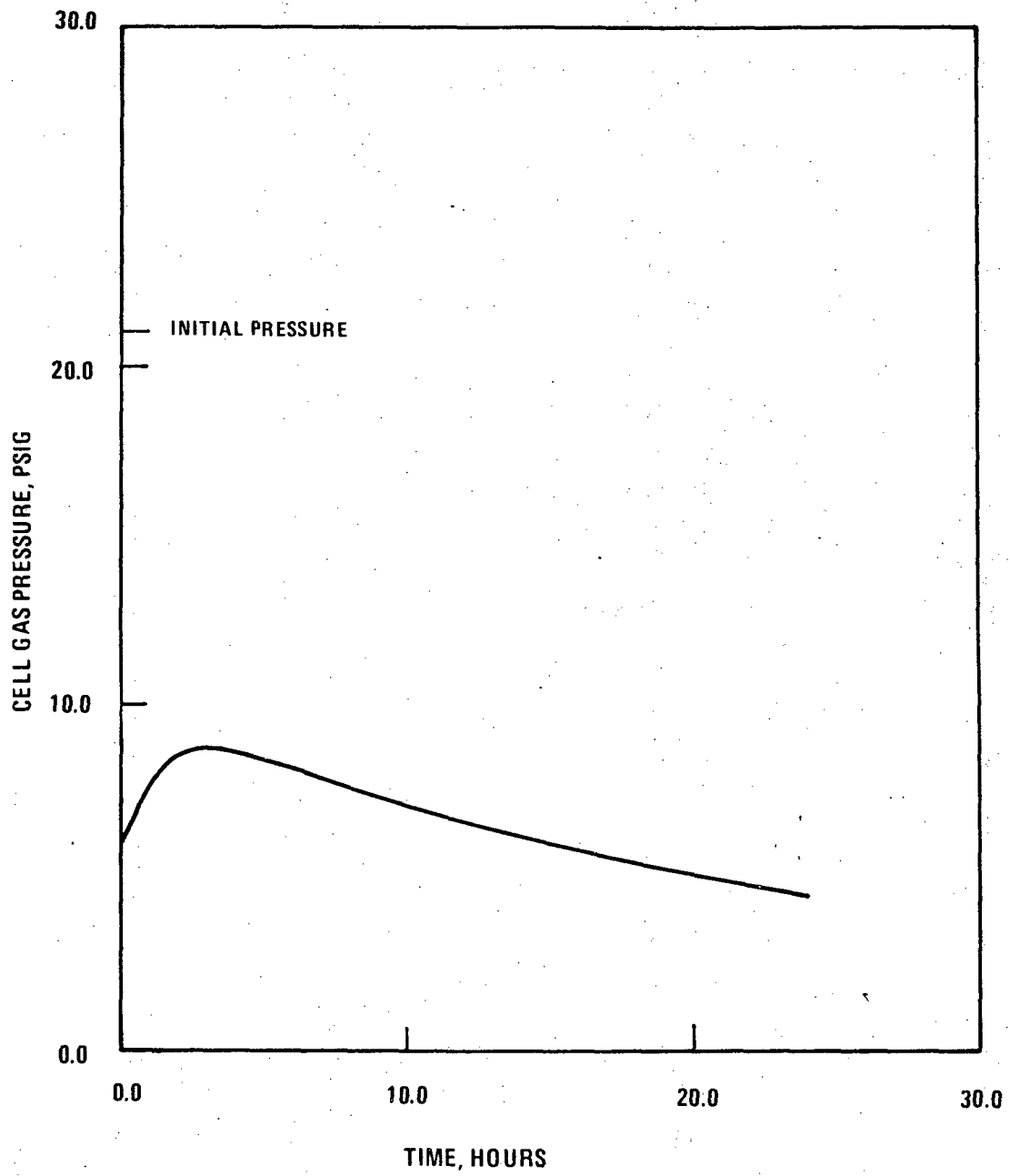


Figure Q001.581-23. Reactor Cavity - Gas Pressure Evaluation Basis Leak

9653-39

Q001.581-50

Amend. 40
July 1977

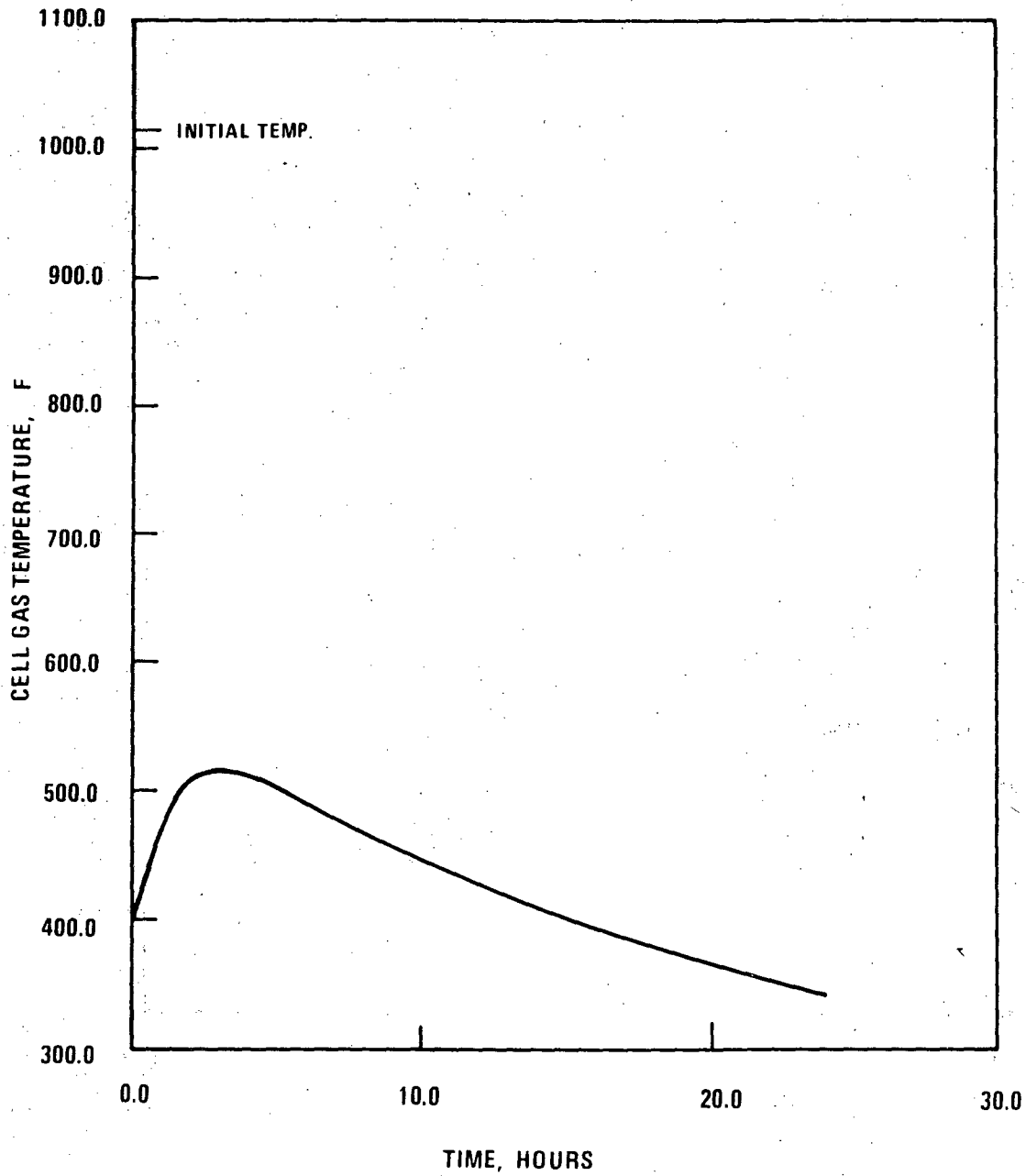


Figure Q001.581-24. Reactor Cavity - Gas Temperature Evaluation Basis Leak

9653-40

Q001.581-51

Amend. 40
1.1. 1977

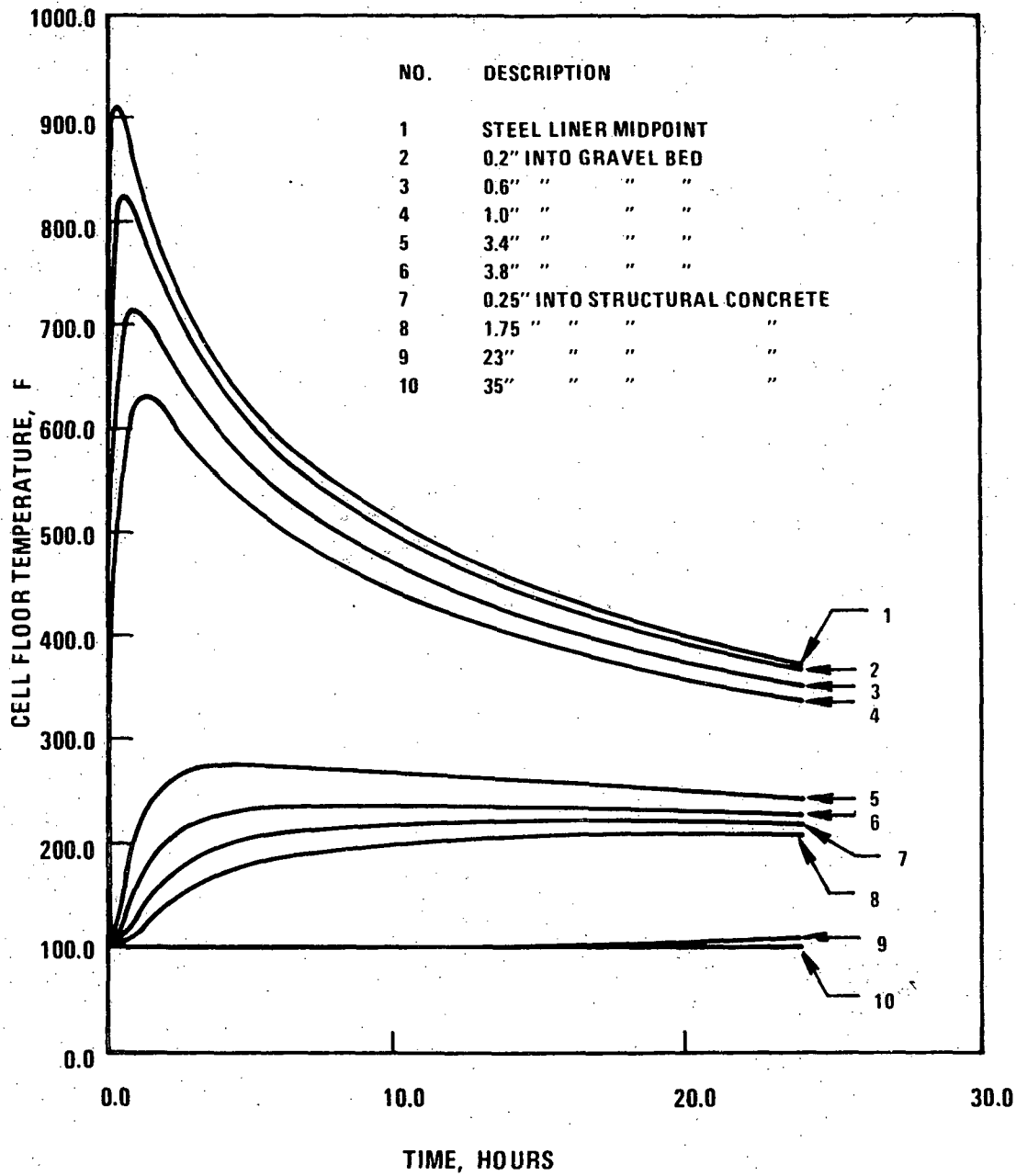


Figure Q001.581-25. Reactor Cavity - Floor Transient Evaluation Basis Leak

9653-43

Q001.581-52

Amend. 40
July 1977

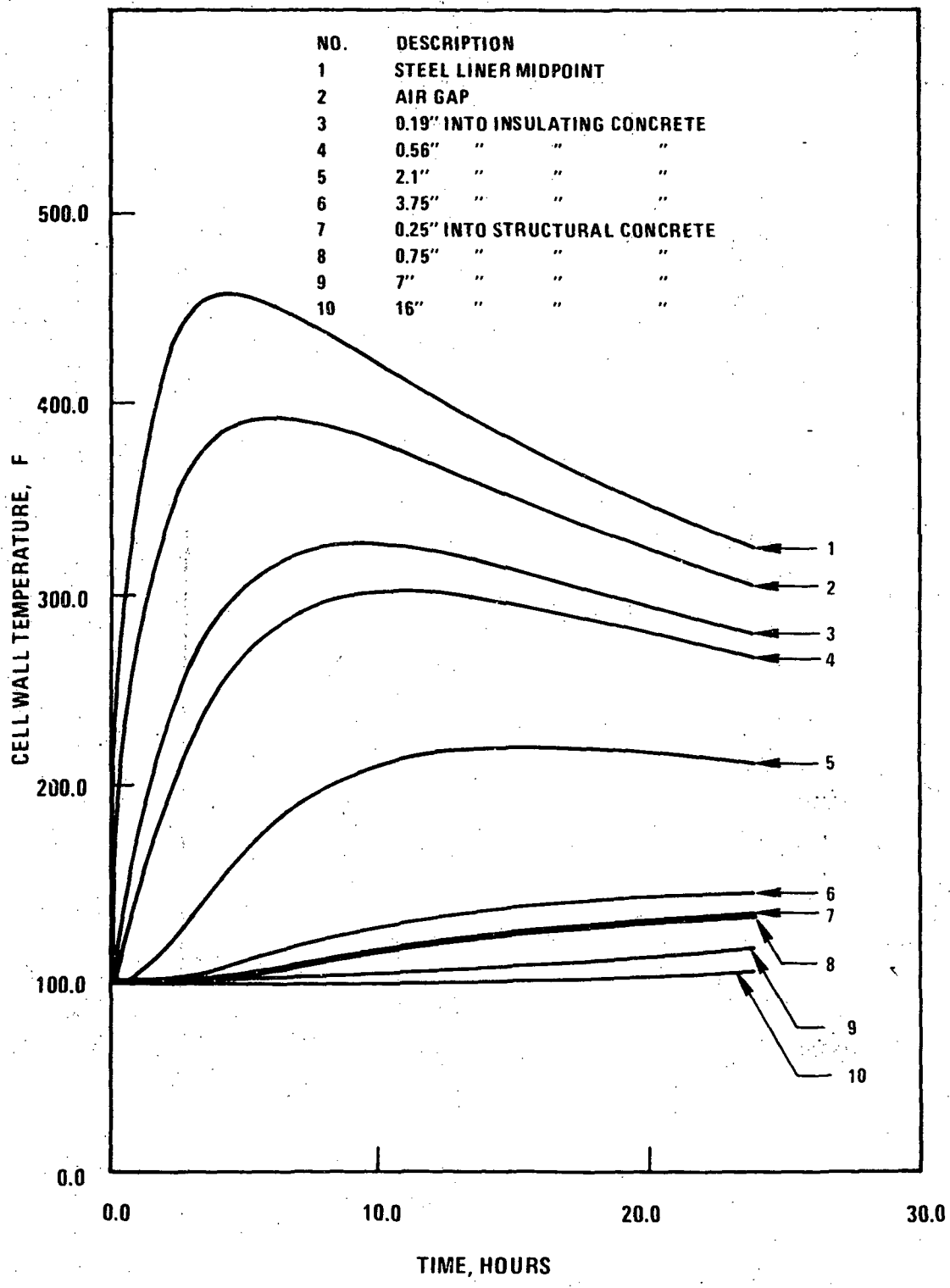


Figure Q001.581-26. Reactor Cavity - Non-Wetted Wall Transient Evaluation Basis Leak

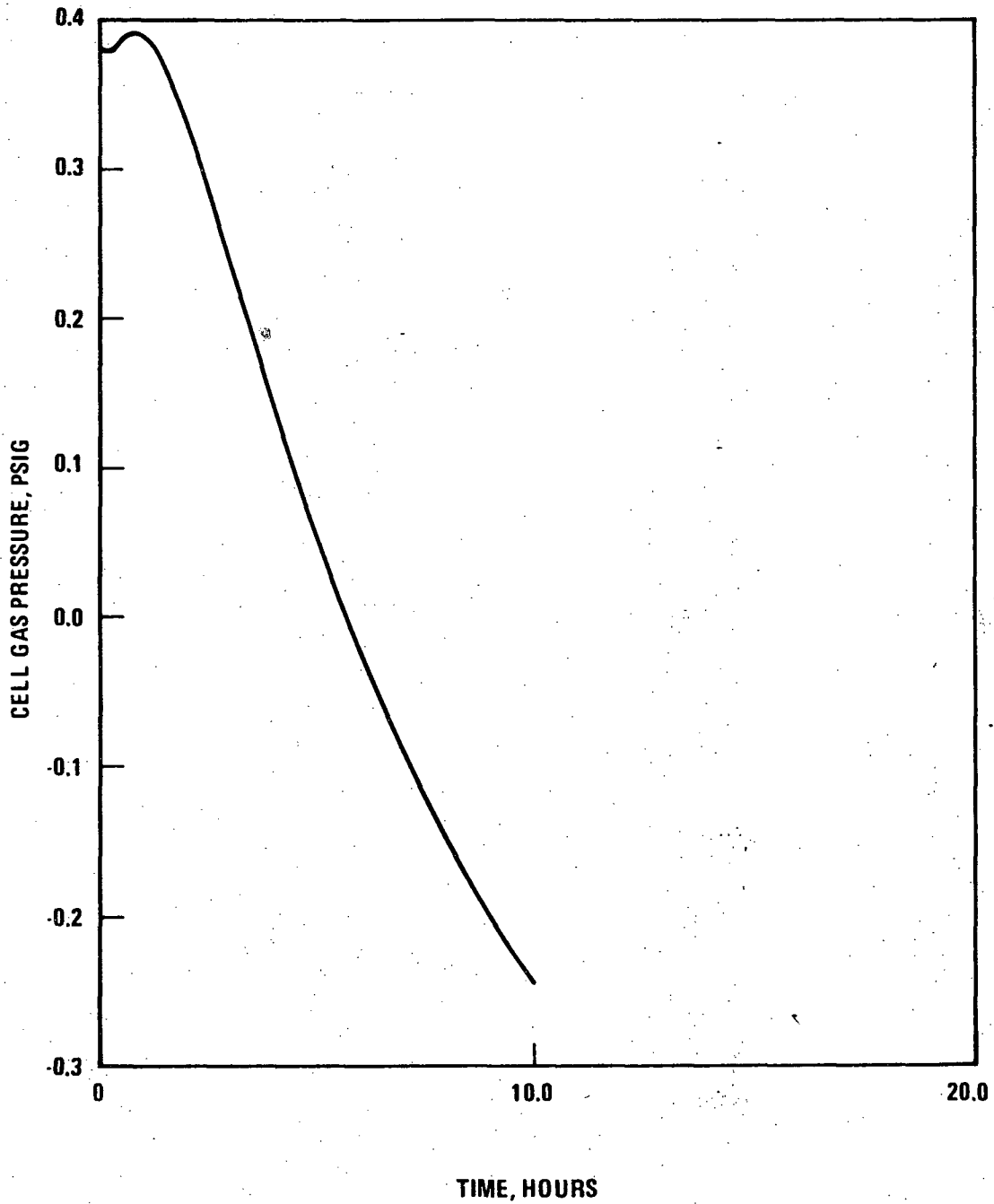


Figure Q001.581-27. Cell 102A - Cell Gas Pressure Design Basis Leak
9653-18

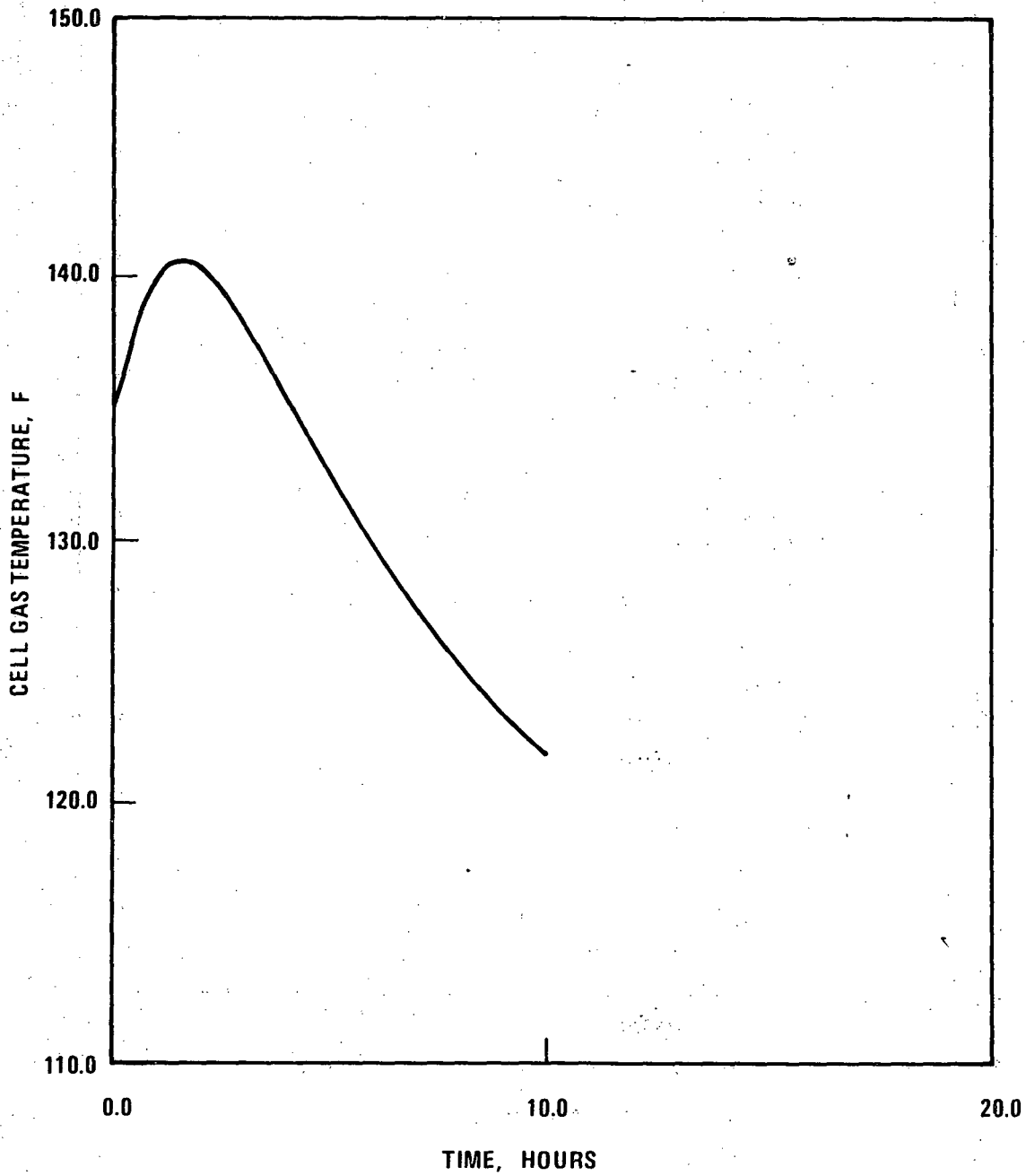


Figure Q001.581-28. Cell 102A - Cell Gas Temperature Design Basis Leak

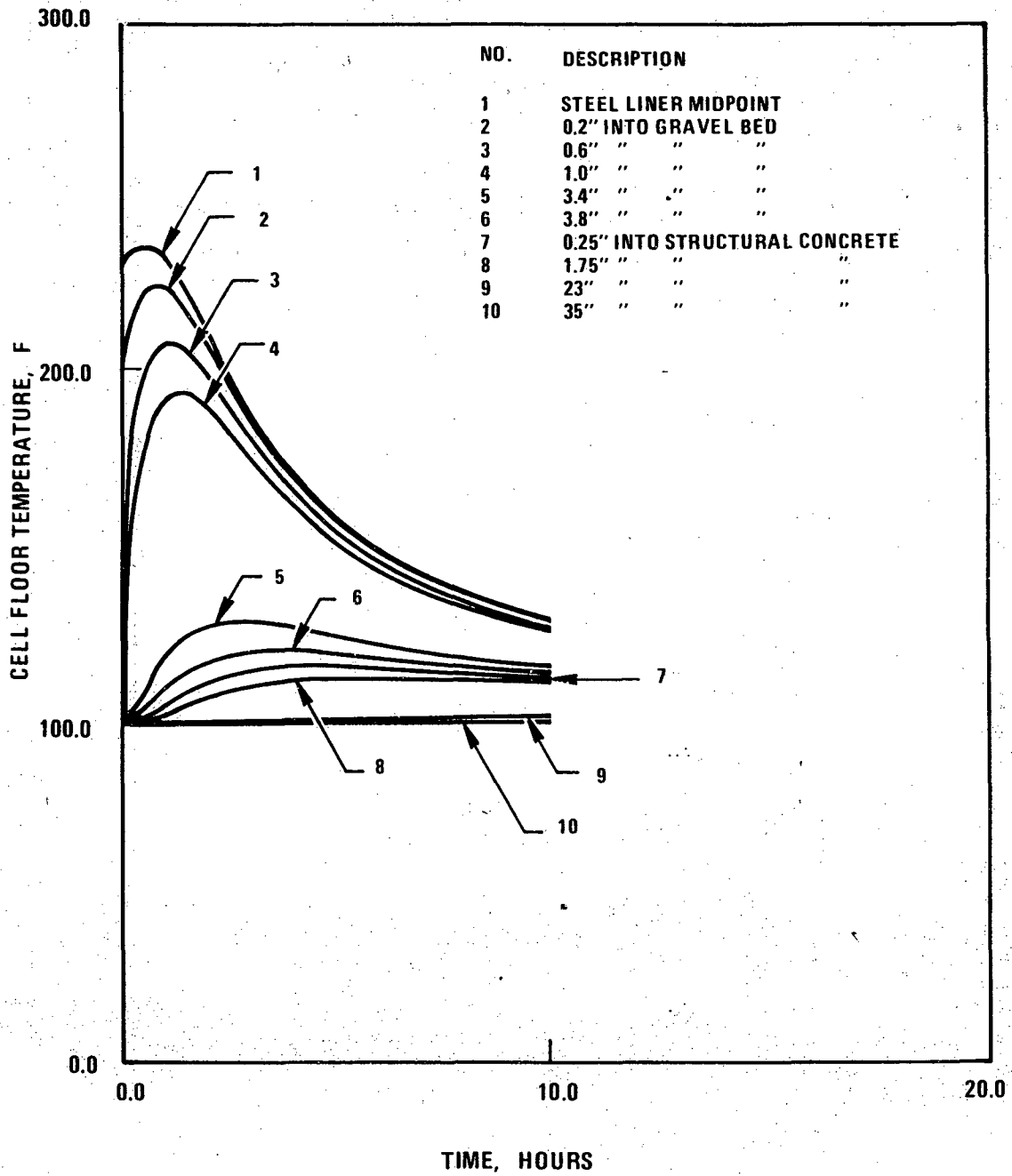


Figure Q001.581-29. Cell 102A - Floor Transient Design Basis Leak

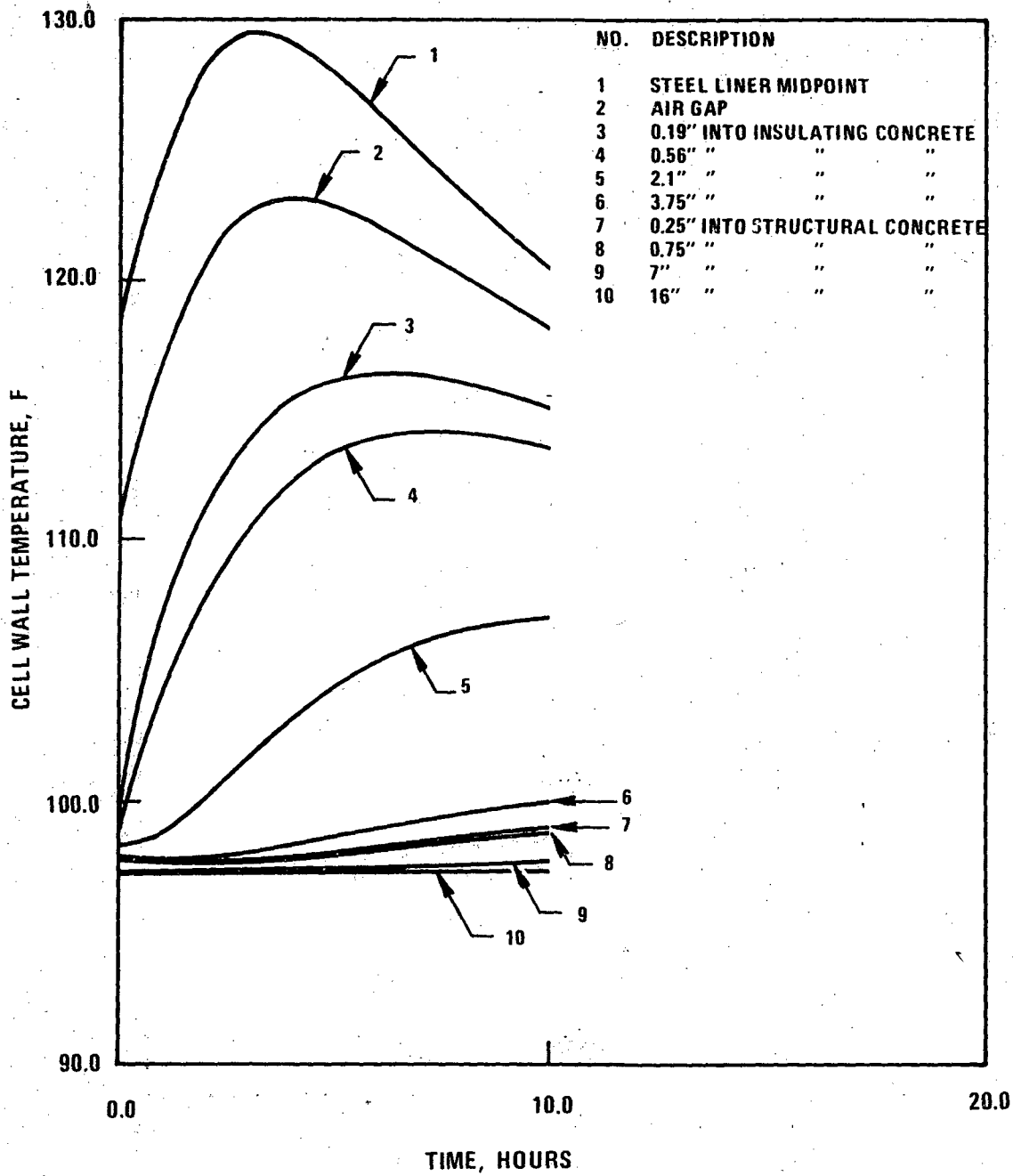


Figure Q001.581-30. Cell 102A - Non-Wetted Wall Transient Design Basis Leak
9653-11

9653-14

Q001.581-58

Amend. 40
July 1977

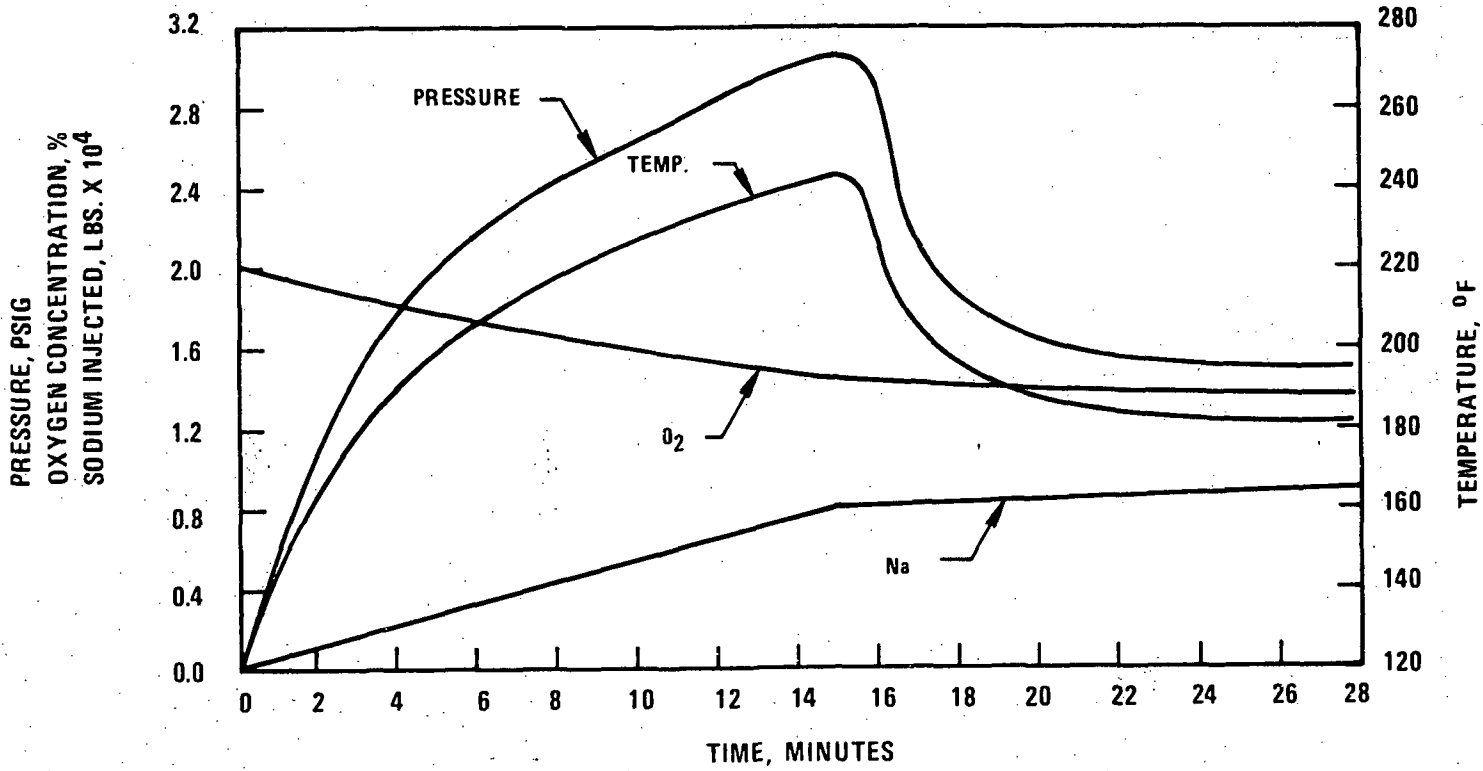


Figure Q001.581-31. Cell 102A - Spray Phase Transient Moderate Energy Fluid System Leak

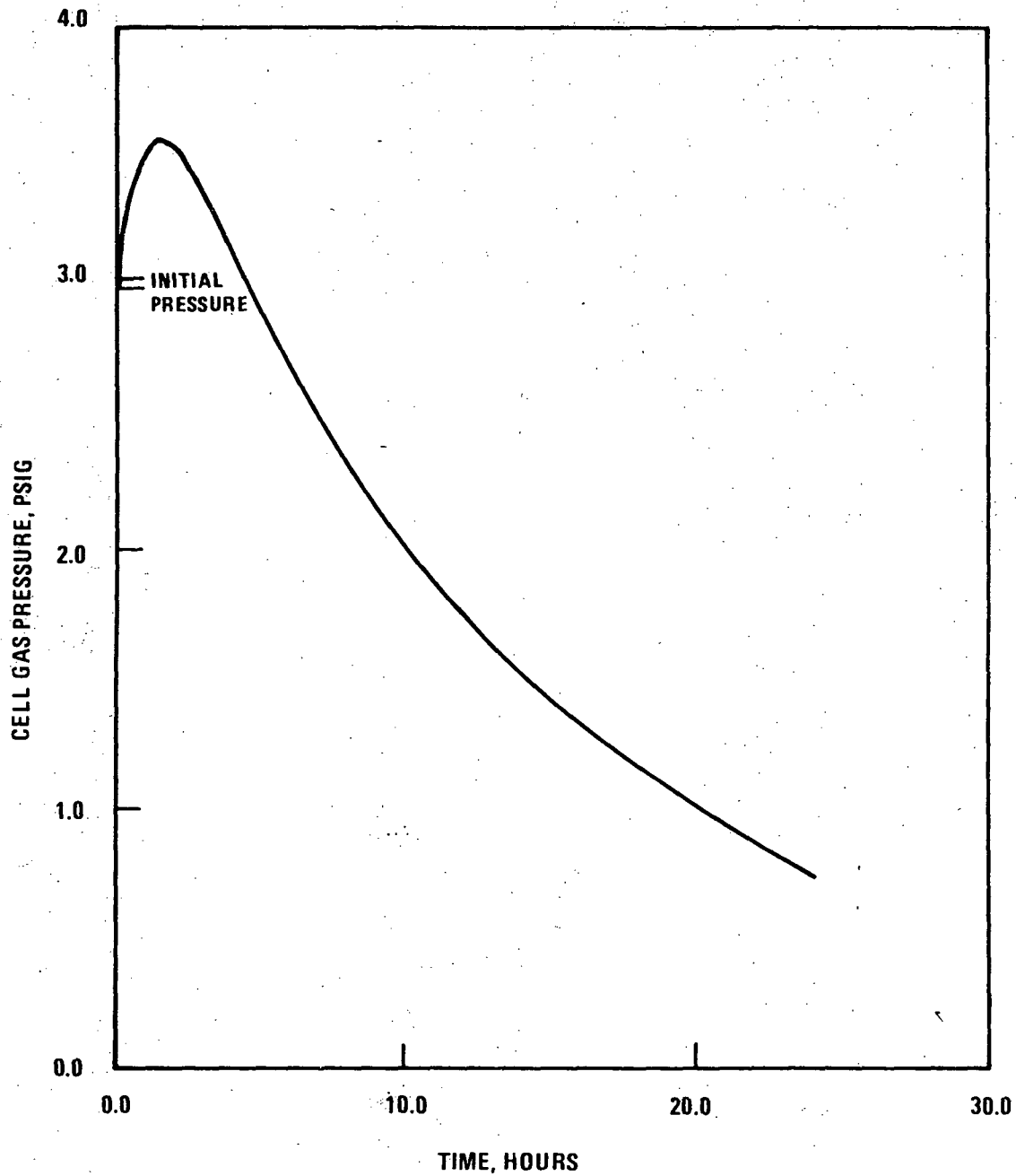


Figure Q001.581-32. Cell 102A - Cell Gas Pressure Moderate Energy Fluid System Leak
9653-15

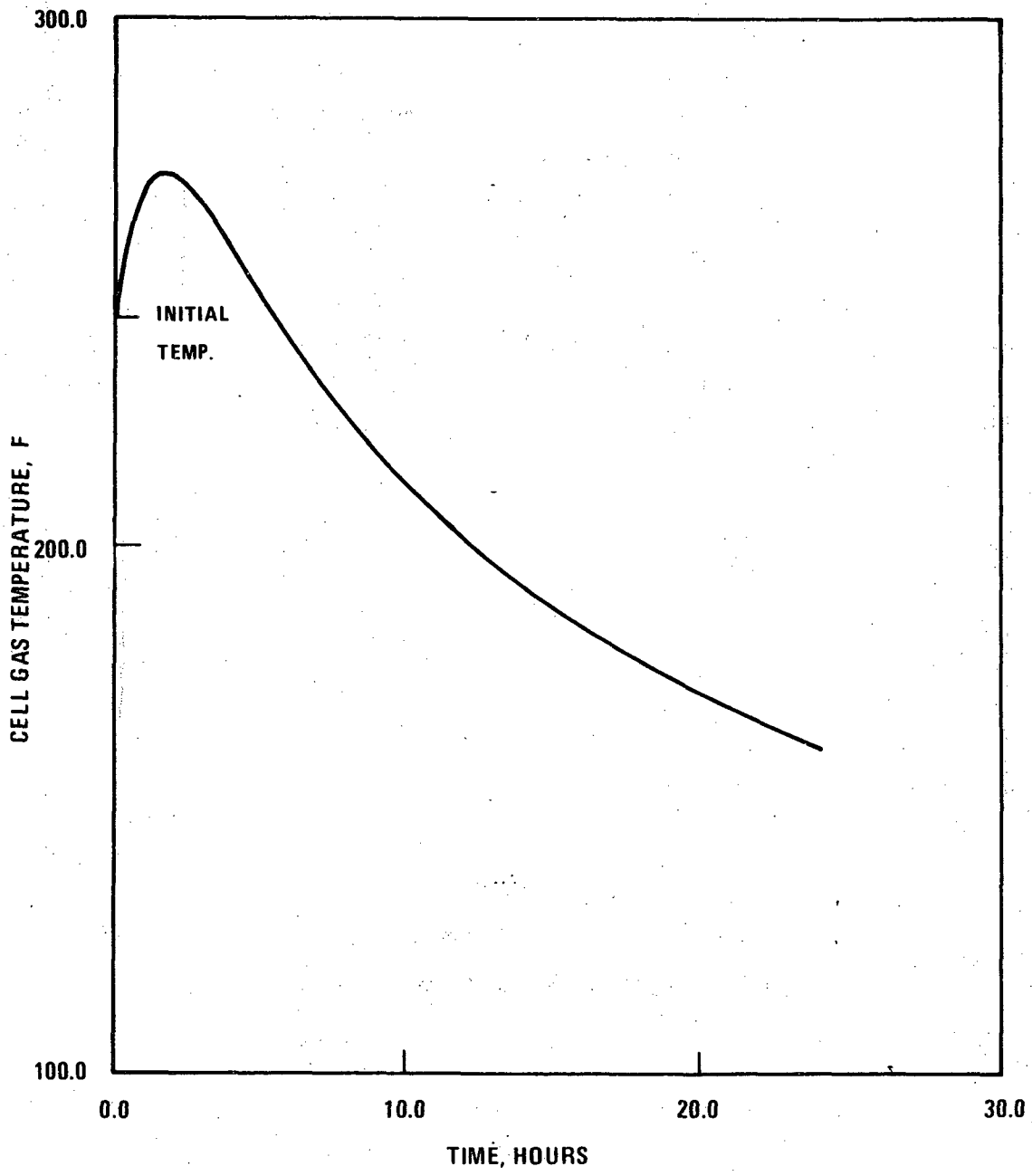


Figure Q001.581-33. Cell 102A - Cell Gas Temperature Moderate Energy Fluid System Leak

9653-17

Q001.581-60

Amend. 40
July 1977

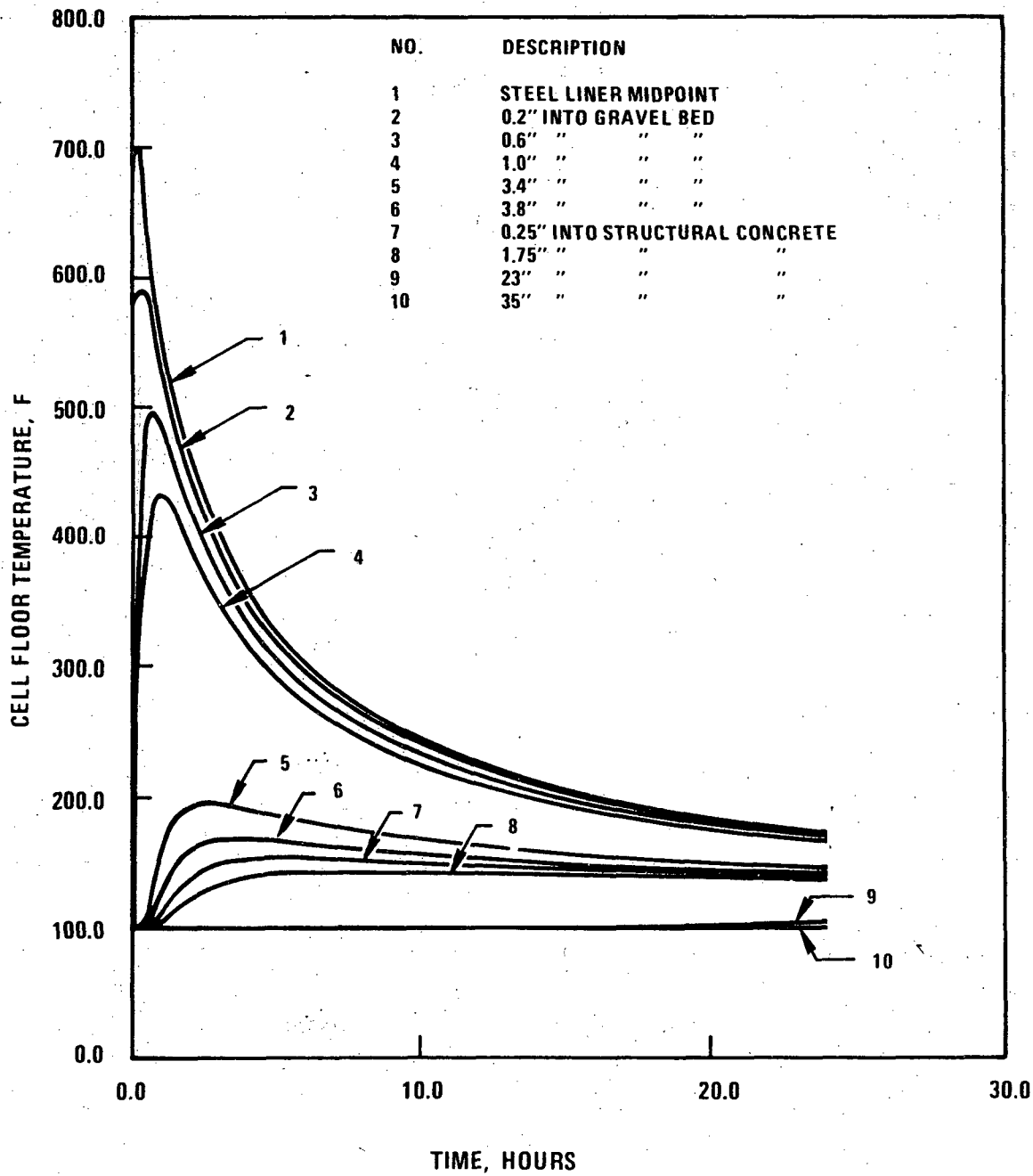


Figure Q001.581-34. Cell 102A - Floor Transient Moderate Energy Fluid System Leak

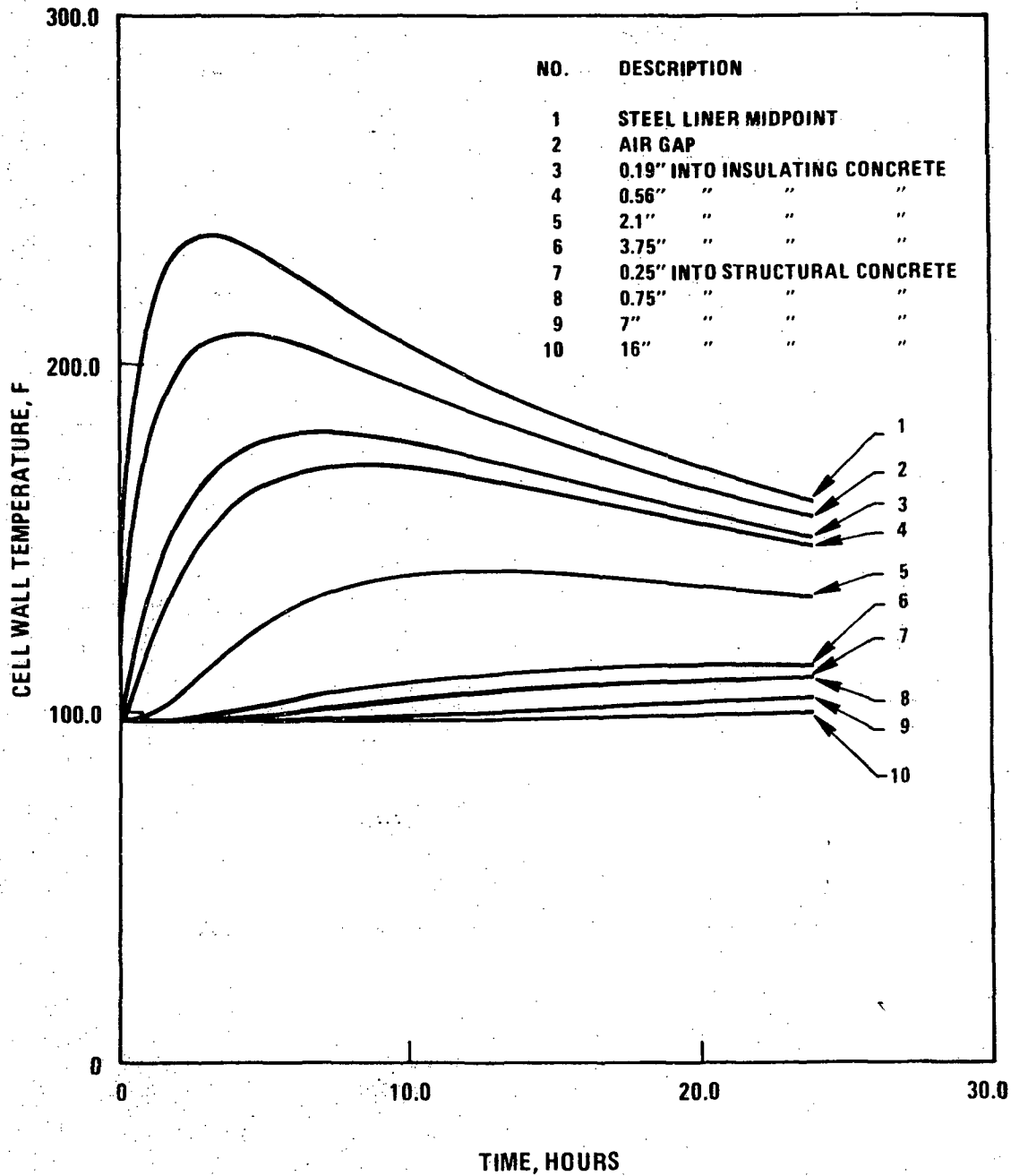


Figure Q001.581-35. Cell 102A - Non-Wetted Wall Transient Moderate Energy Fluid System Leak 9653-19

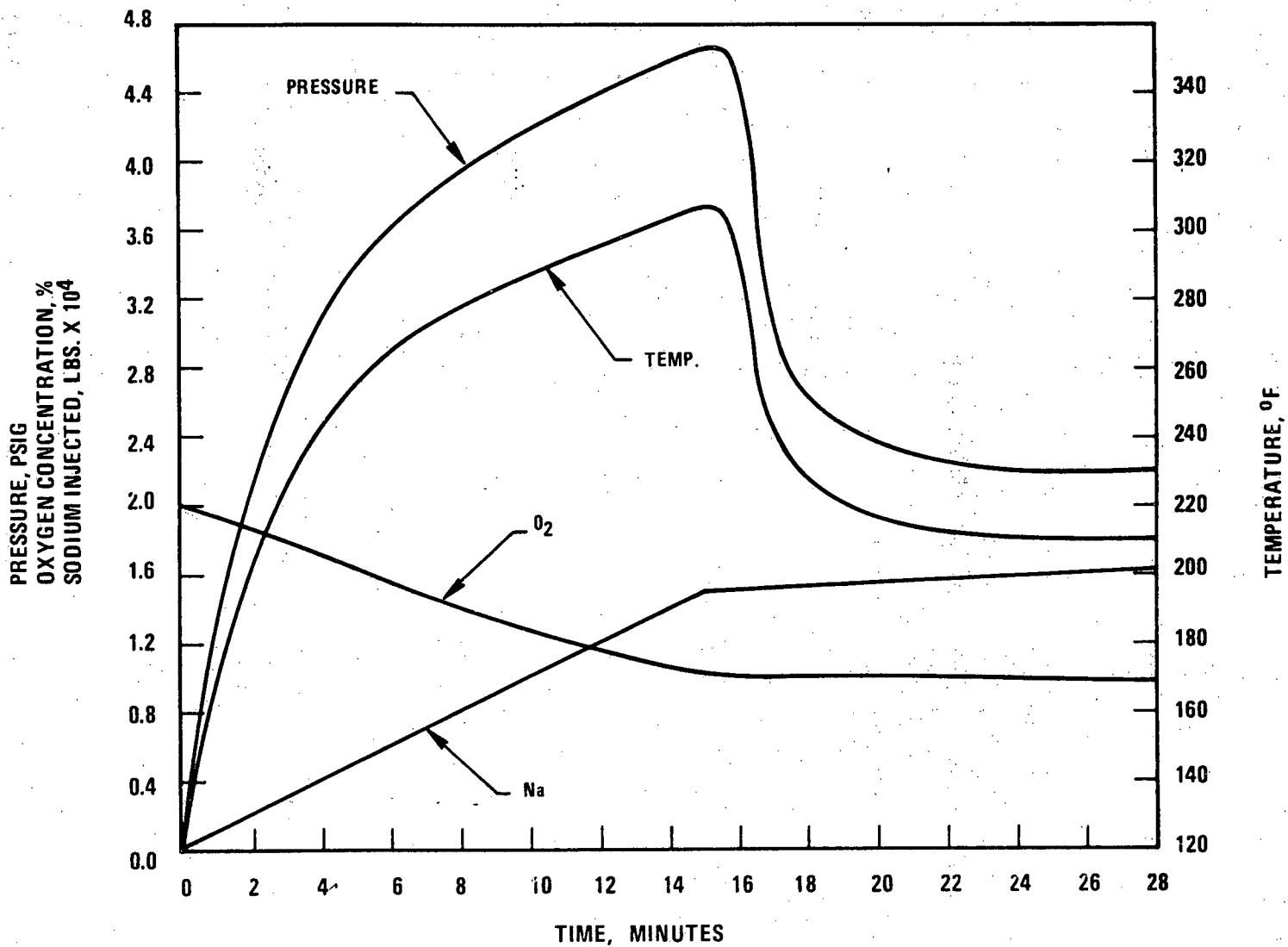


Figure Q001.581-36. Cell 102A - Spray Phase Transient Evaluation Basis Leak

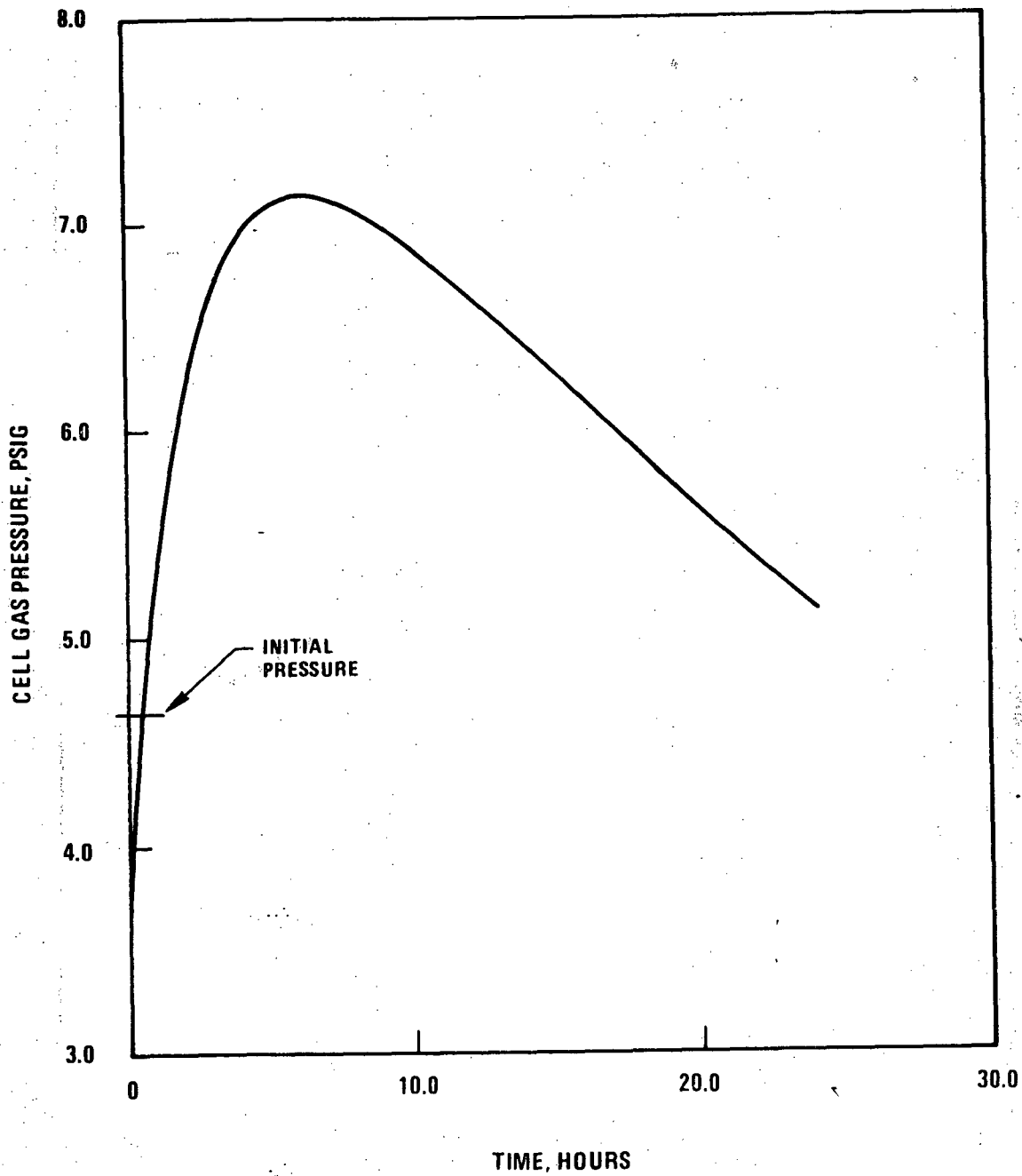


Figure Q001.581-37. Cell 102A - Cell Gas Pressure Evaluation Basis Leak
9653-23

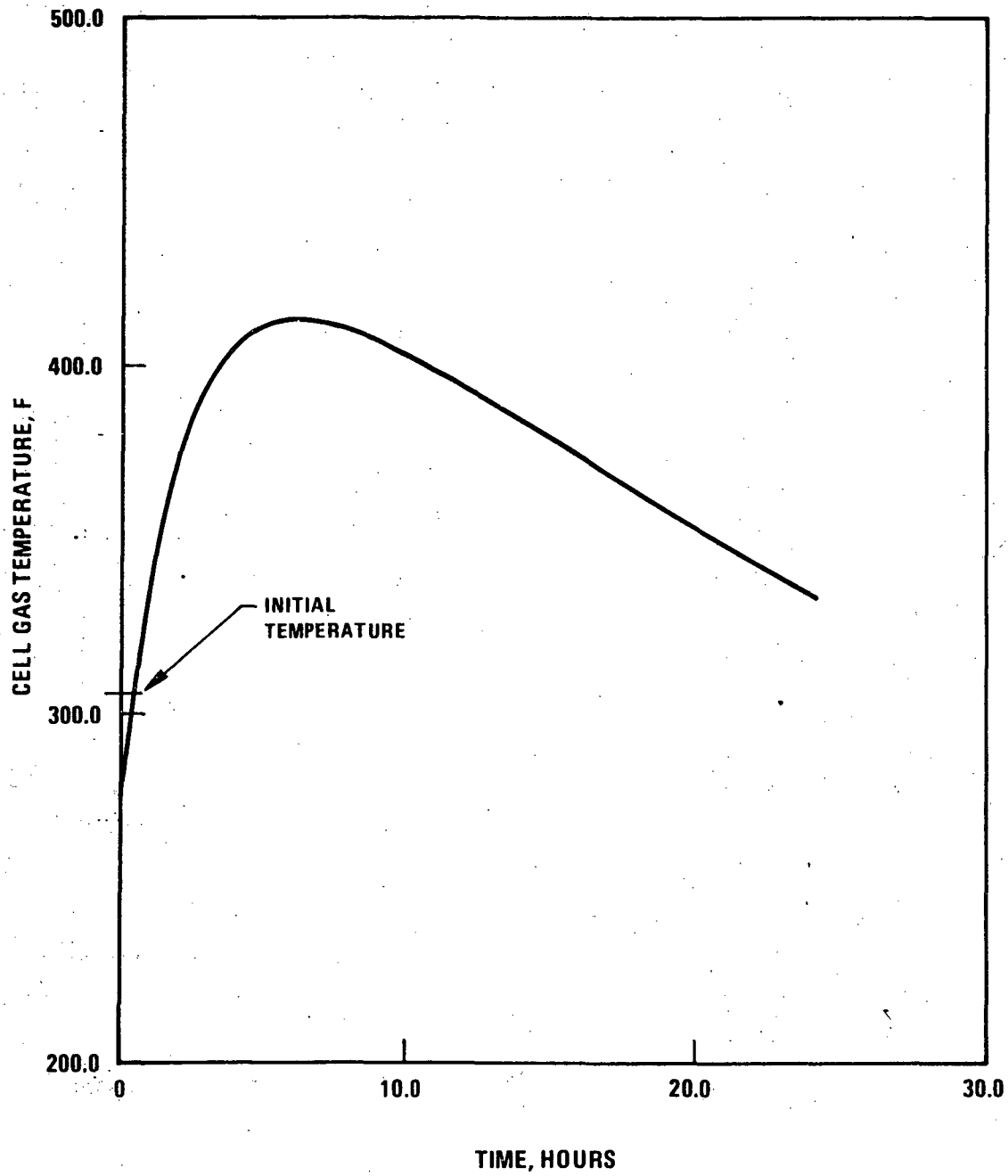


Figure Q001.581-38. Cell 102A - Cell Gas Temperature Evaluation Basis Leak 9653-22.

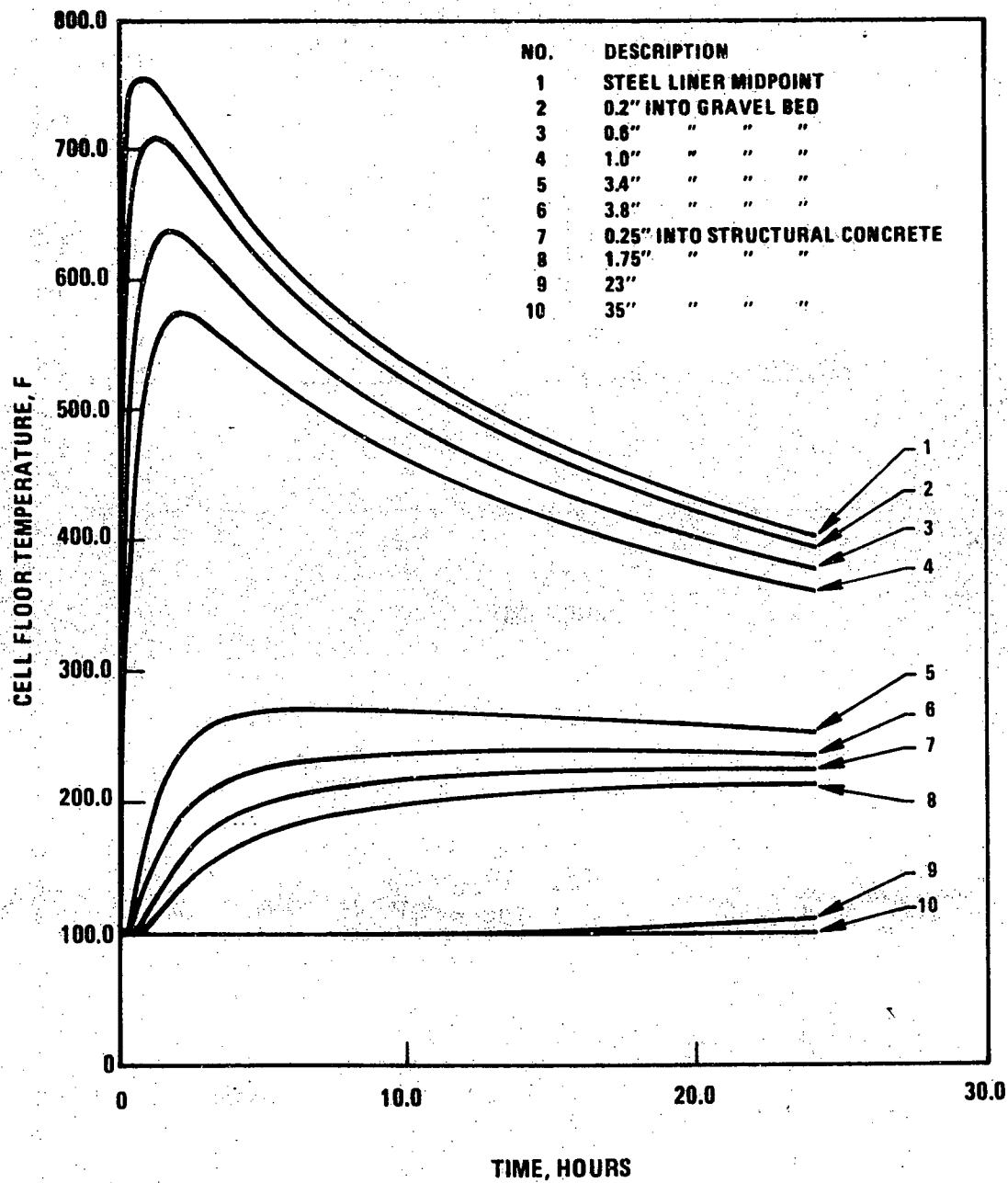


Figure Q001-581-39. Cell 102A - Floor Transient Evaluation Basis Leak

9653-26

Q001.581-56

Amend. 40
July 1977

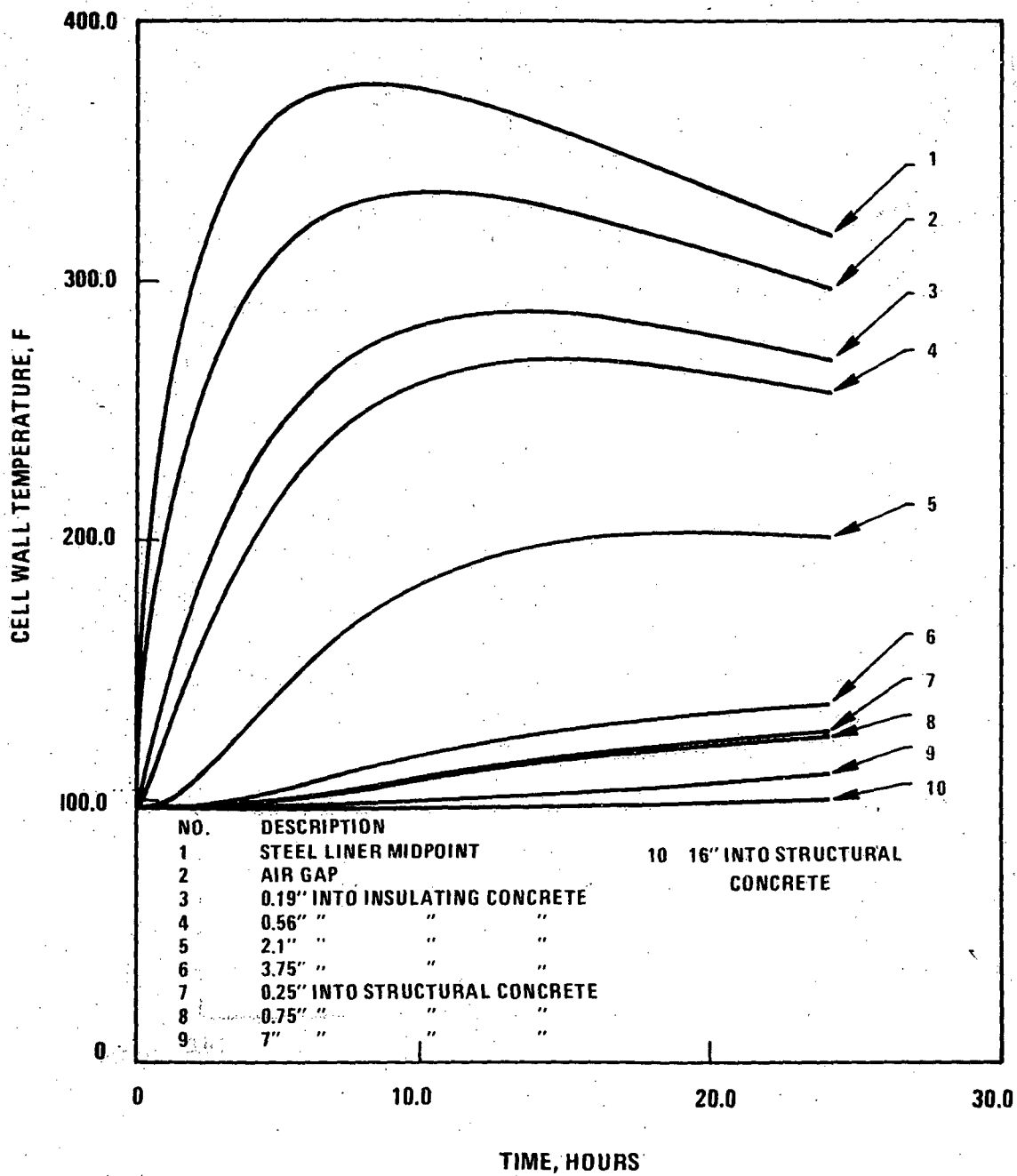


Figure Q001.581-40. Cell 102A - Non-Wetted Wall Evaluation Basis Leak

9653-28

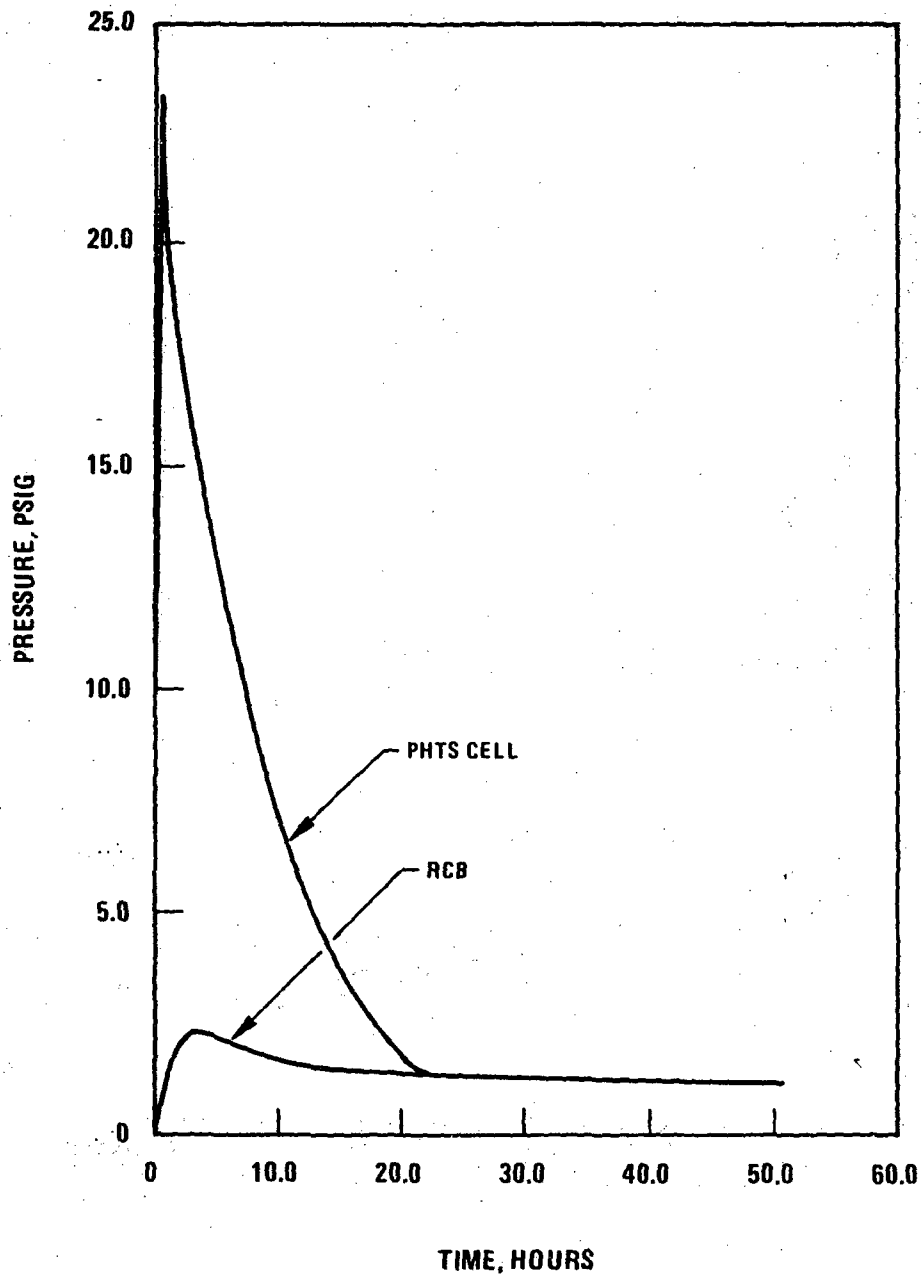


Figure Q001.581-41. PHTS Cell Pressure - Evaluation Basis Leak (25 Percent Failure)

9653-8

Q001.581-68

Amend. 40
July 1977

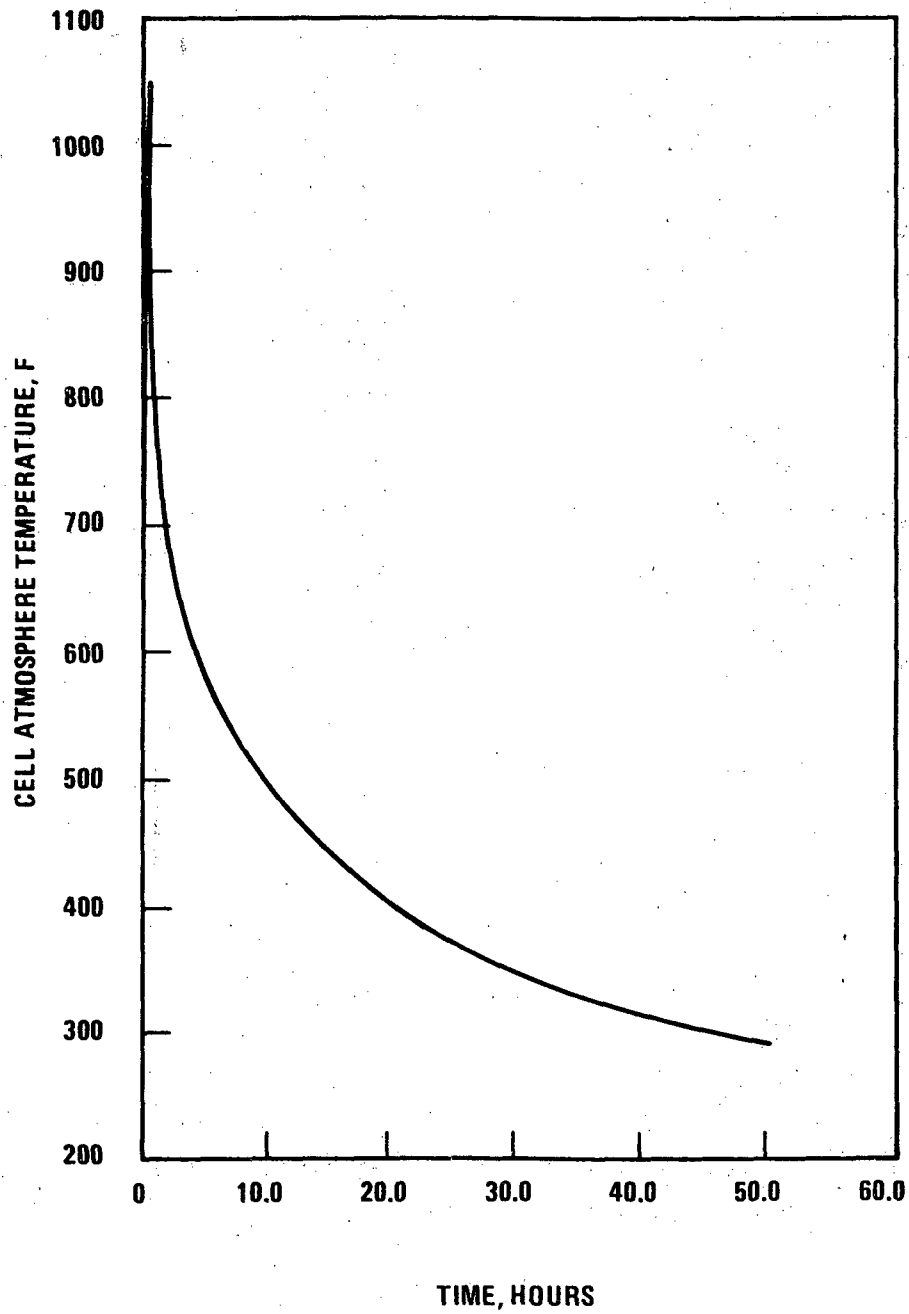


Figure Q001.581-42. PHTS Cell Temperature - Evaluation Basis Leak (25 Percent Failure)

9653-9

Q001.581-69

Amend. 40
July 1977

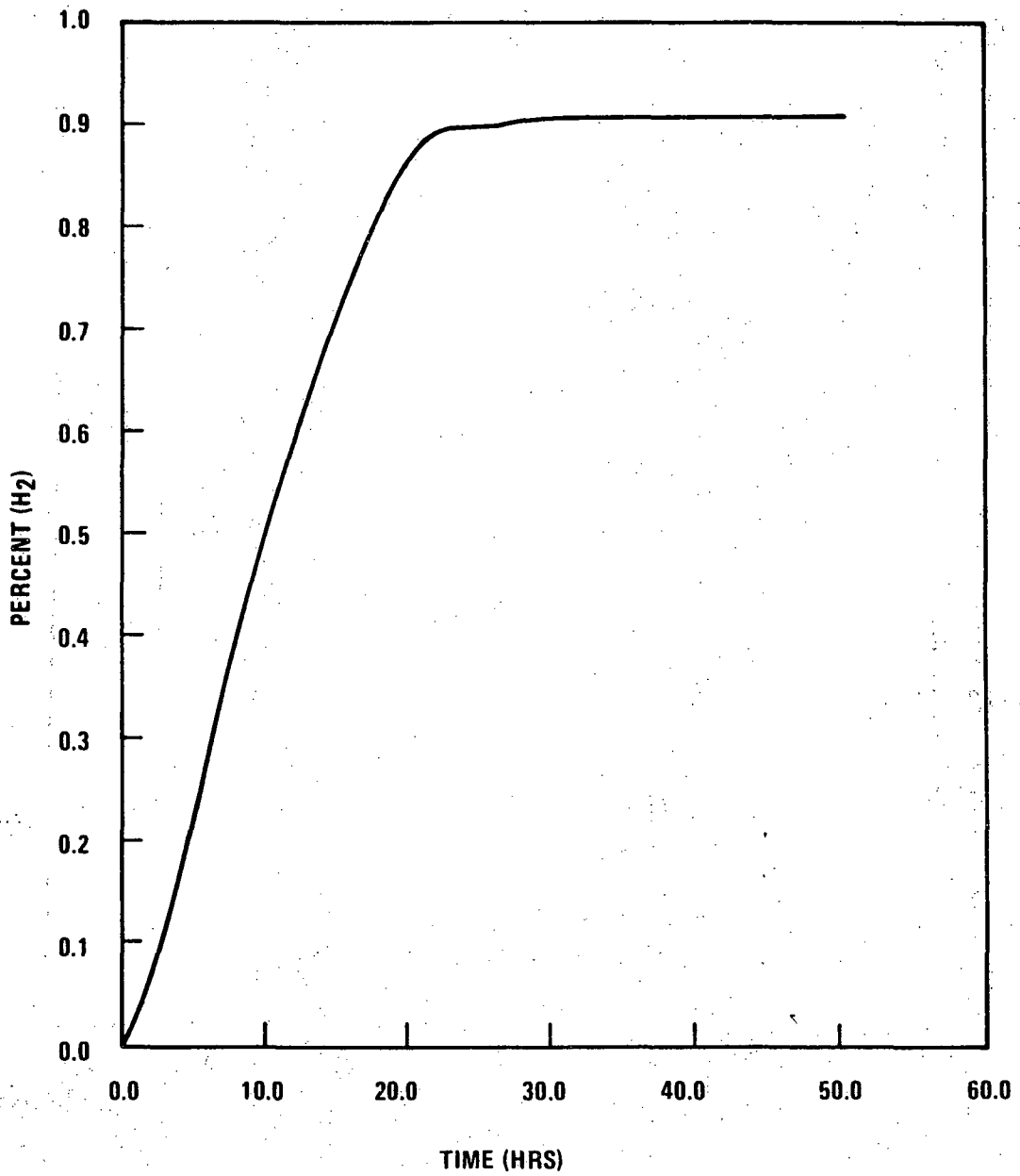


Figure Q001.581-43. RCBC Hydrogen Concentration - Evaluation Basis Leak (25 Percent Failure)

9653-1

Q001.581-70

Amend. 40
July 1977

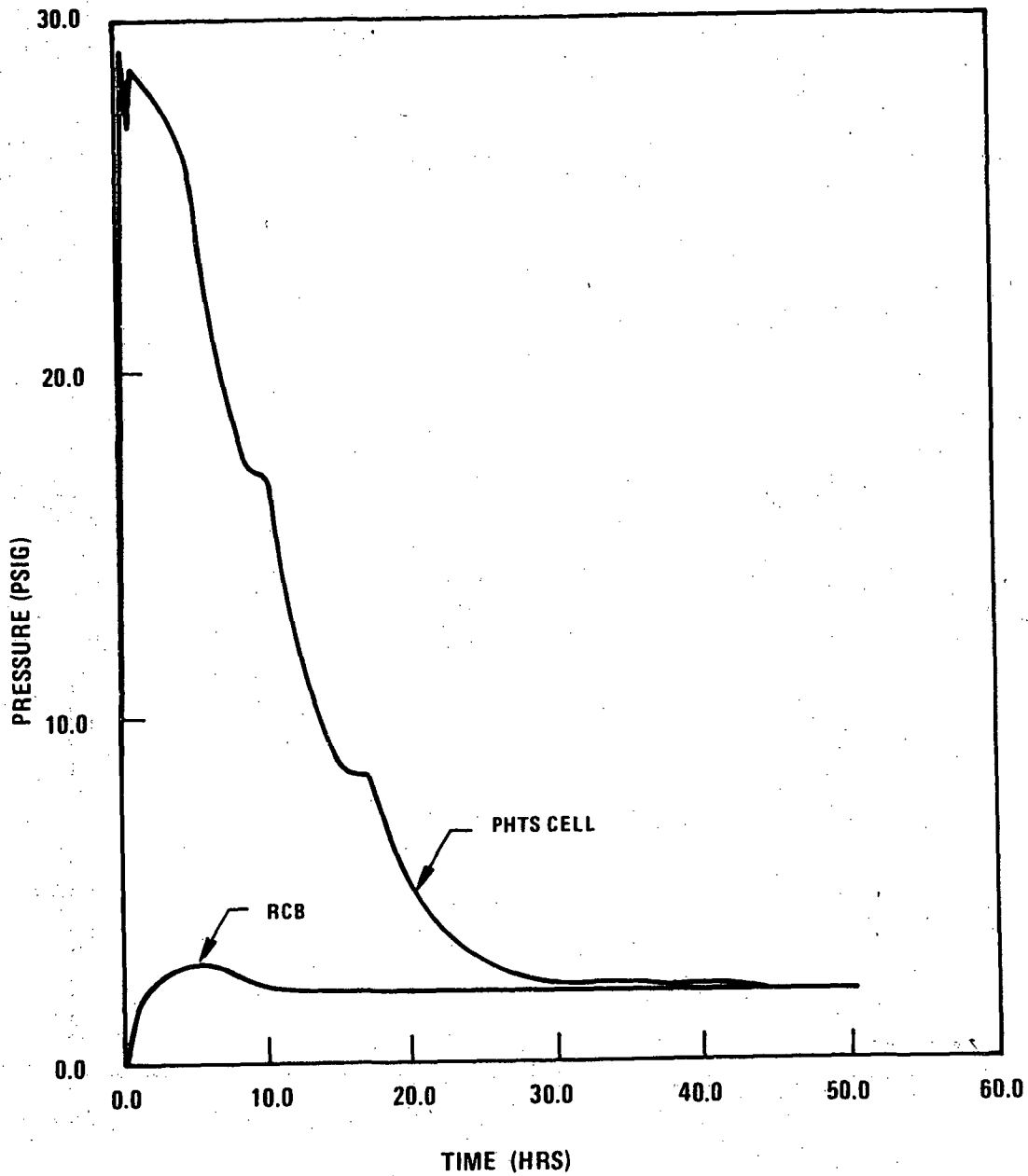


Figure Q001.581-44. PHTS Cell Pressure - Evaluation Basis Leak (50 Percent Failure)

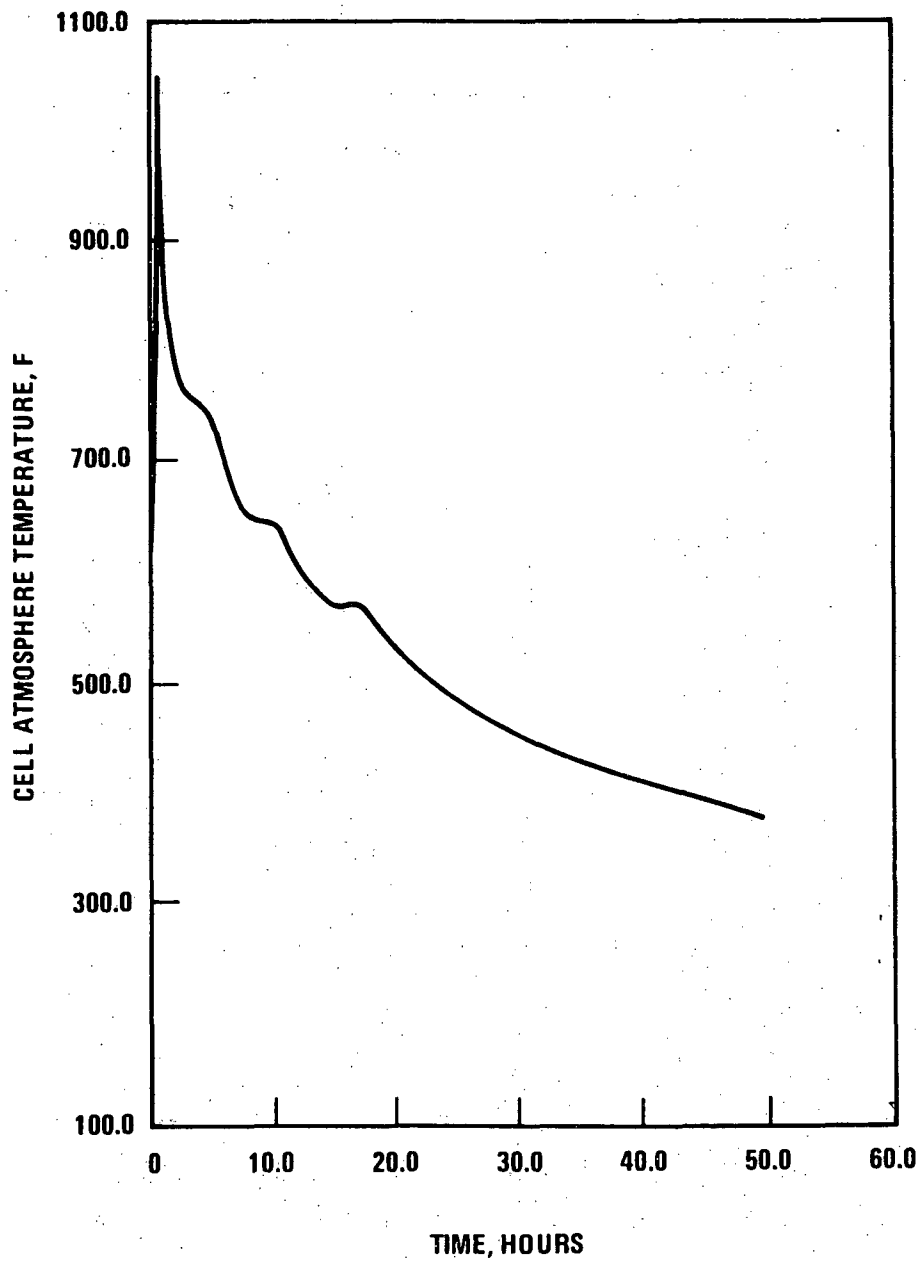


Figure Q001.581-45. PHTS Cell Temperature - Evaluation Basis Leak (50 Percent Liner Failure)

9653-10

Q001.581-72

Amend. 40
July 1977

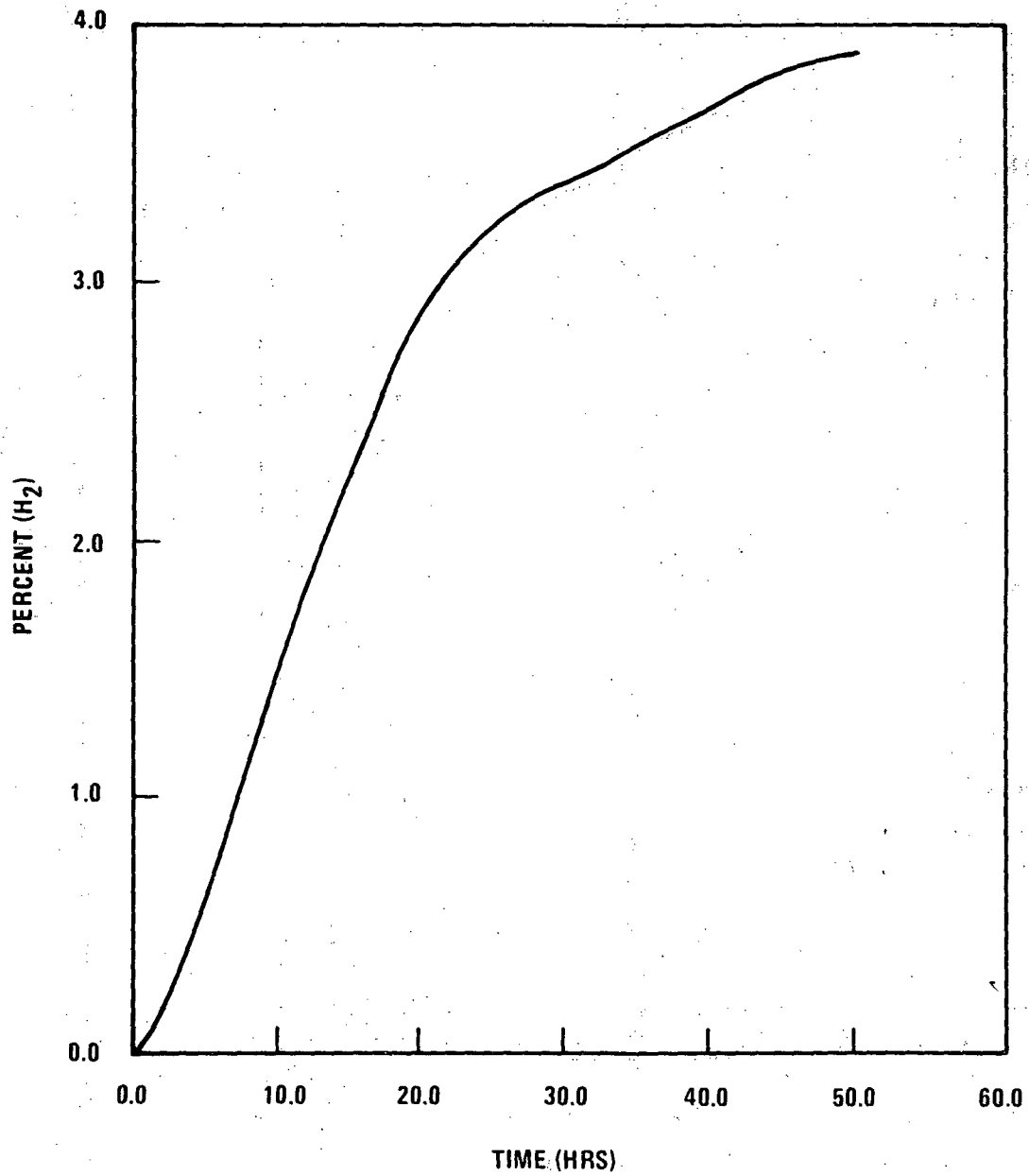


Figure Q001.581-46. RCB Hydrogen Concentration - Evaluation Basis Leak (50 Percent Failure)

9653-3

Q001.581-73

Amend. 40
July 1977

Question 001.583 (F6.3.2.3)

Concerning the thin vessel segment between the coolant level and the reactor vessel flange in a REXCO-HEP calculation, describe:

- (a) **How** it is modeled.
- (b) How it affects the head motion.
- (c) How the head motion affects it.
- (d) From the RESCO-HEP input data listing in Section D6.5, the top of this segment appears to be free in the radial direction which does not represent the constraint of the vessel flange. Explain how this affects the calculation of the upper reactor vessel strain.

Response:

The CRBRP Project has consolidated all considerations given Hypothetical Core Disruptive Accidents into report CRBRP-3 (References 10a and 10b, PSAR Section 1.6) and its associated references; consequently, PSAR Appendices D and F have been withdrawn in Amendments 24 and 60 respectively. The response to this question is now found in Section 5.1.1.3 of Reference 10a, PSAR Section 1.6.

Question 001.584 (F6.3.2.3)

Indicate the effect inclusion of the horizontal thermal baffle would have on the REXCO-HEP generated pressures at the outlet nozzles and on the REXCO-HEP calculated strains of the core barrel and mid-reactor vessel wall.

Response:

The CRBRP Project has consolidated all considerations given Hypothetical Core Disruptive Accidents into report CRBRP-3 (References 10a and 10b, PSAR Section 1.6) and its associated references; consequently, PSAR Appendices D and F have been withdrawn in Amendments 24 and 60 respectively. The response to this question is now found in Section 5.1.1.3 of Reference 10a, PSAR Section 1.6.

60

Question 001.585 (F6.3.2.3)

Describe the effect on the REXCO-HEP calculations of reactor vessel contact with the guard vessel.

Response:

This question requests clarification of information which is no longer a part of the current documentation. The Project has since consolidated all considerations given Hypothetical Core Disruptive Accidents into report CRBRP-3 (References 10a and 10b, PSAR Section 1.6) and its associated references; consequently, PSAR Appendices D and F have been withdrawn in Amendments 24 and 60 respectively. Contact between the reactor vessel and the guard vessel is not predicted.

60

Question 001.586 (001.540)

Expand Table Q001.540-1 to include:

- (a) the work energy in expansion to dynamic equilibrium
- (b) the "average pressure" at dynamic equilibrium

Response:

Revised Table Q001.540-1 includes the requested data.

Question 001.587 (F6.3.3.3)

Clarify further how TRANSWRAP determines the dynamic pipe pressures in Figures F5.4-49 through F5.4-62 up to 200 msec using as input the REXCO-HEP generated pressure histories from Section F5.4 which terminates at 120 msec.

Describe how 20 bars was chosen as the long term steady state pressure, and why 200 msec was selected as the time at which long term steady state pressure is reached.

Using Figure F5.4-50 to exemplify our concern:

- (a) Indicate for what point in the cold leg piping does the figure represent the pressure history.
- (b) Explain how sensitive the shape of the last large pulse is to the boundary assumptions made in Section F6.3.3.3 past 125 msec.
- (c) Indicate if the pressure will continue to fluctuate in time, and if the peak pressures will continue to grow.

Response:

The CRBRP Project has consolidated all considerations given Hypothetical Core Disruptive Accidents into report CRBRP-3 (References 10a and 10b, PSAR Section 1.6) and its associated references; consequently, PSAR Appendices D and F have been withdrawn in Amendments 24 and 60 respectively. The response to this question is now found in Section 5.1.2 of Reference 10a, PSAR Section 1.6.

60

Question 001.588 (F5.4.2)

Verify the labeling time scales on Figures F5.4-63 and F5.4-64.

Response:

This question requests clarification of information which is no longer a part of the current documentation. The Project has since consolidated all considerations given Hypothetical Core Disruptive Accidents into report CRBRP-3 (References 10a and 10b; PSAR Section 1.6) and its associated references; consequently, PSAR Appendices D and F have been withdrawn in Amendments 24 and 60 respectively.

60

Question 001.589 (F2.2)

Update the PSAR to resolve the inconsistencies regarding the attachment of the reactor vessel to the support ring. Question 001.379 (Amendment 17) and Section 5.2.2.1 (Amendment 17) assert that the vessel flange is welded to the support ring, while Table F.2-2 (Amendment 19) and Question 001.544 (Amendment 23) continue to discuss a bolted attachment.

Response:

Details regarding the reactor vessel attachment to the support ring are provided in PSAR Section 5.2 and Figure 5.2-1. Other sections of the PSAR have been revised to be consistent with Section 5.2.

Question 001.590 (F7.0 Addendum 1)

Provide vessel pressure histories corresponding to Figure F5.4-2 for axial locations 2, 6, 12, 17, 22, 26, 32, 37 and 38 in the REXCO-HEP model depicted in Figure F5.4-1 for Case 2, Case 3 and Case 4 analyzed in 1.540, 2, 3 4.

Provide the pressure histories corresponding to Figures F5.4-29 and F5.4-30 for the inlet and outlet nozzle locations for Case 2, Case 3 and Case 4 analyzed in Addendum 1 to Section 7.0. Explain how these histories were obtained, i.e., were the pressures in more than one zone averaged in some was as they slid past the outlet nozzle location? Explain why Figure F5.4-30 has more oscillations than any for the zones in the vicinity of the outlet nozzle (Figures F5.4-15 through F5.4-17).

Response:*

160

A complete set of Reactor Vessel and attached system loadings is provided in Section 5 of Reference 10a. PSAR Section 1.6.

160

*Note that Appendix F has been withdrawn. The text, upon which the question was based, can now be found in Section 5 of Reference 10a, PSAR Section 1.6. 60

Question 001.591 (001.540)

Tabulate the P-V curves used as input to the REXCO-HEP calculations for the four cases.

Response:

The requested P-V curve tabulation is provided in amended Table Q001.540-3.

Question 001.592 (001.540)

Tabulate, as in Table F6.3-2 the energy partition in the REXCO-HEP calculations at the time of slug impact and at dynamic equilibrium for the four cases considered. Include in these tables the average core pressure and the slug surface velocity.

Response:

Table Q001.592-1 provides the requested data.

Table Q001.592-1

ENERGY PARTITION FOR HCDA CASES 1 THROUGH 4

	Case 1		Case 2		Case 3		Case 4	
	Slug Impact	System Equilibrium						
Time (m-Sec)	69.2	122	58.2	120.0	60.0	116.0	62.0	150.0
Total System Energy (MW-Sec)	669.2	661.3	866.6	857.5	301.0	263.7	1304.1	1333.5
Upward KE (MW-Sec)	75.2	20.4	96.4	39.4	41.3	25.9	96.2	42.6
Radial KE (MW-Sec)	2.9	2.3	3.3	3.3	0.9	1.2	5.7	3.1
Cope Barrel Strain Energy (MW-Sec)	16.9	16.9	37.5	37.4	35.3	35.2	39.2	39.1
Vessel Strain Energy (MW-Sec)	4.9	67.7	17.1	120.9	20.9	60.3	21.3	223.7
Coolant Internal Energy (MW-Sec)	1.4	13.25	3.6	9.8	1.9	2.6	3.5	6.6
Vessel Head Energy (MW-Sec)	0	0.2	0	0.5	0	3.6	0.1	15.2
Total Work Energy (MW-Sec)	101.4	140.7	154.6	220.9	100.4	130.9	170.2	349.7
Core Internal Energy (MW-Sec)	567.5	528.6	708.1	641.8	171.7	132.7	1133.9	983.8
Average Core Pressure (psi)	416.2	300.0	523.5	311.8	464.	275.5	775.8	398.8
Slug Surface Velocity (ft/sec)	52.7	0.4	61.9	-2.0*	**	**	68.6	4.9

* The negative value implies that the slug is falling away from the head at this time

**Slug surface velocity not available for this case.

Q001.592-2

Amend. 35
Feb. 1977

Question 001.593 (001.540)

For each of the four cases, provide the maximum values attained by the following and the times at which these maxima occur:

- Core barrel strain
- Mid reactor vessel strain
- Upper reactor vessel strain
- Head holddown bolt strain
- Variation in total system energy from initial total energy

Response:

Table Q001.593-1 provides the requested data based on REXCO calculations. The REXCO results are provided, since detailed structural results are not available for all cases requested. These strain values should be considered to provide comparative results for the various cases, but should not be used as absolute values, since detailed structural evaluation of components are based on more detailed models than used in REXCO.

Also, note that there are no holddown bolts. Data for vessel holddown has been substituted in Table Q001.593-1 for head holddown bolt strain.

160

Table Q001.593-1
 MAXIMUM REACTOR COMPONENT STRAINS AND ENERGY
 DEVIATIONS FOR HCDA CASES 1 THROUGH 4
 (Based on REXCO Results)

	Case 1		Case 2		Case 3		Case 4	
	Time (msec)	Maximum Strain (%)						
Core Barrel Strain	40	6.22	46	9.5	64	8.80	44	9.6
Mid Reactor Vessel Strain	90	0.70	82	1.7	74	1.82	139	3.2
Upper Reactor Vessel Strain	115	6.05	104	8.5	108	3.86	124	10.0
Vessel Holdown	76	0.34	82	0.38	115	1.80	138	2.8

	Time (msec)	Energy Variation (%)						
Variation in Total Energy from Initial Total Energy	120	0.75	122	2.8	116	12.4	128	4.5

Q001.593-2

Amend. 37
 March 1977

Question 001.594 (001.540)

It is understood that mass, momentum, and internal energy are conserved in a rezoning calculation. For each of the four cases, provide the time of each REXCO-HEP mesh rezoning calculation and the resulting change in the total system energy.

Response:

Table Q001.594-1 provides the requested data.

TABLE Q001.594-1
REXCO-HEP REZONING DATA

Case	Rezone Time (msec)	Initial Energy (MJ)	Final Energy (MJ)
1	80	668	680
2	70	867	895
3	No rezone	—	—
4	70	1311	1354

Question 001.595

The following table contains the elastic stiffnesses and yield forces determined through analysis (LRA-75-1109 and Appendix A of Amendment 21) and through experiments (Amendment 21, 001.540) for the three shear rings:

SHEAR RING STIFFNESS - lb/in.

	SRP	IRP	LRP
Analytical	411×10^6	1075×10^6	1552×10^6
Experimental	101.81×10^6	254.53×10^6	392.7×10^6

SHEAR RING YIELD FORCE - lb.

	SRP	IRP	LRP
Analytical	7.13×10^6	22.02×10^6	35.59×10^6
Experimental	24.43×10^6	61.09×10^6	94.24×10^6

Not only do these fundamental input properties, used in the various 1-D analysis submittals differ by as much as 400%, the trends yield force versus stiffness are in opposite directions between the two sets of properties. These conflicting trends in properties imply grossly different deflectors at yield for the analytical and experimental results. Since these input properties are both submitted as credibly derived, provide a detailed explanation for the large differences, differing trends, and confidence expected in analytical solutions based on these properties.

Response:

The analytical predictions of SRP, IRP, and LRP shear ring force-deflection properties were made with preliminary 2D axisymmetric finite element models in early 1974. Only the shear rings and respective locally adjacent notch root regions were modeled. Locally adjacent plug lip regions were not modeled. Axial loads were applied to the shear rings and the outer surfaces of the notch root regions were fixed. The direction of the axial load was parallel to the central axis of the shear rings so as to neglect the wedging action caused by forces applied normally to the inclined shear ring surface. Only elastic analysis was performed. The elastically calculated stress intensities along a vertical strip in the notch root ledge above the shear ring were averaged for the total applied load and ratioed by an allowable stress intensity of 40,000 psi to determine the respective yield forces. The combined elastic stiffness of the shear rings and locally adjacent plug and notch root regions were determined by assuming the plug flexibility to be a small fraction of the flexibility derived for the notch root region.

The experimental scale model force-deflection properties of the LRP shear ring and locally adjacent LRP lip and vessel flange notch root region were determined to eliminate the assumptions associated with earlier elastically calculated analytical predictions. The experimental model included the LRP plug lip flexibility which was essentially neglected in the analytical prediction. Accordingly, experimental elastic stiffnesses would be expected to be lower than those predicted by the early analysis. With regard to yield forces, the wedging action of the shear ring and actual inelastic material behavior which tends to increase the strength of the shear ring region was included in the experimental scale model. In addition, the yield stress of SA-508 rotating plug material is approximately 60,000 psi and not 40,000 psi as was assumed in the analytical prediction. As such, yield forces would be expected to be higher with experimental scale model results than predicted by the early analytical prediction. In this arrangement, the lowering of stiffness and increase in yield forces observed in the scale model experimental results as compared to the earlier analytical predictions are understandable. Earlier analytical predictions are not considered representative of actual SRP, IRP, and LRP shear ring force-deflection behavior and should no longer be considered relevant.

Analytical predictions of CRBRP closure head response based on scale model experimental force-deflection properties for the LRP shear rings are therefore expected to confidently represent actual response to HCDA loadings.

Question 001.596

In the CRBRP Project Report LRA-75-1109 a three-dimensional (3-D) analysis of the Reactor Vessel head-shear ring structure under the CDA SDB load of 661 MW-sec as well as a series of reduced one-dimensional (1-D) analyses are presented. A comparison of the 3-D and 1-D analyses provides the following shear ring plastic deformations:

<u>SHEAR RING FOR:</u>	<u>3-D (inches)</u>	<u>1-D (inches)</u>
Small Rotating Plug (SRP)	0.078	0.01
Intermediate Rotating Plug (IRP)	1.10	0.63
Large Rotating Plug (LRP)	1.45	0.95

Although the comparison of this and other output data is of concern in itself, the analysis on which this output is based also requires explanation.

- a. Justify the idealization of the vessel head (rotating plugs) as elastic thin plate bending only elements since: 1) the restrictions inherent in plate elements make them inapplicable to the axisymmetric solid SRP and IRP structures, and 2) the LRP results imply plastic deformations which cannot be handled by these elastic elements.
- b. Justify the use of 1-D stiffness properties, which are based on a normal mode analysis of a head whose 3 rotating plugs are rigidly coupled, for 1-D and 3-D structural response calculations in which the 3 independent plugs are coupled by flexible 1-D springs.
- c. Explain the use of non-conservative 1-D solutions for design and safety verifications.

Response:

- a. The initial 3-D and series of reduced 1-D analyses were performed primarily to study the configuration characteristics of the system influenced by the HCDA loading. Because of the parametric nature of these studies, many approximations based on engineering judgement were made in the analyses. These include the use of thin elastic plate finite elements to model the plugs in bending while neglecting shear deformations which resulted in efficient and analytically simple solutions. The updated 3-D analysis, which is more detailed and includes both plug plasticity and updated shear ring force-deflection properties, is discussed in Section 4.0 of Reference Q001.596-1.

- b. The use of 1-D stiffness properties of the shear rings and locally adjacent plug materials based on rigid plugs for initial simplified 3-D structural response analysis is an acceptable approach which is consistent with the objectives of the preliminary parametric studies. The effect of the overall plug flexibilities is included in the detailed 3-D response as described in Section 4.0 of Reference Q001.596-1.
- c. The 1-D analyses are only simple indicators of CRBRP closure head response to HCDA loadings and, as noted in the Reference Q001.596-2 transmittal letter for the original reports, were never intended for design and safety verifications.

References:

- Q001.596-1 "CRBRP Closure Head Capability for Third Level Structural Margin Loading", WARD-D-0178, Westinghouse Advanced Reactors Division, Rev. 3, November, 1978.
- Q001.596-2 Letter, A. R. Buhl (ERDA-PO) to R. S. Boyd (USNRC), "Additional Information Supporting the CRBRP Assessment of Plant Margin in HCDA Mechanical Loading Condition," Docket No. 50-537, July 28, 1976.

160

Question 001.597

In the LRA-75-0119 3-D analyses, the shear rings are modeled as 1-D lumped spring-mass elements under the assumption that the shear rings do not greatly influence the overall structural response. At the same time all 3-D and 1-D analysis submittals based on analytically derived shear ring properties show large plastic stresses in the rotating plugs, in contrast to the 1-D submittal (Amendment 21, PSAR) based on experimentally determined shear ring properties, which shows elastic behavior of the plugs.

Provide an explanation of this contradiction between the input assumption and the output results.

Response:

The apparent contradiction between CRBRP closure head response based on earlier analytically derived shear ring force deflection and those derived with scale model experimental shear ring properties is explained in the response to Question 001.595. The rotating plugs were found to undergo only minor plasticity while a moderate and acceptable amount of plasticity in the local shear ring regions was observed in the recent 3-D CRBRP closure head response analysis as described in Section 4.0 of Reference Q001.596-1. 160

Question 001.598

The justification of 1-D analyses based on experimental input is stated in Amendment 21 of the PSAR to be based on a 3-D - 1-D correlation. The background 3-D data for this justification is stated to be found in LRA-75-1109. Although there is a 3-D as well as a series of 1-D analyses, the latter based on the 3-D analysis, presented and compared in LRA-75-1109, a correlation between any of the 1-D analyses in Amendment 21 and the 3-D analysis in LRA-75-1109 is not presented.

Provide a justification for the 1-D analysis used in Amendment 21 to answer question 001.540 by comparing the results for the 661 MWsec CDA loading in Amendment 21 with the 3-D solution in LRA-75-1109.

Response:

The 1-D to 3-D correlation mentioned was based on the analyses in LRA-75-1109. The analysis results in Amendment 21 are not comparable to those of LRA-75-1109, because the shear ring parameters used in the two analytical works were significantly different.

It should be kept in mind that the 1-D analyses were intended to provide indications of system response under HCDA loading. As such, they improved understanding of system behavior and provided a basis for future detailed analysis, as well as serving as efficient tools for parametric evaluations. The completion of the recent 3-D analysis of the Closure Head under SMBDB loading obviates the need for 1-D to 3-D correlations. This analysis is described in Section 4.0 of Reference Q001.596-1.

Question 001.599

The results of Appendix E, LRA-75-1109, show that the addition of crush tubes does not significantly change the accumulated plastic deformation in the vessel head structures. This conclusion is based on a 1-D analysis which has not been justified and may not be acceptable.

Provide a discussion of how the crush tubes and plates below the crush tubes (especially their mass) will be factored into a more complete 3-D analysis of this structural head response problem.

Response:

The initial analysis of the closure head design neglected the effect of the crush tubes between the rotating plugs and the upper shield plate. However, the crush tubes have since been eliminated in the design and replaced with circumferential spacer bars on the inside and outside diameters of each plug. (See Reference Q001.599-1)

The circumferential spacer bars, which have replaced the crush tubes, are represented in the recent 3-D analysis with non-linear spring elements as discussed in Section 4.0 of Reference Q001.596-1.

Reference:

Q001.599-1 Letter from A. R. Buhl (CRBRP-PO) to R. S. Boyd (USNRC), "Summary of December 15 Meeting with NRC Staff to Discuss Reactor Vessel Closure Head Structural Analysis," Docket No. 50-537, January 3, 1977.

Question 001.600

The CRBRP Project Report LRA-76-637 demonstrates that simple 1-D lumped mass models of structural systems can be studied by using simple geometric scaling. However it does not show that this scaling carries back to the original elastic-plastic, dynamic response problem of the 3-D continuum. Provide a justification for the assumption that the scaling holds for the 3-D system. Also, because of the nature of the scaling, any size shear ring would have the same deflection at yield and at the plastic instability point as any other geometrically similar shear ring. Since this is generally not true for scaled elastic-plastic structural members, show how this would be true for the shear rings under consideration.

Response:

The scaling and similitude relationships between the scale model test parameters and the actual systems are discussed in Appendix A of Reference Q001.596-1. In addition, a justification for the scale model simulation follows directly from the fact that the equations of motion in a 3-D continuum are dimensionally homogeneous and therefore are reduceable to non-dimensional form.

For a prototype and scale model structure subjected to similar loads, the strains at corresponding points will be equal. It therefore follows that the deflections will not be equal, but will be proportional to the geometric sizes of prototype and model. This is true for elastic-plastic structures in general, and will therefore be true for the shear rings.

Question 001.601

The margin Shear Ring design and analysis for the Structural Design Basis (SDB), which considers structural loads corresponding to 661 MJ work energy, is required to accommodate a core disruptive accident (CDA). Although the Project has provided its verification of this in the submitted response to Questions 001.540 and 001.554, the input and idealizations in this analysis raise serious questions about its adequacy and its conclusions.

- (a) Justify the adequacy of the experimental data for developing fundamental input to the analysis (e.g., spring constants, yield forces, etc.), considering the following points:
- (1) The reactor vessel flange, which is a full ring, is experimentally represented by a unit circumferential length; thus the CDA loads are transmitted through the shear ring to the flange, failing the shear ring-flange unit in bending in this experiment; a full flange ring provides circumferential support to the shear ring and could result in the shear ring failing in a different mode (e.g., shear) prior to large deformations of the flange.
 - (2) The most recent shear ring design was presented in a revision dated June 22, 1976; the lengthy time to develop experimental data suggests one of the previous designs, with different geometrical shape and contact angle with the large rotating plug, may have been used in the experiment. Submit the experimental details.
 - (3) The response to item 001.554 states that the shear ring material has a considerably higher yield strength than the SA508 base material of the rotating plugs, and since there is so little strain data available for SA508 the Project used data for the "similar SA533 material" for the other reactor head structures; there remains a question as to exactly which materials (i.e., stress-strain curve and material properties) were used in the experiment and which materials were used in the analysis (response to 001.540) and whether these were identical. Submit experimental and analytical details.
- (b) Provide a justification for the use of static and planar experimentally based input and a one dimensional shell model of the vessel for this 3 dimensional nonlinear dynamic analysis.
- (c) Provide a justification for the use of simple linear scaling in the analytical representation of the geometry, loads and failure data developed in the 1/10 scale experiments, when scaling laws for this type of nonlinear structural problem may not exist.
- (d) Provide the justification for the use of an elastic-perfectly plastic stress-strain law approximation for the reactor head material in light of the available stress-strain data for ASTM A533-B steel; the lack of data for SA508, and the undefined shear ring material.

Response:

- (a.1) The experimental representation of a full ring by a unit circumferential length in a plane stress condition is a common simplification made in axisymmetric problems. The analytical treatment of the LRP shear ring in a plane stress or axisymmetric condition showed little difference in deformation modes as described in Appendix C of Reference Q001.596-1. In addition, test results for plane section and full ring specimens indicate that the deformation modes are similar. See Section 5.0 of Reference Q001.596-1. | 60
- (a.2) The shear ring tests were based on the current shear ring design. The test fixtures, specimen geometry and the test set up are given in Appendix B of the Addendum to Response Q001.540. | 60
- (a.3) The analytical work (response to Question 001.540) is based on the experimental shear ring scale model test results using SA-508 material traceable to the prototype CRBRP closure head IRP which inherently does not require assumptions on uniaxial stress-strain behavior. The analytical and experimental details are given in the Addendum to Response Q001.540 (specifically Section 3.4.2.1 and B.2.2.2 of the Addendum). | 60
- (b) The bases for some of the simplification made in the preliminary analytical and experimental studies are discussed in the Addendum 1 to Response Q001.540. Additional analytical and experimental work of a more rigorous nature has since been performed for the shear rings, and is described in Sections 4.0 and 5.0 of Reference Q001.596-1. In the initial stages, effort was made to maintain analytical and experimental simplicity, while at the same time retaining the key features of the closure head configuration. The 1D treatment of the vessel wall in the response to Question 001.540 was consistent with this approach in engineering judgement. | 60
- (c) The justification for scale modeling is discussed in Appendix A of Reference Q001.596-1.
- (d) The direct utilization of the scale model test results in the analytical studies (as was done in the response to Question 001.540) precludes the use of stress-strain curves. Of importance was the load-deflection curve of the load path and this information was obtained experimentally using SA-508 material traceable to the prototype closure head. In modeling the load-deflection curve as an elastic-perfectly plastic curve, the linear elastic stiffness was not changed and the plastic yield force was assumed to be equal to the threshold up to which the force was linearly proportional to deflection. This assumption was made for analytical simplicity and was verified by the results. The analytical and experimental details are given in Sections 3.4.2.1 and B.2.2.2 of the Addendum to Response Q001.540. | 60

Question 001.602

In the convention of the ASME code, your analyses fall into the Inelastic System Analysis and Component Plastic Instability Analysis category. However, Section F-1321.1 of the code, which deals with faulted condition design procedures specifies that in the plastic analysis the actual strain hardening characteristics of the material must be used.

Provide a justification for the use of elastic perfectly-plastic materials models based on the ASME code.

Response:

The selection of the elastic-perfectly plastic material models in the initial analyses was done primarily for analytical simplicity. However, the ASME Code does allow the use of elastic/perfectly plastic material models; see for example, Section NB3213.21, and Section NA, F-1323.2 and F-1324.2. The Code does specify that actual strain hardening characteristics be used in the plastic analysis but it should be noted that in the initial exploratory studies the plugs were simulated by elastic material representations, and the results were mainly used as indicators of the system response characteristics. Furthermore, since an HCDA is not a Design Basis Accident (see Reference Q001.602-1), CRBRP need not meet the Faulted Condition requirements of the ASME Code during the HCDA loading.

It may however, be noted that in the detailed 3-D analysis of the shear ring area, discussed in Section 4.0 of Reference Q001.596-1, actual strain hardening characteristics of the shear ring material and ANSYS kinematic hardening model of the rotating plugs have been used to determine the response characteristics under HCDA loading. 160

Reference:

Q001.602-1 U.S. Nuclear Regulatory Commission, "Final Environmental Statement Related to Construction and Operation of Clinch River Breeder Reactor Plant", NUREG-0139, Appendix I, Docket No. 50-537, February 1977.

Question 001.603

The analysis of the concrete ledge loads show relatively small margins of safety, i.e., loads as large as $46.37(10)^6$ lbs. compared to an allowable of $50 \times (10)^6$ lbs. The analysis indicates that the assumption of an elastic perfectly-plastic material for the vessel flange provides a reduced ledge load.

Provide a justification for the elastic-perfectly plastic idealization of the actual stress-strain relation when the use of the latter could result in decidedly negative safety margins for the concrete ledge loads.

Response:

Since this question was asked, the reactor vessel support ledge material has been changed from reinforced concrete to structural steel.

60

As shown in Figure 3.4.4-1 of the Addendum to Response Q001.540, the elastic-perfectly plastic idealization of the vessel wall was based on an average stress-strain curve in between the low strain rate ($1 \times 10^{-5} \text{ sec}^{-1}$) and the high strain rate (10 sec^{-1}) curves. It was assumed that within the domain of maximum anticipated strains, this idealization does not significantly differ from the actual stress-strain behavior and was used for analytical simplicity. The representation of actual non-linear stress-strain relations over small ranges of inelastic strain beyond yield with elastic-perfectly plastic models is common in engineering analysis. As subsequent vessel wall strains were found to be less than 1%, ledge loads derived with elastic-perfectly plastic models would be slightly higher than those derived using actual non-linear stress-strain relations, as Figure 3.4.4-1 indicates.

60

The upward loads on the ledge are limited by the yield strength of the flange bolts. The bolting material has a stress-strain curve which is close to elastic-perfectly plastic for small strains. The calculated strains in the bolts were small (less than 1%). Hence the elastic-perfectly plastic approximation was reasonable. Also, the yield strength had been augmented to allow for strain rate effects. Hence, the calculated upward ledge load was considered to be conservative.

Question 001.604

A simple spring-lumped mass system is used in the shear ring analysis (001.540) to simulate the response of a complex non-linear structural system, i.e., the reactor vessel head-shear ring-ledge bolt hold down structure.

Provide the justification for excluding with this simplified model important two and possible three dimensional effects. For example, for a thin shell (i.e., the reactor vessel) loaded by internal pressure, failures generally occur at attachments or thickness discontinuities which are not included in the one dimensional longitudinal model of the thin shell. The purely dimensional 1-D model of the thin shell also excludes important bending (rotation) and hoop (circumferential) deformations and their effect on the response of the head-shear ring-vessel flange structure.

Response:

The limitations of using a lumped mass-spring system to simulate the closure head area in the preliminary 1-D analysis are fully realized. However practicality and computing time requirements warrant such a simplification, particularly when the objective of such an analysis is to provide only a representative indicator of the overall CRBRP system response for the wide range of HCDA loadings studies. The preliminary 1-D results are not intended for final design verification. Recent 2-D and 3-D analyses of the CRBRP head closure head area, which involve greater detail and complexity, have been completed and are discussed in Section 4.0 and Appendix C of Reference Q001.596-1.

The simplified 1-D analyses inherently excluded the 2-D and 3-D effects associated with the local response of the reactor vessel under SMBDB loading. Failure modes associated with thin shells at attachments and local discontinuities under internal pressure were not reflected in the 1-D response results as stated. However, 2-D axisymmetric response analysis of the CRBRP reactor vessel under SMBDB loading pressure including the effects of attachments and local discontinuities has been performed. The results indicate that peak equivalent strains of approximately 3% occur as the vessel wall locally bulges near the mid-point along its length. Otherwise the vessel wall along its length behaves in an essentially uniaxial manner as described in the 1-D analysis. In terms of ledge loads, both 1-D and 3-D analyses show comparable downward loads as limited by vessel wall plasticity to be less than the 50 million pound limit.

Question 001.605

Various structural damping coefficients are provided in the shear ring analysis (001.540). Provide the criteria or guidelines used to select the structural damping and structural impact damping coefficients. Indicate if a comparison of the structural response has been made with and without structural damping, noting that nonlinear plastic deformations may provide a more realistic inherent damping mechanism.

Response:

The value of 2% structural damping used in the initial analysis was one of the conservative assumptions made in the analysis and reflects the practice of analytical simplification followed during the preliminary investigations. System and material damping increase as the response amplitude of the equipment increases. This is due to non-linearities in the system introduced by inelastic behavior of both materials and joints (see for example, Reference Q001.605-1). On that basis even a damping value of 4 to 6% of critical is acceptable. It may be noted that the system and material damping value used in the SSE evaluation of major CRBRP equipment is 3% of critical as specified by the NRC Regulatory Guide 1.61.

The value of 20% structural impact damping used in the initial evaluation is based on an FFTF analysis relating the coefficient of restitution to the damping coefficient. The 20% of critical corresponds to a coefficient of restitution of 30%.

No comparison was made of structural response with and without damping, and none was considered necessary. The energy of dissipation associated with structural and impact damping is small compared to the elastic strain energy and is also small compared to the work of plastic deformation. Considerations of the relative energies of elastic deformation, plastic deformation and damping indicated that neglecting structural and impact damping would have little effect on the response predictions.

Reference:

Q001.605-1 Morrone, A., "Damping Values of Nuclear Power Plant Components," Nuclear Engineering and Design, Volume 26, 1974.

Question 001.606

The intermediate rotating and large rotating plugs provide a geometrically nonlinear structural system due to the presence of gaps and sliding interfaces.

Provide the basis for a linear normal mode analysis used to determine natural frequencies for this type of complex structural system.

Response:

Linear normal mode analysis which inherently neglects nonlinearities or alternately assumes that gaps are closed was made for the 3-D closure head to determine the fundamental frequencies which were then used to provide guidance from which the size of the integration time step range of structural damping in the nonlinear dynamic response analysis are selected. The 3-D dynamic response analysis itself, which includes complex nonlinearities and is described in Section 4.0 of Reference Q001.596-1, is otherwise independent of the normal mode analysis approach.

| 60

Question 001.607

Provide an explanation of the analysis in Appendix A of the response to 001.540, involving "minimum possible" shear ring properties. Explain the large plastic deformations and large negative safety margins. Indicate the purpose of this analysis.

Response:

The words "minimum possible" were intended to mean something more restrictive than what these words mean in general. The "minimum possible" shear ring yield properties were those analytically derived during the conceptual design studies in mid-1974 and described in the response to Question 001.595. Later, scale model shear ring tests were conducted (described in the Addendum to the response to Question 001.540 which indicated 160 that the experimentally derived yield forces are significantly higher than the previous analytically derived values. As a result of the differing analytical and test results, the preliminary analysis used both the values (high and low) only to provide an indicator of the range of system responses possible under such assumptions. The experimental (higher) value is included in the analysis described in the main body of the Addendum to the response to Question 001.540, while the initial analytical 160 (lower) value is included in the Appendix A of the same addendum.

Question 001.608

The experimental program at Stanford Research Institute, planned to verify the response of the upper portion of the CRBRP reactor structure, i.e., rotating plugs, reactor head, shear rings, hold down system, upper internal structure, etc., is outlined in Section 1.5.2.9 of the PSAR. Provide in the PSAR the details (sketches or drawings) of the designs to be tested, the loads, the matrix and sequence of tests, the parameters to be studied, the expected accomplishments, and the way the experimental output data will be used to justify the current head design, assuming a 661 MW-sec structural design basis load and a 1200 MW-sec maximum load.

Response:

The CRBRP Project has consolidated all considerations given Hypothetical Core Disruptive Accidents into report CRBRP-3 (References 10a and 10b, PSAR Section 1.6) and its associated references; consequently, PSAR Appendices D and F have been withdrawn in Amendments 24 and 60 respectively. The response to this question is now found in Reference 14, PSAR Section 1.6. 60 | 61

Question 001.609

Provide an outline of the 3-D analysis of the reactor vessel head-shear-ring structure under the CDA load of 1200 MW-sec currently being performed. Include details of the structural idealization (i.e., finite element model); material properties, load distribution, nonlinear assumptions, analysis methodology, and computer codes.

Response:

Reference Q001.609-1 identifies the CRBRP Project position that SMBDB (Third Level Structural Margin) requirements based on an energetic release of 661 MJ provide a reasonable enveloping of HCDA uncertainties. Reference Q001.609-1 further notes that following additional review of the subject, the NRC staff could form a basis for accepting the 661 MJ value. Until the results of the staff review of the Project position are known, the Project considers redesign or analysis based on any energetic release other than 661 MJ to be inappropriate. Consistent with that position, a 3-D analysis of the reactor vessel head shear-ring structure under an HCDA load of 1200 MJ has not been initiated.

| 60

| 60

References:

- Q001.609-1: Letter from R.S. Boyd (NRC) to L.W. Caffey (ERDA), "Implementation of CRBRP 1200 MJ 'Appeal Decision'" dated December 6, 1976.

Question 001.610

Additional descriptive information on the SRI test program is required as indicated:

- (a) Provide drawings of the test models to be used for all phases of testing.
- (b) Provide a technical discussion of the scaling laws and parameters being scaled, and indicate what criteria for acceptability are being used to judge success. Include in this discussion not only the vessel head and its details but the in-vessel components and structures, and nozzle simulation.
- (c) Provide the detailed test plan for all planned tests including a full discussion of the source simulation. Discuss how it relates to the fuel vapor expansion and the NRC specified source term (1200 MJ).
- (d) Provide detailed locations of test instrumentation, descriptions of the response characteristics and data recording. Describe how these locations and recorded data will allow an independent study to be made of the energy distribution.
- (e) Describe the measurements to be taken at the vessel support to verify the loads transmitted to the supports.
- (f) For each test plan discuss all material selections, basis and dynamic properties.
- (g) Indicate if high speed photography will be taken of the experiments and whether the displaced water will be measured.

Response:

The CRBRP Project has consolidated all considerations given Hypothetical Core Disruptive Accidents into report CRBRP-3 (References 10a and 10b, PSAR Section 1.6) and its associated references; consequently, PSAR Appendices D and F have been withdrawn in Amendments 24 and 60 respectively. The response to this question is now found in Section 5.4.2.4 of Reference 10a and 14, PSAR Section 1.6.

Question 001.611

Provide the material properties to be used in the scale tests and indicate how the scale factors were derived. Specifically describe how the shear rings, the shear ring attachment mechanism, and the gaps are to be modeled at 1/20 scale with particular emphasis how the size, material properties and dynamic effects are being modeled. Discuss the plans, if any, to confirm the hydrodynamic-structural response of the 1/20 scale model using a larger model (e.g., 1/10 scale). In a 1/20 scale model small deviations in (1) dimensions (tolerances), (2) the variability in materials or, (3) geometry can produce a response which is not prototypic of the full scale model. Specifically, the shear ring has a nominal dimension of 3-1/2 inches; at 1/20 scale the ring will be 0.175 inches. If one has a 0.005 inch machining tolerance on 4 surfaces this could amount to a 10% change in mechanical simulation. Justify the lack of larger scale tests in this respect.

Response:

For definition of material properties and derivation of scale factors, see the response to Q001.610, parts (b) and (f). No plan is being considered to investigate experimentally the effect of scaling on hydrodynamic structural response as this effect was investigated in the SRI-FFTF series of tests. These tests showed a close similitude of response between 1/30th and 1/10th scale models.

The tolerances used in the scale models are shown on the drawings transmitted to NRC in Reference Q001-611-1. These drawings show that the tolerances around the shear rings are much tighter than those implied in the question. For example, the large shear ring has an interference fit of 0.5 mil with respect to the slot into which it fits (see Note 2 of drawing 1635F16). In addition, when the model is assembled, the shear ring gap is adjusted to 6.0 ± 1.0 mils (see drawing 766J828) by shimming. This latter adjustment is much more important in defining the tolerance held on the gap than prior machining procedures. Such a tolerance will be representative of the scaled-up tolerance on the prototypic head and hence mechanical similitude can be maintained. Since mechanical similitude can be maintained at 1/20 scale, larger scale simulation is unnecessary.

Reference:

Q001.611-1 Letter from A. R. Buhl to R. S. Boyd, "SRI Test Scale Model Drawings", Docket No. 50-537, April 7, 1977.

Question 001.612

Clarify the purpose of the phase II SRI tests (Amendment 34, page 1.5-461, SM-1), and elaborate on what these tests will demonstrate in the absence of a dynamic loading.

Response:

The CRBRP Project has consolidated all considerations given Hypothetical Core Disruptive Accidents into report CRBRP-3 (References 10a and 10b, PSAR Section 1.6) and its associated references; consequently, PSAR Appendices D and F have been withdrawn in Amendments 24 and 60 respectively. The response to this question is now found in Section 5.4.2.4 of Reference 10a and 14, PSAR Section 1.6.

60 | 61

Question 001.613

Provide a detailed schedule of tests SM-1 through SM-6 and specify your schedule for providing the results to the NRC staff.

Response:

The results of the test program are provided in Reference 14, PSAR Section 1.6.

60

Amend. 60
Feb. 1981

Q001,613-1

Question 001.614

Indicate if any complex model or system tests, which include components in the PHTS as well as the reactor, will be undertaken.

Response:

There is no plan to perform complex model or system tests that include the primary heat transport system.

Amend. 60
Feb. 1981

Question 001.615

The Third Level Thermal Margin Report, dated April 22, 1976, and its updating supplement, dated November 5, 1976, describe features which you propose to incorporate in the CRBRP design to "mitigate the results of postulated events beyond the design basis" (Class 9 events). The report states that provision of Third Level Thermal Margin is consistent with the design philosophy of defense-in-depth. In the NRC's defense-in-depth concept, the third level of safety consists of features that provide margins in the plant design, in addition to the first and second levels of safety, to protect the public even in the event of the occurrence of very unlikely accidents. These margins are examined primarily by evaluating the response of the plant to so-called design basis accidents. Such evaluations provide the basis for the incorporation of additional plant features and equipment in the plant design for protecting public health and safety.

In its present form, the Third Level Thermal Margin Report fails to put the design features described therein into the proper perspective. Provide clarification regarding your "Third Level Thermal Margin" philosophy in relation to the third level of safety in the NRC's defense-in-depth concept. Identify (a) those design features which are engineered safety features required to mitigate the consequence of design basis accidents, and (b) those features which will be provided solely to accommodate postulated events beyond the design basis. Indicate (i) the operational chronology of the systems identified in category (b) above, (ii) the capability for identifying accidents beyond the design basis and (iii) the procedures for initiating these systems.

Response:

The nomenclature used by the CRBRP Project has been changed since the Third Level Thermal Margin (TLTM) Report was submitted. The third level of design now includes the accommodation of the most limiting accidents within the design base. This is consistent with NRC's defense-in-depth concept (See Chapter 1.0 of the PSAR). Events beyond the design base, such as hypothetical core disruptive accidents, are accommodated by features associated with Structural Margin Beyond the Design Base (SMBDB) and Thermal Margin Beyond the Design Base (TMBDB). These are discussed in detail in CRBRP-3, Volumes 1 (Reference 10a of PSAR Section 1.6) and 2 (Reference 10b of PSAR Section 1.6) respectively. The differentiation of features between those incorporated for design basis accidents and augmented for TMBDB, and those features incorporated solely for TMBDB is indicated in Figure 1-1 of CRBRP-3, Volume 2. The instrumentation requirements, system initiation requirements and operator actions associated with the Thermal Margin Beyond the Design Base features are discussed in Sections 2.1 and 2.3 of Volume 2 of CRBRP-3. This report supersedes the TLTM Report, including its supplement.

Question 001.616

Provide the specific design criteria (i.e., redundancy, seismic requirements, safety class, quality group, testing requirements and the functional design requirements (i.e., pressure, temperature, flow rate, heat rate, environmental qualification) for the systems identified in part (b) of Item 001.615 above.

Response:

The information requested will be found in CRBRP-3, Volume 2 (Reference 10b of PSAR Section 1.6), Section 2.1, except for testing requirements which have not yet been established.

Question 001.617

In our December 30, 1975 request for additional information, the items delineated below were submitted as part of our review of the CRBRP proposed Parallel Design Ex-Vessel Core Catcher (EVCC). The concerns addressed in these items are equally valid for the Third Level Thermal Margin (TLTM) concept which proposes that the limestone structural concrete function as the core retention material, rather than an EVCC magnesia sacrificial bed. Accordingly, provide responses to each of these items in the context of utilizing concrete instead of a sacrificial bed coupled with an external cooling system.

Item Numbers from 12/30/75 Letter

- | | |
|-------------|--------------|
| (1) 001.505 | (6) 001.520 |
| (2) 001.509 | (7) 001.523 |
| (3) 001.511 | (8) 001.524 |
| (4) 001.512 | (9) 001.525 |
| (5) 001.519 | (10) 001.535 |

Response:

The information pertinent to these questions will be found in CRBRP-3, Volume 2 (Reference 10b of PSAR Section 1.6), Sections 3.1.4, 3.2.1, 3.2.2 and 3.2.3 and Appendices A.3, C.1, C.3, F.5 and G.1.A.

Questions 001.509, 001.519, 001.520 and 001.523 are not applicable because they refer to details of an ex-vessel core catcher which is not part of the design. However, structural evaluations (3.2.2 and 3.2.3) and materials properties (C.1.4 and C.3) are provided for the current design.

The assessment of the effect of various reactor vessel and guard vessel penetration times is provided in Section 3.1.4 and Appendix F.5 (Question 001.505).

Parametric studies have been conducted (3.2.3) to bracket effects of uncertainties in the analyses such as concrete cracking effects, heat transfer coefficients and upward and downward heat splits (Questions 001.511, 001.512 and 001.525).

The CACECO code (A.3) calculates the sodium vapor pressure as a function of average pool temperature, which, because of the pool depth and high sodium conductivity, would approximate the pool surface temperature (Question 001.524).

Debris bed self-leveling (3.2.1 and G.1.A) would limit any asymmetric heating effects to a short time period in the initial time period of the accident. Such effects would be minimal because of the large sodium-to-fuel ratio (Question 001.535).

Question 001.618

The TLTM concept, which relies on the inherent retention capability of the reactor containment building (RCB), involves complex studies of material interactions and predictions of structural behavior of concrete under very severe conditions. These are presently large uncertainties associated with these evaluations. The staff's review of the published Project and/or ERDA R&D in the area of molten core technology indicates that the work has been largely preliminary in nature and confined to establishing important phenomenological aspects in the areas of material interactions and heat transfer. This preliminary R&D does not satisfy our licensing needs. Accordingly, provide a detailed description of your proposed R&D plans, as well as a schedule for completion, for demonstrating the adequacy of your TLTM concept to safely contain a core melt-through accident consistent with the staff requirements as stated in our May 6, 1976 letter to the Project. As indicated in our October 8, 1976 letter the staff would like to meet with the Project to discuss its R&D plans in detail. In the event that the required R&D associated with the TLTM concept cannot be performed on a schedule consistent with CRBRP licensing, provide a description of the positive measures for protection against core meltdown and associated R&D which the Project intends to implement.

Response:

The R&D programs associated with the Thermal Margin Beyond the Design Base will be found in CRBRP-3, Volume 2 (Reference 10b of PSAR Section 1.6), Appendix A.

Question 001.619

Based on our review of the very limited experimental information with small quantities of molten materials (~2kg), you have not adequately justified your assumptions that the molten fuel/steel mixture will fragment, self-level, and attain a coolable debris-bed configuration on the lower reactor cavity floor following melt-through of the reactor and guard vessels. In order for the staff to agree with these assumptions, these phenomena would have to be demonstrated by the conduct of sufficiently large-scale experiments utilizing large quantities of molten materials. Provide your R&D plans for conducting such experiments. In the absence of such experimental results, provide an analysis of the pressure-temperature-hydrogen time history of the containment and penetration into the concrete basemat assuming that the core debris remains in a molten pool form following melt-through of the reactor and guard vessels. Various initial molten pool configurations should be assumed on the lower reactor cavity concrete floor. Your analysis should provide a complete description of assumptions, modeling techniques, and experimental validation.

Response:

Pertinent information will be found in CRBRP-3, Volume 2 (Reference 10b of PSAR Section 1.6), Sections 3.1.1, 3.1.2, 3.2.1, 3.2.2 and 3.2.3 and Appendix G.1.

Sections 3.1.1, 3.1.2, 3.2.1, 3.2.2 and Appendix G.1 present information on fuel debris distributions, debris-bed characteristics, and supporting data. Data on bed leveling, while supportive of the thesis that leveling will occur, has been obtained for relatively small quantities of material only. However, as demonstrated in Appendix G.1, the base scenario is not highly sensitive to leveling, and configurations substantially different from level beds can be readily accommodated.

Analyses prior to sodium boil-dry, following penetration of the reactor vessel and guard vessel, of a molten pool attack on concrete and large scale experiments are not considered necessary since the available data support the coolability of the debris bed. Analyses prior to sodium boil-dry are contained in Sections 3.2.1 and 3.2.2.

Analysis after sodium boil-dry (where a molten pool attack on concrete would occur) are sufficiently conservative and include a large enough variation in the key parameters to encompass all reasonable pool configurations and preclude the need for experimental validation (Section 3.2.3).

Question 001.620

Our review of the core debris/concrete material interactions associated with your TLTM concept indicates a considerable amount of uncertainty because of lack of sufficiently large-scale, prototypic test data for the areas delineated below. For each of these areas, experimental data is crucial to evaluating the safety adequacy of the TLTM concept. For each of these areas, provide the following information where applicable: (1) present test data which you are utilizing to support your TLTM concept, including a description of the experiments; (2) description of future planned R&D; (3) comparison of model predictions to measured test results; and (4) parametric sensitivity studies which show how variations in these parameters affect both the response (pressure-temperature-hydrogen history) of the RCB and the penetration into the concrete basemat.

It should be noted that the general areas of concern listed below are delineated further in subsequent questions in conjunction with specific staff concerns associated with your overall assessment of the RCB melt-down accident:

- (1) Gas and Water Vapor Generation (Rates, Quantity, Species)
- (2) Types of Chemical Reactions and Reaction Products
- (3) Heats of Exothermic Chemical Reactions
- (4) Extent of Particulation, Leveling, and Coolable Debris Bed Formation
- (5) Eutectic Melt/Freezing Temperatures
- (6) Core Debris Penetration Mode (Rate & Depth)
- (7) Mixing and Solubility Rates
- (8) Crust Formation, Inversion, and Flotation Processes
- (9) Heat Transfer Splits (Upward/Downward/Radial)
- (10) Heat & Mass Balances
- (11) Hydrogen Formation & Disposition (Recombination, Burning, Explosions)
- (12) Steam Explosions (refer to Item 001.648)
- (13) Structural Effects (Erosion, Cracking, Spallation)
- (14) High-Temperature Physical, Thermal and Structural Properties of Interaction Materials

Item (11) Hydrogen Formation and Disposition

- (a) Test data employed are located in Appendix H.1. A description of the experiments can be obtained from the cited References.
- (b) Future planned R&D is defined in Appendix A.2.
- (c) Appendix A.3 identifies a planned development program that will compare the model predictions to measured test results.
- (d) Appendix H.1 provides sensitivity studies.

Item (12) Steam Explosions

Steam explosions would be precluded as discussed in Section 3.2.1.

Item (13) Structural Effects (Erosion, Cracking, Spallation)

Sections 3.2.2.5, 3.2.3.3 and Appendix C.3 discuss the structural effects of erosion, cracking and spallation of concrete. Planned R&D can be found in Appendices A.1, A.4 and A.6.

Item (14) High Temperature Physical, Thermal and Structural Properties of Interaction Materials

Appendices C.1, C.2 and C.3 address the high temperature properties of the interaction materials. Planned R&D can be found in Appendices A.1, A.4, A.5 and A.6.

Item (15) Structural Acceptance Criteria, Including Failure Modes and Appropriate Analysis Methods

Sections 3.2.2.5, 3.2.3.3 and Appendix C.3 discuss the various structural acceptance criteria, failure modes and analysis methods.

Question 001.621

With respect to the 1000 scc/sec reactor head leak during the first 1000 sec., provide an evaluation of the consequences of higher leak rates. Provide a description of any R&D to confirm your proposed leak rate.

Response:

The information requested concerning higher leak rates will be found in CRBRP-3, Volume 2 (Reference 10b of PSAR Section 1.6), Sections 4.1.2 and 4.2.2 and Appendix G.4.

Tests describing leak rate verification through the Reactor Vessel Closure Head can be found in Section 5.4.1.5 of CRBRP-3, Volume 1 (Reference 10a of PSAR Section 1.6), Revision 2.

Question 001.622

Clarify the apparent discrepancy between the TLTM report which specifies that the reactor cavity (RC) leaks at 100 volume percent at 15 psig and the PSAR which specifies 100 volume percent at 35 psig. In addition to the pressure differential, provide the temperature for each leak rate specification.

Response:

The PSAR was correct at that time since it represented a stage of design evolution beyond that found in the TLTM Report; however the question is irrelevant to CRBRP-3, Volume 2 (Reference 10b of PSAR Section 1.6), because the current design includes a planned vent path between the reactor cavity and the reactor containment building. Information regarding reactor cavity leakage will be found in CRBRP-3 Volume 2 Sections 2.1.2.1, 2.1.2.6, 2.2.6 and 3.2.1 and Appendix C.1.3.

Sections 2.1.2.1 and 2.1.2.6 describe the reactor cavity leakage and vent requirements. Section 2.2.6 describes the reactor cavity vent design. Section 3.2.1 and Appendix C.1.3 present analyses results and assumptions.

Question 001.623

In addition to providing a steam and CO₂ vent system for the reactor cavity and the Primary Heat-Transport System (PHTS) pipeway cell liners, confirm whether the PHTS cells and the in-containment primary sodium storage tank cell also have a cell liner vent system. If a cell liner vent system is not provided for these cells, provide your justification.

Response:

The Primary Heat Transport System (PHTS) cells and the in-containment Primary Sodium Storage Tank Cell have cell liner venting systems. Cell liner venting is described in Section 3A.8 of the PSAR.

Question 001.624

Provide an evaluation of the consequences of clogging of both the RC to RCB vent lines and the RC liner vent pipes by solid reaction products resulting from sodium and core debris interactions with concrete, which could occur immediately after guard vessel melt-through. Include a description of any tests which will be performed to establish the extent of clogging.

Response:

The response to the question regarding the effects of blockages in the RC to RCB vent lines is discussed in Sections 2.2.6 and G.3 of CRBRP-3, Volume 2 (Reference 10b of PSAR Section 1.6).

The sodium and core debris interaction with the concrete would only affect the reactor cavity floor liner which is assumed to immediately fail following a guard vessel melt-through. In this case, the function of the cell liner is not necessary anymore, since no protection is needed for the failed floor liner. Additionally, liner vent pipes are provided with loop seals to prevent escape of sodium vapor from the cavity area into the cells below the operating floor (see Section 2.2.5.3 of CRBRP-3, Volume 2). Also, the cell liner walls are provided with baffles (see Figure 3.34 of CRBRP-3, Volume 2) to inhibit any sodium and core debris interaction with concrete from penetrating around the wall liner to the cells below the operating floor.

Question 001.625

Provide an evaluation of the consequences of failure of the RC liner vent system pipes. Provide your structural evaluation to show that structural integrity of these pipes is maintained. Include consideration of loads caused by: (1) high temperature transients, and (2) weight of degraded concrete resulting from cracking.

Response:

Structural evaluations and considerations of loads on the RC liner vent system pipes are provided in Section 2.2.5 of the CRBRP-3, Volume 2 (Reference 10b of PSAR Section 1.6).

Evaluation of consequences of failure of the RC liner vent system pipes have not been performed due to design redundancy and margins inherent in the system which indicate that total failure of this system is not probable.

Question 001.626

Provide a justification for the statement that steam and CO₂ from the reactor cavity bottom and submerged wall liners are vented directly above the operating floor so that, in the event those bottom liners fail, the steam, CO₂ and sodium reaction products would not enter the cavity. Include an evaluation of the consequences of RC submerged wall liner failure resulting in the steam, CO₂ and sodium reaction products being introduced into the RC instead of being vented.

Response:

This question is not entirely relevant to the design as described in CRBRP-3 Volume 2. However, related information will be found in CRBRP-3, Volume 2 (Reference 10b of PSAR Section 1.6), Sections 2.1.2.4, 2.1.2.5, 2.2.4, 2.2.5, 3.2.1 and 3.2.2 and Appendix F.7.

Sections 2.1.2.5 and 2.2.5 discuss the design requirements and design description of the reactor cavity liner venting system. Note that the design provides venting from the reactor cavity floor to containment. Sections 2.1.2.4 and 2.2.4 provide requirements and design details of the physical barriers separating various liner segments.

Sections 3.2.1 and 3.2.2 provide detail results of the consequences of various reactor cavity liner failures. Appendix F.7 provides further detail on the sensitivity of containment conditions to liner failure times. After liner failure, gases released from the concrete and the reaction products are considered to be released to the reactor cavity.

Question 001.627

Explain in more detail the purpose and design of the RC vapor barriers, including a materials description.

Response:

The response to this question is provided in Section 2.2.4 of the CRBRP-3, Volume 2 (Reference 10b of PSAR Section 1.6).

Question 001.628

Explain in more detail and provide a design of the special reinforcing truss bars that tie the degraded concrete to the non-degraded concrete. Include a justification that the degraded concrete will not impose additional loads on the liner.

Response:

The special reinforcing truss bars have been deleted. The response to this question with regard to the degraded concrete imposing additional loads on the liner is provided in Section 2.2.5 of the CRBRP-3, Volume 2 (Reference 10b of PSAR Section 1.6).

Question 001.629

For your proposed liner vent system, the steam and CO₂ will have to travel a large distance in the 1/4 inch gap. Provide an evaluation as to the adequacy of this gap size under the TLTM pressure and temperature conditions.

Response:

The response to this question is provided in Section 2.2.5 of the CRBRP-3, Volume 2 (Reference 10b of PSAR Section 1.6).

Question 001.630

Provide the bases for the 19 ft. submerged liner assumption, including consideration of the effects of local gas pressurization in the reactor vessel causing the level outside the vessel to rise.

Response:

The information requested will be found in CRBRP-3, Volume 2 (Reference 10b of PSAR Section 1.6), Section 3.2.2. The horizontal baffle behind the reactor cavity wall liner, previously at the 19 foot level, has been raised to an elevation of 26 feet above the reactor cavity floor. This was done to accommodate the possible pressurization of the reactor vessel relative to the reactor cavity atmosphere.

Question 001.631

With respect to your structural analyses of the RC and RCB, we have the following concerns:

- (1) The conclusion (TLTM Report Section 2.7.2) that the reactor cavity, including the reactor closure head and vessel support ledge, retains its structural capability for 215 hours could presumably be used as a basis to claim satisfaction of the staff requirement for 24 hour containment system integrity in a conservative manner and with a high degree of confidence. The conclusion of 215 hours is not adequately substantiated and any conclusions regarding 24 hours are therefore also not substantiated. Please provide structural analyses, including analysis methods, assumptions, structural acceptance criteria, materials properties, and loading combinations. Include consideration of the structural effects of core debris remaining in a molten pool form and attacking the concrete immediately following reactor vessel melt-through.
- (2) Likewise, you have not adequately substantiated your conclusion (TLTM Report Section 2.7.1) that the RCB retains its structural integrity indefinitely, and we could not, therefore, conclude that you meet our requirement for 24 hour containment system integrity in a conservative manner and with a high degree of confidence. Please provide structural analyses, including analysis methods, assumptions, structural acceptance criteria, materials properties, and loading combinations. Include consideration of the structural effects of core debris remaining in a molten pool form and attacking the concrete immediately following reactor vessel melt-through.

Response:

Structural analyses are provided in Sections 3.2.2, 3.2.3 and C.3 of CRBRP-3, Volume 2 (Reference 10b of PSAR Section 1.6).

This response does not include consideration of core debris remaining in a molten pool because of reasons stated in the response to Question Q001.619.

Question 001.632

Provide a description and design of the steel expansion joints, which are referred to in Figure B7 but are not shown there. Describe the potential leak paths referred to. Provide an evaluation of the consequences of collapse of the reactor cavity (as stated on page II-30 of the TLTM report) for times less than 215 hours, including consideration of the associated impact loads on the RCB basemat.

Response:

The steel expansion joint referred to has been deleted from the TMBDB design. This design feature has been replaced by a steel liner on the exterior of the reactor cavity wall which will function to prevent sodium that may leak through wall cracks from reaching Cell 105. The potential leak paths are the wall cracks which will be the result of the high bending moment and radial shear forces acting at the base of the Reactor Cavity and at other restraints. As described in Section 3.2.2.5.1.2 of CRBRP-3, Volume 2 (Reference 10b, PSAR Section 1.6) no collapse of the Reactor Cavity is expected before sodium boil dry.

Question 001.633

Provide the evaluations which support your conclusion that melt-through times ranging from 100 to 10,000 seconds do not affect the TLTM accident scenario. Include the effects of rate dependent phenomena, as well as total energy deposition considerations as discussed in your response to Item 001.505.

Response:

The information requested will be found in CRBRP-3, Volume 2 (Reference 10b of PSAR Section 1.6), Section 3.1.4 and Appendix F.5 which provide an evaluation of reactor vessel and guard vessel penetration times ranging from 100 to 10,000 seconds.

Question 001.634

The pressure in the RC is capable of pushing sodium through the failed liner, up the liner vent line, and out into the RCB prior to RC venting. Provide an evaluation of this event, including specifically the consequences of a sodium spray fire in the RCB.

Response:

The question is not entirely relevant to the design as described in CRBRP-3, Volume 2 (Reference 10b of PSAR Section 1.6). However, related information will be found in Sections 2.1.2.4, 2.1.2.5, 2.2.4, 2.2.5 and Appendix G.4.

Sections 2.1.2.4, 2.1.2.5, 2.2.4 and 2.2.5 provide details of the requirements and design features of the reactor cavity and pipeway cell liners and the respective liner vent system.

Appendix G.4 provides results describing the sensitivity of containment from a thermal standpoint to various assumed head leak rates (i.e. simulating a spray fire).

Question 001.635

The manner in which the core debris and sodium penetrate the reactor and guard vessels and spill onto the cavity floor has not been discussed in the TLTM report. These effects are important in determining the initial conditions in the reactor cavity. Provide a discussion of the consideration that has been given to these effects, as well as a description of your proposed R&D program in this area.

Response:

The information requested will be found in CRBRP-3, Volume 2 (Reference 10b of PSAR Section 1.6), Sections 3.1.4, 3.2.1 and 3.2.2 and Appendices B, C.1, G.1 and F.

Sections 3.1.4, 3.2.1, 3.2.2 and Appendix G.1 present information on core debris behavior considerations after melt through.

Appendix B discusses the basis for the assumed vessel penetration time.

Sections 3.2.1, 3.2.2 and Appendix C.1 contain information on other key assumptions concerning reactor cavity initial conditions.

Appendix F provides sensitivity analyses for a range of assumed initial conditions.

Question 001.636

With regard to fuel melting through the PHTS piping, we have the following information needs:

- (1) Provide the justification necessary to support your assumption that fuel which melts through the PHTS piping will not cause PHTS cell liner failure and will not affect the TLTM accident scenario.
- (2) For the fuel which penetrates the piping in the PHTS pipe chase ways, provide an evaluation of the penetration depth, effect on RCB response, and structural consequences on the chase ways due to the existence of high temperatures and cracking in the concrete.
- (3) The TLTM report states that a separate analysis has been made to determine the consequences of the scenario where fuel is assumed to melt through the PHTS piping into the PHTS cells, including an assessment of cell structural capability. Provide this separate analysis.

Response:

The information requested will be found in CRBRP-3, Volume 2 (Reference 10b of PSAR Section 1.6), Appendices F.7 and I. Appendix I addresses the consequences of fuel in the PHTS piping. Appendix F.7 addresses the consequences of earlier liner failure times in the pipeway cells, which might result from fuel penetrating the piping in this area.

Item 3 has not been addressed because the analyses in Appendix I show that the piping in the PHTS cell would not melt during the nominal case, and the PHTS cell liner would not be penetrated for a range of more severe assumptions.

Question 001.637

During normal operation a considerable amount of water will be released from the concrete. Explain in more detail how this water release is accounted for in your TLTM analyses.

Response:

The information requested will be found in CRBRP-3, Volume 2 (Reference 10b of PSAR Section 1.6), Section 2.2.5 and Appendix C.1.4.

Section 2.2.5 describes the design features provided for the removal of water that would be released from heated concrete. Appendix C.1.4 provides the experimental basis for concrete water release.

Question 001.638

For the case where only the reactor vessel sodium (740,000 lbs.) drains into the reactor cavity, provide your evaluation of this scenario, including the effect on core debris penetration into the RC concrete.

Response:

CRBRP-3, Volume 2 (Reference 10b of PSAR Section 1.6), Appendix F.4 "Sensitivity to Sodium Inventory Variations" shows that the containment conditions are not very sensitive to the initial amount of sodium that drains into the reactor cavity.

Core debris behavior after vessel penetration is described in Sections 3.2.1 and 3.2.2 and Appendix G.1.

Question 001.639

If melt-through takes longer than 1000 sec., initial sodium temperatures in excess of 1075°F can be experienced in the RC. Provide an evaluation of the consequences of higher initial sodium temperatures up to and including boiling in the RC. Include an assessment of the radiological consequences.

Response:

The information requested will be found in CRBRP-3, Volume 2 (Reference 10b of PSAR Section 1.6), Section 3.1.4 and Appendix F.5.

Section 3.1.4 and Appendix F.5 discuss penetration times of 100 to 10,000 seconds. The containment conditions were found not to be sensitive to the penetration times investigated. Although the associated sodium temperature did not reach boiling at the time of penetration in these cases, similar results would be expected for higher sodium temperatures up to the boiling point. Since the containment conditions are not sensitive to the penetration time, venting and purging conditions would also be similar. Therefore the radiological consequences would not be sensitive to the penetration times investigated.

Question 001.640

Clarify whether the TLTM features are designed to Seismic Category I requirements and whether such features are located in Seismic Category I buildings. Provide an explanation of why the building, which houses the RCB Filtration System and the Annulus Air Cooling System, is not on a common basemat with the other Seismic Category I buildings. (you may wish to coordinate this response with Item 001.615).

Response:

The response to this question is provided in Sections 2.1.1 and 2.2.11 of the CRBRP-3, Volume 2 (Reference 10b of PSAR Section 1.6).

TMBDB features are designed to Safety Class 3 and Seismic Category I requirements.

Question 001.641

Your TLTM report states, "A substantial part of the lower reactor cavity wall would be melted or heated excessively and it would be expected to fail." Provide the evaluation of the failure time, as well as the consequence of RC failure on the RCB. In this context, your Parallel Design core catcher incorporated a Separator Dome and a Core Debris Receptacle, both of which would improve the core debris retention effectiveness and decrease the heat load on the RC walls (i.e., the Separator Dome would tend to improve spreading of the core debris and the Core Debris Receptacle would increase the radial thickness of concrete for retaining the lateral penetration of core debris). Include a discussion of the consideration that has been given to incorporating these features into your TLTM concept. (You may wish to coordinate this response with Items 001.631 and 001.632).

Response:

The structural analyses for the TMBDB scenario are provided in CRBRP-3, Volume 2 (Reference 10b of PSAR Section 1.6), Sections 3.2.2 and 3.2.3. The methods and data are provided in Appendix C.3. The results of these analyses indicate that venting of containment would not be required for at least 24 hours and containment capability above the basemat would be maintained indefinitely. Therefore, the additional features noted in the question are not required.

Question 001.642

Provide your structural evaluation to support your claim that basemat integrity is maintained while the core debris is penetrating RC floor concrete. Include structural evaluations of the basemat for the scenario outlined in Item 001.619 where core debris fragmentation does not occur. (You may wish to coordinate this response with Item 001.631).

Response:

The response to this question is provided in Sections 3.2.2, 3.2.3.1, 3.2.3.2 and 4.3 of the CRBRP-3, Volume 2 (Reference 10b of PSAR Section 1.6).

See also the response to Question Q001.619.

Question 001.643

The temperature profiles in the concrete basemat indicate that a significant amount of heat is being taken out of the molten pool at the sidewalls. Provide a discussion of what is providing the energy sink. Indicate what fraction of the decay heat goes neither up nor down but radially outward. For a given upward/downward split in the molten pool decay power, provide an explanation of how the radial heat transfer is determined.

Response:

The post sodium boildry analyses are provided in CRBRP-3, Volume 2 (Reference 10b of PSAR Section 1.6), Section 3.2.3. The model and data base are provided in Appendix C.2.

Question 001.644

The fuel debris when spread evenly over the floor of the 40 ft. diameter RC creates a layer less than one inch thick. Provide the evidence that exists which supports this extent of self-leveling, including the consideration that has been given to the influence of sodium sub-cooling and the guard vessel support skirt on the self-leveling tendency. (You may wish to coordinate this response with Item 001.619.)

Response:

The information requested will be found in CRBRP-3, Volume 2 (Reference 10b of PSAR Section 1.6), Sections 2.1.2.3, 2.2.3, 3.2.1 and 3.2.2 and Appendix G.1.

Sections 2.1.2.3 and 2.2.3 present the requirements and design configuration for the guard vessel support skirt, which were developed to allow for flow of material outside the guard vessel support skirt and across the entire reactor cavity floor.

Sections 3.2.1 and 3.2.2 describe the debris behavior after vessel penetration. Appendix G.1 contains a sensitivity study which demonstrates that the base scenario is not highly sensitive to leveling of the debris bed.

Question 001.645

Your CACECO modeling in TLTM is confined to sodium-concrete reactions when, in fact, fuel is also present to interact with concrete. Provide the evidence that CACECO is able to predict the results of sodium/fuel/concrete interactions.

Response:

The information requested will be found in CRBRP-3, Volume 2 (Reference 10b of PSAR Section 1.6), Sections 3.2.1 and 3.2.2 and Appendices C.1.2, C.2 and G.1.

Sections 3.2.1, 3.2.2 and Appendix G.1 discuss core debris behavior after vessel penetration. These sections provide the basis for debris bed coolability before sodium boil-dry. Coolability would preclude any significant molten fuel concrete interactions prior to sodium boil-dry.

Sections 3.2.2 and Appendix C.2 provide the experimental basis for non-energetic fuel/concrete interactions.

Appendix C.1.2 provides the experimental basis for sodium/concrete interactions.

Question 001.646

Provide an evaluation of the RCB pressure-temperature-hydrogen history and molten pool penetration into the basemat for conditions where concrete cracking and spallation occur resulting in increased exposure of concrete to sodium and core debris. This should include the effects of increased water vapor and CO₂ releases that will occur in the presence of concrete cracking. Also include an evaluation of the sensitivity of the RCB response and the basemat penetration to the extent of concrete cracking and spallation.

Response:

The information requested will be found in CRBRP-3, Volume 2 (Reference 10b of PSAR Section 1.6), Section 3.2.3 and Appendices G.2, C.1 and C.2 and in the response to Question 001.654.

The consequences of increased sodium-concrete penetration rate and the extent of penetration due to sodium-concrete interaction during the TMBDB scenario prior to sodium boil-dry are provided in Appendix G.2 and discussed in the response to Question 001.654. During this pre-boil-dry phase, experimental results show that all of the CO₂ released from the concrete reacts with the sodium pool, so that CO₂ is not a significant contributor to containment pressurization. The exothermic heats of reaction between sodium and CO₂ and sodium and water vapor are included as a heat source in the TMBDB evaluations as indicated in Table C.1-4.

Following boil-dry of the sodium in the reactor cavity the basemat would interact with the remaining molten steel and core debris. This post-boil-dry analysis is presented in Appendix C.2. The rate of penetration of the basemat under post-boil-dry conditions is assumed to be governed by the rate of heat conduction into the concrete and its subsequent melting. Penetration therefore is limited by the amount of energy available for melting concrete. The overall effect of concrete spalling and cracking can be simulated by increasing the percent of the fission product decay power that is assumed to be directed downward into the basemat. This has been accomplished in the model by adjusting the thermal resistance to heat loss from the pool surface to obtain the desired fraction of the decay heat being transferred into the concrete. The melted concrete is assumed to be mixed with the molten steel and core debris. The energy due to the reaction of iron with concrete has not been explicitly included; however, its magnitude is small relative to the decay power and if included would only result in a slight shift in the quoted energy transfer split. The analyses of Appendix C.2 considered a range of 10% to 90% of the decay energy being directed downward which is considered to conservatively cover the range of possible effects of concrete cracking and/or spalling. As additional heat is forced downward, more water vapor and CO₂ are released and reactions from these gases are considered in the analyses discussed in Section 3.2.3.

Question 001.647

A high heat transfer coefficient will develop at the stagnation point of the molten fuel/steel stream impinging on the floor of the RC. This may cause local melting of the floor liner and lead to the development of localized concrete penetration prior to reparticulation by the sodium deluge. Molten fuel in this depression and under the liner may not readily self-level. Provide an evaluation of this proposed accident scenario. (You may wish to coordinate this response with Items 001.619 and 001.644).

Response:

The information requested will be found in CRBRP-3, Volume 2 (Reference 10b of PSAR Section 1.6), Section 3.2.2 and Appendix G.1.

Section 3.2.2 addresses the possibility of liner melting, and Appendix G.1 discusses non-uniform bed distributions and the experimental data that support the assessments.

Question 001,648

Heating of the concrete by the hot core debris can result in water collecting in local pockets and voids within the RC concrete floor. If molten core debris comes in contact with this water, a steam explosion may result. Provide a discussion of the consideration that has been given to this concern, as well as a description of your planned R&D in this area.

Response:

The information requested will be found in CRBRP-3, Volume 2 (Reference 10b of PSAR Section 1.6), Sections 2.1.2.5, 2.2.5 and 3.2.1.

Section 2.1.2.5 describes the reactor cavity and pipeway cell liners vent functional requirements, Section 2.2.5 describes the liner vent design and Section 3.2.1 indicates how the liner vent design prevents accumulation of water and therefore steam explosions.

Question 001.649

Provide a discussion and evaluation of the potential for recriticality to occur if the core debris does not self-level across the entire RC floor and form a particulate debris bed. Various molten core debris configurations should be examined. Include a discussion of why the TLTM concept does not include neutron absorbing material in the lower RC, similar to that proposed for the parallel design EVCC.

Response:

The potential for recriticality in the reactor cavity is addressed in CRBRP-3, Volume 2 (Reference 10b of PSAR Section 1.6), Section 3.2.4.

Question 001.650

If the RC floor liner fails, sodium can reach and react with the RC concrete sidewalls. Provide the justification for not allowing sodium and/or core debris to react with the RC sidewalls. Provide estimates of the pressure-temperature-hydrogen-time history of the RCB if the aforementioned reactions are allowed to occur along the sidewalls of the RC.

Response:

The information requested will be found in CRBRP-3, Volume 2 (Reference 10b of PSAR Section 1.6), Sections 2.1.2.4, 2.2.4, 3.2.1 and 3.2.2.

Sections 2.1.2.4 and 2.2.4 provide the design requirements and associated features that would prevent sodium interaction with the cavity sidewall when the reactor cavity floor liner fails and would limit the interactions when liners in other areas fail.

The analyses in Sections 3.2.1 and 3.2.2 include the effects of various reactor cavity and pipeway cell liner failures.

Question 001.651

Noble gas, volatile, and sodium soluble fission products may be vented from the RC to the RCB following a core melt-through accident. The decay heat associated with these radioisotopes can represent a significant fraction of the total decay heat load. Provide an evaluation of the consequences on the RC and RCB conditions caused by this energy source.

Response:

These effects are included in the analyses in CRBRP-3, Volume 2 (Reference 10b of PSAR Section 1.6), Sections 3.2.1, 3.2.2 and Appendix C.1.2.

Question 001.652

Provide a discussion of the evidence that exists to substantiate your claim that sodium reactions will reparticulate molten fuel, including an evaluation of the consequences if reparticulation does not occur. (You may wish to coordinate this response with Items 001.619, 001.635, and 001.644).

Response:

The information requested will be found in CRBRP-3, Volume 2 (Reference 10b of PSAR Section 1.6), Sections 3.2.1 and 3.2.2 and Appendix G.1. These sections discuss the behavior of fuel debris after vessel penetration and the experimental support for the assessments. An evaluation of consequences assuming reparticulation does not occur was not performed as explained in the response to Question 001.619.

Question 001.653

It is not clear how the chemical reactions associated with molten fuel/ steel interacting with concrete are accounted for in your analyses. Discuss this aspect in more detail. (You may wish to coordinate this response with Item 001.645).

Response:

The information requested will be found in CRBRP-3, Volume 2 (Reference 10b of PSAR Section 1.6), Section 3.2.3 and Appendix C.2.1.

Question 001.654

The assumptions that sodium-concrete reactions will stop after 4 hours due to accumulation of reaction products may not be justified and conservative. The combination of concrete cracking and agitation due to gas and vapor release may enhance the capability of sodium to react with fresh concrete at a rate greater than 1/2 inch per hour and continue to react beyond 4 hours. Provide an evaluation of these concerns as well as planned R&D to quantify these effects.

Response:

The information requested will be found in CRBRP-3, Volume 2 (Reference 10b of PSAR Section 1.6), Section 3.2.3, and Appendices A.1, C.1, and G.2 and is amplified below.

The conclusion that a reaction product barrier would form to limit sodium penetration is based on experiments that show that when limestone concrete is restrained (as it will be in the CRBRP reactor cavity floor) such a barrier consistently forms to limit penetration depth (See Reference C.1-4 of CRBRP-3, Volume 2). Appendix A.1 briefly describes the R&D conducted to further verify the penetration model. The LSC-2 test was a larger scale restrained limestone concrete test (3 ft. x 3 ft. surface area) exposed to sodium at temperatures up to ~1600°F for 100 hours. The penetration was limited to ~3 inches, similar to the penetrations observed in the smaller HEDL tests. Some tests conducted by Sandia Laboratories with unrestrained limestone concrete and by HEDL with other types of concrete (some of which were dehydrated specimens) have indicated that there are situations where the reaction product barrier may not limit penetration. The formation of the reaction product barrier may depend upon the strength of the concrete, with stronger concrete less prone to cracking and penetration. Additional testing is being considered to verify that the reaction product barrier would form reliably in the TMBDB scenario for CRBRP.

Appendix G.2 presents results of sensitivity analyses of containment conditions for more severe sodium-concrete reactions than considered in the base case. The results show that the predicted containment conditions are not very sensitive to the sodium-concrete reaction assumptions. This is due to the fact that the reaction energy from sodium-concrete reactions is a small part of the total energy involved in the scenario from the decay heat, chemical reactions in containment and other chemical reactions in the sodium pool. Adequate margins exist in the design to accommodate the most severe case investigated, which was a penetration rate of 1 inch per hour for 12 hours.

Question 001.655

In addition to the concern raised in Item 001.654, the presence of dense molten fuel may float off the reaction products which are assumed to terminate sodium-concrete reactions in 4 hours. Provide a discussion of the consideration that has been given to this removal process. In addition, even if the fuel is in particulate form, the sodium boiling which it causes may more rapidly remove reaction products than has been observed when sodium alone was poured onto concrete. Provide an evaluation of this concern along with any proposed R&D to quantify these effects.

Response:

Pertinent information will be found in CRBRP-3, Volume 2, (Reference 10b of PSAR Section 1.6), Section 3.2.1 and Appendices A.1, C.1 and G.

Section 3.2.1 (Item 4) shows that the geometric configuration of core debris and sodium on the reactor cavity floor would result in a coolable debris bed. Appendix G.1 provides the experimental bases to support this conclusion and shows that the results are not highly sensitive to bed leveling. Therefore there would be no molten fuel to react with concrete until after sodium boil-dry. Section 3.2.1 (Item 5) discusses the expected behavior of the sodium-concrete reaction products. The sodium-concrete reaction parameters used in this study are based on testing as discussed in Section C.1.2.3. Appendix G.2 provides sensitivity analyses of containment conditions to various sodium-concrete reaction rates. Appendix A.1 presents the planned development tests to confirm the limited extent of sodium-concrete reactions.

Question 001.656

Fuel debris may enter the PHTS and melt-through into the PHTS cells. Provide an evaluation of the pressure-temperature-hydrogen history under conditions of various fuel fractions being introduced into the PHTS cells, as well as the RC, in order to establish whether fuel relocation into the RC is indeed the most severe case. (You may wish to coordinate this response with Item 001.636.)

Response:

The information requested will be found in CRBRP-3, Volume 2 (Reference 10b of PSAR Section 1.6), Appendices F.7 and I. Appendix I assesses the consequences of fuel in the PHTS piping and predicts that melt-through of the piping in the PHTS cells would not occur. Appendix F.7 provides the effect of earlier pipeway cell floor liner failure times, which could result from the penetration of the piping.

Question 001.657

Fuel penetration into concrete is calculated on the basis of heat transfer coefficients derived from quiescent thermal convection heat transfer in a single-phase fluid. Because of gas and vapor generation caused by fuel melting into concrete, the heat transfer rate from the agitated molten pool may be substantially greater than the single-phase pool. Provide an evaluation of this concern as well as planned R&D to quantify this effect.

Response:

The analyses of fuel penetration into concrete will be found in CRBRP-3, Volume 2 (Reference 10b of PSAR Section 1.6), Section 3.2.3. The post sodium boildry model and data base are provided in Appendix C.2.

Question 001.658

Provide a discussion of the effects that shorter melt-through times (i.e., less than 1000 seconds) will have on required operator action to activate the proposed TLTM features. (You may want to coordinate this response with Item 001.633.)

Response:

The information requested will be found in CRBRP-3, Volume 2 (Reference 10b of PSAR Section 1.6), Sections 2.3 and 3.1.4.

Section 3.1.4 addresses the effects of shorter reactor vessel and guard vessel penetration times. It was determined that the effects of shorter penetration times would not significantly impact containment conditions. Consequently no impacts to the operator action sequence described in Section 2.3 have been identified.

Question 001.659

The current analyses are based on the assumption of uniform hydrogen mixing in the RCB. Provide a discussion of the consideration that has been given to the potential for development of locally high concentrations of hydrogen and the attendant possibility of local hydrogen explosions within the RCB. Discuss any planned R&D to address this concern.

Response:

The potential for hydrogen stratification is addressed in CRBRP-3, Volume 2 (Reference 10b of PSAR Section 1.6), Section 3.2.1. The hydrogen control features are considered adequate without additional R&D beyond that defined in Appendix A.2.

Question 001.660

The GROWS code, which models the growth of a molten pool into a melting solid, is being used to predict penetration of core debris into either a sacrificial bed or concrete. Provide the following information in regard to the GROWS code:

- (1) Explain in detail the interface between use of the GROWS and AYER computer codes.
- (2) Provide the criteria used to determine the point at which the molten pool stops growing, including the rationale and specification of the freezing point of the pool material.
- (3) The pool side heat transfer correlations all include a ΔT terms as the driving temperature difference. Provide justification for using the same ΔT magnitude for all the pool surfaces (i.e., bottom, top, and side). Explain and justify the boundary condition which is being used as the top of the pool.
- (4) A subroutine within the GROWS code computes physical properties of the molten pool as weighted averages of UO_2 and catcher material (MgO or concrete) properties. Provide the rate of solubility of catcher material into UO_2 which is required to cause this assumed instantaneous mixing process to be a realistic model. Provide any experimental measurements on solubility rates of the materials in question to justify your assumption.
- (5) The use of GROWS is referred to in the TLTM Report (p. D-3, Ref. D3) when establishing the upward/downward energy split for computing penetration into concrete. Because of appreciable release of vapor and gas from the concrete, vigorous agitation of the molten pool will occur. With respect to the pool-side heat transfer correlations described in Reference D3, provide justification that these correlations are valid for an agitated pool condition.
- (6) For the amount of energy which is transferred in the downward direction, provide further discussion on the sideward versus downward split, including a parametric sensitivity evaluation to show whether your design is adequate for a wide range of variations in the sideward/downward energy split.

- (7) The molten core debris pool is continually diluted by the addition of concrete material which is assumed to be miscible in UO_2 . Since large amounts of steel are also expected to be present and since the steel is immiscible with the concrete, provide an evaluation of the consequences of molten steel dropping to the bottom of the molten pool as the pool density decreases to a value less than the steel density.
- (8) The GROWS code assumes a cylindrical geometry for the molten pool shape. The molten pool can take on other shapes either initially as core debris is introduced into the RC or later as it grows into the catcher material. Provide justification that the cylindrical geometry assumed is satisfactory in regard to predicting the maximum extremities of the molten pool boundary.
- (9) For each of the Items (2) through (8) above, provide a discussion and description of your proposed R&D programs that will yield quantitative information relative to understanding these uncertainties. In addition, recently published experimental results (Reference: R. Farhadieh, L. Baker, "Simulation Experiments of the Growth of a Hot Fuel Pool in a Sacrificial Bed," ANL/RAS 76-27, September 1976) provide an opportunity to check the heat transfer models incorporated in the GROWS computer code. Accordingly, for the transient molten pool temperature and growth, provide a comparison between the GROWS predictions and the experimental results provided in the aforementioned reference.

Response:

The question refers to a previous design and its analysis. The GROWS code is not used in the analysis of the present design. CRBRP-3, Volume 2 (Reference 10b of PSAR Section 1.6); Section 3.2.3.2 contains the present post-boildry evaluation, which is a similar analysis. Uncertainties in various physical phenomena are investigated by doing parametric analyses. Appendix C.2 provides the details of the thermal model.

Question 001.661

Provide the following information in regard to the AYER computer code which models molten pool growth in concrete or a sacrificial bed material.

- (1) As the molten pool grows in size, the volume throughout which decay heat is being generated increases accordingly. Provide clarification on whether the AYER code assigns a volumetric power generation to more nodes as time progresses or does it have some other means of expanding the total volume which generates decay heat. In addition, provide a discussion of whether the limit on the number of nodes which can generate power in the code is a factor in its application.
- (2) The boundary conditions pertinent in the application of AYER to the concrete basemat are not well defined. Appendix D of the TLTM Report indicates that a large amount of decay heat is being removed at the side of the molten pool, as evidenced by the steep temperature gradients shown on pages D-11 to D-14. Provide an explanation of the conditions being modeled by the code at the outer boundary.
- (3) The AYER code does not include any convection processes. Attempts to circumvent this problem appear to be based on using an anisotropic thermal conductivity for UO_2 . The use of an anisotropic thermal conductivity seems to depart markedly from reality. Provide justification for this approach as well as an assessment of its impact. In addition, your approach raises the following concerns:
 - (a) The UO_2 is continually diluted by base material to the extent that UO_2 eventually comprises only 5% or less of the molten material. The conductivity of the pool is then very nearly that of the base material which is not anisotropic. Discuss whether this dilution would quickly wash out any effort to simulate a desired energy distribution by manipulating UO_2 properties alone.
 - (b) Supposedly the AYER code is to establish the magnitude of energy transfer in the sideward, downward, and upward directions with respect to the molten pool. Instead, the two thermal conductivities input for UO_2 have, at least initially, a direct impact in the resultant energy distribution. Therefore, discuss whether this technique requires, in effect, that one know the answer before the code input is prepared. Provide a discussion of the information used to select the two conductivities.

- (c) The expressions for the heat transfer coefficients at pool boundaries all involve the pool thermal conductivity. Discuss what conductivity is used and how it is computed.
- (d) Example 5 in the report "A Thermal Model of Molten Core Debris in a Concrete Basemat" (WARD-D-0107, Rev. 1) details the application of AYER to pool growth in concrete. Anisotropic UO_2 thermal conductivities are shown on the load sheets. Both are much higher than any UO_2 data commonly used (also the concrete conductivity appears to be in the wrong units and the density of UO_2 is surprisingly low). Provide an explanation of this situation.
- (4) Provide clarification as to whether the AYER code makes allowance for the porosity of the solid material. This would be particularly important in analyzing a sacrificial bed, such as MgO which would have a 15% to 20% porosity.
- (5) The report WARD-D-0107, "A Thermal Model of Molten Core Debris in Concrete Basemat," was apparently first written to describe a sacrificial bed situation, as evidenced by a few minor changes in the report which substituted phrases appropriate to concrete. It is not clear why no computational results are shown for concrete and no required physical properties or characteristics of concrete are included. Provide in detail your position on whether the molten pool growth process in concrete is any different from the expected in a sacrificial bed.
- (6) Carrying over the pool-side heat transfer correlations from the GROWS code appears to be unrealistic if the catcher material is concrete. This reasoning stems from the fact that appreciable vapor and gas release from the concrete will thoroughly disrupt the assumed natural convection pattern in the molten pool. In addition, the bottom and side faces may be blanketed with a continuous gas film. Since these effects differ from conditions assumed to exist when the GROWS code correlations were developed, provide a detailed discussion and evaluation of these concerns.
- (7) An upward-downward split in decay power is assumed to be 50%-50% for concrete as the catcher material. This cannot be taken as conservative until consideration is given to the pool conditions which would be unique to concrete. Provide an evaluation of the effect of vapor and gas agitation on the heat transfer split for concrete.

- (8) Describe in detail the manner in which steel, both on the top and below the molten pool, will affect pool growth in concrete.
- (9) In the event that the core debris does not self-level across the 40 ft. diameter reactor cavity floor, a pile of debris may form and early dryout would occur resulting in a concentrated melting attack on a local area of the concrete floor. Provide an evaluation of the penetration of molten core debris into concrete assuming that the core debris remains in a molten pool form following melt-through of the reactor and guard vessels. Various initial molten pool configurations should be examined on the lower reactor cavity concrete floor. Your analysis should include a complete description of assumptions and modeling techniques. (You may wish to coordinate this response with Item 001.619.)
- (10) For each of the Items (5) through (9) above, provide a discussion and description of your proposed R&D programs that will yield quantitative information relative to understanding these uncertainties.

Response:

The question refers to a previous design and its analysis. The AYER code is not used in the present analysis. CRBRP-3, Volume 2 (Reference 10b of PSAR Section 1.6), Section 3.2.3 contains the thermal and structural evaluation following sodium boil-dry. The effects of uncertainties are encompassed by the results of the parametric studies. Appendix C.2 provides the details of the thermal model and data base. Appendix G.1 contains an evaluation of the sensitivity of bed leveling characteristics.

Question 001.662

Provide the sequence of operator actions and corresponding times to manually activate the TLTM features in the event of a CDA. In addition, provide a discussion of the necessary instrumentation that will be provided to assist the operator in determining the actions to be taken. Address the potential for and consequences of incomplete or inadequate operator action. (You may wish to coordinate this response with Item 001.658.)

Response:

The information requested will be found in CRBRP-3, Volume 2 (Reference 10b of PSAR Section 1.6), Sections 2.1.2.12, 2.2.12, and 2.3.

Section 2.3 discusses the operator actions associated with the TMBDB features. As shown throughout the report, no operator actions with respect to operation of these features would be required for at least 24 hours. Section 2.1.2.12 provides the requirements for instrumentation that would be used by the operator to determine actions to be taken and Section 2.2.12 discusses the instrumentation design. Studies of the potential for and consequences of incomplete or inadequate operator actions are in progress.

Question 901.663

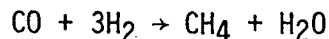
Under the TLTM accident conditions, provide an evaluation of the potential for and consequences of combustible gas formation, other than hydrogen, such as CO, CH₄, C₂H₄, and C₃H₆.

Response:

The information requested will be found in CRBRP-3, Volume 2 (Reference 10b of PSAR Section 1.6), Sections 3.2.2.1 and 3.2.3.1.

Section 3.2.2.1 discusses chemical reactions prior to sodium boil-dry when the presence of sodium governs the reactions and hydrogen is the only significant combustible gas produced. Section 3.2.3.1 discusses reactions after sodium boil-dry when temperatures would increase to the melting point of steel. The resulting production of hydrogen and carbon monoxide is discussed.

Under certain conditions, after sodium boil-dry, hydrocarbons such as those noted in the question could be formed from the hydrogen and the oxides of carbon. The potential for formation would depend on the temperature, reactant concentration, and the presence of a catalyst such as iron. Even if the hydrocarbon were formed, its concentration would be low compared to the potential concentrations of carbon monoxide and hydrogen that have been considered. For example, CH₄ could be formed by the following reaction:



In this case four moles of reactants (CO and H₂) are required to produce one mole of CH₄. Considering this reduced concentration of CH₄ relative to the H₂, the hydrocarbons would be less limiting from the standpoint of flammability, and the reaction energy, if the gases burn, would not exceed 500,000 Btu/hr estimated in Section 3.2.3.1 of CRBRP-3, Volume 2.

Consequently, it is conservative to assume that hydrogen and carbon monoxide are the gases produced from the reactions following sodium boil-dry. Since the containment purge system can maintain the hydrogen and carbon monoxide concentrations below potentially explosive concentrations, it would also provide adequate control of the hydrocarbons if they should be formed.

Question 001.664

Provide the bases for the thickness (4 in.) of insulating concrete behind the reactor cavity wall liners and pipeway cell liners.

Response

The following criteria was used in the selection of the insulating concrete thickness and thermal properties in the Reactor Cavity and the Pipeway Cells.

- a. To limit the temperature in the structural concrete to acceptable levels under Design Base Accident (DBA) conditions.
- b. Under TMBDB conditions to limit the temperature in the structural concrete to levels that structural integrity requirements can be satisfied and at the same time allow heat to flow through so that the concrete structures can be used as heat sinks.

Question 001.665

Section II of the TLTM report (April 1976) describes a three-region liner vent system to account for the fact that certain regions of the cell liner have a greater potential for failure than others, and if the liner fails, the reaction products are isolated from the other liner venting subsystems. However, the TLTM update report (November 1976) states that the reactor cavity wall liners and pipeway cell liners will be vented to non-inerted spaces below the operating floor. Confirm whether you now only have a one-region liner vent system. Include an evaluation of the consequences of blocking the vent passages by reaction products resulting from sodium and core debris interactions with concrete behind the wall liner where failure has occurred. In addition, if wall liner failure occurs, sodium can be forced through the vent passages into non-inerted spaces below the operating floor. Provide an evaluation of (1) the consequences of venting sodium into these non-inerted spaces below the operating floor, and (2) venting one liner section to a non-inerted space which is also the vented space for another liner section. (You may wish to coordinate this response with Items 001.624 and 001.625.)

Response:

A description of the region liner vent system (which now contains four regions) is contained in Section 2.2.4 of the CRBRP-3, Volume 2 (Reference 10b, PSAR Section 1.6). An evaluation of the consequences of venting sodium into non-inerted spaces below the operating floor was not performed due to the design features discussed in the response to Question Q001.624 and Section 2.2.5.3 of CRBRP-3 Volume 2. The response to the remaining portion of this Question is contained in the response to Question Q001.624, Q001.632 and Section 2.2.5.3 of CRBRP-3, Volume 2.

Question 001.666

With respect to the TLTM update of concrete thermophysical properties, carbon dioxide release, water release, sodium-concrete reaction energy, and hydrogen-oxygen reaction, our review of the cited references indicates that the data are still preliminary and subject to change. Provide in the PSAR the above data and their bases, as well as a description of any planned R&D to firm up this data base. Include a sensitivity study on the response of the RCB to changes in each of the above parameters.

Response:

The information requested will be found in CRBRP-3, Volume 2 (Reference 10b of PSAR Section 1.6), Appendices A.1, A.2, A.6, C.1.2, C.1.4, G.2 and H.1.

The experimental basis for concrete thermophysical properties is contained in Appendix C.1.4.

The experimental basis for carbon dioxide and water release from concrete is contained in Appendix C.1.4.

The experimental basis for sodium-concrete reaction energy is contained in Appendix C.1.2.

The experimental basis for hydrogen-oxygen reactions is contained in Appendix H.1.

Planned R&D efforts are contained in the following Appendices: Appendix A.1 sodium-concrete interaction; Appendix A.2, hydrogen auto-catalytic recombination; and Appendix A.6, concrete thermophysical property data.

Sensitivity analyses of increased sodium-concrete interactions are contained in Appendix G.2.

Sensitivity analyses of hydrogen-oxygen recombination are contained in Appendix H.1.

Carbon dioxide and water release data were developed in a conservative manner as indicated in Appendix C.1.4 and sensitivity analyses were not performed.

Question 001.667

The TLTM update report states that operation of the annulus cooling system after 24 hours would make the annulus filtration system inoperative. Provide clarification of this planned mode of operation and its radioactivity release consequences considering such related operations as "burping" the containment vessel through filters (after 24 hours) to relieve over-pressure (not total pressure), but otherwise retaining the containment as a leak-tight barrier with filtration of the leakage by the annulus filtration system. It is our general position that the operation of TLTM features should not negate operation of the engineered safety features after 24 hours, consistent with further reducing residual risks, but with consideration of the practicalities involved; relief of over-pressure by "burping" through filters is an example of a temporary defeat of the containment leak-tight barrier which may be acceptable as a reasonable measure compared to other alternatives. Please discuss your design and its operation in light of the above, including alternatives considered to reduce released radioactivity (coordinate with 312.63).

Response:

The operator action sequence will be found in CRBRP-3, Volume 2 (Reference 10b of PSAR Section 1.6), Section 2.3.

The annulus between the confinement concrete structure and the containment steel vessel is kept at a slightly negative pressure ($\sim 1/2$ " H₂O) under all plant design base conditions and events. The annulus filter system, which is an engineered safety feature, is provided to mitigate radiological consequences to an acceptable level when subjected to the non-mechanistic Site Suitability Source Term (SSST) within the containment without destroying vacuum in the annulus. No TMBDB features would be activated by the operator for any design basis events.

The scenario with continuous venting and purging after 24 hours described in CRBRP-3, Volume 2, results in acceptably low radiological consequences (See Tables 4-3 and 4-4). A qualitative assessment has been made of the radiological consequences of a scenario in which the containment is vented and purged intermittently (burping) to control pressure and hydrogen concentration. The radiological release would not be substantially changed because a large part of the fission products (>95% noble gases, Cs, Rb) would be released during the initial venting period (after 24 hours) that is necessary with both the reference scenario and the burping scenario. After the initial release, the lower releases when containment is sealed are compensated by higher releases when burping occurs. The burping scenario would also result in TMBDB features which would be inherently less reliable because of their intermittent operating mode. The longer term operation of the containment at a slightly negative rather than positive pressure is also desirable to minimize leakage to the environment in the event of long term seal degradation.

Question 001.668

Consistent with our May 6, 1976 letter, provide an evaluation of the response of the containment building for the CDA consequences which include release of 1000 lbs. of sodium to the head access area, and vaporization of 10% of the core fuel inventory and direct release of this fraction from the reactor head.

Response:

CRBRP-3, Volume 2 (Reference 10b of PSAR Section 1.6), Section 4 discusses the radiological consequences of various initial head releases. Similarly Appendix G.4 presents data regarding radiological consequences and also the thermal consequences in containment from a wide range of initial releases through the reactor vessel closure head.

Question 001.669

In view of the uncertainties associated with the inherent retention capability of the containment to contain a core meltdown accident, provide an evaluation of the consequences of core debris penetrating the RCB basemat and entering the surrounding soil. Include consideration of the effects of ground-water interaction in terms of radioactivity motion and migration outside containment, and in terms of interactions which generate pressure in the containment.

Response:

The information requested will be found in CRBRP-3, Volume 2 (Reference 10b of PSAR Section 1.6), Sections 3.2.3.3 and 4.3. Section 3.2.3.3 discusses the long term structural assessments and Section 4.3 discusses the radiological consequences associated with an assumed penetration of the basemat and the resultant interactions with groundwater.

Question 001.670

In the supplemental updating of the Third Level Thermal Margin Report, dated November 5, 1976, the reactor cavity venting provisions have been modified. According to Figure 6 of this document, each line running from the vent header to above the operating floor of the containment building contains a rupture disc and a remotely operated shutoff valve. We are concerned about the effect of partial or complete blockage of the vent lines on the results of the analysis described in this document. Describe how your analysis considered uncertainties in rupture disc performance (i.e., disc ruptures at pressure differentials less than or greater than 15 psi). The remotely operated shutoff valve will normally be in the open position. Discuss the effect on the analytical results if one of these valves is inadvertently in the closed position when the scenario described in Section 4 of the document occurs. Describe how the CRBRP operator will be assured that the shutoff valves are in the correct position.

Response:

The response to this question is provided in Sections 2.2.6 and G.3 of the CRBRP-3, Volume 2 (Reference 10b of PSAR Section 1.6).

Question 001.671

Provide a complete description of the CACECO computer code, including details of the mathematical models, the equations used, subroutines and supporting data. Provide a discussion of the limitations of the code and describe the method used for verification of the code. Provide a description, including a schedule, of any future experimental work which will be used to obtain data for verification of the code. (You may wish to coordinate this response with Item 001.645.)

Response:

The information requested will be found in CRBRP-3, Volume 2 (Reference 10b of PSAR Section 1.6), Appendices A.3 and C.1.

Appendix C.1 presents a brief description of the CACECO computer code, together with a reference to the detailed description.

Appendix A.3 provides the program for further analytical and experimental validation of the code.

Question 001.672

Provide a description of the test program which will be implemented to determine the leak rate characteristics of the inner barrier or inner containment cells under the conditions described in the Third Level Thermal Margin Report.

Response:

The present scenario and design to provide Thermal Margin Beyond the Design Base, as described in CRBRP-3, Volume 2 (Reference 10b of PSAR Section 1.6), do not require the inner cells to be leak tight. Section 2.2.6 of the report describes the reactor cavity vent system which vents the Reactor Cavity to the Reactor Containment Building.

Question 001.673

Provide the analytical and/or experimental basis which was used to develop the functional design requirements for the reactor containment annulus cooling system. In particular, address the heat transfer characteristics within the annulus.

Response:

The response to this question is contained in Sections 2.1.2.10, 2.2.10, and 3.2.2.2 of the CRBRP-3, Volume 2 (Reference 10b of PSAR Section 1.6).

Section 2.1.2.10 provides the design requirements for the annulus cooling system. Section 2.2.10 provides a description of the system. Section 3.2.2.2 provides the thermal analysis of the Containment-Confinement structures used to develop the functional design requirements.

Question 001.674

Discuss the operation of the vents and cap at the top of the reactor containment building annulus. Provide a discussion of any impact that these features have on the annulus filtration system for accommodation of design basis accidents.

Response:

A discussion of the operation of the Annulus Cooling System, including the vents (dampers) at the top of the Reactor Containment Building Annulus, is included in Section 2.2.10 of the CRBRP-3, Volume 2 (Reference 10b of PSAR Section 1.6).

These features have no impact on the Annulus Filtration System for accommodation of design basis accidents. An evaluation of the impact of these features on the Annulus Filtration System operation has been conducted, the results of which are indicated in PSAR Section 6.2.5.3.

Question 001.675

Provide the assumptions made or data correlations used in the determination of the heat transfer coefficients used in the CACECO analysis described in Appendix A of the Third Level Thermal Margin Report and updated in the November 5, 1976 submittal.

Response:

The basis for the heat transfer correlations used in the current CACECO analyses will be found in CRBRP-3, Volume 2. (Reference 10b of PSAR Section 1.6), Appendix C.1.

Question 001.676

There appears to be a number of inconsistencies between the stated conditions for the analyses and certain parameters plotted in the November 5, 1976 update of the Third Level Thermal Margin Report. Accordingly, please address the following:

- (1) Explain why the reactor cavity pressure shown in Figure 1 has an initial value of 14 psi, whereas the initial pressure in the containment building was 0 psi.
- (2) Explain why the initial temperatures of the reactor cavity atmosphere and the steel dome of the containment shown in Figure 2 are 1200°F and 0°F, respectively.
- (3) Explain why the initial value of the concentration of sodium entering containment is approximately 40 grams per cubic meter.

Response:

This question is not relevant to the current analyses contained in CRBRP-3, Volume 2 (Reference 10b of PSAR Section 1.6), since the information has been completely updated. The specific numbers which appear in the question are not those appropriate to the current analysis. Explanation follows:

- (1) The initial reactor cavity and containment building pressures are shown on Figure 3-7 of CRBRP-3, Vol. 2. It will be noted that in the early stages of the scenario, the reactor cavity pressure is higher than that for the containment. This reflects the fact that events in the reactor cavity are essentially driving the whole scenario. Thus there is, in this phase, a small time lag between the containment and cavity pressure time histories.
- (2) The reactor cavity and containment building temperatures are shown on Figure 3-6 of CRBRP-3, Vol. 2. The steel dome temperature remains substantially below that of the reactor cavity atmosphere because of the large volume of containment atmosphere and because of heat losses from the containment outer surface.
- (3) Figure 3-10 provides the sodium concentration entering containment as a function of time.

Question 001.677

Describe the method that will be used during the operating life of the plant to determine whether the vent lines are open between the reactor cavity, the PHTS Pipeways Cells, the vent header, and the vent lines into the reactor containment building. Provide an analysis which shows the transient response of the containment building to the accident scenario postulated in the November 5, 1976 document assuming that a vent line between the reactor cavity and a PHTS Pipeways Cell is completely plugged. (You may wish to coordinate this response with Item 001.670.)

Response:

Prior to operation, the vent system will be completely tested for flow to ensure that all passages are clear. Since the vent system is totally passive, no further tests will be made subsequent to reactor operations.

The second portion of this question is responded to in Sections 2.2.6 and G.3 of the CRBRP-3, Volume 2 (Reference 10b of PSAR Section 1.6).

Question 001.678

On page 3 of the November 5, 1976 update of the Third Level Thermal Margin Report, it states that the bases for auto-ignition of hydrogen Criteria I and II may be found in Reference 2 (G. R. Armstrong and R. W. Wierman, "Hydrogen Formation and Control Under Postulated LMFBR Accident Conditions," HEDL-SA-119, presented at the LMFBR Safety Technology Meeting on PAHR, September 27, 1976). On page 3.4-16 of Reference 2, in the General Summary, it states, "Caution should be exercised at this time, however, in drawing any general conclusions since (1) the test program has not yet been completed, (2) each reactor design will likely be different, and (3) postulated accident conditions resulting in hydrogen release will likely vary for each reactor. Because of these differences, an independent assessment of each LMFBR design is indicated if hydrogen auto-ignition is cited as a significant mitigating factor in the overall safety analyses."

In view of the above-quoted disclaimer, justify your reliance on Reference 2 as the bases for Criteria I and II.

Response:

The information requested will be found in CRBRP-3, Volume 2 (Reference 10b of PSAR Section 1.6), Appendices A.2 and H.1. Appendix H.1 references the completed test program referred to in the question. Appendix A.2 details further R&D to substantiate the burning criteria.

Question 001.679

Page 3 of the November 5, 1976 update of the Third Level Thermal Margin Report states that the bases for hydrogen auto-ignition Criterion I are found in Reference 2 and those for Criterion II are found in References 2 and 3. Identify the reference which serves as the basis for Criterion III.

Response:

The references for the hydrogen burning criteria presently employed can be found in Appendix H.1 of CRBRP-3, Volume 2 (Reference 10b of PSAR Section 1.6).

Question 001.680

On page 7 of the November 5, 1976 update of the Third Level Thermal Margin Report, the reference to Reference 4 for data regarding carbon dioxide release from heated concrete is in error. Identify the correct reference. Provide seventy (70) copies of this reference to facilitate our review if it was not included in the list of references contained in the Enclosure to the December 2, 1976 letter from Themis P. Speis to Mr. Lochlin W. Caffey.

Response:

The information requested will be found in CRBRP-3, Volume 2 (Reference 10b of PSAR Section 1.6), Appendix C.1.4.

The data previously employed in the TLTM report were conservatively selected, recognizing the lack of detailed data on carbon dioxide release as a function of temperature. Appendix C.1.4 provides information with respect to the present data used, accompanied with appropriate references. Copies of the requested references were provided in Reference Q001.680-1.

Reference:

Q001.680-1 Letter from A. R. Buhl to R. S. Boyd, "Transmittal of Requested TLTM References," PS:77:074, January 25, 1977.

Question 001.681

The value of 268 calories/gram used for the sodium-concrete heat of reaction in the analyses described in the Third Level Thermal Margin Report included a probable error of $\pm 100\%$ (J. A. Hassberger, R. K. Hilliard, and L. D. Muhlestein, "Sodium-Concrete Reaction Tests," HEDL-TME 74-36, June 1974).

Describe how the determination of the sodium-limestone heat of reaction of 184 calories/gram (used in the November 5, 1976 update) considered the uncertainties in the Differential Thermal Analysis measurement technique.

Response:

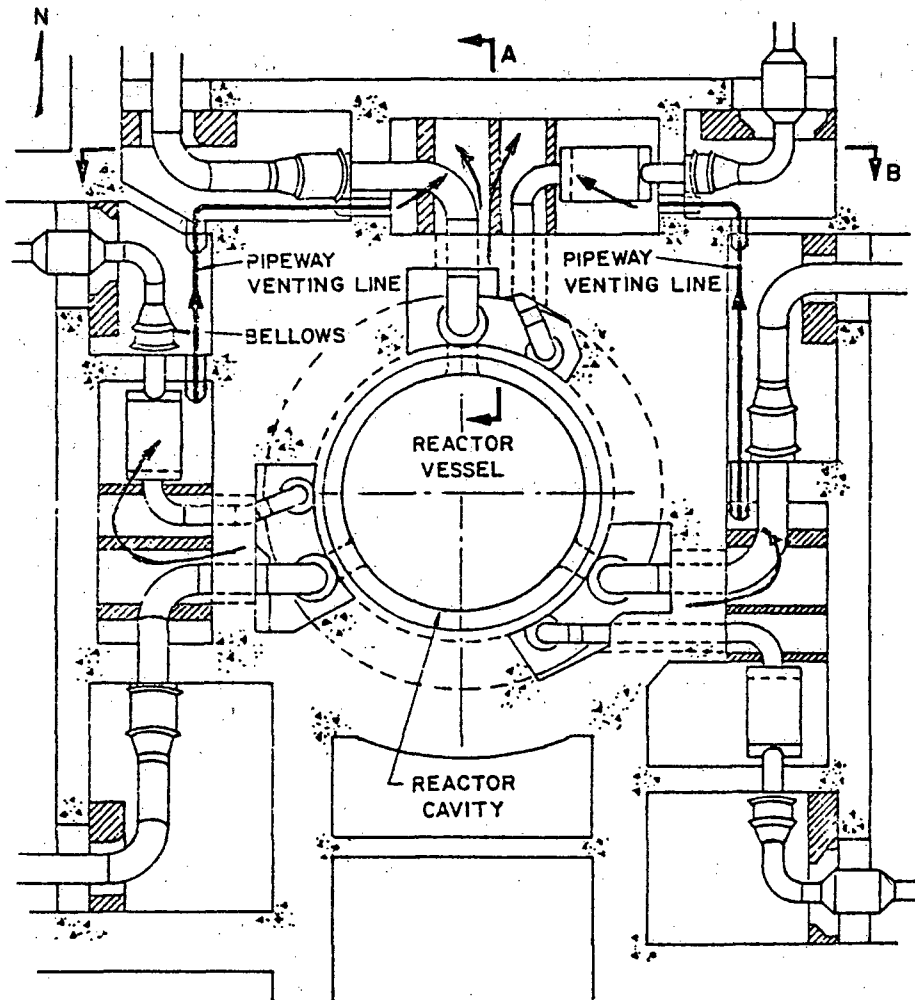
The information requested will be found in WARD-D-0141 which is referenced in CRBRP-3, Volume 2 (Reference 10b of PSAR Section 1.6), Appendix C.1.2, and which has been transmitted to the NRC in Reference Q001.680-1.

Question 001.682

Describe and provide detailed drawings showing the physical location of the piping and header of the reactor cavity - PHTS pipeways cells-reactor containment building venting system.

Response:

The response to this question is provided in Section 2.2.6 of the CRBRP-3, Volume 2 (Reference 10b of PSAR Section 1.6) and figures Q001.682-1, 2, and 3.



REACTOR CAVITY VENTING ARRANGEMENT EL 780'-0"

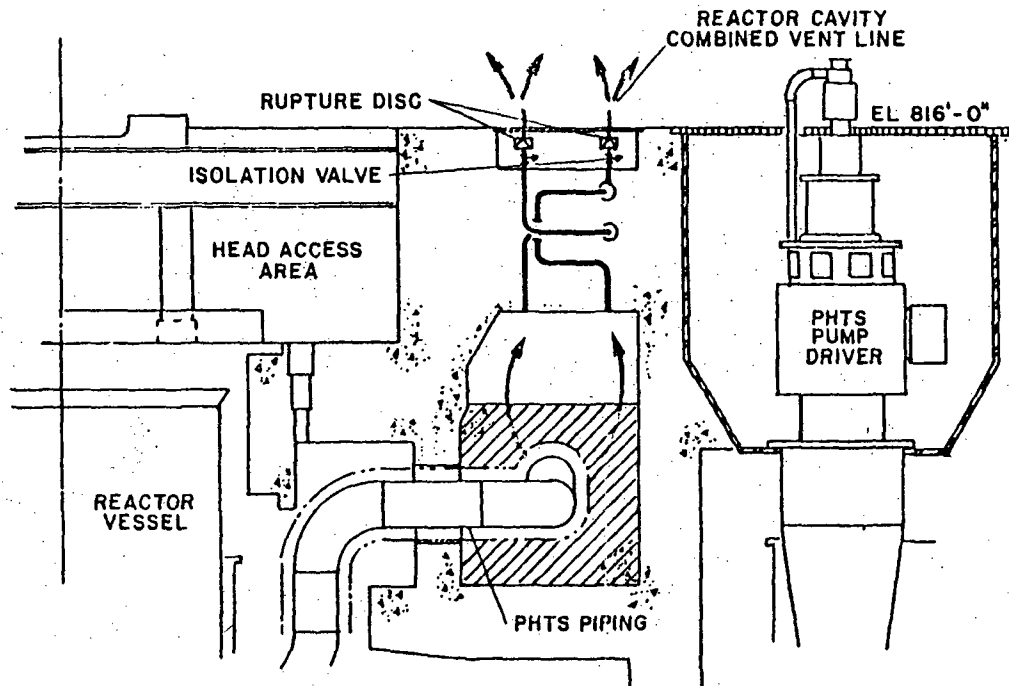
Figure Q001.682-1

Q001.682-2

Amend. 60
Feb. 1981

Figure Q001.682-2

REACTOR CAVITY VENTING ARRANGEMENT SECTION A - A

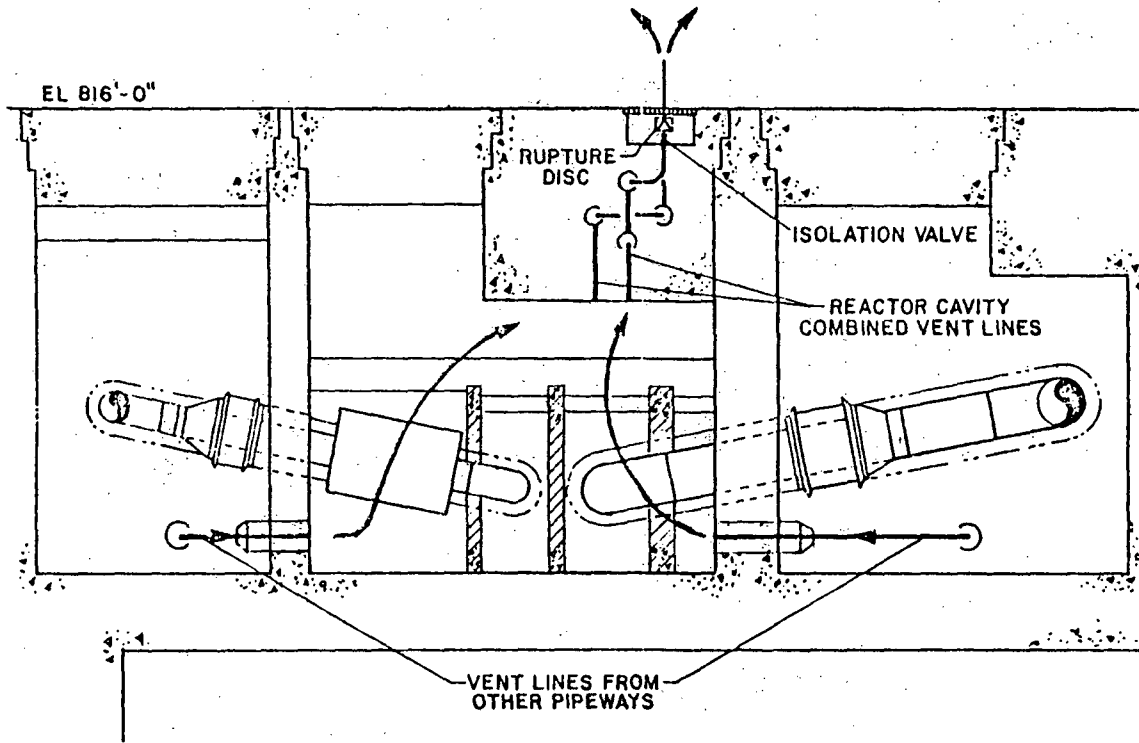


Q001.682-3

Amend. 60
Feb. 1981

Figure Q001.682-3

REACTOR CAVITY VENTING ARRANGEMENT SECTION B - B



Q001.682-4

Amend. 60
Feb. 1981

Question 001.683

Your response to Item 001.500 is not acceptable. The staff is not able to identify relevant material in the reference document (ANL/RAS 75-44) which supports the contention that added fines will be produced by quenching of a two-phase fuel mixture. In addition, recent work at Stuttgart University by Professor Dr. Ing Frolich indicates that complete fragmentation may not occur if a threshold in quantity of molten mass is exceeded. Reassess your response to Item 001.500 in light of these comments and provide the requested evaluation, including the applicability of any experimental data to the UO_2 /sodium combination.

Response:

Pertinent information will be found in CRBRP-3, Volume 2 (Reference 10b of PSAR Section 1.6), Section 3.2.1 and Appendix G.1.A.

Section 3.2.1 addresses particle size and its effect on the analysis.

Appendix G.1.A addresses the experimental bases for debris particulation. Data from Argonne National Laboratory provided in Appendix G.1.A show that particulation is complete unless the fuel mass approaches the sodium mass. For situations of interest in the TMBDB scenario, the sodium mass exceeds the fuel mass and complete particulation would be expected.

Question 001.684

Your response to Item 001.507 provided an evaluation for the EVCC Parallel Design concept of the consequences of debris beds which remain within the reactor vessel constituting a long term heat source. Provide a similar evaluation for your proposed Third Level Thermal Margin (TLTM) concept. Justify your assumed guard vessel surface temperature (1000°F assumed in Section F6.4.1.4). The conclusions which you reached regarding internal temperatures and residue debris quantities are a direct consequence of this assumption. Include a structural evaluation of the reactor vessel, guard vessel, reactor cavity and support ledge. If reactor vessel and guard vessel rupture occurs, provide a structural evaluation of the resulting impact loads.

Response:

CRBRP-3, Volume 2 (Reference 10b of PSAR Section 1.6), Appendix F.6 describes a revised scenario in which a portion of the core remains within the reactor vessel following penetration of the reactor vessel and guard vessel. The assumptions for this scenario are included in Appendix F.6.

Question 001.685

With regard to your response to Item 001.508, provide a discussion for your proposed TLTM concept of any credit you are taking for natural convection heat removal through steam generators following a core melt-down accident while the core debris is within the reactor vessel. Provide an evaluation of the consequences of no natural convection heat removal through the main heat transport loops, including an evaluation of the consequences (both in-reactor vessel and ex-reactor vessel) of boiling sodium before reactor vessel melt-through occurs. (You may wish to coordinate this response with Item 001.639).

Response:

The information requested will be found in CRBRP-3, Volume 2 (Reference 10b of PSAR Section 1.6), Section 3.2.1 and Appendices C.1.1 and F.5.

Section 3.2.1 indicates that no heat loss from the vessel is assumed prior to penetration. However, Appendix F.5 includes some sensitivity studies in which decay heat removal is assumed until penetration.

Appendix C.1.1 identifies the key assumptions made with respect to heat removal mechanisms after vessel penetration.

Appendix F.5 includes a sensitivity study of the consequences of in-vessel boiling prior to vessel penetration.

Question 001.686

Both Section F6.4.3.5 and your response to Item 001.517 (Including Reference Q001.517-1) appear to conclude that the Parallel Design External Cooling System (ECS) is necessary to remove heat from the core debris and overlying sodium to keep temperatures low enough to prevent structural failures within the reactor cavity. If this was the case for your Parallel Design, which also included a sacrificial bed for removing part of the decay heat load, provide a detailed assessment of why a cooling system is not required for your proposed TLTM concept as a means of removing heat from the core debris and sodium, thereby keeping reactor cavity components, structures, and concrete temperatures from reaching unacceptable levels where structural failures would occur. Include your structural acceptance criteria if different than existing code criteria.

Response:

The requested information can be found in CRBRP-3, Volume 2 (Reference 10b of PSAR Section 1.6), Sections 2.1.2.14 and 3.2.2.5 and Appendix C.3.

The Reactor Cavity has been evaluated and has been found to meet the requirements (Section 2.1.2.14) for structural integrity and thus a cooling system is not required. The description of the structural evaluation and the criteria are provided in Sections 3.2.2.5 and Appendix C.3.

Question 001.687

Your response to Item 001.514 is not acceptable. Delete the word "sealed" in Item 001.514. The point is that even for your proposed TLTM concept, we are still concerned about how structural integrity of the head access area concrete, including the reactor support ledge, is assured considering the additional dynamic loads and heat loads introduced following a CDA. (You may wish to coordinate this response with Item 001.631.)

Response:

A response to this question is provided in Section 3.2.2.5.1.2 of the CRBRP-3, Volume 2 (Reference 10b of PSAR Section 1.6). Based on preliminary assessments, it is expected that the ledge will be capable of carrying the vessel weight considerably beyond 24 hours and the head access area will survive at least to sodium boil dry.

Question 001.688

With regard to your response to Item 001.503, we agree that the information presently available to describe the settling of particles is probably adequate. However, our concern mainly stems from uncertainty in your analysis regarding particle size distribution and initial conditions established by the injection into the upper plenum. Provide an assessment of these concerns. Section F6.4.1.2.1 provides experimental results from sand injection experiments. Clarify how the sand experiments relate to real reactor conditions. Provide a discussion of any R&D program to address the above concerns.

Response:

The information requested will be found in CRBRP-3 Volume 2 (Reference 10b of PSAR Section 1.6), Section 3.1.1. Better analysis techniques have been used in this evaluation, and the portion of the question regarding sand experiments is no longer applicable.

Question 001.689

Your response to Item 001.501 is not entirely acceptable. You have not adequately substantiated your assumptions regarding particle size distribution, bed porosity, gas entrainment, and wall interference effects. Reasonable variations in these parameters can reduce the dryout heat flux substantially when compared to the ANL data. Provide an evaluation as to whether your proposed TLTM concept envelopes these uncertainties in the dryout heat flux, especially considering the fact that gaseous constituents released from the heated concrete into the particulate debris bed will substantially lower the dryout heat flux. Also include the consideration that has been given to the adverse effects that hyperstoichiometric oxide fuel will have on the bed dryout heat flux characteristics. Specifically, include an assessment of the effect of the above parameters on the 215 hr dryout time and start of core debris penetration into the concrete basemat.

Response:

The information on debris bed behavior will be found in CRBRP-3, Volume 2 (Reference 10b of PSAR Section 1.6), Section 3.2.1 and Appendix G.1.

Question 001.690

Your response to Item 001.502 is not entirely acceptable. We have a number of concerns with the response which you have provided. Reassess your response to Item 001.502 in light of the concerns delineated below; your reassessment should include an evaluation for each of items provided below:

- (1) The statement that the particles entrained in fluid above the Upper Internal Structure (UIS) experience little radial movement is misleading. On the contrary, according to calculations performed with the MIX code (Reference: Figure 23, ANL-CT-75-41, "MIX-A Computer Code for Transient Thermal-Hydraulic Analysis of LMFBR Outlet Plenums," May 1975) after 35 sec of flow coastdown, the flow is essentially a stratified recirculation flow, with fluid immediately above the UIS moving horizontally. Therefore, the debris particles initially situated above the UIS would be carried away by the recirculation flow, resulting in little settlement of the debris on top of the UIS. As a result, the assumption that all debris particles directly above the UIS settle on its surface may lead to serious error and the settled fraction could be well below the 27% claimed in the response.
- (2) As is evident from Figure 23 of the aforementioned reference, only the fluid near the outlet nozzle moves essentially radially. In the recirculation flow region, both the vertical and horizontal flow velocities are equally important. Therefore, the assumption that the sodium in the settling zones moves only in the radial direction may lead to substantial error in calculating the fraction settled in the upper sodium plenum.
- (3) The assumption that the fraction settled in the reactor vessel is the ratio of the vertical distance traveled to the initial height of the column of particles is difficult to conceive physically. This assumption needs further elaboration and justification. Since this assumption plays an important role in the whole theory, provide your plans for experimental verification.
- (4) Equation (2) in your response to Item 001.502 appears to be incorrect because the actual particle settling velocity (relative to the vessel wall) is not the terminal velocity. Instead, it should be equal to the vector sum of the terminal velocity and the fluid vertical velocity. If this equation is only an approximation, this is not a good approximation since in most of the flow regions the vertical flow velocity is equally important.
- (5) The significance of the upper plate area on the UIS is not understood, as well as why this area establishes the fraction of material to be swept toward the upper plenum outlets.
- (6) In your analyses of settling rate and particle concentrations per linear foot of piping, you have not accounted for particle interactions. Provide us with your assessment of this effect.

- (7) The equation at the bottom of page Q001.502-4 is not valid for the verticle piping segments. By streaming through the verticle pipe, the debris may disperse again, resulting in redistribution of the debris particles in the verticle pipe and at its outlet.

Response:

The assessment of in-vessel debris behavior has been updated and is provided in CRBRP-3, Volume 2 (Reference 10b of PSAR Section 1.6), Section 3.1. Specific comments contained in the question are discussed below.

161

- (1) The analysis of the settling of fuel particles in the reactor vessel plenum and their transport to the PHTS piping is currently based on two dimensional sodium flow that is predicted with the VARR II computer code (see Appendix A of the PSAR) and the particle mechanics discussed in Section 3.1.1.1 of CRBRP-3, Volume 2. With this model only a small fraction of the fuel particles would be predicted to settle on the top of the UIS. Table 3-7 of CRBRP-3, Volume 2, contains the predicted fuel fraction remaining in the reactor vessel and the fraction exiting through the outlet piping.
- (2) As indicated in (1) above, a new analytical model has been developed which removes the approximation previously followed that only radial flow occurs in the settling zone. The particles move due to the forces of gravity and drag forces from the two dimension fluid flow streamlines.
- (3) This assumption is not used in the current model. Approximations were made in the previous model to conservatively predict the amount of fuel material transported to the PHTS piping. The revised model has reduced this amount to 18-25 percent (see Table 3.7 of CRBRP-3, Volume 2) of the core fuel as compared to the previous prediction of 35% reported in the response to Question 001.502.
- (4) In the revised model, the fluid drag forces on the particles are based on the relative velocity of the particle and the flowing sodium. The particle terminal velocity relative to the reactor vessel wall is properly calculated.
- (5) The geometry of the UIS in the present model is shown on Figure 3-1 of CRBRP-3, Volume 2. The total fuel debris is introduced into the flowing stream in the region between the top of the core and the bottom of the UIS. Particle deposition is calculated on the basis of the forces exerted upon them. It is no longer assumed that deposition on the top of the UIS is proportional to the solid area of the top of the UIS.
- (6) Particle interaction was considered in Section 3.1.1.1 of CRBRP-3, Volume 2. It was concluded that because of the low particle concentration (0.7 v/o), settling would occur without hinderance. Since agglomeration of particles would enhance in-vessel settling and reduce fuel carried into the piping, it is conservative to exclude this potential interaction.

- (7) The settling of particles in vertical pipe sections is discussed in CRBRP-3, Volume 2, Section 3.1.1.1. For coolant flowing upward, if the particle terminal velocity is greater than the coolant velocity, the particle will settle to the bottom of the section. It has been assumed in the analysis that all particles that reach the top of the outlet pipe downcomer (see Figure 5.1-1B and Figure 5.1-3 of the PSAR) will be uniformly distributed in the coolant at the beginning of the horizontal run. Essentially all of the material will settle in this horizontal run within the reactor cavity and pipeway cells prior to reaching the PHTS cells.

Question 001.691

Your response to Item 001.504 is not entirely acceptable. We have some concerns with the response which you have provided. Reassess your response to Item 001.504 in light of the concerns delineated below; your reassessment should include an evaluation for each of the items provided below:

- (1) It is not clear from the information presented in Figure Q001.502-2 how you arrive at 0.46% of the debris is deposited in the first foot of piping in each of the three chaseway cells and 0.1% debris per foot of piping for the HTS cell. It is also not clear how these numbers translate into the numbers you are specifying in Table Q001.504-1 for the amount of debris deposited in the piping before the HTS cell and in the piping inside the HTS cell.
- (2) Boiling of sodium within the primary piping may provide sufficient agitation to cause settled particles to move together at system low points. Such action could concentrate debris which was initially distributed along many feet of pipe. Subsequent material release following dryout into either the pipe chaseway cells or the HTS cells would then be much more localized and concentrated.
- (3) It is not clear what technique was used to judge the spreading of debris dropped onto cell liners in the absence of sodium.
- (4) If core debris penetrated the PHTS piping and cell liner, it would be expected that sodium, which vaporized in the reactor cavity, would be carried into the HTS cells, condense on the walls, and collect on the floor where it would be able to react with concrete.

Response:

The assessment of debris behavior within the reactor vessel and within the primary heat transport system has been updated and is reported in CRBRP-3, Volume 2 (Reference 10b of PSAR Section 1.6), Section 3.1 and Appendix I. Current evaluations of items (1) through (4) are as follows:

- (1) A new analytical model has been developed to evaluate the amount of core debris carried to the PHTS piping and its deposition in the piping. This model is described in CRBRP-3, Volume 2, Section 3.1.1.1. The final disposition of the debris within the reactor vessel and the piping is summarized in Table 3-3 of the reference. Maximum concentrations of debris at selected locations are given in Table I-1 of the reference.
- (2) Concentration of debris at low points within the piping system as a result of agitation due to sodium boiling has not been considered for the following reasons:
 - a. Most of the fuel is predicted to settle in the piping upstream of the high point in the piping. Any motion of this fuel would be toward the pipeway cells and reactor cavity, where the consequences of piping and liner penetration have already been considered.

- b. The horizontal sections of the piping within the PHTS cells downstream of the high point have a slope of less than 1 degree. Debris bed leveling studies at ANL (CRBRP-3, Volume 2, Reference 3-5) have shown that debris beds tend to remain stationary on surfaces inclined at up to 10-15 degrees even with boiling agitation. Thus motion along the slightly inclined pipes is not anticipated.
- c. The quantity of fuel predicted to settle in the piping downstream of the system high point within the confines of the PHTS cell is less than 0.1% of the total quantity of fuel and blanket. Heat would be removed from this material by conduction rather than bed boiling; thus, boiling induced bed movement which could have a concentrating effect is not expected downstream of the system high point.
- (3) No spreading of the fuel debris on the cell liners has been assumed after melt through of the PHTS piping. (See CRBRP-3, Volume 2, Appendix I.3)
- (4) Penetration of the PHTS cell liners is not expected and consequently sodium would not contact the underlying concrete. (See Appendix I.3 of CRBRP-3, Volume 2)

Question 001.692 (5.2.1.3)

Your response to Item 001.73 is not acceptable. You make the assumption that, in a CDA, no sodium will leak out of the head seals because they are designed that way. However, the SRI model tests on FFTF seals indicated that coolant would leak out. In view of the fact that CDA energetics will most probably be higher than your initial proposals and that model tests for CRBR have not yet been performed, we cannot accept the conclusion that all sodium will be retained. With no evidence to the contrary, it is our position that some sodium will leak out. The clearances on the plugs have led us to the conclusion that the leakage of 1000 lbs. of sodium through the head seals should be considered in a CDA situation. Discuss and provide an evaluation of how a sodium release of this quantity could be prevented from leading to an extensive spray fire and overpressurization of the containment. (You may wish to coordinate this response with Items 001.621 and 001.668).

Response:

The information requested will be found in CRBRP-3, Volume 2 (Reference 10b of PSAR Section 1.6), Sections 3.2.1 and 3.2.2, and Appendices C.1.1.3 and G.4.

Sections 3.2.1 and 3.2.2 describe the effect of 1000 lbs. initial sodium head leakage. Appendix G.4 provides sensitivity of the TMBDB calculated results to the amount of the initial head release.

Question 001.700

For the case of sodium being injected (guillotine pipe rupture) into an inerted cell as a spray, splash or other form of dispersion, the March 5, 1976 presentation focused narrowly on comparison of the SPRAY Code with data from four AI LTV tests which were very limited with respect to key parameters such as mass of sodium injected (relative to the mass of N₂ in the vessel), mean sodium droplet size, and volume fraction of vessel occupied by the sodium spray. The single example shown was maximum pressure vs. droplet diameter, but only for an LTV test. We are concerned that this presentation was misleading in its implications.

Provide the results of sensitivity analyses for important parameters in the SPRAY Code (e.g., droplet diameter, mass of sodium sprayed and volume fraction) for the case of a double-ended pipe rupture in the hot leg of CRBRP.

Response:

Sensitivity analyses for important input parameters to the SPRAY Code for sodium leaks from the hot leg of the Primary Heat Transport System (PHTS) piping into the PHTS cell have been performed. These sensitivity analyses were performed for (a) a sodium leak equivalent to the PHTS loop full flow condition (33500 gpm) for 35.5 seconds during which the total available sodium is spilled and (b) a sodium leak of three percent of full flow conditions lasting for 400 seconds. Following these leak durations, the flow was ramped to zero in 5 seconds. This latter leak is representative of, but more severe than, the leak for which the PHTS cell liners are designed. The nominal parameters about which variations were made are an average sodium drop size of 0.18 inches (see PSAR Section 15.6), a spray volume fraction occupying 30 percent of the cell volume and a spray cone angle of zero degrees. These values are used for CRBRP accident analyses. The variation considered for these parameters are shown in Table Q001.700-1. In all cases, the sodium temperature was 1015°F; all of the sodium leaked was converted to sodium drops; and the initial cell atmosphere consisted of nitrogen with two percent oxygen and 1000 ppm water vapor at 120°F.

The most significant consequence of a sodium leak that is predicted by the SPRAY Code in the inerted cells is the cell pressurization. This result has been used to demonstrate the sensitivity of consequences to the input parameters. The rate of pressurization of the cell for the two reference conditions are shown on Figures Q001.700-1 and Q001.700-2. For the full flow leak, a peak pressure is reached in 22 seconds and additional flow beyond that point maintains the pressure. The pressure drops following oxygen depletion and termination of maximum flow. It should be noted that even for this large flow rate, the peak pressure attained is substantially below the PHTS cell design pressure of 30 psig.

For the three percent full flow leak, the initial rate of pressurization is much lower, the maximum pressure attained is lower and an equilibrium condition had not been reached when the analysis was terminated.

The results of the sensitivity analyses are shown in Figures Q001.700-3 through Q001.700-5. Figure Q001.700-3 shows the effect of drop size on peak pressure. The effect is somewhat different in the two cases. While the initial rate of pressurization is greater for smaller size drops, the maximum pressure reached for the full flow case (i.e., the plateau on Figure Q001.700-1) does not vary significantly with drop size. For the 0.5 inch drop size, the initial rate of pressurization is low enough that the maximum achievable pressure has not been attained within the 35.5 seconds leak period. There is a slight increase in peak pressure with drop size for the full flow leak. For the smaller drop size, more rapid pressurization and oxygen depletion occurs and less sodium is leaked to the pool at the time of peak pressure to displace the cell atmosphere. This results in a slightly lower peak cell atmosphere pressure for the smaller drops.

For the three percent of full flow spill (Figure Q001.700-3), the true peak cell pressure is not reached before the analysis is terminated. Larger droplet diameters result in a lesser rate of pressurization, thus giving the appearance that the cell pressure decreases with increasing droplet diameter. Regardless of this effect, even for drop sizes, a factor of 2 lower, the peak cell pressure is not significantly higher than that for 0.18 inch diameter drops.

To determine if leaks greater than the full flow leak would result in higher pressurization, a leak rate of 150 percent of the full flow (50,250 gpm) with nominal parameters was analyzed. The peak pressure as shown in Figure Q001.700-3 is the same as that for the full flow case.

The effect of cell volume fraction occupied by the zone containing the sodium drops on cell pressurization was discussed in PSAR Section 15.6.1.4.2. It was concluded that the reported results were not strongly dependent upon the spray volume fraction or the spray cone angle. Additional data have been obtained in this study. The spray volume fraction was changed by increasing the diameter of the spray region while keeping the spray zone angle constant at zero degrees. The results are presented in Figure Q001.700-4. The results indicate that the peak pressure increases with increasing spray volume fraction, but that the peak pressure reaches a plateau at a spray volume fraction of approximately 30% of the cell volume. The spray volume fraction can also be changed by changing the spray cone angle. While maintaining a constant spray volume fraction of 0.3, the spray region diameter at the top of the cell and the spray cone angle were varied. The resulting peak pressures are shown in Figure Q001.700-5. This demonstrates that there is essentially no change in the peak pressure due to the changes in the spray cone angle.

The data presented above indicate the sensitivity of important input parameters for the SPRAY Code on the predicted consequences of sodium leaks into the PHTS Cell. Both an extremely large leak and a leak representative of that for which the PHTS cell and its liner are designed were considered. The results show that the sensitivity to the input parameters is moderate. Considering the conservatism of the nominal input parameters (0.18 in. diameter droplet, 100 percent conversion of the sodium leak to drops, 30 percent spray volume fraction) and the lack of strong sensitivity to any of the parameters, they will continue to be used for safety analysis of sodium spills.

Table Q001.700-1

RANGE OF VALUES FOR PARAMETER STUDY

<u>Parameter</u>	<u>Range of Values</u>
Drop Diameter (in)	0.075 to 0.50
Spray Volume (Fraction of Cell Volume)	0.075 to 0.45
Spray Cone Angle (Degrees)	0.0 to 57.0

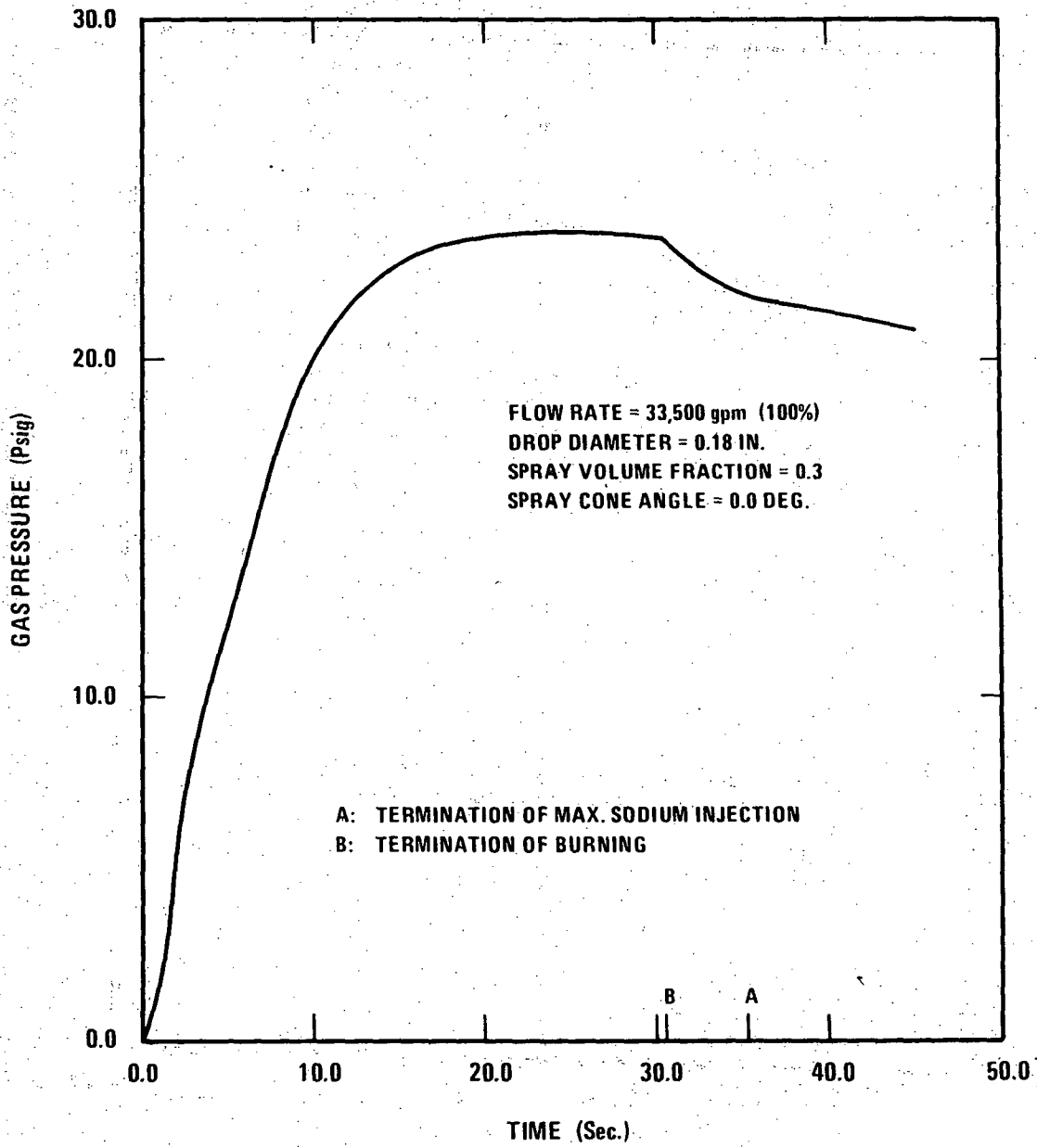


Figure Q001.700-1

0966-4

Q001.700-5

Amend. 48
 Feb. 1979

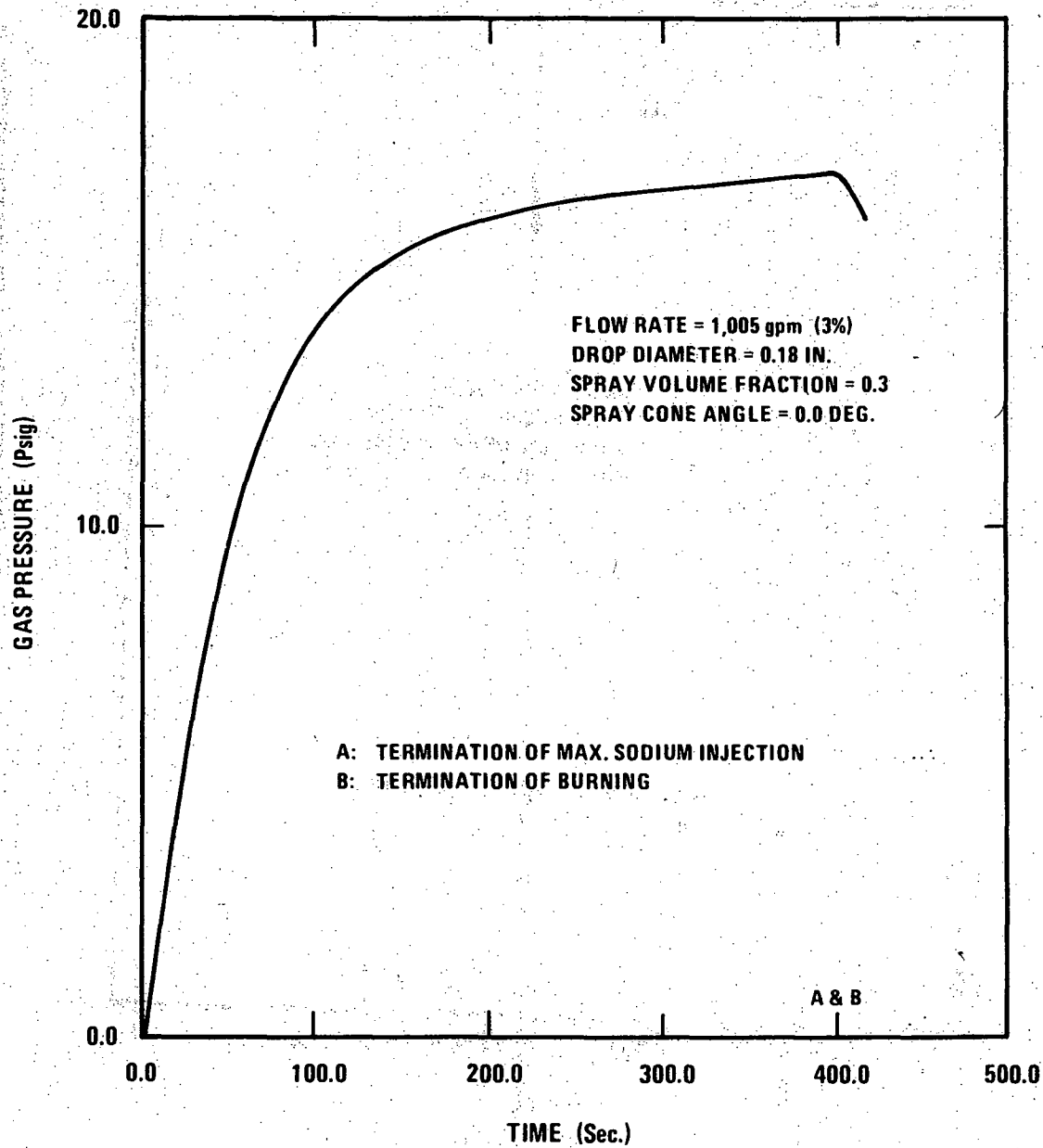


Figure Q001.700-2

0966-44

Amend. 48
Feb. 1979

Q001.700-6

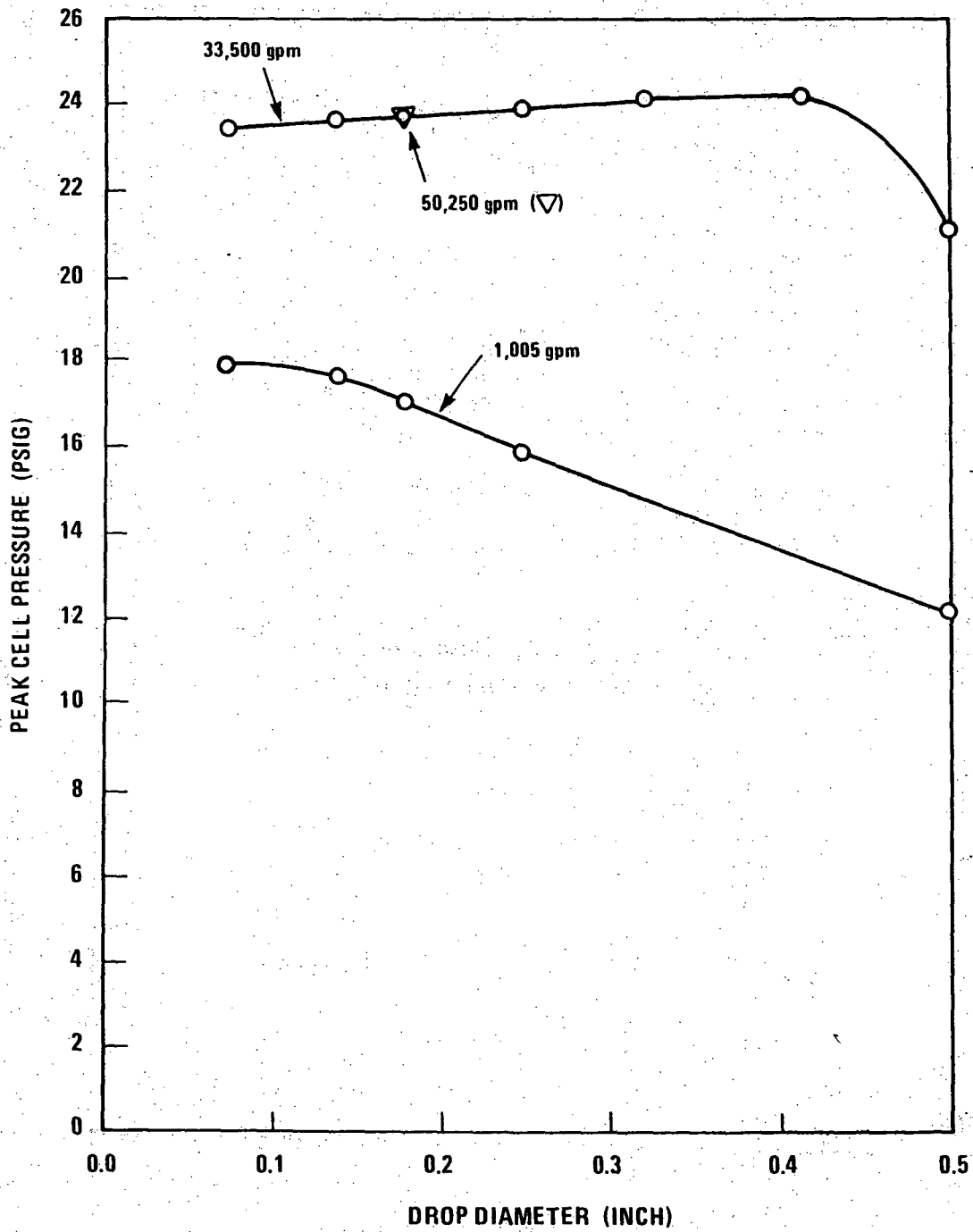


Figure Q001.700-3 Peak Pressure vs. Drop Diameter

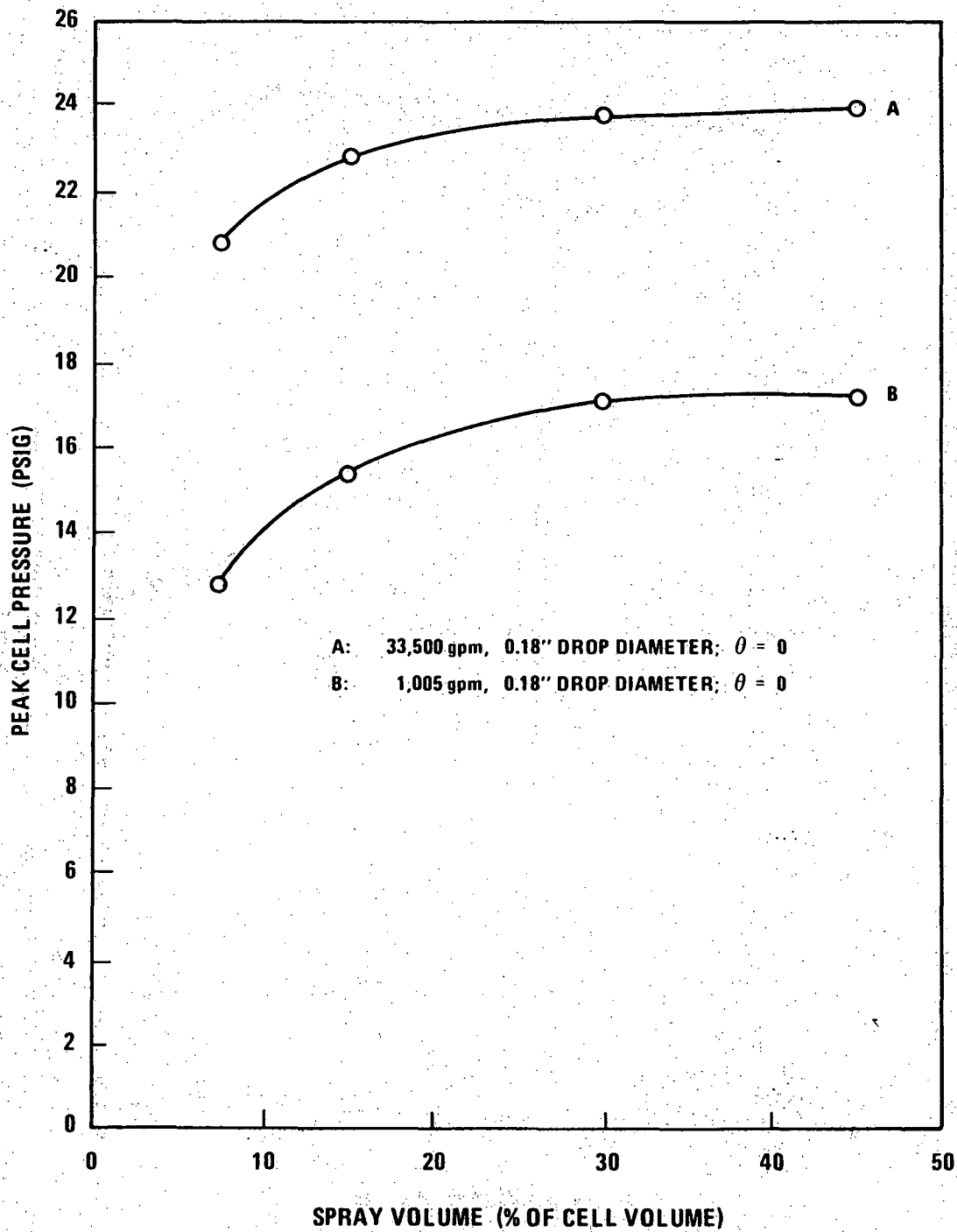


Figure Q001.700-4 Peak Pressure vs. Spray Volume

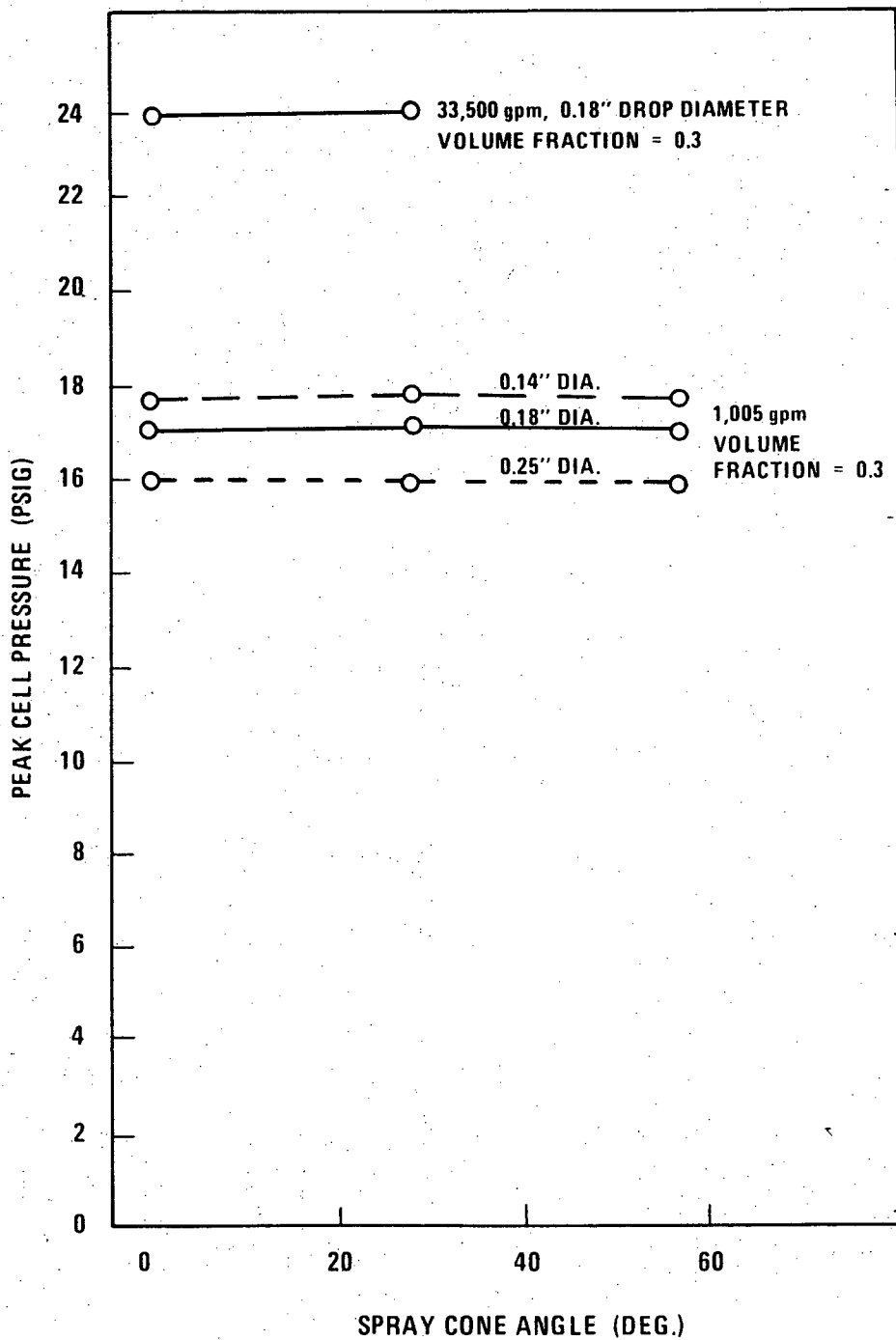


Figure Q001.700-5 Peak Pressure vs. Spray Cone Angle

Question 001.701

The work presented at the March 5, 1976 meeting regarding the characterization of sodium breakup following impact of a vertical jet (simulating double-ended pipe rupture) for the inerted PHTS cell case was limited to jet velocities of about 20 ft/sec. Higher velocity jets from partial pipe breaks or splits will yield smaller droplet sizes resulting in higher PHTS pressure rises at probably even lower sodium discharge flow rates. Published data on the stability of liquid jets and sheets show that the dependence of droplet diameter at breakup or stream velocity changes at velocities (Re numbers) of interest of partial breaks, which are higher than the velocity range shown during the presentation.

Discuss the characteristics of sodium sprays from partial pipe breaks and the higher stream velocities resulting therefrom. Extend the sensitivity studies requested in item 001.700 above to include the full range of parameter values associated with partial pipe breaks (e.g., pipe cracks and breaks of process lines at the weld joint to the primary loop).

Response:

The parameters studied in the sensitivity study for question 001.700 are (1) drop size, (2) spray volume fraction and (3) spray cone angle. These three parameters are those utilized in SPRAY which would vary with jet velocity and leak configuration. Exit velocity of the jet is not a parameter input to SPRAY. As reported in the response to Question 001.700, the peak cell pressure is not sensitive to the spray cone angle nor to spray volume fraction for spray volume fractions greater than 30%. The peak pressure resulting from drops smaller than the nominal 0.18" in diameter increases only slightly for drops down to a diameter of 0.075". The 0.18" diameter drops are consistent with experimental data (see PSAR Section 15.6.1.4.2) for leak rates as low as 15 gpm. This leak rate is considerably lower than the leak which formed the lower bounds of the parameter study in 001.700. Therefore, the parameter study envelops the values associated with partial pipe breaks and higher velocity jets.